Advancing Aluminyl Anions:
Synthesis of Acyclic and Four-Membered Metallocyclic Aluminium Nucleophiles

Aidan James Richard Matthews

Thesis presented to the Research School of Chemistry, Australian National University
for the degree of Doctor of Philosophy

October 2024

Australian National University

© Copyright by A. J. R. Matthews 2024
All rights reserved

Declaration

The research described within this thesis is the owner's original work, with exception of that to which reference is made in the text.

A. J. R. Matthews

This thesis is dedicated to my friend and mentor

Richard Ruff

the giant on whose shoulders I have stood.

Acknowledgements

I would like to express my sincere gratitude to Dr. Jamie Hicks for the invaluable opportunity to pursue my PhD studies within his research group as its inaugural candidate. This experience has profoundly impacted my academic and personal journey, and I have never regretted my decision to relocate from Melbourne. Discussions of the "main group paper of the week" and recent Formula 1 races have always been a Monday morning highlight whilst walking to group morning coffee. His unwavering support and guidance in exploring opportunities both within Australia and internationally have been instrumental in the completion of this work. His mentorship, generosity, and dedication to the growth of all his students will forever resonate with me.

To Prof. Dr. Christian Sindlinger, I am incredibly appreciative to work and learn within his research group for over 7 months at the Universität Stuttgart. Arriving only a few weeks after the group had arrived at a new institution provided an exceptional opportunity to deepen my understanding of diverse areas of chemistry and broader academic processes. His encouragement, structured approach, and teaching have significantly shaped my research inquiries both in Germany and upon my return to Australia.

To all members of the Hicks Group, past and present, thank you for fostering a vibrant and dynamic laboratory environment. I am particularly grateful to my fellow PhD students – Li Feng Lim, Liam Pascoe, Emily Nahon, Gareth Nelmes, and Ryan Huo – for the collaborative atmosphere we shared while pursuing our respective research goals and all the many, many laughs we have shared together. I wish you all the very best when the time comes to write each of your theses and for your careers ahead. I extend special thanks to Dr. Fabian Kallmeier for his meticulous review of this thesis and unwavering promotion of Scooter Fridays. Additionally, I appreciate the contributions of the Honours and project students who have enriched the group during their tenure, and often left a lasting impact.

To the Arbeitskreis Sindlinger, I am grateful for your warm welcome, which made Stuttgart feel like a second home. My thanks go especially to Dr. Tobias Heitkemper, Julijan Sarcevic, Thibault Damiens, and Michael Jochum for creating an engaging lab atmosphere filled with diverse music and camaraderie over coffee and lunch. I would also like to acknowledge the support staff and research groups within the Institute of Anorganische Chemie, particularly those from Sarkar, Gudat, and Niewa, whose assistance and hospitality were invaluable during my time in Stuttgart.

To the collaborators who have contributed work to this thesis, thank you. Dr. David Liptrot and Ross Jackson (University of Bath), who were close contributors in developments of acyclic aluminium(III) precursors and the first acyclic aluminyl anion in chapters 2 and 3. Dr Petra Vasko (University of Helsinki) who performed computational studies on compounds in Chapter 3. Gareth Nelmes (Australian National University) who performed computational studies on compounds in Chapter 4. Dr Tobias Heitkemper, Julijan Sarcevic and Michael Jochum (Universität Stuttgart) who assisted with providing reagents, synthetic precursors and optimisation techniques for compounds reported in Chapter 5. Fridolin Hennhöfer (Universität Stuttgart) and Lim Li Feng (Australian National University) who assisted with the collection, interpretation and simulation of EPR spectroscopic measurements and reporting of radical species in Chapter 5.

I would like to express my heartfelt gratitude to my parents, Tracey and Iain Matthews, for their unwavering support and encouragement throughout my academic and educational journey. I would also like to thank my sister Carly, brother-in-law Shay, grandparents Lola and Alby Irwin, Michael and Jewel Matthews, aunty Kerry Ruff and my further extended family for their consistent curiosity and support throughout this endeavour. Notably, would like to thank Damian Ruff whose passion for science has fostered much of my career. I am equally grateful to my friends in Melbourne and beyond, who have continually shown interest in my research inquiries.

To my partner, Clara-Rike Niemeyer, your steadfast support and encouragement throughout this journey have been nothing short of extraordinary. Thank you for your willingness to accompany me through our relocations from Melbourne to Canberra, then Stuttgart, and back to Canberra. Your support has been a cornerstone of my success. Thank you for everything you have done to support me on this adventure.

Lastly, this thesis is dedicated to Richard Ruff. His generosity of time, tutelage and mentorship are foundational to my education and career within chemistry, and the wider scientific community. For this, I am infinitely grateful.

Abbreviations

Ad	1-adamantyl
Ar	a general aryl substituent
Ar^{Dipp}	2,6-$Dipp_2$-C_6H_3
Ar^{Mes}	2,6-Mes_2-C_6H_3
$[^{Ar}Nacnac]^-$	$[(ArNCMe)_2CH]^-$
Ar^{Tripp}	2,6-$Tripp_2$-C_6H_3
bipy	2,2′-bipyridine
br.	broad
ca.	*circa*
CAAC	cyclic alkyl amino carbene
CDP	Contact Dimeric Pair
cm^{-1}	unit of wavenumber
Cp	cyclopentadienyl, $[C_5H_5]^-$
Cp*	pentamethylcyclopentadienyl, $[C_5Me_5]^-$
$[C^{Ph*}N^{Dipp}]^{2-}$	$[(Ph*)_2C(CH)_2NDipp]^{2-}$
crypt-222	cryptand [2.2.2]
$[C^{Si}]^{2-}$	$[\{C(SiMe_3)_2CH_2\}_2]^{2-}$
$[C^{Si}N^{Ad}]^{2-}$	$[(Me_3Si)_2C(CH)_2NAd]^{2-}$
Cp^{3t}	1,2,4-tris(*tert*-butyl)cyclopentadienyl
Cy	cyclohexyl
d	doublet
$[DAS]^{2-}$	$[Ph_2Si(DippN)_2]^{2-}$
$[DBDI^{Dipep}]^{2-}$	$[H_2C=C(N^{Dipep})-C(H)=C(Me)-N^{Dipep}]^{2-}$
$[DBDI^{Dipp}]^{2-}$	$[H_2C=C(N^{Dipp})-C(H)=C(Me)-N^{Dipp}]^{2-}$
DCM	Dichloromethane
dec.	decomposition
DFT	density functional theory
Dipep	2,6-$CEt_2(H)$-C_6H_3
Dipp	2,6-diisopropylphenyl
$[^{Dipp}DAB]^{2-}$	$[\{(DippNC(CH_3)\}_2]^{2-}$
$[^{Dipp}Nacnac]^-$	$[(DippNCMe)_2CH]^-$

DMAP	4-dimethylaminopyridine
DME	1,2-dimethoxyethane
DMF	dimethylformamide
DOSY	Diffusion Ordered Spectroscopy
EPR	electron paramagnetic resonance
Et	ethyl
eq.	equivalents
$[Giso]^-$	$[(DippN)_2CN^iPr_2]^-$
HMDS	hexamethyldisilylamide
HOMO	highest occupied molecular orbital
Hz	hertz, s^{-1}
Idipp	$C\{N(Dipp)CH\}_2$
Idipp*	$C\{N(Dipp)C(Me)\}_2$
IMe	$C\{N(Me)CH\}_2$
Imes	$C\{N(Mes)CH\}_2$
IiPr	$C\{N(^iPr)CH\}_2$
^{i}Pr	isopropyl
IiPr*	$C\{N(^iPr)C(Me)\}_2$
IR	infrared spectroscopy
J_{xy}	coupling constant between nuclei X and Y in Hz
K	Kelvin
kJ	kilojoule
L	a general ligand
LUMO	lowest occupied molecular orbital
LEP	Ligand encapsulated pair
m	*meta*-substituent
m	multiplet (NMR) or medium (IR)
M	a general metal or molar (mol dm^{-3})
m/*z*	mass/charge ratio
M^+	a molecular ion
Me	methyl
Mes	mesityl (2,4,6-trimethylphenyl)

Mes*	2,4,6-tri-*tert*-butylphenyl
^{Mes}Nacnac	$[(MesNCMe)_2CH]^-$
MIP	Monomeric Ion Pair
mol	mole
Mp	melting point
MS/EI	electron ionisation mass spectrometry
MS/LIFDI	Liquid Injection Field Desorption/Ionization Mass Spectrometry
mT	Millitesla
mW	Milliwatt
*m*Xyl	3,5-dimethylphenyl
N_2P_2	^{t}BuN$^{(-)}$SiMe$_2$N-(CH$_2$CH$_2$P^{i}Pr$_2$)$_2$
^{n}Bu	primary butyl
NCCCN	bis(2,6-diisopropylphenyl)-1,3-propanediamine
NHBO	N-heterocyclic boryloxy, $[\{OB(NDippCH)_2\}_2]^-$
NHC	N-heterocyclic carbene
$[NON]^{2-}$	4,5-bis(2,6-diisopropylanilido)-2,7-di-*tert*-butyl-9,9-dimethylxanthene
NMR	Nuclear Magnetic Resonance
o	*ortho*-substituent
p	*para*-substituent
Ph	phenyl
Ph*	3,5-^{t}Bu$_2$-C$_6$H$_3$
Piso	$[(DippN)_2CH]^-$
ppm	parts per million
*p*Xyl	3,6-dimethylphenyl
ppm	parts per million
*p*Xyl	3,6-dimethylphenyl
q	quartet
R, R′, R″	general organic substituent
r.t.	Room temperature (25 °C)
s	singlet (NMR) or strong (IR)
S	spin state
SCXRD	Single crystal X-Ray Diffraction

sept	septet
$[SiN^{Dipp}]^{2-}$	$[\{CH_2SiMe_2N(Dipp)\}_2]^{2-}$
$[SiN^{Mes}]^{2-}$	$[\{CH_2SiMe_2N(Mes)\}_2]^{2-}$
$[^{Si}NON]^{2-}$	$[O\{Si(Me)_2N(Dipp)\}_2]^{2-}$
SIP	Separated Ion Pair
sol.	solvent
t	triplet
^{t}Bu	tertiary butyl
$[^{tBu}DAB]^{2-}$	$[\{(^t BuNC(CH_3)\}_2]^{2-}$
THF	tetrahydrofuran
TMEDA	tetramethylethylenediamine
TMS	trimethylsilyl or tetramethylsilane
Tripp	2,4,6-triisopropylphenyl
UV	ultraviolet
WBI	Wiberg bond index
X	a general halide
Xyl	2,6-dimethylphenyl
δ	chemical shift in NMR spectroscopy (*ppm*)
λ	wavelength
μ	bridging
ν	wavenumber
12-crown-4	1,4,7,10-tetraoxacyclododecane
18-crown-6	1,4,7,10,13,16-hexaoxacyclooctadecane

Abstract

Chapter 1 presents a general introduction to modern organometallic chemistry and its subsequent paradigm shift encompassing the developing roles of the main group elements, their fundamental considerations and challenges in low oxidation state element synthesis. It includes an overview of the frontiers of research interests and the pursuit of transition-metal metallomimetic species for small molecule activation. Finally, the focus of the chapter shifts to group 13, highlighting its elemental members, and a chronological summary of research discoveries in developing a new class of group 13 anionic nucleophiles.

Chapter 2 focuses on the preparation of bulky silylamido aluminium(III) halide complexes incorporating both monodentate and bidentate chelating ligand scaffolds. The rationalisation and role of ligand design in modern organometallic chemistry, and previous applications of the utilised ligand scaffolds are discussed. The necessitated synthetic routes, isolation and structure of prepared species are explored and compared with related aluminium(III) halide complexes. The complexes reported in the chapter will serve as precursors for the novel aluminyl anions presented in Chapters 3 and 4.

Chapter 3 discusses the preparation and isolation of low oxidation state, aluminium(I) nucleophiles. These include the isolation and characterisation of the first acyclic aluminyl anion $[K_2(Al\{N(Dipp)SiMe_3\}_2)_2]$, synthesised by the reduction of $[AlI\{N(Dipp)SiMe_3\}_2]$ with potassium graphite. The reduction of the bulkier analogue, $[AlI\{N(Dipp)Si(^iPr)_3\}_2]$, yielded intramolecular activation products consistent with the transient generation of an aluminyl anion. The reactivity of the resulting acyclic aluminyl anion was explored briefly towards a range a small molecules, and applied in the preparation of the magnesium aluminyl complexes $[(^{Ar}Nanac)Mg–Al\{N(Dipp)SiMe_3\}_2]$ ($[^{Ar}Nacnac]^– = [(ArNCMe)_2CH]^–$, Ar = mesityl, 2,6-diisopropylphenyl). Structural classifications of related aluminyl anions are explored from the conversion of the parent acyclic aluminyl anion contact dimeric pair toward both monomeric and charge-separated ion pairs.

Chapter 4 further expands on the isolated examples of low oxidation state aluminium(I) nucleophiles. This includes the isolation and characterisation of the first aluminyl anion contained within a four-membered metallocycle. This anion was synthesised by the reduction of the aluminium(III) iodide precursor [AlI(DAS)] ([DAS]$^{2-}$ = [$Ph_2Si(NDipp)_2$]$^{2-}$) with potassium graphite under short timeframes, [K{Al(DAS)}] was isolated as a 1-dimensional coordination polymer in the solid state. Synthesis and characterisation of the corresponding iron aluminyl coordination complex [$(CO)_2CpFe$–Al(DAS)] (Cp = cyclopentadienyl) is also discussed. The reactivity of [K{Al(DAS)}] was briefly explored and utilised in the preparation of complexes featuring unsupported bonds of Mg–Al [(^{Ar}Nanac)Mg–Al(DAS)] and Al–Al [{Al(DAS)}$_2$]. The published library and presented aluminyl anions [K_2(Al{N(Dipp)$SiMe_3$}$_2$)$_2$] and [K{Al(DAS)}] are compared, concerning their ligand scaffolds and the imparted electronic and nucleophilic effects present in reactivity is reported.

Chapter 5 concentrates on research investigations undertaken on exchange at the University of Stuttgart. Hückel antiaromatic group 13 metalloles incorporating boron and aluminium, and their reduction to give aromatic and radical species are discussed. The redox applications of the acyclic aluminyl anion [K_2(Al{N(Dipp)$SiMe_3$}$_2$)$_2$] with 2,5-disilyl-3,4-diaryl boroles is presented through reductions to analogous boroldiide and borole radical anions, and coinciding oxidation yielding an acyclic dialane [(Al{N(Dipp)$SiMe_3$}$_2$)$_2$]. A catalogue of new 2,5-disilyl-3,4-diaryl alumole complexes are reported, their synthesis, structure and reactivity are explored, and investigations undertaken toward new NHC-stabilised alumole cations are discussed.

Contents

Declaration ii

Dedication iii

Acknowledgements iv

Abbreviations vi

Abstract x

Contents xii

1. Chapter 1: General Introduction 1

1.1. Modern Organometallic Chemistry 1

1.2. Main Group Elements 1

1.3. Frontiers in Main Group Organometallic Chemistry 2

1.4. Group 13: The Boron Group 4

1.4.1. Trends, Physical and Chemical Properties 4

1.4.2. Boron 5

1.4.3. Aluminium 5

1.4.4. Gallium 6

1.4.5. Indium 6

1.4.6. Thallium 7

1.5. Low Oxidation State Group 13 Chemistry 7

1.5.1. Singly Bonded $E^{(II)}$-$E^{(II)}$ Group 13 Dimers 8

1.5.2. Neutral Compounds Featuring $E^{(I)}$ centres 10

1.5.3. Multiply Bonded $E^{(I)}$-$E^{(I)}$ Group 13 Dimetallenes and Dimetallynes 16

1.6. Anionic Group 13 Nucleophiles 19

1.6.1. Gallyl Anions: Synthesis and Structural Arrangements 20

1.6.2. Boryl Anions: Synthesis and Structural Arrangements 21

1.6.3. Indyl Anions: Synthesis and Structural Arrangements 23

1.6.4. Aluminyl Anions: A New Class of Group 13 Nucleophiles 24

1.7. Overview of Literature Review 25

1.8. References 26

2. Bulky Silylamido Aluminium(III) Iodide Precursors 30

2.1. Introduction 30
2.1.1. The First Aluminyl Anion 30
2.1.2. Ligand Design 30
2.1.3. Synthetic Methodologies 31

2.2. Literature Outline and Target Rationalisation 33
2.2.1. Library of Aluminium(III) Halide Precursors for Aluminyl Anion Preparation 33
2.2.2. Ligand Rationalisation 35

2.3. Research Rationales 39
2.3.1. Acyclic Aluminium(III) Precursor Rationale 39
2.3.2. 4-Membered Aluminium(III) Precursor Rationale 40

2.4. Acyclic Aluminium(III) Halide Precursors: Results and Discussion 41
2.4.1. Synthesis of Bulky Monodentate *N*-Silylanilines 41
2.4.2. Trimethylaluminium Metalations of Monodentate *N*-Silylanilines 41
2.4.3. Halogenation of the Amido Aluminium(III) Dimethyl Complexes 46
2.4.4. Salt Metathesis Transformations with Silyl(aryl)amido Alkali Metal Salts 49
2.4.5. Contemporary Li[AlH_4] Metalations 60

2.5. A Four-Membered Aluminium(III) Halide Precursor: Results and Discussion 63
2.5.1. Synthesis of a Bulky Bidentate Silyldiamine Proligand 63
2.5.2. Trimethylaluminium Metalations of Bidentate Silyldiamine Proligand 63
2.5.3. Iodination of Aluminium Methyl Silyldiamido Complexes 67
2.5.4. Contemporary Li[AlH_4] Metalations 68
2.5.5. Salt Metathesis involving Silyldiamido Alkali Metal Salts 70
2.5.6. Exploring the Reactivity of a 4-Membered Aluminium(III) Iodide Precursor 2-XXXIII 78

2.6. Conclusions 79

2.7. Experimental 80

2.8. References 100

3. An Acyclic Aluminyl Anion 102

3.1. Introduction 102
3.1.1. Previous Aluminyl Anions Accessible in the form of Transition Metal Complexes 102
3.1.2. Synthetic Library of Aluminyl Anions 103
3.1.3. Cation Influences on Structural Arrangements 107
3.1.4. Reactivity of Aluminyl Anions 112

3.2. Research Rationale 124
3.2.1. Acyclic Precursors for Aluminyl Complexes 124

3.3. Results and Discussion 124
3.3.1. Attempted Preparations of Iron-Aluminyl Coordination Complexes 124
3.3.2. Reductions of the Bis-triisopropylsilyl(aryl)amido Aluminium(III) Iodide 127
3.3.3. Reductions of Bis-trimethylsilyl(aryl)amido Aluminium(III) Iodide 134
3.3.4. *In-silico* Investigations of Acyclic Aluminyl Anions 138
3.3.5. Initial Reactivity Studies 141
3.3.6. Attempted Preparation of MIP and SIP complexes 144
3.4. Conclusions 147
3.5. Experimental 148
3.6. References 155

4. A 4-Membered Aluminyl Anion 158

4.1. Preamble 158
4.2. Research Rationale 159
4.2.1. A 4-Membered Precursor for Reduction Inquiries 159
4.3. Results and Discussion 160
4.3.1. Preparations of an Iron-Aluminyl Coordination Complex 160
4.3.2. Alkali Metal Reductions of a 4-Membered Aluminium(III) Iodide Precursor 163
4.3.3. *In-silico* Investigations of a 4-Membered Aluminyl Anion 170
4.3.4. Initial Reactivity Studies of a 4-Membered Aluminyl Anion 172
4.3.5. Inquiries toward Isolating MIP and SIP Complexes of 4-Membered Aluminyl Systems 179
4.4. Conclusion 185
4.5. Experimental 186
4.6. References 193

5. Developments of Group 13 Metalloles 194

5.1. Introduction 194
5.1.1. Hückel Antiaromatic Metalloles and their Initial Reports 194
5.1.2. Boroles: A Structural Overview 195
5.1.3. Boroles: Synthesis 197
5.1.4. Boroles: Reactivity 199
5.1.5. Borole Reduction and Derivatisation 203
5.1.6. Boroles: An Outlook 205
5.1.7. Alumoles: A Structural Overview 206
5.1.8. Alumoles: Synthesis 209
5.1.9. Alumoles: Reactivity 213

5.1.10. Alumoles: An Outlook 216

5.2. Research Rationale 217

5.2.1. Applying an Acyclic Aluminyl Anion with Boroles 217

5.2.2. Expanding the Alumole Catalogue 217

5.3. Results and Discussion: Boroles 218

5.3.2. Reduction Chemistry of Boroles with an Acyclic Aluminyl Anion 220

5.3.3. Targeted Preparations of an Acyclic Aluminium(II) Dimer 229

5.3.4. Summary of Borole Reductions with an Acyclic Aluminyl Anion 230

5.4. Results and Discussion: Alumoles 231

5.4.1. Synthesis of Haloalumoles and their Lewis Acid-Base Adducts 231

5.4.2. Investigations to Afford Aryl-Coordinated Alumoles 240

5.4.3. Reactivity of NHC-Stabilised Chloroalumoles toward a Cationic Alumole 243

5.5. Conclusion 246

5.6. Experimental 247

5.7. References 261

6. Conclusions 265

7. Future Work 266

8. Appendix 267

8.1. Publications in Support of this Thesis 267

8.2. X-ray Crystallography 267

8.3. Computational Studies 267

8.4. Summary of Crystallographic Data 268

8.4.1. Crystallographic and Refinement Parameters for the Structures in Chapter 2 268

8.4.2. Crystallographic and Refinement Parameters for the Structures in Chapter 3 271

8.4.3. Crystallographic and Refinement Parameters for the Structures in Chapter 4 272

8.4.4. Crystallographic and Refinement Parameters for the Structures in Chapter 5 274

8.5. References 275

1. Chapter 1: General Introduction

1.1. Modern Organometallic Chemistry

The last half century has seen contemporaneous development of the main group and transition metal organometallic frontiers. Representing a rendezvous of traditional inorganic and organic chemistry concepts, organometallic chemistry encompasses burgeoning fields that underpin industrial applications of catalysis, and small-molecule activation and functionalisation.

Prior to the 1980's, the chemistry of transition metals was viewed as being inherently more rich than that of main group elements. Previous dogma highlighted transition metal elements as typically having partially filled valence *d* orbitals (which are relatively close in energy) that can interact with small molecules (CO, C_2H_4, or H_2) and subsequently yield value added products on up to industrial scales. In contrast, the main group elements present valence *s* or *p* orbitals, which are traditionally unambiguously fully occupied or empty. Such being separated by relatively large energy gaps are, therefore, generally inert toward small molecules. As such, the belief was held that main group chemistry was devoid of further major discoveries.[1]

The dawn of modern main group chemistry seeded the paradigm shift towards elements of valence *s* or *p* orbitals. In 1981, the isolation of a number of compounds, previously considered to be inaccessible, meant that the traditional rules governing the understanding of the main group were overhauled.[1] Since then, the access of isolable species has seen the ongoing and continual acceleration of the field.[2] Such compounds have been reported to adopt unusual electronic configurations,[3] display increased reactivity through activating strong chemical bonds,[4] and facilitate a range of catalytic processes.[5] The renaissance of modern main group elements continues to represent unprecedented developments within organometallic chemistry.

1.2. Main Group Elements

Main group elements include those of groups 1-2 and 13-18 of the periodic table. The *s*-block subsumes the elements of the first two groups with ground state configuration electrons populating the valence *s* orbitals. *s*-Block metals (irrespective of radioactive examples) were all discovered by the middle of the 19th century.[6] Along with ionisation energies, atomic radii and ionic radii are governing factors in the chemical properties of group 1 and 2 elements.[7] The *p*-block elements (groups 13-18) encompass a variation of metals, non-metals, metalloids, variable oxidation states, and valencies constituting a breadth of structures ranging from polymers and covalent molecules to metals, alloys, and ionic solids with varied properties.[3] *p*-Block elements feature ground state electrons occupying

the valence *p* orbitals of p_x, p_y, and p_z orientations.[7] Moreover, the early *p*-Block encompasses the groups 13-15, highlighting the inclusion of post-transition metal elements.[8]

Traditionally, main group elements are limited in their oxidation states, governed by their element electron configuration.[9] This is in stark contrast to *d*-block elements, which present an assortment of oxidation states.[7] Main group compounds orthodoxly feature large HOMO-LUMO gaps (Highest Occupied Molecular Orbital, Lowest Unoccupied Molecular Orbital), and often lack multiple stable oxidation states, subsequently increasing the barrier to reliable small molecule activation and applications within catalytic processes. Furthermore, as per the "Double Bond rule" elements of principle quantum number >2 were conventionally understood not to form stable multiply bonded species.[3] This was reinforced by challenges faced with degeneracy, symmetry, and poor overlap exhibited in the main group frontier orbitals of such species.[7, 9]

In recent years, efforts toward cheaper and "greener" chemical processes have bolstered investigations transitioning main group elements toward the applications previously held by late transition metals.[10] The abundance of main group elements within the Earth's crust (silicon 28.2%, aluminium 8.2%, calcium 4.2%, and sodium 2.4%),[11] bolsters the interest in such elements toward industrial applications.[12] The affordability of the main group elements is sustained by their existing prevalence within manufacturing and industrial applications. Irrespective of outliers, main group elements are considered environmentally benign and relatively non-toxic.[10]

In conjunction with their abundance, affordability and non-toxicity, the diversity of physical and chemical properties spanning the main group accentuates these elements for innumerable applications of environmental, economic and industrial significance further developing previously inaccessible synthetic routes.[13]

1.3. Frontiers in Main Group Organometallic Chemistry

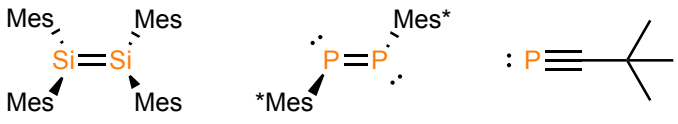

1.1 **1.2** **1.3**

Figure 1.1: First reported examples of disilene, diphosphene, and phosphaalkyne. (Mes = 2,4,6-trimethylphenyl, Mes=2,4,6-tri-tert-butylphenyl).*

Following the conclusion of 1981, the renaissance of main group chemistry was initiated, forgoing dogmatic preconceptions.[1] The doctrine concerning the traditionally accepted understandings was inverted upon the report of three novel compounds (Figure 1.1). These included West and coworkers

disilene $Mes_2Si{=}SiMes_2$ (**1.1**),[14] Yoshifuji and coworkers diphosphene Mes*P=PMes* (**1.2**),[15] and Becker and coworkers phosphaalkyne P≡C^{t}Bu (**1.3**).[16] The isolation of these novel compounds saw the transgression of the strongly accepted "Double Bond rule", through the formation of multiple bonds by elements of principle quantum number >2.[17] Kinetic stabilisation through an increase in ligand steric bulk was prominent across all of these novel compounds, proving key in their isolation.[18] This revelation stimulated the paradigm shift in main group chemistry, from which over four decades of research has followed.[1, 17]

At the beginning of the recent millennium, comprehensions developed toward the applicability of modern main group species through ongoing synthetic and burgeoning computational inquiries. Investigations reiterated that low oxidation state main group compounds could emulate similar electronic properties and frontier orbital arrangements to those of many late transition metal complexes.[3, 18] Transition metal complexes are highly applied within small molecule activation due to their electronic configurations and the degeneracy and symmetry of their *d*-orbitals. The relatively moderate HOMO-LUMO energy gap, ability to undergo oxidative addition at the metal centre, and the vacancy of orbitals supporting ligand coordination endorse transition metal complexes for small molecule activation.[7] When interacting with various species, transition metals may interact in a σ acceptor/π donor approach through a combination of vacant and occupied frontier orbitals facilitating small molecule activation (Figure 1.2 (a, b)).[18-19]

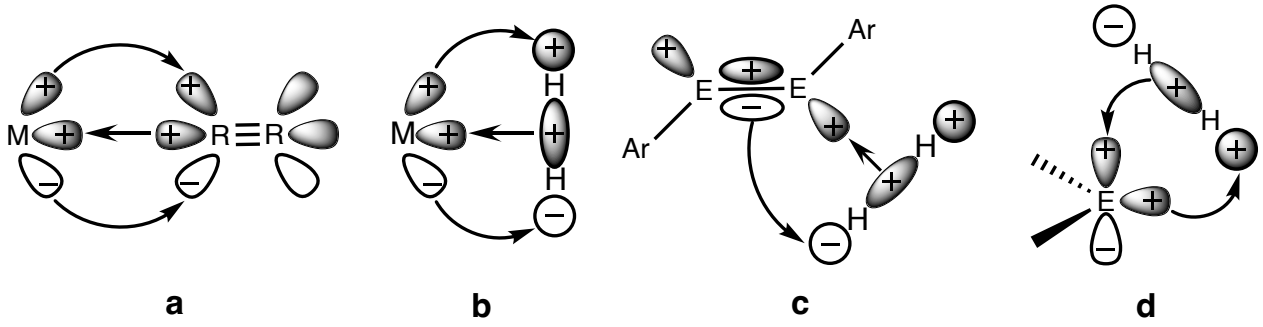

Figure 1.2: Frontier orbital interaction of a: (a) transition metal (M) and CO/N_2 (R=C, N, O) (b) transition metal and H_2 (c) multiply bonded main group species and H_2 (d) carbene analogue singlet main group species and H_2.

The principle exemplification for main group elements to mimic the reactivity of transition metals was published by Power and coworkers in 2005.[20] A formally triply bonded heavy alkyne analogue, digermyne ($Ar^{Dipp}Ge{\equiv}GeAr^{Dipp}$), stabilised by bulky aryl ligands (Ar^{Dipp} = 2,6-$(Dipp)_2$-C_6H_3, Dipp = 2,6-diisopropylphenyl) was reported as the first purely main group compound to split dihydrogen under ambient conditions. This was possible through the synergistic interactions of the frontier orbitals with H_2, seeing the electron density of the π-HOMO orbital of $Ar^{Dipp}{}_2Ge{\equiv}GeAr^{Dipp}{}_2$ donated into the

σ*-orbital of H_2 (Figure 1.2 (c)). This donation of electron density weakened the H-H bond, facilitating oxidative addition by the metal centre. Moreover, the reactivity of singlet state group 14 tetrylenes (heavier analogues of highly reactive, neutral two-coordinate carbenes, i.e. silylenes, germylenes, stannylenes, and plumbylenes) have also been identified to react similarly, aided by an empty *p*-orbital *and* a pair of electrons at the main group centre (Figure 1.2 (d)).[21] The orbital overlap and comparatively analogous reactivity of the transition metal and main group centres with the substrate, postulates opportunities for main group species as metallomimetics in catalysis.[18, 22] However, challenges remain in the application of main group species as catalysts, limiting their implementation within industry.[5]

Highly relevant to industry and presenting key challenges, catalytic transformations featuring main groups species are a growing investigative focus within academic literature. Drawing parallels to transition metal-based catalysis, *s*-block systems have been developed that are capable of insertion and σ-bond metathesis reactions, however, featuring fixed rather than fluxional main group element oxidation state cycles.[3] Conversely, a small number of reports have highlighted low valent *p*-block species capable of undergoing redox based-catalytic cycles (including FLP-catalyzed hydrogenation of imines and alkynes, Catalytic CO_2 reduction, and Phosphonium catalysis),[3] however, examples remain limited. Principal challenges faced in main group catalytic cycles include oxidative addition reactions yielding stable products, consequently hampering reductive elimination steps, and halting implementation in reductive elimination processes.[5]

Confronting these challenges, ongoing inquiries feature new and varied ligands/substituents for kinetic and electronic stabilisation of these species within applicable redox configurations and consequently broadening their potential for utilisation.[22-23]

1.4. Group 13: The Boron Group

1.4.1. Trends, Physical and Chemical Properties

In contrast to the exclusively metallic nature of *s*- and *d*-block elements, the *p*-block covers elements of non-metal, metalloid and metallic characters.[7] Progression down the group sees an increase in metallic character from boron as a metalloid (highlighting its anomalous nature), to gallium, indium and thallium as metals. Boron's small atomic radius and its chemical properties as the first congener of group 13 differ from those of the other elements. This anomalous nature highlights a diagonal relationship with silicon of group 14, illustrated in the physical characteristics and binary compounds of both elements.[7]

Electronically, three electrons occupy the elemental ground state as an ns^2 np^1 configuration, with the +3 oxidation state dominating in the lighter group 13 elements.[7, 9] Conversely, heavier group 13 congeners favour the +1 oxidation state. Concurrent to this progression is the shift from predominantly covalent to ionic bonding modes, rationalised by the increase in atomic radii and the decreasing ionisation energy down the group.[7] The tendency of the heavier group 13 elements to favour an oxidation state 2 less than their lighter counterparts is attributed to the "inert pair effect", which is exhibited within Groups 13 – 16.[24] Exemplified by thallium of period 6, this sees the *s*-orbital electron pair contract due to relativistic effects. This is presented as 6*s* orbital electrons being more tightly bound by the nucleus and more defiant in forming chemical bonds, as evident through anomalously high ionisation energies.[24] Transitionally, indium of period 5 presents the potential to be stabilised in the +1 oxidation state; however, it prevalently remains in the +3 state.

The extraction, toxicity, and applications of the group 13 elements vary notably, with an overview of the naturally occurring elements (except synthetic Nihonium of period 7) discussed herein.

1.4.2. Boron

Evidence of boron as a once newly discovered element was first isolated following the work of French chemists Gay-Lussac and Thénard in 1808,[25] and independently replicated in 1809 by Davy.[26] Constituting a relatively low amount of the Earth's crust (0.001%, 10 ppm), commercial boron extractions primarily include areas of former geologic volcanic activity.[11] Within naturally occurring minerals (ulexite, borax, and kernite) boron is exclusively bound to oxygen as a borate.[27] However, in its elemental state, several allotropes (crystalline solid ranging red to black, amorphous powders) of boron are accessible, inclusive of an amorphous brown powder or crystalline as shiny black crystals.[7] The applications of boron through its mineral borax ($Na_2[B_4O_5(OH)_4]\cdot 8H_2O$) are of great historical significance, with reported uses from ancient Babylonian and Egyptian societies.[28] Within modern settings, boron's main use is within borosilicate glass, however, further avenues of boron utilisation are continually expanding into medicinal, optoelectronic, aerospace, and industrial and catalytic applications including in borane sources for Suzuki-Miyaura coupling reactions.[29] Further, borax continues its use as a mild pesticide, cleaner and water softener.[7]

1.4.3. Aluminium

Aluminium is the most abundant metal in the Earth's crust (8.23%, 82,300 ppm).[11] First isolated in its metallic state in 1824 by Danish chemist Hans Christian Ørsted,[30] aluminium is a soft and relatively lightweight metal which is rapidly oxidised by air.[7, 31] It is readily found in numerous sedimentary clays and minerals, including bauxite ($Al_2O_3\cdot 2H_2O$).[7] Globally, over one hundred

million tonnes is mined annually, with the largest producer of bauxite being Australia. The Bayer process converts bauxite to alumina (Al_2O_3), which is smelted to aluminium through an electrolytic process.[32] Aluminium is the most widely used non-ferrous metal, with technological applications stretching from consumer and household goods,[7] to aerospace and critical technologies,[33] to medicinal and antiperspirants,[34] and industrial scale chemical processing and catalysis.[35] Specifically, organoaluminium species are highly applied alkylating reagents in chemical synthesis, and aluminium trihalides serve as potent Lewis Acids.[7, 9, 36] Aluminium is widely recycled within society, with 52% of the world's elemental aluminium being of recycled material.[37] Furthermore, the development of recycling methodology is a key focus of academic research.[38] Widespread use and processing of aluminium and its subsequent compounds, ensure it is an attractive candidate for academic and industrial investigation.

1.4.4. Gallium

First discovered in 1875 as a trace constituent of sphalerite (ZnS), gallium is a silvery, brittle metal which melts just above room temperature (29.6 °C).[7, 39] Within the Earth's crust, gallium is of low relative natural abundance (0.0019%, 19 ppm).[11] Due to their elemental geochemical affinity, gallium is commonly found as the intergrowth of aluminium within bauxite.[40] Primarily, the isolation of gallium is a by-product of bauxite, sulphidic zinc ore, and coal processing, whereby the production of alumina from bauxite ores serves as the most viable source of gallium.[41] Once of little commercial interest prior to the 1960's, developments within integrated circuits utilising gallium arsenide and gallium nitrides have been employed within military and mobile telecommunication applications.[41] Subsequently, the application of gallium within critical technologies is considered crucial for the function of modern economies.[42]

1.4.5. Indium

Present in similar abundance as silver, cadmium and mercury within the Earth's crust (2.5×10^{-5}%, 0.25 ppm), Indium was first discovered in 1863 following analysis of ZnS ores.[11, 43] A soft semi-precious non-ferrous metal, indium presents as silvery white in colour.[44] A trace amount and by-product of zinc metal processing operations, indium may be recovered upon the processing of extracted metal concentrates or via extractive metallurgy upon treatable residues.[7, 44] Applications within semiconductor systems reaffirm indium's use within high-speed transistors, high-efficiency photovoltaic devices and infrared detectors.[44-45] Primary uses are within thin-film coatings for liquid crystal display screens (LCD's) including touch screens, and in solar cells through the development of

indium tin oxides (ITO).[44-45] The relative scarcity of indium and global shifts toward sustainable manufacturing practices promote considerations and investigations toward elements and compounds other than those featuring indium.[46]

1.4.6. Thallium

In its elemental state as a silvery white metal, thallium is the second least abundant of the naturally occurring group 13 elements (8.5×10^{-5} %, 0.85 ppm).[11] During the smelting processes of lead and zinc, thallium dust is generated as a by-product from trace amounts present within a range of minerals. Its capture and eventual extraction via electrolysis yields precipitated thallium(I) chloride.[7] Thallium's severe toxicity is attributed to an ionic radius similar to that of potassium ions (Tl: 2.42, K: 2.34 Å).[47] Subsequently, it may enter cells and disrupt imperative sodium and potassium transport mechanisms.[7] Previously applied in pesticides and rodenticides in the 1930s, the advent of criminal and unintentional poisonings saw thallium's prohibition within the United States in 1965 and much of the wider Western world.[48] Growing demand for thallium is attributed to its contemporary application within advanced technology fields, including optical systems (infrared spectrometers), electronic devices, alloys, and the laser industry.[49] Thallium's cellular absorptive aptitude further increases in tumour cells, promoting its use within nuclear medicine as an imaging agent.[7]

1.5. Low Oxidation State Group 13 Chemistry

The various capabilities of group 13 elements have seen growing developments and applications, furthered through expansions into various available oxidation states. Classes of low oxidation or valence state main group compounds are a key focus in the rapidly developing field of organometallic chemistry.[1] In such compounds, the combination of both occupied and unoccupied orbitals, as well as low coordination numbers, serve to heighten and differentiate the modes of reactivity with respect to higher oxidation state relatives.[50] Subsequently, the development of viable low oxidation state group 13 metallomimetic species capable of the fundamental processes of widely applied transition metals, *viz.* oxidative addition and reductive elimination, are of great significance.[2-3]

Irrespective of the propensity of some heavier group 13 elements to exist in the +1 oxidation state, the pursuit of low oxidation state group 13 compounds includes species in the atypical +2, +1 and 0 oxidation states.[50] In kinetically stabilising such highly reactive species, the employment of sterically demanding ligands/substituents is required in disfavouring thermodynamic disproportionation and/or oligomerisation processes. Through the variation of ligands/substituents and coordination numbers, different valence states are accessible, thereby expanding the structural richness and chemical diversity

of complexes.[7] The diversity of low oxidation state group 13 compounds featuring monoanionic ligand systems is extensive and continues to expand, and a brief overview is discussed herein.

1.5.1. Singly Bonded $E^{(II)}$-$E^{(II)}$ Group 13 Dimers

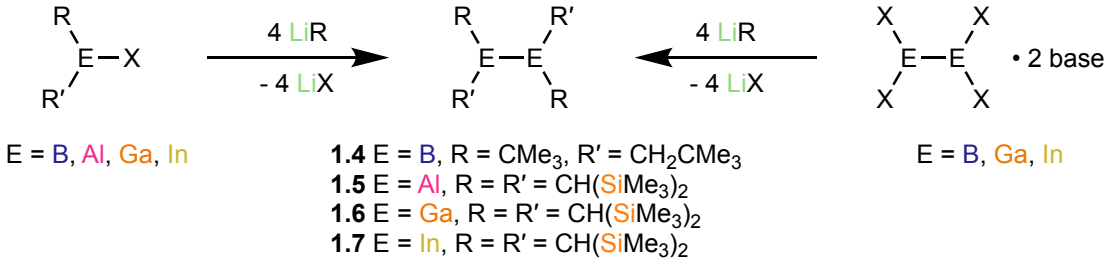

Scheme 1.1: First reported examples of low-oxidation state organo-group 13 element complexes featuring a single element(II)-element(II) bond. (X = Halide).[51]

Low oxidation state organometallic group 13 chemistry emerged at the point of the wider renaissance of main group chemistry featuring compounds in the +2 oxidation state and an E-E single bond. Previously, species featuring element-element single bonds were restricted to boron(II) compounds stabilised with nitrogen, oxygen and halogen substituents.[51] In 1980, the first organoboron species, diborane(4) **1.4**, featuring a single B-B bond was independently reported by the research groups of Nöth and Berndt.[52] Later in the decade, this series was expanded to the heavier element analogues, with Uhl and coworkers reporting the first isolation of an aluminium dimetallane **1.5** in 1988,[53] and analogous gallium **1.6** and indium **1.7** compounds in 1989 (Scheme 1.1).[54]

These novel compounds [R_2E-ER_2] could be accessed through the alkali metal reduction of halide precursors [R_2EX] (E = B, Al, Ga, In, X = halide) or the metathesis of [X_2E-EX_2] (E = B, Ga, In) reagents with a pre-embedded E-E bond featuring element(II) centres stabilised by Lewis bases (Scheme 1.1). Moreover, extensive investigations have expanded the series to include R groups of alkyl, aryl, alkoxy, bis(trimethylsilyl)methyl, tris(trimethylsilyl)methyl, and other sterically encumbered silyl derivatives, commonly featuring sterically demanding and/or highly σ- and π-donating ligand systems.[50, 55]

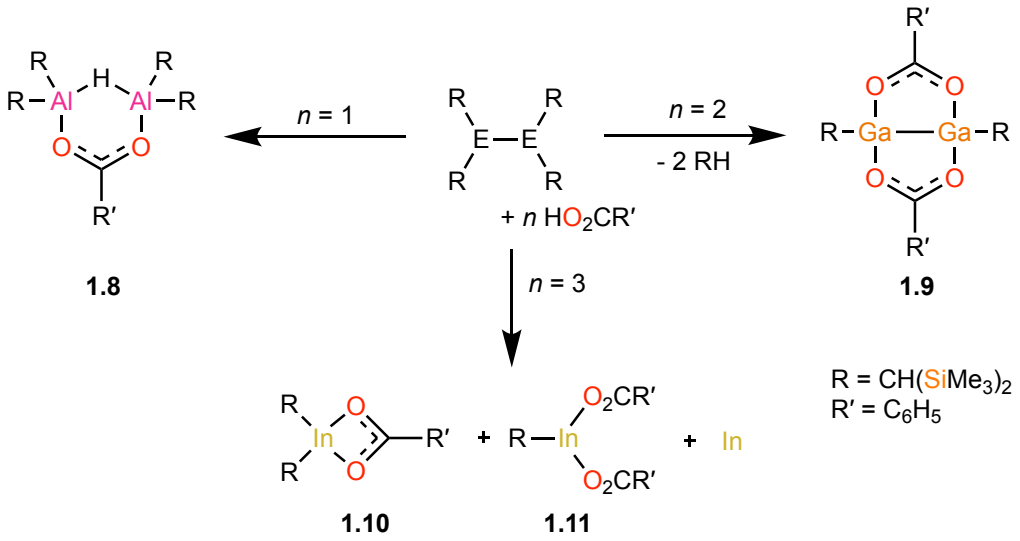

Scheme 1.2: Varied and metal specific reactivity of group 13 dimetallanes of aluminium(II), gallium(II) and indium(II) with carboxylic acids.

Stabilisation of group 13 centres in the formal +2 oxidation state presents the opportunity for further reduction to the +1 oxidation state, yielding multiply-bonded radical anions and tetrameric metal(I) compounds (examined in subsequent sections). The oxidation and reactivity of dimetallanes R_2EER_2 have been extensively examined through investigations of substrate insertion into the E-E bond, explicit cleavage of the E-E bond, and addition to the E-E bond. Exemplified in the reactions of carboxylic acids to $[R_2E\text{-}ER_2]$ compounds (E = Al, Ga, In, R = $CH(SiMe_3)_2$) highlights the metal specificity observed in yielding varied element(III) oxidation products. The Al-Al bond dialane is cleaved yielding a hydrido-bridged and bridging carboxylato dialuminium species **1.8** (Scheme 1.2). The Ga-Ga bond digallane is conserved but supported via two bridged carboxylato moieties having cleaved two previously coordinated ligands **1.9** (Scheme 1.2). Finally, the In-In bond diindane is cleaved, undergoing disproportionation to indium(III) containing species **1.10**, **1.11**, and indium metal (Scheme 1.2).[50, 56]

The applications of dimetallanes as ligands toward transition metals has also been examined, but largely restricted to diborane(4) species **1.4** and isostructural analogues. In the case of diboranes, a monoanionic boron-centred boryl ligand is prepared through heterolytic cleavage of the B-B bond, which may bond to the transition metal through a terminal or a bridging coordination mode.[57] Comprehensive investigations have utilised these transition metal complexes as reagents and models for hydroboration, Suzuki coupling and small molecule functionalisation reactions.[58]

The preparation of the first low oxidation state group 13 compounds of the +2 oxidation state further extended the applications of these elemental centres and ushered the extensive developments and findings of intriguing characteristics found in the +1 oxidation state.

1.5.2. Neutral Compounds Featuring $E^{(I)}$ centres

The possibility for differentiated reactivity of group 13 elements in the +1 oxidation state has remained a key area of research interest for the last 30 years. In accessing subvalent species, two general synthetic methods have been employed and dictated initial research focuses. These have included the salt metathesis of metastable metal(I) halides and the reduction of metal(III) halide precursors. Despite the commercial availability of indium(I) and thallium(I) halide reagents, aluminium(I) and gallium(I) analogues were first prepared by Schnöckel and coworkers in the 1980's using a specifically designed apparatus.[59] In the Schnöckel system, a high-temperature gas phase reaction (~1000 °C) yields the targeted $M^{I}X$ (where M = Al, Ga, and X = Cl, Br, I) from the reaction of the metal with HX. Metastable solutions of the salts could be condensed and stored at -78 °C within donor solvents. Being highly reactive, the isolation of metal(I) species proves a considerable challenge due to their propensity toward disproportionation into elemental metal(0) and trivalent metal(III) species.[4, 51, 60]

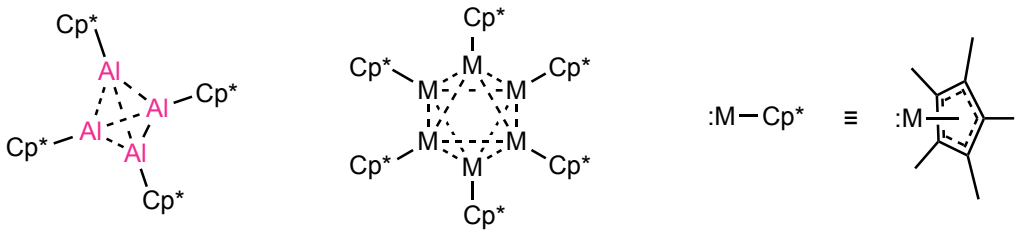

1.12

1.13 M = Ga
1.14 M = In

1.15 M = Al
1.16 M = Ga
1.17 M = In
1.18 M = Tl

*Figure 1.3: First examples of isolated neutral metal(I) aggregates (**1.12-1.14**) and corresponding solution state monomers observed at elevated temperatures (**1.15-1.18**).*

In 1991, the first example of an isolable aluminum(I) "diyl" complex $[(AlCp^*)_4]$ **1.12** ($Cp^* = C_5Me_5^-$) as a tetramer was reported by Schnöckel and coworkers (Figure 1.3).[61] The reaction of metastable aluminium(I) chloride and $[MgCp^*_2]$ yielded the $[(AlCp^*)_4]$ **1.12** tetrahedron in the solid state, featuring kinetic stabilisation of the complex via the bulky η^5 Cp* ligands capping the Al centres. Further investigations identified the possibility of preparing **1.12** through the reduction of the metal(III) precursor $[AlCp^*Cl_2]$ with alkali metals, and reductive elimination reactions of $[AlCp^*_2H]$.[62] Concurrent to investigations of Al diyls, the $[(GaCp^*)_6]$ **1.13** species was synthesised analogously from salt metathesis of metastable gallium(I) halide with $[MgCp^*_2]$,[60] and later via reductions of $[GaCp^*X_2]$ with K metal (where X = Cl, Br, I).[63] Notably, in contrast to the tetramer **1.12**, **1.13** aggregates in the solid state as a hexamer and is therefore isomorphous to the $[(InCp^*)_6]$

1.14 first published in 1989.[64] The report of gallium(I) and indium(I) analogues completed the series, as monomeric [TlCp*] **1.18** was originally reported in 1986.[65]

When exposed to increased temperature in solution, **1.12** undergoes dissociation into monomeric [AlCp*] diyl **1.15** as identifiable via ^{27}Al NMR spectroscopy.[60] Hexamers **1.13** and **1.14** also dissociate into to monomers **1.16** and **1.17** at elevated temperatures.[59b] Exploited directly, **1.12** and **1.13** have served as valuable starting materials in the preparation of new metal(I) organoaluminium and organogallium species, spurring the expansion of similar tetrameric aluminium(I) and hexameric gallium(I) structures using monodentate alkyl and silyl ligand systems.[59b, 66] However, within the aggregated structure, diyls **1.12**, **1.13**, and **1.14** feature decreased reactivity and are rendered a less potent reducing agent, highlighting the potential for new species development.[55]

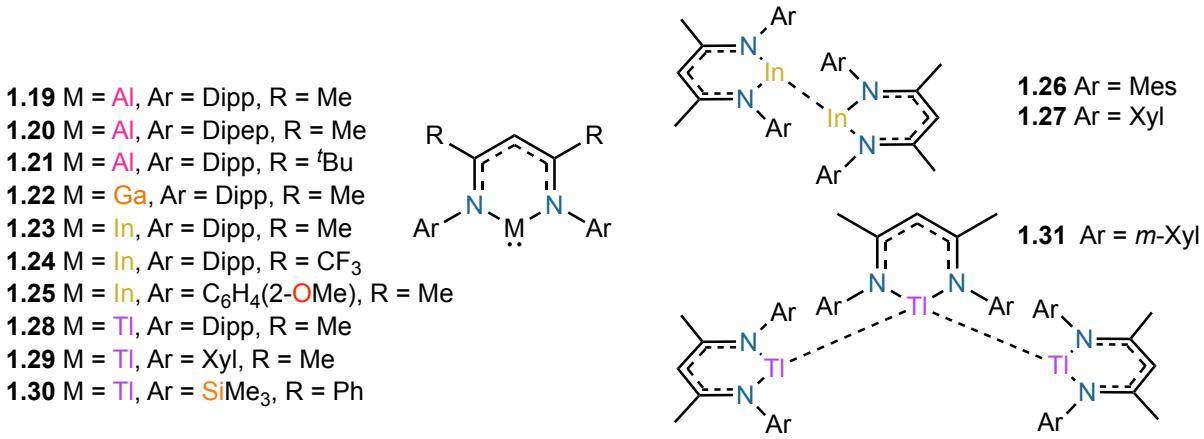

Figure 1.4: Selected catalogue of isolable metal(I) species containing group 13 metal centre within a six-membered metallocycle. (Dipep = 2,6-CH(Et)$_2$-C$_6$H$_3$, Xyl = Xylyl = 2,6-dimethylphenyl, m-Xyl = meta- Xylyl = 3,5-dimethylphenyl).

In 2000, the preparation of the first isolable monomeric aluminium(I) compound [Al(^{Dipp}Nacnac)] **1.19** ([^{Dipp}Nacnac]$^-$ = ß–diketiminato [(DippNCMe)$_2$CH]$^-$) was reported by Roesky and coworkers.[67] This ß-diketiminato complex features a two-coordinate aluminium(I) centre and was crystallographically characterised (Figure 1.4). A group 13 analogue of a singlet *N*-heterocyclic carbene (NHC),[68] the aluminium(I) centre in **1.19** is stabilised within a 6-membered metallocycle, featuring a lone pair and an empty *p*-orbital localised on the metal.[67] **1.19** was prepared in a 21% yield from a potassium reduction of a ligated aluminium dihalide precursor over 3 days. The reactivity exhibited at the aluminim(I) centre offered many exciting possibilities, including extensive examples of oxidative additions,[67] activations of small molecules (CO, C_2H_4),[69] cycloadditions,[70] reduction chemistry,[71] and the activation of C−H and C−F bonds.[72] Notably, investigations have been primarily centred on **1.19**, with only two further analogous aluminium(I) species being reported employing "superbulky" diisopentylphenyl (Dipep) aryl groups **1.20** in 2020,[73] and increased

backbone steric hinderance via introducing ^{t}Bu groups **1.21** in 2007.[74] Repeatedly, **1.19** has extensively highlighted the potential reactivity of aluminium(I) as a reducing agent in further inorganic chemical syntheses.

Also in 2000, the isoelectronic monomeric gallium(I) species, [Ga(^{Dipp}Nacnac)] **1.22**, was reported by Power and coworkers.[75] **1.22** was prepared via the salt metathesis of Li[^{Dipp}Nacnac] with metastable gallium(I) iodide reagents, and subsequent potassium reduction of the product in toluene. Extensive investigations of **1.22** have yielded over forty Ga-containing complexes, and identified the nucleophilicity of the gallium centre found to be greater than that of the **1.15** and **1.16** diyls, however, less electrophilic than that of the aluminium(I) centre of **1.19**.[76] Extensive investigations have been conducted exploiting the nucleophilicity of the gallium(I) centre including unsaturated fragments coordination,[77] transition metal complex ligand displacement,[78] gallium(I) centre insertion into E−X bonds (E = H, *d*- or *p*-block element; X = halide, alkyl, etc.),[79] main group halide reduction,[80] Gallium imide and amide preparation from organo-azides,[81] and oxidation of the gallium(I) centre.[82] **1.22** has been highlighted in its applicability as a highly reactive source of Ga toward further inorganic syntheses.[76]

Investigations targeting indium(I), and thallium(I) analogous ß-diketiminato species contained within six-membered metallocycles have yielded solid-state structures of varied aggregations (Figure 1.4). The employed ß–diketiminato ligand offers fine-tuning of steric and electronic properties through the variation of substituents at the backbone α- and β-carbons, and via the alkyl and aryl substituents at the nitrogens.[83] Ligand steric variability is consequential in the aggregations of indium(I) heterocycles, whereby monomeric structures in the solid state are observed when employing more sterically encumbered aryl groups (**1.23** - **1.25**).[76, 84] Conversely, less bulky aryl groups (Xyl, Mes) have resulted in dimeric complexes **1.26** and **1.27** featuring weak In–In interactions, which dissociate into their monomeric forms in solutions of low polarity solvents.[85] Similarly ß-diketiminato substituted thallium(I) species can be prepared via salt metathesis of thallium(I) halide salts. Derivatives have primarily observed the isolation of monomeric thallium(I) species (**1.28** - **1.30**) in the solid-state.[76] However, unlike previously reported aluminium(I), gallium(I) and indium(I) analogues, the use of xyl aryl moieties in preparing thallium(I) species yielded a trimer **1.31** in the solid state.[85b] Compared to the aluminium(I) and gallium(I) six-membered species, the reactivity and applications of the indium(I) and thallium(I) analogues are under investigated, which can be attributed to the relatively lower energy of the lone pairs of the indium(I) and thallium(I) centres (i.e. more stable), comparative toxicity and poor natural abundance.[76]

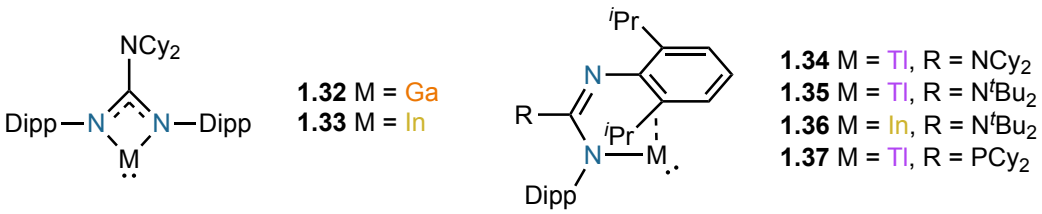

Figure 1.5: Isolable metal(I) complexes containing gallium and indium centres within a four-membered metallocycle, and pseudo-five-membered isomeric indium and thallium compounds. (Cy = cyclohexyl).

To date, no examples of boron(I), aluminium(I) or thallium(I) compounds exclusively within a four-membered ligand heterocycle have been crystallographically characterised. However, through employing the bulky guanidinate ligand Giso (Giso = $\{(Dipp)N\}_2CNCy_2$), the monomeric four-membered NHC analogous [Ga(Giso)] **1.32** and [In(Giso)] **1.33** species were isolated by Jones and coworkers in 2004 (Figure 1.5).[86] Similar to the preparation of **1.19**, salt metathesis of the [M^IX] (where M = Ga and X = I, M = In and X = Cl, M = Tl and X = Br) with the lithium guanidinate Li[Giso] yielded metal(I) products in moderate to good yields. When preparing the thallium(I) analogue, rather than the identified *N*,*N*-chelated species (**1.32**, **1.33**), the isomeric *N*, arene-chelated species [Tl(η^1-N:η^3-Ar-Giso)] **1.34** was isolated as a pseudo-five membered metallocycle featuring weak Tl-arene interactions. This structural motif is attributed to the increased ionic radius of the heavier ion disfavouring the *N*,*N*-chelation.[86] Notably, this pseudo-five membered motif is replicated with indium(I) and thallium(I) species when analogous guadinate (**1.35**, **1.36**), and phosphaguanidinate (**1.37**) ligand scaffolds are employed.[86] Attempts in the preparation of aluminium(I) species with the Giso and related ligand frameworks have been unsuccessful, despite calculations indicating experimental viability.[76]

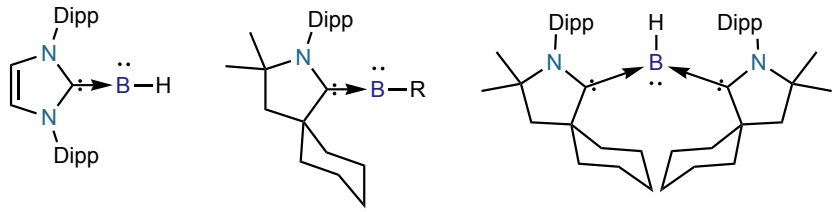

Figure 1.6: Attempts toward preparation of isolable mono- and bis(Lewis base)-stabilised borylene species.

The pursuit of neutral boron(I) systems isostructural to carbenes (borylenes) has been heavily investigated. Initially applied within borylene-transition metal complexes, investigations have since spawned a substantive field of research toward "free" borylenes [:B-R], however, isolation of these species remains elusive.[57] The inherent difficulty of isolation can be attributed to their one coordinate

boron(I) centre and subsequent two vacant orbitals, ensuring they are even more electron-deficient and reactive than carbenes.[58b] Consequently, these species have thus far only been spectroscopically characterised within the gas phase or in low temperature matrix preparations.[87]

In-situ experimentation of mono-coordinated borylenes has reinforced immense interest through transition metal metallomimetic behaviour in reactions with alkynes, C-H and C-C single bonds, carbon monoxide and dinitrogen.[23, 88] Ongoing attempts at isolating these transient species have been undertaken through trapping experiments, however, challenges have prompted the taming of reactivity and subsequent isolation through stabilisation with one or two Lewis bases.[87]

In 2007, Robinson and coworkers reported the transient generation of a mono(Lewis base)-stabilised borylene [B(H)(Idipp)] **1.38** (Idipp = C{N(C_6H_3-2,6-^{i}Pr$_2$)CH}$_2$), from the reduction of a boron(III) halide precursor [B(Br)$_3$(Idipp)].[89] Subsequent focuses on adduct variation would not yield an isolable species; this was attributed to the inherent reactivity of the electron rich and electropositive boron(I) centre.[87] Seven years later, Bertrand and coworkers utilised a cyclic(alkyl)(amino)carbene (CAAC) and a bulky silylamido group to yield the first isolable Lewis-base stabilised borylene [B(CAAC)N(SiMe$_3$)$_2$] **1.39**.[90] This species features a two-coordinate boron(I) centre and notably exhibited transition metal metallomimetic behaviour at the boron centre with both carbon monoxide and dihydrogen.[90] Despite attempts, the transiently identified parent CAAC borylene [B(CAAC)H] **1.40** could not be isolated, highlighting the steric requirement of the bulky silylamido substituent.

In isolating a bis(Lewis base)-stabilised borylene, Bertrand and coworkers reported the first example [B(H)(CAAC)$_2$] **1.41** in 2011.[91] The species is similar to the transiently prepared parent compound [B(H)(CAAC)] **1.40**,[90] but features a second CAAC substituent aiding in its isolation. Prepared in moderate yields from the potassium graphite reduction of the brominated [B(Br)$_3$(CAAC)] precursor, this species is a viable precursor to a wide range of new compounds. Subsequently, over 20 analogous planar tricoordinate bis(Lewis base)-stabilised borylene species have been since reported, aided in their isolation by significant π-backdonation and steric protection afforded from coordinated Lewis base adducts.[87] Often stable for multiple months under inert -conditions, these species have been employed as viable ligands for transition metal complexes aiding in catalytic applications.[92]

Despite attempts toward this highly reactive boron(I) species, the isolation of a “free” borylene [:B-R] to date remains unreported.

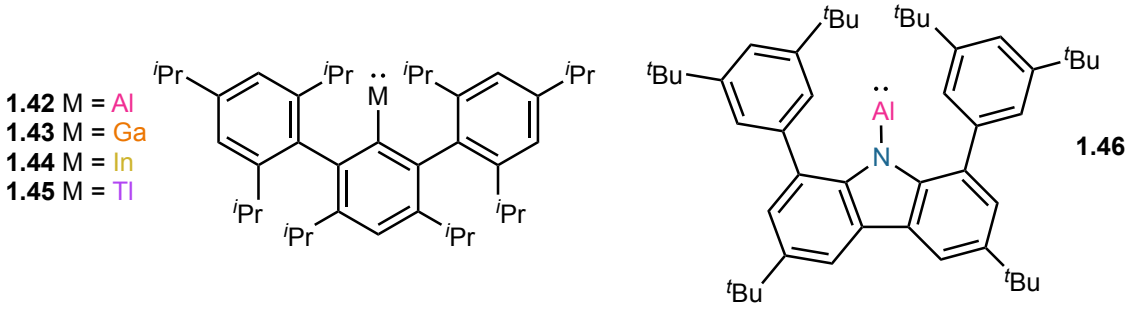

Figure 1.7: Isolated monomeric metal(I) group 13 -ylene complexes incorporating terphenyl and carbazolyl scaffolds.

Following initial investigations of metal(I) species incorporating Cp*, one coordinate alkyl and silyl ligands, and two coordinate ß-diketiminato and amidinato ligands have been employed in the isolation of various new systems. In 2020, Power, Tuononen and coworkers reported the first example of a free monomeric aluminylene [:Al-R], isolable at room temperature, [AlAr^{iPr8}] **1.42** Ar^{iPr8} = C_6H-2,6-(C_6H_2-2,4,6-$^i Pr_3$)$_2$-3,5-$^i Pr_2$ stabilised with a bulky terphenyl ligand.[93] **1.42** was prepared from the reduction corresponding dihalide [Al(Ar^{iPr8})I_2] with a 5% weight Na on NaCl, a reducing agent developed by Jones and coworkers.[94] Utilising the same sterically demanding terphenyl ligand, Power and coworkers had previously reported the solution state coordination isomers of gallium(I) **1.43**,[95] indium(I) **1.44**,[96] and thallium(I) **1.45** (discussed in Section 1.5.3).[97] Further advances from the groups of Hinz and coworkers,[98] and Zhang and Liu identified the analogous free *N*-aluminylene **1.46** employing a carbazolyl ligand scaffold.[99] Reduction of the corresponding dihalde precursor with excess 5% weight K on KI as a reducing agent over 2 days at -15 to 13 °C yielded the targeted free *N*-aluminylene **1.46** in good yields (67%). Both **1.42** and **1.46** were found to be inaccessible by reductions of their precursor complexes with potassium graphite or an Na mirror.[100]

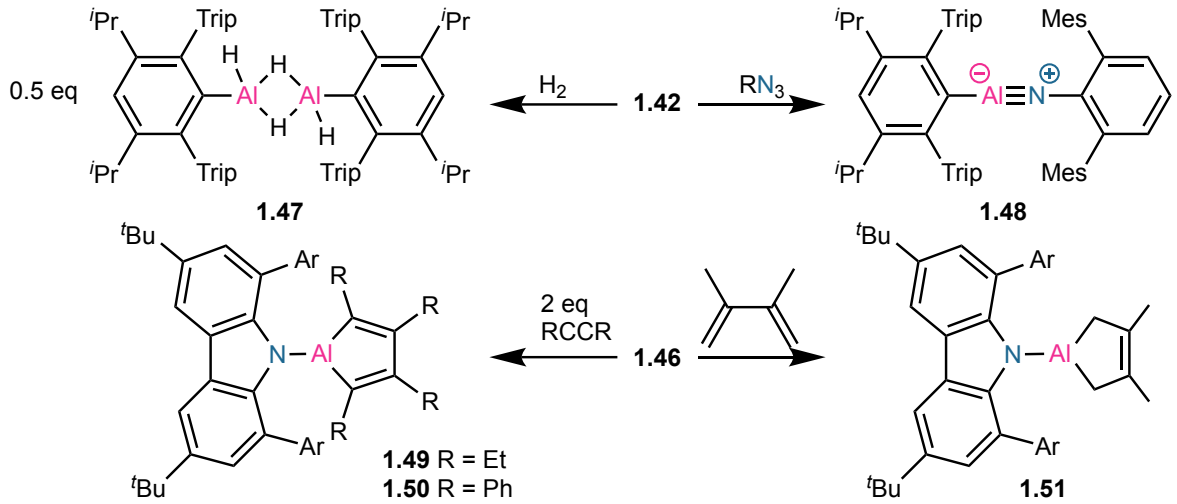

*Scheme 1.3: Redox reactivity of isolated free C- and N-aluminylene species **1.42** and **1.46**.*

Highlighting the thermodynamically favourable process of oxidation from aluminium(I) to aluminium(III),[35a] investigations of both **1.42** and **1.46** aluminylenes have yielded a variety of value-added aluminum(III) products. Notably, the reaction of **1.42** with H_2 rapidly produced the hydrogenation product [{AlH(μ-H)Ar^{iPr8}}$_2$] **1.47** (Scheme 1.3).[93] Upon addition to organic azides, **1.42** would yield the first isolable monomeric aluminium imide featuring an Al≡N triple bond **1.48**.[101] In the preparation of Al-heterocycles and C-C bond formation, treatment of excess alkyne with *N*-aluminylene **1.46** yielded alumole species **1.49** and **1.50**, consequential of a [2+1] cycloaddition and subsequent ring expansion.[102] This highlighted a new route in potential alumole synthesis through simple unsaturated hydrocarbons. Further expanding applicability, a facile [4+1] cycloaddition was undertaken upon addition of 2,3-dimethyl-1,3-butadiene to **1.46** yielding the Al-heterocycle **1.51**.[100] The preparation of value-added Al-containing products from simple substrates emphasises the potency of the free aluminylenes as synthons for wider reactivity.

Previous research focusses have yielded extensive investigations into the isolation and applications of borylenes, and now aluminylenes; however, the development of analogous gallium(I), indium(I) and thallium(I) species is ongoing, often observing the formation of low oxidation state multiply bonded species.[103]

1.5.3. Multiply Bonded E$^{(I)}$-E$^{(I)}$ Group 13 Dimetallenes and Dimetallynes

In defiance of the once dogmatic "double bond rule",[1] the formation of complexes with multiple bonds between heavier group 13 element centres is a field of growing development.[17]

The isolation of heavier congeners of gallium(I), indium(I) and thallium(I) species presenting homoatomic multiple bonds is extremely challenging due to featuring significant singlet diradical character and subsequent extreme reactivity.[104] Extremely bulky terphenyl ligands are employed to provide sufficient steric shielding to kinetically stabilise heavier element dimetallenes and dimetallynes,[95-97] (as in free aluminylene **1.42**).[95] Primarily dissociating to monomers within hydrocarbon solvents (**1.42**, - **1.44**), the solid state structures and indicative descriptive bond multiplicity and structural motifs within this class has been of extensive investigation and dispute.[105]

In the solid state, the heavier +1 oxidation state diligated (R_2EER_2) (Ga^I, In^I, Tl^I) and monoligated (REER) (E = Ga^I, In^I, Tl^I) homoatomic bonded species present structural arrangements of a *trans*-bent geometry, the degree of bending increases upon atomic number.[106] The Carter-Goddard-Malrieu-Trinquier model attributes this geometry to the avoidance of steric clash between bulky ligands, with the combined down-the-group singlet ground state stability increase and decrease in E-E bond strength.[105] This manifests the double bonds as a double dative bond between two monomers. Molecular Orbital theory attributes this geometry to the increased mixing of the π and σ* orbitals down

the group. The degree by which compounds are bent and the consequent weakening of the π bond is manifest through increased lone pair character, and increased localisation of electron density upon the E centre. Extensive theoretical and reactivity studies upon the heavier congeners have revealed transition metal metallomimetic reactivity at the heavier group 13 centres and insight into multiple bond nature.[17, 105]

In developing the analogous lighter R_2EER_2 and REER congeners (E = B^I, Al^I), coordination of NHC's have afforded previously non-isolable homoatomic multiply bonded species (Figure 1.8).[89]

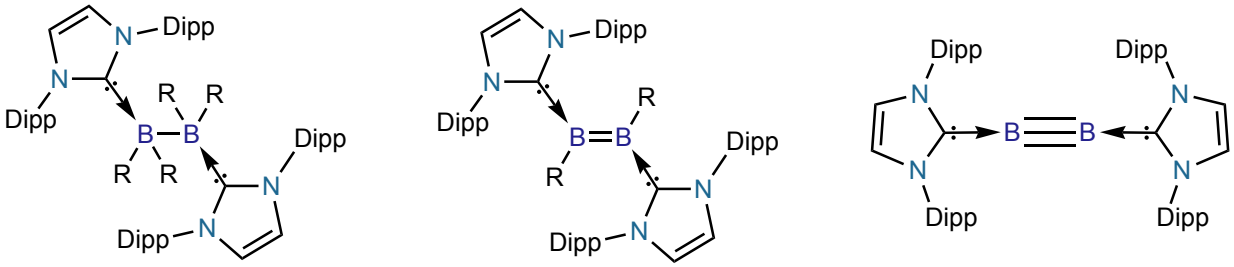
Dipp
N
R
B
Dipp
N
R
B
Dipp
N
R
B
Dipp
N
Dipp
N
Dipp
N

reactions of diboryne **1.55** with tetrabromodiborane **1.56** (Figure 1.8). Investigations further reiterated the donor strength of NHC's and their applicability in preparing isolable species only previously identified within argon matrices.[108]

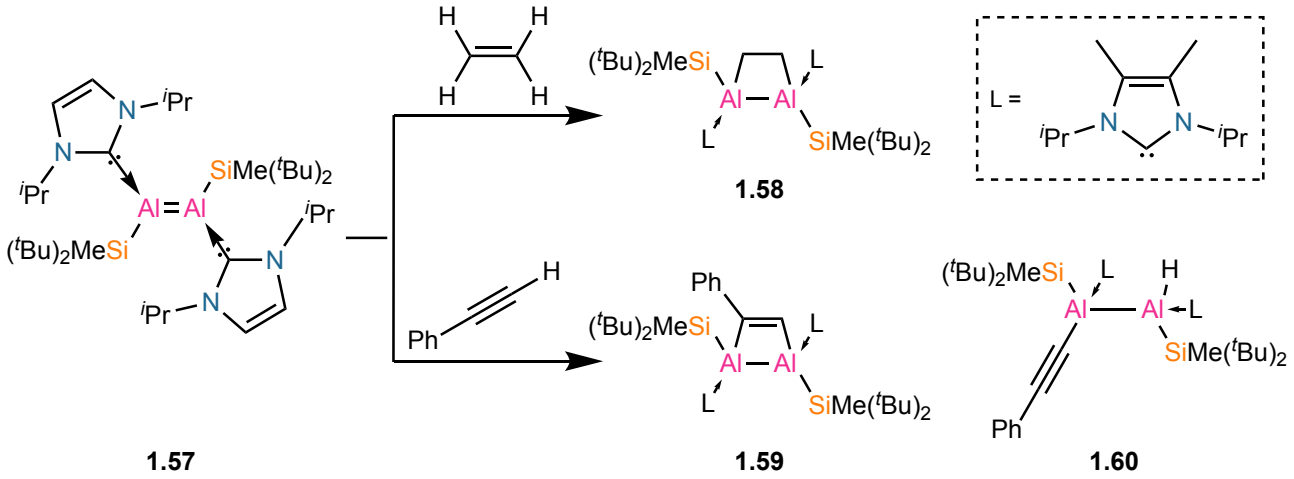

*Scheme 1.4: First isolated neutral dialumene (**1.57**) species, and its reported recativity with unsaturated organic molecules (ethylene and phenyl acetylene).*

Through the combination of the strong donor capabilities of NHC ligands and σ-electron-donating bulky silyl groups, the first example of a neutral dialumene **1.57** was reported by Inoue and coworkers in 2017 (Scheme 1.4).[109] Prior, a reliable method toward the clean and high yielding synthesis of NHC-coordinated organoaluminium(III) precursors with silyl, aryl or alkyl dihalides had not been developed. As such, efficient precursor synthesis was of principle focus to provide the foundation necessary in developing the highly reactive dialumene species. Despite previous reports of aluminium systems with bond orders >1,[110] **1.57** represented the first isolable species of this aluminium(I) analogue of an alkene. Upon addition of ethylene, **1.57** undergoes a formal [2+2] cycloaddition yielding **1.58**, whereas upon addition of phenyl acetylene, the reaction proceeds via both a formal [2+2] cycloaddition **1.59**, and C-H insertion **1.60** (Scheme 1.4).[109] This presented the opportunity for reactions with a wide array of molecules accessing organoaluminium compounds and aluminium-based functional materials, the developments of which are continually ongoing.[105]

The chemistry of low oxidation state group 13 compounds has been extensively investigated through the coordination of monoanionic ligand and neutral NHC systems. Aligning with developments in organometallic chemistry, the main group has been acceleratingly extended into transition metal metallomimetic applications exemplified within group 13. Correspondingly, the applications of dianionic ligand scaffolds have amplified research pursuits to develop a novel class of nucleophilic and highly reactive group 13 anions.

1.6. Anionic Group 13 Nucleophiles

Strategies toward uncovering distinctive chemistry within group 13 has motivated targets toward inverse, or umpolung, reactivity through the exhibition of nucleophilic character at metal centres.[3]

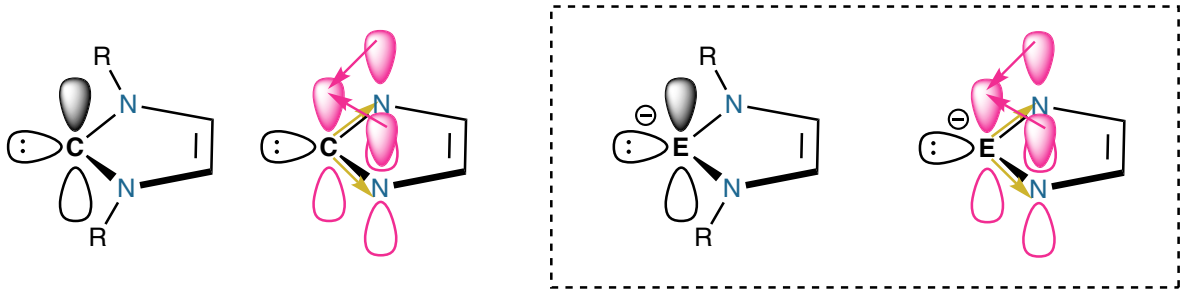

Figure 1.9: A generic N-heterocyclic carbene (left) and the isoelectronic anionic group 13 metal centre (E) systems with monocationic counterion omitted (right). Electronic stabilisation of the frontier orbitals shown by arrows demonstrating electron donation.

Pursuits have targeted structures isoelectronic to singlet state N-heterocyclic carbenes, identifiable via two coordinate species incorporating a lone pair within a non-bonding sigma orbital, and an empty *p*-orbital localised the metal centre (Figure 1.9). NHCs are neutral species featuring a carbon centre with 6-valence electrons, however, systems incorporating group 13 centres require a negative charge and necessitate a counterion M^+ (often an alkali metal) to remain isoelectronic.[111] Similar to NHCs, electronic stabilisation is possible through concurrent electronic σ-withdrawing (gold arrows) and π-donating (pink arrows) nature of the nitrogen atoms (Figure 1.9). Through this configuration, withdrawal of electron density from the reactive centre lone pair serves to stabilise this high energy orbital (often the HOMO). Concurrently, donation of electron density from the nitrogen lone pairs into the empty group 13 element-based *p*-orbital of π-symmetry raises the energy of the LUMO. The σ-withdrawing and π-donating ability of the nitrogen atoms can be manipulated through 1) varying the N-bound substituents and/or 2) employing steric bulk or strain to disrupt these stabilising interactions. As such, electronic stabilisation through the widening of the HOMO-LUMO gap supports the isolation of singlet carbene and isoelectronic anionic group 13 species and the tuning of reactivity through electronic implications.

1.6.1. Gallyl Anions: Synthesis and Structural Arrangements

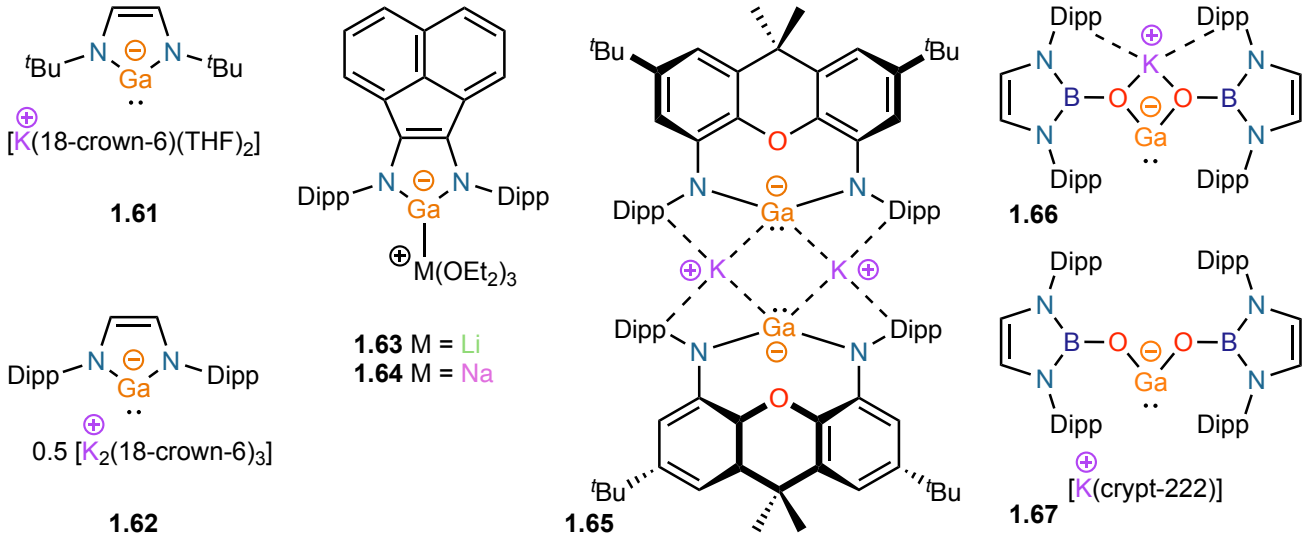

Figure 1.10: Selected examples of reported gallyl anions.

The first examples of complexes featuring an anionic, +1 oxidation state group 13 centre were that of gallium systems (gallyl anions) (Figure 1.10). The first gallyl anion **1.61** was reported by Schmidbaur and coworkers in 1999.[112] Incorporating a diazabutadiene ([^{R}DAB]$^{2-}$, R = alkyl or aryl) based dianionic ligand featuring *tert*-butyl substituents, [K(18-crown-6)(THF)$_2$][Ga(^{tBu}DAB)] **1.61** gallyl anion presented the first example containing an anionic gallium(I) centre with 6 valence electrons. However, to counteract the negative charge of the anionic gallyl species, the potassium counterion is sequestered within a crown ether (18-crown-6) and two tetrahydrofuran molecules. Within the solid state, **1.61** was identified as a separated ion pair.[4]

Further expanding the [^{Dipp}DAB]$^{2-}$ ligand scaffold, aryl (Dipp) substituents were employed by Jones and coworkers in 2002, furnishing the complex [K$_2$(18-crown-6)$_3$][{Ga(^{Dipp}DAB)}$_2$] **1.62** featuring the sequestering of the potassium cation within 18-crown-6 molecules.[113] Thereafter, in 2008, Fedushkin, Schumann and coworkers reported a gallyl anion species **1.63** and **1.64** stabilised via a BIAN ligand (BIAN = bis(Dipp)acenaphthenequinonediimine) featuring diethyl ether tri-solvated lithium and sodium counterions, and crystallising as monomeric ion pairs in the solid state.[114] The coordination chemistry of gallyl anions has been thoroughly investigated, however, investigations toward their applications within small molecule activation are limited.[4]

Since 2018, the library of free gallyl anion ligand frameworks have been expanded through the collective works of Aldridge, Goicoechea and coworkers. Within the seminal report of a low valent main group species stabilised by a bulky rigid diamido xanthene ligand system [NON]$^{2-}$, the gallyl anion [K$_2${Ga(NON)}$_2$] **1.65** was reported and is isostructural to the first reported aluminium analogue (see **section 1.6.4**).[115] Subsequent studies have optimised the synthesis of **1.65**, achieved by reduction

of the gallium iodide precursor complex with two equivalents of potassium naphthalenide [K($C_{10}H_8$)], and yielded **1.65** on a multigram scale with over 90 % yield. Furthermore, reactivity studies have highlighted the varied reactivity of **1.65** toward carbon and metal centred electrophiles, especially with reference to more Lewis acidic aluminium(III) products.[116]

In 2024, Aldridge and coworkers reported the first *O*-ligated gallyl anion **1.66** encompassing two N-heterocyclic boryloxy [NHBO]$^-$ groups (Figure 1.10).[117] Exploiting the salt metathesis of [GaCp*] **1.16** with potassium K[OB(^{Dipp}DAB)] at 80 °C in benzene yielded **1.66** with the elimination of [KCp*]. Sequestration of the K^+ counterion with 2.2.2-cryptand (crypt-222) yielded the first acyclic "naked" gallyl anion **1.67**, whereby the anionic EO_2 centre is unperturbed by presence of the potassium.

1.6.2. Boryl Anions: Synthesis and Structural Arrangements

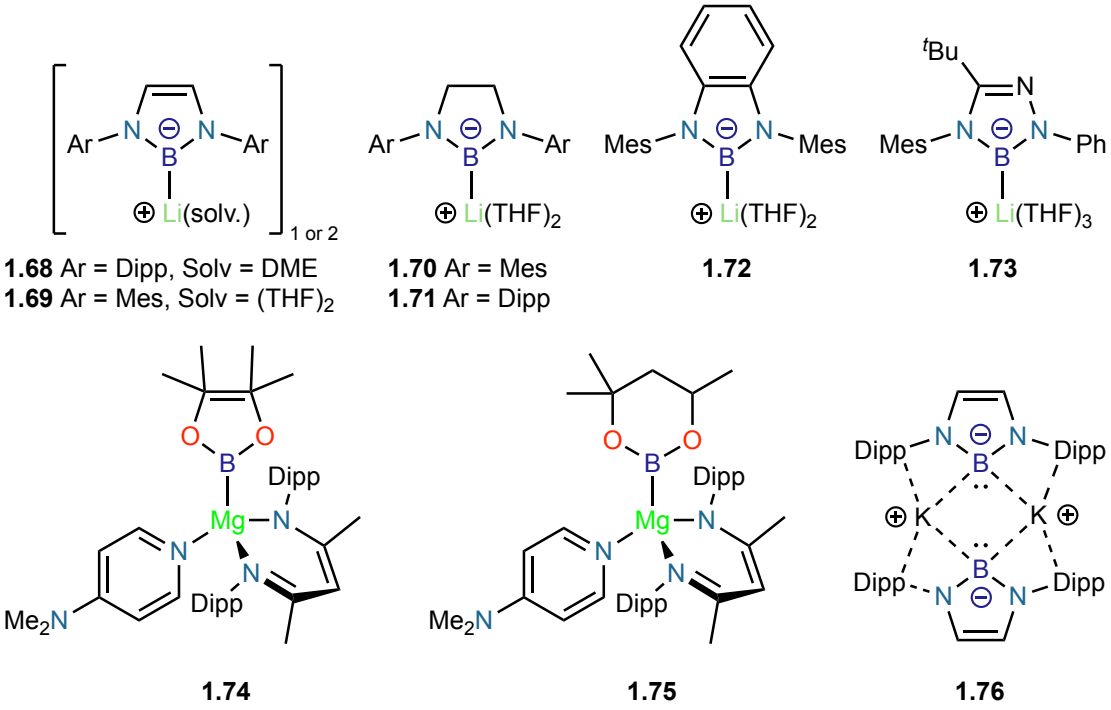

1.68 Ar = Dipp, Solv = DME
1.69 Ar = Mes, Solv = $(THF)_2$

1.70 Ar = Mes
1.71 Ar = Dipp

1.72

1.73

1.74

1.75

1.76

*Figure 1.11: Examples of reported "free" boryl anions from the research groups of Nozaki (**1.68 – 1.72**), Kinjo (**1.73**), Hill, McMullin (**1.74**, **1.75**), and Aldridge (**1.76**). (DME = 1,2-dimethoxylethane, DMAP = 4-dimethylaminopyridine)*

Isoelectronic to gallyl anions, "free" (*i.e.* not transition metal-bound) systems incorporating the lightest congener of group 13, boron, were first reported in 2006 and has since seen ongoing investigative focus (Figure 1.11). Incorporating the [^{Dipp}DAB]$^{2-}$ ligand applied by Jones and coworkers in their gallyl anion **1.62**,[113] Nozaki and coworkers reported the boryl lithium complex [{Li(DME)B(^{Dipp}DAB)}$_2$] **1.68**, stabilised within the unsaturated 1,3,2-diazaborolyl 5 membered heterocycle.[118] As determined through the solid-state structure, a strong electrostatic interaction is

observed between the lone pair of the boryl anion and the lithium cation. **1.68** was identified as a contact ion pair, which would crystallise as a dimer through the lithium bridged DME moieties.

Following the landmark isolation of **1.68**, further boryl lithium complexes have since been isolated incorporating a range of dianionic chelating ligands of varying steric bulk (Figure 1.11).[119] For example, Yamashita, Nozaki and coworkers prepared species **1.68** - **1.72** by manipulations of the original 1,3,2-diazaboryl 5-membered heterocycle. These included the incorporation of a saturated C−C backbone (**1.71**), and substituting the bulky Dipp substituents for Mes groups was also reported with both unsaturated C=C **1.69**, and saturated C−C backbones **1.70**.[119] Further modification of the backbone was reported by the incorporation of a benzannulated unit **1.72**.[119]

In 2016, Kinjo and coworkers prepared the 1,2,4,3-triazaboryl anion **1.73** (Figure 1.11).[120] Further steric bulk is also included through a *tert*-butyl group at the C group of the backbone, and mixed aryl groups (Dipp and Ph) upon the nitrogen coordination atoms. Additional studies in 2017 by Hill, McMullin and coworkers led to the boryl anion **1.74** that contains a di-oxygen five-membered heterocycle generated from a bis(pinacolato)diboron precursor.[121] Later in 2018, the same group published the first example of an isoelectronic B^{I} centre within a six-membered di-oxygen heterocycle **1.75**.[121-122] Both species presented notable synthetic ease in their preparation from oxygen ligated diboron starting materials treated with mononuclear organomagnesium reagents. This method proved more synthetically straight-forward in the preparation of boron(I)-containing species and saw the incorporation of a magnesium cation as opposed to more widely applied alkali metals (Figure 1.11).[122]

Toward isolating a truly "free" boryl system (i.e. no interaction between the anion and the cation), in 2021 Aldridge and coworkers reported the generation of the first non-lithium boryl complex with a group 1 element counterion **1.76**.[123] This saw further advances toward more ionic character in the bonding between the boron centre and the cation, which previously featured highly covalent interactions of the boryl anion with its counterion. In the solid state, **1.76** is a contact dimeric pair, whereby the K^{+} ions form interactions with the flanking aryl groups of the ligands and only weakly interact with the boron centres in the 1,3,2-diazaborolyl heterocycle. As such, this highly polar example **1.76** highlights the "freest" example of a boryl system. Further varied boryl anions have been reported with an array of counterions and ligand scaffolds, however, despite the various methods of stabilisation for boryl systems, all are confined to cyclic examples included in a sole six-membered (**1.75**), but primarily five-membered heterocycles.

1.6.3. Indyl Anions: Synthesis and Structural Arrangements

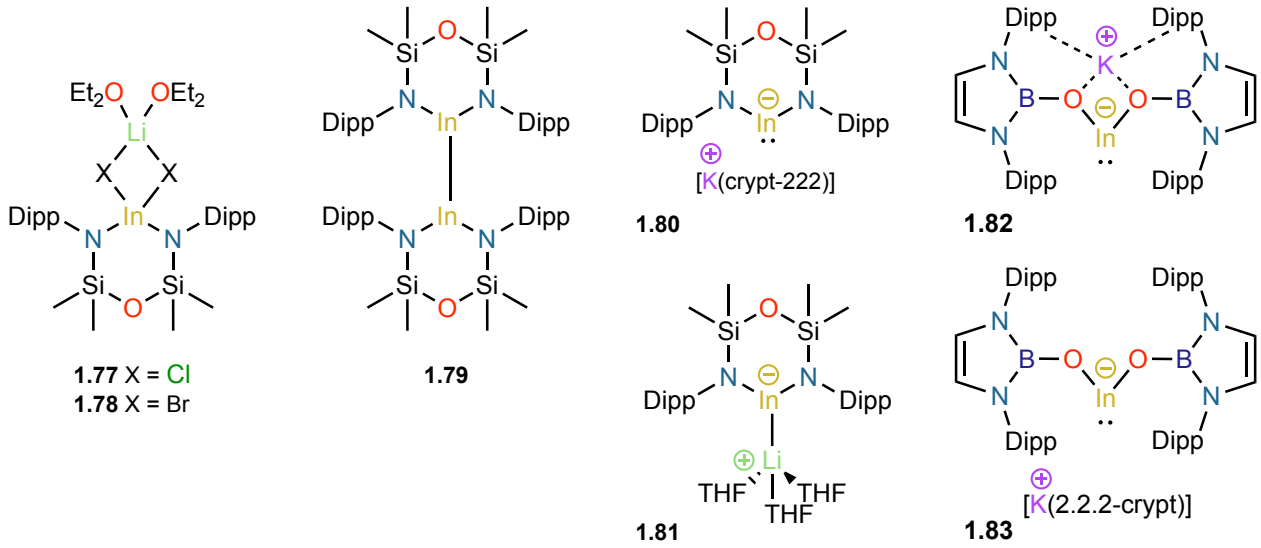

*Figure 1.12: First reported indyl anions and their synthons described by Coles and coworkers (**1.77**-**1.81**), and expansions by Aldridge and coworkers toward acyclic and "naked" analogues (**1.82**, **1.83**).*

Obverse to boryl systems, the heaviest reported congener of the nucleophilic group 13 anions feature few examples of indyl anions. Reported by Coles and coworkers in early 2018, the indyl anion is stabilised with a sterically encumbered dianionic bis(amidodimethyl)disiloxane ligand $[O\{SiMe_2NR\}_2]^{2-}$ $[^{Si}NON]^{2-}$. The indyl anion was prepared through the reduction of the indium(III) indate $[Li(OEt_2)][InCl_2(^{Si}NON)]$ **1.77** to the indium(II) diindane **1.79**. Further treatment of dimeric **1.79** with potassium metal in the presence of [crypt-222] yielded the first indyl anion as a separated ion pair [K(crypt-222)][In(^{Si}NON)] **1.80**.[124] Whereas addition of Li to the bromo indate **1.78**, would yields the monomeric ion pair $[Li(THF)_3][In(^{Si}NON)]$ **1.81** featuring a tri-THF solvated lithium counterion.[124] Investigations via DFT analysis and preliminary reactivity studies, confirmed the metal centred HOMO in **1.81**, its nucleophilic character,[125] and applicability as a reducing agent.[126]

As observed with developments towards a "naked" acyclic gallyl anion, **1.67**, Aldridge and coworkers concurrently developed the indium(I) analogues. Employing again two highly stabilising $[NHBO]^-$ boryloxy ligands, both as the contact ion pair **1.82** featuring the η^6-arene interactions of the K^+ counterions with the boryloxy Dipp groups, and as the separated ion pair **1.83**.[117] Similarly investigated with the gallium(I) analogues **1.66** and **1.67**, the nucleophilicity of the metal and oxygen centres was established through reactivity with carbon- and silicon-based electrophiles.

Group 13 anions once confined to gallyl and boryl anions from 1999,[112] and 2006 respectively,[118] were expanded through the implementation of new ligand systems. Confined to only a few examples, indyl anion systems continue to be developed as their reactivity toward varied substrates is expanded. Prior to the end of 2018, a new generation of aluminium(I) species was to be isolated.[4]

1.6.4. Aluminyl Anions: A New Class of Group 13 Nucleophiles

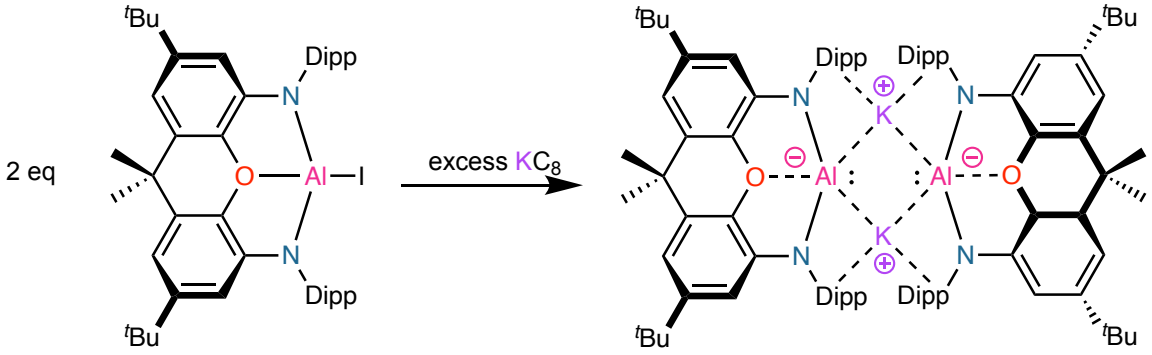

Scheme 1.5: First reported aluminyl anion [K_2{Al(NON)}$_2$] and its related aluminium(III) iodide precursor [AlI(NON)] by Aldridge, Goicoeceha and coworkers.

Later in 2018, the series of group 13 anions was completed through the report of the first aluminium(I) nucleophile (aluminyl anion) by Aldridge, Goicoechea and coworkers (Scheme 1.5: First reported aluminyl anion [K_2{Al(NON)}$_2$] and its related aluminium(III) iodide precursor [AlI(NON)] by Aldridge, Goicoeceha and coworkers.).[115] Exploiting the bulky rigid diamido xanthene $[NON]^{2-}$ ligand system (simultaneously reported with the gallyl analogue **1.65**), the reduction of aluminium(III) iodide precursor [AlI(NON)] with potassium graphite afforded the first aluminyl anion [K_2{Al(NON)}$_2$]. Extensive *in-silico* and *in-vitro* studies of [K_2{Al(NON)}$_2$] have reinforced the applicability and varied reactivity afforded by the aluminium(I) centre.[4, 111] In combination with the minimal elemental toxicity, vast abundance and novel reactivity of aluminium presented by this principle system, the field of aluminyl anions with expansion through diverse ligand systems, has seen accelerating advancement.[4]

Of key relevance to this work, the preparation of precursors, and subsequent synthesis and reactivity of this novel class of aluminium nucleophiles will be presented and discussed in chapters 2 and 3 respectively.

1.7. Overview of Literature Review

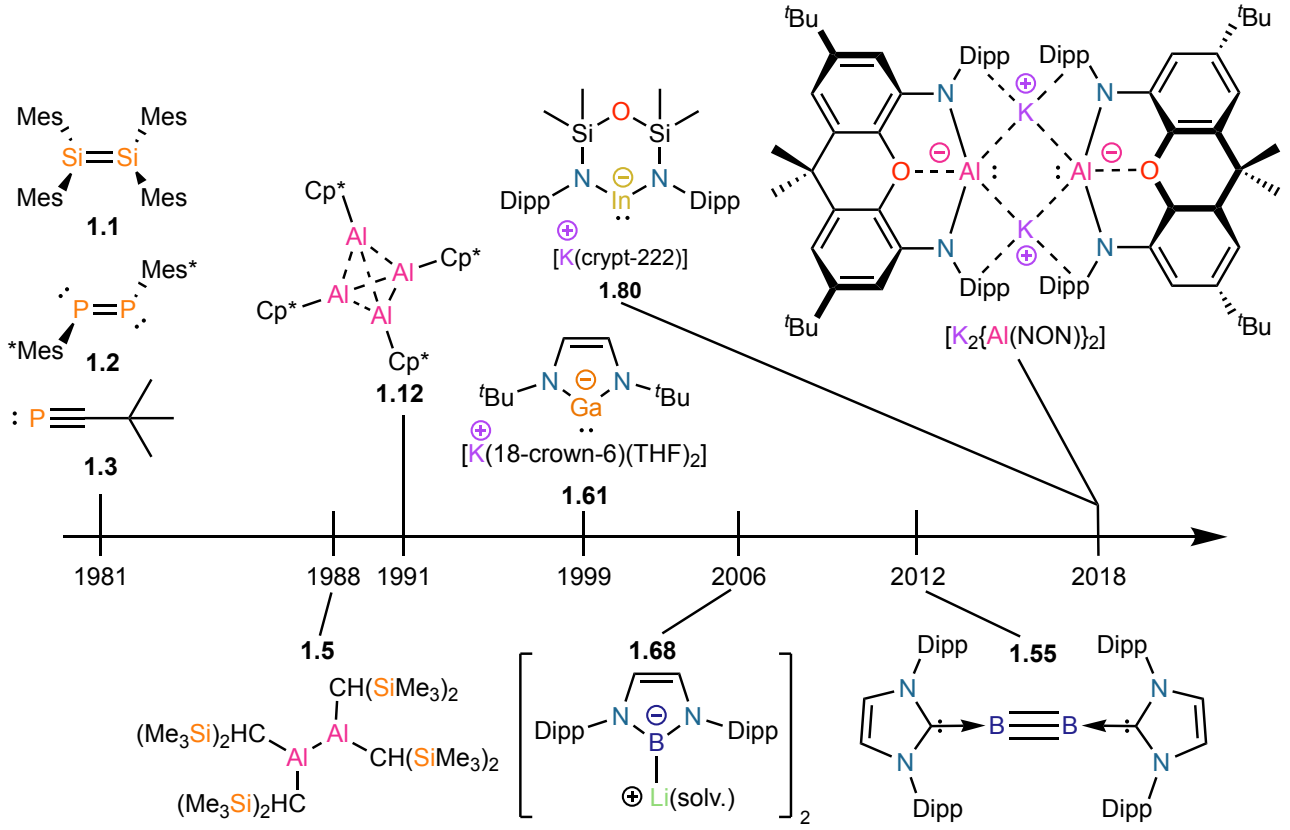

Figure 1.13: Timeline of selected main group organometallic species highlighted throughout Chapter 1.

The paradigm shift within organometallic chemistry as extending from the transition metals to the main group has promoted the exploration of reactivity, coordination and application of *s*- and *p*-block elements (Figure 1.13).[1] Featuring diverse chemical and physical properties, group 13 elements presents an exciting focus toward further expanding the organometallic renaissance since report of **1.1**-**1.3** in 1981.[3, 105] A now extensive field, low oxidation state group 13 compounds stabilised in the +2 (**1.5**), +1 (**1.12**), and 0-oxidation states (**1.55**) are underlined by their highly reactive nature, leading to opportunities for transition metal metallomimetic applications.[2] Developments of +1 oxidation state group 13 anions present exciting advancements in the capabilities of such systems for umpolung reactivity arising from the nucleophilicity of the metal centre.[3] Following the initial report in 1999 of a gallyl anion **1.61**,[112] the isolation of the first isoelectronic boryl **1.68**,[118] and indyl **1.80** anions,[124] has initiated the continued development of this field of research. The completion of the series in 2018 with the report of the first aluminyl anion $[K_2\{Al(NON)\}_2]$,[115] set investigations into overdrive ensuring extensive advances in the years that followed.[4, 111] Advancements within the novel class of aluminium(I) nucleophiles have seen the application of new and diverse ligand systems in tuning and broadening the reactivity of the metal centre, implicating these compounds in developments toward a new generation of main group organometallics.

1.8. References

[1] C. Jones, G. A. Koutsantonis, *Aust. J. Chem.* **2013**, *66*, 1115-1117.
[2] P. P. Power, *Nature* **2010**, *463*, 171-177.
[3] R. L. Melen, *Science* **2019**, *363*, 479-484.
[4] J. Hicks, P. Vasko, J. M. Goicoechea, S. Aldridge, *Angew. Chem. Int. Ed. Engl.* **2021**, *60*, 1702-1713.
[5] M. S. Hill, D. J. Liptrot, C. Weetman, *Chem. Soc. Rev.* **2016**, *45*, 972-988.
[6] S. Krieck, M. Westerhausen, *Inorganics* **2017**, *5*, 17.
[7] M. Weller, T. Overton, J. Rourke, F. Armstrong, *Inorganic Chemistry*, 6th ed., Oxford University Press, USA, **2014**.
[8] a) W. L. Masterton, C. N. Hurley, *Chemistry: Principles and Reactions*, Cengage Learning, **2015**; b) J. M. Goicoechea, in *Clusters–Contemporary Insight in Structure and Bonding*, **2016**, pp. 63-97.
[9] C. E. Housecroft, A. G. Sharpe, *Inorganic Chemistry, Vol. 1*, Pearson Education, **2008**.
[10] S. Yadav, S. Saha, S. S. Sen, *ChemCatChem* **2016**, *8*, 486-501.
[11] W. M. Haynes, *CRC Handbook of Chemistry and Physics*, CRC Press, **2016**.
[12] A. A. Yaroshevsky, *Geochem. Int.* **2006**, *44*, 48-55.
[13] G. Bertrand, *Chem. Rev.* **2010**, *110*, 3851.
[14] R. West, M. J. Fink, J. Michl, *Science* **1981**, *214*, 1343-1344.
[15] M. Yoshifuji, I. Shima, N. Inamoto, K. Hirotsu, T. Higuchi, *J. Am. Chem. Soc.* **1981**, *103*, 4587-4589.
[16] G. Becker, G. Gresser, W. Uhl, *Z. Naturforsch. B* **1981**, *36*, 16-19.
[17] R. C. Fischer, P. P. Power, *Chem. Rev.* **2010**, *110*, 3877-3923.
[18] C. Weetman, S. Inoue, *ChemCatChem* **2018**, *10*, 4213-4228.
[19] M.-A. Légaré, G. Bélanger-Chabot, R. D. Dewhurst, E. Welz, I. Krummenacher, B. Engels, H. Braunschweig, *Science* **2018**, *359*, 896-900.
[20] G. H. Spikes, J. C. Fettinger, P. P. Power, *J. Am. Chem. Soc.* **2005**, *127*, 12232-12233.
[21] N. Tokitoh, W. Ando, in *Reactive Intermediate Chemistry*, **2003**, pp. 651-715.
[22] H. Braunschweig, I. Krummenacher, M.-A. Légaré, A. Matler, K. Radacki, Q. Ye, *J. Am. Chem. Soc.* **2017**, *139*, 1802-1805.
[23] M.-A. Légaré, C. Pranckevicius, H. Braunschweig, *Chem. Rev.* **2019**, *119*, 8231-8261.
[24] P. Schwerdtfeger, G. A. Heath, M. Dolg, M. A. Bennett, *J. Am. Chem. Soc.* **1992**, *114*, 7518-7527.
[25] J. L. Gay-Lussac, L. J. Thénard, *Ann. Chim. Phys* **1808**, *68*, 169-174.
[26] H. Davy, *Philos. Trans. R. Soc. A* **1809**, 39-104.
[27] P. P. Power, W. G. Woods, *Plant Soil* **1997**, *193*, 1-13.
[28] W. G. Woods, *Environ. Health Perspect* **1994**, *102 Suppl 7*, 5-11.
[29] a) N. S. Hosmane, *Boron Science*, **2011**; b) R. Martin, S. L. Buchwald, *Acc. Chem. Res.* **2008**, *41*, 1461-1473.
[30] H. C. Ørsted, *Physisk Classe* **1825**, *1*, 15-16.
[31] F. Habashi, *Nano studies* **2013**, *8*, 333-344.
[32] A. Bagshaw, *Bauxite to Alumina: The Bayer Process. An Introductory Text*, **2017**.
[33] P. Rambabu, N. Eswara Prasad, V. V. Kutumbarao, R. J. H. Wanhill, in *Aerospace Materials and Material Technologies: Volume 1: Aerospace Materials* (Eds.: N. E. Prasad, R. J. H. Wanhill), Springer Singapore, Singapore, **2017**, pp. 29-52.
[34] I. Iqbal, S. Sharma, A. R. Pathania, *Mater. Today. Proc.* **2022**, *62*, 4365-4369.
[35] a) G. I. Nikonov, *ACS Catal.* **2017**, *7*, 7257-7266; b) A. Arbaoui, C. Redshaw, *Polym. Chem.* **2010**, *1*, 801-826; c) J. Wu, T.-L. Yu, C.-T. Chen, C.-C. Lin, *Coord. Chem. Rev.* **2006**, *250*, 602-626.
[36] E. Zurek, T. Ziegler, *Prog. Polym. Sci.* **2004**, *29*, 107-148.

[37] X. Lu, Z. Zhang, T. Hiraki, O. Takeda, H. Zhu, K. Matsubae, T. Nagasaka, *Nature* **2022**, *606*, 511-515.
[38] S. Van Den Eynde, E. Bracquené, D. Diaz-Romero, I. Zaplana, B. Engelen, J. R. Duflou, J. R. Peeters, *J. Waste Manag.* **2022**, *137*, 231-240.
[39] L. de Boisbaudran, *C. R. Hebd. Seances Acad. Sci.* **1875**, *81*, 493-495.
[40] Z. Liu, H. Li, *Hydrometallurgy* **2015**, *155*, 29-43.
[41] F. Max, P. K. Marina, S. Thomas, G. Jens, *Resour. Policy* **2016**, *47*, 38-50.
[42] G. Angerer, L. Erdmann, F. Marscheider-Weidemann, M. Scharp, A. Lüllmann, V. Handke, M. Marwede, *Rohstoffe für Zukunftstechnologien*, **2009**.
[43] F. Reich, T. Richter, *J. Prakt. Chem.* **1863**, *90*, 172-176.
[44] A. M. Alfantazi, R. R. Moskalyk, *Miner. Eng.* **2003**, *16*, 687-694.
[45] Z. Chen, W. Li, R. Li, Y. Zhang, G. Xu, H. Cheng, *Langmuir* **2013**, *29*, 13836-13842.
[46] Y. Zhang, M. Kim, L. Wang, P. Verlinden, B. Hallam, *Energy Envirom. Sci.* **2021**, *14*, 5587-5610.
[47] M. Rahm, R. Hoffmann, N. W. Ashcroft, *Chem. Eur. J.* **2017**, *23*, 4017-4017.
[48] G. Genchi, A. Carocci, G. Lauria, M. S. Sinicropi, A. Catalano, *Appl. Sci.* **2021**, *11*, 8322.
[49] M. Razeghi, J. Kim, S. Park, Y. Choi, D. Wu, E. Michel, J. Xu, E. Bigan, in *Compound Semiconductors 1995, Proceedings of the Twenty-Second INT Symposium on Compound Semiconductors held in Cheju Island, Korea, 28 August-2 September, 1995*, CRC Press, **2020**, pp. 1085-1090.
[50] C. L. Macdonald, B. D. Ellis, A. a. Swidan, *Encyclopedia of Inorganic and Bioinorganic Chemistry* **2011**.
[51] W. Uhl, *Angew. Chem. Int. Ed.* **1993**, *105*, 1449-1461.
[52] a) W. Biffar, H. Nöth, H. Pommerening, *Angew. Chem. Int. Ed. Engl.* **1980**, *19*, 56-57; b) K. Schlüter, A. Berndt, *Angew. Chem. Int. Ed.* **1980**, *92*, 64-65.
[53] W. Uhl, *Z. Naturforsch. B Chem. Sci.* **1988**, *43*, 1113-1118.
[54] a) W. Uhl, M. Layh, T. Hildenbrand, *J. Organomet. Chem.* **1989**, *364*, 289-300; b) W. Uhl, M. Layh, W. Hiller, *J. Organomet. Chem.* **1989**, *368*, 139-154.
[55] K. Hobson, C. J. Carmalt, C. Bakewell, *Chem. Sci.* **2020**, *11*, 6942-6956.
[56] W. Uhl, *Chem. Soc. Rev.* **2000**, *29*, 259-265.
[57] H. Braunschweig, R. D. Dewhurst, A. Schneider, *Chem. Rev.* **2010**, *110*, 3924-3957.
[58] a) H. Braunschweig, M. Colling, *Coord. Chem. Rev.* **2001**, *223*, 1-51; b) H. Braunschweig, M. Colling, *Eur. J. Inorg. Chem.* **2003**, 393-403; c) U. Kaur, K. Saha, S. Gayen, S. Ghosh, *Coord. Chem. Rev.* **2021**, *446*, 214106.
[59] a) A. Schnepf, H. Schnöckel, *Angew. Chem. Int. Ed. Engl.* **2002**, *41*, 3532-3554; b) G. Linti, H. Schnöckel, *Coord. Chem. Rev.* **2000**, *206-207*, 285-319.
[60] C. Dohmeier, D. Loos, H. Schnöckel, *Angew. Chem. Int. Ed. Engl.* **1996**, *35*, 129-149.
[61] C. Dohmeier, C. Robl, M. Tacke, H. Schnöckel, *Angew. Chem. Int. Ed. Engl.* **1991**, *30*, 564-565.
[62] a) S. Schulz, H. W. Roesky, H. J. Koch, G. M. Sheldrick, D. Stalke, A. Kuhn, *Angew. Chem. Int. Ed. Engl.* **1993**, *32*, 1729-1731; b) C. Ganesamoorthy, S. Loerke, C. Gemel, P. Jerabek, M. Winter, G. Frenking, R. A. Fischer, *Chem. Commun.* **2013**, *49*, 2858-2860.
[63] P. Jutzi, B. Neumann, G. Reumann, H. G. Stammler, *Organometallics* **1998**, *17*, 1305-1314.
[64] O. T. Beachley, R. Blom, M. R. Churchill, K. Faegri, J. C. Fettinger, J. C. Pazik, L. Victoriano, *Organometallics* **1989**, *8*, 346-356.
[65] H. Werner, H. Otto, H. J. Kraus, *J. Organomet. Chem.* **1986**, *315*, C57-C60.
[66] a) A. Purath, H. Schnöckel, *J. Organomet. Chem.* **1999**, *579*, 373-375; b) A. Purath, C. Dohmeier, A. Ecker, H. Schnöckel, K. Amelunxen, T. Passler, N. Wiberg, *Organometallics* **1998**, *17*, 1894-1896; c) M. Schormann, K. S. Klimek, H. Hatop, S. P. Varkey, H. W. Roesky,

C. Lehmann, C. Röpken, R. Herbst-Irmer, M. Noltemeyer, *J. Solid State Chem.* **2001**, *162*, 225-236.
[67] C. Cui, H. W. Roesky, H.-G. Schmidt, M. Noltemeyer, H. Hao, F. Cimpoesu, *Angew. Chem. Int. Ed. Engl.* **2000**, *39*, 4274-4276.
[68] A. J. Arduengo, III, R. L. Harlow, M. Kline, *J. Am. Chem. Soc.* **1991**, *113*, 361-363.
[69] R. Y. Kong, M. Batuecas, M. R. Crimmin, *Chem. Sci.* **2021**, *12*, 14845-14854.
[70] C. Bakewell, M. Garçon, R. Y. Kong, L. O'Hare, A. J. P. White, M. R. Crimmin, *Inorg. Chem.* **2020**, *59*, 4608-4616.
[71] A. Paparo, A. J. R. Matthews, C. D. Smith, A. J. Edwards, K. Yuvaraj, C. Jones, *Dalton Trans.* **2021**, *50*, 7604-7609.
[72] a) C. Bakewell, A. J. P. White, M. R. Crimmin, *Chem Sci.* **2019**, *10*, 2452-2458; b) T. N. Hooper, M. Garçon, A. J. P. White, M. R. Crimmin, *Chem. Sci.* **2018**, *9*, 5435-5440.
[73] S. Grams, J. Eyselein, J. Langer, C. Färber, S. Harder, *Angew. Chem. Int. Ed. Engl.* **2020**, *132*, 16116-16120.
[74] X. Li, X. Cheng, H. Song, C. Cui, *Organometallics* **2007**, *26*, 1039-1043.
[75] N. J. Hardman, B. E. Eichler, P. P. Power, *Chem. Commun.* **2000**, 1991-1992.
[76] M. Asay, C. Jones, M. Driess, *Chem. Rev.* **2011**, *111*, 354-396.
[77] N. J. Hardman, P. P. Power, J. D. Gorden, C. L. B. Macdonald, A. H. Cowley, *Chem. Commun.* **2001**, 1866-1867.
[78] A. Kempter, C. Gemel, T. Cadenbach, R. A. Fischer, *Organometallics* **2007**, *26*, 4257-4264.
[79] a) A. Kempter, C. Gemel, R. A. Fischer, *Inorg. Chem.* **2008**, *47*, 7279-7285; b) A. Kempter, C. Gemel, N. J. Hardman, R. A. Fischer, *Inorg. Chem.* **2006**, *45*, 3133-3138.
[80] G. Prabusankar, A. Kempter, C. Gemel, M.-K. Schröter, R. A. Fischer, *Angew. Chem. Int. Ed. Engl.* **2008**, *47*, 7234-7237.
[81] N. J. Hardman, P. P. Power, *Chem. Commun.* **2001**, 1184-1185.
[82] N. J. Hardman, P. P. Power, *Inorg. Chem.* **2001**, *40*, 2474-2475.
[83] C. Jones, *Nat. Rev. Chem.* **2017**, *1*, 0059.
[84] M. S. Hill, P. B. Hitchcock, *Chem. Commun.* **2004**, 1818-1819.
[85] a) M. S. Hill, P. B. Hitchcock, R. Pongtavornpinyo, *Dalton Trans.* **2007**, 731-733; b) M. S. Hill, R. Pongtavornpinyo, P. B. Hitchcock, *Chem. Commun.* **2006**, 3720-3722.
[86] C. Jones, P. C. Junk, J. A. Platts, A. Stasch, *J. Am. Chem. Soc.* **2006**, *128*, 2206-2207.
[87] M. Soleilhavoup, G. Bertrand, *Angew. Chem. Int. Ed. Engl.* **2017**, *56*, 10282-10292.
[88] K. Edel, M. Krieg, D. Grote, H. F. Bettinger, *J. Am. Chem. Soc.* **2017**, *139*, 15151-15159.
[89] Y. Wang, B. Quillian, P. Wei, C. S. Wannere, Y. Xie, R. B. King, H. F. Schaefer, P. v. R. Schleyer, G. H. Robinson, *J. Am. Chem. Soc.* **2007**, *129*, 12412-12413.
[90] F. Dahcheh, D. Martin, D. W. Stephan, G. Bertrand, *Angew. Chem. Int. Ed. Engl.* **2014**, *126*, 13375-13379.
[91] R. Kinjo, B. Donnadieu, M. A. Celik, G. Frenking, G. Bertrand, *Science* **2011**, *333*, 610-613.
[92] L. Kong, R. Ganguly, Y. Li, R. Kinjo, *Chem. Sci.* **2015**, *6*, 2893-2902.
[93] J. D. Queen, A. Lehmann, J. C. Fettinger, H. M. Tuononen, P. P. Power, *J. Am. Chem. Soc.* **2020**, *142*, 20554-20559.
[94] J. Hicks, M. Juckel, A. Paparo, D. Dange, C. Jones, *Organometallics* **2018**, *37*, 4810-4813.
[95] Z. Zhu, R. C. Fischer, B. D. Ellis, E. Rivard, W. A. Merrill, M. M. Olmstead, P. P. Power, J. D. Guo, S. Nagase, L. Pu, *Chem. Eur. J.* **2009**, *15*, 5263-5272.
[96] S. T. Haubrich, P. P. Power, *J. Am. Chem. Soc.* **1998**, *120*, 2202-2203.
[97] M. Niemeyer, P. P. Power, *Angew. Chem. Int. Ed. Engl.* **1998**, *37*, 1277-1279.
[98] A. Hinz, M. P. Müller, *Chem. Commun.* **2021**, *57*, 12532-12535.
[99] X. Zhang, L. L. Liu, *Angew. Chem. Int. Ed. Engl.* **2021**, *60*, 27062-27069.
[100] X. Zhang, Y. Mei, L. L. Liu, *Chem. Eur. J.* **2022**, *28*, e202202102.

[101] J. D. Queen, S. Irvankoski, J. C. Fettinger, H. M. Tuononen, P. P. Power, *J. Am. Chem. Soc.* **2021**, *143*, 6351-6356.
[102] X. Zhang, H. Wang, X. Lan, Y. Mei, D. A. Ruiz, L. L. Liu, *CCS Chem.* **2023**, *5*, 2059-2068.
[103] a) R. J. Wright, A. D. Phillips, N. J. Hardman, P. P. Power, *J. Am. Chem. Soc.* **2002**, *124*, 8538-8539; b) R. J. Wright, A. D. Phillips, S. Hino, P. P. Power, *J. Am. Chem. Soc.* **2005**, *127*, 4794-4799.
[104] J. Moilanen, P. P. Power, H. M. Tuononen, *Inorg. Chem.* **2010**, *49*, 10992-11000.
[105] P. Bag, C. Weetman, S. Inoue, *Angew. Chem. Int. Ed. Engl.* **2018**, *57*, 14394-14413.
[106] R. J. Wright, M. Brynda, P. P. Power, *Angew. Chem. Int. Ed. Engl.* **2006**, *45*, 5953-5956.
[107] H. Braunschweig, R. D. Dewhurst, K. Hammond, J. Mies, K. Radacki, A. Vargas, *Science* **2012**, *336*, 1420-1422.
[108] M. Zhou, N. Tsumori, Z. Li, K. Fan, L. Andrews, Q. Xu, *J. Am. Chem. Soc.* **2002**, *124*, 12936-12937.
[109] P. Bag, A. Porzelt, P. J. Altmann, S. Inoue, *J. Am. Chem. Soc.* **2017**, *139*, 14384-14387.
[110] R. J. Wehmschulte, K. Ruhlandt-Senge, M. M. Olmstead, H. Hope, B. E. Sturgeon, P. P. Power, *Inorg. Chem.* **1993**, *32*, 2983-2984.
[111] M. P. Coles, M. J. Evans, *Chem. Commun.* **2023**, *59*, 503-519.
[112] E. S. Schmidt, A. Jockisch, H. Schmidbaur, *J. Am. Chem. Soc.* **1999**, *121*, 9758-9759.
[113] R. J. Baker, R. D. Farley, C. Jones, M. Kloth, D. M. Murphy, *Dalton Trans.* **2002**, 3844.
[114] I. L. Fedushkin, A. N. Lukoyanov, G. K. Fukin, S. Y. Ketkov, M. Hummert, H. Schumann, *Chem. Eur. J.* **2008**, *14*, 8465-8468.
[115] J. Hicks, P. Vasko, J. M. Goicoechea, S. Aldridge, *Nature* **2018**, *557*, 92-95.
[116] M. Edwards, J. Hicks, C. McManus, J. M. Goicoechea, S. Aldridge, *Polyhedron* **2023**, *242*, 116520.
[117] D. Sarkar, P. Vasko, T. Gluharev, L. P. Griffin, C. Bogle, J. Struijs, J. Tang, A. F. Roper, A. E. Crumpton, S. Aldridge, *Angew. Chem. Int. Ed. Engl.* **2024**, *63*, e202407427.
[118] Y. Segawa, M. Yamashita, K. Nozaki, *Science* **2006**, *314*, 113-115.
[119] Y. Segawa, Y. Suzuki, M. Yamashita, K. Nozaki, *J. Am. Chem. Soc.* **2008**, *130*, 16069-16079.
[120] W. Lu, H. Hu, Y. Li, R. Ganguly, R. Kinjo, *J. Am. Chem. Soc.* **2016**, *138*, 6650-6661.
[121] A.-F. Pécharman, A. L. Colebatch, M. S. Hill, C. L. McMullin, M. F. Mahon, C. Weetman, *Nature Comm.* **2017**, *8*, 15022.
[122] A.-F. Pécharman, M. S. Hill, M. F. Mahon, *Dalton Trans.* **2018**, *47*, 7300-7305.
[123] A. V. Protchenko, P. Vasko, M. Á. Fuentes, J. Hicks, D. Vidovic, S. Aldridge, *Angew. Chem. Int. Ed. Engl.* **2021**, *60*, 2064-2068.
[124] R. J. Schwamm, M. D. Anker, M. Lein, M. P. Coles, C. M. Fitchett, *Angew. Chem. Int. Ed. Engl.* **2018**, *57*, 5885-5887.
[125] M. D. Anker, Y. Altaf, M. Lein, M. P. Coles, *Dalton Trans.* **2019**, *48*, 16588-16594.
[126] M. D. Anker, M. Lein, M. P. Coles, *Chem. Sci.* **2019**, *10*, 1212-1218.

2. Bulky Silylamido Aluminium(III) Iodide Precursors

2.1. Introduction

2.1.1. The First Aluminyl Anion

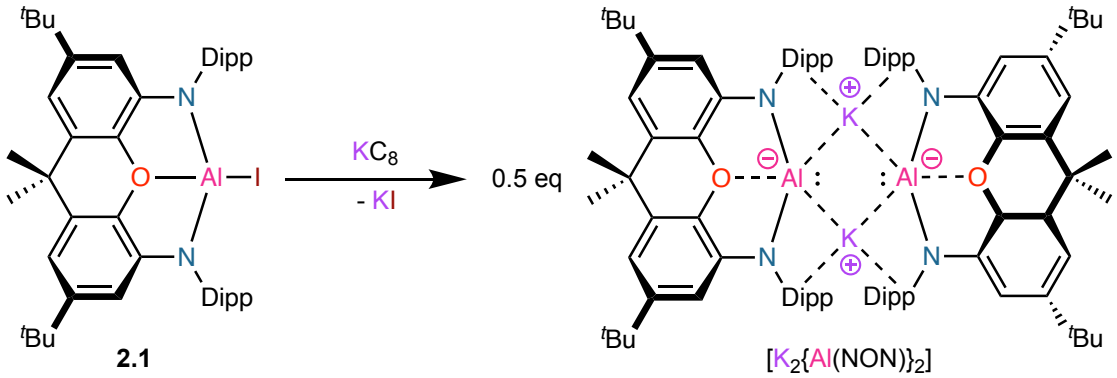

*Figure 2.1: Reduction of aluminium iodide precursor **2.1** yielding the first reported aluminyl anion [K₂{Al(NON)}₂] (Dipp = 2,6-diisopropylphenyl).*[1]

In establishing a new class of aluminium(I) nucleophile, the seminal report of the highly reactive species [K₂{Al(NON)}₂] was foundational upon its precursor complex. Shrouded with a rigid diamido xanthene [NON]$^{2-}$ ligand system ([NON]$^{2-}$ = 4,5-bis(2,6-diisopropylanilido)-2,7-di-*tert*-butyl-9,9-dimethylxanthene), the aluminium(III) halide precursor **2.1** was treated with potassium graphite, leading to a two-electron reduction and the formation of the novel aluminyl anion [K₂{Al(NON)}₂] (Figure 2.1).[1] Subsequent reports have replicated or applied similar synthetic methodologies in the preparation of varied aluminium(I) nucleophiles.[2] By design, precursors are similarly as diverse as reported aluminium(I) frameworks, however, the library of aluminium(III) halide precursors for reduction to aluminyl anions remains restricted to ten examples.

In advancing aluminyl anions, rationalised and synthetical viable precursor preparations are imperative due to the highly reactive nature of the targeted species.[3] Observing the reported library and literature considerations, this Chapter shall explore the preparation of new aluminium(III) halide complexes employing sterically encumbered ligand scaffolds as potential precursors to novel aluminyl anions.

2.1.2. Ligand Design

Modern main group chemistry advancements hinge on the development and application of stabilising ligand systems.[4] Fundamentally, ligands form the primary coordination sphere of a complex, contributing to the coordination number of the central metal atom. Through the variation of ligands, the stabilisation of a wide range of coordination numbers and valence states are accessible, further supporting the structural richness and chemical diversity of metal complexes.[5]

Denticity dictates the number of attachment sites through which a ligand binds to a metal centre, (mono- one, bi- two, tri- three, poly- many). Increasing complex stability, the entropy-driven chelate effect sees increased denticity, which increases metal centre affinity compared to monodentate examples. Moreover, it is possible for anionic charges to be delocalised across multiple coordination sites, further defining the oxidation state of their coordinated metal.[6] However, despite the entropic advantages of bi- and polydentate ligands, monodentate scaffolds remain significant in main group organometallic chemistry, yielding new and varied species.[4]

The stabilising properties of a ligand can be tuned through steric and electronic manipulations. Steric considerations, whereby the coordination of bulky, sterically demanding moieties and ligand systems are utilised to support the kinetic stabilisation of otherwise unstable bonding motifs and oxidation states.[7] Consequently, highly reactive species may be kinetically trapped, and the decomposition via disproportionation, comproportionation and aggregation pathways are greatly hindered. Electronically, ligands allow the electron density upon a metal centre to be manipulated. This is evident through the broadening and narrowing of frontier orbital (HOMO and LUMO) energy gaps, fundamental in explaining the reactivity of metal centres.[8] This can be imparted through employing relatively hard (*N*, *O*, and *F*) and soft (*C*, *P*, *S*, and *X*) coordination atoms, and the inclusion of electron-withdrawing (carbonyl C=O, cyano C≡N) and/or electron donating (amine -NR_2, ether -OR) functional groups. Moreover, steric and electronic manipulations of such substituents can further influence the solubility and solid-state isolation of the derived coordination complexes.

2.1.3. Synthetic Methodologies

Two key methodologies (and their variants) are notably employed in the preparation of aluminium(III) halide complexes and wider organometallic precursors: salt metathesis and metalation.[2-3] A brief overview of these methods and their relation to precursor synthesis is provided herein.

2.1.3.1. Salt Metathesis

*Equation 2.1: (**a**) Generic salt metathesis equation of a metal halide (M'Xn) organoalkali metal compound (RM). (M and M' = metal; R = organic group, X = halide).*

Halide (or 'salt') metathesis is widely utilised within organometallic chemistry and is applicable to elements across the periodic table.[5] This is typically the reaction of a metal halide ($M'X_n$) (M′ = metal) and an organoalkali metal compound (RM; R = organic fragment, M = Li, Na, K), affording the

corresponding alkali metal halide salt (MX) and the organometallic target (RM') (Equation 2.1 **a**).[9] To drive the reaction effectively, M should be more electropositive than M' to maximise hard–soft acid–base interactions. Moreover, the formation of the insoluble by-products or salts serves as a thermodynamic driving force, shifting the equilibrium position of the reaction towards the targeted products.[10] Within the formation of aluminium(III) halide precursors, salt metathesis pathways are widely applied (M' = Al).

2.1.3.2. Metalation

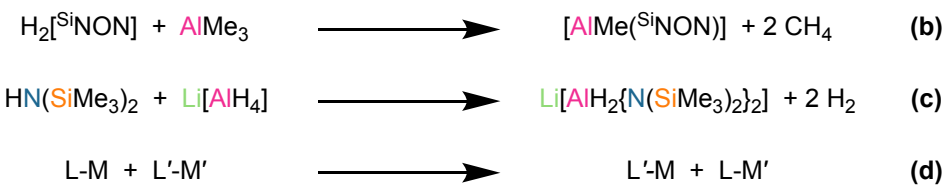

*Equation 2.2: **(b)** Equation outlining direct double metalation with an organoaluminium base, $[^{Si}NON]^{2-}$ = $[O\{Si(Me)_2N(Dipp)\}_2]^{2-}$.[11] **(c)** Equation describing contemporary method utilising lithium aluminium hydride as a metalation source.[12] **(d)** Generic transmetalation equation when ligands (L, L') of metals (M, M') are exchanged.[13]*

Metalation within organometallic chemistry describes any metal-organic bond formation, and commonly features a metal atom or ion incorporated into an organic molecule by replacing a hydrogen atom or other substituent.[5] Direct metalation relates a metal directly replacing a hydrogen atom or another substituent in the organic molecule, and is often facilitated by a strong base metallic reagent (i.e. organoaluminium bases).[14] Within the preparation of aluminium(III) complexes, trimethylaluminium can be applied with amines to yield amido ligated aluminium methyl starting materials as viable reagents for halogenation (Equation 2.2 **b**).[11] Contemporary reports by Heine and Stalke in 1992 highlighted the application of $Li[AlH_4]$ as a source of aluminium for yielding a range of aluminium complexes, expanding on previous reducing and hydrogenating applications.[12] For example, addition of $Li[AlH_4]$ to the bulky hexamethyldisilylamine (HMDS) affords a four coordinate diligated lithium aluminate $[Li(OEt_2)_2][AlH_2\{N(SiMe_3)_2\}_2]$ and two equivalents of H_2 (Equation 2.2 **c**). Once isolated the aluminate complex can serve as an immediate towards halogenation, and subsequent purification to a viable aluminium(III) halide precursor. Finally, transmetalation involves the transfer of a metal from one organic molecule to another, typically through the interaction of two metal-containing species featuring different metal identities (Equation 2.2 **d**). Predominantly applied in ligand preparation rather than precursor synthesis, this process is crucial in cross-coupling reactions, such as the Sonogashira and Stille reactions, where the transfer of an organic fragment to a catalytically active metal (palladium) enables the formation of new carbon-carbon bonds.[13, 15]

In previous reports, organoaluminium compounds with terminal alkyl ligands (usually methyl) have undergone halogenation with methyl groups substituted for halides. Consequently yielding viable aluminyl anion precursors.[11, 14] Consequently, this methodology is the second most applied in the preparation of aluminium(III) halide aluminyl anion precursors within the literature.[2-3]

2.2. Literature Outline and Target Rationalisation

2.2.1. Library of Aluminium(III) Halide Precursors for Aluminyl Anion Preparation

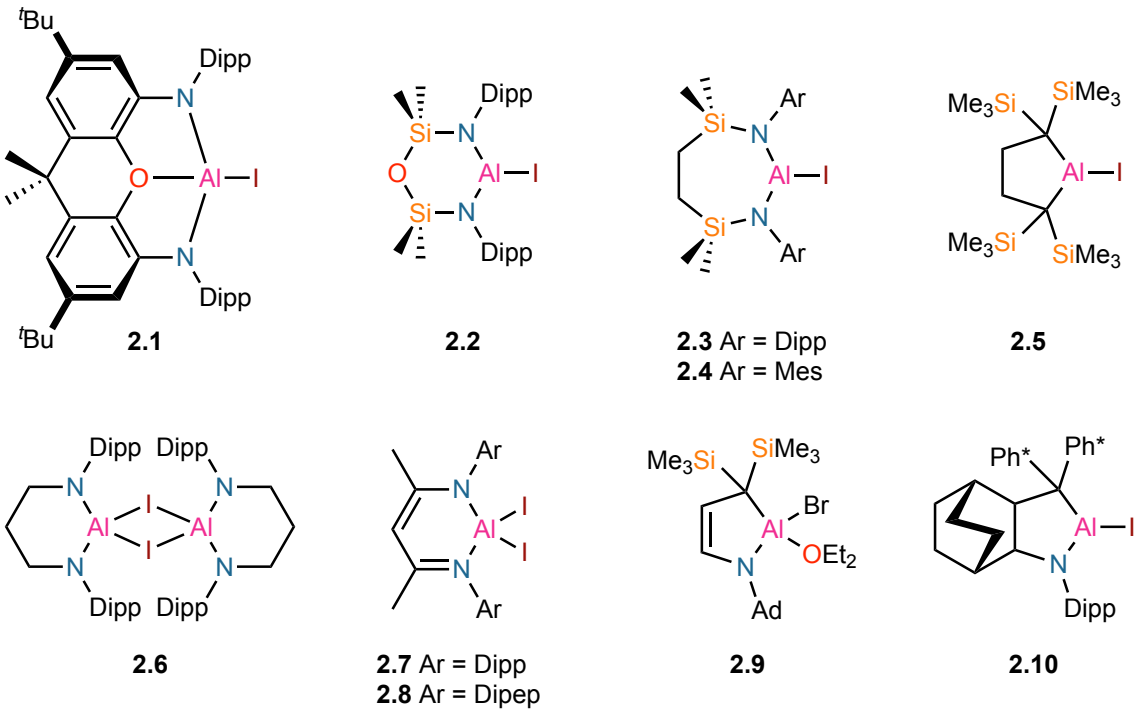

Figure 2.2: Library of reported aluminium(III) halide precursors utilised in the preparation of aluminyl anions. (Ad = 1-adamantyl, Dipep = 2,6-C(H)Et$_2$-C$_6$H$_3$, Mes = 2,4,6-trimethylphenyl, Ph = 3,5-^{t}Bu$_2$-C$_6$H$_3$).*

Figure 2.2 shows the library of reported aluminium(III) halide precursors utilised in the preparation of aluminyl anions via reduction methodologies.[2] Of particular note to this thesis is that all precursors are cyclic, constraining the aluminium(III) centre within a 5- to pseudo-8-membered metallocycles (Figure 2.2). The report of the first analogue **2.1** by Aldridge, Goicoechea and coworkers in 2018 utilised the dianionic $[NON]^{2-}$ ligand scaffold to coordinate the metal centre within a pseudo-tridentate, 8-membered metallocycle, whereby electron donation from the backbone oxygen atom assists in species stabilisation.[1] The complex was synthesised through a salt metathesis reaction between the potassium salt of the ligand and aluminium triiodide. Reported shortly thereafter, Coles and coworkers utilised the bulky $[^{Si}NON]^{2-}$ scaffold ($[^{Si}NON]^{2-}$ = $[O\{Si(Me)_2N(Dipp)\}_2]^{2-}$) in preparing the 6-membered metallocyclic species **2.2** from routes of metalation with trimethylaluminium and halogenation with elemental iodine.[11] Following a similar route in 2020,

further expansions to include examples of 7-membered metallocycles were first reported respectively by Hill, McMullin and coworkers, **2.3**, and **2.4**, respectively, utilising a diamido $[SiN^{Ar}]^{2-}$ scaffold ($[\{CH_2SiMe_2N(Ar)\}_2]^{2-}$, Ar = Dipp,[16] Mes).[14] In the same year, Yamashita and coworkers used lithium salt metathesis syntheses to yield the first 5-membered aluminyl precursor **2.5** featuring a dialkyl dianionic $[\{C(SiMe_3)_2CH_2\}_2]^{2-}$ scaffold.[17] Subsequent reports have since expanded 6- (**2.6**,[18] **2.7**,[19] **2.8**),[20] and 5- (**2.09**,[21] **2.10**)[22] membered aluminium metallocycles, varying both the heterocycle-contained atoms and their substituents (Figure 2.2). Notably, outside the ligand scaffolds highlighted within Figure 2.2, aluminyl anions have been reported employing further diverse ligand systems.[23] However, access to aluminiyl anions utilise methods other than traditional reduction approaches, which will be discussed within **Chapter 3**.

Notably, all aluminium(III) halide precursors feature *N*- or *C*-donors, primarily applying diamido (**2.1**-**2.4**, **2.6**-**2.8**), or mixed alkyl-amido scaffolds (**2.9**, **2.10**),[21-22] with a single dialkyl system (**2.5**) reported.[17] Generally, *N*-donor substituents feature bulky organo-moieties of varying steric hinderance including Dipp, Dipep, and Mes aryl moieties, and 1-adamantyl alkyl moieties. *C*-donors almost exclusively feature trimethylsilyl moieties. Similar to aryl substituents, varied steric influences can be incorporated from the vast catalogue of synthetically available reagents. The exception is **2.10**, which features the bulky bis(*tert*-butyl)phenyl upon its singular *C*-donor (Figure 2.2).

Despite the variability of moieties and heterocycle size in aluminium(III) halide precursors, further structural characteristics are consistent across the library. Within the solid-state, all precursors except **2.6** are monomeric; **2.6** as reported by Yamashita and coworkers; features a bis(2,6-diisopropylphenyl)-1,3-propanediamine ligand which is isolated as an iodide-bridged dimer.[18] Moreover, within the precursors, all ligands are dianionic, except for the $[^{Ar}Nacnac]^-$ ($[^{Ar}Nacnac]^-$ = ß–diketiminato $HC[C(Me)Ar]_2$, Ar = Dipp, Dipep) scaffolds applied in **2.7**, and **2.8**.[19-20] Following initial precursor reduction, subsequent deprotonation of ligand yields a dianionic scaffold affording the related aluminyl anion (**Chapter 3**).

Aluminium(III) halide aluminyl precursors observe minimal variation of the halide identity. Primarily, iodide ligands are applied with just a single bromide example **2.9**. Whilst comparative analysis of bond dissociation energies has not been performed upon alkyl and amido aluminium(III) halides specifically, values corresponding to diatomic Al-X species can highlight trends present within the series.[24] As such, the Al-I library prevalence can be attributed to the bond dissociation energy being the lowest of the Al-halide series (Table 2.1). Experimentally, the lower bond dissociation energy of associated iodide ligands is highlighted through the ease of reduction to the targeted aluminyl anions.[3]

Table 2.1: Bond dissociation energies (Enthalpy, BDE) of aluminium halide diatomic molecules.[24]

Al – X Bond	BDE^0 298 /kJ mol^{-1}
Al – F	675
Al – Cl	502
Al – Br	429
Al – I	370

Further to the BDE of aluminium-halide bonds, the solubility and lattice energies of corresponding alkali metal-halide salts aids in the preparation of reduced species. Widely applied within preparation of reduced species (further discussed in **Chapter 3**) and the salt metathesis reactions in forming precursor species, generated potassium and lithium halide salts commonly precipitate from hydrocarbon solutions thermodynamically driving reactions forward. Of keynote, potassium halides (and particularly potassium iodide) feature decreased within organic solvents and are less commonly retained with products (comparative with Lithium halide salts).[25]

At the outset of this PhD project, two coordination motifs on the structural extremes of aluminyl anions were absent within the literature. These were (i) acyclic derivatices featuring two monodentate monoanionic ligands, and (ii) 4-memebered metallocycles. Accordingly, the remainder of this Chapter will focus on aluminium(III) halide precursor complexes used to target novel aluminyl anions.

2.2.2. Ligand Rationalisation

2.2.2.1. Monodentate Ligands Towards an Acyclic Aluminyl Anion

Previously unreported within aluminyl anion chemistry, monodentate ligands have been foundational in the establishment of the modern main group field.[4] Sterically demanding aryl and silyl substituents have featured widely in isolating low oxidation state species encompassing both transition metal and main group centres.

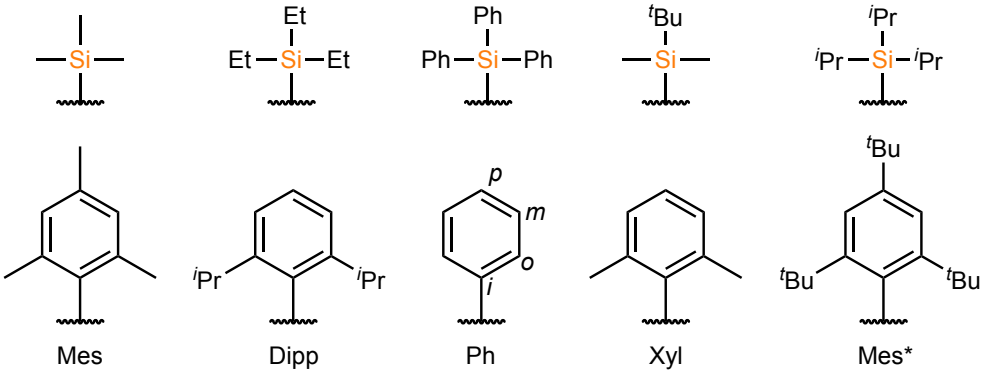

Figure 2.3: Sterically encumbering aryl and silyl moieties applied within main group chemistry.

Applying aryl substituents, West's disilene [$Mes_2Si{=}SiMes_2$] (**1.1**, **Chapter 1**) featuring monodentate bulky Mes groups, and Yoshifuji's disphosphene [Mes*P=PMes*] (**1.2**, **Chapter 1**) with Mes* groups (Mes* = 2,4,6-tris-*tert*-butylphenyl) helped promote the renaissance of main group chemistry.[26] Aryl substituents have become widely applied as a consequence of their ease of functionalisation and tunability with diverse groups at the *ortho*, *meta*, and *para* positions thereby varying the steric bulk and the electronic properties of the aryl ring (Figure 2.3). *Ortho*-positioned substituents can promote the kinetic protection of the metal centre, whereas *meta* and *para* substituents can direct steric bulk progressively away from the metal centre. Importantly, this functionality can be incorporated into more complex ligand systems by employing aryl units as functional groups (Figure 2.3). Consequently, aryl groups are foundationally applied within ligand scaffolds of aluminium(III) halide precursors and their reduction products, aluminyl anions.

Silyl substituents have proven to be highly applicable within organometallic systems and applied in the initial isolation of low oxidation state group 13 dimetallanes [$\{(Me_3Si)_2HC\}_2M$-$M\{CH(SiMe_3)_2\}_2$] (M = Al, Ga, In).[27] Traditionally, these moieties are readily available as organosilyl halides due to their wide application as silyl protecting groups for alcohols and amines. However, these moieties can be utilised as accessible steric bulk in the synthesis of amido or alkyl ligands (Figure 2.4). Applied within aluminium(III) halide precursors **2.5** and **2.9**, trimethylsilyl represents a relatively less sterically bulky moiety within the series (Figure 2.2). As such, increased steric encumberment can be exemplified with triethylsilyl, triisopropylsilyl, triphenylsilyl, and combinations thereafter including *tert*-butyldimethylsilyl groups (Figure 2.3).

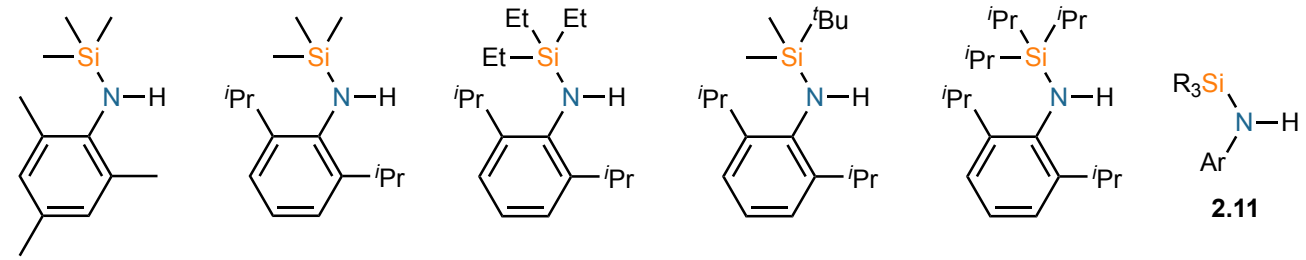

Figure 2.4: Applied bulky N-silylaniline proligands of varied aryl and silyl moieties and generic HN(Ar)SiR₃.

In combining varied sources of steric bulk, the application of aryl and silyl groups can be furthered through silyl(aryl)amido ligand systems of the corresponding *N*-silylaniline (Figure 2.4). These bulky amide ligands have seen intense research interest due to their high-yielding and economical one-step proligand *N*-silylaniline preparations and growing applications in transition metal,[28] and main group organometallic chemistry.[29] Once deprotonated, their monoanionic bulky amido counterparts **2.11**

$[N(Ar)SiR_3]^-$ (Ar = aryl, R = alkyl) impart steric and electronic effects tuneable through the variation of Ar and R groups (Figure 2.4).[29] Similarly applied in the synthesis of group 13 nucleophiles, amido ligands offer added stabilisation by participating in metal-ligand π-bonding.[30]

Toward the preparation of acyclic aluminium(III) halide precursors for aluminyl anion synthesis, the application of bulky monodentate silyl(aryl)amido monoanionic ligands offer a tuneable and economical synthon for targeted species development.

2.2.2.2. Bidentate Ligands Toward a 4-Membered Aluminyl Anion

Bidentate ligand systems stabilising smaller metallocycles with reactive metal centres have seen growing investigational focus. Notably, neither an aluminyl anion nor a neutral "free" aluminium(I) centre has been reported as stabilised within a 4-membered metallocycle.[3, 31] Rather, the library of aluminium(III) halide precursors (Figure 2.2), feature 5-membered metallocycles as the current smallest arrangements. Toward the preparation of new 4-membered aluminium(III) halides as precursors to the first 4-membered aluminyl anion, a previously minimally applied ligand system within aluminium chemistry was sought.

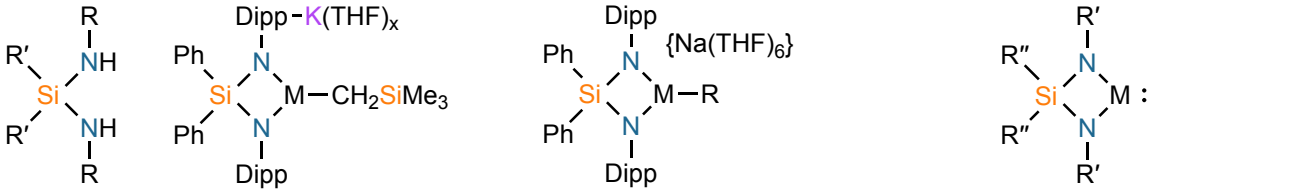

2.12

2.13 M = Zn, x = 4
2.14 M = Mg(THF), x = 3
2.15 M = Mn, x = 3

2.16 M = Zn, R = CH_2SiMe_3
2.17 M = Zn, R = $N(SiMe_3)_2$
2.18 M = Mg, R = CH_2SiMe_3
2.19 M = Mg(THF), R = Bu

2.20 M = Ge, R′ = Dipp, R″ = ^{i}Pr
2.21 M = Sn, R′ = Dipp, R″ = ^{i}Pr
2.22 M = Ge, R′ = $SiPh_3$, R″ = ^{i}Pr
2.23 M = Sn, R′ = $SiPh_3$, R″ = ^{i}Pr
2.24 M = Sn, R′ = Dipp, R″ = Ph

Figure 2.5: Generic Bis(amine)silane proligand $[R_2Si(R'NH)_2]$ ***2.12****. Applied silyldiamido ligand within alkali salt metalates* ***2.13-2.19****. Sterically varied silyldiamido ligands utilised in stabilising low coordinate germylene and stannylene heterocycles* ***2.20-2.24****.*

Prevalent within diamido ligand scaffolds for aluminium(III) halide precursors, the incorporation of silyl groups within precursor heterocycles (**2.2**-**2.4**) and growing applications of monodentate silyl(aryl)amido systems in stabilising low oxidation organometallic compounds, was of key interest (Figure 2.5). Synthetically, bis(amino)silanes **2.12** can be prepared on multigram scales through one-step synthesis and purification via crystallisation, highlighting applications as dianionic diamido ligand scaffolds (Figure 2.5).

Toward 4-membered metallocycles, silyldiamido ligands $[R_2Si(R'N)_2]^{2-}$ (R and R′ = aryl, alkyl, silyl) present similar tunability to their monodentate counterparts through the incorporating of varied

R and R′ substituents (Figure 2.5).[32] Through minimal backbone span, the bite angle with which the hard nitrogen donors bind to the metal centre is greatly narrowed with respect to larger metallocycles (Figure 2.2). This can lead to the varied isolation and reactivity potential of low valent metal centres compared with 5- and 6-membered metallocycle species. Within the literature, these kinetically stabilising σ-accepting, and π-donating ligand systems incorporating sufficient steric bulk have seen application with low-coordinate, reactive metal centres and wider investigation within *s*-, *d*- and *p*-block chemistry (Figure 2.5).[33] Hevia and coworkers have investigated extensively the complexation of metals within a silyldiamido metallocycle. Investigations have explored bimetallic systems toward highly functionalised aryl and heteroaryl organometallics with potassium metal(ates) with **2.13**-**2.15**,[34] varied and enhanced basicity toward enolates with sodium zincates with **2.16** and **2.17**,[35] and enolate metalation with sodium magnesiates with **2.18**,[35] and the promotion of single electron transfer processes,[36] direct Mg-H exchange, and selective C-2 metalation reactions with **2.19**.[37]

Relevant to this work, low oxidation state monomeric germylene and stannylene complexes have been reported by the groups of Rivard **2.20**-**2.23**,[38] and Russell **2.24**.[39] Stabilising the +2 oxidation state of two-coordinate group 14 metal centres within a planar 4-membered metallocycle, varied steric encumberment is imparted through the variation of Dipp (**2.20**, **2.21** and **2.24**) and umbrella-shaped $SiPh_3$ (**2.22** and **2.23**) groups at the coordinating *N* atoms. Moreover, the steric bulk upon the Si centre can directly impart and direct steric shielding of the *N* moieties.[38-39]

For targeting the first four-membered aluminyl anion, the above mentioneddianionic bidentate silyldiamido ligands are ideally suited for their stabilising properties and easy synthesis.

2.3. Research Rationales

2.3.1. Acyclic Aluminium(III) Precursor Rationale

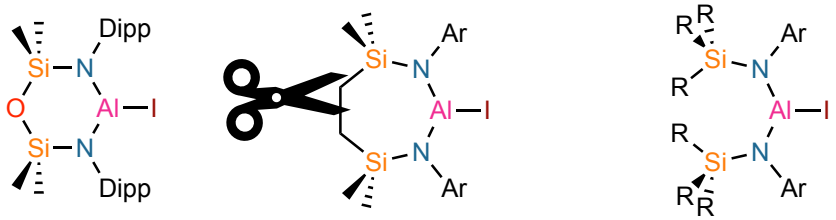

2.2 **2.3** Ar = Dipp **2.4** Ar = Mes **2.25**

*Figure 2.6: Previously reported 6- and 7-membered aluminium(III) iodide aluminyl anion precursors incorporating N-coordination atoms and Si groups within the heterocycles **2.2-2.4**. Structurally inspired motif to be pursued toward acyclic aluminium(III) iodide precursors **2.25**.*

As discussed previously, all reported aluminyl anions are heterocycles.[2] The chelating effect of these ligands could be seen to potentially dampen the reactivity of these reduced complexes. Consequently, acyclic analogues may present enhanced reactivity over their cyclic counterparts.

Inspired by the previously published cyclic analogues **2.2**-**2.4**, the implementation of two monodentate monoanionic bulky silyl(aryl)amido systems toward an acyclic aluminium(III) iodide precursor **2.25** was sought as a viable candidate (Figure 2.6). The generic targeted precursor **2.25** is reminiscent of a cyclic congener, whereby the related backbone linkers (**2.2** "O", **2.3** **2.4** "C-C") had been cleaved.

In targeting the first acyclic aluminyl anion, a library of acyclic aluminium(III) iodide precursors **2.25** incorporating varied silyl(aryl)amido ligands had to be developed for further reduction and reactivity investigations.

2.3.2. 4-Membered Aluminium(III) Precursor Rationale

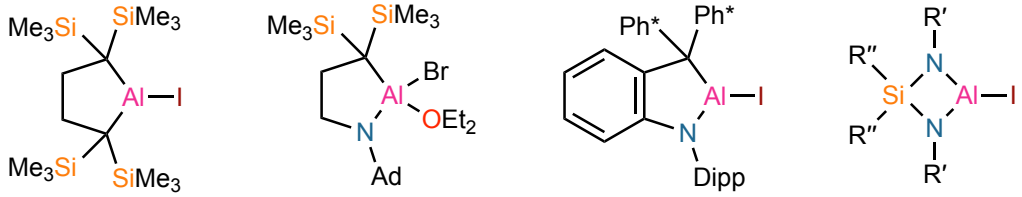

2.5 **2.9** **2.10** **2.26**

*Figure 2.7: Previously reported 5-membered heterocyclic aluminum(III) iodide aluminyl anion precursors **2.5**, **2.09**, **2.10**. Targeted 4-membered aluminium(III) iodide **2.26** as a potential precursors to the first 4-membered aluminyl anion.*

Previous attempts to isolate aluminium(I) species within 4-membered heterocycles have thus far been unsuccessful. Reductions of aluminium(III) halide complexes featuring amidinate, guanidinate and iminophosphonamides have observed decomposition and immediate reactivity of the low oxidation state species yielding them non-isolable.[40] The growing applications, varied species and oxidation states stabilised by silyldiamido ligands highlight this as a viable scaffold to stabilise the first 4-membered aluminium(I) species as an aluminyl anion (Figure 2.5).

The generic targeted precursor **2.26**, by design, imparts a narrower *N*-Al-*N* bond angle than previously reported 5-membered species (**2.5**, **2.9**, **2.10**) (Figure 2.7). Highlighted in the varied reactivity and synthesis of 5-membered metallocycles, 4-membered metallocycles present the potential for new and varied reactivity at the aluminium(I) centre. Despite extensive amidinate and guanidinate investigations, aluminium(III) species with silyldiamido ligands are of growing academic focus,[41] with further extensions into low-oxidation state chemistry through this work.

In the preparation of the first 4-membered aluminyl anion, new aluminium(III) iodide precursors incorporating silyldiamido ligands are targeted for further reduction and reactivity investigations. Therefore, a range of synthetic methodologies are employed to yield targeted precursor complex **2.26**.

2.4. Acyclic Aluminium(III) Halide Precursors: Results and Discussion

2.4.1. Synthesis of Bulky Monodentate *N*-Silylanilines

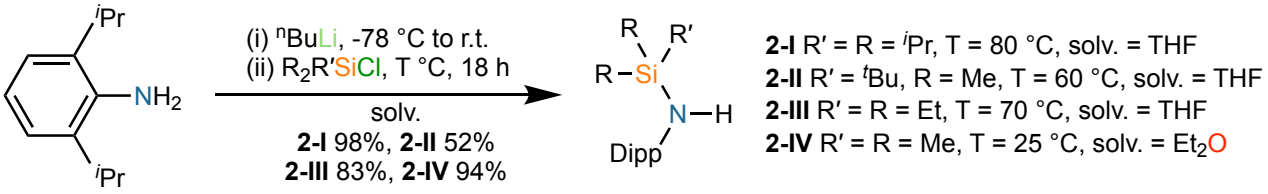

*Scheme 2.1: Synthesis of N-silylaniline proligands (**2-I** – **2-IV**), incorporating varied organosilyl substituents.*

Nitrogen-based silyl(aryl)amido ligand systems were sought as an attractive candidate for developing aluminium(III) iodide precursors **2.25** (Figure 2.6). To this end, *N*-silylaniline proligands were synthesised through one-pot preparations with commercially available starting materials, as per literature methods, and subsequently purified in moderate-to-high yields (**2-I** 98%,[42] **2-II** 52%,[43] **2-IV** 94%[44]) (Scheme 2.1). Previously unreported, the triethylsilyl analogue **2-III** was prepared in high yield (83%) via a similar synthetic route to bridge a steric gap between trimethyl, *tert*-butyldimethyl and triisopropyl analogues. Optimised on multigram scales, purification via vacuum distillation afforded the targeted *N*-silylaniline proligands in yields greater than those previously reported (where applicable) (Scheme 2.1).[42-44]

To date, the coordination of monodentate ligands affording diligated silyl(aryl)amido aluminium halide systems **2.25** are unreported. However, monoligated silyl(aryl)amido aluminium dihalide complexes are known and applied as a precursor to access the $[Al\{N(Dipp)SiMe_3\}]_4$ tetramer.[45] This tetramer features four aluminium(I) metal centres with "capping" ligands, analogous to Schnöckel's first low valent species $[AlCp^*]_4$ **1.12** (**Chapter 1**).[46]

The preparation of bis-silyl(aryl)amido aluminium halide complexes required investigations toward reliable and efficient synthetic routes. Exploring this, procedures incorporating organoaluminium bases and successive halogenation, alkali metal salt metathesis, and lithium aluminium hydride and subsequent halogenation routes were explored and the results discussed herein.

2.4.2. Trimethylaluminium Metalations of Monodentate *N*-Silylanilines

The use of alkyl aluminium reagents is a widely applicable synthetic method in aluminium(III) precursor preparation. Notably, this route was utilised in the preparation of precursor **2.7**, which allowed access to the first monomeric neutral aluminium(I) species [Al(Nacnac)] **1.19** (**Chapter 1**).[47] More recently, this methodology has been utilised in the formulation of multiple aluminum(III) iodide precursors (**2.2**-**2.4**,[11, 14, 16] **2.7**,[19] **2.8**[20]) before reduction to their corresponding aluminium(I) nucleophiles, as highlighted within reviews.[2-3]

Preparations utilising alkyl aluminium bases have been previously applied with monodentate silyl(aryl)amido ligand systems featuring the trimethyl and *tert*-butyldimethyl motifs of **2-II** and **2-IV**. In 1997, treatment of *N*-silylaniline proligands with trimethylaluminium yielded the first examples of methyl-bridged aminodimethylalanes $[AlMe_2\{N(Dipp)SiR_2R'\}]_2$ (R = R′ = Me, and R = Me, R′ = ^{t}Bu).[43] To date, no examples of bulkier monoligated aluminium dimethyl complexes featuring triethyl- and triisopropyl- silyl(aryl)amido ligand scaffolds have been crystallographically reported. Moreover, minimal literature precedence of diligated aluminium methyl complexes exists with silyl(aryl)amido frameworks,[48] highlighting an area of potential development. To this end, attempts at isolating ligated aluminium synthons were investigated.

2.4.2.1. Attempted Synthesis of Diamido Aluminium(III) Methyl Complexes

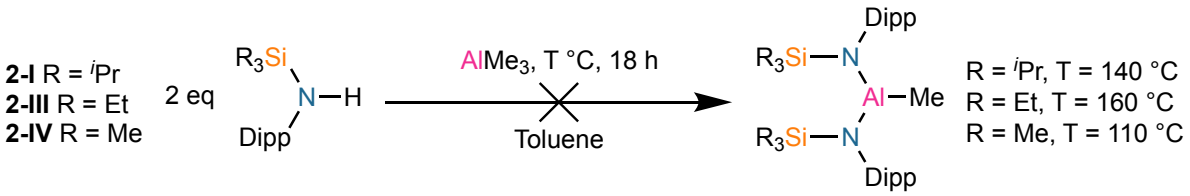

Scheme 2.2: Attempted synthesis of diamido aluminium methyl complexes from corresponding N-silylanilines.

To form diamido aluminium methyl complexes, the preparation of the most and least bulky analogues (trimethylsilyl and triispropylsilyl respectively) were pursued, along with the previously unreported triethylsilyl ligand system. Following investigations using benzene and hexane as solvents which gave mixtures of products, toluene was applied for reactions at elevated temperatures (Scheme 2.2). To toluene solutions of the corresponding *N*-silylanilines (**2-I**, **2-III**, **2-IV**), was added half an equivalent of trimethylaluminium. Whilst kept at room temperature, slow reaction progression towards a speculated monoligated silyl(aryl)amido aluminium dimethyl was observed. Aiding reaction progression and endeavouring to coordinate both bulky silyl(aryl)amido ligands, toluene solutions were refluxed for trimethylsilyl the system (110 °C) and superheated for bulkier analogues (triispropylsilyl 140 °C, triethylsilyl 160 °C) within J. Young's-valve sealed glassware overnight. In every case, ^{1}H NMR spectra identified the formation of a single new silyl(aryl)amido-containing product, but in an approximate 1:1 ratio with the starting *N*-silylaniline, suggesting mono-coordination.

Further attempts to prepare diligated species through increased equivalents of starting *N*-silylaniline were also conducted; however, these similarly led to unreacted proligand and the proposed mono-ligated aluminium dimethyl species (identified from ^{1}H NMR spectroscopy integrations). These findings suggested that the high degree of steric bulk is a significant barrier to ligand coordination through an organoaluminium metalation method.

To confirm preparations, crystallisations of the proposed mono-amido aluminium dimethyl species were attempted, but all attempts were unsuccessful in yielding single crystals from concentrated hydrocarbon solutions (toluene, hexane, pentane). The monoligated trimethylsilyl analogue $[AlMe_2\{N(Dipp)SiMe_3\}]_2$ isolated by Roesky and coworkers,[43] reportedly crystalised following the removal of hexane *in vacuo*. Despite multiple attempts, such crystallisations could not be replicated. The formation of targeted mono-amido aluminium dimethyl species in a mixture with unreacted proligand could be confirmed via ^{1}H NMR spectroscopic patterns analogous to that reported by Roesky and coworkers.[43] Similarly, crystallisation challenges could also be accredited to the additional equivalents of *N*-silylaniline proligand oil within the mother liquor, hindering crystallisation.

In ascertaining species identities, subsequent decreased equivalencies and the use of coordinating solvents were undertaken.

2.4.2.2. Confirmation of Monoligated Aluminium(III) Dimethyl Complexes

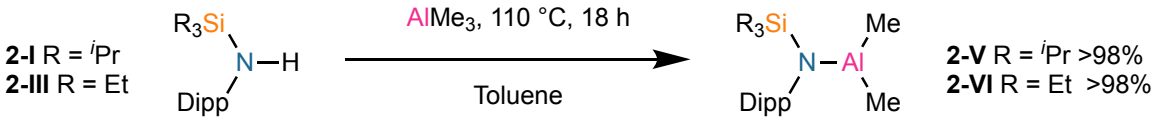

Scheme 2.3: Preparations of monoligated aluminium dimethyl complexes from the corresponding N-silylanilines.

Toward the confirmation of previously postulated mono-amido aluminium dimethyl species, inquiries were undertaken with bulkier triisopropylsilyl and triethylsilyl derivatives of the proligand (Scheme 2.3). Consequently, pursuing aluminium compounds had not been previously reported. Toluene solutions of the corresponding *N*-silylanilines (**2-I**, **2-III**) were treated with one equivalent of trimethylaluminium and heated to 110 °C overnight. This yielded a single clean product as identified by ^{1}H NMR spectroscopy. Postulating formation of the monoamido species $[AlMe_2\{N(Dipp)Si^iPr_3\}]$ **2-V** and $[AlMe_2\{N(Dipp)SiEt_3\}]$ **2-VI**, new signals were found that were identical to those observed in reactions with two equivalents of the proligand. Again, ^{1}H NMR spectra highlighted two methyl groups (6 H) coordinated to the aluminium centre via relative integrations to one $[N(Dipp)SiR_3]^-$ ligand system from diisopropyl methyl groups (12 H). Repeating reactions to yield triisopropylsilyl **2-V** were conducted on scales up to 3 g, with products utilised *in situ* for further investigations, rather than isolated. Both **2-V** and **2-VI** were afforded as transparent oils (yellow **2-V** and colourless **2-VI**), with **2-VI** characterised via heteronuclear NMR spectroscopic techniques. To aid in the isolation and solid-state characterisation of the amido aluminium(III) dimethyl species, the uses of Lewis bases were investigated with the objective of isolating solid products.

2.4.2.3. Addition of Lewis Bases to the Amido Aluminium(III) Dimethyl Complexes

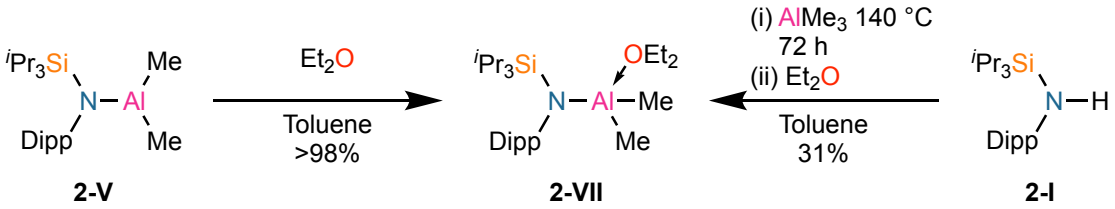

*Scheme 2.4: Two synthetic methods yielding diethyl ether coordinated aluminium dimethyl species **2-VII**.*

Following the preparations of **2-V** and **2-VI**, diethyl ether was added as a Lewis base in an attempt to coordinate to the aluminium(III) centres and aid in crystallisations (Scheme 2.4). Initial NMR-scale investigations found that the addition of excess diethyl ether to a C_6D_6 solution of **2-V** gave a single new product according to ^{1}H NMR spectroscopy (>98%). The removal of residual uncoordinated diethyl ether was further possible through co-evaporation of the mother liquor. Towards crystallisations, the reaction was repeated on a multigram scale, first isolating **2-V** as a yellow oil. Dissolution of the oil within diethyl ether, concentration and extraction afforded a precipitated yellow powder, although in poor yields (<20 %). The solid-state structure of **2-VII** was confirmed by X-ray crystallography which confirmed the formation of the diethyl ether adduct of the amido aluminium(III) dimethyl species **2-VII** (Figure 2.8).

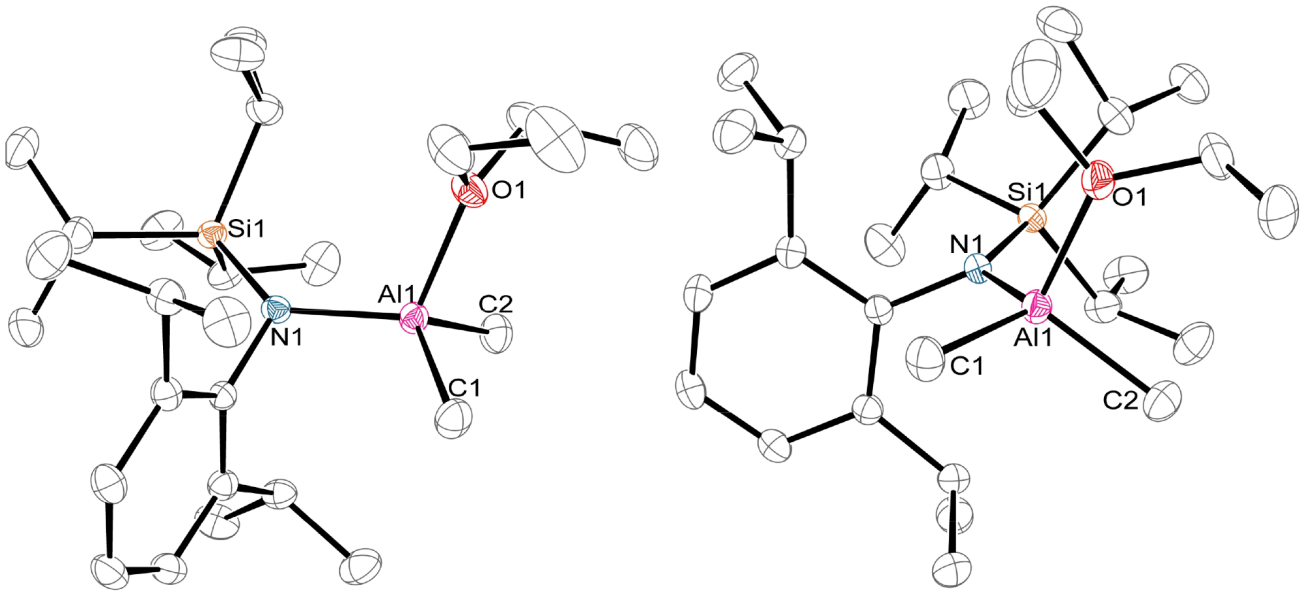

*Figure 2.8: Molecular structure of [AlMe$_2${N(Dipp)Si^{i}Pr$_3$}] **2-VII**, shown from two different orientations, as determined by X-ray crystallography. Hydrogen atoms omitted. Thermal ellipsoids set to 50% probability. Selected bond lengths (Å) and angles (°): Al1-O1 1.9539(10), Al-N1 1.8720(11), Al1-C2 1.9791(14), Al1-C1 1.9711(14), Si1-N1 1.7572(11), O1-Al1-C2 99.74(6), O1-Al1-C1 101.82(6), C1-Al1-C2 110.91(7).*

2-VII is a monomeric Lewis acid-base diethyl ether adduct in the solid-state, furnished with two terminal methyl groups and a single silyl(aryl)amido ligand at aluminium. The tetracoordinate aluminium metal centre presents a tetrahedral arrangement featuring bond angles of 110.9° (C1–Al1–C2), 101.8° (O1–Al1–C1), and 99.7° (O1–Al1–C2) being notably distorted when compared with ideal tetrahedral arrangement angles (109.5°) (Figure 2.8).

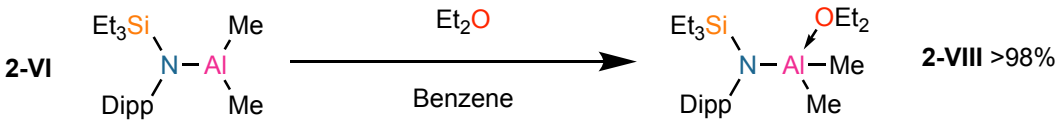

*Scheme 2.5: Synthesis of diethyl ether-coordinated aluminium dimethyl species **2-VIII**.*

Attempting to replicate the success in isolating **2-VII** as a crystalline solid, diethyl ether was added to a benzene solution of **2-VI** (Scheme 2.5). Similarly, clean conversion to the diethyl ether coordinated compound was observed by ^{1}H NMR spectroscopy to yield the target solvated species **2-VIII** (>98%). Removal of volatiles *in vacuo*, however, did not produce a solid as with **2-VII**, but instead a colourless oil. Dissolution of the oil and analysis via ^{1}H NMR spectroscopy identified the clean formation of a single product **2-VIII**, which was characterised by heteronuclear NMR spectroscopy. Even though crystallisation attempts of **2-VIII** were unsuccessful, an interesting decomposition species **2-IX** was crystallised from a saturated hexane solution of **2-VII** following 32 days at –40 °C (Figure 2.9).

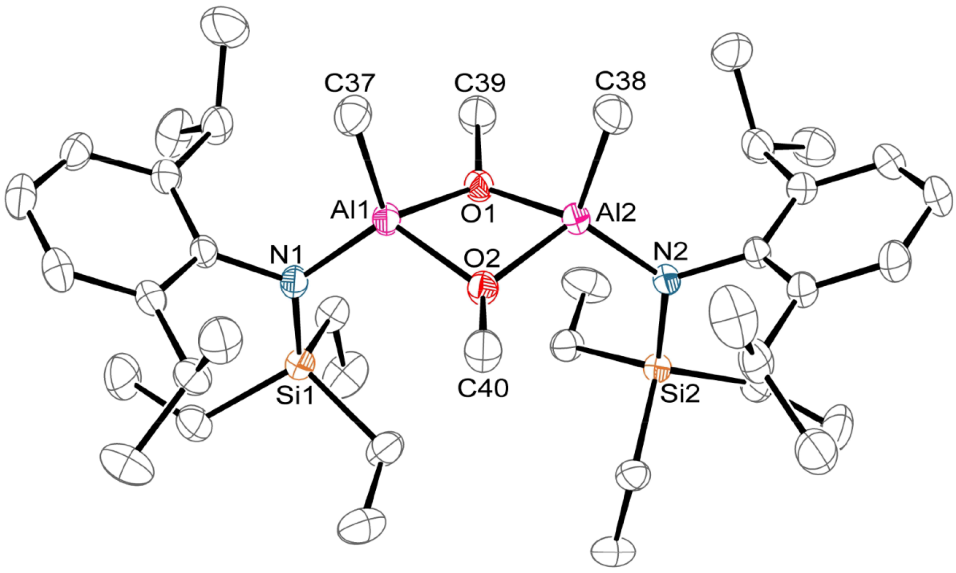

*Figure 2.9: Molecular structure of [AlMe(OMe){N(Dipp)SiEt$_3$}]$_2$ **2-IX** as determined by X-ray crystallography. Hydrogen atoms omitted. Thermal ellipsoids set to 50% probability. Selected bond lengths (Å) and angles (°): Al1···Al2 2.7875(7), Al1-O1 1.8505(12), Al1-O2 1.8472(13), Al1-N1 1.8153(15), Al2-O1 1.8528(13), Al2-O2 1.8483(12), Al2-N2 1.8179(15), Si1-N1 1.7481(15), Si2-N2 1.7485(14), Al1 O1 Al2 97.65(6), C39-O1-Al1 126.67(12), C39-O1-Al2 126.04(11), N1-Al1-C37 116.41(8), C38-Al2-N2 115.96(8).*

As identified from the solid-state structure, the decomposition product **2-IX** is a dimethoxy-bridged dimer whereby both aluminium centres feature a distorted tetrahedral configuration and feature a singular $[N(Dipp)SiEt_3]^-$ ligand and methyl group. Consequently, the presence of oxygen highlights the decomposition of the **2-VIII**, likely from advantageous oxygen given the extended crystallisation period. Unfortunately, the conditions to yield **2-IX** could not be replicated, so the single crystal X-ray diffraction data is the only characterisation data acquired on this complex (Figure 2.9).

2.4.3. Halogenation of the Amido Aluminium(III) Dimethyl Complexes

Since the end of the 20th century, aluminium methyl complexes have been utilised as a synthon for halogenated aluminium halides.[47a] Within the literature, aluminium species employing silyl(aryl)amido ligands, monoligated amido aluminium(III) dimethyl complexes $[(AlMe_2\{N(Dipp)SiR_2R'\})_2]$ (R = R′ = Me, and R = Me, R′ = ^{t}Bu) have been halogenated with a trimethyltin fluoride to yield novel amido aluminium(III) difluorides $[(AlF_2\{N(Dipp)SiR_2R'\})_2]$ (R = R′ = Me, and R = Me, R′ = ^{t}Bu).[43] Moreover, halogenation with elemental iodine afforded the isostructural amido aluminium(III) diiodides $[(AlI_2\{N(Dipp)SiMe_3\})_2]$, from which reductions yielded $[Al\{N(Dipp)SiMe_3\}]_4$ as the first exclusively *N*-based tetrameric aluminium(I) complex.[45]

Iodine is widely applied as a source of iodide ligands via halogenation, and is used in the preparation of precursors for aluminyl anions and [Al(^{Dipp}Nacnac)] **1.18**.[47a] Synthetically, the common volatile side product methyliodide may be removed *in vacuo*, and the installed Al-I bond presents the most weakly bonded aluminium-halide, aiding subsequent reductions (Table 2.1).[24] Moreover, correct stoichiometry yields a visible indicator whereby a reaction colour change from iodine deep purple/red toward colourless aligns with the consumption of I_2.

The literature presents varied reaction conditions when halogenating aluminium centres with monoanionic and dianionic ligand frameworks. In both monoanionic and dianionic ligated systems, stoichiometric I_2 (one and two equivalents, respectively) is added to the associated aluminium(III) (di)methyl species, ensuring halogenation of all Al-Me bonds is completed in one step. In yielding aluminium(III) iodide precursors with a dianionic ligand framework, monomethyl-halide exchange occurs only once upon metal centres, often requiring high temperatures (**2.2**-**2.4**).[11, 14, 16] Meanwhile, aluminium(III) species **1.18** enswathed with the monoanionic $[^{Dipp}Nacnac]^-$ frameworks yield double halogenation of two methyl groups at ambient temperatures.[47a] Most relevant to this work, in 2003, Roesky and coworkers reported that the halogenation of the trimethylsilyl analogue $[(AlMe_2\{N(Dipp)SiMe_3\})_2]$ with I_2 afforded the amido aluminium(III) diiodide following stirring overnight at ambient temperatures.[45]

To aid in the synthetic comprehension of silyl(aryl)amido aluminium(III) complexes, the preparation of analogous monoligated aluminium(III) diiodides was undertaken. After preparations, analysis assisted in identifying monoligated diiodide species generated through salt metathesis routes, and in exploring silyldiamido species incorporating aluminium centres.

2.4.3.1. Double Iodination of Amido Aluminium(III) Dimethyl Complexes

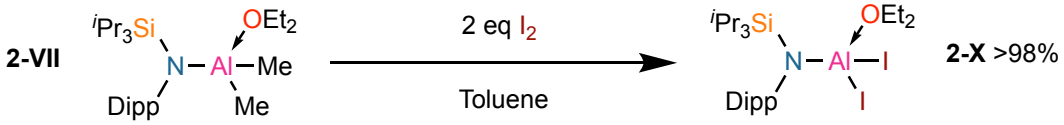

*Scheme 2.6: Synthesis of diethyl ether-solvated triisopropylsilyl(aryl)amido aluminium diiodide species **2-X**.*

Similarly applied within the less sterically bulky trimethylsilyl analogue [$AlMe_2${N(Dipp)$SiMe_3$}] by Roesky and coworkers,[45] the addition of two equivalents of I_2 to a toluene solution of **2-VII** initially gave a deep red/purple solution (Scheme 2.6). Vigorous stirring overnight yielded a pink-tinged solution. Analysis by ^{1}H NMR spectroscopy identified the clean conversion to a single targeted diiodide **2-X** product and the production of methyl iodide side-product (Supporting Information Figure S.9). Signals corresponding to Al-Me signals were notably absent. Concentration of the mother liquor and crystallisation at ambient temperature afforded **2-X** in high crystalline yields (>80%) and its the solid-state structure was confirmed by X-ray crystallography (Figure 2.10). The monoligated aluminium(III) features solvation with a single diethyl ether moiety yielding a distorted tetrahedral arrangement of coordination about the aluminium(III) centre. Consequently, a monomeric arrangement occurs in **2-X**, analogous to the previously known monoligated aluminium(III) dimethyl complex **2-VII** (Figure 2.8).

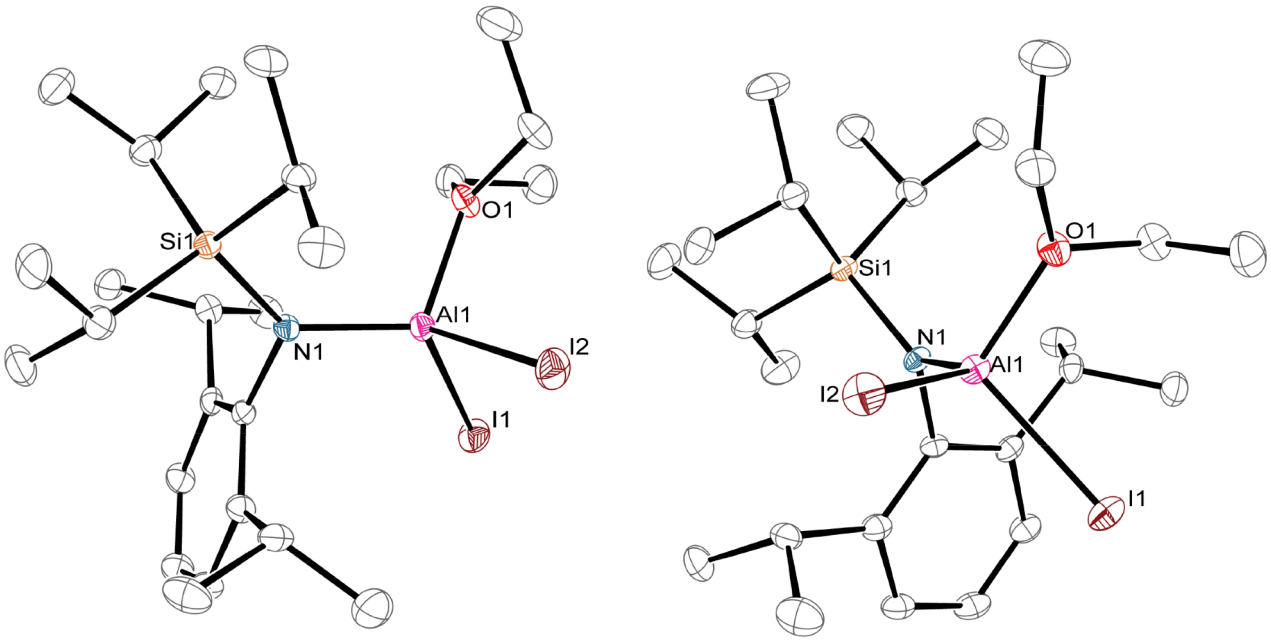

*Figure 2.10: Molecular structure of [AlI$_2$\{N(Dipp)Si^{i}Pr$_3$\}(OEt$_2$)] **2-X**, shown from two different orientations, as determined by X-ray crystallography. Hydrogen atoms omitted. Thermal ellipsoid set to 50% probability. Selected bond lengths (Å) and angles (°): Al1-O1 1.907(3), Al1-N1 1.830(3), I1-Al1 2.5465(10), I2-Al1 2.5512(10), Si1-N1 1.769(3), I1-Al1-I2 103.37(4), O1-Al1-I1 103.52(9),O1-Al1-I2 102.14(8), N1-Al1-I1 112.66(10).*

2.4.3.2. Sequential Iodination of Amido Aluminium(III) Dimethyl Complexes

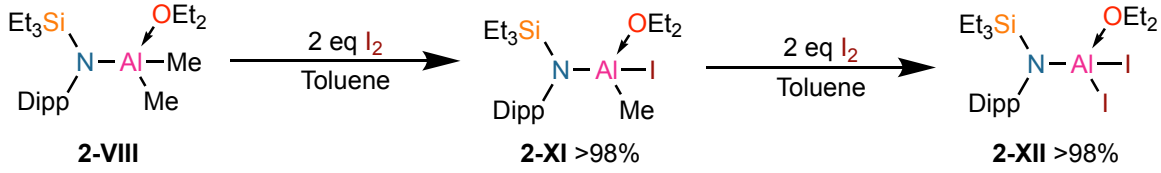

2-VIII **2-XI** >98% **2-XII** >98%

*Scheme 2.7: Stepwise halogenation yielding diethyl ether solvated iodoaluminium complexes with [N(Dipp)SiEt$_3$]$^-$ ligand framework **2-XI** and **2-XII**.*

Attempts to conduct the direct double iodination of **2-VIII** i.e. the less sterically bulky triethylsilyl analogue of **2-VII**, yielded indiscernible mixtures of products. Repeating the reaction on small (50 mg) and larger (1 g) scales identified no differences, nor the preferential formation of a single product. Further attempts toward driving a singular species were unsuccessful at elevated temperatures (>60 °C). To this end, the sequential halogenation of each methyl group was attempted (Scheme 2.7). One equivalent of I_2 was added to a toluene solution of **2-VIII**, which led to a colour change from red-purple to colourless over 10 minutes. The reaction proceeded cleanly by ^{1}H NMR spectroscopy, leading to a single mixed amido-iodo-methyl aluminium(III) **2-XI** product and one equivalent of iodomethane. **2-XI** was obtained as a colourless oil, once again preventing solid-state characterisation.

To yield the diiodide species, a further equivalent of I_2 was added to the *in-situ* prepared solution of **2-XI**. Similarly, the initial red/purple solution changed toward colourless, but occurring relatively slowly over 19 hours. ^{1}H NMR spectroscopy identified the formation of targeted diiodide **2-XII** and an additional equivalent of iodomethane. Purification of the species via removal of volatiles *in vacuo* yielded a pink-tinged oil, which was confirmed to be the pure amido aluminium diiodide complex **2-XII** via heteronuclear NMR spectroscopy. As with the other monoligated $[N(Dipp)SiEt_3]^-$ aluminium(III) complexes, isolation of **2-XII** as an oil prevented solid-state characterisation via X-ray crystallography.

2.4.3.3. Summary of Silyl(aryl)amido Aluminium(III) Complex Formation via Metalation

In summary of this sub-chapter, metalation via alkyl aluminium reagents was unsuccessful in the preparation of diligated aluminium(III) species. Instead, monoligated dimethyl complexes (**2-V**, **2-VI**, **2-VII**, **2-VIII**) were selectively yielded. Further enquiries afforded routes yielding the desired mono- and diiodide silyl(aryl)amido aluminium(III) complexes (**2-X**, **2-XI**, **2-XII**). To yield the targeted diligated aluminium(III) species, another common synthetic methodology was explored.

2.4.4. Salt Metathesis Transformations with Silyl(aryl)amido Alkali Metal Salts

Alkali metal salt metathesis is a reliable and scalable approach to prepare aluminium(III) halide precursors for aluminyl synthesis.[2-3] Commonly, lithium and potassium ligand salts are first generated by deprotonation of the proligand with a variety of alkali metal bases (e.g. butyllithium, potassium hydride, benzyl potassium). Subsequent treatment with aluminium halides serves to coordinate the ligand to the metal centre and eliminate the metal halide salt.

Within the literature, the [AlI(NON)] precursor **2.1** was prepared via reaction between the potassium salt of the ligand, K_2[NON], and aluminium iodide.[1] Subsequently, Yamashita and coworkers reported the preparation of heterocycles through metathesis of the corresponding lithium ligand salts with aluminium iodide in hexane and toluene to yield the 5- and 6-membered species, **2.5** and **2.6**, respectively.[17-18] The preparation of **2.9** by Kinjo and coworkers is conducted from the corresponding lithium ligand salt and aluminium bromide in diethyl ether.[21]

To date, minimal examples of silyl(aryl)amido ligand systems that have been coordinated to aluminium metal centres through salt metathesis routes.[49] To this end, attempts at isolating diligated silyl(aryl)amido aluminium(III) halide complexes were investigated.

2.4.4.1. Preparation of Alkali Metal Silyl(aryl)amides

The corresponding alkali metal complexes of silyl(aryl)amido ligands were prepared according to literature procedures for Li[N(Dipp)SiMe$_3$],[50] K[N(Dipp)SiMe$_3$],[51] K[N(Dipp)Si^{t}BuMe$_2$],[52] Li[N(Dipp)Si^{i}Pr$_3$],[30] and K[N(Dipp)Si^{i}Pr$_3$].[30] Investigations were also completed by manipulating the reaction mixture temperature and the solvent to enable the *in-situ* preparation of the targeted silyl(aryl)amides. These methods were then applied in the preparation of the corresponding unknown M[N(Dipp)SiEt$_3$] derivatives (M = Li **2-XIV**, K **2-XIII**).

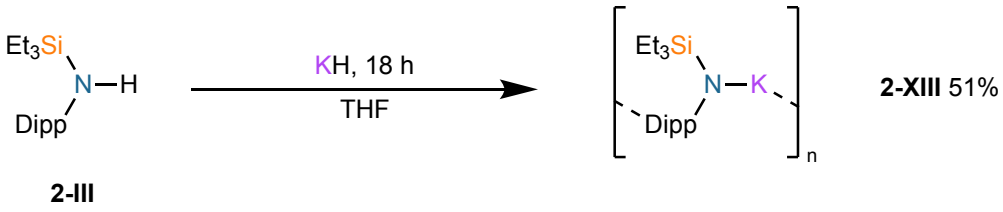

*Scheme 2.8: Synthesis of K[N(Dipp)SiEt$_3$]$_n$ alkali metal starting material **2-XIII**.*

Proligand **2-III** was deprotonated with potassium hydride by stirring over 18 h in tetrahydrofuran (Scheme 2.8). **2-XIII** was isolated as a dark grey solid in moderate yields (51%). Crystallisation was accomplished by dissolving the solid in benzene and leaving for 9 days at ambient temperature. The polymeric solid-state structure of **2-XIII** was confirmed by X-ray crystallography (Figure 2.11).

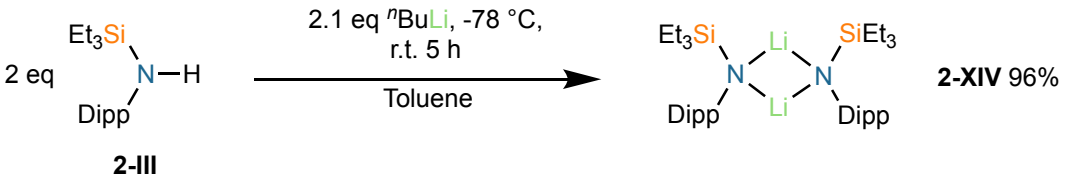

*Scheme 2.9: Synthesis of [Li{N(Dipp)SiEt$_3$}]$_2$ alkali metal starting material **2-XIV**.*

Similarly, proligand **2-III** was deprotonated with *n*-butyllithium under kinetic control at -78 °C, followed by stirring at ambient temperature for 5 hours (Scheme 2.9). Following the removal of volatiles, the targeted lithium amide **2-XIV** was isolated as a yellow powder in near quantitative yield (96%). Further validating the preparation of **2-XIV**, a saturated toluene solution left over a weekend at ambient temperature afforded crystals of **2-XIV**, and the resulting structure was identified by X-ray crystallography (Figure 2.11).

Both **2-XIII** and **2-XIV** feature deprotonated *N*-centres with a cation to balance the corresponding negative charge of the amide. The K^+ analogue **2-XIII** is observed as a one-dimensional polymer, stabilised by *N*- and arene interactions with the cation. The Dipp and SiEt$_3$ moieties are mutually positioned in alternating arrangements above and below the syndiotactic *N*-K-Dipp-*N* polymeric chain.

Conversely, **2-XIV** crystallises as a lithium-bridged dimer whereby silyl and Dipp groups are situated upon the opposing sides of the NLi_2N plane. A high degree of steric encumberment is noted down the N,N axis and the dihedral angle by which the two ligands are rotated (Figure 2.11).

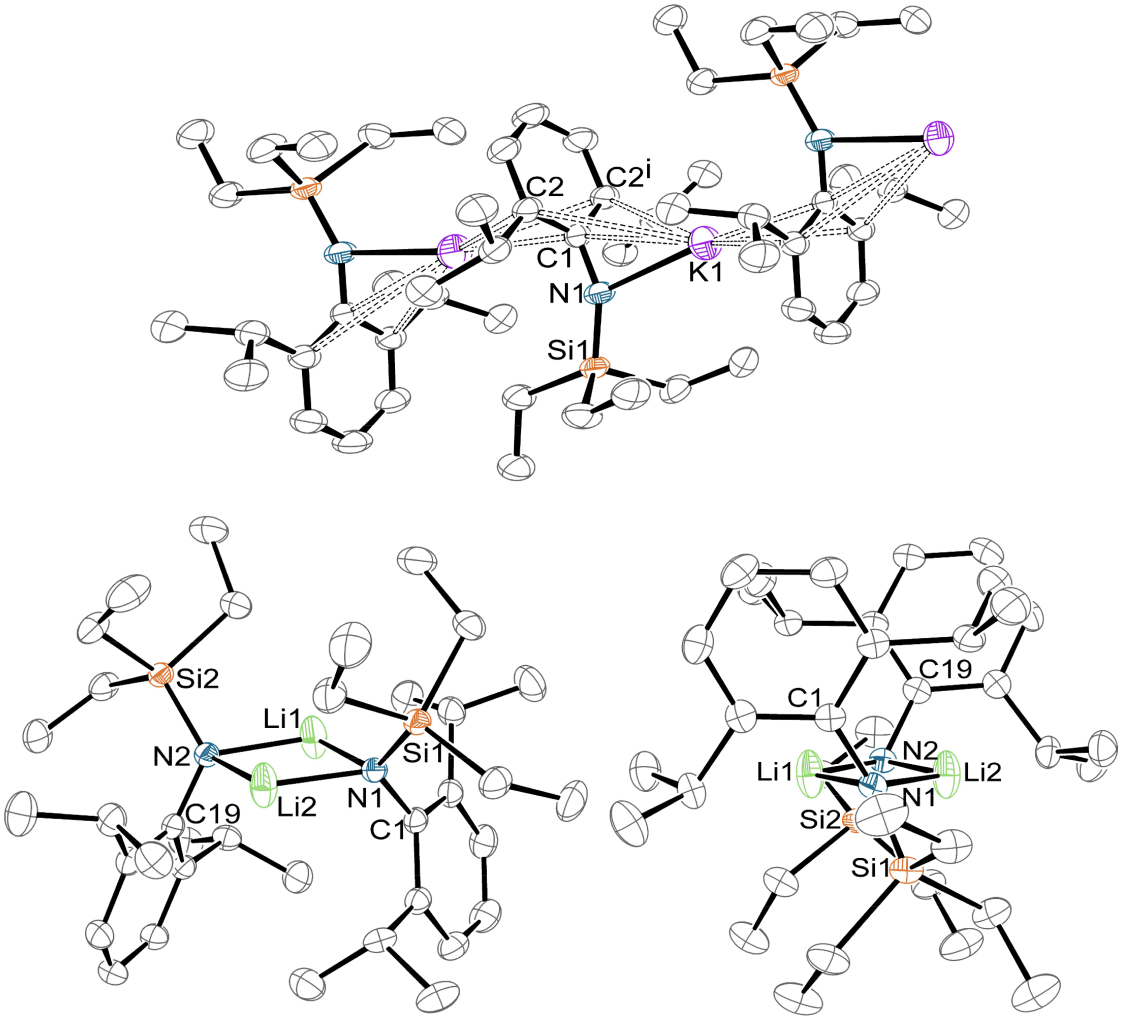

*Figure 2.11: Molecular structures of alkali metal starting materials incorporating the $[N(Dipp)SiEt_3]^-$ ligand framework as potassium **2-XIII** (top) and lithium **2-XIV** (bottom) salts, as determined by X-ray crystallography. Hydrogen atoms and solvent molecules omitted. Thermal ellipsoids set to 50% probability. **2-XIII** Selected bond lengths (Å) and angles (°): K1-N1 2.698(2), Si1-N1 1.647(2), N1-C1 1.356(3), C1-N1-K1 87.29(14), C1-N1-Si1 153.97(19), Si1-N1-K1 118.74(10). **2-XIV** Selected bond lengths (Å) and angles (°): Li1-N1 1.960(5), Li1-N2 1.979(4), Li2-N1 1.978(4), Li2-N2 1.964(4), N1-Si1 1.7112(18), N1-C1 1.422(3), N2-Si2 1.7129(17), N2-C19 1.421(3), Li2-N1-Li1 72.19(18), Li2-N2-Li1 72.06(18), Si1-N1-C1 121.50(14), Si2-N2-C19 122.05(14).*

With the alkali metal starting materials of ligands prepared and *in-situ* methodologies optimised, salt metathesis investigations with potassium and lithium reagents were undertaken.

2.4.4.2. Salt Metathesis Investigations from Potassium Silyl(aryl)amido Reagents

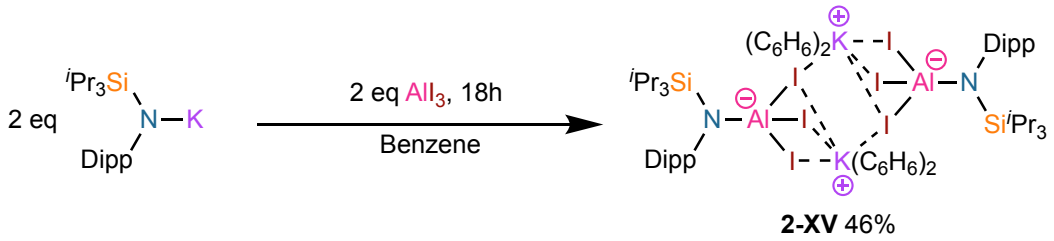

*Scheme 2.10: Attempted synthesis of diamido [AlI{N(Dipp)Si^{i}Pr$_3$}$_2$] from the potassiated ligand K[N(Dipp)Si^{i}Pr$_3$], yielding the potassium aluminate salt [K(C$_6$H$_6$)$_2${AlI$_3$(N{Dipp}Si^{i}Pr$_3$)}]$_2$ **2-XV**.*

Analogous to preparations affording the [AlI(NON)] precursor **2.1**, initial attempts pursued potassiated ligand investigations.[1] Treatment of a benzene solution of K[N(Dipp)Si^{i}Pr$_3$] with a stoichiometric amount of aluminium triiodide yielded a colourless solution, which was stirred at room temperature for 16 h, affording a white precipitate (Scheme 2.10). Extraction of the mother liquor, and analysis of an aliquot identified two unknown species in a 2.5 : 1 ratio. Further separation and concentration of the pale-yellow filtrant afforded small colourless block crystals, which could be isolated and confirmed as the observed major product via ^{1}H NMR spectroscopy in fair yield (46%) identifiable via protons in environments of Dipp-isopropyl methine (4.17 ppm), and Dipp-methyl (1.87-1.46 ppm) groups (Supporting Information Figure S.27). Further analysis of the isolated crystalline material via X-ray diffraction determined this species as a monoamido potassium aluminate salt [K(C$_6$H$_6$)$_2${AlI$_3$(N{Dipp}Si^{i}Pr$_3$)}$_2$] **2-XV** (Figure 2.12).

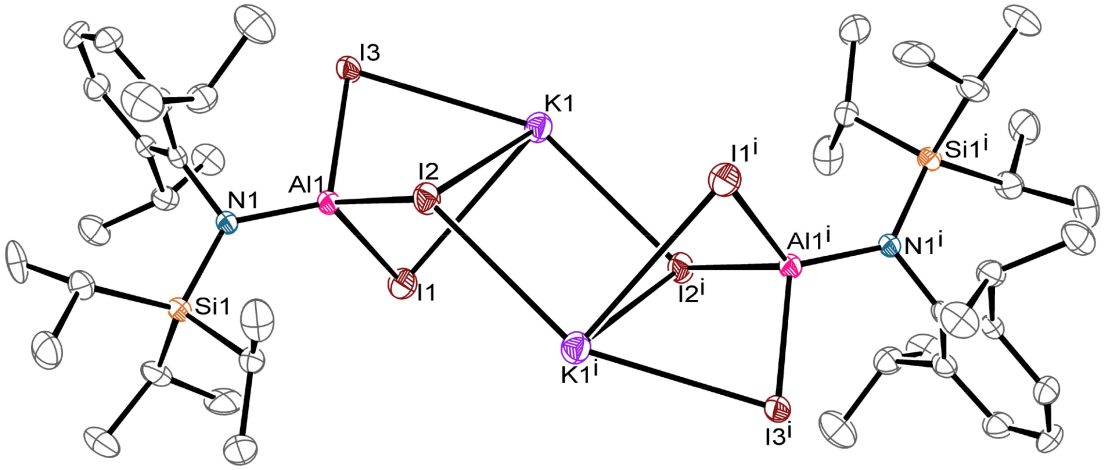

*Figure 2.12: Molecular structure of dimeric [K(C$_6$H$_6$)$_2${AlI$_3$(N{Dipp}Si^{i}Pr$_3$)}]$_2$ **2-XV** potassium aluminate salt as determined by X-ray crystallography. Hydrogen atoms and solvent molecules omitted. Thermal ellipsoids set to 50%. Selected bond lengths (Å) and angles (°): Al1-I1 2.5580(9), Al1-I2 2.6164(9), Al1-I3 2.5798(9), Al1-N1 1.819(2), K1-I1 3.7643(7), K1-I2 3.7784(8), K1-I3 3.5227(7), K1-I2^i 3.603(8), N1-Si1 1.777(2), I1-Al1-I2 100.43(3), I2-Al-I3 100.49(3), N1-Al1-I2 118.92(8).*

In the solid-state, **2-XV** exists as a potassium-bridged dimer feature potassium interactions with all three coordinated iodides. The tetracoordinate aluminium metal centre presents a distorted tetrahedral arrangement, as evidenced by bond angles of 100.4° (I1–Al1–I2) ,100.5° (I2–Al1–I3), and 118.9° (N1–Al1–I2) when compared with ideal tetrahedral arrangement angles (109.5°) (Figure 2.12).

Repeating the reaction identified that irrespective of temperature (r.t. – 80 °C), primary formation of aluminate salt **2-XV** was presented with varying ratios of proligand impurity (5 – 55%) as a potential contaminant and decomposition product. Further inquiries within varied aliphatic solvents (hexane, pentane) yielded intractable mixture of products. Worthy of note is that the addition of diethyl ether to **2-XV** lead to the elimination of potassium iodide and subsequent diethyl ether coordination, yielding the diethyl ether adduct of the monoamido aluminium(III) diiodide [AlI_2{N(Dipp)Si^{i}Pr$_3$}(OEt$_2$)] **2-X**.

Investigations with less sterically bulky silyl species were largely unsuccessful. Addition of both the triethylsilyl and trimethylsilyl potassium amides to solutions of aluminium iodide in a variety of solvents yielded a mixture of products, with the *N*-silylaniline proligands **2-III** and **2-IV** being the major product in every case.

Despite the success of potassium salt metathesis methods applied by Aldridge, Goicoechea and coworkers in the preparation of [AlI(NON)] precursor **2.1**,[1] the same was not observed with attempts to generate systems employing monodentate ligands. Despite reports of potassium salts as potentially advantageous for salt metathesis reactions due to decreased potassium iodide solubility within organic solvents,[25] this appeared to not translate nor assist in the coordination of a second ligand to the metal centre. Consequently, focus was shifted to lithium salt metathesis methodologies.

2.4.4.3. Salt Metathesis Investigations from Lithium Silyl(aryl)amido Reagents

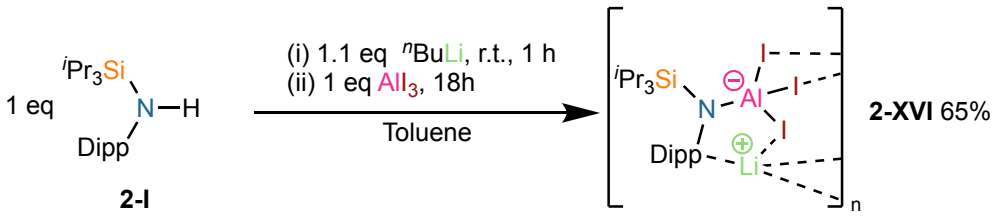

*Scheme 2.11: Attempted synthesis of diamido [AlI{N(Dipp)Si^{i}Pr$_3$}$_2$] from in-situ prepared Li[N(Dipp)Si^{i}Pr$_3$] and AlI$_3$, instead yielding lithium aluminate salt Li[AlI$_3${N(Dipp)Si^{i}Pr$_3$}]$_n$ **2-XVI**.*

Lithium salt metathesis routes serve as viable methodologies as previously applied by Yamashita and coworkers for the preparation of the aluminium(III) iodide precursors **2.5** and **2.6**.[17-18] Notably, in the synthetic ease associated with the *in-situ* preparation of lithiated silyl(aryl)amido stating materials promoted this synthetic approach. Therefore, efforts toward the preparation of diamido

aluminium(III) iodide precursors were initially explored with the $[N(Dipp)SiR_3]^-$ ligand system in non-polar solvents (benzene, toluene, hexane).

At ambient temperature, aluminium iodide was charged into solutions of $Li[N(Dipp)Si^iPr_3]$ (Scheme 2.11). Analysis of the reaction mixtures via ^1H NMR spectroscopy determined the presence of the proligand **2-I** and two new inequivalent $[N(Dipp)Si^iPr_3]^-$ containing species in a ratio of 1.7 : 1. Comparison of spectra with those from potassium salt metathesis inquiries identified the same minor product generated via both lithium and potassium salt metathesis routes. It was hypothesised that this species could be the target diligated aluminium(III) iodide species. Crystallisation attempts from saturated hexane solutions afforded colourless plate-like crystals, which were confirmed by X-ray diffractometry to be the incidental lithium aluminate salt $Li[AlI_3\{N(Dipp)Si^iPr_3\}]_n$ **2-XVI** (Figure 2.13). Within the solid-state, the lithium aluminate also presented a distorted tetrahedral aluminium centre incorporating angles of 117.5° (N1-Al1-I2) and 100.8° (I1-Al1-I3). Differing from potassium aluminate dimer **2-XV**, the lithium species was observed as a 1-dimensional coordination polymer with lithium-arene interactions and bridging the greater system through interactions with the corresponding iodide ligands.

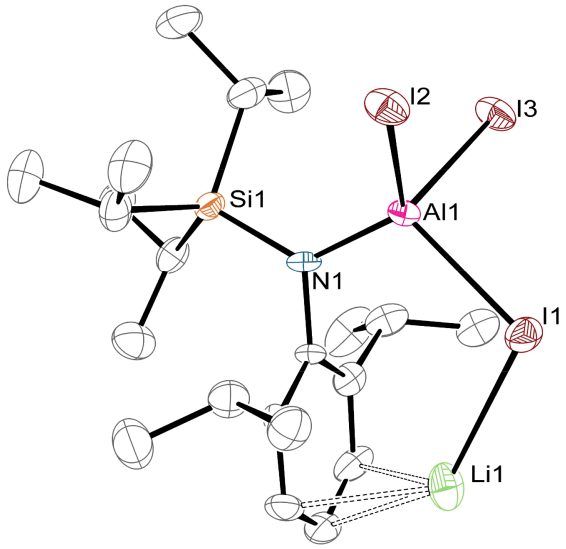

*Figure 2.13: Molecular structure of $Li[AlI_3\{N(Dipp)Si^iPr_3\}]_n$ **2-XVI** as determined by X-ray crystallography. Hydrogen atoms omitted. Thermal ellipsoids set to 50%. Selected bond lengths (Å) and angles (°): Al1-I1 2.587(3), Al1-I2 2.574(3), Al1-I3 2.580(3), Al1-N1 1.842(8), Li1···I1 2.79(2), Ni1-Si1 1.769(8), N1-Al1-I2 117.5(3), I1-Al1-I3 100.81(9).*

Isolation and analysis of **2-XVI** by ^1H NMR spectroscopy confirmed it as the identified major species identifiable via protons in environments of Dipp-isopropyl methine (3.82 ppm), and Dipp-methyl (1.51-1.25 ppm) groups (Supporting Information Figure S.29). As with the analogous chemistry involving potassium amides, the isolation of the aluminate salt species prompted inquiries

as to the role of temperature toward the thermodynamically-promoted target product formation. Upon increase from ambient to 40 °C and 60 °C, the amount of minor product (hypothesised to be the diamido aluminium iodide) grew in comparison to aluminate major species. Such findings supported postulations that an increase of temperature could inverse the distribution of products, yielding the preferential formation of the unknown minor product.

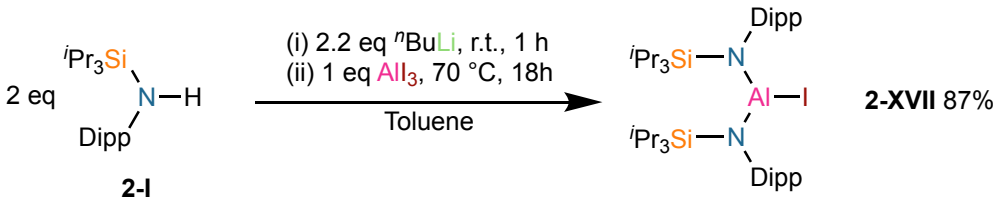

*Scheme 2.12: Synthesis of the diamido aluminium(III) iodide complex [AlI{N(Dipp)Si^{i}Pr$_3$}$_2$] **2-XVII** from in-situ prepared Li[N(Dipp)Si^{i}Pr$_3$] and aluminium triiodide in toluene at elevated temperatures.*

The addition of aluminium triiodide to *in-situ* prepared Li[N(Si^{i}Pr$_3$)Dipp] in toluene, and heating to 65 °C overnight yielded a burnt-orange solution containing a colourless precipitate. Extraction via cannula filtration and concentration gave colourless crystals of **2-XVII** at -30 °C. Repeating this reaction at 70 °C, and crystallisation afforded crystals of nearly 6-millimetre square in high yields (87%), which were used in characterisation via multinuclear NMR spectroscopy and single crystal X-ray diffraction, confirming the identity of targeted [AlI{N(Dipp)Si^{i}Pr$_3$}$_2$] **2-XVII** (Figure 2.14).

^{1}H NMR spectroscopy performed on a pure sample of isolated **2-XVII** confirmed it to be the minor product in the initial reactions performed at ambient and at the moderately-elevated temperatures of 40 °C and 60 °C). Of note, the signal corresponding to the four isopropyl methine protons upon the Dipp moiety, traditionally featuring a refined septet splitting pattern, appeared as a broad, stepped resonance at 3.72 ppm. This was attributed to the steric crowding within the molecule and slight inequivalence of environments, causing the resultant signal to be broad rather than well-resolved septets identified for less sterically crowded Li[N(Si^{i}Pr$_3$)Dipp] and proligand **2-I** species. This was also reinforced through half of the protons of Dipp-methyl environments appearing as a broad signal 0.91 ppm, and the other a traditional doublet at 1.28 ppm (Supporting Information Figure S.30).

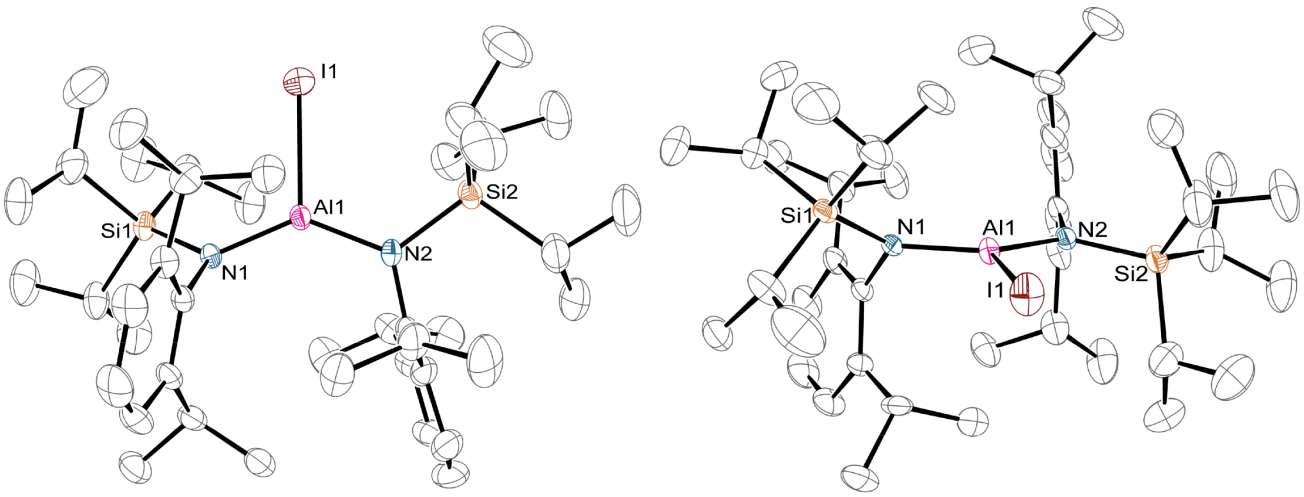

*Figure 2.14: Molecular structure of [AlI{N(Dipp)Si^{i}Pr$_3$}$_2$] **2-XVII**, shown from two different orientations, as determined by X-ray crystallography. Hydrogen atoms omitted. Thermal ellipsoids set to 50% probability. Selected bond lengths (Å) and angles (°): Al1-I1 2.5506(13), Al1-N1 1.820(3), Al1-N2 1.825(4), N1-Si1 1.792(3), N2-Si2 1.811(4), N1-Al1-I1 112.68(12), N1-Al1-N2 135.01(17).*

Evident from the solid-state structure of **2-XVII**, this aluminium(III) complex features a terminal iodide and two bulky monodentate [N(Dipp)Si^{i}Pr$_3$]$^-$ ligands. The planar 3-coordinate metal centre featured significant distortion from an ideal trigonal planar geometry, identifiable from the N–Al–N bond angle of 135° (*cf.* 120° for non-distorted trigonal planar).[5] Furthermore, the N–Al–N angle being closer to linear than trigonal planar highlights more significant *s* character in these bonding orbitals. The steric crowding around the aluminium centre hinders ligand rotation about the Al–N bonds, with one ligand rotated such that the Dipp moiety is slightly above the plane, and the Dipp moiety of the other ligand is below the plane at >30°. The aluminium-iodide bond length of 2.5506(13) Å is longer than all other diamido aluminium(III) iodide precursor complexes [AlI(NON)] (2.497(1) Å),[1] [AlI(SiN^{Dipp})] (2.4690(5) Å),[16] and [AlI(^{Si}NON)] (2.4539(8) Å).[11] This strain highlights the increased steric encumberment around the aluminium metal centre, which was hoped to assist in kinetically stabilising the targeted acyclic aluminyl anion following reductions.

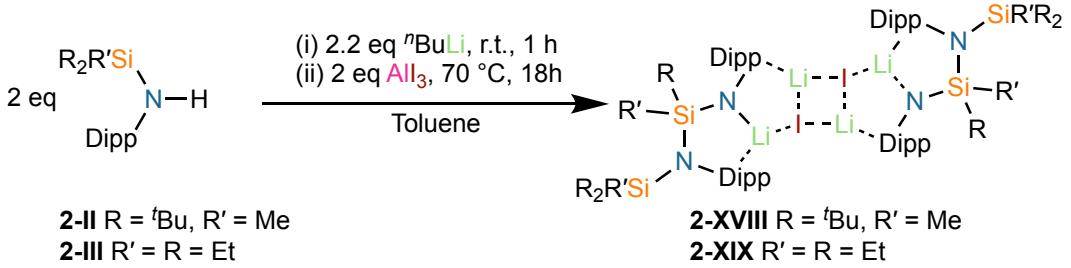

*Scheme 2.13: Attempted synthesis of the diamido [AlI{N(Dipp)SiR₂R′}₂] complexes from in-situ prepared lithiated amides Li[N(Dipp)SiR₂R′], instead yielding incidental lithium iodide salts **2-XVIII** and **2-XIX**.*

Following success in isolating the target diamido aluminium(III) precursor **2-XVII**, a variety of less sterically bulky substrates were examined for the preparation of an aluminyl precursor library. Subsequently, initial attempts were replicated through the reaction between 2 equivalents of Li[N(Dipp)SiR₂R′] (R = Me, R′ = ^{t}Bu; R, R′ = Et) with aluminium iodide in toluene at 65 °C for 18 h (Scheme 2.13). However, contrary to the formation of diamido precursor complex **2-XVII**, the corresponding less bulky aluminium(III) iodide precursors could not be isolated via this route, nor was any evidence of their formation identified by ^{1}H NMR spectroscopy. Rather, spectroscopic evidence was consistent with the formation of multiple silyl(aryl)amido-containing products. Crystallisation attempts were undertaken within non-polar solvents, affording single crystals of one of the species, in addition to a significant proportion of microcrystalline material and amorphous precipitate. Following X-ray crystallographic analysis, it was possible to determine the incidental formation of the substituted products **2-XVIII** and **2-XIX** (Figure 2.15). Attempts to identify the other reaction products were carried out but were unsuccessful despite changes in reaction temperature and solvent variations.

The solid-state structures of **2-XVIII** and **2-XIX** appear to result from a nucleophilic substitution reaction at a silyl group of the amide, with the nucleophile being a second equivalent of the amide substituting either a methyl (**2-XVIII**) or ethyl (**2-XIX**) group. Within the wider dimeric structure, two inequivalent lithium environments are identified, one associated with the deprotonated N^- centre of the amide, and another as a lithium iodide salt supporting bridging interactions with a Dipp group and two iodides. **2-XIX** was notable given the role of the ethyl as a leaving group, previously hoped to be a barrier to the formation being more sterically encumbered than that of the smaller methyl group in **2-XVIII**. The presence of iodide in structures **2-XVIII** and **2-XIX** highlighted the required involvement of aluminium iodide in formation.

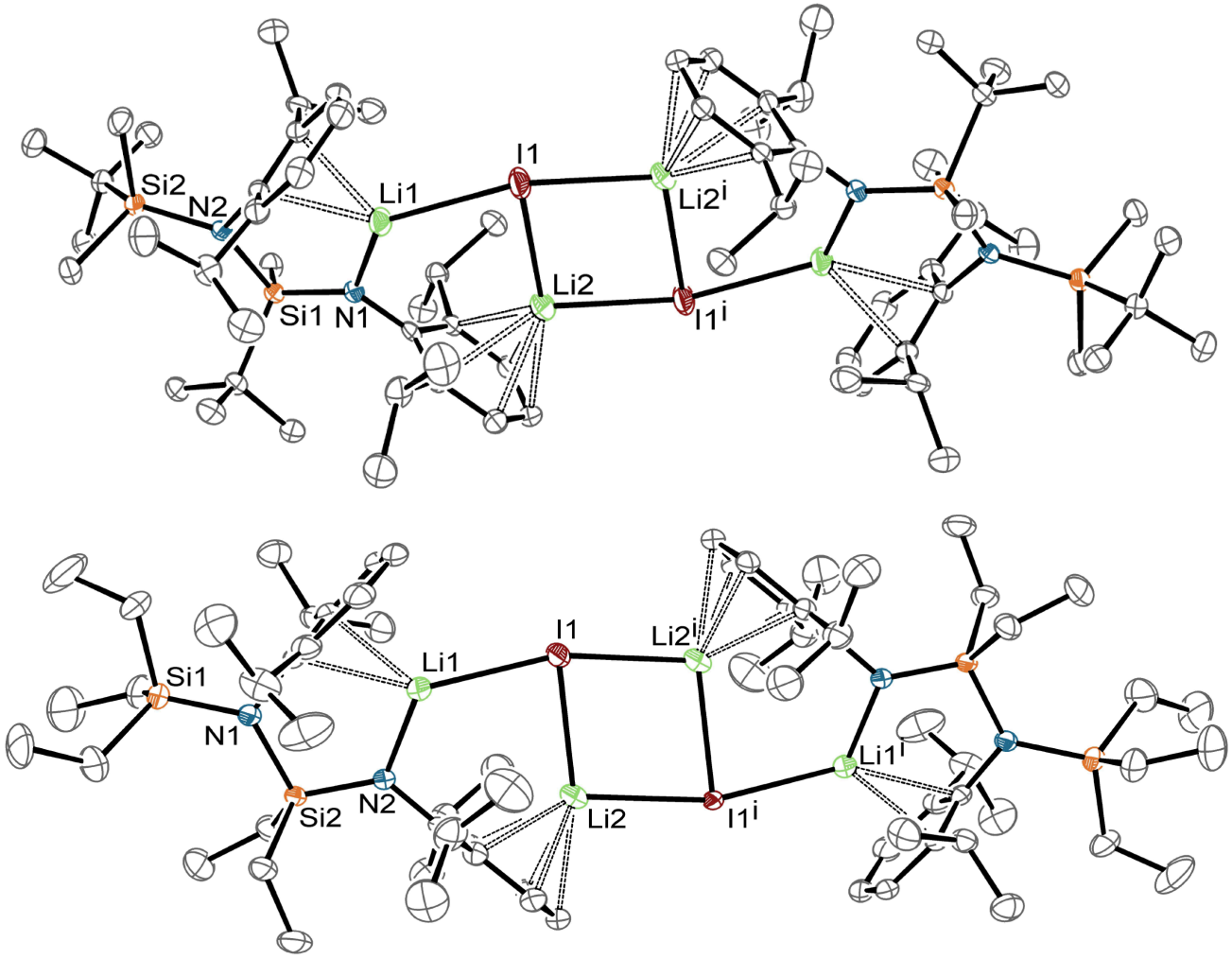

*Figure 2.15: Molecular structures of [Li$_4${Dipp(^{t}BuMe$_2$Si)NSi^{t}Bu(Me)NDipp}$_2$I$_2$] **2-XVIII** and [Li$_4${Dipp(Et$_3$Si)NSiEt$_2$NDipp}$_2$I$_2$] **2-XIX** as determined by X-ray crystallography. Hydrogen atoms and solvent molecules omitted. Thermal ellipsoids set to 50% probability. **2-XVIII** Selected bond lengths (Å) and angles (°): I1-Li1 2.760(5), I1-Li2 2.731(5), N1-Si1 1.702(2), N2-Si1 1.808(2), N2-Si2 1.781(2), N1 -Si1-N2 107.09(10), Si2-N2-Si1 132.14(13), Si1-N1-Li1 121.45(19). **2-XIX** Selected bond lengths (Å) and angles (°): I1-Li1 2.805(9), I1-Li2 2.718(9), Li2-N1 1.925(9), N1-Si1 1.694(4), N1-C1 1.390(6), N2-Si1 1.790(4), N2-Si2 1.761(4), Li1-I1-Li2 83.3(3), Li2-N1-C1 113.2(4), C1-N1-Si1 126.8(3), N1-Si1-N2 107.36(18), C2-N2-Si2 117.3(3)*

To investigate the requirement of aluminium triiodide the formation of the **2-XVIII** and **2-XIX**, toluene solutions solely containing the corresponding lithium amides Li[N(Dipp)SiEt$_3$] and Li[N(Dipp)Si^{t}BuMe$_2$] were heated at 65 °C for 66 h. Utilising ^{1}H NMR spectroscopy to monitor the reaction, no reaction progress was observed after this time. Thereafter, the solutions were heated to reflux for 18 h, however the starting materials remained unchanged or exhibited slight decomposition to their corresponding *N*-silylaniline proligands.

The role of the elevated temperature was also probed in the formation of the **2-XVIII** and **2-XIX**. In replications of the reactions between the lithium amides Li[N(Dipp)SiEt$_3$] and

Li[N(Dipp)Si^{t}BuMe$_2$] and aluminium triiodide at ambient temperature, both systems presented evidence of **2-XVIII** and **2-XIX** formation but requiring 36 and 48 h, respectively. The increased and differing time requirements were attributed to the varied steric hinderance from reactions with ethyl substituents as opposed to the smaller methyl groups.

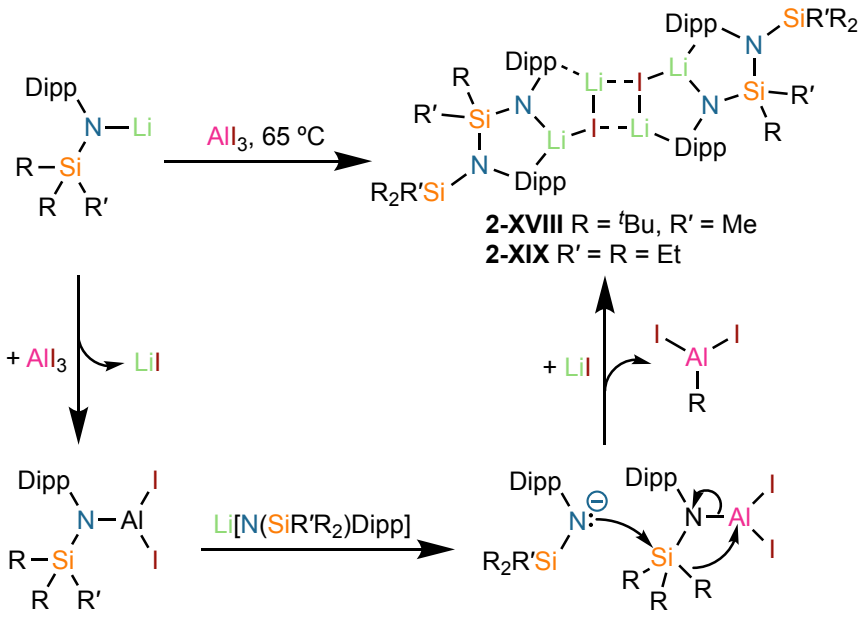

*Scheme 2.14: Postulated mechanism affording species **2-XVIII** and **2-XIX**.*

From the above mentioned synthetic investigations, a mechanism for the formation of **2-XVIII** and **2-XIX** can be postulated (Scheme 2.14). Evident by the iodide in the structures and no reactions occurring without aluminium triiodide being present, the mechanism was dependent upon aluminium iodide. Consequently, it is hypothesised that a monoamido complex, possibly the lithium aluminate equivalent of the previously observed **2-XVI** $[LiAlI_3\{N(Dipp)SiR_2R'\}]_n$ is generated as an intermediate. To this, a molecule of the lithium amide $[N(Dipp)SiR_2R']^-$ acts as a nucleophile upon the silyl group of the coordinated ligand and promotes a nucleophilic substitution reaction causing the corresponding methyl (**2-XVIII**), or ethyl (**2-XIX**) group to leave. These small and strongly nucleophilic alkyl anions then attack the aluminium centre and consequently eliminate the associated $[AlI_2Me]$ or $[AlEtI_2]$ species, yielding the isolated products **2-XVIII** and **2-XIX**.

In supporting the postulated mechanism (Scheme 2.14), ^{1}H NMR spectroscopy was sought in identifying the generation of the organoaluminium diiodide species. In reactions generating **2-XVIII**, the by-product $[AlMeI_2]$ was postulated from an upfield singlet (–0.27 ppm), within the region common for alkyl aluminium species. Moreover, in generating **2-XIX**, ^{1}H NMR spectroscopy

identified the formation of the [$AlEtI_2$] by-product via a quartet (–0.20 ppm) and triplet (0.22 ppm) of the aluminium coordinated –CH_2– and –CH_3 groups respectively.

Due to the isolation of **2-XVIII** and **2-XIX**, it was clear that for the preparation of diamido aluminium(III) iodide species via this salt metathesis pathways, more sterically demanding silyl groups were needed to prevent the silicon-centred nucleophilic substitution. This sentiment was echoed in investigations with the smallest analogue trimethylsilyl, whereby unidentified product mixtures were generated through lithium salt metathesis reactions. In all cases, irrespective of temperature or solvent (benzene, toluene, tetrahydrofuran), the major species dominating formation was that of the proligand **2-IV**.

Whilst salt metathesis had been effective in the preparation of the highly sterically encumbered disilyl(aryl)amido aluminium(III) iodide complex [$AlI\{N(Dipp)Si^iPr_3\}_2$] **2-XVII**, the reduction of steric hindrance around the silicon centre saw the formation of multiple side products, including proligand and those resulting from nucleophilic substitution at the silicon centre. Consequently, other methods sought in the preparation of less sterically bulky silyl(aryl)amido stabilised aluminium(III) iodide precursors.

2.4.5. Contemporary Li[AlH_4] Metalations

Through a collaboration with Dr. David Liptrot and Ross Jackson from the University of Bath, an alternate, less common contemporary metalation method was explored. Inspired by the route employed by Heine and Stalke,[12] the application of the lithium aluminium hydride as an aluminium source was investigated.

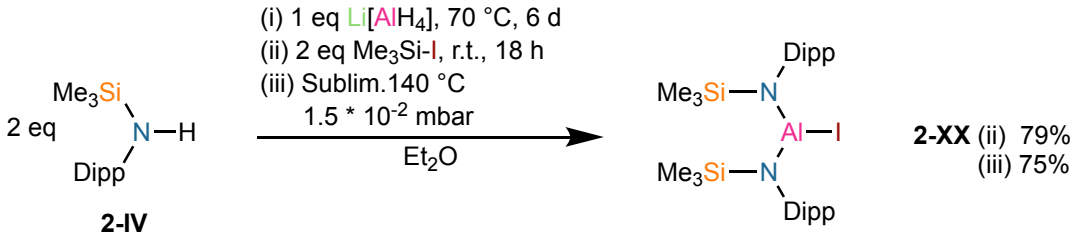

*Scheme 2.15: Synthesis of diligated [$AlI\{N(Dipp)SiMe_3\}_2$] **2-XX**.*

A diethyl ether solution with two equivalents of the smallest alkylsilyl *N*-silylaniline [$HN(Dipp)SiMe_3$] **2-IV** was superheated with lithium aluminium hydride in diethyl ether for six days. Treatment of the resultant colourless solution with stoichiometric trimethylsilyl iodide and subsequent sublimation furnished the targeted diamido aluminium iodide **2-XX** in good yields (79% and 75%).

The solid-state structure of [AlI{N(Dipp)SiMe$_3$}$_2$] **2-XX** was confirmed by X-ray crystallography from colourless crystals grown from a -30 °C saturated pentane solution (Figure 2.8).

Analogous to the triisopropylsilyl **2-XVII** species, **2-XX** featured a trigonal planar aluminium centre with two monodentate [N(Dipp)SiMe$_3$]$^-$ ligands and a single terminal iodide. Corresponding to the slight decrease in steric encumberment, the distorted trigonal arrangement featured a wide N–Al–N bond angle of 131°, but slightly narrower than in **2-XVII** (135°). Similar ligand rotation about the Al–N bond again was identified, however, to a decreased degree than the bulkier **2-XVII**., the Al–I bond length of 2.5085(9) Å was greater than that of all previously reported aluminium(III) iodide precursors, but was slightly less than that of the bulkier analogous triisopropylsilyl **2-XVII** species 2.5506(13) Å.

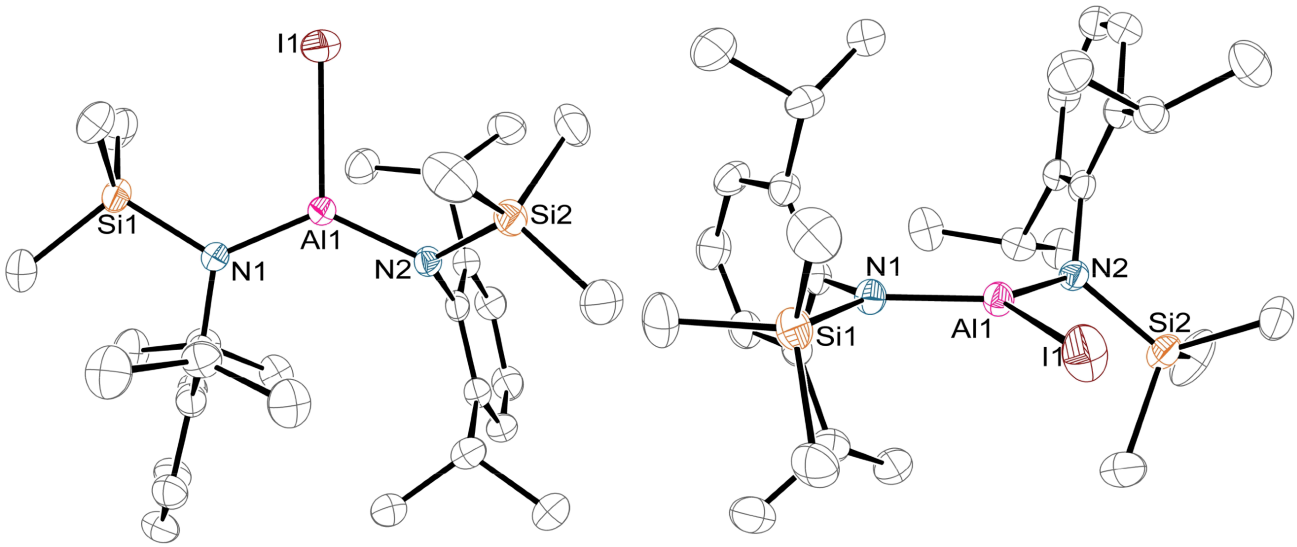

*Figure 2.16: Molecular structure of [AlI{N(Dipp)SiMe$_3$}$_2$] **2-XX**, shown from two different orientations, as determined by X-ray crystallography. Hydrogen atoms omitted. Thermal ellipsoids set to 50%. Selected bond lengths (Å) and angles (°): Al1-I1 2.5085(9), Al1-N1 1.785(3), Al1-N2 1.800(3), N1-Si1 1.776(3), N2-Si2 1.757(3), N1-Al1-I1 112.86(9), N1-Al1-N2 131.35(12).*

The slight reduction in the steric encumberment was further notable via ^{1}H NMR spectroscopy. The isopropyl methine protons of Dipp groups were identified as a traditional septet splitting pattern at 3.54 ppm, as opposed to the broad stepped resonance observed for **2-XVII** at 3.72 ppm (Supporting Information Figure S.30). Further variation was identifiable in protons in the Dipp-methyl (1.20 and 0.91 ppm) environments both appearing in a doublet splitting pattern (Supporting Information Figure S.33).

Unlike other previously reported aluminium(III) iodides for aluminyl anion synthesis, the rotation afforded by the unsupported Al–N bond saw the location of aryl groups “behind” the terminal Al–I bond. This is in contrast to all other species (**2.1-2.4**, **2.6-2.8**, **2.10**) that feature aryl groups traditionally

pointing in the direction of the Al–I bond. Consequently, the location of the trimethylsilyl moieties is reminiscent of **2.5**, as reported by Yamashita and coworkers (Figure 2.2).[17] As such the flexibility presented by the acyclic coordination motif, could present differing reactivity and isolation of previously unobserved species from aluminyl anions.[2-3]

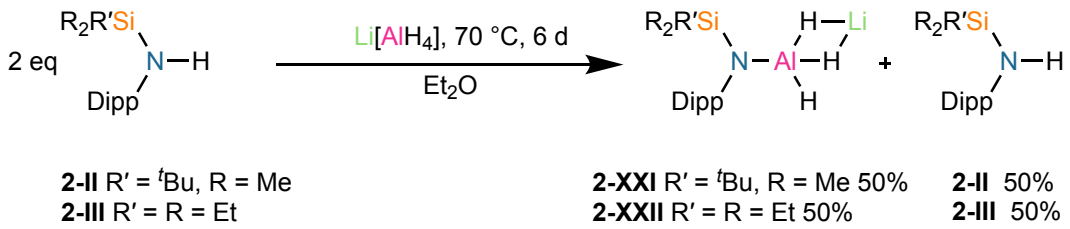

*Scheme 2.16: Attempted synthesis of diamido [AlI{N(Dipp)SiR$_2$R'}$_2$] via lithium aluminium hydride metalation routes, yielding postulated monoligated complexes **2-XXI** and **2-XXII**.*

Inspired by the success with the least bulky trimethylsilyl **2-IV**, reactions between Li[AlH$_4$] and the larger amines **2-II** and **2-III** were undertaken. Diethyl ether solutions of *N*-silylanilines **2-II** and **2-III** were treated with lithium aluminium hydride and superheated to 70 °C for six days (Scheme 2.16). Preparation of an aliquot and analysis of the reaction solutions via ^{1}H NMR spectroscopy observed the formation of a monoamido aluminium species **2-XXI** and **2-XXII** and corresponding unreacted of *N*-silylanilines **2-II** and **2-III**, respectively. Despite attempts, crystals of SCXRD quality could not be prepared for the hypothesised monoamido aluminium species **2-XXI** and **2-XXII**. Similarly observed in previously explored metalation pathways, the high degree of steric encumbrance about the aluminium(III) centres appeared a further challenge in the coordination of a second ligand.

2.4.5.1. Summary of Acyclic Aluminium(III) Iodide Precursor Preparations

Following investigations of the reaction of *N*-silylanline proligands with organoaluminium bases, reproducible and reliable synthetic methods were identified via lithium salt metathesis and metalation with lithium aluminium hydride. Despite challenges with moderately bulky *N*-silylanilines **2-II** and **2-III**, findings assisted in directing further investigations and purification techniques. Acyclic aluminium(III) iodide precursors **2-XVII** and **2-XX** were isolated as pure and crystalline compounds serving as potential starting materials for reduction investigations towards the first acyclic aluminyl anion (**Chapter 3**). Following synthetic successes in the preparation of two acyclic aluminium(III) iodide precursors **2-XVII** and **2-XX**, inquiries shifted toward developing an isoelectronic four-membered aluminium(III) metallocycle precursor.

2.5. A Four-Membered Aluminium(III) Halide Precursor: Results and Discussion

2.5.1. Synthesis of a Bulky Bidentate Silyldiamine Proligand

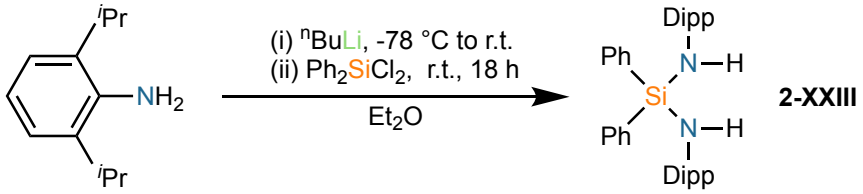

*Scheme 2.17: Synthesis of the bulky silyldiamine proligand [(DippNH)$_2$SiPh$_2$] **2-XXIII** (H$_2$DAS).*

Highlighted within literature, the silyldiamido ligand class provides kinetic stabilisation to a variety of species, including low coordinate, low oxidation state main group compounds **2.21**-**2.25** featuring germanium and tin centres (Figure 2.5).[38-39] The corresponding bulky silyldiamine proligand [H$_2$(NDipp)$_2$SiPh$_2$] **2-XXIII** (H$_2$DAS) was prepared through a one-pot synthesis on a multigram scales at greater than 95% yields.[53] Isolated in high purity as a crystalline solid, **2-XXIII** was advantageous in its ease of use compared to the *N*-silylaniline **2-I**–**2-IV** proligand oils.

Like the monodentate amido donors, once deprotonated, **2-XXIII** features hard *N*-coordination centres with bulky Dipp substituents. Both *N*-centres are bridged by a bulky diphenylsilyl linker. When deprotonated or coordinated within a metal complex, the bidentate [DAS]$^{2-}$ ligand is dianionic and chelating, reminiscent of nearly all reported cyclic aluminium(III) iodide precursors.

Emulating investigations with the acyclic aluminium(III) iodide precursors, focus was centred on the development of reliable and efficient synthetic routes. Previously highlighted, varied investigations incorporating metalation via organoaluminium and lithium aluminium hydride with successive halogenation, and alkali metal salt metathesis were explored and the results discussed herein.

2.5.2. Trimethylaluminium Metalations of Bidentate Silyldiamine Proligand

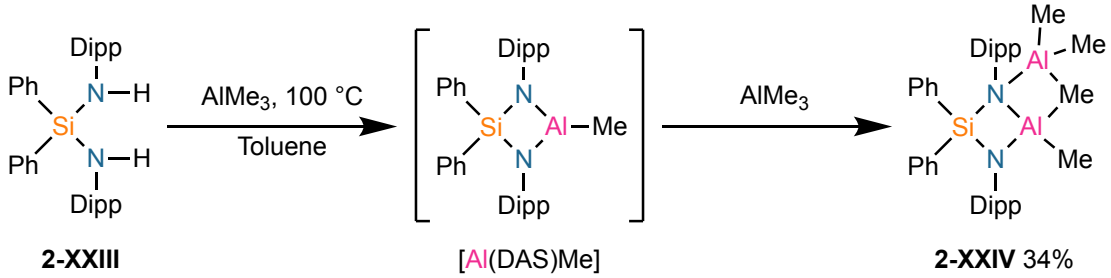

*Scheme 2.18: Attempted synthesis of the targeted monomethylated aluminium complex from corresponding silyldiamine proligand, yielding incidental trimethylaluminium adduct species **2-XXIV**.*

A toluene solution of H$_2$[DAS] **2-XXIII** was treated with trimethylaluminium and heated to 100 °C for 48 h (Scheme 2.18). After the initial 24 h, analysis of the mother liquor identified a mixture of monomethylated [Al(DAS)Me] with unreacted proligand and trimethylaluminium. After 48 h, the

targeted monomethylated species was identified as the majority (>80%). Consequently, attempts to isolate the targeted [Al(DAS)Me] were undertaken from a variety of non-coordinating solvents (toluene, benzene, hexane, pentane). Extractions yielded a colourless powder in low yields (34%), which was identified via ^{1}H NMR spectroscopy to feature very broad signals and different integrations to that of identified [Al(DAS)Me] intermediate (Supporting Information Figure S.35). This was attributed to fluxionality within the solution being hindered at lower temperatures, with VT analysis identifying sharp signals at 75 °C. However, recrystallisation of the white solid from benzene afforded the confirmation of trimethylaluminium adduct species [Al_2(DAS)Me_4] **2-XXIV** (Figure 2.17).

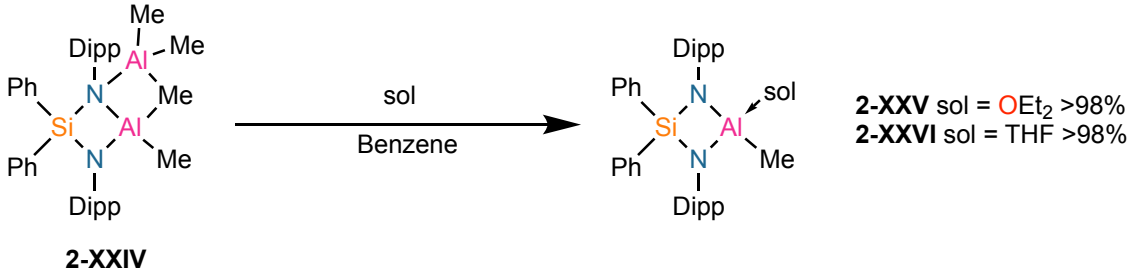

*Scheme 2.19: Treatment of adduct species **2-XXIV** with coordinating solvents to displace the coordinated trimethylaluminium and yield corresponding solvated aluminium methyl complexes **2-XXV** and **2-XXVI**.*

Due to ^{1}H NMR spectroscopic evidence yielding differing spectra when crystallised as opposed to when prepared *in-situ*, it was hypothesised the process of crystallisation was dependent upon adduct formation. Despite attempts, isolation of the targeted tricoordinate aluminium [Al(DAS)Me] species was not possible. Therefore, to displace the coordinated trimethylaluminium adduct and afford synthetically preferably four-coordinate species for crystallisations, coordinating solvents were introduced (Scheme 2.19). Adding diethyl ether and tetrahydrofuran to **2-XXIV**, ^{1}H NMR spectroscopy identified the clean formation of a single product, leading to the displacement of the trimethylaluminium, yielding solvated species. In both cases, reactions were undertaken on small (<40 mg) scales, as reactions on a larger scale or when attempted via *in situ* routes without the isolation of adduct species **2-XXIV** would afford an intractable mixture of products. From these small-scale reactions, concentration of the reaction mixtures yielded the corresponding solvated aluminium(III) methyl species of diethyl ether **2-XXV**, and tetrahydrofuran **2-XXVI** in quantitative yields (Figure 2.17).

Highlighted by their solid-state structures, all three species (**2-XXIV**, **2-XXV**, **2-XXVI**) feature 4-coordinate aluminium centres (Figure 2.17). In all examples, the 4-membered heterocycle is serves a horizontal plate, featuring steric bulk above and below its plane. All species contain one Dipp group as perpendicular to the Al–Me units; however, the other Dipp group deviates above and backward of

the cyclic plane corresponding to the encumbrance of the corresponding adduct. The deviation is most prevalent in the trimethylaluminium adduct **2-XXIV**, further identifiable in the greater Al–N bond length and narrower N–Al–N bond angle forcing *N*,*N*-coordinated Al1 centre out of the ligand pocket (Table 2.2). Within this species, the trimethylaluminium adduct interacts with the central complex through one *N*-coordination atom and a bridging methyl group with the empty *p*-orbital of the ligated aluminium centre. This was analogous to previously reported ethyl,[41c] and phenyl bridged adduct species,[41b] formed from the corresponding silyldiamine ligands and aluminium bases.

In solvated products **2-XXV** and **2-XXVI**, the central aluminium p-orbital is occupied via electron donation from the oxygen of the coordinating solvent moiety. Both **2-XXV** and **2-XXVI** are noticeably similar in bond lengths and angles, with slight deviations present from the varied greater and less steric bulk of coordinated diethyl ether and tetrahydrofuran substituents, respectively (Table 2.2).

Notably, removing all volatiles prior to crystallisation would yield an intractable mixture of products. To this end, the solvated species **2-XXV** and **2-XXVI** were preferential for further investigations.

Having prepared three different aluminium methyl species incorporating the $[DAS]^{2-}$ ligand framework, these species were hoped to serve as viable synthons for halogenation, yielding the corresponding iodide species.

Table 2.2: Selected bond lengths (Å) and angles (°) of aluminium methyl silyldiamido adduct species $[Al_2(DAS)Me_4]$ ***2-XXIV****, $[Al(DAS)Me(OEt_2)]$* ***2-XXV****, and [Al(DAS)Me(THF)]* ***2-XXVI****:*

Atoms	*2-XXIV*	*2-XXV*	*2-XXVI*
Al1-C37	1.940(5)	1.9474(12)	1.9492(14)
Al1-O1	-	1.9298(10)	1.9150(11)
Al1···Si1	2.6368(17)	2.5483(6)	2.5531(6)
Al1-N1,N2	2.000(3), 1.828(4)	1.8364(10), 1.8357(10)	1.8429(10), 1.8322(11)
Si1-N1,N2	1.808(3), 1.722(3)	1.7356(10), 1.7344(10)	1.7346(10), 1.7372(10)
N1-Al1-N2	83.74(15)	85.67(4)	85.59(4)
N1-Si1-N1	92.89(16)	92.03(4)	91.97(4)
O1-Al1-C37	-	99.53(5)	99.60(6)
S1···Al1-C37	152.34(16)	151.50(4)	149.85(5)

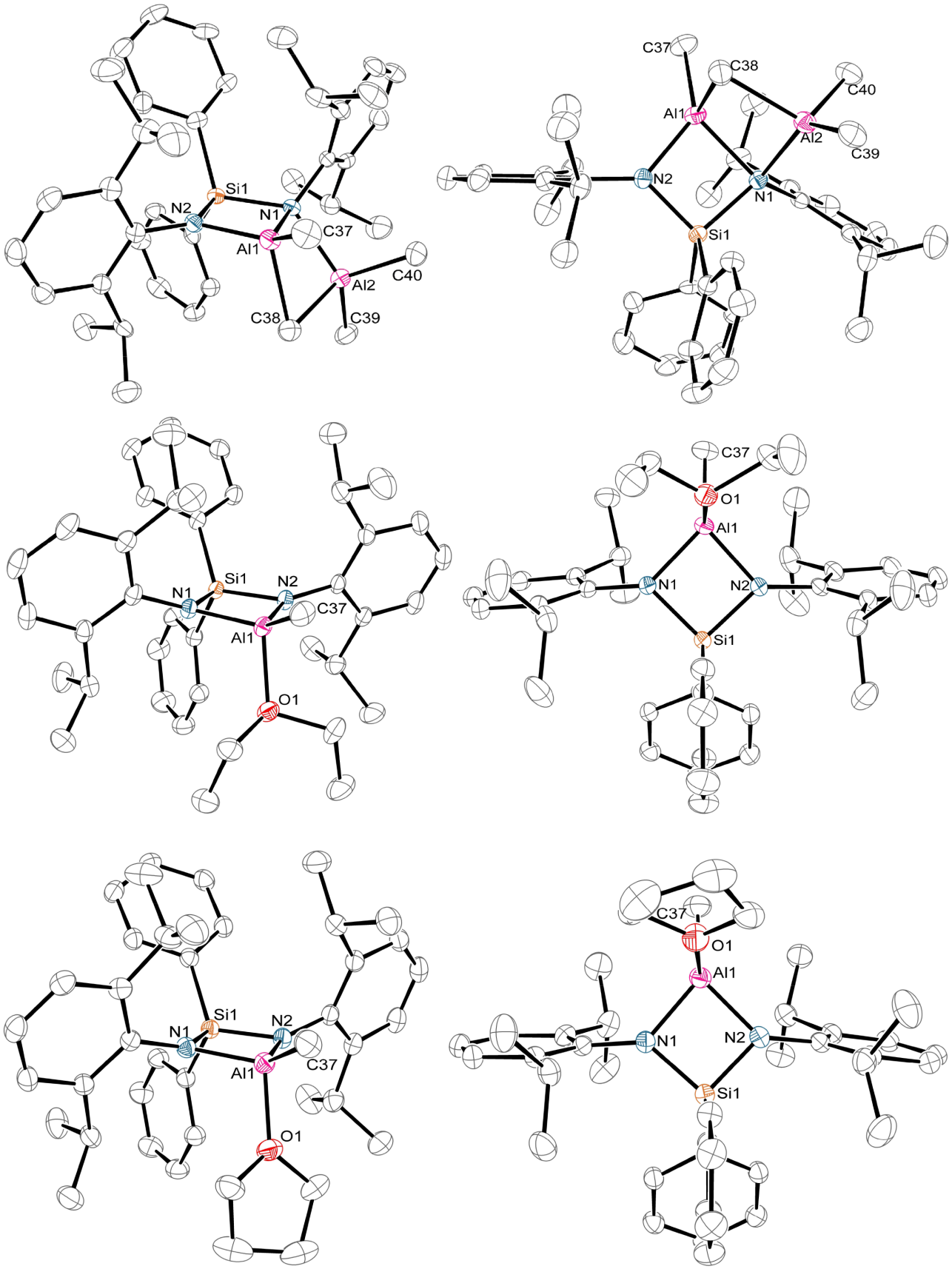

*Figure 2.17: Molecular structure of [Al_2(DAS)Me_4] **2-XXIV** (top), [Al(DAS)Me(OEt_2)] **2-XXV** (middle), and [Al(DAS)Me(THF)] **2-XXVI** (bottom), shown from two different orientations, as determined by X-ray crystallography. H atoms omitted. Thermal ellipsoids set to 50% probability.*

2.5.3. Iodination of Aluminium Methyl Silyldiamido Complexes

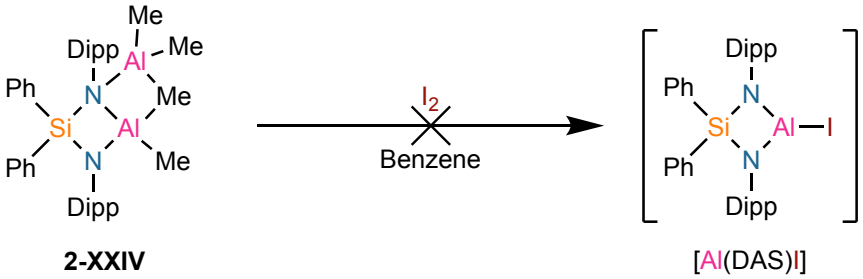

2-XXIV [Al(DAS)I]

*Scheme 2.20: Attempted treatment of trimethylaluminium adduct species **2-XXIV** with elemental iodine.*

Inspired by applied halogenation methods in the preparation of viable aluminyl anion precursors (*vide supra* **section 2.1.3.2**),[11, 14, 16] iodine was introduced to the isolated aluminium methyl **2-XXIV** toward preparing target [Al(DAS)I] (Scheme 2.20). The addition of iodine to both isolated and *in-situ* prepared solutions of **2-XXIV** and intermediate [Al(DAS)Me] gave a mixture of products. From this mixture, the expected by-product of methyl iodide could be identified via ^{1}H NMR spectroscopy from a singlet at 1.42 ppm. Moreover, multiple previously unidentified $[DAS]^{2-}$ containing species were present. Attempts toward isolating any species yielded a further intractable mixture of species, including proligand **2-XXIII**.

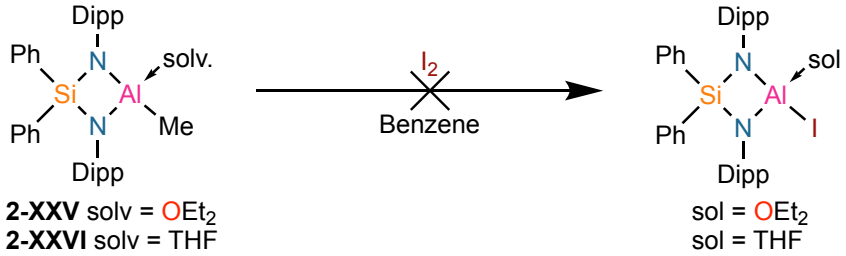

2-XXV solv = OEt_2
2-XXVI solv = THF

sol = OEt_2
sol = THF

*Scheme 2.21: Treatment of solvated aluminium methyl complexes **2-XXV** and **2-XXVI** with elemental iodine.*

Applying similar methodologies to the solvated species [Al(DAS)Me(sol)] **2-XXV** (sol = Et_2O) and **2-XXVI** (sol = THF), the corresponding benzene solutions were treated with iodine (Scheme 2.21). Methyl iodide was identified from ^{1}H NMR spectroscopy, however, as in investigations with the trimethylaluminium adduct species, these reactions yielded many species. Within the ^{1}H NMR spectrum, small signals relating to the target iodide complexes were identified [Al(DAS)I], which would be later confirmed through contemporary metalations routes and solvent coordination to [Al(DAS)I]. However, the majority of the isolated material was identified as decomposition products consisting primarily of the proligand **2-XXIII** and diisopropylaniline ($DippNH_2$).

Despite the challenges presented in the preparation of targeted aluminium(III) iodide complexes (Scheme 2.21), successes included the development of reproducible and reliable methodologies to

afford aluminium complexes featuring a silyldiamido ligand. Toward further progression in the preparation of target aluminium(III) iodide precursors, other synthetic methodologies were investigated.

2.5.4. Contemporary Li[AlH$_4$] Metalations

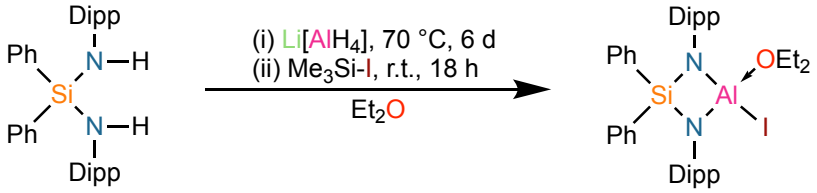

2-XXIII **2-XXVII** 81%

*Scheme 2.22: Preparation of diethyl ether solvated silyldiamido aluminium iodide **2-XXVII** from lithium aluminium hydride and the proligand **2-XXIII**.*

Following successes in the preparation of the acyclic aluminium(III) iodide precursor **2-XX**, a diethyl ether solution with two equivalents of silyldiamine **2-IV** and one equivalent of lithium aluminium hydride was superheated at 70 °C for 6 days. Treatment of the resultant colourless solution with stoichiometric trimethylsilyl iodide afforded the diethyl ether coordinated silyldiamido aluminium iodide **2-XXVII** in good yields (81%). Analysis of ^{1}H NMR spectrum identified signals previously observed as a minor product (5%) generated through halogenations of methyl species **2-XXV**. This was identified through protons in environments of Dipp-isopropyl methine (4.02 ppm), and Dipp-methyl (1.11-1.01 ppm) groups, and coordinated diethyl ether molecule (3.52 and 0.69 ppm) (Supporting Information Figure S.37). Confirming the preparation of aluminium halide species, single crystals suitable for SCXRD could be isolated from saturated diethyl ether solution and identified as **2-XXVII** (Figure 2.18).

From the solid-state structure, the four-coordinate aluminium centre in **2-XXVII** is constrained within the silyldiamido ligand framework. Similar to the solvated methyl systems **2-XXV** and **2-XXVI**, the terminal iodide and diethyl ether ligands in **2-XXVII** are located above and below the plane of the 4-membered heterocycle. The Al–I (2.5082(11) Å) bond length is identical (within error) to the corresponding Al–I bonds formed within the acyclic trimethylsilyl **2-XX** (2.5085(9) Å), and triisopropylsilyl **2-XVII** (2.5506(13) Å). However, the Al–O bond length (1.895(3) Å) is shorter when compared in the methyl analogue **2-XXV** (1.9298(10) Å). Both Dipp groups are identified to deviate from trigonal planar arrangements at the nitrogen centre with minor twisting toward the silyl backbone, and away from the substituents about the aluminium centre.

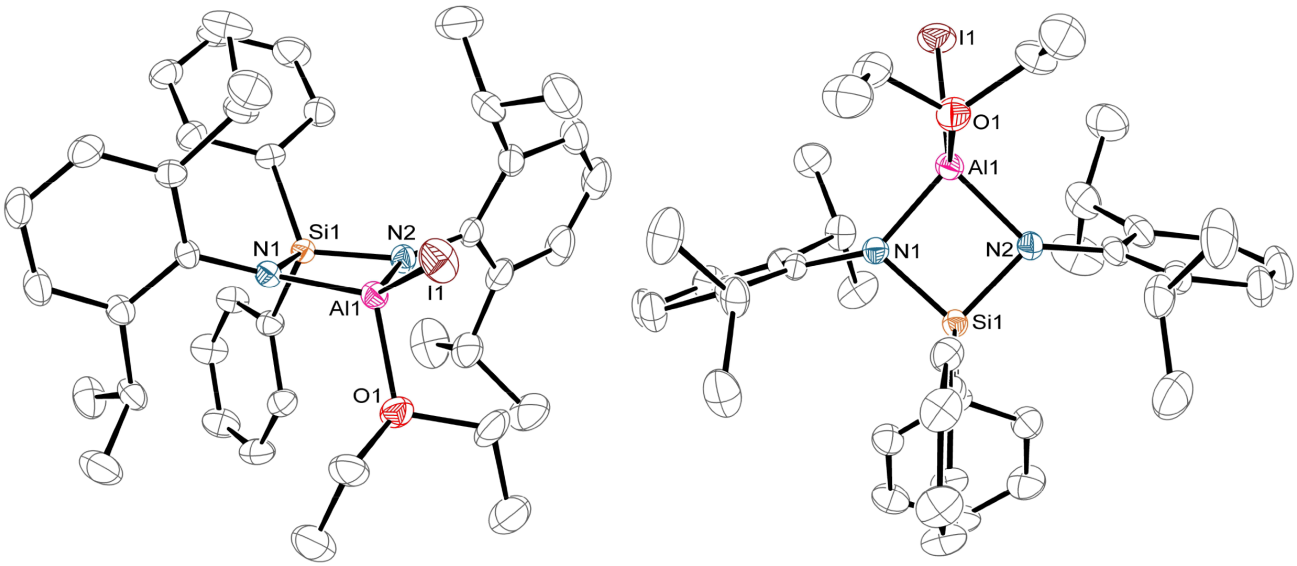

Figure 2.18: Molecular structure of [Al(DAS)I(OEt₂)] ***2-XXVII****, shown from two different orientations, as determined by X-ray crystallography. Hydrogen atoms omitted. Thermal ellipsoids set to 50%. Selected bond lengths (Å) and angles (°): Al1-I1 2.5082(11), Al1-O1 1.895(3), Al1-N1 1.819(3), Al1-N2 1.833(3), Si1-N1 1.746(3), Si1-N2 1.747(3), N1-Al1-N2 86.66(14), N1-Si1-N2 91.64(14), Si1···Al1-I1 143.38, O1-Al1-I1 97.10(10).*

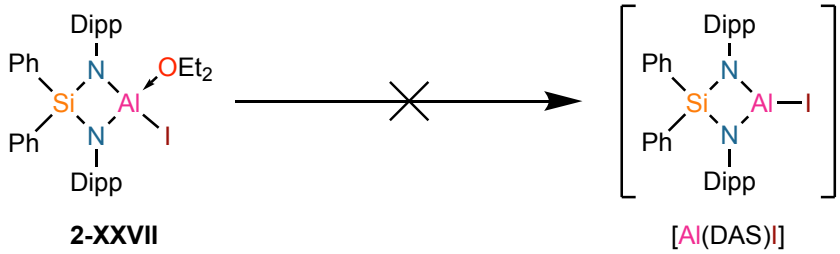

Scheme 2.23: Attempted removal of coordinated diethyl ether solvent via sublimation and extended reduced pressure toward the preparation of [Al(DAS)I].

In attempts to prepare the tricoordinate aluminium complex [Al(DAS)I], efforts were undertaken to remove the coordinated diethyl ether from **2-XXVII** (Scheme 2.23). As highlighted from the development of analogous aluminyl anion species, tri-coordinate neutral aluminium(III) halide precursors were preferential in the formation of low valent species.[2-3, 7] Extended periods of decreased pressure under a dynamic vacuum were unsuccessful in removing the coordinated solvent molecule from **2-XXVII**. Moreover, inspired by the purification of the acyclic precursor **2-XX**, sublimation was also attempted with **2-XXVII**. Conducted at various scales (50 mg, 250 mg, 500 mg), sublimations under dynamic vacuum (1.5×10^{-2} mbar) and varied temperatures (80 °C, 100 °C, 180 °C) all yielded yellow oils. These were identified to be mixtures of decomposition products via ^{1}H NMR

spectroscopy. Nevertheless, focus continued toward the preparation of tricoordinate [Al(DAS)I] through salt metathesis methods.

2.5.5. Salt Metathesis involving Silyldiamido Alkali Metal Salts

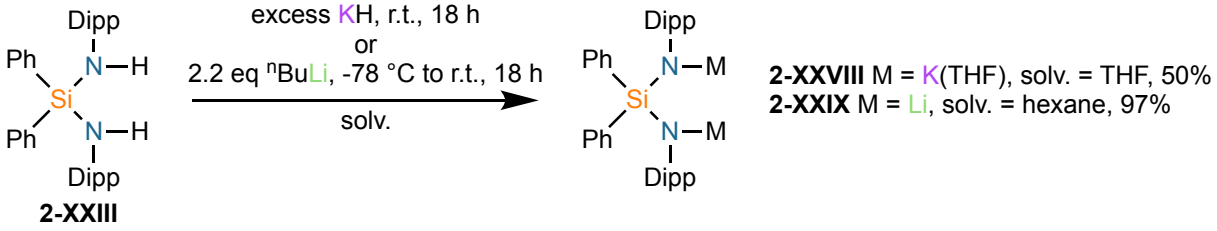

Scheme 2.24: Optimised procedures for the preparation of DAS ligand alkali metal salts.

Fundamental in undertaking salt metathesis procedural routes, the corresponding alkali metal ligand salts were prepared according to literature procedures for **2-XXVIII**,[54] and optimised procedures for **2-XXIX** (Scheme 2.24).[55] The already highly yielding literature procedure (87%) was improved to yield the isolation of analytically pure **2-XXIX** in near-to-quantitative amounts (97%) (Scheme 2.24). Moreover, as identified from the literature and the Cambridge Crystallographic Data Centre (CCDC), the solid-state structure of **2-XXIX** was previously unreported, therefore X-ray diffraction on SCXRD quality crystals of **2-XXIX** obtained from saturated hexane solutions was performed (Figure 2.19). Throughout the optimisation process of synthesising the lithium ligand salt, an unexpected species was also isolated. When the preparation of **2-XXIX** was undertaken in hexane at ambient temperatures, the target species was yielded. However, a by-product in minimal yield (15%), the thrice deprotonated species **2-XXX** could be isolated as pure crystalline material, and its identity was confirmed via NMR spectroscopy and X-ray diffractometry (Figure 2.19).

From the solid-state structure, **2-XXIX** and **2-XXX** were identified to crystallise as lithium-bridged dimers featuring 4 and 6 lithium atoms, respectively. In **2-XXIX**, the two ligand scaffolds are stacked with each coordination pocket facing in opposing directions; supporting this dimer, one lithium is situated within the *N,N*-coordination pocket, and the other interacts with an *N*-centre and corresponding Dipp groups of two ligands. A similar motif is observed in the thrice deprotonated system, with an additional lithium interacting with the deprotonated *ortho*-C32 centre of the backbone phenyl group. Resultant of a slight excess of butyl lithium, the *ortho*-positioned proton of the silyl backbone is identified as the next most acidic following the deprotonation of amines (N-H) (Figure 2.19).[56]

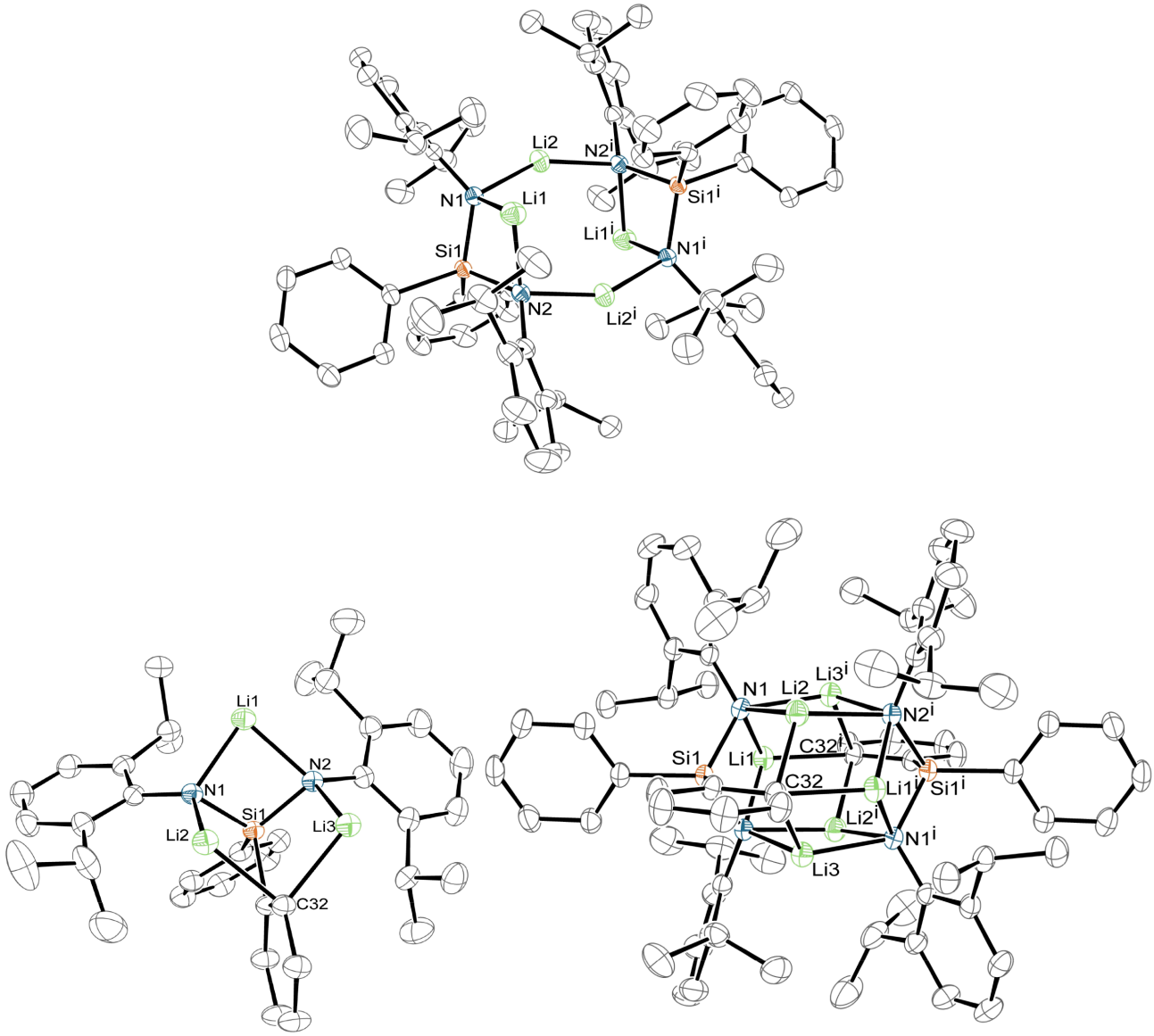

*Figure 2.19: Molecular structure of [Li_4{DAS}$_2$] **2-XXIX** (top) and [Li_6{(NDipp)$_2$SiPh(C_6H_4)}$_2$] **2-XXX** (bottom as both asymmetric unit and dimer) as determined by X-ray crystallography. H atoms omitted. Thermal ellipsoids set to 50% probability. **2-XXIX** Selected bond lengths (Å) and angles (°):N1-Li1 1.977(2), N1-Li2 1.981(2), N2-Li1 1.986(2), N2-Li2 1.972(2), Si1-N1 1.7228(9), Si1-N2 1.7258(10), N1-Si1-N2 99.86(4), N1-Li1-N2 83.50(9), N2-Li2-N1 147.94(12). **2-XXX** Selected bond lengths (Å) and angles (°): N1-Li1 2.063(2), N1-Li2 2.093(3), N1-Li3 2.121(3), N2-Li1 2.083(3), N2-Li2 2.162(3), N2-Li3 2.118(3), C32-Li1 2.181(3), C32-Li2 2.139(3), C32-Li3 2.224(3), Si1-N1 1.7570(11), Si1-N2 1.7461(11), N2-Si1-N1 103.32(5).*

Given the highly reactive and basic nature of aluminyl anions, the relative acidity of the ligands system was valuable in understanding the sites of potential reactivity within the proposed ligand framework. Fortunately, **2-XXX** could be easily separated from the preferential dilithium ligand salt **2-XXIX**, ensuring it is not a hindrance in salt metathesis investigations.

2.5.5.1. Salt Metathesis Investigations from Potassium Silyldiamido Reagents

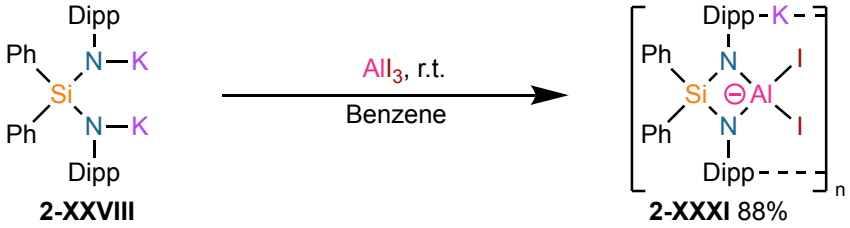

*Scheme 2.25: Synthesis of the potassium diiodide aluminate salt **2-XXXI** via salt metathesis.*

Emulating synthetic routes employed by Aldridge, Goicoechea and coworkers in the preparation of the aluminium(III) iodide precursor **2.1** (Figure 2.1),[1] aromatic hydrocarbon solutions of **2-XXVIII** were treated with stoichiometric aluminium triiodide (Scheme 2.25). At ambient temperatures, reactions afforded two previously unidentified products identified via ^{1}H NMR spectroscopy. From the orange-yellow solutions, the major of the two species was identified as the potassium diiodide aluminate salt **2-XXXI**, which was confirmed via X-ray diffraction and NMR spectroscopy (Figure 2.20).

Identified from the X-ray structure, the aluminium centre in **2-XXXI** is contained within the 4-membered DAS scaffold and features four monoanionic coordinated substituents. Consequently, the imparted negative charge of the complex is balanced by the +1 charged potassium cation. Again, as an aluminate salt **2-XXXI** features an aluminium centre with a distorted tetrahedral arrangement, however, this is greatly impacted by the steric restriction imparted by the 4-membered metallocycle. Notably, this species crystalises as a one-dimensional coordination polymer supported by η^6-arene interactions with the Dipp groups. This resulted in an alternating arrangement of aluminium iodide bond direction. Moreover, the previously identified motif of Dipp group bending is attributed to the potassium bridging interactions rather than steric encumberment around the aluminium centre, as previously within solvated and adduct species (Figure 2.20).

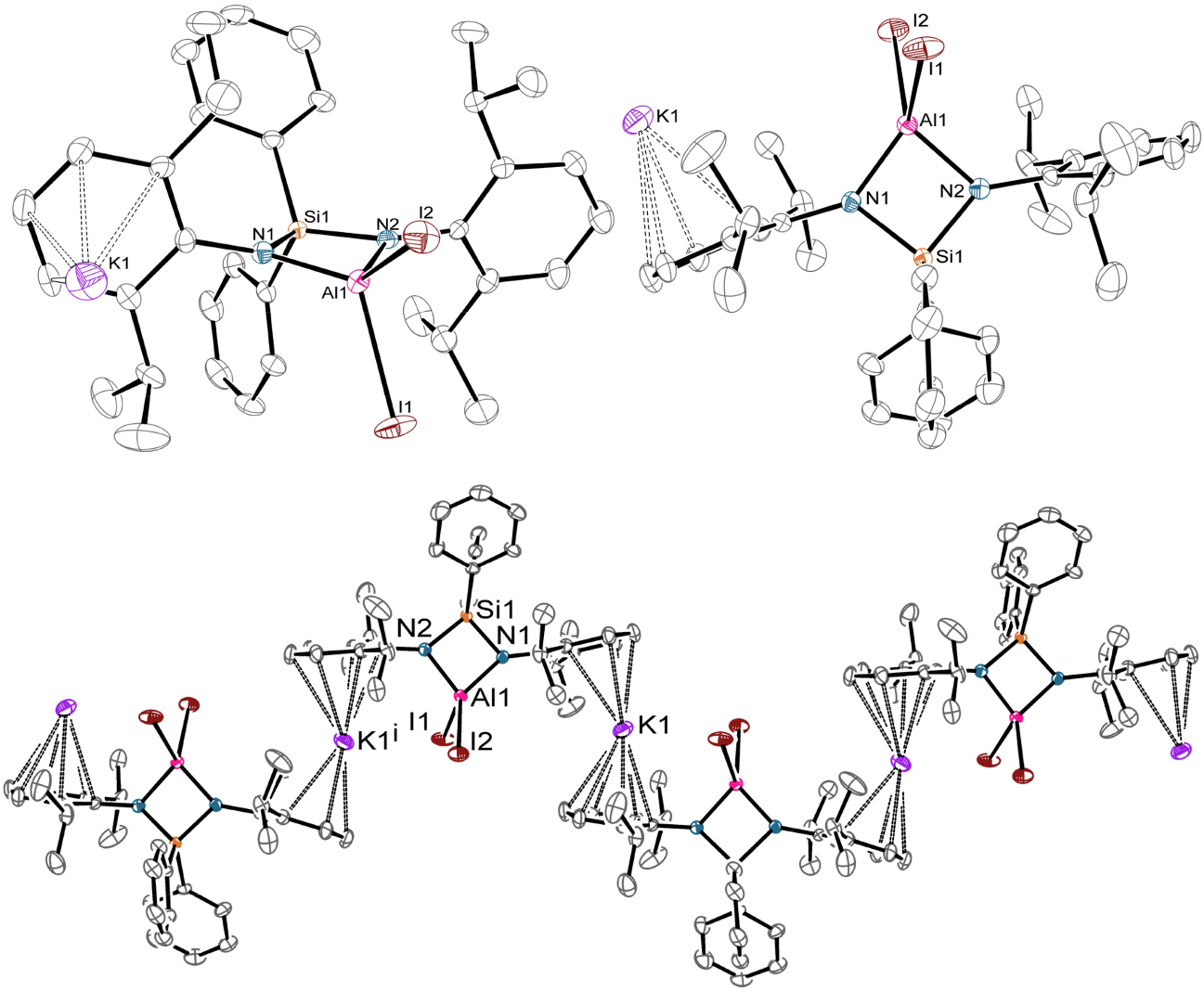

*Figure 2.20: Solid-state structure of the potassium aluminate K[Al(DAS)I$_2$] **2-XXXI** as asymmetric unit shown from two different orientations (top), and polymeric arrangement (bottom) as determined by X-ray crystallography. Hydrogen atoms omitted. Thermal ellipsoids set at 50% probability. Selected bond lengths (Å) and angles (°): Al1-I1 2.5783(9), Al1-I2 2.5459(9), K1-I1 3.8610(12), K1-I1 3.9870(9), Al1-N1 1.822(3), Al1-N2 1.854(3), Si1-N1 1.748(2), Si1-N2 1.730(2), K1···Ct^{Dipp} 2.879, 2.925, N1-Al1-N2 84.83(11), I1-Al1-I2 100.51(3), N1-Si1-N2 90.97(12).*

In the optimisation of the synthesis, utilising toluene as a solvent gave the potassium aluminate **2-XXXI** in good yields (88%). This product could be identified by protons in environments of Dipp-isopropyl methine (4.39 ppm), and Dipp-methyl (1.20 ppm) groups. Toward the identification of other species within solution featuring signals of Dipp-isopropyl methine (4.11 ppm), and Dipp-methyl (1.11 ppm) groups (Supporting Information Figure S.47), attempts were investigated within further aliphatic solvents (pentane, hexane, cyclohexane), however, did not afford the second species as a majority

product. As opposed to attempts undertaken with the bulkier acyclic precursor species, an increase in reaction mixture temperature did not afford the targeted [Al(DAS)I] compound, rather assisting in the further generation of **2-XXXI**, potentially from aiding potassium iodide solubility in hydrocarbon solutions. The unidentified second species was hypothesised to be targeted tri-coordinate species [Al(DAS)I], however, it could not be crystallised despite extensive attempts (all yielding the **2-XXXI**). Reactions in tetrahydrofuran were also unsuccessful, yielding an intractable mixture of products.

Given the successes of lithium salt metathesis reactions previously within this work and literature, further experiments were undertaken through this line of inquiry.

2.5.5.2. Salt Metathesis Investigations from the Lithium Silyldiamido Reagent 2-XXIX

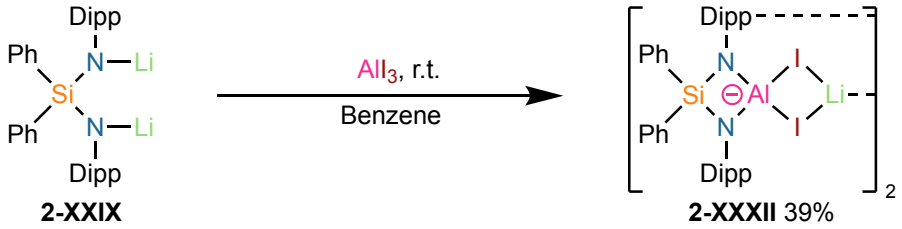

*Scheme 2.26: Synthesis of lithium aluminate salt **2-XXXII** via salt metathesis.*

Intending to emulate successes with lithium salt metathesis routes in preparing the acyclic aluminium(III) precursor [AlI{N(Dipp)Si^{i}Pr$_3$}$_2$] **2-XVII**, analogous investigations were undertaken with [DAS]$^{2-}$ scaffolds. To this end, benzene solutions of **2-XXIX** were treated with stoichiometric aluminium triiodide and sonicated at room temperature for 2 h. Subsequent analysis via ^{1}H NMR spectroscopy identified the formation of a single [DAS]$^{2-}$ containing product featuring signals in environments of Dipp-isopropyl methine (4.25 ppm), and Dipp-methyl (1.15 ppm) groups (Supporting Information Figure S.49). As with the potassium analogue, the crystallisation of the product was very quick (< 1 h) from aromatic solvents, yielding crystals of SCXRD quality at ambient temperatures. Isolated in a relatively low yield (39%), the structure of the lithium aluminate salt **2-XXXII** was confirmed via X-ray diffraction (Figure 2.21).

As observed with the preparation of **2-XXXI**, coordination of the aluminium centre within a *N*–Si–*N* coordination pocket had been successful in **2-XXXII**, however, the elimination of a lithium iodide equivalent had not seceded. This could be attributed to the near perpendicular location of Dipp substituents not serving as sufficiently sterically enshrouding as presented within analogous aluminum(III) iodides species (**2.2-2.4**, **2.6-2.8**). Analogous to **2-XXXI**, the aluminate centre is contained within the 4-membered [DAS]$^{2-}$ scaffold and with two halide ligands. Conversely, the lithium coutercation does not afford a polymeric motif, but rather a dimeric structure. This is attributed

to metal prevalence toward contacts with halide substituents, yielding the dimer bridge by the combinative $(\mu\text{–I})_2$–Li–η^3–Dipp interactions (Figure 2.21).

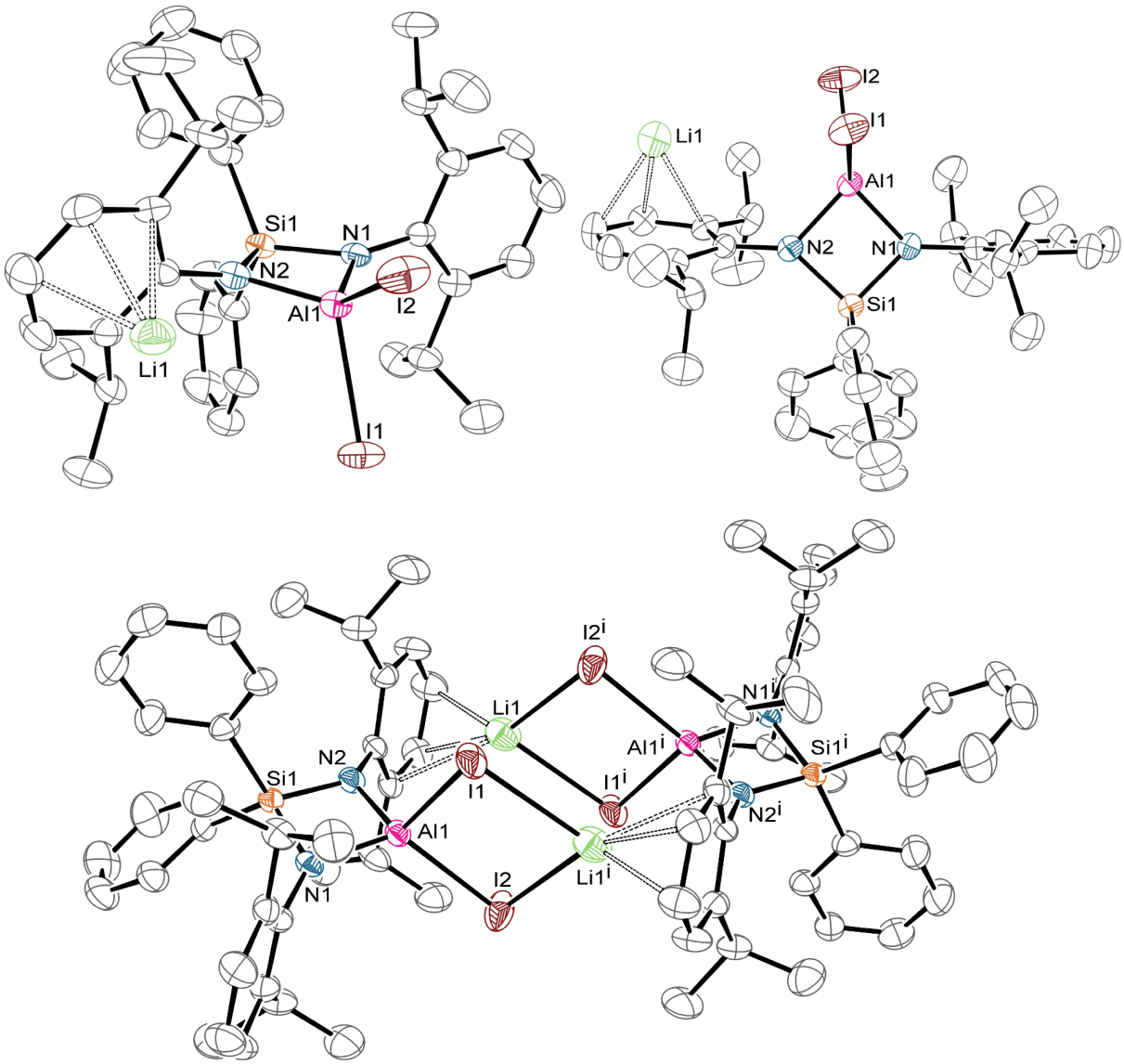

*Figure 2.21: Molecular structure of the lithium aluminate salt Li[Al(DAS)I$_2$] **2-XXXII** as asymmetric unit shown from two different orientations (top) and dimeric arrangement (bottom) as determined by X-ray crystallography. Hydrogen atoms omitted. Thermal ellipsoids set to 50% probability. Selected bond lengths (Å) and angles (°): Al1-I1 2.5950(15), Al1-I2 2.5736(15), Li-I1 2.846(11), Li1-I2 2.776(10), Al1-N1 1.823(4), Al1-N2 1.849(4), Si1-N1 1.741(4), Si1-N2 1.745(4), Li1···Ct^{Dipp} 2.132, N1-Al1-N2 85.07(19), I1-Al1-I2 95.94(5), I1-Li1-I2 86.1(3), N1-Si1-N2 90.81(19).*

To understand **2-XXXII** formation, small-scale reactions at ambient temperatures in J. Young's NMR tubes were undertaken followed by immediate ^{1}H NMR spectroscopic analysis. Similar to observations with the potassium analogue, the same signals corresponding an unknown $[DAS]^{2-}$

containing product were identified. This further supported the hypothesis of the target [Al(DAS)I] species being formed within solution. Consequently, the identified aluminates were formed through incomplete elimination of the associated alkali metal halide salt or the subsequent salt coordination in solution following the salt metathesis. In attempting to preferentially form the targeted aluminium(III) iodide precursor [Al(DAS)I], large-scale investigations were undertaken.

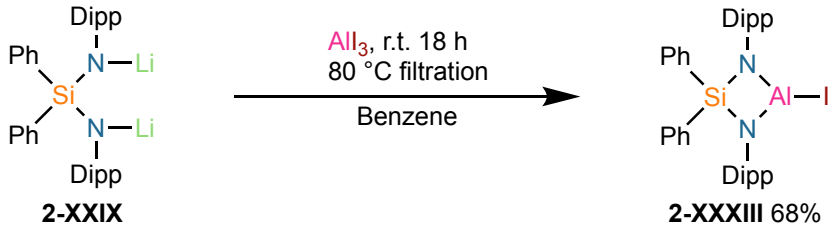

Scheme 2.27: Synthesis of aluminium(III) iodide precursor coordinated within a 4-membered metallocycle .

Large-scale preparations (500 mg, 1 g, 2 g) identified a viable and reliable method for the isolation of the targeted LiI-free precursor **2-XXXIII** (Scheme 2.27). In such investigations, benzene solutions of lithiated ligand salt **2-XXIX** were charged with aluminium triiodide and stirred at room temperature overnight. The initial extraction of the mother liquor was identified to yield mixtures of species including the previously identified lithium aluminate **2-XXXII**, proligand H_2DAS **2-XXIII**, and the target [Al(DAS)I] hypothesised previously during salt metathesis reactions. However, the isolated material in previous trials was notably minimal (35 mg) compared to that expected from larger reaction scales (500 mg of **2-XXIX**). Consequently, further benzene was added to the reaction flask and extraction conducted at elevated temperatures (70 °C). Following substantial investigations, extraction from refluxing benzene was identified to ensure the highest yield of the product **2-XXXIII**. This was isolated as a colourless powder in good yield (~45%), and confirmed via ^{1}H NMR spectroscopy (Supporting Information Figure S.51).

This cross-referencing of ^{1}H NMR spectra identified signals of Dipp-isopropyl methine (4.11 ppm), and Dipp-methyl (1.11 ppm) groups observed in the synthesis of alkali metal aluminate species **2-XXXI** and **2-XXXII** and in the baseline of ^{1}H NMR spectra from the sublimation attempts of **2-XXVII** (Scheme 2.23). By optimising the synthesis and isolation of the targeted aluminium(III) iodide precursor **2-XXXIII**, a reliable synthesis was identified and replicated to isolate the compound in moderate yield (68%). Notably, **2-XXXIII** is sparingly soluble in hydrocarbons, requiring either vigorous agitation or elevated temperatures to aid in its solubility and isolation.

In attempts to characterise **2-XXXIII** crystallographically, extensive crystallisation attempts were undertaken. Due to the low solubility of the species, hexane, pentane, and cyclohexane solutions of **2-XXXIII** were observed to yield precipitate at ambient and very minimal solubility at elevated

temperatures (contrary to aluminate species). Similarly, solutions in aromatic solvents at ambient temperatures saw minimal solubility and primarily the precipitation of **2-XXXIII**. In attempts when SCXRD quality crystalline material was grown, the amount and mass of crystalline material was minimal (< 5 crystals per 25 mg investigation) and confirmed via X-ray diffraction as lithium aluminate **2-XXXII** by-product in multiple different polymorphs. Also attempted, a benzene solution of **2-XXXIII** was slowly cooled from reflux in a large oil bath, which did yield single crystals, however these turned out to be an example of a C-C bonded decomposition product **2-XXXIV** (Figure 2.22). Exhibiting an interesting motif through the C-C coupling of two Dipp groups, **2-XXXIV** unfortunately featured two iodide ligands upon the aluminium(III) centre. As a direct result of the coupling, the Dipp phenyl rings exhibited a pseudo-boat conformation with the slight puckering of *ortho*- and *ipso*-carbons within the ring. Despite attempts, a reliable and reproducible route to this species could not be found.

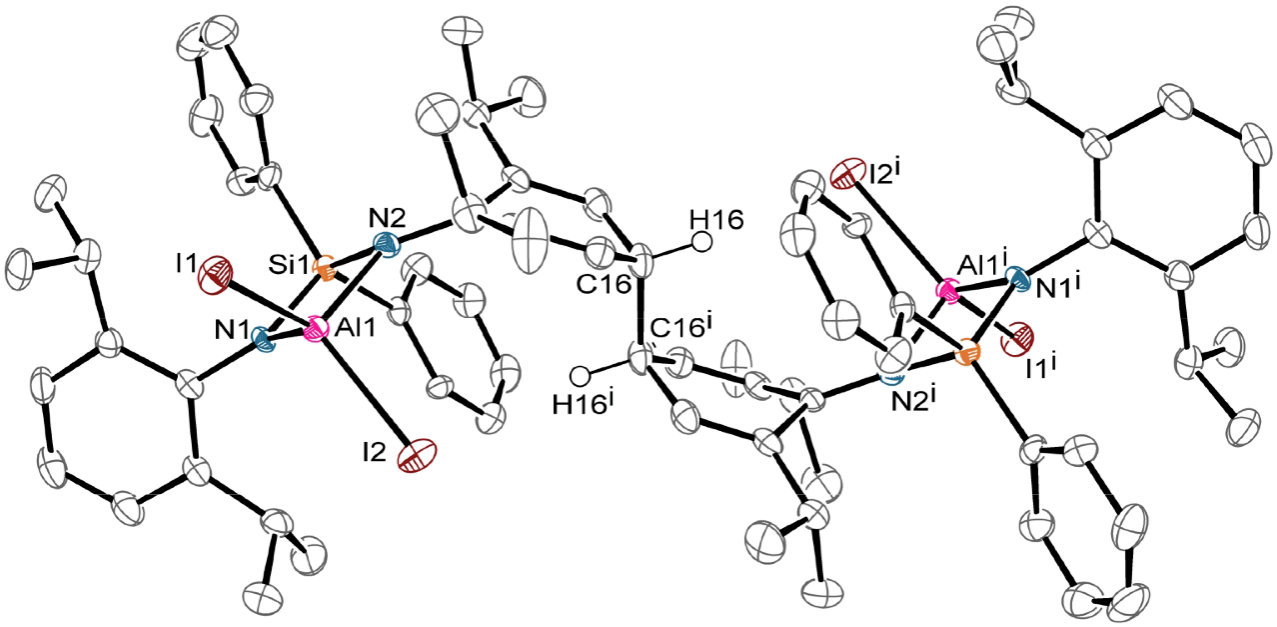

*Figure 2.22: Molecular structure of C-C coupled species **2-XXXIV** as determined by X-ray crystallography. Hydrogen atoms omitted and phenyl groups represented as wireframe for clarity. Thermal ellipsoids set to 50% probability. Selected bond lengths (Å) and angles (°): C16-C16 1.580(8), Al1- I1 2.5191(13), Al1- I2 2.5483(13), Al1-N1 1.818(3), Al1-N2 1.954(3), Al1···Si1 2.6824(17), Si1-N1 1.724(3), Si1-N2 1.829(4), N1-Al1-N2 82.46(15), N1-Si1-N2 88.87(16), I1-Al1-I2 110.41(5).*

2.5.6. Exploring the Reactivity of a 4-Membered Aluminium(III) Iodide Precursor 2-XXXIII

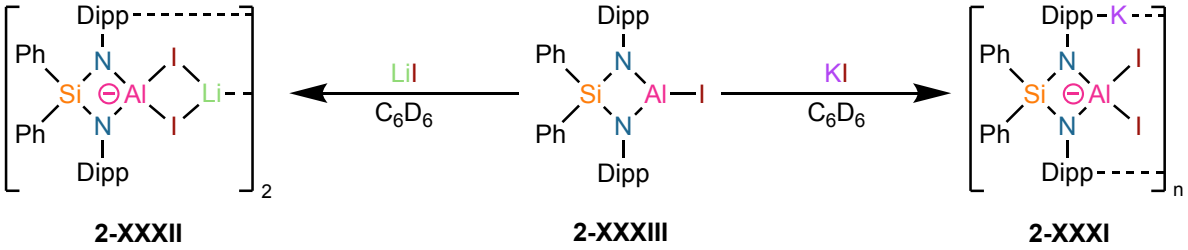

2-XXXII **2-XXXIII** **2-XXXI**

*Scheme 2.28: Preparation of alkali metal aluminate salts **2-XXXI** and **2-XXXII** from reactions of aluminium(III) iodide precursor **2-XXXIII** with corresponding alkali metal iodide.*

Following the optimisation and highly replicable purification of the target precursor **2-XXXIII**, reactivity investigations were undertaken with Lewis bases and coordinating solvents to yield previously identified compounds. On a *circa* 20 mg scale, J. Young's NMR tube investigations were undertaken with the introduction of alkali metal iodide salts. The salts (lithium iodide, potassium iodide) available as pellets were first ground with a mortar and pestle to increase surface area to aid solubility. Consequently, the addition of the salts to C_6D_6 solutions of **2-XXXIII**, followed by analysis via ^{1}H NMR spectroscopy, identified the quantitative conversion to the associated target **2-XXXI** and **2-XXXII** aluminate complexes (Scheme 2.28).

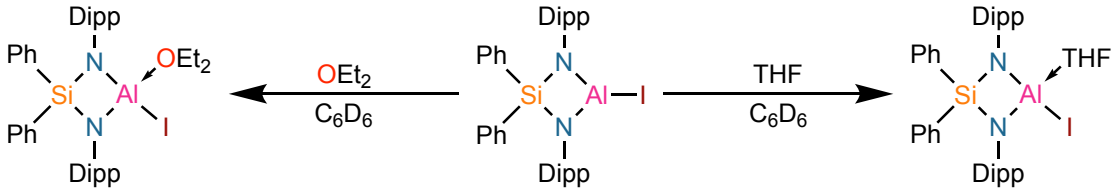

2-XXVII **2-XXXIII** **2-XXXV**

*Scheme 2.29: Preparation of solvated aluminium(III) iodide species **2-XXVII** and **2-XXXV** from the addition of coordinating solvents to the aluminium(III) iodide precursor **2-XXXIII**.*

Additions of coordinating solvents to solutions of **2-XXXIII** were undertaken with diethyl ether and tetrahydrofuran (Scheme 2.29). Investigations with diethyl ether identified the clean formation of single product featuring a single diethyl ether molecule coordinated to aluminium, yielding the previously identified solvated complex **2-XXVII**. Excess diethyl ether was removed through subsequent co-evaporation of the benzene solvent, yielding target species **2-XXVII** with minimal decomposition. Investigations with tetrahydrofuran also presented evidence of a single solvent molecule coordination to the aluminium centre, cleanly yielding the solvated species **2-XXXV** with excess tetrahydrofuran, as identified by ^{1}H NMR spectroscopy. The solvated species **2-XXXV** was identifiable via the signals of proton environments of Dipp-isopropyl methine (4.11 ppm), and Dipp-

methyl (1.11 ppm) groups as well as signals of a coordinated THF molecule (3.94-3.90 and 1.23-1.19 ppm) (Supporting Information Figure S.53). Removal of excess tetrahydrofuran through multiple co-evaporations with benzene and toluene ensured the excess majority was removed. However, unlike diethyl ether investigations, all residual non-coordinated THF could not be removed without degradation of target compound **2-XXXV** and further attempts to purify target species via crystallisation was unsuccessful.

The optimisation of precursor **2-XXXIII** ensured the investigative success in the preparation of an aluminium(III) precursor featuring a 4-membered metallocycle. Highlighted through Lewis base coordination, relatively minimal steric encumberment about the aluminium centre (compared with acyclic analogues) reinforced exciting structural differences with the opportunity to impart varied reactivity observed following reduction investigations toward the first 4-membered aluminyl anion.

2.6. Conclusions

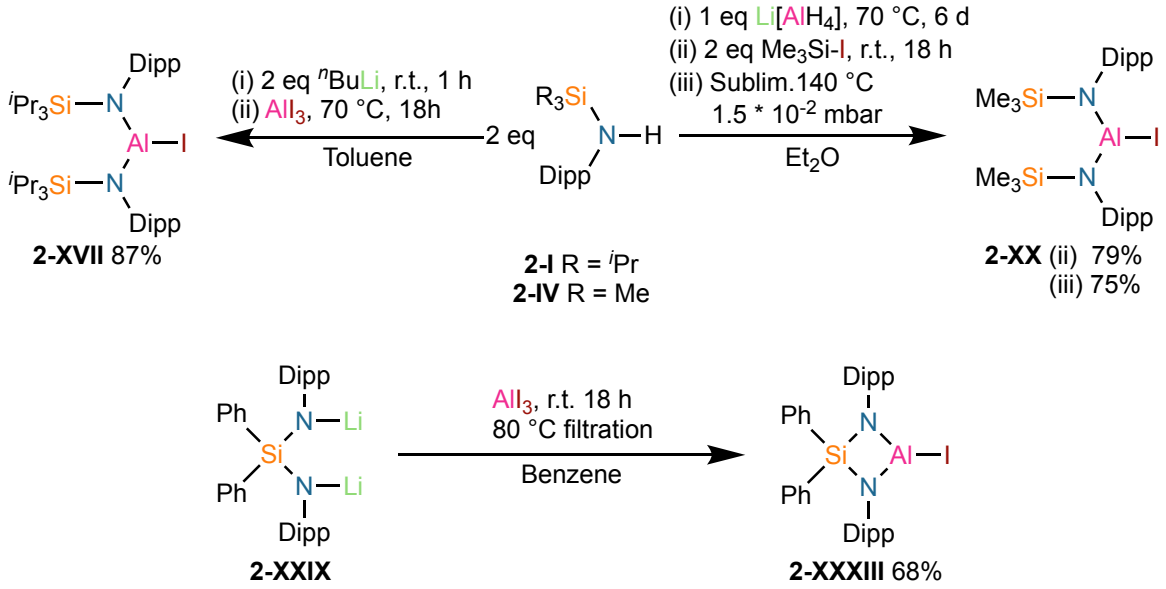

Scheme 2.30:Successful synthetic routes affording target diamido aluminium(III) iodide precursor complexes.

Aluminium(III) halide precursors for the synthesis for aluminyl anion have seen increased variability since their first report in 2018.[2] All reported halide precursors feature the aluminium centre within a 5-, 6-, 7- or pseudo-8-membered metallocycle.[3] No examples of aluminium(III) iodide precursors featuring acyclic or 4-membered co-ordinational motifs have been previously reported.

Investigations of lithium aluminium hydride and organoaluminium metalations, and alkali metal salt metathesis reactions were undertaken with four silylamido systems of varying steric bulk (**2-I** – **2-IV**). Consequently, synthetic attempts afforded two targeted acyclic aluminium(III) iodide precursors [AlI{N(Dipp)Si^{i}Pr$_3$}$_2$] **2-XVII** (87%) and [AlI{N(Dipp)SiMe$_3$}$_2$] **2-XX** (79% and 75%) in good

yields. These species adopted similar arrangements to cyclic aluminium(III) iodide precursors **2.3**-**2.5** incorporating *N*-coordination atoms and substituted silyl groups. With optimised and reproducible synthetic routes, both species are promising reagents for reductions toward the isolation of the first acyclic aluminyl anions (**Chapter 3**).

Applying understandings gained through the acyclic precursor developments, the bidentate silyldiamido $[DAS]^{2-}$ ligand derived from proligand (H_2DAS) **2-XXIII** was also investigated extensively. Following these investigations, the targeted precursor [Al(DAS)I] **2-XXXIII**, was isolated in moderate yields (68%). Featuring an aluminium centre constrained within a metallocycle, crystalline examples of the 4-membered motif were identified and confirmed through reactivity investigations with various Lewis bases. Featuring a reproducible and optimised synthesis, **2-XXXIII** presents a candidate for reduction towards the first 4-membered aluminyl anion (**Chapter 4**).

With the successes yielded in precursor preparation, the stage was set to synthesise previously unreported aluminyl anions and explore their related reactivities.

2.7. Experimental

General Methods and Considerations

All reactions dealing with air- and moisture-sensitive compounds were carried out under an argon atmosphere using standard Schlenk line and glovebox techniques. NMR experiments using air sensitive compounds were conducted in J. Young's tap NMR tubes prepared and sealed in a glovebox under argon. Toluene, hexane, and pentane were purified using an MBraun Solvent Purification System and stored over 4Å molecular sieves or sodium mirror and degassed with argon before use. Diethyl ether was dried using sodium suspended with benzophenone. C_6D_6 and toluene-d_8 were dried over potassium mirrors prior to vacuum transfer into sealed ampoules and stored in a glove box under argon. All NMR data, unless otherwise stated, were acquired at 298 K on either an Agilent ProPulse instrument for ^{1}H (500 MHz), $^{13}C\{^{1}H\}$ (126 MHz) and $^{29}Si\{^{1}H\}$ (99 MHz), a Bruker Ascend 400 for ^{1}H (400 MHz), $^{13}C\{^{1}H\}$ (101 MHz) and $^{29}Si\{^{1}H\}$ (79 MHz) or Bruker Ascend 700 for $^{13}C\{^{1}H\}$ (176 MHz) and $^{29}Si\{^{1}H\}$ (139 MHz). ^{1}H and ^{13}C NMR spectra were referenced using residual solvent resonances. IR spectroscopy was acquired on a Brucker Alpha II or a PerkinElmer UATR Two FT-IR spectrometer. Elemental analyses of **2-III**, **2-VII**, **2-X**, **2-XIV**, **2-XV**, and **2-XVII** were performed by Elemental Analysis Services, London Metropolitan University, London, U.K, Elemental analyses of **2-XX** were performed by Elemental Microanalysis Ltd., Okehampton, Devon, U.K. Li[N(Dipp)SiMe$_3$],[50] K[N(Dipp)SiMe$_3$],[51] K[N(Dipp)Si^{t}BuMe$_2$],[52] Li[N(Dipp)Si^{i}Pr$_3$],[30] K[N(Dipp)Si^{i}Pr$_3$],[30] AlI$_3$,[1] **2-XXIII**,[53] **2-XXVIII**,[54] and **2-XXIX**,[55] were all prepared as per

literature methods. $LiAlH_4$ was recrystallised from diethyl ether before use. All other reagents were used as received.

Optimised synthesis of HN(Dipp)Si^{i}Pr$_3$ (2-I)

To a stirred brown solution of 2,6-diisopropylphenylaniline (14.9 g, 15.8 mL, 84 mmol, 1.0 eq.) in tetrahydrofuran (30 mL), *n*-butyllithium (55.2 mL of 1.6 M solution in hexanes, 88.3 mmol, 1.1 eq.) was added dropwise over 5 min at –78 °C. Following 3 h stirring at ambient temperature, chlorotriisopropylsilane (16.2 g, 18 mL, 84 mmol, 1.0 eq.) was added dropwise. The red solution was stirred at 80 °C for 25 h. The resultant red solution was filtered, and the volatiles were removed *in vacuo*. Distillation at 100 °C (2.8×10^{-1} mbar) yielded HN(Dipp)Si^{i}Pr$_3$ **2-I** as a vibrant orange oil (27.3 g, 98%). Characterisation data was consisted with that previously reported.[42]

Optimised synthesis of HN(Dipp)Si(^{t}Bu)Me$_2$ (2-II)

To a stirred brown solution of 2,6-diisopropylphenylaniline (3.53 g, 3.74 mL, 19.9 mmol, 1.0 eq.) in tetrahydrofuran (10 mL), *n*-butyllithium (13.75 mL of 1.6 M solution in hexane, 22 mmol, 1.1 eq.) was added dropwise over 2 min at –78 °C. Following 3 h stirring at ambient temperature, a tetrahydrofuran solution (5 mL) of *tert*-butylchlorodimethylsilane (3.00 g, 19.9 mmol, 1.0 eq.) was added dropwise. 3 h stirring at ambient temperature did not lead to noticeable salt formation, but subsequent heating to 60 °C led to precipitation of a colourless solid. The wine red mixture was stirred at 60 °C for 18 h. The volatiles removed *in vacuo* gave a maroon oily solid product. Distillation at 70 °C (2.3×10^{-1} mbar) yielded HN(Dipp)Si(^{t}Bu)Me$_2$ **2-II** as a pale-yellow oil (3.02 g, 52%). Characterisation data was collected since this was not previously reported in the literature.[43] **^{1}H NMR** (400 MHz, C_6D_6, 298 K): δ = 7.14 – 7.05 (m, 3H, Dipp-aryl-*H*), 3.60 (sept, $^3J_{HH}$ = 6.8 Hz, 2H, Dipp-C*H*$(CH_3)_2$), 2.22 (s, 1H, N-*H*), 1.21 (d, $^3J_{HH}$ = 6.9 Hz, 12H, Dipp-CH(C*H*$_3)_2$), 1.00 (s, $^3J_{HH}$ = 7.8 Hz, 9H, Si$(CH_3)_2$(C(C*H*$_3)_3$), 0.06 (s, 6H, Si(C*H*$_3)_2$(C$(CH_3)_3$). **^{13}C{^{1}H} NMR** (101 MHz, C_6D_6, 298 K): δ = 145.2 (Dipp-*o*-*C*), 139.2 (Dipp-*i*-*C*), 124.5 (Dipp-*p*-*C*), 123.5 (Dipp-*m*-*C*), 28.4 (Dipp-*C*H$(CH_3)_2$), 26.8 ((Si$(CH_3)_2$(C(*C*H$_3)_3$), 23.9 (Dipp-CH(*C*H$_3)_2$), 18.3 (Si$(CH_3)_2$(*C*$(CH_3)_3$), –3.6 (Si(*C*H$_3)_2$(C$(CH_3)_3$). **IR** ν_{max} (cm^{-1}) (Nujol): 3385(w), 1590(w), 1438(m), 1382(w), 1325(m), 1194(m) 1111(w), 1055(w), 1043(w), 1007(w), 933(w), 898(s), 877(m), 837(s), 822(s), 897(s), 778(s), 759(m), 677(w), 575(w), 412(w).

Synthesis of HN(Dipp)SiEt$_3$ (2-III)

To a stirred brown solution of 2,6-diisopropylphenylaniline (10.0 g, 56.4 mmol, 1.0 eq.) in tetrahydrofuran (50 mL), *n*-butyllithium (38.9 mL of 1.6 M solution in hexanes, 62.3 mmol, 1.1 eq.) was added dropwise over 15 min at –78 °C. Warming over 20 min of stirring to ambient temperature, Chlorotriethylsilane (8.50 g, 9.47 mL, 56.4 mmol, 1.0 eq.) was added dropwise. The mango orange mixture was stirred at 70 °C for 18 h, and a gold coloured filtrate was isolated via cannula filtration. Removal of the solvent from the filtrate under reduced pressure, followed by distillation of the product at 80 °C (7.6×10^{-2} bar) yielded HN(Dipp)SiEt$_3$ **2-III** as a pale-yellow oil (13.6 g, 83%). **^{1}H NMR** (400 MHz, C_6D_6, 298 K): δ = 7.12 – 7.02 (m, 3H, Dipp-aryl-*H*), 3.49 (sept, $^3J_{HH}$ = 6.8 Hz, 2H, Dipp-C*H*(CH$_3$)$_2$), 2.22 (s, 1H, N-*H*), 1.22 (d, $^3J_{HH}$ = 6.9 Hz, 12H, Dipp-CH(C*H*$_3$)$_2$), 0.96 (t, $^3J_{HH}$ = 7.8 Hz, 9H, SiCH$_2$C*H*$_3$), 0.64 (q, $^3J_{HH}$ = 7.9 Hz, 6H, SiC*H*$_2$CH$_3$). **^{1}H NMR** (400 MHz, Toluene-d_8, 298 K): δ = 7.04 – 6.96 (m, 3H, Dipp-aryl-*H*), 3.45 (sept, $^3J_{HH}$ = 6.8 Hz, 2H, Dipp-C*H*(CH$_3$)$_2$), 2.19 (s, 1H, N-*H*), 1.18 (d, $^3J_{HH}$ = 7.0 Hz, 12H, Dipp-CH(C*H*$_3$)$_2$), 0.93 (t, $^3J_{HH}$ = 7.9 Hz, 9H, SiCH$_2$C*H*$_3$), 0.62 (dq, $^3J_{HH}$ = 7.5 Hz, $^4J_{HH}$ = 0.7 Hz, 6H, SiC*H*$_2$CH$_3$). **^{13}C{^{1}H} NMR** (101 MHz, C_6D_6, 298 K): δ = 144.0 (Dipp-*o*-*C*), 140.1 (Dipp-*i*-*C*), 123.9 (Dipp-*p*-*C*), 123.4 (Dipp-*m*-*C*), 28.4 (Dipp-*C*H(CH$_3$)$_2$), 23.9 (Dipp-CH(*C*H$_3$)$_2$), 7.5 (SiCH$_2$*C*H$_3$), 6.0 (Si*C*H$_2$CH$_3$). **^{29}Si{^{1}H} NMR** (79 MHz, C_6D_6, 298 K): δ = 6.6 (N-*Si*-CH$_2$CH$_3$). **IR** ν_{max} (cm^{-1}) (Nujol): 3063(w), 2912(m), 2874(s), 1586(w), 1499(w), 1438(s), 1416(m), 1360(m), 1326(s), 1240(m), 1158(w), 1111(w), 1055(w), 1043(w), 1008(s), 973(m), 932(m), 896(s), 875(m), 810(w), 774(s), 745(s), 685(m), 573(w), 430(m), 414(m). **E.A:** Anal. Calc. for $C_{18}H_{33}NSi$: C 74.15; H 11.41; N 4.80%. Found C 74.52; H 11.56; N 4.87%.

Optimised synthesis of HN(Dipp)SiMe$_3$ (2-IV)

To a stirred brown solution of 2,6-diisopropylphenylaniline (5.32 g, 5.66 mL, 30 mmol, 1.0 eq.) in diethyl ether (150 mL), *n*-butyllithium (19.7 mL of 1.6 M solution in hexanes, 33 mmol, 1.1 eq.) was added dropwise at –78 °C over 2 min. Following 2 h of stirring at ambient temperature, Chlorotrimethylsilane (3.59 g, 4.08 mL, 31.5 mmol, 1.05 eq.) was added dropwise. The resultant yellow slurry was stirred for 18 h at ambient temperature. The volatiles were removed under reduced pressure, and distillation at 40 °C (4.8×10^{-2} mbar) yielded HN(Dipp)SiMe$_3$ **2-IV** as a pale-yellow oil (7.00 g, 94%). Characterisation data was consisted with that previously reported.[44]

Preparation of [AlMe$_2${N(Dipp)Si^{i}Pr$_3$}] (2-V), isolation of [AlMe$_2${N(Dipp)Si^{i}Pr$_3$}(OEt$_2$)] (2-VII)

To a 100 mL J. Young's reaction flask containing a toluene (10 mL) solution of HN(Dipp)Si^{i}Pr$_3$ (528 mg, 1.6 mmol, 1.0 eq.), was added trimethylaluminium (0.8 mL of 2 M solution in toluene, 1.6

mmol, 1.0 eq.). The lightly burnt-orange solution was heated to 140 °C. Following 72 h stirring vigorously at this temperature, the yellow solution was cooled slowly to ambient temperature. Volatiles were removed under reduced pressure, yielding a yellow oil that was identified by ^{1}H NMR spectroscopy as a single product, [AlMe$_2${N(Dipp)Si^{i}Pr$_3$}] (**2-V**). The oil was dissolved in diethyl ether (5 mL), with the reaction solution then being concentrated to a volume of *ca.* 2 mL, precipitating a yellow powder. The solid was isolated via cannula filtration and the filtrate evaporated to dryness giving [AlMe$_2${(N(Dipp)Si^{i}Pr$_3$}(OEt$_2$)] **2-VII** as a yellow powder (262 mg, 31%). **N.B.** SCXRD quality crystals of **2-VII** were obtained from a concentrated diethyl ether solution at ambient temperature for 2 h.

Characterisation data for monoligated aluminium(III) dimethyl complex (**2-V**):

^{1}H NMR (400 MHz, toluene-d_8, 298 K): δ = 6.97 (s, 3H, Dipp-aryl-*H*), 3.61 (sept, $^3J_{HH}$ = 6.9 Hz, 2H, Dipp-C*H*(CH$_3$)$_2$), 1.32 – 1.23 (m, 3H, SiC*H*(CH$_3$)$_2$), 1.24 (d, $^3J_{HH}$ = 6.7 Hz, 6H, Dipp-CH(C*H*$_3$)$_2$), 1.10 (d, $^3J_{HH}$ = 7.2 Hz, 18H, SiCH(C*H*$_3$)$_2$), 1.08 (d, $^3J_{HH}$ = 6.8 Hz, 6H, Dipp-CH(C*H*$_3$)$_2$), -0.48 (s, 6H, Al-C*H*$_3$).

Characterisation data for Lewis base monoligated aluminium(III) dimethyl adduct (**2-VII**):

^{1}H NMR (400 MHz, C$_6$D$_6$, 298 K): δ = 7.12 – 7.10 (m, 3H, Dipp-aryl-*H*), 3.90 (sept, $^3J_{HH}$ = 7.0 Hz, 2H, Dipp-C*H*(CH$_3$)$_2$), 3.55 (q, $^3J_{HH}$ = 7.1 Hz, 4H, Al-OC*H*$_2$CH$_3$), 1.34 – 1.41 (m, 3H, SiC*H*(CH$_3$)$_2$), 1.40 (d, $^3J_{HH}$ = 6.7 Hz, 6H, Dipp-CH(C*H*$_3$)$_2$), 1.26 (d, $^3J_{HH}$ = 6.8 Hz, 6H, Dipp-CH(C*H*$_3$)$_2$), 1.22 (d, $^3J_{HH}$ = 7.3 Hz, 18H, SiCH(C*H*$_3$)$_2$), 0.75 (t, $^3J_{HH}$ = 7.0 Hz, 6H, Al-OCH$_2$C*H*$_3$), -0.55 (s, 6H, Al-C*H*$_3$). **^{13}C{^{1}H} NMR** (101 MHz, C$_6$D$_6$, 298 K): δ = 146.8 (Dipp-*i*-*C*), 146.7 (Dipp-*o*-*C*), 124.4 (Dipp-*p*-*C*), 123.5 (Dipp-*m*-*C*), 65.8 (Al-O*C*H$_2$CH$_3$), 27.2 (Dipp-*C*H(CH$_3$)$_2$), 26.5 (Dipp-CH(*C*H$_3$)$_2$), 25.2 (Dipp-CH(*C*H$_3$)$_2$), 19.8 (SiCH(*C*H$_3$)$_2$), 14.9 (Si*C*H(CH$_3$)$_2$), 13.1 (Al-OCH$_2$*C*H$_3$), –5.1 (Al-*C*H$_3$). **^{29}Si{^{1}H} NMR** (79 MHz, C$_6$D$_6$, 298 K): δ = 1.8 (N-*Si*CH(CH$_3$)$_2$). **IR** ν_{max} (cm^{-1}) (Nujol): 2050(w), 1588(w), 1424(m), 1382(m), 1361(w), 1327(w), 1302(w), 1225(w), 1193(m), 1164(m), 1147(w), 1102(w), 1068(w), 1029(m), 1000(m), 985(m), 924(w), 889(s), 875(s), 838(s), 795(s), 770(m), 744(w), 657(s), 604(w), 561(m), 546(w), 527(w), 496(m), 253(w), 435(w). **E.A:** Anal. Calc. for C$_{27}$H$_5$AlN$_2$Si$_2$O: C 69.92; H 11.74; N 3.02%. found C 69.33; H 11.70; N 3.19%.

Synthesis of [AlMe$_2${N(Dipp)SiEt$_3$}] (2-VI)

In a J. Young's NMR tube containing a deuterated toluene (0.4 mL) solution of HN(Dipp)SiEt$_3$ **2-III** (140 mg, 480 μmol, 1.0 eq.) was added trimethylaluminium (240 μmL of 2.0 M solution in toluene, 480 μmol, 1eq.). The mixture was heated to 110 °C for 1 h and ^{1}H NMR spectroscopy identified the clean conversion to a single species identified as the monosubstituted [AlMe$_2${N(Dipp)SiEt$_3$}] **2-VI**

(>98% yield based on NMR spectroscopy). **N.B.** Crystallisation attempts were unsuccessful, and the removal of volatiles yielded a colourless oil. **^{1}H NMR** (400 MHz, toluene-d_8, 298 K): δ = 7.00 (s, 3H, Dipp-aryl-*H*), 3.53 (sept, $^3J_{HH}$ = 6.8 Hz, 2H, Dipp-C*H*(CH_3)$_2$), 1.24 (d, $^3J_{HH}$ = 6.8 Hz, 6H, Dipp-CH(C*H*$_3$)$_2$), 1.09 (d, $^3J_{HH}$ = 6.9 Hz, 6H, Dipp-CH(C*H*$_3$)$_2$), 0.95 (dt, $^3J_{HH}$ = 8.3 Hz, $^4J_{HH}$ = 0.7 Hz, 9H, $SiCH_2CH_3$), 0.67 (dq, $^3J_{HH}$ = 7.8 Hz, $^4J_{HH}$ = 0.9 Hz, 6H, $SiCH_2CH_3$), –0.51 (s, 6H, Al-Me). **^{13}C{^{1}H} NMR** (101 MHz, toluene-d_8, 298 K): δ = 144.9 (Dipp-*o*-*C*), 143.7 (Dipp-*i*-*C*), 124.2 (Dipp-*p*-*C*), 123.7 (Dipp-*m*-*C*), 28.1 (Dipp-*C*H(CH_3)$_2$), 25.0 (Dipp-CH(*C*H$_3$)$_2$), 24.0 (Dipp-CH(*C*H$_3$)$_2$), 8.3 ($SiCH_2CH_3$), 7.6 ($SiCH_2CH_3$), –7.4 (Al-*C*H$_3$).

Preparation of [AlMe$_2${N(Dipp)SiEt$_3$}(OEt$_2$)] (2-VIII) and isolation of [Al{N(Dipp)SiEt$_3$}(μ-OMe)]$_2$ (2-IX) degradation product.

Method A: To a J. Young's NMR tube containing a deuterated benzene (0.5 mL) solution of [AlMe$_2${N(Dipp)SiEt$_3$}] **2-VI** (167 mg , 480 μmol, 1.0 eq.) was added diethyl ether (0.1 mL). Following brief agitation and subsequent removal of volatiles under reduced pressure yielded a colourless oil following 2 h under dynamic vacuum. Further dissolution of the product in deuterated benzene (0.5 mL) identified the clean conversion to [AlMe$_2${N(Dipp)SiEt$_3$}(OEt$_2$)] **2-VIII** as identified via ^{1}H NMR spectroscopy (>98%). **Method B:** To a 100 mL J. Young's reaction flask containing a toluene (15 mL) solution of HN(Dipp)SiEt$_3$ **2-III** (530 mg, 1.82 mmol, 1.0 eq.) was added trimethylaluminium (910 μmL of 2.0 M solution in toluene, 1.82 mmol, 1.0 eq.) at 0 °C. Following warming to ambient temperature, the reaction mixture was then heated and stirred at 160 °C for 18 h. After allowing the reaction mixture to cool to ambient temperature, the volatiles were removed under reduced pressure, yielding a yellow oil. Diethyl ether (0.1 mL) was added and ^{1}H NMR spectroscopy revealed the clean conversion of all HN(Dipp)SiEt$_3$ into [AlMe$_2${N(Dipp)SiEt$_3$}(OEt$_2$)] **2-VIII** (>98%). **N.B.** Attempts to crystallise SCXRD quality samples of **2-VIII** were conducted using diethyl ether and aromatic solvents. From a concentrated hexane solution after 32 days at –40 °C, only SCXRD quality crystals of the methoxy-bridged degradation product [Al{N(Dipp)SiEt$_3$}(μ-OMe)]$_2$ **2-IX** were isolated, the synthesis of which could not be replicated. **^{1}H NMR** (400 MHz, C_6D_6, 298 K): δ = 7.11 – 7.03 (m, 3H, Dipp-aryl-*H*), 3.90 (sept, $^3J_{HH}$ = 6.8 Hz, 2H, Dipp-C*H*(CH_3)$_2$), 3.57 (q, $^3J_{HH}$ = 7.0 Hz, 4H, Al-OC*H*$_2$CH$_3$), 1.34 (d, $^3J_{HH}$ = 6.9 Hz, 6H, Dipp-CH(C*H*$_3$)$_2$), 1.25 (d, $^3J_{HH}$ = 6.9 Hz, 6H, Dipp-CH(C*H*$_3$)$_2$), 1.07 (dt, $^3J_{HH}$ = 8.3 Hz, $^4J_{HH}$ = 0.7 Hz, 9H, $SiCH_2CH_3$), 0.80 (dq, $^3J_{HH}$ = 7.9 Hz, $^4J_{HH}$ = 0.9 Hz, 6H, $SiCH_2CH_3$), 0.73 (t, $^3J_{HH}$ = 7.1 Hz, 6H, Al-OCH$_2$C*H*$_3$), –0.62 (s, 6H, Al-Me). **^{1}H NMR** (400 MHz, toluene-d_8, 298 K): δ = 7.05 – 6.97 (m, 3H, Dipp-aryl-*H*), 3.85 (sept, $^3J_{HH}$ = 6.8 Hz, 2H, Dipp-C*H*(CH_3)$_2$), 3.57 (q, $^3J_{HH}$ = 7.1 Hz, 4H, Al-OC*H*$_2$CH$_3$), 1.32 (d, $^3J_{HH}$ = 6.9 Hz, 6H, Dipp-CH(C*H*$_3$)$_2$), 1.22 (d, $^3J_{HH}$ = 6.9 Hz, 6H, Dipp-CH(C*H*$_3$)$_2$), 1.04 (t, $^3J_{HH}$ = 8.0 Hz, 9H, $SiCH_2CH_3$), 0.80

– 0.72 (m, 12H, SiCH_2CH$_3$, Al-OCH$_2$CH_3), –0.67 (s, 6H, Al-CH_3). **^{13}C{^{1}H} NMR** (101 MHz, toluene-d_8, 298 K): δ = 146.6 (Dipp-*o*-*C*), 146.2 (Dipp-*i*-*C*), 123.8 (Dipp-*m*-*C*), 123.0 (Dipp-*p*-*C*), 65.7 (Al-O*C*H$_2$CH$_3$), 27.3 (Dipp-*C*H(CH$_3$)$_2$), 25.7 (Dipp-CH(*C*H$_3$)$_2$), 25.3 (Dipp-CH(*C*H$_3$)$_2$), 12.8 (Al-OCH$_2$*C*H$_3$), 8.8 (SiCH$_2$*C*H$_3$), 8.0 (Si*C*H$_2$CH$_3$), –6.8 (Al-*C*H$_3$). **^{29}Si{^{1}H} NMR** (79 MHz, toluene-d_8, 298 K): δ = 2.4 (N-Si(CH$_2$*C*H$_3$)$_3$). **IR** ν_{max} (cm^{-1}) (Nujol): 3047(w), 2962(m), 2873(m), 2162(w), 2050(w), 1980(w), 1587(w), 1429(m), 1389(m), 1382(m), 1361(w), 1309(m), 1289(w), 1233(m), 1191(m), 1173(s), 1148(m), 1103(m), 1032(m), 1011(m), 1002(m), 930(w), 901(s), 881(m), 847(s), 795(s), 773(m), 714(s), 665(s), 566(m), 536(w), 518(w), 441(m), 420(w).

Synthesis of [AlI$_2${(N(Dipp)Si^{i}Pr$_3$}(OEt$_2$)] (2-X)

Method A: In a glovebox, K[N(Dipp)Si^{i}Pr$_3$] (200 mg, 538 μmol, 1.0 eq.) and aluminium triiodide (219 mg, 538 μmol, 1.0 eq.) were charged within a 50 mL Schlenk flask. Addition of benzene (10 mL), gave a yellow solution that was stirred at ambient temperature for 1.5 h. The mother liquor was separated via cannula filtration, and volatiles were removed from the filtrate *in vacuo*. To the resultant orange oil, diethyl ether (0.5 mL) was added and once dissolved, was stored at 4 °C. Following 14 days, colourless crystals of SCXRD quality were isolated and confirmed as [AlI$_2${(N(Dipp)Si^{i}Pr$_3$}(OEt$_2$)] **2-X** (92 mg, 25%). **Method B:** [AlMe$_2${N(Dipp)Si^{i}Pr$_3$}(OEt$_2$)] **2-VII** (185 mg, 399 μmol, 1.0 eq.) and iodine (438 mg, 798 μmol, 2 eq.) were charged in a 25 mL Schlenk flask and toluene (15 mL) was added. The resultant red/violet solution was stirred vigorously at ambient temperature for 18 h. The pink solution was concentrated under reduced pressure to a final volume of *ca.* 2 mL. Following 4 days at ambient temperature, colourless crystalline material was isolated and washed with cold hexane (3 × 2 mL). Once dried under reduced pressure, crystalline material was isolated and confirmed via ^{1}H NMR spectroscopy as [AlI$_2${(N(Dipp)Si^{i}Pr$_3$}(OEt$_2$)] **2-X** (245 mg, 89%). **^{1}H NMR** (400 MHz, C$_6$D$_6$, 298 K): δ = 7.05 (s, 3H, Dipp-aryl-*H*), 3.95 – 3.82 (m, 2H, Dipp-C*H*(CH$_3$)$_2$, 4H, Al-OCH_2CH$_3$), 1.56 (sept, $^3J_{HH}$ = 7.5 Hz, 3H, SiC*H*(CH$_3$)$_2$), 1.41 (d, $^3J_{HH}$ = 6.7 Hz, 6H, Dipp-CH(CH_3)$_2$), 1.35 (d, $^3J_{HH}$ = 6.6 Hz, 6H, Dipp-CH(CH_3)$_2$), 1.23 (d, $^3J_{HH}$ = 7.5 Hz, 18H, SiCH(CH_3)$_2$), 0.73 (t, $^3J_{HH}$ = 7.0 Hz, 6H, Al-OCH$_2$CH_3), **^{13}C{^{1}H} NMR** (101 MHz, C$_6$D$_6$, 298 K): δ = 147.6 (Dipp-*o*-*C*), 144.3 (Dipp-*i*-*C*), 125.3 (Dipp-*m*-*C*), 125.1 (Dipp-*p*-*C*), 70.9 (Al-O*C*H$_2$CH$_3$), 27.6 (Dipp-*C*H(CH$_3$)$_2$), 27.3 (Dipp-CH(*C*H$_3$)$_2$), 25.8 (Dipp-CH(*C*H$_3$)$_2$), 20.4 (SiCH(*C*H$_3$)$_2$), 15.3 (Si*C*H(CH$_3$)$_2$), 12.8 (Al-OCH$_2$*C*H$_3$). **E.A:** Anal. Calc. for C$_{25}$H$_{48}$AlI$_2$NOSi: C 43.67; H 7.04; N 2.04%. Found C 44.20; H 7.22; N 2.17%.

Preparation of [Al(I)Me{N(Dipp)SiEt$_3$}(OEt$_2$)] (2-XI)

To a deuterated toluene (0.5 mL) solution of [AlMe$_2${N(Dipp)SiEt$_3$}(OEt$_2$)] **2-VIII** (86.5 mg, 20.5 µmol, 1.0 eq.) was added iodine (52 mg, 20.5 µmol, 1.0 eq.). An immediate colour change was observed from colourless to a deep red. After 10 minutes of agitation, the solution turned from being yellow to colourless. ^{1}H NMR spectroscopy identified clean conversion to [Al(I)Me{N(Dipp)SiEt$_3$}(OEt$_2$)] **2-XI** and iodomethane. Removal of all volatiles under reduced pressure yielded a colourless oil. The addition of deuterated toluene (0.5 mL) and subsequent analysis identified as clean conversion to the product [Al(I)Me{N(Dipp)SiEt$_3$}(OEt$_2$)] **2-XI** via ^{1}H NMR spectroscopy (>98%). **N.B.** Despite attempts, no crystals of SCXRD quality could be isolated. **^{1}H NMR** (400 MHz, toluene-d_8, 298 K): δ = 7.03 – 6.97 (m, 3H, Dipp-aryl-*H*), 3.90 (sept, $^3J_{HH}$ = 6.9 Hz, 1H, Dipp-C*H*(CH$_3$)$_2$), 3.79 (sept, $^3J_{HH}$ = 6.8 Hz, 1H, Dipp-C*H*(CH$_3$)$_2$), 3.57 (dq, $^3J_{HH}$ = 7.0 Hz, $^4J_{HH}$ = 4.1 Hz, 4H, Al-OC*H*$_2$CH$_3$), 1.30 – 1.27 (m, 9H, Dipp-CH(C*H*$_3$)$_2$), 1.21 (d, $^3J_{HH}$ = 6.9 Hz, 3H, Dipp-CH(C*H*$_3$)$_2$), 1.03 (dt, $^3J_{HH}$ = 7.9 Hz, 9H, SiCH$_2$C*H*$_3$), 0.85 (qd, $^3J_{HH}$ = 7.9 Hz, $^4J_{HH}$ = 5.8 Hz, 6H, SiC*H*$_2$CH$_3$), 0.67 (t, $^3J_{HH}$ = 7.1 Hz, 6H, Al-OCH$_2$C*H*$_3$), –0.18 (s, 3H, Al-C*H*$_3$). **^{13}C{^{1}H} NMR** (101 MHz, toluene-d_8, 298 K): δ = 146.6 (Dipp-*o*-*C*), 146.5 (Dipp-*o*-*C*), 145.0 (Dipp-*i*-*C*), 124.3 (Dipp-*m*-*C*), 124.1 (Dipp-*m*-*C*), 123.8 (Dipp-*p*-*C*), 68.2 (Al-O*C*H$_2$CH$_3$), 27.5 (Dipp-*C*H(CH$_3$)$_2$), 27.3 (Dipp-*C*H(CH$_3$)$_2$), 26.2 (Dipp-CH(*C*H$_3$)$_2$), 25.7 (Dipp-CH(*C*H$_3$)$_2$), 25.6 (Dipp-CH(*C*H$_3$)$_2$), 12.3 (Al-OCH$_2$*C*H$_3$), 8.7 (SiCH$_2$*C*H$_3$), 7.9 (Si*C*H$_2$CH$_3$), –0.9 (Al-*C*H$_3$).

Synthesis of [AlI$_2${N(Dipp)SiEt$_3$}(OEt$_2$)] (2-XII)

Method A: To a deuterated toluene (0.5 mL) solution of [Al(I)Me{N(Dipp)SiEt$_3$}(OEt$_2$)] **2-XI** (109 mg, 20.5 µmol, 1.0 eq.) was added iodine (52 mg, 20.5 µmol, 1.0 eq.). An immediate colour change was observed from colourless to a deep purple-red colour. A yellow solution was obtained after 19 h of stirring. ^{1}H NMR spectroscopy identified clean conversion to a single product [AlI$_2${N(Dipp)SiEt$_3$}(OEt$_2$)] **2-XII** and iodomethane. Removal of the volatiles under reduced pressure yielded a pale-pink oil. Addition of deuterated toluene (0.5 mL) and subsequent analysis identified pure [AlI$_2${N(Dipp)SiEt$_3$}(OEt$_2$)] **2-XIII** via ^{1}H NMR spectroscopy (>98%). Despite attempts, no crystals of SCXRD quality could be isolated. **Attempted Method B:** To a deuterated benzene (0.5 mL) solution of [AlMe$_2${N(Dipp)SiEt$_3$}(OEt$_2$)] **2-VI** (202 mg, 480 µmol, 1.0 eq.) was added iodine (381 mg, 1.50 mmol, 3.1 eq.). An immediate colour change was observed from colourless to deep red. The mixture was then heated to 80 °C for 18 h, and ^{1}H NMR spectroscopy identified an indiscernible mixture of products. Removal of the volatiles under reduced pressure yielded a dark red oily solid. Crystallisation attempts were undertaken with a combination of aromatic and aliphatic solvents, however, no crystals of SCXRD quality could be isolated. **^{1}H NMR** (400 MHz, toluene-d_8, 298 K): δ

= 7.01 – 6.97 (m, 3H, Dipp-aryl-*H*), 3.89 – 3.81 (m, 2H, Dipp-C*H*(CH_3)$_2$, 4H, Al-OCH_2CH$_3$), 1.28 (d, 12H, $^3J_{HH}$ = 6.9 Hz, Dipp-CH(CH_3)$_2$), 1.04 – 0.95 (m, 9H, Si(CH_2CH_3)$_3$, 6H, Al-OCH$_2$CH_3), 0.71 (t, 6H, $^3J_{HH}$ = 7.0 Hz, Si(CH_2CH$_3$)$_3$). **^{13}C{^{1}H} NMR** (101 MHz, Toluene-d_8, 298 K): δ = 146.9 (Dipp-*o*-*C*), 143.9 (Dipp-*i*-*C*), 124.6 (Dipp-*p*-*C*), 124.5 (Dipp-*m*-*C*), 70.4 (Al-O*C*H$_2$CH$_3$), 27.6 (Dipp-*C*H(CH$_3$)$_2$), 26.3 (Dipp-CH(*C*H$_3$)$_2$), 25.6 (Dipp-CH(*C*H$_3$)$_2$), 12.4 (Al-OCH$_2$*C*H$_3$), 8.7 (SiCH$_2$*C*H$_3$), 7.8 (Si*C*H$_2$CH$_3$). **^{29}Si{^{1}H} NMR** (79 MHz, C_6D_6, 298 K): δ = 8.1 (N-Si(CH_2CH_3)$_3$)

Synthesis of K[N(Dipp)SiEt$_3$] (2-XIII)

In a 250 mL Schlenk flask, HN(Dipp)SiEt$_3$ **2-III** (1.00g, 3.43 mmol, 1 eq) and potassium hydride (275 mg, 6.86 mmol, 2 eq) were added. Addition of tetrahydrofuran (100 mL) afforded a deep yellow solution with small bubbles of gas formation. The reaction mixture was stirred at ambient temperature for 18h whilst open to a slow flow of argon. The targeted product was extracted via cannula filtration and removal of the volatiles gave a grey solid. This was washed with hexane (3 × 10 mL) to afford K[N(Dipp)SiEt$_3$] **2-XIII** as a dark-grey solid (575 mg, 51%). **N.B.** SCXRD quality crystals of **2-XIII** as thin plates were obtained from a concentrated benzene solution kept at room temperature for 9 days. **^{1}H NMR** (400 MHz, C_6D_6, 298 K): δ = 7.04 (d, $^3J_{HH}$ = 7.4 Hz, 2H, Dipp-*m*-*H*), 6.60 (t, $^3J_{HH}$ = 7.4 Hz, 1H, Dipp-*p*-*H*), 3.93 (sept, $^3J_{HH}$ = 6.8 Hz, 2H, Dipp-C*H*(CH_3)$_2$), 1.26 – 1.21 (m, $^3J_{HH}$ = 6.7 Hz, 21H, 12H Dipp-CH(CH_3)$_2$, 9H Si-CH$_2$CH_3), 0.81 (q, $^3J_{HH}$ = 7.9 Hz, 6H, Si-CH_2CH$_3$).

Synthesis of Li[N(Dipp)SiEt$_3$] (2-XIV)

To a stirred pale-yellow solution of HN(Dipp)SiEt$_3$ **2-III** (0.53 g, 1.82 mmol, 1.0 eq.) in toluene (10 mL), was added dropwise *n*-butyllithium (1.18 mL of 1.6 M solution in hexanes, 1.89 mmol, 1.05 eq.) at –78 °C. The reaction mixture was slowly warmed to ambient temperature where it was stirred for a further 5 h, yielding a yellow solution, from which volatiles were removed under reduced pressure to give Li[N(Dipp)SiEt$_3$] **2-XIV** as a pale-yellow solid (0.49 g, 96%). **N.B.** SCXRD quality crystals of Li[N(Dipp)SiEt$_3$] **2-XIV** were obtained from a saturated toluene solution after 3 days at ambient temperature. **^{1}H NMR** (400 MHz, C_6D_6, 298 K): δ = 6.93 (d, $^3J_{HH}$ = 6.8 Hz, 2H, Dipp-aryl-*H*), 6.83 (dd, $^3J_{HH}$ = 8.2 Hz, $^4J_{HH}$ = 6.8 Hz, 1H, Dipp-aryl-*H*), 3.50 (sept, $^3J_{HH}$ = 6.8 Hz, 2H, Dipp-C*H*(CH_3)$_2$), 1.22 (d, $^3J_{HH}$ = 6.7 Hz, 6H, Dipp-CH(CH_3)$_2$), 1.04 (t, $^3J_{HH}$ = 7.9 Hz, 9H, SiCH$_2$CH_3), 0.81 (d, $^3J_{HH}$ = 6.8 Hz, 6H, Dipp-CH(CH_3)$_2$), 0.72 (q, $^3J_{HH}$ = 7.6 Hz, 6H, SiCH_2CH$_3$). **^{13}C{^{1}H} NMR** (101 MHz, C_6D_6, 298 K): δ = 149.7 (Dipp-*o*-*C*), 142.8 (Dipp-*i*-*C*), 124.0 (Dipp-*p*-*C*), 120.0 (Dipp-*m*-*C*), 27.1 (Dipp-CH(CH$_3$)$_2$), 25.3 (Dipp-CH(*C*H$_3$)$_2$), 25.0 (Dipp-CH(*C*H$_3$)$_2$), 8.8 (SiCH$_2$*C*H$_3$), 8.1 (Si*C*H$_2$CH$_3$). **^{29}Si{^{1}H} NMR** (79 MHz, C_6D_6, 298 K): δ = 5.8 (N-*Si*CH$_2$CH$_3$). **IR** ν_{max} (cm^{-1}) (Nujol): 3050(w), 2870(s), 1593(w), 1456(m), 1419(s), 1363(w), 1306(m), 1233(s), 1187(s), 1106(m), 1039(m), 1012(s),

977(m), 961(m), 939(m), 916(s), 878(w), 811(w), 770(s), 754(m), 708(s), 683(s), 671(m), 584(m), 555(w), 533(s), 454(s), 439(s). **E.A:** Anal. Calc. for $C_{18}H_{32}LiNSi$: C 72.68; H 10.84; N 4.71%. Found C 71.28; H 10.75; N 4.73%.

Synthesis of K[AlI$_3${N(Dipp)Si^{i}Pr$_3$}] (2-XV)

To a 50 mL Schlenk flask, K[N(Dipp)Si^{i}Pr$_3$] (0.219 g, 538 µmol, 1.0 eq.) and aluminium triiodide (0.2 g, 538 µmol, 1.0 eq.) were added. The mixture was dissolved in benzene (15 mL), and the resulting pale-yellow solution was stirred vigorously at ambient temperature for 18 h. The yellow solution was separated from a colourless precipitate via cannula filtration, and the filtrate was concentrated under reduced pressure to a volume of *ca.* 5 mL. From this solution, SCXRD quality crystals of K[AlI$_3${N(Dipp)Si^{i}Pr$_3$}] **2-XV** were isolated as large colourless blocks (0.211 g, 46%). **^{1}H NMR** (400 MHz, C_6D_6, 298 K): δ = 7.26 – 7.18 (m, 3H, Dipp-aryl-*H*, C_6H_6), 4.17 (sept, $^3J_{HH}$ = 7.5 Hz, 2H, Dipp-C*H*(CH$_3$)$_2$), 1.87 – 1.80 (m, 9H, Dipp-CH(C*H*$_3$)$_2$, SiC*H*(CH$_3$)$_2$), 1.50 (d, $^3J_{HH}$ = 6.7 Hz, 6H, Dipp-CH(C*H*$_3$)$_2$), 1.46 (d, $^3J_{HH}$ = 7.5 Hz, 18H, SiCH(C*H*$_3$)$_2$). **^{13}C{^{1}H} NMR** (101 MHz, C_6D_6, 298 K): δ = 150.1 (Dipp-*o*-*C*), 148.0 (Dipp-*i*-*C*), 146.0 (Dipp-*p*-*C*), 124.8 (Dipp-*m*-*C*), 28.2 (Dipp-*C*H(CH$_3$)$_2$), 27.4 (Dipp-CH(CH$_3$)$_2$), 25.7 (Dipp-CH(CH$_3$)$_2$), 20.8 (SiCH(*C*H$_3$)$_2$), 15.2 (Si*C*H(CH$_3$)$_2$). **IR** ν_{max} (cm^{-1}) (Nujol): 3100(w), 2863(s), 2722(s), 2544(m), 1853(w), 1615(w), 1572(m), 1544(m), 1489(m), 1385(m), 1366(w), 1344(w), 1304(w) 1161(w), 1048(m), 1028(m), 911(w), 866(m), 847(m), 796(s), 7345(w), 708(w), 656(m), 605(w), 544(w), 528(w), 446(w) **E.A:** Anal. Calc. for $C_{21}H_{38}AlI_3KNSi$: C 32.36; H 4.91; N 1.80%. Found C 31.07; H 5.03; N 2.21%.

Synthesis of Li[AlI$_3${N(Dipp)Si^{i}Pr$_3$}]$_n$ (2-XVI)

Method A: To a solution of [HN(Dipp)Si^{i}Pr$_3$] **2-I** (500 mg, 1.50 mmol, 1.0 eq.) in toluene (10 mL) was added *n*-butyllithium (1.03 mL of 1.6 M solution in hexanes, 1.65 mmol, 1.1 eq.) at ambient temperature. After stirring for 1 h, the yellow solution was added to a colourless solution of aluminium triiodide (612 mg, 1.5 mmol, 1.0 eq.) in toluene (10 mL) at ambient temperature. The reaction mixture was stirred at ambient temperature for 18 h. The subsequent yellow supernatant was separated from LiI precipitate via cannula filtration, and the filtrate concentrated toa volume of *ca.* 2 mL. Following 3 days at ambient temperature, crystals of SCXRD quality were isolated and identified as Li[AlI$_3${N(Dipp)Si^{i}Pr$_3$}]$_n$ **2-XVI**. After three further crystallisation crops, Li[AlI$_3${N(Dipp)Si^{i}Pr$_3$}]$_n$ **2-XVI** was obtained in a combined yield as a colourless solid (731.3 mg, 65%). **Method B:** In a J Young's NMR tube, a deuterated benzene (0.6 mL) solution of Li[N(Dipp)Si^{i}Pr$_3$] (5 mg, 14.7 µmol, 1.0 eq.) was charged with aluminium iodide (6 mg, 14.7 µmol, 1.0 eq.). Following sonication for 10 min, ^{1}H NMR spectroscopy identified the formation of targeted species Li[AlI$_3${N(Dipp)Si^{i}Pr$_3$}]$_n$ **2-**

XVI as the major product (77%), with by-product being decomposition to the proligand HN(Dipp)Si^{i}Pr$_3$ **2-I** (23%). **^{1}H NMR** (400 MHz, C_6D_6, 298 K): δ = 7.09 – 7.06 (m, 3H, Dipp-aryl-*H*), 3.82 (sept, $^3J_{HH}$ = 6.9 Hz, 2H, Dipp-C*H*(CH$_3$)$_2$), 1.55 (sept, $^3J_{HH}$ = 7.5 Hz, 3H, SiC*H*(CH$_3$)$_2$), 1.51 (d, $^3J_{HH}$ = 6.7 Hz, 6H, Dipp-CH(C*H*$_3$)$_2$), 1.29 (d, $^3J_{HH}$ = 6.8 Hz, 6H, Dipp-CH(C*H*$_3$)$_2$), 1.25 (d, $^3J_{HH}$ = 7.4 Hz, 18H, SiCH(C*H*$_3$)$_2$). **IR** ν_{max} (cm^{-1}) (Nujol): 3062(w), 2866(m), 1587(w), 1424(m), 1363(w), 1328(w), 1305(w), 1228(w), 1197(w), 1159(m), 1101(m), 1041(m), 875(s), 842(s), 814(s), 795(s), 771(s), 747(m), 706(s), 656(s), 598(m), 554(m), 542(m), 505(m), 445(m).

Synthesis of [AlI{N(Dipp)Si^{i}Pr$_3$}$_2$] (2-XVII)

To a solution of HN(Dipp)Si^{i}Pr$_3$ **2-I** (3.00 g, 9.0 mmol, 1.0 eq.) in toluene (30 mL) was added *n*-butyllithium (6.18 mL of 1.6 M solution in hexanes, 9.9 mmol, 1.12 eq.) at –78 °C dropwise. The colourless solution was warmed to ambient temperature, becoming yellow after 2 h, whereupon it was added to a colourless solution of aluminium iodide (1.83 g, 4.5 mmol, 0.5 eq.) in toluene (20 mL). The combination immediately yielded small amounts of colourless precipitate, and then the mixture was heated and stirred vigorously at 70 °C for 48 h. The yellow supernatant was separated from the colourless precipitate via cannula filtration at 70 °C. Upon cooling to ambient temperature, the solution was concentrated under reduced pressure to a volume of *ca.* 2 mL. The burnt-orange filtrate was stored overnight at room temperature to give [AlI{N(Dipp)Si^{i}Pr$_3$}$_2$] **2-XVII** as large colourless crystals, which were isolated via cannula filtration. The subsequent concentration of the filtrate to a volume of *ca*. 1 mL gave two more crystallisation crops of **2-XVII** in a combined yield as a colourless solid (3.19 g, 87%). **^{1}H NMR** (400 MHz, C_6D_6, 298 K): δ = 6.93 – 6.99 (m, 6H, Dipp-aryl-*H*), 3.71 (br, 4H, Dipp-C*H*(CH$_3$)$_2$), 1.69 (sept, $^3J_{HH}$ = 7.6 Hz, 6H, SiC*H*(CH$_3$)$_2$), 1.28 (d, $^3J_{HH}$ = 6.6 Hz, 12H, Dipp-CH(C*H*$_3$)$_2$), 1.16 (d, $^3J_{HH}$ = 7.6 Hz, 36H, SiCH(C*H*$_3$)$_2$), 0.91 (br., 12H, Dipp-CH(C*H*$_3$)$_2$). **^{13}C{^{1}H} NMR** (101 MHz, C_6D_6, 298 K): δ = 147.2 (Dipp-*o*-*C*), 143.5 (Dipp-*i*-*C*), 125.6 (Dipp-*p*-*C*), 125.5 (Dipp-*m*-*C*), 28.2 (Dipp-*C*H(CH$_3$)$_2$), 24.8 (Dipp-CH(*C*H$_3$)$_2$), 21.0 (SiCH(*C*H$_3$)$_2$), 17.2 (Si*C*H(CH$_3$)$_2$), **^{29}Si{^{1}H} NMR** (79 MHz, C_6D_6, 298 K): δ = 9.3 (N-*Si*CH(CH$_3$)$_2$). **IR** ν_{max} (cm^{-1}) (Nujol): 3057(w), 2867(m), 2727(w), 2544(w), 2050(w), 1574(w), 1543(w), 1454(m), 1422(m), 1385(m), 1364(w), 1302(w), 1230(w), 1157(m), 1145(w), 1067(w), 1040(w), 1017(w), 1004(w), 965(w), 918(w), 872(s), 848(m), 820(s), 790(s), 742(w), 706(s), 661(m), 636(w), 626(w), 605(w), 597(w) 541(w), 535(m), 505(w), 490(w), 458(w), 434(w), 405(w). **E.A:** Anal. Calc. for $C_{42}H_{76}AlIN_2Si_2$: C 61.58; H 9.35; N 3.42%. Found: C 61.72; H 9.45; N 3.48%.

Attempted synthesis of [AlI{N(Dipp)Si(^{t}Bu)Me$_2$}$_2$] from *in-situ* Li[N(Dipp)Si(^{t}Bu)Me$_2$], and isolation of [Li$_4${Dipp(^{t}BuMe$_2$Si)NSi^{t}Bu(Me)NDipp}$_2$I$_2$] (2-XVIII)

To a solution of HN(Dipp)Si(^{t}Bu)Me$_2$ **2-II** (500 mg, 1.7 mmol, 1.0 eq.) in toluene (20 mL) was added dropwise *n*-butyllithium (1.25 mL of 1.6 M solution in hexanes, 2.0 mmol, 1.2 eq.) at –78 °C. The colourless solution was warmed to ambient temperature and stirred for 18 h. A toluene (10 mL) solution of aluminium triiodide (357 mg, 875 μmol, 1.03 eq.) was prepared and added the stirred yellow solution of Li[N(Dipp)Si(^{t}Bu)Me$_2$]. The subsequent mixture was stirred at ambient temperature for 36 h, giving a pale-yellow mother liqour, which was separated from a grey precipitate via cannula filtration and the filtrate concentrated (*ca.* 3 mL) to crystallise the product. Following 11 days, SCXRD quality crystals were grown as colourless plates (2 – 5 examples) which could be picked and confirmed via X-ray diffraction as [Li$_4${Dipp(^{t}BuMe$_2$Si)NSi^{t}Bu(Me)NDipp}$_2$I$_2$] **2-XVIII**. Attempts to isolate the remaining material were conducted via the removal of volatiles under reduced pressure and washing with cold hexane (3 × 1 mL). Drying *in vacuo* yielded a pale-yellow oily powder (205 mg). However, ^{1}H NMR spectroscopy identified this solid to be an indiscernible mixture of products. **N.B.** Further attempts of purification or recrystallisation of a single species from the mixture were unsuccessful.

Attempted synthesis of [AlI{N(Dipp)SiEt$_3$}$_2$] from *in-situ* Li[N(Dipp)SiEt$_3$], and isolation of [Li$_4${Dipp(Et$_3$Si)NSiEt$_2$NDipp}$_2$I$_2$] (2-XIX)

Method A: To a deuterated toluene (0.5 mL) solution of Li[N(Dipp)SiEt$_3$] **2-XIV** (81 mg, 272 μmol, 2.0 eq.) in a J. Young's NMR tube, was added aluminium triiodide (56 mg. 136 μmol, 1.0 eq.). Immediate precipitation of a colourless solid from the yellow solution was observed. Following agitation at ambient temperature for 18 h, ^{1}H NMR spectroscopy identified that minimal reaction had occurred. Subsequently, the reaction mixture was heated to 68 °C for 23 h, following which the complete consumption of Li[N(Dipp)SiEt$_3$] **2-XIV** was observed via ^{1}H NMR spectroscopy and an indiscernible mixture of products was obtained. Following 48 h at ambient temperature, colourless crystals (2 – 5 examples) of SCXRD quality could be picked and confirmed via X-ray diffraction as [Li$_4${Dipp(Et$_3$Si)NSiEt$_2$NDipp}$_2$I$_2$] **2-XIX**. **N.B.** Crystals isolated within Nujol were also immediately analysed via infrared spectroscopy. **Attempted Method B:** To a solution of HN(Dipp)SiEt$_3$ **2-III** (250 mg, 857 μmol, 2 eq.) in toluene (20 mL) was added *n*-butyllithium (600 μL of 1.6 M solution in hexanes, 960 μmol, 1.1 eq.) dropwise at –78 °C. The colourless solution was warmed to ambient temperature, becoming yellow following 5 h of stirring at ambient temperature. Addition of this solution to a toluene (10 mL) solution of aluminium triiodide (174 mg, 427 μmol, 0.53 eq.) at ambient temperature led to immediate precipitate formation. Following stirring for 16 h, the pale-yellow supernatant was separated from the grey precipitate via cannula filtration. Analysis of the reaction

mixture via ^{1}H NMR spectroscopy identified the formation of a mixture of products. Recombination of crops and removal of volatiles under reduced pressure yielded an oily yellow solid (92 mg). **N.B.** Further attempts of purification or recrystallisation of a single species from the mixture were unsuccessful.

Optimised synthesis of [AlI{N(Dipp)SiMe$_3$}$_2$] (2-XX)

In a 350 mL J. Young's reaction flask, HN(Dipp)SiMe$_3$ **2-IV** (3.00 g, 12 mmol, 2 eq.) and $LiAlH_4$ (235 mg, 6.2 mmol, 1.03 eq.) were charged. The vessel was cooled to 0 °C, and diethyl ether (30 mL) was added. The resultant colourless suspension was stirred at 60 °C for 6 days. Upon cooling to ambient temperature, the transparent colourless solution was separated from the grey solid via cannula filtration. The filtrate was cooled to 0 °C, and iodotrimethylsilane (2.41 g, 1.64 mL, 12 mmol, 2 eq.) was added dropwise. Following 18 h of stirring at ambient temperature, the volatiles were removed under reduced pressure. The resultant colourless powder was washed with hexane (3 × 6 mL) and dried under reduced pressure. The isolated solid was identified via ^{1}H NMR spectroscopy as Li(OEt$_2$)[AlI$_2${N(Dipp)SiMe$_3$}$_2$] (3.67 g, 79%) prior to sublimation. To a 250ml Schlenk flask was charged Li(OEt$_2$)[AlI$_2${N(Dipp)SiMe$_3$}$_2$] (538 mg, 692 μmol, 1.0 eq.). Sublimation for 4 h at 143 °C (1.5×10^{-2} mbar) yielded [AlI{N(Dipp)SiMe$_3$}$_2$] **2-XX** as a colourless solid deposited as a band upon the glass walls above level of oil bath. Recrystallisation from pentane (3 mL) at –40 °C afforded [AlI{N(Dipp)SiMe$_3$}$_2$] **2-XX** as a white crystalline solid (339 mg, 75%). **N.B.** SCXRD quality crystals of [AlI{N(Dipp)SiMe$_3$}$_2$] **2-XX** were obtained from a saturated solution of pentane at –30 °C. **^{1}H NMR** (400 MHz, C_6D_6, 298 K): δ = 6.97 – 6.93 (m, 6H, Dipp-aryl-*H*), 3.54 (sept, $^{3}J_{HH}$ = 6.8 Hz, 4H, Dipp-C*H*(CH$_3$)$_2$, 1.20 (d, $^{3}J_{HH}$ = 6.8 Hz, 12H, Dipp-CH(C*H*$_3$)$_2$), 0.91 (d, $^{3}J_{HH}$ = 6.9 Hz, 12H, Dipp-CH(C*H*$_3$)$_2$), 0.29 (s, 18H, Si(C*H*$_3$)$_3$). **^{1}H NMR** (500 MHz, Toluene-d_8): δ = 6.94 – 6.88 (m, 6H, Dipp-aryl-*H*), 3.51 (d, $^{3}J_{HH}$ = 6.7 Hz, 4H, Dipp-C*H*(CH$_3$)$_2$), 1.18 (d, $^{3}J_{HH}$ = 6.8 Hz, 12H, Dipp-CH(C*H*$_3$)$_2$), 0.86 (d, $^{3}J_{HH}$ = 6.9 Hz, 12H, Dipp-CH(C*H*$_3$)$_2$), 0.26 (s, 18H, Si(C*H*$_3$)$_3$). **^{13}C{1H} NMR** (101 MHz, C_6D_6): δ = 145.9 (Dipp-aryl-*C*), 142.6 (Dipp-aryl-*C*), 125.2 (Dipp-aryl-*C*), 124.6 (Dipp-aryl-*C*), 28.5 (Dipp-*C*H(CH$_3$)$_2$), 26.0 (Dipp-CH(*C*H$_3$)$_2$), 24.3 (Dipp-CH(*C*H$_3$)$_2$), 4.5 (Si(*C*H$_3$)$_3$). **^{13}C{1H} NMR** (125 MHz, Toluene-d_8): δ = 145.8 (Dipp-aryl-*C*), 142.5 (Dipp-aryl-*C*), 125.2 (Dipp-aryl-*C*), 124.5 (Dipp-aryl-*C*), 28.5 (Dipp-*C*H(CH$_3$)$_2$), 25.9 (Dipp-CH(*C*H$_3$)$_2$), 24.2 (Dipp-CH(*C*H$_3$)$_2$), 4.4 (Si(*C*H$_3$)$_3$). **^{29}Si{^{1}H} NMR** (99 MHz, Toluene-d_8): δ = 8.1 (*Si*(CH$_3$)$_3$). **E.A:** Anal. Calc. for $C_{30}H_{52}AlIN_2Si_2$: C, 55.37; H, 8.05; N, 4.30%. Found: C, 55.44; H, 8.22; N, 4.30%.

Attempted synthesis of $Li(OEt_2)[AlI_2\{N(Dipp)Si(^tBu)Me_2\}_2]$, and consequential preparation of $Li[AlH_3\{N(Dipp)Si(^tBu)Me_2\}]$ (2-XXI)

In a 100 mL J. Young's reaction flask, $HN(Dipp)Si(^tBu)Me_2$ **2-II** (508 mg, 1.74 mmol, 2 eq.) and $LiAlH_4$ (33 mg, 871 μmol, 1.0 eq.) were added. The vessel was cooled to 0 °C, and the reactants dissolved in diethyl ether (5 mL). The reaction mixture was then stirred at 60 °C for 6 days. Upon cooling to ambient temperature, the resulting pale-yellow solution was separated from the grey solid via cannula filtration. Analysis of the reaction solution by ^1H NMR spectroscopy identified the formation of the postulated species $Li[AlH_3\{N(Dipp)Si(^tBu)Me_2\}]$ **2-XXI** (50%) along with $HN(Dipp)Si(^tBu)Me_2$ **2-II** (50%) in a 1:1 ratio. The reaction mixture was cooled to 0 °C, and iodotrimethylsilane (349 mg, 248 μL, 1.74 mmol, 2 eq.) was added, followed by warming to ambient temperature and stirring for 18 h. Analysis of the reaction solution by ^1H NMR spectroscopy identified the formation of the postulated species $[AlI_2\{N(Dipp)Si(^tBu)Me_2\}(OEt_2)]$ (50%) and $HN(Dipp)Si(^tBu)Me_2$ **2-II** (50%) in a 1:1 ratio. **^1H NMR** (400 MHz, C_6D_6, 298 K): δ = 7.14 – 6.98 (m, 3H, Dipp-aryl-*H*), 4.05 (sept, $^3J_{HH}$ = 6.8 Hz, 2H, Al-NDipp-C*H*$(CH_3)_2$), 3.60 (sept, $^3J_{HH}$ = 6.9 Hz, 2H, HNDipp-C*H*$(CH_3)_2$), 3.10 (q, $^3J_{HH}$ = 7.1 Hz, 4H, Li-OC*H*$_2$CH$_3$), 2.23 (s, 1H, N-*H*), 1.40 (d, $^3J_{HH}$ = 6.9 Hz, 6H, Al-NDipp-CH(C*H*$_3)_2$), 1.32 – 1.29 (m, 6H, Al-NDipp-CH(C*H*$_3)_2$, 9H, Al-NSi(CH$_3)_2$(C(C*H*$_3)_3$), 1.21 (d, $^3J_{HH}$ = 6.9 Hz, 12H, HNDipp-CH(C*H*$_3)_2$), 0.99 (sept, $^3J_{HH}$ = 7.8 Hz, 9H, HNSi(CH$_3)_2$(C(C*H*$_3)_3$), 0.93 (t, $^3J_{HH}$ = 7.1 Hz, 6H, Li-OCH$_2$C*H*$_3$), 0.23 (s, 6H, Al-NSi(C*H*$_3)_2$(C(CH$_3)_3$), 0.06 (s, 6H, HNSi(C*H*$_3)_2$(C(CH$_3)_3$).

Attempted synthesis of $Li(OEt_2)[AlI_2\{N(Dipp)SiEt_3\}_2]$, and preparation of $Li(OEt_2)[AlH_3\{N(Dipp)SiEt_3\}]$ (2-XXII)

In a 100 mL J. Young's reaction flask, $HN(Dipp)SiEt_3$ (791 mg, 2.71 mmol, 2.0 eq.) and $LiAlH_4$ (51 mg, 1.35 mmol, 1.0 eq.) were charged. The vessel was cooled to 0 °C and the reactants dissolved in diethyl ether (5 mL). The mixture was then stirred at 60 °C for 6 days. Upon cooling to ambient temperature, the resulting pale-yellow solution was separated from the grey solid via cannula filtration. Analysis of the reaction solution by ^1H NMR spectroscopy identified the formation of the postulated species $Li(OEt_2)[AlH_3\{N(Dipp)SiEt_3\}]$ (**2-XXII**) (50%) and $HN(Dipp)SiEt_3$ (50%) in a 1:1 ratio. The filtrate was cooled to 0 °C, and iodotrimethylsilane (543 mg, 586 μmol, 2.71 mmol, 2.0 eq.), followed by warming to ambient temperature and stirring for 18 h. Analysis of the reaction solution by ^1H NMR spectroscopy identified a mixture of species present within solution. **^1H NMR** (400 MHz, C_6D_6, 298 K): δ = 7.12 – 6.82 (m, 6H, Dipp-aryl-*H*), 3.49 (sept, $^3J_{HH}$ = 7.1 Hz, 2H, Al-NDipp-C*H*$(CH_3)_2$), 3.49 (sept, $^3J_{HH}$ = 6.9 Hz, 2H, HNDipp-C*H*$(CH_3)_2$), 3.09 (q, $^3J_{HH}$ = 7.1 Hz, 4H, Li-OC*H*$_2$CH$_3$), 2.22 (s, 1H, N-*H*), 1.42 (d, $^3J_{HH}$ = 6.9 Hz, 6H, Al-NDipp-CH(C*H*$_3)_2$), 1.30 (d, $^3J_{HH}$ = 6.7 Hz, 6H, Al-NDipp-

$CH(CH_3)_2$), 1.22 (d, $^3J_{HH}$ = 6.9 Hz, 12H, HNDipp-$CH(CH_3)_2$), 1.11 (t, $^3J_{HH}$ = 8.0 Hz, 9H, Al-$NSiCH_2CH_3$), 0.95 (t, $^3J_{HH}$ = 7.9 Hz, 9H, $HNSiCH_2CH_3$), 0.90 – 0.85 (m, 6H, Al-$NSiCH_2CH_3$, 6H, Li-OCH_2CH_3), 0.64 (q, $^3J_{HH}$ = 7.9 Hz, 6H, $HNSiCH_2CH_3$).

Synthesis of [Al_2(DAS)Me_4] (2-XXIV)

To a colourless toluene (5 mL) solution of H_2[DAS] **2-XXIII** (545 mg, 1.02 mmol, 1.0 eq.) in a 25 mL J. Young's reaction flask was added dropwise trimethylaluminium (1.1 mL, 1.0 M solution in toluene, 1.1 mmol, 1.1 eq.). Following 5 min of stirring, the reaction mixture was heated to 100 °C and stirred vigorously for 48 h. A colourless suspension formed, and the volatiles were removed from the reaction mixture under reduced pressure. The resultant colourless solid was washed with hexane (3 x 10 mL) and then extracted with toluene (5 mL) to give a yellow solution. Concentration of this solution (*ca.* 2 mL) and storage at –40 °C for 3 days yielded [Al_2(DAS)Me_4] **2-XXIV** as a white powder (217 mg, 34%). **N.B.** SCXRD quality crystals were prepared from saturated benzene solutions to a volume of *ca*. 1 mL, yielding **2-XXIV** as large colourless blocks. **^{1}H NMR** (400 MHz, C_6D_6, 349 K): δ = 7.25 (br, 4H, Ph-o-C*H*), 7.07 – 6.93 (m, 12H, Dipp-aryl-C*H*, Ph-aryl-C*H*), 3.77 (sept, $^3J_{HH}$ = 6.8 Hz, 4H, Dipp-C*H*$(CH_3)_2$), 0.99 (br, 24H, Dipp-$CH(CH_3)_2$), 0.01 (br, 12H Al-CH_3). **^{13}C{^{1}H} NMR** (101 MHz, C_6D_6, 348 K): δ = 145.3 (Aryl-*C*), 141.0 (Aryl-*C*), 136.8 (Aryl-*C*), 136.1 (Aryl-*C*), 129.8 (Aryl-*C*), 127.3 (Aryl-*C*), 125.0 (Aryl-*C*), 124.5 (Aryl-*C*), 29.1 (Dipp-*C*$H(CH_3)_2$), 25.5 (Dipp-$CH(CH_3)_2$), –1.9 (Al-CH_3). **IR** ν_{max} (cm^{-1}) (Nujol): 3370(w), 3069(w), 3052(w), 2961(s), 2933(s), 2870(m), 1590(w), 1428(s), 1383(m), 1363(m), 1332(w), 1252(m), 1198(m), 1156(w), 1108(m), 1042(w), 942(w), 913(w), 882(w), 852(w), 826(w), 787(m), 735(m), 698(s), 678(s), 645(s), 617(m), 591(m), 563(m), 537(w), 510(m), 487(m), 475(m), 460(m), 425(w).

Synthesis of [Al(DAS)Me(OEt_2)] (2-XXV)

Method A: To a J. Young's NMR tube containing a deuterated benzene (0.5 mL) solution of [Al_2(DAS)Me_4] **2-XXIV** (22 mg, 33.8 μmol, 1.0 eq.) was added diethyl ether (0.1 mL). No colour change from the colourless transparent solution was observed. ^{1}H NMR spectroscopy revealed the formation of a single product, identified as the targeted species **2-XXV** (>98%). **N.B.** Following transfer to a 10 mL Schlenk flask, the volatiles were removed under reduced pressure. Toluene (0.5 mL) was added to redissolve the colourless powder and concentrated to *ca.* 0.2 mL to crystallise. Following 4 days at –40 °C, crystals of SCXRD quality were isolated, which confirmed the formation of [Al(DAS)Me(OEt_2)] **2-XVII**. **Method B:** To a J. Young's NMR tube containing a deuterated benzene (0.5 mL) solution of [Al(DAS)I] **2-XXXIII** (25 mg, 36.4 μmol, 1.0 eq.), was added methyllithium powder (2.4 mg, 109 μmol, 3 eq.). Following overnight agitation, ^{1}H NMR

spectroscopy identified the predominant formation of targeted [Al(DAS)Me] (72%). In a glovebox, diethyl ether (0.1 mL) was added. Excess diethyl ether was removed *in vacuo* via co-evaporation of the deuterated benzene. The colourless oily solid was redissolved in deuterated benzene (0.5 mL), and ^{1}H NMR spectroscopy identified the formation of the targeted species [Al(DAS)Me(OEt$_2$)] **2-XXV** (83%). **N.B.** Attempts to purify and isolate **2-XXV** were unsuccessful. **^{1}H NMR** (400 MHz, C_6D_6, 298 K): δ = 7.48 (dd, $^{3}J_{HH}$ = 7.8 Hz, $^{4}J_{HH}$ = 1.7 Hz, 4H, Ph-*o*-C*H*), 7.14 – 6.96 (m, 6H, Dipp-aryl-C*H*, 6H, Ph-aryl-C*H*), 4.03 (sept, $^{3}J_{HH}$ = 7.1 Hz, 4H, Dipp-C*H*(CH$_3$)$_2$), 2.65 (br., 4H, Al-OC*H*$_2$CH$_3$), 1.05 (d, $^{3}J_{HH}$ = 6.7 Hz, 24H, Dipp-CH(C*H*$_3$)$_2$), 0.58 (br., 6H, Al-OCH$_2$C*H*$_3$), –0.06 (s, 3H, Al-C*H*$_3$). **^{13}C{^{1}H} NMR** (101 MHz, C_6D_6, 298 K): δ = 145.5 (Dipp-*o*-*C*), 145.2 (Dipp-*i*-*C*), 144.2 (Ph-*o*-*C*), 135.9 (Ph-*i*-*C*), 127.5 (Ph-*m*-*C*), 124.6 (Ph-*p*-*C*), 124.2 (Dipp-*p*-*C*), 122.3 (Dipp-*m*-*C*), 65.8 (Al-O*C*H$_2$CH$_3$), 28.5 (Dipp-*C*H(CH$_3$)$_2$), 25.7 (Dipp-CH(*C*H$_3$)$_2$), 13.8 (Al-OCH$_2$*C*H$_3$), –2.9 (Al-*C*H$_3$).

Synthesis of [Al(DAS)Me(THF)] (2-XXVI)

Method A: To a J. Young's NMR tube containing a deuterated benzene (0.5 mL) solution of [Al$_2$(DAS)Me$_4$] **2-XXIV** (35 mg, 53.9 μmol, 1.0 eq.) was added tetrahydrofuran (0.1 mL). No colour change from the colourless transparent solution was observed. ^{1}H NMR spectroscopy identified the clean formation of the targeted species **2-XXVI** (>98%). **N.B.** The solution was transferred to a 10 mL Schlenk flask where the volatiles were removed under reduced pressure. Toluene (0.5 mL) was added to redissolve the colourless powder and the solution concentrated to a volume of *ca*. 0.2 mL to crystallise. Following 6 days at -40 °C, crystals of SCXRD quality were isolated, which confirmed the formation of [Al(DAS)Me(THF)] **2-XXVI**. **Method B:** To a J. Young's NMR tube containing a deuterated benzene (0.5 mL) solution of [Al(DAS)I(THF)] **2-XXXV** (12 mg, 15.8 μmol, 1.0 eq.) was added methyllithium powder (1 mg, 47.4 μmol, 3.0 eq.). Following heating at 60 °C for 5 days, ^{1}H NMR spectroscopy identified near stoichiometric formation of the targeted compound. Residual tetrahydrofuran was removed through co-evaporation of deuterated benzene under reduced pressure. The solid was redissolved in deuterated benzene (0.5 mL), and ^{1}H NMR spectroscopy identified the formation of the targeted species [Al(DAS)Me(THF)] **2-XXVI** (88%). **N.B.** Attempts to purify and isolate **2-XXVI** were unsuccessful. **^{1}H NMR** (400 MHz, C_6D_6, 298 K): δ = 7.62 (dt, $^{3}J_{HH}$ = 7.9 Hz, $^{4}J_{HH}$ = 1.7 Hz, 2H, Ph-*o*-C*H*), 7.23 – 7.21 (m, 2H, Ph-*o*-C*H*), 7.14 – 7.03 (m, 6H, Dipp-aryl-C*H*, 6H, Ph-aryl-C*H*), 6.89 (t, $^{3}J_{HH}$ = 7.4 Hz, 2H, Ph-*p*-C*H*), 4.11 (sept, $^{3}J_{HH}$ = 6.8 Hz, 4H, Dipp-C*H*(CH$_3$)$_2$), 3.73 – 3.61 (m, 4H, Al-OC*H*$_2$CH$_2$), 1.22 – 1.18 (m, 4H, Al-OCH$_2$C*H*$_2$), 1.15 (d, $^{3}J_{HH}$ = 6.8 Hz, 12H, Dipp-CH(C*H*$_3$)$_2$), 0.99 (d, $^{3}J_{HH}$ = 6.7 Hz, 12H, Dipp-CH(C*H*$_3$)$_2$), -0.40 (s, 3H, Al-C*H*$_3$). **^{13}C{^{1}H} NMR** (101 MHz, C_6D_6, 298 K): δ = 145.4 (Dipp-*o*-*C*), 144.3 (Dipp-*i*-*C*), 137.1 (Ph-*i*-*C*), 135.2 (Ph-*o*-*C*), 129.2 (Ph-*p*-*C*), 126.9 (Ph-*m*-*C*), 124.0 (Dipp-*m*-*C*), 122.2 (Dipp-*p*-*C*), 70.9 (Al-O*C*H$_2$CH$_2$), 28.5

(Dipp-*C*H(CH_3)$_2$), 26.1 (Dipp-CH(*C*H_3)$_2$), 25.2 (Al-OCH$_2$*C*H$_2$), 24.7 (Dipp-CH(*C*H_3)$_2$), –10.6 (Al-*C*H_3). **^{29}Si{^{1}H} NMR** (79 MHz, C_6D_6, 298 K): δ = –40.0 (NDipp)$_2$*Si*Ph$_2$; from ^{1}H/^{29}Si HMBC. **IR** ν_{max} (cm^{-1}) (Nujol): 2863(m), 1589(w), 1432(m), 1381(w), 1360(w), 1311(w), 1249(m), 1200(m), 1109(m), 1098(m), 1040(m), 1011(w), 934(m), 863(w), 827(s), 792(s), 775(m) 743(w), 731(m), 711(m), 699(s), 675(m), 652(m), 595(w), 543(w), 507(m), 489(m), 448(w), 427(w).

Synthesis of [Al(DAS)I(OEt$_2$)] (2-XXVII)

Method A: To a 10 mL Schlenk flask, [Al(DAS)I] **2-XXXIII** (0.100 g, 0.146 mmol, 1.0 eq.) was charged. Diethyl ether (5mL) was added via cannula, quickly yielding a transparent colourless solution as part of an exothermic reaction. After standing for 30 min to return to room temperature, the colourless solution was concentrated to a volume of *ca.* 0.5 mL under reduced pressure, and placed in a –40 °C freezer. Following 16 h, large colourless crystalline blocks of SCRXD quality were grown, which were isolated, dried *in vacuo*, and washed with cold hexane (3 × 2 mL). Following the removal of volatiles, [Al(DAS)I(OEt$_2$)] **2-XXVII** was isolated as large colourless crystalline blocks (93 mg, 84%). **N.B.** Adding diethyl ether to [Al(DAS)I] **2-XXXIII** dropwise observes instantaneous boiling of the solvent; replications were conducted by initial dissolution in benzene (5 mL) followed by the addition of diethyl ether (1 mL). **Method B:** To a 350 mL J. Young's reaction flask, H$_2$[DAS] **2-XXIII** (300 mg, 561 μmol, 1.0 eq.) and Li[AlH$_4$] (21.3 mg, 617 μmol, 1.1 eq.) were added. Diethyl ether (5 mL) was added via cannula, and the reaction mixture was heated to 57 °C and stirred. Following 6 days at this temperature, the colourless solution was cooled to ambient temperature and iodotrimethylsilane (79 μL, 112 mg, 561 μmol, 1.0 eq.) was added dropwise. Following stirring at ambient temperature for 18 h, the volatiles were removed under reduced pressure, yielding a colourless solid. The solid was washed with hexane (3 × 5 mL), and dried *in vacuo* to give [Al(DAS)I(OEt$_2$)] **2-XXVII** as a colourless solid (344 mg, 81%). **Method C:** To a J. Young's NMR tube containing a colourless solid of Li[Al(DAS)I$_2$] **2-XXXII** (12 mg) contaminated with [Al(DAS)I] **2-XXXIII** (8 mg) in benzene (0.6 mL), diethyl ether (0.1 mL) was added, and the colourless transparent solution became slightly opaque with a fine colourless precipitate (presumably LiI). Following 30 min of standing at room temperature, analysis via ^{1}H NMR spectroscopy identified the clean formation of a single product identified as [Al(DAS)I(OEt$_2$)] **2-XXVII** (>98%). **^{1}H NMR** (400 MHz, C_6D_6, 343 K): δ = 7.67 (dd, $^3J_{HH}$ = 7.6 Hz, 1.9 Hz, 2H, Ph-*o*-C*H*), 7.23 (dd, $^3J_{HH}$ = 7.6, $^4J_{HH}$ = 1.9 Hz, 2H, Ph-*o*-C*H*), 7.18 (br, 2H, Aryl-*H*), 7.15 – 7.06 (m, 6H, Aryl-C*H*), 6.87 (t, $^3J_{HH}$ = 7.4z Hz, 2H, Ph-*m*-C*H*), 4.02 (sept, $^3J_{HH}$ = 6.8 Hz, 4H, Dipp-C*H*(CH_3)$_2$), 3.52 (q, $^3J_{HH}$ = 7.1 Hz, 4H, Al-OC*H*$_2$CH$_3$), 1.11 (d, $^3J_{HH}$ = 6.9 Hz, 12H, Dipp-CH(C*H*$_3$)$_2$), 1.01 (br., 12H, Dipp-CH(C*H*$_3$)$_2$), 0.69 (t, $^3J_{HH}$ = 7.1 Hz, 12H, Al-OCH$_2$C*H*$_3$). **^{13}C{^{1}H} NMR** (101 MHz, C_6D_6, 298 K): δ = 145.4 (Dipp-*o*-*C*), 144.0 (Dipp-*i*-*C*), 136.8 (Ph-*i*-*C*),

134.8 (Ph-*o*-*C*), 129.4 (Ph-*p*-*C*), 127.6 (Ph-*m*-*C*), 124.1 (Dipp-*m*-*C*), 122.3 (Dipp-*p*-*C*), 67.6 (Al-O*C*$H_2$$CH_3$), 28.6 (Dipp-*C*H($CH_3$)$_2$), 26.6 (Dipp-CH(*C*$H_3$)$_2$), 24.3 (Dipp-CH(*C*$H_3$)$_2$), 13.2 (Al-O$CH_2$*C*$H_3$). **IR** ν_{max} (cm^{-1}) (Nujol): 3070(w), 1845(m), 1585(w), 1429(s), 1312(w), 1248(s), 1199(m), 1109(m), 1102(m), 1039(w), 1029(w), 933(s), 828(s), 793(s), 777(m), 742(m), 731(m), 709(s), 699(s), 634(w), 625(w), 573(m), 547(m), 504(s), 488(m), 449(m), 432(m).

Optimised synthesis of Li_2[DAS] (2-XXIX)

To a hexane (30 mL) solution of H_2[DAS] **2-XXIII** (3.46 g, 6.47 mmol, 1.0 eq.) was added dropwise *n*-butyllithium (7.2 mL of 1.98 M solution in cyclohexane, 14.2 mmol, 2.2 eq.) at 0 °C. The reaction mixture was warmed to ambient temperature and stirred vigorously for 18 h. Subsequent cannula filtration isolated a colourless solid, which was washed with hexane (4 × 5 mL). Concentration of the mother liquor and washings afforded colourless blocks of SCXRD-quality crystals following standing for 18 h at 4 °C. Isolation of these crystals yielded pure Li_2[DAS] **2-XXIX** as identified via ^{1}H NMR spectroscopy (3.43 g, 97%). Characterisation data was consistent with that previously reported. However, NMR spectroscopic data was also collected in deuterated benzene (previous study used different solvents). **^{1}H NMR** (400 MHz, C_6D_6, 343 K): δ = 7.36 (br, 2H, Ph-o-C*H*), 7.10 – 6.87 (m, 12H, 4H Dipp-aryl-C*H,* 8H Ph-aryl-C*H*), 6.73 (t, $^3J_{HH}$ = 7.5 Hz , 2H, Ph-o-C*H*), 3.92 (br., 2H, Dipp-C*H*(CH_3)$_2$), 3.21 (br., 2H, Dipp-C*H*(CH_3)$_2$), 1.59 (br, 6H, Dipp-CH(C*H*$_3$)$_2$), 1.03 (br, 6H, Dipp-CH(C*H*$_3$)$_2$), 0.6 (br, 6H, Dipp-CH(C*H*$_3$)$_2$), 0.37 (br, 6H, Dipp-CH(C*H*$_3$)$_2$). **^{13}C{^{1}H} NMR** (101 MHz, C_6D_6, 298 K): δ = 160.0 (Aryl-*C*), 152.9 (Aryl-*C*), 149.0 (Aryl-*C*), 141.3 (Aryl-*C*), 135.7 (Aryl-*C*), 127.0 (Aryl-*C*), 124.7 (Aryl-*C*), 119.0 (Aryl-*C*), 29.2 (Dipp-*C*H(*C*H_3)$_2$), 28.0 (Dipp-*C*H(CH_3)$_2$), 24.6 – 23.8 (Dipp-CH(*C*H_3)$_2$).

Synthesis of Li_3[(NDipp)$_2$Si(Ph)(C_6H_4)] (2-XXX)

To a hexane (20 mL) solution of H_2[DAS] **2-XXIII** (3.03 g, 5.66 mmol, 1.0 eq.) was added *n*-butyllithium (6.1 mL of 1.98 M solution in cyclohexane, 11.9 mmol, 2.1 eq.) at ambient temperature. The reaction mixture was stirred vigorously for 18h, yielding a colourless precipitate, which was identified via ^{1}H NMR spectroscopy as Li_2[DAS] **2-XXIX**. Following filtration, the colourless solid was washed with hexane (3 × 5 mL). Concentration of the mother liquor and washings afforded yellowish block SCXRD quality crystals following standing for 18 h at 4 °C. Isolation of the afforded crystalline solid gave Li_3[(NDipp)$_2$Si(Ph)(C_6H_4)] **2-XXX** in a low combined yield (487 mg, 15%). **^{1}H NMR** (400 MHz, C_6D_6, 343 K): δ = 8.51 (d, $^3J_{HH}$ = 7.8 Hz, 1H, Ph-*o*-C*H*), 7.05 – 6.75 (m, 15H, Dipp-aryl-C*H*, Ph-aryl-C*H*), 3.33 (sept, $^3J_{HH}$ = 6.8 Hz, 2H, Dipp-C*H*(CH_3)$_2$), 2.57 (sept, $^3J_{HH}$ = 6.8 Hz, 2H,

Dipp-C*H*(CH_3)$_2$), 1.58 (d, $^3J_{HH}$ = 6.9 Hz, 6H, Dipp-CH(CH_3)$_2$), 1.06 (d, $^3J_{HH}$ = 6.5 Hz, 6H, Dipp-CH(CH_3)$_2$), 0.67 (d, $^3J_{HH}$ = 6.2 Hz, 6H, Dipp-CH(CH_3)$_2$), 0.26 (d, $^3J_{HH}$ = 7.2 Hz, 6H, Dipp-CH(CH_3)$_2$). **^{13}C{^{1}H} NMR** (101 MHz, C_6D_6, 298 K): δ = 165.1 (Aryl-*C*), 151.8 (Aryl-*C*), 138.8 (Aryl-*C*), 136.2 (Aryl-*C*), 133.7 (Aryl-*C*), 127.0 (Aryl-*C*), 125.9 (Aryl-*C*), 125.3 (Aryl-*C*), 120.8 (Aryl-*C*), 31.2 (Dipp-*C*H(CH_3)$_2$), 28.2 (Dipp-*C*H(CH_3)$_2$), 26.4 (Dipp-CH(*C*H_3)$_2$), 25.7 (Dipp-CH(*C*H_3)$_2$), 25.2 (Dipp-CH(*C*H_3)$_2$), 23.2 (Dipp-CH(*C*H_3)$_2$). **IR** ν_{max} (cm^{-1}) (Nujol): 3677(w), 2959(m), 2926(w), 2868(w), 1590(w), 1455(w), 1437(w), 1411(m), 1385(w), 1362(w), 1252(w), 1217(w), 1169(m), 1147(w), 1105(m), 1041(w), 897(m), 899(m), 760(s), 737(m), 701(s), 647(m), 574(w), 554(w), 532(w), 495(m), 456(m), 432(m).

Synthesis of K[Al(DAS)I$_2$] (2-XXXI)

Method A: To a 10 mL Schlenk flask, [Al(DAS)I] **2-XXXIII** (120 mg, 175 μmol, 1.0 eq.) and freshly ground (with a mortar and pestle) potassium iodide (120 mg, 723 μmol, 4.1 eq.) were charged. The addition of benzene (3 mL) and sonication for 5 min yielded a pale-yellow solution. The flask was left to stand at ambient temperature for 30 min, allowing the precipice to settle, after which the reaction mixture was filtered and concentrated to a volume of *ca.* 1 mL. Standing overnight at ambient temperature yielded K[Al(DAS)I$_2$] **2-XXXI** as an orange-tinged colourless crystalline solid (52 mg, 35%). **N.B.** Reactions were undertaken with freshly ground potassium iodide (15 mg, 90.3 μmol, 3 eq.) added to a deuterated benzene (0.5 mL) solution of [Al(DAS)I] (20 mg, 29.1 μmol, 1.0 eq.). Following 5 min of sonication, clean conversion to K[Al(DAS)I$_2$] **2-XXXI** was identified via ^{1}H NMR spectroscopy (>98%). **Method B:** To a 100 mL Schlenk flask, K_2[DAS] **2-XXVIII** (110 mg, 180 μmol, 1.0 eq.) and AlI_3 (77 mg, 177 μmol, 1.1 eq.) were charged. Following dissolution in toluene (5 mL), the colourless mixture was stirred at room temperature for 16 h. The precipitate was left to settle and was then separated from the pale-yellow solution via cannula filtration. Removal of volatiles from the filtrate under reduced pressure yielded an orange powder which was subsequently washed with hexane (3 x 1 mL). The orange powder was dried *in vacuo* and isolated as K[Al(DAS)I$_2$] **2-XXXI** (136 mg, 88%). **N.B.** SCXRD quality crystals were grown from a concentrated benzene solution of K[Al(DAS)I$_2$] **2-XXXI**, which was left at room temperature overnight. **^{1}H NMR** (400 MHz, C_6D_6, 298 K): δ = 7.71 (d, $^3J_{HH}$ = 7.8 Hz, 4H, Ph-*o*-C*H*), 7.11 – 7.06 (m, 4H, Dipp-aryl-C*H,* 6H, Ph-aryl-C*H*), 6.98 – 6.94 (m, 2H, Dipp-*p*-C*H*), 4.39 (sept, $^3J_{HH}$ = 6.6 Hz, 4H, Dipp-C*H*(CH_3)$_2$), 1.20 (d, $^3J_{HH}$ = 6.7 Hz, 24H, Dipp-CH(CH_3)$_2$). **^{13}C{^{1}H} NMR** (101 MHz, C_6D_6, 298 K): δ = 147.3 (Dipp-*o*-*C*), 143.7 (Dipp-*i*-*C*), 137.0 (Ph-*o*-*C*), 131.2 (Ph-*i*-*C*), 129.4 (Ph-*p*-*C*), 127.3 (Ph-*m*-*C*), 124.3 (Dipp-*p*-*C*), 122.8 (Dipp-*m*-*C*), 28.3 (Dipp-*C*H(CH_3)$_2$), 26.6 (Dipp-CH(*C*H_3)$_2$). **IR** ν_{max} (cm^{-1}) (Nujol): 2280(w),

2050(w), 1589(w), 1428(m), 1317(w), 1250(w), 1202(w), 1160(w), 1100(w), 1041(w), 928(w), 828(w), 791(m), 741(w), 701(m), 623(w), 596(w), 539(w), 497(m).

Synthesis of Li[Al(DAS)I$_2$] (2-XXXII)

Method A: Li_2[DAS] **2-XXIX** (22 mg, 40.2 μmol, 1.0 eq.) and AlI_3 (17 mg, 41.7 μmol, 1.05 eq.) were charged into a J. Young's NMR tube and deuterated benzene (0.5 mL) was added. The vessel was sonicated for 2 h at room temperature, which resulted in the clean conversion of Li[Al(DAS)I_2] **2-XXXII**, as identified by ^{1}H NMR spectroscopy (>98%). **NB:** Allowing this reaction mixture to stand at room temperature for two days afforded colourless crystals of sufficient quality for SCXRD. **Method B:** In a 10 mL Schlenk flask, [Al(DAS)I] **2-XXXIII** (120 mg, 175 μmol, 1.0 eq.) and freshly ground lithium iodide (120 mg, 897 μmol, 5.1 eq.) were added. The addition of benzene (3 mL) and sonication of the flask for 5 min yielded a yellow solution. The flask was left to stand at ambient temperature for 30 min, allowing the precipice to settle, after which the reaction mixture was filtered and the filtrate concentrated to a volume of *ca*. 1 mL. Standing overnight at ambient temperature yielded Li[Al(DAS)I_2] **2-XXXII** as a colourless crystalline solid (47 mg, 39%). **N.B.** To a solution of [Al(DAS)I] **2-XXXIII** (20 mg, 29.1 μmol, 1.0 eq.) in deuterated benzene (0.5 mL), freshly ground lithium iodide (15 mg, 112 μmol, 3.8 eq.) was added. Following 5 min of sonication, clean conversion to single product of Li[Al(DAS)I_2] **2-XXXII** was observed via ^{1}H NMR spectroscopy (>98%). **^{1}H NMR** (400 MHz, C_6D_6, 298 K): δ = 7.61 (d, $^3J_{HH}$ = 5.6 Hz, 4H, Ph-*o*-C*H*), 7.09 – 7.01 (m, 4H, Dipp-aryl-C*H,* 6H, Ph-aryl-C*H*), 6.91 (t, $^3J_{HH}$ = 7.5 Hz, 2H, Dipp-*p*-C*H*), 4.25 (sept, $^3J_{HH}$ = 6.8 Hz, 4H, Dipp-C*H*(CH_3)$_2$), 1.15 (d, $^3J_{HH}$ = 6.7 Hz, 24H, Dipp-CH(CH_3)$_2$). **^{13}C{^{1}H} NMR** (101 MHz, C_6D_6, 298 K): δ = 147.4 (Dipp-*o*-*C*), 146.3 (Dipp-*i*-*C*), 138.8 (Ph-*o*-*C*), 136.6 (Ph-*i*-*C*), 129.6 (Ph-*p*-*C*), 127.4 (Ph-*m*-*C*), 124.5 (Dipp-*p*-*C*), 122.5 (Dipp-*m*-*C*), 28.6 (Dipp-*C*H(CH_3)$_2$), 26.2 (Dipp-CH(CH_3)$_2$). **IR** ν_{max} (cm^{-1}) (Nujol): 3050(w), 2281(w), 1590(w), 1428(m), 1316(w), 1251(w), 1201(w), 1160(w), 1101(m), 1041(w), 998(w), 931(w), 828(m), 792(m), 759(w), 740(m), 700(s), 622(w), 596(w), 540(w), 497(s).

Synthesis of [Al(DAS)I] (2-XXXIII)

To a 25 mL Schlenk flask, Li_2[DAS] **2-XXIX** (575 mg, 1.05 mmol, 1.0 eq.) and AlI_3 (437 mg, 1.41 mmol, 1.02 eq.) were charged. Following dissolution of the solids in benzene (40 mL), the colourless solution was stirred at room temperature for 18 h. The mother liquor was separated from the colourless precipitate via cannula filtration. Benzene (40 mL) was added to the insoluble material within the mother reaction flask, which was heated to reflux and filtered at this temperature. The volatiles were

removed from the colourless filtrate *in vacuo*, and the residue was washed with hexane (10 mL). Drying the solid under reduced pressure afforded [Al(DAS)I] **2-XXXIII** as a colourless powder (492 mg, 68%). **N.B.** Despite numerous attempts, SCXRD quality crystals from aromatic and aliphatic solvents could not be yielded. Crystallisation attempts within coordinating solvents yielded the associated [Al(DAS)I(OEt_2)] **2-XXVII** and [Al(DAS)I(THF)] **2-XXXV** species reported herein. The attempted crystallisation by slowly cooling a saturated boiling benzene solution yielded a single crystalline sample of C-C bonded decomposition product (**2-XXXIV**). **^{1}H NMR** (800 MHz, C_6D_6, 343 K): δ = 7.54 (dd, $^3J_{HH}$ = 8.1 Hz, $^4J_{HH}$ = 1.4 Hz, 4H, Ph-*o*-C*H*), 7.10 (d, $^3J_{HH}$ = 7.6 Hz, 4H, Dipp-*m*-C*H*), 7.07 (tt, $^3J_{HH}$ = 7.5 Hz, $^4J_{HH}$ = 1.4 Hz, 2H, Ph-*p*-C*H*), 7.02 (t, $^3J_{HH}$ = 7.6 Hz, 4H, Ph-*m*-C*H*), 6.95 (t, $^3J_{HH}$ = 7.6 Hz, 2H, Dipp-*p*-C*H*), 4.11 (sept, $^3J_{HH}$ = 6.7 Hz, 4H, Dipp-C*H*(CH_3)$_2$), 1.11 (d, $^3J_{HH}$ = 6.8 Hz, 24H, Dipp-CH(C*H*$_3$)$_2$). **^{13}C{^{1}H} NMR** (201 MHz, C_6D_6, 298 K): δ = 147.1 (Dipp-*o*-*C*), 143.4 (Dipp-*i*-*C*), 138.3 (Ph-*i*-*C*), 136.5 (Ph-*o*-*C*), 129.7 (Ph-*p*-*C*), 127.5 (Ph-*m*-*C*), 124.4 (Dipp-*p*-*C*), 122.7 (Dipp-*m*-*C*), 28.9 (Dipp-*C*H(CH$_3$)$_2$), 25.8 (Dipp-CH(*C*H$_3$)$_2$). **^{29}Si NMR** (79 MHz, C_6D_6, 298 K): δ = –37.4 ((NDipp)$_2$*Si*Ph$_2$) Value inferred from ^{29}Si HSQC. **IR** ν_{max} (cm^{-1}) (Nujol): 3050(w), 1591(w), 1426(m), 1368(w), 1314 (w), 1280(m), 1201(w), 1098(m), 1040(w), 929(m), 898(w), 826(m), 814(w), 793(s), 776(m), 741(m), 726(m), 704(s), 677(m), 623(w). 595(w), 540(w), 501(s), 487(m), 452(w), 432(w).

Synthesis of [Al(DAS)I(THF)] (2-XXXV)

Method A: To a 10 mL Schlenk flask, [Al(DAS)I] **2-XXXIII** (100 mg, 146 μmol, 1.0 eq.) was added as a colourless solid. The addition of toluene (3 mL) yielded a pale-yellow suspension, to which tetrahydrofuran (1 mL) was added dropwise leading to the dissolution of the precipitate. Following 10 min of agitation, the reaction mixture was kept at ambient temperature for 3 h, which gave a dark-yellow solution. Co-evaporation of excess tetrahydrofuran with toluene (3 mL) was completed three times. This gave [Al(DAS)I(THF)] **2-XXXV** as a dark-yellow solid (82 mg, 74%). **Method B:** To a J. Young's NMR tube containing a suspension of [Al(DAS)I] **2-XXXIII** (12 mg, 17.5 μmol, 1.0 eq.) in benzene (0.4 mL) was added tetrahydrofuran (0.1 mL). An immediate colour change was observed to a pale-yellow solution. Following 30 min of sonication, analysis via ^{1}H NMR spectroscopy identified the clean formation of a single product [Al(DAS)I(THF)] **2-XXXV**. Excess tetrahydrofuran was removed through co-evaporated four times with deuterated benzene (0.5 mL) (>98%). **^{1}H NMR** (400 MHz, C_6D_6, 298 K): δ = 7.51 (dt, $^3J_{HH}$ = 6.6 Hz, $^4J_{HH}$ = 1.5 Hz, 2H, Ph-*o*-C*H*), 7.14 – 6.94 (m, 6H, Dipp-aryl-C*H,* 6H, Ph-aryl-C*H,*), 6.86 (t, $^3J_{HH}$ = 7.5 Hz, 2H, Ph-*m*-C*H*), 4.11 (sept, $^3J_{HH}$ = 6.8 Hz, 4H, Dipp-C*H*(CH_3)$_2$), 3.94 – 3.90 (m, 4H, Al-OC*H*$_2$CH$_2$), 1.23 – 1.19 (m, 4H, Al-OCH$_2$C*H*$_2$), 1.11 (d, $^3J_{HH}$ = 6.8 Hz, 12H, Dipp-CH(C*H*$_3$)$_2$), 1.07 (d, $^3J_{HH}$ = 6.7 Hz, 12H, Dipp-CH(C*H*$_3$)$_2$). **^{13}C{^{1}H} NMR** (101

MHz, C_6D_6, 298 K): δ = 145.7 (Dipp-*o*-*C*), 142.2 (Dipp-*i*-*C*), 136.8 (Ph-*i*-*C*), 135.4 (Ph-*o*-*C*), 129.0 (Ph-*p*-*C*), 127.1 (Ph-*m*-*C*), 124.4 (Dipp-*m*-*C*), 123.2 (Dipp-*p*-*C*), 72.8 (Al-O*C*$H_2$$CH_2$), 27.0 (Dipp-CH(*C*$H_3$)$_2$), 24.9 (Dipp-CH(*C*$H_3$)$_2$), 24.5 (Al-OC$H_2$*C*$H_2$). **IR** ν_{max} (cm^{-1}) (Nujol): 3362(w), 3047(w), 2865(m), 1589(s), 1428(m), 1360(w), 1335(w), 1311(w), 1256(m), 1227(w), 1198(w), 1172(w), 1100(m), 1041(m), 931(w), 902(m) 853(m), 826(m), 787(s), 742(m), 730(m), 701(s), 624(w), 595(w), 544(w), 502(m), 490(m), 465(w), 454(w), 431(w), 406(w).

2.8. References

[1] J. Hicks, P. Vasko, J. M. Goicoechea, S. Aldridge, *Nature* **2018**, *557*, 92-95.
[2] J. Hicks, P. Vasko, J. M. Goicoechea, S. Aldridge, *Angew. Chem. Int. Ed. Engl.* **2021**, *60*, 1702-1713.
[3] M. P. Coles, M. J. Evans, *Chem. Commun.* **2023**, *59*, 503-519.
[4] C. Jones, G. A. Koutsantonis, *Aust. J. Chem.* **2013**, *66*, 1115-1117.
[5] M. Weller, T. Overton, J. Rourke, F. Armstrong, *Inorganic Chemistry*, 6th ed., Oxford University Press, USA, **2014**.
[6] S. Ganguly, A. Ghosh, *Acc. Chem. Res.* **2019**, *52*, 2003-2014.
[7] R. L. Melen, *Science* **2019**, *363*, 479-484.
[8] J. Clayden, N. Greeves, S. Warren, *Organic Chemistry*, OUP Oxford, **2012**.
[9] O. Kysliak, H. Görls, R. Kretschmer, *Dalton Trans.* **2020**, *49*, 6377-6383.
[10] C. Jones, S. Aldridge, T. Gans-Eichler, A. Stasch, *Dalton Trans.* **2006**, 5357-5361.
[11] R. J. Schwamm, M. D. Anker, M. Lein, M. P. Coles, *Angew. Chem. Int. Ed. Engl.* **2019**, *58*, 1489-1493.
[12] A. Heine, D. Stalke, *Angew. Chem. Int. Ed. Engl.* **1992**, *31*, 854-855.
[13] R. Martin, S. L. Buchwald, *Acc. Chem. Res.* **2008**, *41*, 1461-1473.
[14] R. J. Schwamm, M. S. Hill, H.-Y. Liu, M. F. Mahon, C. L. McMullin, N. A. Rajabi, *Chem. Eur. J.* **2021**, *27*, 14971-14980.
[15] R. Chinchilla, C. Nájera, *Chem. Rev.* **2007**, *107*, 874-922.
[16] R. J. Schwamm, M. P. Coles, M. S. Hill, M. F. Mahon, C. L. McMullin, N. A. Rajabi, A. S. S. Wilson, *Angew. Chem. Int. Ed. Engl.* **2020**, *59*, 3928-3932.
[17] S. Kurumada, S. Takamori, M. Yamashita, *Nat. Chem.* **2020**, *12*, 36-39.
[18] G. Feng, K. L. Chan, Z. Lin, M. Yamashita, *J. Am. Chem. Soc.* **2022**, *144*, 22662-22668.
[19] S. Grams, J. Eyselein, J. Langer, C. Färber, S. Harder, *Angew. Chem. Int. Ed. Engl.* **2020**, *132*, 16116-16120.
[20] S. Grams, J. Mai, J. Langer, S. Harder, *Organometallics* **2022**, *41*, 2862-2867.
[21] K. Koshino, R. Kinjo, *J. Am. Chem. Soc.* **2020**, *142*, 9057-9062.
[22] C. Yan, R. Kinjo, *Angew. Chem. Int. Ed. Engl.* **2022**, *61*, e202211800.
[23] D. Sarkar, P. Vasko, A. F. Roper, A. E. Crumpton, M. M. D. Roy, L. P. Griffin, C. Bogle, S. Aldridge, *J. Am. Chem. Soc.* **2024**, *146*, 11792-11800.
[24] Y. R. Luo, *Comprehensive Handbook of Chemical Bond Energies*, CRC Press, **2007**.
[25] H. Nicholas, C. Goodwin, J. Kragskow, S. Lockyer, D. Mills, *Molecules* **2018**, *23*, 1138.
[26] a) R. West, M. J. Fink, J. Michl, *Science* **1981**, *214*, 1343-1344; b) M. Yoshifuji, I. Shima, N. Inamoto, K. Hirotsu, T. Higuchi, *J. Am. Chem. Soc.* **1981**, *103*, 4587-4589.
[27] a) A. Sekiguchi, S. Inoue, M. Ichinohe, Y. Arai, *J. Am. Chem. Soc.* **2004**, *126*, 9626-9629; b) P. J. Davidson, M. F. Lappert, R. Pearce, *Acc. Chem. Res.* **1974**, *7*, 209-217.
[28] J. Hicks, C. Jones, *Inorg. Chem.* **2013**, *52*, 3900-3907.
[29] D. L. Kays, *Chem. Soc. Rev.* **2016**, *45*, 1004-1018.

[30] I. C. Cai, M. I. Lipschutz, T. D. Tilley, *Chem. Commun.* **2014**, *50*, 13062-13065.
[31] M. Asay, C. Jones, M. Driess, *Chem. Rev.* **2011**, *111*, 354-396.
[32] M. S. Hill, P. B. Hitchcock, *Organometallics* **2002**, *21*, 3258-3262.
[33] M. Veith, *Chem. Rev.* **1990**, *90*, 3-16.
[34] P. Mastropierro, A. R. Kennedy, E. Hevia, *Eur. J. Inorg. Chem.* **2021**, 1016-1022.
[35] P. Mastropierro, Z. Livingstone, S. D. Robertson, A. R. Kennedy, E. Hevia, *Organometallics* **2020**, *39*, 4273-4281.
[36] Z. Livingstone, A. Hernán-Gómez, S. E. Baillie, D. R. Armstrong, L. M. Carrella, W. Clegg, R. W. Harrington, A. R. Kennedy, E. Rentschler, E. Hevia, *Dalton Trans.* **2016**, *45*, 6175-6182.
[37] D. R. Armstrong, W. Clegg, A. Hernán-Gómez, A. R. Kennedy, Z. Livingstone, S. D. Robertson, L. Russo, E. Hevia, *Dalton Trans.* **2014**, *43*, 4361-4369.
[38] S. M. I. Al-Rafia, P. A. Lummis, M. J. Ferguson, R. McDonald, E. Rivard, *Inorg. Chem.* **2010**, *49*, 9709-9717.
[39] S. M. Mansell, C. A. Russell, D. F. Wass, *Inorg. Chem.* **2008**, *47*, 11367-11375.
[40] B. Nekoueishahraki, H. W. Roesky, G. Schwab, D. Stern, D. Stalke, *Inorg. Chem.* **2009**, *48*, 9174-9179.
[41] a) M. Veith, J. Frères, P. König, O. Schütt, V. Huch, J. Blin, *Eur. J. Inorg. Chem.* **2005**, 3699-3710; b) M. Veith, H. Lange, O. Recktenwald, W. Frank, *J. Organomet. Chem.* **1985**, *294*, 273-294; c) M. Khandelwal, D. R. Powell, R. J. Wehmschulte, *Eur. J. Inorg. Chem.* **2011**, 521-526.
[42] B. Shen, L. Ying, J. Chen, Y. Luo, *Inorganica Chim. Acta* **2008**, *361*, 1255-1260.
[43] S. D. Waezsada, F.-Q. Liu, E. F. Murphy, H. W. Roesky, M. Teichert, I. Usón, H. G. Schmidt, T. Albers, E. Parisini, M. Noltemeyer, *Organometallics* **1997**, *16*, 1260-1264.
[44] Y. W. Chao, P. A. Wexler, D. E. Wigley, *Inorg. Chem.* **1989**, *28*, 3860-3868.
[45] M. Schiefer, N. D. Reddy, H. W. Roesky, D. Vidovic, *Organometallics* **2003**, *22*, 3637-3638.
[46] C. Dohmeier, C. Robl, M. Tacke, H. Schnöckel, *Angew. Chem. Int. Ed. Engl.* **1991**, *30*, 564-565.
[47] a) C. Cui, H. W. Roesky, H.-G. Schmidt, M. Noltemeyer, H. Hao, F. Cimpoesu, *Angew. Chem. Int. Ed. Engl.* **2000**, *39*, 4274-4276; b) B. Qian, D. L. Ward, M. R. Smith, *Organometallics* **1998**, *17*, 3070-3076.
[48] S. D. Waezsada, C. Rennekamp, H. W. Roesky, C. Röpken, E. Parisini, *ZAAC* **1998**, *624*, 987-990.
[49] M. A. Petrie, K. Ruhlandt-Senge, P. P. Power, *Inorg. Chem.* **1993**, *32*, 1135-1141.
[50] D. K. Kennepohl, S. Brooker, G. M. Sheldrick, H. W. Roesky, *Chem. Ber.* **1991**, *124*, 2223-2225.
[51] C. Schädle, C. Meermann, K. W. Törnroos, R. Anwander, *Eur. J. Inorg. Chem.* **2010**, 2841-2852.
[52] I. C. Cai, M. S. Ziegler, P. C. Bunting, A. Nicolay, D. S. Levine, V. Kalendra, P. W. Smith, K. V. Lakshmi, T. D. Tilley, *Organometallics* **2019**, *38*, 1648-1663.
[53] R. Murugavel, N. Palanisami, R. J. Butcher, *J. Organomet. Chem.* **2003**, *675*, 65-71.
[54] C.-L. Pan, W. Chen, J. Song, *Organometallics* **2011**, *30*, 2252-2260.
[55] D. Yang, J. Guo, H. Wu, Y. Ding, W. Zheng, *Dalton Trans.* **2012**, *41*, 2187-2194.
[56] V. Snieckus, *Chem. Rev.* **1990**, *90*, 879-933.

3. An Acyclic Aluminyl Anion

3.1. Introduction

3.1.1. Previous Aluminyl Anions Accessible in the form of Transition Metal Complexes

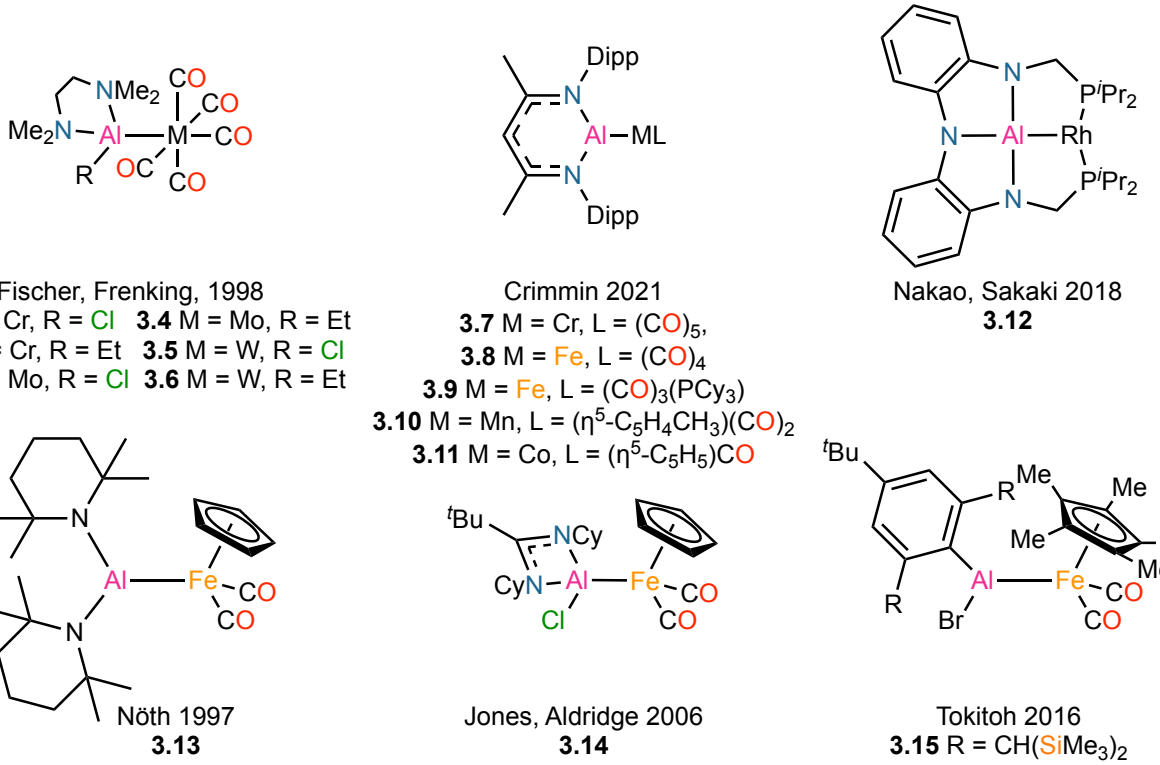

Figure 3.1: Selected aluminium metalloligands incorporated into transition metal complexes: neutral aluminylene centres (L-type) ***3.1-3.6****,[1] and* ***3.7-3.11****,[2] Lewis acidic acceptor (Z-type)* ***3.12****[3] and anionic aluminyl centres (b) (X-type) coordination* ***3.13****,[4]* ***3.14****[5] and* ***3.15****.[6]*

Previously, neutral and anionic aluminium systems have served as a metalloligand within a variety of transition metal complexes (Figure 3.1).[2] These metalloligands were reported to form supported or unsupported metal-metal bonds with transition metal centres.[2] Neutral metalloligands may bond as a two-electron donor aluminylene **3.1-3.11** (L-type),[1-2] or as a two-electron acceptor **3.12** (Z-type) system.[3] More relevant to this work, aluminyl metalloligands **3.13-3.15** serve one-electron donor (X-type) ligands generating complexes of $X_2Al–M$ or $LX_2Al–M$ forms (Figure 3.1) (M = transition metal, X_2 = two monoanionic ligands or one dianionic ligand, L = neutral ligand).[7] These examples serve as the heavier analogues of the more widely known boryl ligands, and were previously the most common examples of anionic aluminium organometallics.[8] The reactive and catalytic functions of these complexes are of ongoing inquiry,[2, 9] with focusses upon metalloligand lability and reactivity at the M-Al bond.[9] Aluminyl-stabilised transition metal complexes have expanded with the report of isolable alkali metal aluminyl anions. These new systems featuring nucleophilic aluminium(I) centres serve as valuable reagents for a variety of new and applicable chemical transformations.

3.1.2. Synthetic Library of Aluminyl Anions

Following the initial report of aluminyl anions in 2018,[10] the synthetic library of these complexes has seen ongoing development and advancement in coordination motif and reactivity.[11] Whilst the majority of these nucleophiles are accessible through the reduction of corresponding aluminium(III) halide precursors (as presented in **Chapter 2**), a handful of species are afforded through other synthetic methodologies. All currently reported aluminyl anions and their preparative methods are reported herein.

3.1.2.1. *N,N*-Diamido Aluminyl Anions

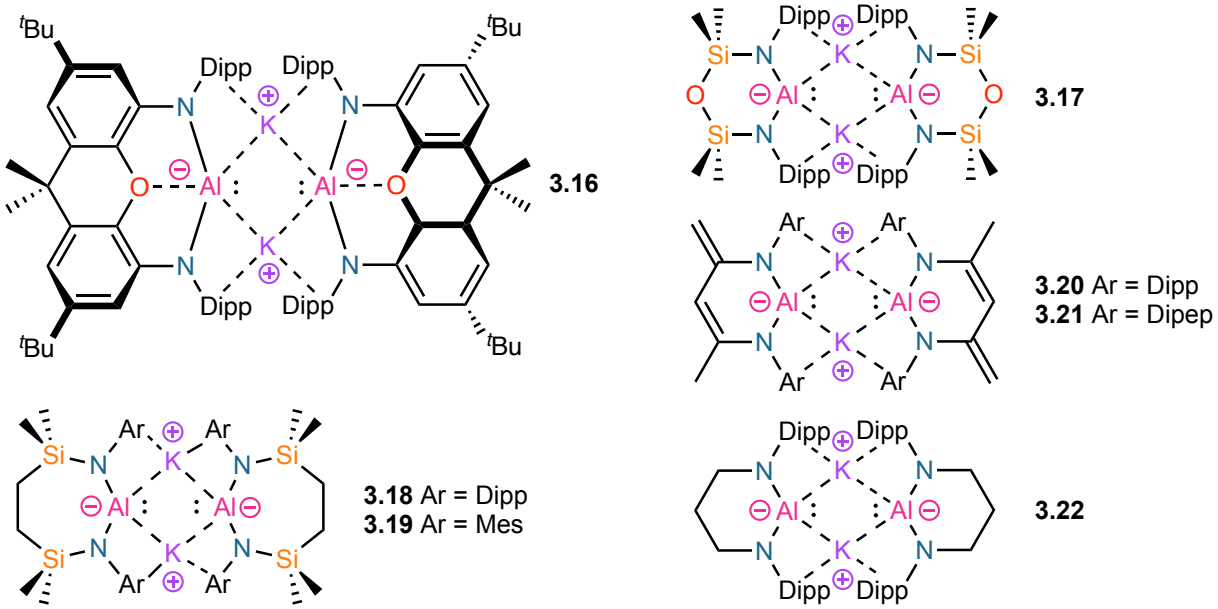

Figure 3.2: Library of N,N-diamido-bound aluminyl anion complexes as reported from groups of Aldridge and Goicoechea ***3.16****,[10] Coles* ***3.17****,[12] Hill and McMullin* ***3.18-3.19****,[13] Harder* ***3.20-3.21****,[14] and Yamashita* ***3.22****.[15] (Dipep = 2,6-C(H)Et$_2$-C$_6$H$_3$)*

Reported by Aldridge, Goicoechea and coworkers, the first aluminyl anion **3.16** employed the bulky rigid diamido xanthene $[NON]^{2-}$ ligand system (Figure 3.2).[10] The highly reactive species, $[K_2\{Al(NON)\}_2]$ **3.16** was isolated as bold-yellow crystals. From the solid-state structure, the aluminium(I) centres were >6 Å apart, highlighting a lack of Al-Al bonding interaction. Moreover, the O backbone to aluminium interactions were identified as being relatively weak from their corresponding distance (2.28(2) Å), accompanying the pseudo-tridentate, 8-membered metallocycle of the $[NON]^{2-}$ ligand. Supported through bridging potassium-arene interactions, **3.16** exists as a dimer within the solid state, the preservation of which in the solution state was confirmed via ^{1}H DOSY NMR (Diffusion Ordered Spectroscopy) spectroscopic experiments.[10]

Following this initial report in 2018,[10] further aluminyl anions were reported featuring dianionic amido ligands (Figure 3.2). In 2019, Coles and coworkers reported the 6-membered metallocyclic potassium aluminyl anion $[K_2\{Al(^{Si}NON)\}_2]$ **3.17** employing the $[^{Si}NON]^{2-}$ ligand scaffold (^{Si}NON = $[O\{Si(Me)_2N(Dipp)\}_2]^{2-}$).[12] This 6-membered system featured a strictly bidentate coordination made of the ligand, as identifiable from long Al···O distances of 3.418(2) and 3.356(2) Å via X-ray crystallography. An observed lack of residual electron density in Al–H ligand expected regions, spectroscopic data, and later reactivity profiles confirmed **3.17** as the second isolable aluminyl anion.[12]

In 2020, Hill, McMullin and coworkers reported the isolation of the first 7-membered metallocycle aluminyl anion $[K_2\{Al(SiN^{Dipp})\}_2]$ **3.18** ($[SiN^{Dipp}]^{2-}$ = $[\{CH_2SiMe_2N(Dipp)\}_2]^{2-}$).[13a] In 2021, the same group also reported the first aluminyl anion $[K_2\{Al(SiN^{Mes})\}_2]$ **3.19** ($[SiN^{Mes}]^{2-}$ = $[\{CH_2SiMe_2N(Mes)\}_2]^{2-}$) to feature the less bulky Mes aryl substituents upon the hard *N*,*N*-coordination atoms.[13b] All of the *N*,*N*-diamido aluminyl anions discussed to this point were prepared from the direct reduction of neutral aluminium(III) iodide precursors by 2-electron reductions with a potassium reducing agent (potassium graphite **3.16**,[10] potassium mirror **3.17**,[12] **3.18**,[13a] **3.19**).[13b] However, these are not the only methods through which *N*,*N*-diamido aluminyl anions have been prepared.

Reported by Harder and coworkers in 2020, ligand deprotonation of Roesky's neutral aluminium(I) species $[Al(^{Dipp}Nacnac)]$ ($[^{Dipp}Nacnac]^-$ = ß–diketiminate $[HC\{C(Me)Dipp\}_2]^-$),[16] enabled the isolation of 6-membered metallocycle aluminyl anion **3.20**.[14a] Stabilised by another diamido, dianionic ligand $[DBDI^{Dipp}]^{2-}$ ($DBDI^{Dipp}$ = $[H_2C{=}C(NDipp){-}C(H){=}C(Me){-}NDipp]^{2-}$), this species was accessed through the addition of K[R] (R = CH_2SiMe_3, $N(SiMe_3)_2$) to $[Al(^{Dipp}Nacnac)]$, whereby the potassium base yielded a facile deprotonation of a methyl group in the monoanionic $[^{Dipp}Nacnac]^{1-}$ backbone. As such, the $[DBDI^{Dipp}]^{2-}$ ligand is unsymmetric about the backbone (Figure 3.2). Analogously, deprotonation of the bulkier analogue $[Al(^{Dipep}Nacnac)]$ with K[R] yielded the "superbulky" Dipep stabilised system $[K_2\{Al(DBDI^{Dipep})\}_2]$ **3.21** (Dipep = 2,6-C(H)Et_2-C_6H_3).[14b] Notably, the isolation of **3.21** was solvent dependent, whereby deprotonation within benzene afforded a mixture of **3.21** and a ligand C–H activation product, whereas hexane exclusively yielded the target aluminyl anion **3.21**.[14b]

In 2022, Yamashita and coworkers reported the latest *N*,*N*-diamido metallocyclic aluminyl anion **3.22** accessed from the reduction of corresponding aluminum(III) iodide precursor with NaK_2.[15] Incorporating a saturated bis(2,6-diisopropylphenyl)-1,3-propanediamine $[NCCCN]^{2-}$ ligand framework, the species $[K_2\{Al(NCCCN)\}_2]$ **3.22** was reminiscent of aluminyl anions **3.20** and **3.21** featuring two hard *N*-coordination atoms and containing the aluminium(I) centre within a 6-membered

organo-amido-metallocycle. Despite the prevalence of *N*,*N*-diamido aluminyl anions within the literature, advancement within mixed *C*,*N*-(alkyl)(amido) and *C*,*C*-dialkyl systems have further expanded the catalogue and capabilities of this novel class of main group species.[11, 17]

3.1.2.2. *C*,*N*-(Alkyl)(Amido) and *C*,*C*-Di(Alkyl) Aluminyl Anions

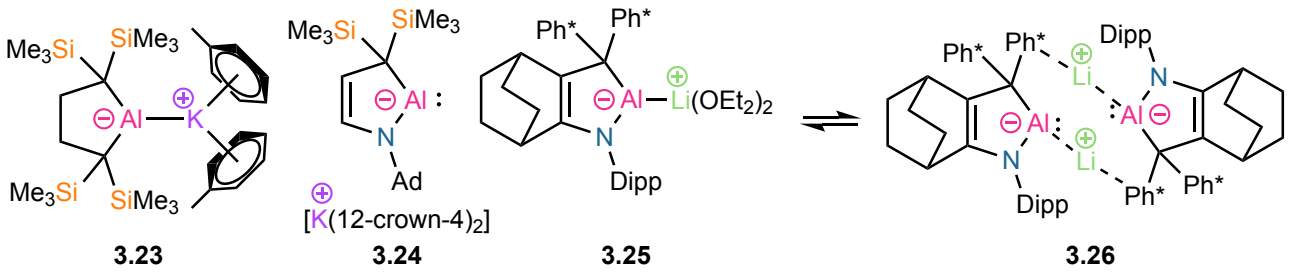

3.23 **3.24** **3.25** **3.26**

Figure 3.3: Library of C,N-(alkyl)(amido) and C,C-dialkyl aluminyl anions as reported from the groups of Yamashita ***3.23****,*[18] *and Kinjo* ***3.24****,*[19] *and* ***3.25*** *and its analogous dimer* ***3.26****.*[20]
(Ad = 1-adamantyl, Ph = 3,5-^{t}Bu$_2$-C$_6$H$_3$)*

Different from the *N*,*N*-diamido-stabilised species reported above, three further aluminyl anion systems were reported utilising alkyl substitutions within their supporting ligands (Figure 3.3). Initially reported in 2020, the aluminyl anion complexes [(toluene)$_2$K−Al(C^{Si})] **3.23** ([C^{Si}]$^{2-}$ = [{C(SiMe$_3$)$_2$CH$_2$}$_2$]$^{2-}$),[18] and [K(12-crown-4)$_2$][Al(C^{Si}N^{Ad})] **3.24** ([C^{Si}N^{Ad}]$^{2-}$ = [(Me$_3$Si)$_2$C(CH)$_2$NAd]$^{2-}$),[19] were isolated by the groups of Yamashita and Kinjo, respectively (Figure 3.3). Markedly, these species both feature the stabilised aluminyl anion centre within a 5-membered metallocycle. The electronic structures of **3.23** and **3.24** were calculated by DFT and showed that the incorporation of less electronegative alkyl-groups at aluminium raised the HOMO energy relative to the diamido derivatives.[11]

Chiefly different to the abovementioned species (diamido aluminyl anions **3.16**-**3.19**) prepared via two-electron reductions of corresponding aluminium(III) halide precursors, the alkyl-substituted aluminyl anions **3.23** and **3.24** were prepared via two single-electron reductions of aluminium(III) halide precursors (Scheme 3.1). First the halide precursors were reduced to the isolable and corresponding homoatomic aluminium(II) dialanes [R$_2$Al–AlR$_2$] with excess lithium and potassium graphite respectively. The aluminium(II) species were further reduced with Na:K or potassium congruently in yielding the corresponding aluminium(I) aluminyl anions **3.23** and **3.24**.

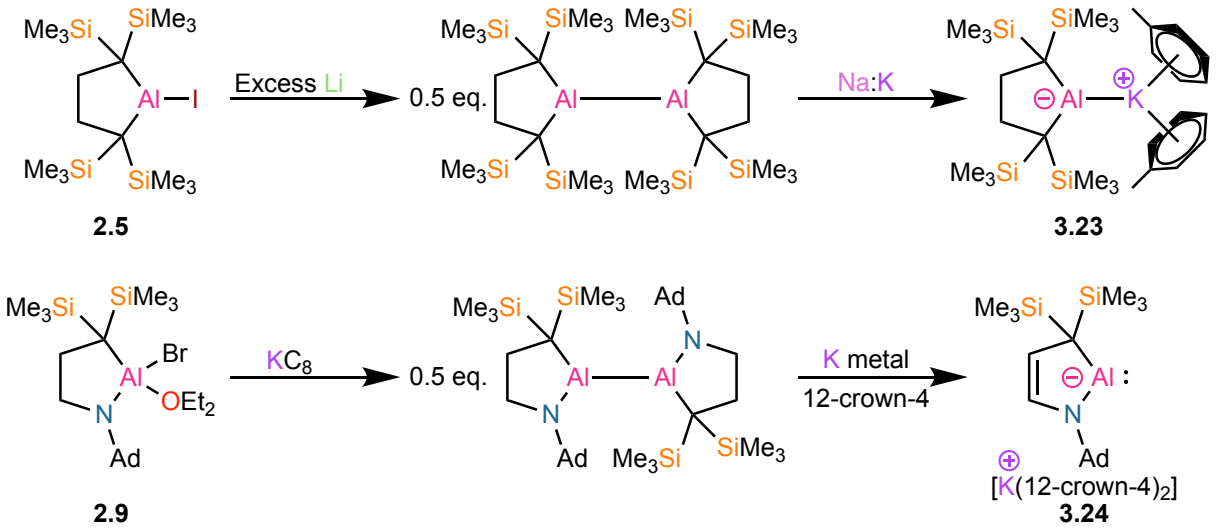

*Scheme 3.1: Preparation of the aluminyl anions (**3.23**, **3.24**) via the subsequent reductions of aluminium(III) halides.*

Expanding the ligand scaffold and varying the alkyl substituents, Kinjo and Yan reported the 5-membered aluminyl anion **3.25** featuring a rigid bicyclic backbone.[20] $[(Et_2O)_2Li–Al(C^{Ph*}N^{Dipp})]$ **3.25** was prepared via reduction of the corresponding aluminium(III) iodide precursor with excess lithium metal afforded and crystallised from diethyl ether ($[C^{Ph*}N^{Dipp}]^{2-} = [(Ph*)_2C(CH)_2NDipp]^{2-}$, Ph* = 3,5-^{t}Bu$_2$-C$_6H_3$). Recrystallisation of the species from hexane afforded the dimeric system $[Li_2\{Al(C^{Ph*}N^{Dipp})\}_2]$ **3.26** supported by lithium interactions with Ph* substituents. **3.25** highlighted the capacity for alkali metals other than potassium to be utilised as counterions. Since significant expansion has occurred, the further structural variability of such species is covered in more depth in **sub-chapter 3.1.3.1**.

3.1.2.3. *O,O*-Dioxo Aluminyl Anions

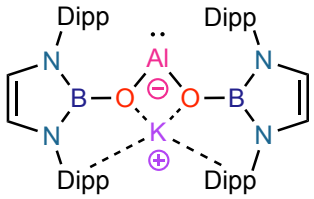

3.26

*Figure 3.4: Known example of an O,O-dioxo aluminyl anion **3.26**, reported by Aldridge, Sarkar and coworkers.[21]*

Typically, aluminyl anions have been stabilised through *N*,*N*-, *C*,*C*-, and *C*,*N*-based dianionic donor sets within chelating frameworks.[17] Acyclic analogues offer the potential for increased flexibility in ∠X–Al–X angles (compared with cyclic counterparts), and consequently greater scope for modifying the HOMO and LUMO energies (thereby impacting reactivity).[21] As part of investigating this, Sarkar, Aldridge and coworkers reported in 2024 the second acyclic aluminyl anion (the first I reported as part

of the Results and Discussion section of this Chapter) stabilised with two *N*-heterocyclic boryloxy [NHBO]$^-$ ligands [K{Al(NHBO)$_2$}] **3.26** ([NHBO]$^-$ = [{OB(NDippCH)$_2$}$_2$]$^-$).[21] The [NHBO]$^-$ ligand was found to be capable of preventing aggregation on steric grounds, and stabilizing the HOMO (a metal-centred lone pair) through two highly electronegative *O*-coordination atoms.[22] Initial preparations of **3.26** were attempted through the corresponding alkali metal reductions of aluminium(III) halide precursor, but these led to an intractable mixture of products. Consequently, the preparation of **3.26** was achieved through salt metathesis of an aluminium(I) reagent [AlCp*] **1.15** (**Chapter 1**) with K[NHBO] yielding the elimination of KCp* and targeted **3.26** in high yields. The solid-state structure revealed a two-coordinate aluminium(I) centre with two [NHBO]$^-$ ligands and the potassium counterion encapsulated between two oxygen atoms. Moreover, the structure of **3.26** features a markedly narrow ∠O–Al–O bond angle (∠O1–Al1–O2, 92.3(1)°), similar to those of the 5-membered aluminyl complexes **3.23** (∠C1–Al1–C2, 90.40(5)°) and **3.24** (∠C1–Al1–N1, 86.8(1)°).[18-19, 21]

3.1.3. Cation Influences on Structural Arrangements

Despite the prevalence of potassium reagents in aluminyl anion synthesis, subsequent inquiries of lighter and heavier alkali metal aluminyl systems have identified aluminium-ion interactions as well.[17] Ongoing investigations of reactivity and solution-state NMR spectroscopy have aided in application considerations and arrangement perseverance. The varied reactivity attributed to the alkali metal cation has become evident in unlocking previously inaccessible reaction pathways.[23] The implications of the alkali metals variation, reactivity, and structural arrangements are discussed herein.

3.1.3.1. Extended Alkali Metal Aluminyl Anions

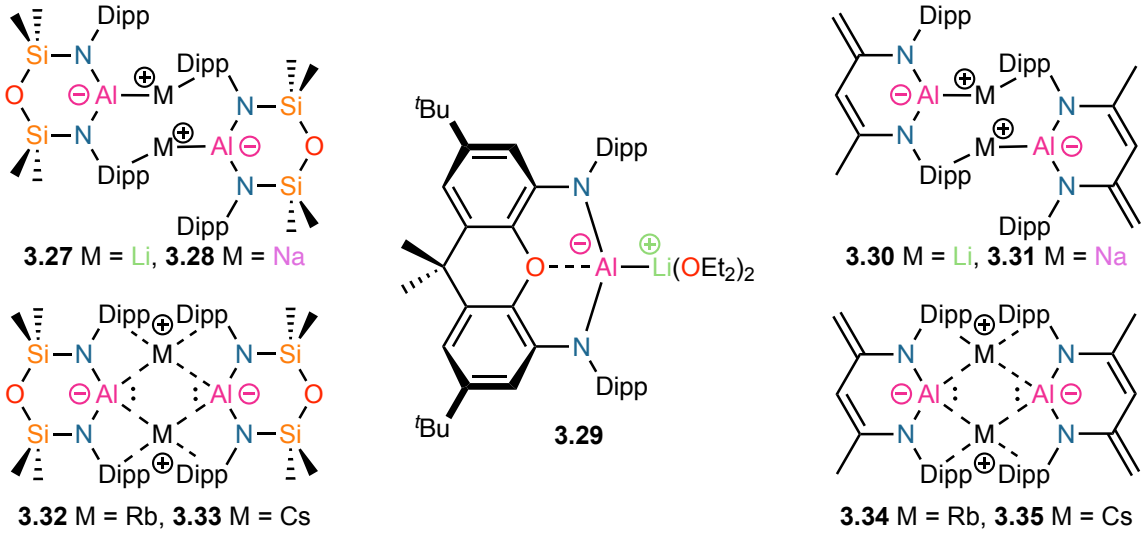

Figure 3.5: Selected aluminyl anions featuring non-potassium alkali metal cations.

Developments within wider organometallic chemistry have highlighted the applicability for synergistic interactions of group 1 metals.[24] Specifically within low valent aluminium species, alkali-metal-mediated reactivity has enhanced accessibility to reaction pathways once inefficient or inaccessible as summarised in the above figure.[17] Within aluminyl anion systems, widely employed potassium cations serve as a border of difference in the varied alkali metal systems of the lighter (lithium, sodium) and heavier (rubidium, caesium) congener derivatives (Figure 3.5).

Lighter alkali metal cation congeners of aluminyl anions have proven accessible through two synthetic protocols.[17] As exemplified in $[^{Si}NON]^{2-}$ stabilised aluminyl anions, direct reduction of the aluminium(III) halide precursor [AlI(^{Si}NON)] with corresponding group 1 element reductant (excess lithium or sodium metal), yielded the respective $[Li_2\{Al(^{Si}NON)\}_2]$ **3.27** and $[Na_2\{Al(^{Si}NON)\}_2]$ **3.28** species.[25] Similarly, the previously discussed lithium-bound aluminyl species incorporating the $[C^{Ph*}N^{Dipp}]^{2-}$ ligand system **3.25** and **3.26** were prepared through reductions of the corresponding halide precursor with excess lithium (Figure 3.3). However, this approach is not universally applicable. In xanthene-based [AlI(NON)] system, halide precursor reduction with lithium afforded the proligand H_2[NON], and analogous sodium reductions yielded the dialane $[Al(NON)]_2$.[26] Consequently, a cation exchange method was employed whereby potassium aluminyl anion **3.16** was treated with lithium iodide salt in diethyl ether to yield the corresponding lithium aluminyl $[(Et_2O)_2Li{-}Al(NON)]$ **3.29**.[26] Similar cation exchange reactions have also afforded both lithium $[Li_2\{Al(DBDI^{Dipp})\}_2]$ **3.30** and sodium $[Na_2\{Al(DBDI^{Dipp})\}_2]$ **3.31** aluminyl species by Harder and coworkers through reactions of the potassium aluminyl $[K_2\{Al(DBDI^{Dipp})\}_2]$ **3.20** with corresponding $M[BPh_4]$ (M = Li, Na) salts.[23]

The preparation of the heavier rubidium and caesium congeners have thus far been accessed through direct reduction methods. Treating the corresponding aluminium(III) halide or aluminium(I) [Al(^{Dipp}Nacnac)] starting materials with graphitic RbC_8 or CsC_8 has been reported to yield the targeted aluminyl systems **3.32** and **3.33** as reported by Coles, McMullin, Mulvey and coworkers,[27] and **3.34** and **3.35** by Harder and coworkers.[23] Initial investigations yielding **3.34** and **3.35** highlighted their accessibility in the solution state, however, further mechanochemical investigations led to their preparation via the solvent-free ball-milling of starting materials with the corresponding alkali metal graphites.[17] The analogous symmetric rubidium and caesium aluminyl anions stabilised with the $[SiN^{Dipp}]^{2-}$ ligand scaffold, have recently been reported by Hill, McMullin, Mahon and coworkers.[28]

3.1.3.2. Contacted Dimeric Pairs (CDPs)

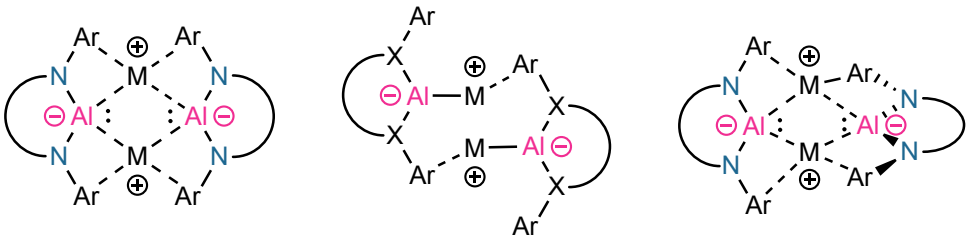

Figure 3.6: Generic structural arrangements of contacted dimeric pairs (CDPs) and associated sub-categories of symmetric, slipped and twisted relative arrangements.

In the solid state, potassium-, rubidium- and caesium-based aluminyl systems have been identified as dimers, thus far. Termed contacted dimeric pairs (CDPs), the resulting structural arrangement features the linkage of two aluminyl anion frameworks through the flanking π interactions of the ligand-based arenes (within Dipp and Mes groups), and the associated alkali metal cation (potassium **3.16**–**3.22**,[10, 12-15] rubidium **3.32**, **3.34**,[23, 27] or caesium **3.33**, **3.35**).[23, 27] Extensive investigations of potassium systems have also confirmed the retention of these dimeric arrangements within solution, as identified through DOSY NMR experiments.[11, 17]

Influenced by both the alkali metals and ligand scaffolds, three sub-categories of CDP have been identified based upon the relative orientations of the aluminyl anions within the dimer (Figure 3.6). Prevalent within potassium aluminyl systems, symmetrical orientations feature relatively equivalent cation interactions with arenes of both flanking aryl groups and aluminium centres. However, within the lighter congeners of aluminyl anions, slipped CDPs have been identified via X-ray crystallography. Slipped orientations feature significantly dissimilar and unsymmetrical aluminium-alkali metal interactions (range $\Delta d_{Al\cdots M}$ = 0.40–0.62 Å), with further investigations by DFT computations having identified single Al-M bonds,[20, 23, 25] this notably contrasts with the symmetric and twisted systems, which feature aluminium interactions with both M^+ cations (M = K, Rb, Cs) (Figure 3.6).

The least prevalent CDP orientation is the twisted arrangement. Within such species, the aluminium metallocycle units are both coplanar, however, observe a rotational twist of a single whole aluminyl framework. The degree of twisting can be quantified from the least squares plane of each aluminium metallocycle unit, observed as a rotational twist of 66.55(4)° in **3.34** and 66.31(5)° in **3.35**. [27] This orientation is attributed to the steric influence of large rubidium and caesium cations, ligand-alkali metal interactions and/or crystal packing effects.[17]

3.1.3.3. Monomeric Ion Pairs (MIPs)

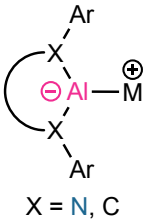

3.23 [(Toluene)$_2$K-Al(C^{Si})]
3.25 [(Et$_2$O)$_2$Li-Al(C^{Ph*}N^{Dipp})]
3.29 [(Et$_2$O)$_2$Li-Al(NON)]
3.36 [(Et$_2$O)$_2$Li-Al(DBDI^{Dipp})]
3.37 [(Et$_2$O)(TMEDA)Na-Al(DBDI^{Dipp})]

[(Et$_2$O)$_2$M-Al(^{Si}NON)] M = Li **3.38**, Na **3.39**
[(THF)$_3$M-Al(^{Si}NON)] M = Li **3.40**, Na **3.41**
[(18-c-6)K-Al(NON)] **3.42**
[(TMEDA)Li-Al(^{Si}NON)] **3.43**
[(TMEDA)$_2$M-Al(^{Si}NON)] M = Na **3.44**, K **3.45**

Figure 3.7: Generic monomeric ion pair (MIPs) structural arrangement and corresponding species examples. (18-c-6 = 18-crown-6, TMEDA = Tetramethylethylenediamine).

Highly prevalent within, but not exclusive to alkyl-containing aluminyl anions, monomeric ion pair (MIPs) arrangements feature a highly polarised Al–M bond (Figure 3.7). As exemplified in the first isolated example [(toluene)$_2$K−Al(C^{Si})] **3.23**, significant interaction exists between the aluminium centre and potassium cation (Al-K 3.4549(5) Å),[18] however, being longer than the sum of aluminium and potassium covalent radii (3.24 Å) this is attributed to a predominantly electrostatic interaction.[11] Despite the toluene cation solvation of **3.23**, the preparation of MIPs has featured predominantly within coordinating solvents, or with *N*- or *O*- coordinating ligands (TMEDA, 18-crown-6). Notably, many species observe structural interconversion relationships such as that highlighted between slipped CDP **3.26** and derivative MIP **3.25** reported by Kinjo and coworkers (Figure 3.3).[20]

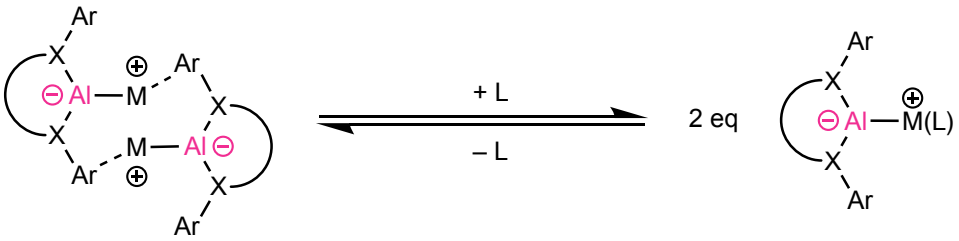

Scheme 3.2: Generic representation of the CDP↔MIP aluminyl arrangement interconversion relationship. X = C or N, L = Ligand or Solvent.

The CDP↔MIP interconversion has also been observed to occur for other aluminyl systems in diethyl ether solutions (Figure 3.3). Specifically, lithium and sodium aluminyl species featuring the [DBDI^{Dipp}]$^{2-}$ ligand (slipped CDPs **3.30** and **3.31**) yield respective derivative MIPs (**3.36** and **3.37**),[23] and [^{Si}NON]$^{2-}$ ligand MIPs (**3.38** and **3.39**) are accessible from the corresponding slipped CDPs (**3.27** and **3.28**) (Scheme 3.2).[25] Whilst nearly all diethyl ether-solvated MIP species have been crystallised, the [DBDI^{Dipp}]$^{2-}$ stabilised **3.37** could only be identified within the solution state, requiring the coordination of TMEDA to induce crystallisation.[23] Notably, solvent coordination can also hinder the CDP↔MIP interconversion relationship, as observed in the application of tetrahydrofuran. Treatment of lithium and sodium [^{Si}NON]$^{2-}$ ligated slipped CDPs (**3.27** and **3.28**), with tetrahydrofuran yielded

the corresponding MIPs (**3.40** and **3.41**), however, reversion to the CDP was found not to be possible, attributed to the greater alkali metal-oxygen bond strength present from increased σ-donor property of tetrahydrofuran.[29]

Further exploring the coordination of ligands to alkali metal centres, the potassium sequestering reagent 18-crown-6 was applied in the preparation of MIP [(18-c-6)K–Al(NON)] **3.42** from the CDP **3.18,** and the bidentate donor ligand TMEDA systems [(TMEDA)$_n$M–Al(^{Si}NON)] have been reported with various cations (M= Li, n = 1; **3.43**, M = Na, n = 2; **3.44**, M = K, n = 2; **3.45**).[10, 25] Moreover, the application of varied ligands and sequestering reagents has afforded a further class of aluminyl, separated ion pairs (SIPs).

3.1.3.4. Separated Ion Pairs (SIPs)

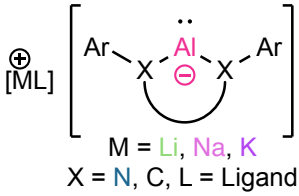

3.24 [K(12-c-4)][Al(C^{Si}N^{Ad})]
3.46 [K(crypt-222)][Al(NON)]
3.47 [K(crypt-222)][Al(^{Si}NON)]
3.48 [K(crypt-222)][Al(SiN^{Dipp})]
3.49 [K(crypt-222)][Al(NCCCN)]
3.50 [K(crypt-222)][Al(NHBO)]
3.51 0.5[K$_2$(18-c-6)$_3$][Al(SiN^{Dipp})]
3.52 [Li(TMEDA)$_2$][Al(NON)]
3.53 [Na(crypt-222)][Al(^{Si}NON)]

Figure 3.8: Generic separated ion pair (SIP) structural arrangement and reported examples.

Assisted through the ligation or sequestering of alkali metal cations, CDPs serve as the basis for the third arrangement type; separated ion pairs (SIPs) (Figure 3.8). The first example was reported by Aldridge, Goicoechea and coworkers in 2019, employing [2.2.2]cryptand (crypt-222) as a potassium sequestering reagent to yield [K(crypt-222)][Al(NON)] **3.46**.[30] This was shortly followed by the previously discussed [K(12-crown-4)$_2$][Al(C^{Si}N^{Ad})] **3.24**.[19] Highlighted through X-ray crystallography, these SIPs feature alkali metal cations sequestered from aluminyl anion, yielding a "naked" aluminium(I) centre with no strong interaction with the cation. In **3.46,** a lack of close interactions between the potassium cation and the [Al(NON)] anion confirmed the charged-separated species, with all K···Al distances >7 Å.[30]

Since the two initial reports, further species have also been prepared from the corresponding potassium aluminyl anions (**3.17**, **3.18, 3.22**, **3.26**) via treatment with crypt-222 to yield [K(crypt-222)][Al(^{Si}NON)] **3.47**,[29] [K(crypt-222)][Al(SiN^{Dipp})] **3.48**,[13b] [K(crypt-222)][Al(NCCCN)}] **3.49** and [K(crypt-222)][Al(NHBO)] **3.50**,[21] or via excess 18-crown-6 to yield 0.5[K$_2$(18-crown-6)$_3$][Al(SiN^{Dipp})] **3.51**.[13b] Notably, **3.50** was the first isolated example of an acyclic "naked" aluminyl anion published in 2024.[21] To date, only the [^{Si}NON]$^{2-}$ stabilised SIP system are lithium [Li(TMEDA)$_2$][Al(^{Si}NON)] **3.52** and sodium [Na(crypt-222)][Al(^{Si}NON)] **3.53** aluminyl anions.[29]

3.1.3.5. Ligand Encapsulated Pairs (LEPs)

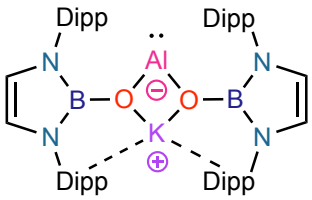

3.26 [K{Al(NHBO)$_2$}]

Figure 3.9: Generic ligand encapsulated pair (LEPs) structural arrangement and corresponding species examples.

A previously unidentified ligand encapsulated pair (LEPs) structural arrangement was observed in the second acyclic aluminyl anion [K{Al(NHBO)$_2$}] **3.26** (Figure 3.9).[21] Identified via X-ray crystallography, the potassium cation in the species is supported solely through ligand interactions with a single aluminyl anion framework.[21] This arrangement was present with cation encapsulation by the *O*-coordination atoms and arene interactions with Dipp groups of [NHBO]$^-$ ligands observed in the AlO_2K core. Within the literature, **3.26** is the only species featuring this arrangement. However, investigations targeting further aluminyl anions of this arrangement are ongoing and are highlighted in **Chapter 4**.

3.1.4. Reactivity of Aluminyl Anions

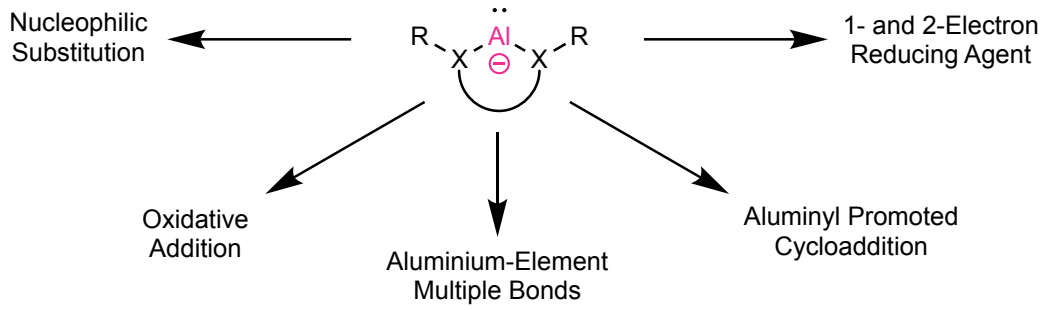

Scheme 3.3: General overview of the diverse reactivity in aluminyl anion chemistry.

Since their inception, the diverse reactivity of aluminyl anions has expanded rapidly, yielding new substrates and applications.[11, 17] As highlighted, reactivity developments have aligned with 5 key applications: nucleophilic substitution, oxidative addition, the formation of aluminium-element multiple bonds, cycloaddition reactions and their use as novel reducing reagents (Scheme 3.3).[17] Through these methodologies, aluminyl anions as transition metal metallomimetics have continued to be explored.

In relevance to this work, the remainder of this introduction will concentrate on aluminyl anions undertaking 1) nucleophilic substitution reactions, 2) oxidative addition pathways and 3) use as reducing agents.

3.1.4.1. Aluminyl anions as Nucleophiles: Nucleophilic Substitution

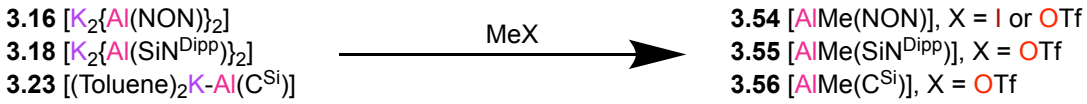

*Scheme 3.4: Preparation of aluminium(III) methyl compounds **3.54**, **3.55**, **3.56** via nucleophilic substitution.*

A defining feature of aluminyl anions is their nucleophilic character at the aluminium(I) centre.[11] This notable reactivity has been shown by aluminyl anions **3.16**, **3.18**, and **3.23**, presenting nucleophilic attack upon carbon-centred electrophiles (MeI, MeOTf), yielding aluminium(III) methyl compounds (**3.54**,[10] **3.55**,[13b] **3.56**) (Scheme 3.4).[18] This aluminium-centred nucleophilicity has also been applied to metal-centred electrophiles (M-X).[11]

Employing aluminyl anions in the preparation of Al-M bonds, nucleophilic substitution reactions have been widely reported in furnishing homo- and heterobimetallic species.[10, 13a, 31] Initial reports highlighted the use of weakly coordinating anions (OTf^-, I^-, BPh_4^-) containing electrophile reagents to assist with salt elimination.[11] Initially presented as isolable species in the stepwise reductions to alkyl-substituted aluminyl anions [(toluene)$_2$K−Al(C^{Si})] **3.23** and [K(12-crown-4)$_2$][Al(C^{Si}N^{Ad})] **3.24**, aluminium(II) dialane complexes have been reported to be accessible via nucleophilic substitution reactions. From the aluminyl anion [K$_2${Al(NON)}$_2$] **3.16**, treatment with aluminium(III) iodide [AlI(NON)] yielded the unsupported aluminium(II)-aluminium(II) bonded complex [{Al(NON)}$_2$]$_2$ **3.57**. Notably, **3.57** was also found accessible through treatment of the corresponding precursor [AlI(NON)] with stoichiometric amounts of potassium graphite, or excess sodium graphite, or excess lithium graphite.[10, 26]

Recently, aluminyl-containing heterobimetallic products have expanded in metal and ligand identity, often featuring an unsupported aluminium–metal bond, reminiscent of MIP complexes. Moreover, covering metals from the *s*- and *p*-block, early and late transition metals, the catalogue presents varied electronics within the complexes (**3.58-3.77**) highlighted in Figure 3.10.[17]

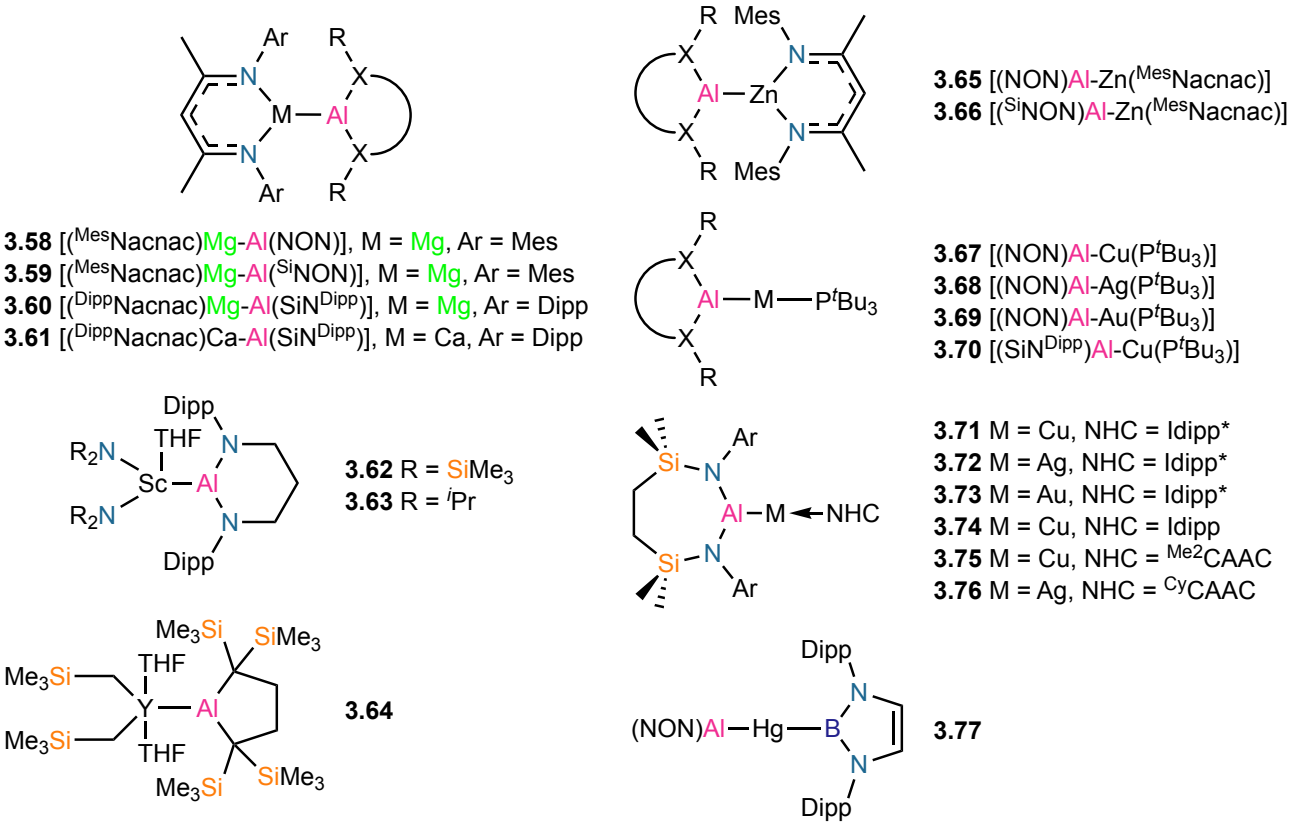

Figure 3.10: Selected examples of metal-aluminium bonded species prepared from their corresponding aluminyl anion. (Idipp = N,N-diisopropyl-4,5-dimethyl-2-ylidene, Idipp = N,N-bis(2,6-diisopropylphenyl)-imidazol-2-ylidene, ^{Me2}CAAC = 1-(2,6-diisopropylphenyl)-3,3,5,5-tetrame-thylpyrrolidin-2-ylidene, ^{Cy}CAAC = 2-[2,6-bis(1-methylethyl)phenyl]-3,3-dimethyl-2-azaspiro[4.5]dec-1-ylidene.)*

Al-M bimetallic complexes generated through nucleophilic substitution reactions may be divided into two classes relating the polarisation of the aluminium–metal bond. In complexes which the bound metal features an electronegativity less than that of aluminium (< 1.61 Pauling scale), polarisation of the bond would reflect a retained pseudo aluminium-centred nucleophile Al(δ–)-M(δ+). Initially reported through reactions with magnesium electrophiles, the consequential magnesium-aluminyl complex **3.58** was highlighted as reacting as a nucleophile. Employing the previously highlighted [^{Ar}Nacnac]$^-$ ligand framework (Ar = aryl), **3.58** served as a vanguard in the preparation of metal-aluminyl species stabilising the electrophilic bound M centres with [^{Ar}Nacnac]$^-$ ligands (M = Mg, Ca). More recent investigations have afforded [^{Mes}Nacanc]$^-$ stabilised metal-aluminyls (**3.58** and **3.59**) accessible from different potassium aluminyl reagents, including [K$_2${Al(NON)}$_2$] **3.16** and [K$_2${Al(^{Si}NON)}$_2$] **3.17** affording the respective magnesium-aluminyl derivatives **3.58** and **3.59** respectively.[10, 32] Utilising a bulkier [^{Dipp}Nacnac]$^-$ ligand at the group 2 centre, Hill, McMullin and coworkers also prepared the corresponding Mg **3.60** and Ca **3.61** aluminyl derivatives from [K$_2${Al(SiN^{Dipp})}$_2$] **3.18**.[13a] Notably, whilst **3.58** was accessible through the nucleophilic substitution

pathways, subsequent developments successfully sought reductions of the corresponding aluminium(III) iodide complexes with the 2-electron magnesium(I) reducing agent [Mg(^{Mes}Nacncac)]$_2$ reported by Jones and coworkers in 2007.[33] Metal-aluminyl complexes have since been developed by employing varied ligands, featuring the early transition metals scandium and yttrium. Employing [K$_2${Al(NCCCN)}$_2$] **3.22**, Yamashita, Lin and coworkers presented the first scandium-aluminyl complexes **3.62** and **3.63** featuring bulky amido donors of the transition metal centre.[15] Analogously, from the highly reactive dialkyl aluminyl [(toluene)$_2$K−Al(C^{Si})] **3.23**, the first yttrium-aluminyl complex **3.64** was isolated notably featuring an unsupported Y–Al bond.[31b]

Complexes featuring a more electronegative metal than aluminium (> 1.61 Pauling scale), tend to adopt Al(δ+)-M(δ–) bonding with an electron-rich metal and electrophilic aluminium centres. Similarly applied within previously discussed metal-aluminyl species, the ^{Mes}Nacnac ligand scaffold has also supported electron-rich metal centres within heterobimetallic complexes. [K$_2${Al(NON)}$_2$] **3.16** and [K$_2${Al(^{Si}NON)}$_2$] **3.17** were also applied in the preparation of the respective zinc-aluminyl derivatives **3.65** and **3.66** (Zn = 1.65 Pauling scale).[26, 32, 34] Al(δ+)-M(δ–) complex examples were further developed with bulky phosphine ligand system (P^{t}Bu$_3$) coordinated upon coinage metals (M = Cu **3.67**,[35] M = Ag **3.68**,[35] M = Au **3.69**),[31a] with the analogous copper-aluminyl complex **3.70** prepared with the 7-membered aluminyl system **3.18**.[36] Further applying [K$_2${Al(SiN^{Dipp})}$_2$] **3.18**, a catalogue of Al(δ+)-M(δ–) coinage metal complexes have been prepared stabilised with carbenes of varying steric bulk (**3.71**-**3.76**).[36-37] In further exploring metal-aluminium species with the seminal aluminyl anion **3.16**, the mercury-aluminium complex **3.77** was prepared, featuring boron and aluminium ligation upon the mercury centre.[38]

Notably, but outside the scope of this work, the reactivity of Al-M complexes generated from aluminyl anions has been extensively investigated.[17] Primarily investigations have focussed upon the small molecule activation, including the reduction of carbon monoxide and carbon dioxide.[31a, 35-37]

3.1.4.2. Oxidative Addition Reactions with Aluminyl Anions

IUPAC defines an oxidative addition reaction as “the insertion of a metal complex into a covalent bond involving formally an overall two-electron loss on one metal or a one-electron loss on each of two metals”.[39] Observed with both neutral and anionic aluminium(I) centres,[40] reactions with various substrates can lead to the oxidation of the metal centre to aluminium(III).[41] Ongoing investigations have presented reactivity involving the selective cleavage of strong σ-bonds.

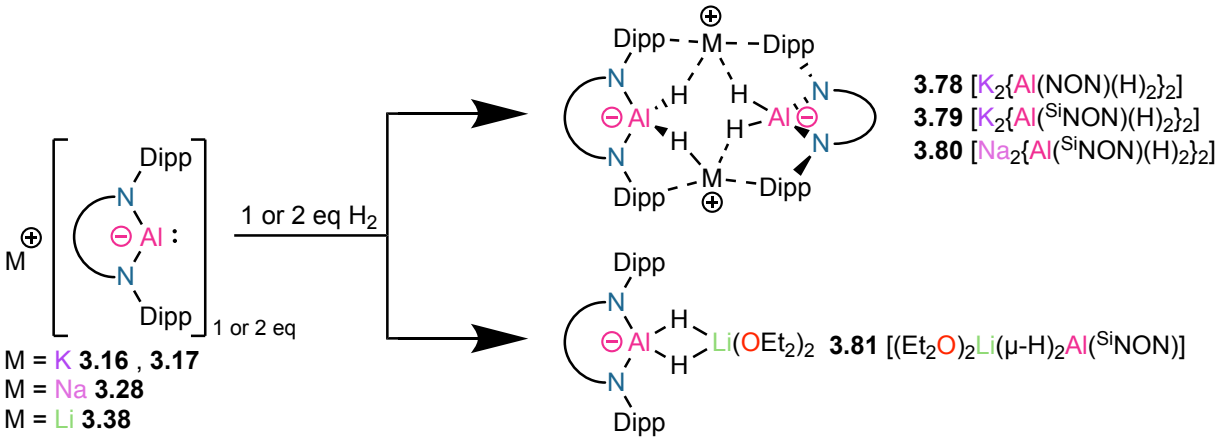

Scheme 3.5: Oxidative addition of H_2 with potassium, sodium and lithium aluminyl anion species.

First exemplified with the simplest molecule, H_2, treatment with the aluminyl anion **3.16** led to cleavage of the H-H, yielding the formal oxidative addition product **3.78** (Scheme 3.5).[10] Subsequent investigations from Coles and coworkers showed the capability of MIP lithium **3.38**, and CDP sodium **3.28**, and potassium $[K_2\{Al(^{Si}NON)\}_2]$ **3.17** aluminyl anions to also oxidatively add H_2.[25] Similar to reactions with $[K_2\{Al(NON)\}_2]$ **3.16**, dihydroaluminate species featuring potassium (**3.78**, **3.79**) and sodium (**3.80**) cations were isolated as dimers, whilst the lithium species (**3.81**) was isolated as a monomeric species. [10, 25] Relating $[(^{Si}NON)]^{2-}$ stabilised aluminyl species, the counterion alkali metal was identified to influence reaction progression rates. Inferring rates of reaction based on the 50% conversion ($t_{1/2}$) with corresponding aluminyl species, the relative trend of Li^+ **3.28** > Na^+ **3.38** > K^+ **3.17**, was observed from $t_{1/2}$ reaction times of 1.5, 6 and 12 days respectively.[17]

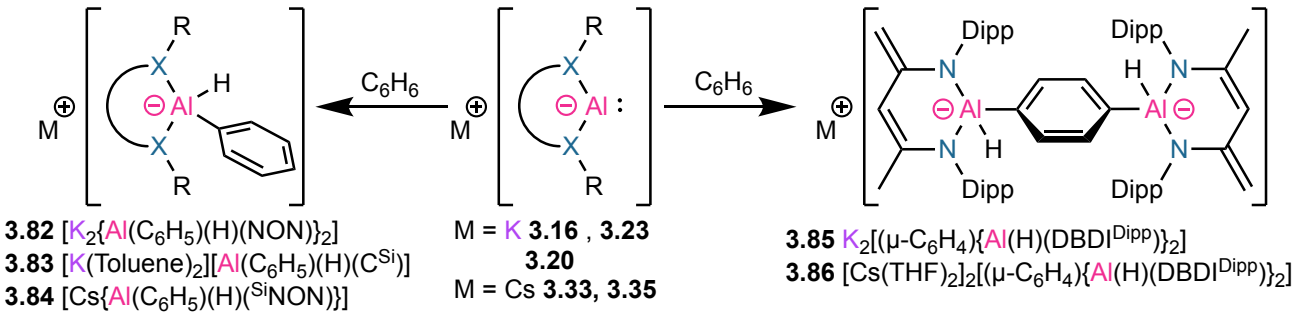

*Scheme 3.6: Oxidative addition of C–H bond with potassium (**3.16**, **3.23**, **3.20**) and caesium (**3.33**, **3.35**) aluminyls.*

In addition to H_2, $[K_2\{Al(NON)\}_2]$ **3.16** was first example of a main group compound to oxidatively add the C-H bond of benzene, affording (hydrido)(phenyl)aluminate species $[K\{Al(H)(C_6H_5)(NON)]_2$ **3.82** (Scheme 3.6).[10] The preparation of the analogous products **3.83** and **3.84**, also via the C-H oxidative addition of benzene, has been highlighted at ambient temperatures with dialkyl aluminyl anion $[(toluene)_2K{-}Al(C^{Si})]$ **3.23**,[18] and 80 °C with caesium aluminyl anion **3.33,** respectively.[27]

Conversely, reactions with the $[DBDI^{Dipp}]^{2-}$ stabilised aluminyl species **3.20** and **3.35** did not afford the (hydrido)(phenyl)aluminate species, but rather the corresponding 1,4-activation products $K_2[(\mu\text{-}C_6H_4)\{Al(H)(DBDI^{Dipp})\}_2]$ **3.85** following 1 week at 35 °C,[14a] and $[Cs(THF)_2]_2[(\mu\text{-}C_6H_4)\{Al(H)(DBDI^{Dipp})\}_2]$ **3.86** as a byproduct later crystallised as THF adduct.[23]

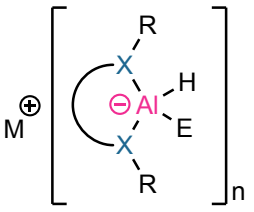

3.87 E = NHDipp, $[K_2\{Al(NHDipp)(H)(NON)\}_2]$, n = 2
3.88 E = NHDipp, $[K(Et_2O)_2][Al(NHDipp)(H)(^{Si}NON)]$, n = 1
3.89 E = NH_2, $[K(12\text{-}c\text{-}4)][Al(NH_2)(H)(C^{Si}N^{Ad})]$, n = 1
3.90 E = SiH_2Ph, $[K(12\text{-}c\text{-}4)][Al(SiH_2Ph)(H)(C^{Si}N^{Ad})]$, n = 1
3.91 E = SiH_2Ph, $[K(Et_2O)_2][Al(SiH_2Ph)(H)(^{Si}NON)]$, n = 1
3.92 E = OAr″, $[K\{Al(OAr'')(H)(^{Si}NON)\}]$, n = 1
3.93 E = PHMes, $[K(Et_2O)_2][Al(PHMes)(H)(^{Si}NON)]$, n = 1

Figure 3.11: Selected aluminate products generated by oxidative additions with aluminyl anions toward acidic, hydridic, and non-polar E-H bonds. (Ar″ = 2,6-^{t}Bu$_2$-4-MeC$_6$H$_3$)

Expanded to further varied E-H bonds, oxidative addition reactions with aluminyl anions have been investigated with acidic (N-H, O-H), hydridic (Si-H), and non-polar (P-H) bonds, in addition to previously discussed C-H bonds (Figure 3.11).[17] Highlighted by Aldridge, Goicoechea and coworkers in their seminal report, N-H activation by an aluminyl anion **3.16** of $DippNH_2$ affording corresponding (amido)(hydrido)aluminate **3.87**.[42] This capability was replicated by Coles and coworkers aluminyl anion $[K_2\{Al(^{Si}NON)\}_2]$ **3.17** with the similar activation of $DippNH_2$ to give **3.88**,[43] then expanded by Kinjo and coworkers with the report of the analogous species **3.89**[19] prepared from N-H activation of ammonia with $[K(12\text{-crown-}4)_2][Al(C^{Si}N^{Ad})]$ **3.24**. Further extending aluminyl reactivity, Kinjo and coworkers reported the hydridic Si-H activation of phenylsilane by **3.24**, yielding corresponding aluminate **3.90**.[19] This was later proved possible with $[K_2\{Al(^{Si}NON)\}_2]$ **3.17** in the preparation of analogous aluminate **3.91**.[43] Moreover, Coles and coworkers reported the reactivity of **3.17** toward acidic O-H and non-polar P-H bonds in the respective isolation of aluminates **3.92** and **3.93**, from the formal oxidative addition of Ar″OH and $MesPH_2$ respectively.[43]

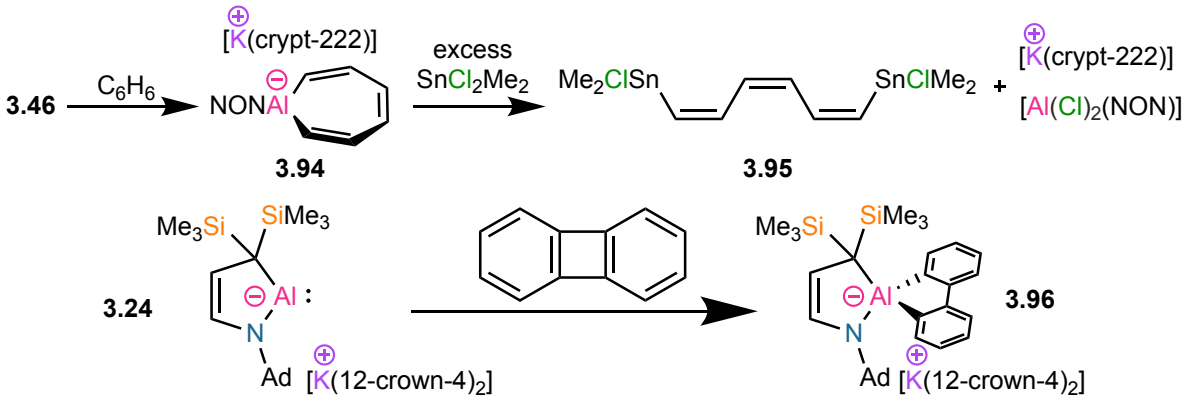

*Scheme 3.7: (Above) C-C activation of benzene by SIP [K(crypt-222)][Al(NON)] **3.46**, and resultant elimination of cis,cis,cis-triene **3.95**. (Below) C-C bond activation of biphenylene by SIP [K(12-crown-4)$_2$][Al(C^{Si}N^{Ad}] **3.24**.*

The activation of more challenging C-C bonds was first achieved remarkably with the "naked" aluminyl anion [K(crypt-222)][Al(NON)] **3.46**.[30] Consequential to the elevated reactivity of the SIP arrangement, **3.46** reacts at room temperature with benzene, affording the 7-membered heterocycle **3.94** from the oxidative addition of an aromatic C-C bond.[30] Subsequent treatment of **3.94** with 2 equivalents of $SnCl_2Me_2$ afforded the elimination of value added *cis*,*cis*,*cis*-triene **3.95** and consequential potassium dichloroaluminate [K(crypt-222)][$AlCl_2$(NON)]. These findings supported aluminyl anions as viable reagents in the preparation of functionalised acyclic products from aromatic molecules.[11] Analogously, Kinjo and coworkers reported that [K(12-crown-4)$_2$][Al(C^{Si}N^{Ad})] **3.24** could oxidatively add the strained C-C bond of biphenylene, yielding the bis-5-membered metallocyclic product **3.96**.[19]

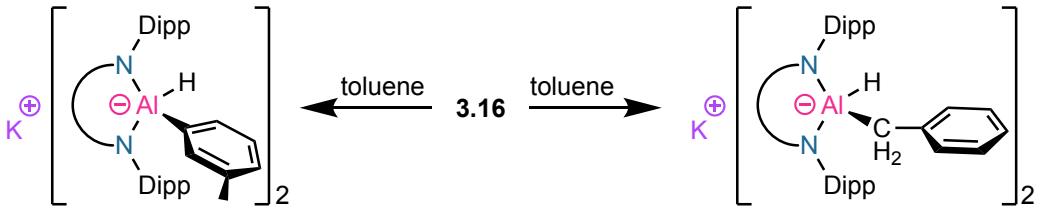

*Scheme 3.8: C-H activation of toluene by the CDP [K$_2${Al(NON)}$_2$] **3.16**.*

Highlighted in recent reports, the reactivity of aluminyl species towards methyl-substituted aromatic molecules can lead to multiple products. Aluminyl species [K$_2${Al(NON)}$_2$] **3.16**, [K$_2${Al(SiN^{Dipp})}$_2$] **3.18**, and [(toluene)$_2$K−Al(C^{Si})] **3.23** have all presented varied selectivity towards toluene, with **3.16** capable of activations upon both the *meta*-C-H bond, yielding [K$_2${Al(3-MeC$_6$H$_4$)(H)(NON)}$_2$] **3.97** and benzylic CH_3 group, yielding [K$_2${Al(CH_2Ph)(H)(NON)}$_2$] **3.98** (Scheme 3.8).[44] Markedly, **3.18** and **3.23** were identified to exclusively form the analogous benzylic-

activated [K{Al(CH_2Ph)(H)(SiN^{Dipp})}]$_n$ polymer **3.99** and *meta*-activated K[Al(3-MeC_6H_4)(H)(C^{Si})] **3.100** species respectively.[13b, 45] Subsequent synthetic and computational investigations have expanded comprehensions toward the activation of dialkylated aromatic substrates with aluminyl anions **3.16**, **3.18** and **3.24**.[44-46] Consequently, *meta*-aromatic activations of various substrates were identified as more energetically accessible than competing *ortho*, *para*, and benzylic activation pathways.[44] This aligns with the aluminium anion undergoing transformations at the most δ+ carbon centre, in toluene systems being that of the *meta*-position.

3.1.4.3. Reduction of Small Molecules with Aluminyl Anions

Treatment with a range of oxidisable reagents highlight the reducing nature of aluminyl anions. Consequent to the umpolung reactivity of nucleophilic aluminium, previously inaccessible complexes and oxidations of small molecules via this route have become available. Recent reports have demonstrated the widely applicable reduction-oxidation reactivity of aluminyl anions toward organic azides,[42, 47] ketones,[41, 48] white phosphorus,[49] and chalcogens (selenium[50] and tellurium[51]). Relevant to this work, reactivity profiles of aluminyl anions toward nitrous oxide, carbon dioxide and carbon monoxide is discussed.

In late 2019, reports from the groups of Aldridge and Goicoechea,[52] and Coles,[53] described the oxidation of aluminyl anions with carbon dioxide and nitrous oxide. Under 1 atm of carbon dioxide, both **3.16** and **3.17** yielded the respective carbonate complexes **3.101** and **3.102** (Scheme 3.9). Analogously, the treatment of **3.16** with phenyl isocyanate afforded the isoelectronic aluminium carbamate complex **3.103**.[52] Mechanistic investigations have identified these reactions to occur via a two-step process, whereby initial reduction of the substrate affords a highly reactive aluminium oxide intermediate and corresponding carbon monoxide or PhNC. With another equivalent of the substrate, the intermediates react via a [2+2] cycloaddition to afford the corresponding aluminate products **3.101**–**3.103**. In targeting the highly reactive oxide intermediate (aluminoxane), more controlled preparations with nitrous oxide and aluminyl anions **3.16** and **3.17** afforded the oxo-anions **3.104** and **3.105** (Scheme 3.9). Analogous to the starting reagents, aluminoxanes **3.104** and **3.105** were isolated as dimeric species supported by potassium-arene interactions but featured extremely polarised terminal Al-O bonds. Confirming the intermediate identity and stepwise formation of previously isolated species, treatment of **3.104** and **3.105** with carbon dioxide afforded the previously mentioned carbonates **3.101** and **3.102**, respectively, whilst addition of further equivalents of nitrous oxide yielded the *cis*-hyponitrite complexes **3.106** and **3.107** via a [2+3] cycloaddition (Scheme 3.9); the latter of which required the sequestering of the potassium cation with crypt-222 to aid in isolation. Addition of

crypt-222 to **3.105** in the absence of nitrous oxide or carbon dioxide led to intramolecular C-H activation of the ligand scaffold across the Al-O bond. **3.106** and **3.107** are the first reports of *cis*-hyponitrites ligands prepared directly from nitrous oxide.[11, 17] Subsequent investigations of the aluminoxanes have highlighted their ability to form C-C coupled products (e.g. **3.108** and **3.109**)[42] upon treatment with isonitriles and carbon monoxide, respectively (Scheme 3.9).[50b] Remarkably, **3.104** showed reactivity toward H_2 at room temperature, affording the hydride/hydroxide aluminate product **3.110**.[52]

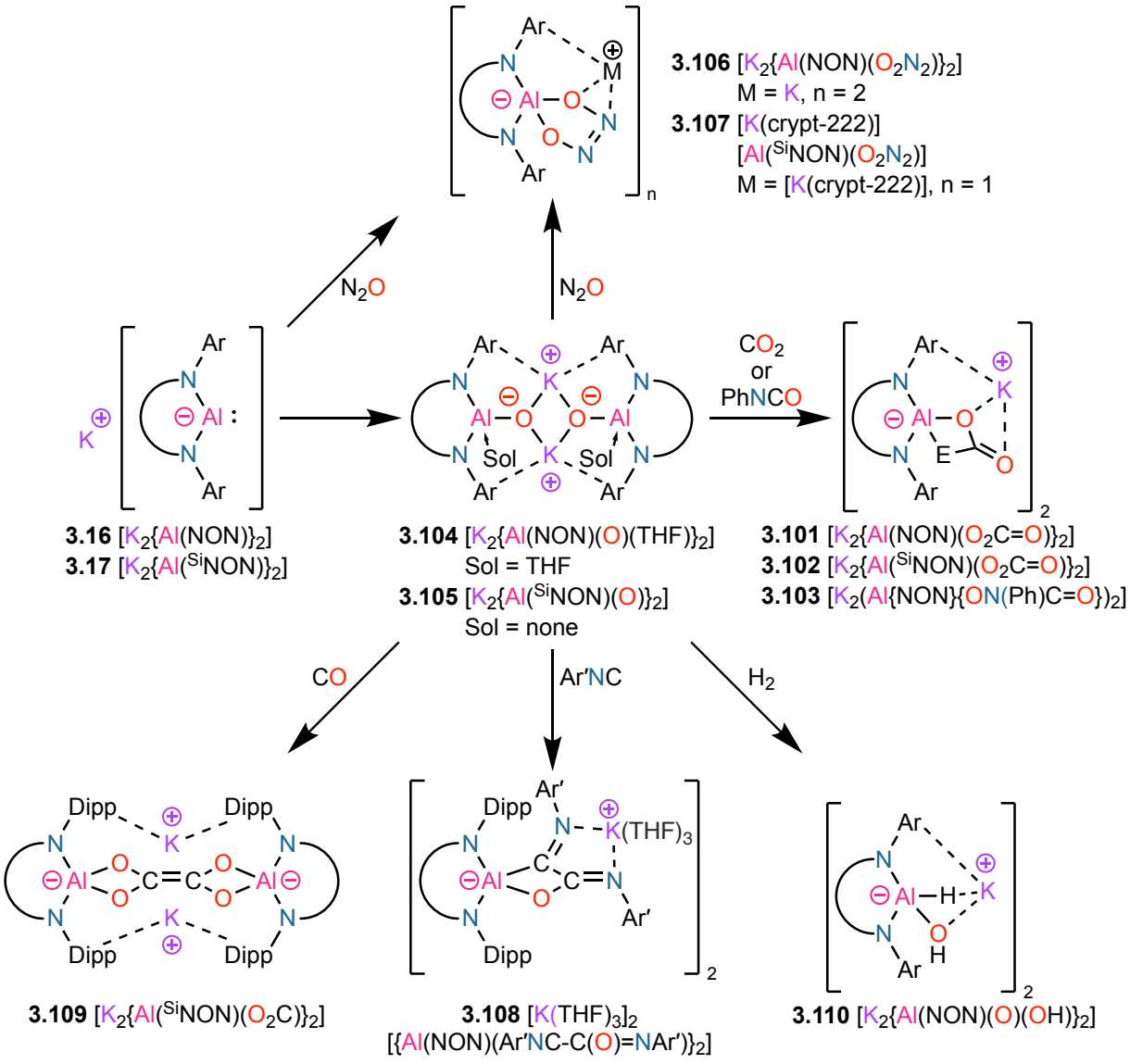

*Scheme 3.9: Preparation of aluminoxane species (**3.104** and **3.105**) and an overview of their reactivity.*

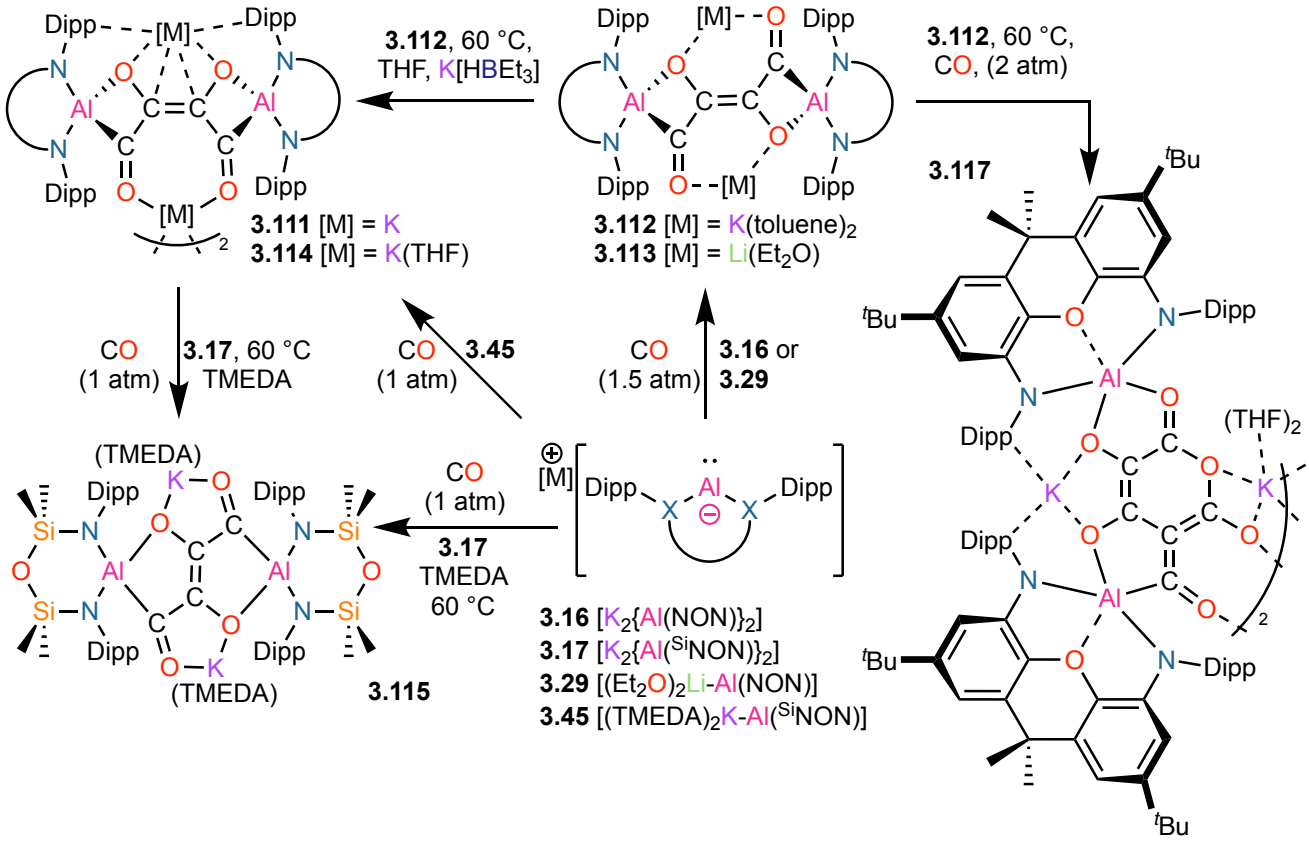

*Scheme 3.10: Reactivity of the aluminyl anions (CDP **3.16**, **3.17** and MIP **3.29**, **3.45**) towards carbon monoxide.*

Reactivity of aluminyl anions toward carbon monoxide has further promoted aluminyl compounds as transition metal metallomimetics.[54] Crimmin and Kong showed in 2018, that the neutral aluminium(I) reagent [Al(DippNacnac)] participated in CO homologation with $[W(CO)_6]$ as a carbonyl source.[55] Markedly, the reductively coupled products, via C-C bond formation, are reminiscent of products from the industrial Fischer-Tropsch process whereby carbon monoxide serves a C_1 building block (Scheme 3.10).[56]

Aluminyl anions were first reported as being capable of conducting carbon monoxide homologation in 2022 by Coles and coworkers.[41] Exposure of the TMEDA-solvated MIP **3.45** to carbon monoxide afforded the 4-electron reduced $[C_4O_4]^{4-}$ containing product aluminium(III) dimer $[K_2\{Al(^{Si}NON)(C_4O_4)\}_2]$ **3.111** (C_4O_4 = 1,4-dioxido-2,3-diolato(Z)-but-2-en-1,4-diyl) (Scheme 3.10).[41] Interacting with aluminate fragments via both *C*-,*O*-centres, the newly formed $[C_4O_4]^{4-}$ ligand forms a 4-membered heterocycle with the Al centres. This ligand adopts a *cis*-{anti, anti} configuration about central C=C double bond, featuring a C_4 chain consisting of alternating single and double bonds. Shortly after, Aldridge, Goicoechea and coworkers reported the reduction of carbon monoxide, achieving similar 4-electron reduced products $[C_4O_4]^{4-}$ with both CDP **3.16** and MIP **3.29**, as well as a $[C_6O_6]^{4-}$ product through the coupling of six molecules of CO by CDP **3.16** (Scheme 3.10).[54]

Treatment of **3.16** and **3.29** under a slight carbon monoxide over-pressure afforded the *trans*-{syn,syn} $[C_4O_4]^{4-}$ configured products $[\{K(toluene)_2\}_2\{Al(NON)\}_2(C_4O_4)]$ **3.112** and $[\{Li(Et_2O)\}_2\{Al(NON)\}_2(C_4O_4)]$ **3.113**. Similar to **3.111**, the aluminium centres are additionally contained within a 4-membered heterocycle. Strikingly, the *trans*-{syn,syn} $[C_4O_4]^{4-}$ ligand **3.112** undergoes a thermally-induced isomerisation at 65–70 °C in the presence of $K[HBEt_3]$ to yield the *cis*-{anti, anti} arrangement **3.114**.[54] This isomer is analogous to the previously isolated dimer $[K_2\{Al(^{Si}NON)\}_2(C_4O_4)]$ **3.111**.[41]

In applications of CDP $[K_2\{Al(^{Si}NON)\}_2]$ **3.17** by Coles and coworkers, varied products were generated compared with the previously discussed MIP **3.45**.[54] Exposing **3.17** to a carbon monoxide atmosphere in the presence of TMEDA at 60 °C afforded the tetraanionic $[C_4O_4]^{4-}$ containing product of *trans*-{syn,syn} configuration $[\{K(TMEDA)\}_2\{Al(^{Si}NON)\}_2(C_4O_4)]$ **3.115**. Comparatively, **3.115** features aluminium centres within an additional 5-membered heterocycle, rather than the 4-membered arrangements in **3.112** and **3.113**. Conversion of *cis*-{anti, anti} **3.111** to to *trans*-{syn,syn} **3.115** was achieved by addition of TMEDA under a carbon monoxide atmosphere at elevated temperatures.[41]

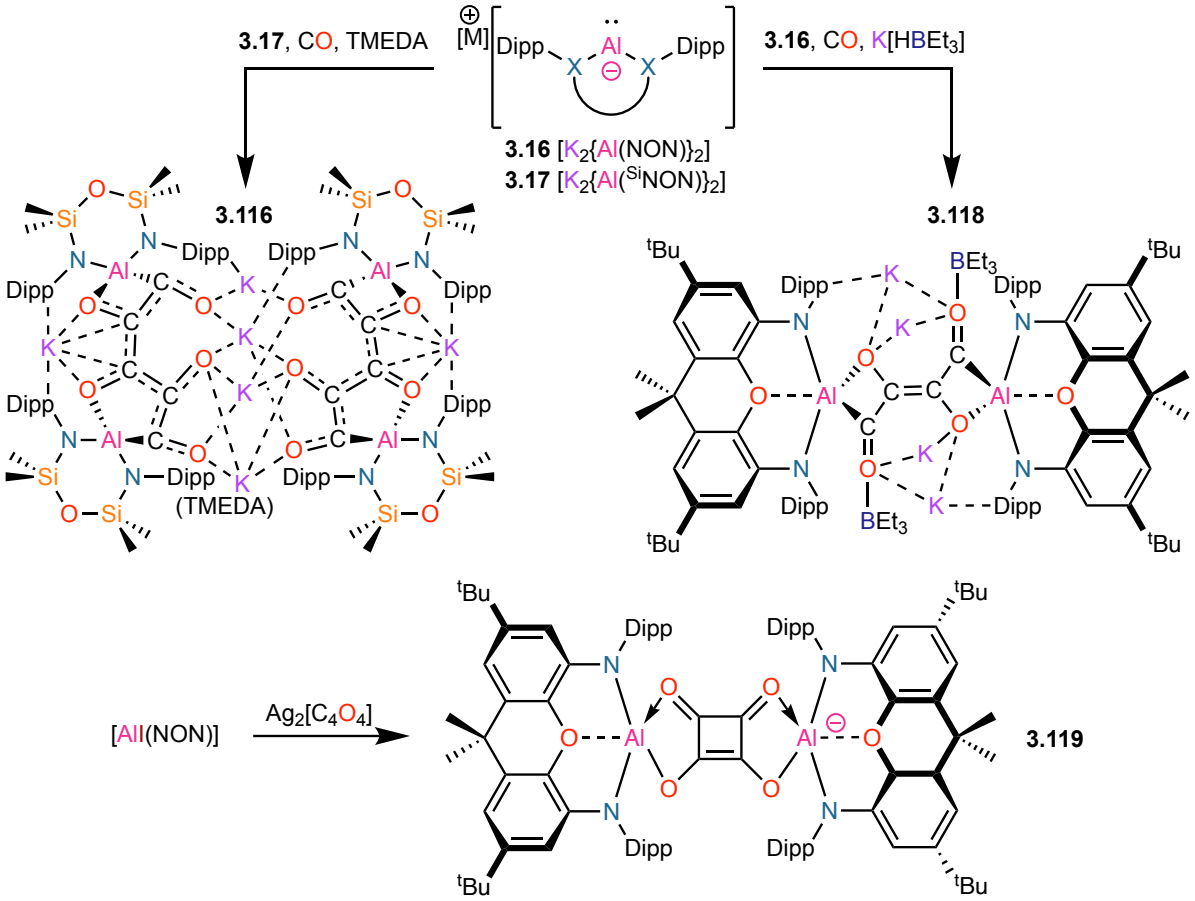

*Scheme 3.11: (top) Reactivity of aluminyl anions (CDP **3.16**, **3.17**) towards carbon monoxide and (bottom) installation of a $[C_4O_4]^{2-}$ ligand by salt metathesis.*

Unlike CDP [K_2{Al(^{Si}NON)}$_2$] **3.17**, exposing MIP **3.45** to 1 atmosphere of carbon monoxide notably did not afford a $[C_4O_4]^{4-}$ containing product (Scheme 3.11). Rather, this reaction yielded a pentaanionic $[C_5O_5]^{5-}$ bridged dimer species [K_6{Al(^{Si}NON)}$_4$(C_5O_5)$_2$(TMEDA)] **3.116**.[41] This C_5 fragment was identified as the first non-cyclic oligomer generated from CO and featured aluminium centres contained within both additional 4-membered and 5-membered heterocycles.

In further expanding CO homologation, $[C_6O_6]^{4-}$ fragments were generated as downstream products from preparations with CDP [K_2{Al(NON)}$_2$] **3.16**. From the previously prepared *trans*-{syn,syn} $[C_4O_4]^{4-}$ homologation product **3.112** in a tetrahydrofuran solution, heating to 65 °C under an additional two atmospheres of carbon monoxide resulted in the incorporation of two further carbon monoxide molecules into the previous generated $[C_4O_4]^{4-}$ ligand. Consequently, the novel *cyclo*-$[C_6O_6]^{4-}$ unit within [K{K(THF) $_2$}{Al(NON)}$_2$(C_6O_6)] **3.117** contains bridging two aluminium centres within 5-membered heterocycles (Scheme 3.10).[54] As a result of a sum four-electron reduction of six carbon monoxide molecules, the tetraanionic $[C_6O_6]^{4-}$ ligand featured a C_5O-pyran core. This species was the first example of solution-phase CO homologation yielding chain branching via complete C–O bond cleavage.[54]

In preparing a homologation resultant hexa-anionic ligand system, direct treatment of **3.16** with K[$HBEt_3$] under a carbon monoxide atmosphere afforded the targeted C-C coupled species. **3.118** contains a formal linear hexa-anionic $[C_4O_4]^{6-}$ ligand.[54] Furthermore, in completing the series of C-C coupled products, the treatment of [AlI(NON)] **2.1 Chapter 2** with a pre-formed squarate salt $Ag_2[C_4O_4]$ in diethyl ether affording targeted product [{Al(NON)}$_2$(C_4O_4)] **3.119** bearing a central $(C_4O_4)^{2-}$ unit (Scheme 3.11).

The chemistry of aluminyl anions has seen rapid growth since their discovery, with a wide array of reactions now documented. Although certain reactivity patterns resemble those of established aluminium(I) compounds, aluminyl anions exhibit greater reactivity and can engage with new substrates by activating otherwise inert bonds. Presented in their diverse reported reactivity, aluminyl anions serve as viable candidates toward applications as transition metal metallomimetics and highly reactive reagents for chemical synthesis.

3.2. Research Rationale

3.2.1. Acyclic Precursors for Aluminyl Complexes

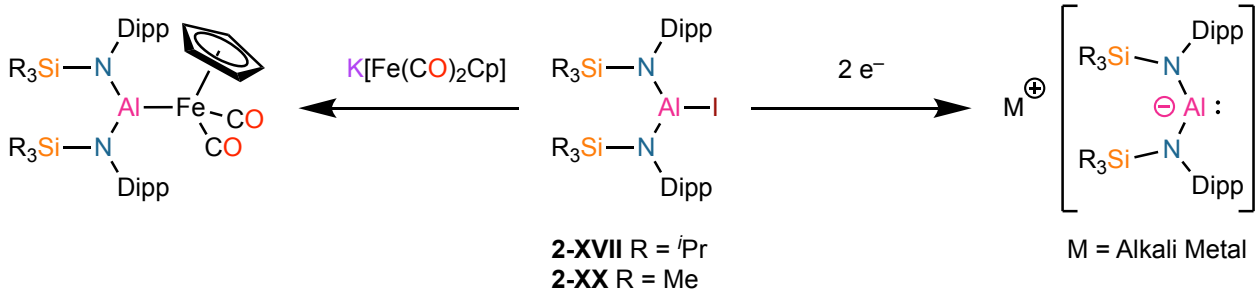

Figure 3.12: Acyclic aluminium(III) iodide precursors stabilised with bulky monodentate silyl(aryl)amido ligands prepared for transformations toward acyclic aluminyl complexes.

Outlined within **Chapter 2**, synthetic investigations into developing an acyclic precursor system afforded two aluminium(III) iodide complexes **2-XVII** and **2-XX**. Both complexes feature varied steric bulk upon silyl moieties and a consequentially distorted trigonal planar aluminium centre featuring two monoanionic silyl(aryl)amido ligands bonding through *N*-donors. Emulating developed aluminium centres as aluminyl metalloligands for transition metals, attempts to afford iron aluminyl complexes were undertaken. Thereafter and aligning more closely with overarching aims of this work, inquiries targeted the preparation of alkali metal aluminyl complexes.

Reminiscent of precursors affording 6-membered (**3.17**) and 7-membered (**3.18** and **3.19**) aluminyl species, reduction attempts were undertaken targeting the corresponding potassium aluminyls. Conditional upon successful isolations, attempts to undergo reductions with other alkali metals were investigated toward alkali metal stabilised aluminyl anions potential inaccessible via potassium reduction routes.

The catalogue of reactivity of the aluminium(I) species was then explored and the varied steric encumberment, and consequential electronics of the acyclic species were explored *in silico*.

3.3. Results and Discussion

3.3.1. Attempted Preparations of Iron-Aluminyl Coordination Complexes

Inspired by transition metal aluminyl complex developments **3.13** – **3.15**,[4-6] initial research investigations sought the preparation of iron-aluminyl complexes. Further reflecting growing research trends within main group synthesis,[57] mechanochemical preparative methods were also explored.

The benefits of mechanochemical methods for "green chemistry" include being near solvent free, safer, cheaper and less energy intensive than traditional solution state chemistry.[58] Within the literature, examples of metal-metal bond formation from mechanochemical methods are scarce. In

2022, Harder and coworkers reported the preparation of magnesium(I)–magnesium(I) bonded dimers through ball-milling of corresponding magnesium(II) iodide precursors.[59] Expanding aluminyl chemistry, Yamashita and coworkers in 2024 reported the preparation of non-solvated dialkylaluminyl anion [K{Al(C^{Si})}$_2$] from the mechanochemical reduction of precursor [AlBr(C^{Si})] with a Na/K alloy.[60]

In collaborations within the Hicks group, findings reported within this thesis contributed to developing mechanochemical synthesis methods for generating heterobimetallic complexes with unsupported metal-metal bonds.[61]

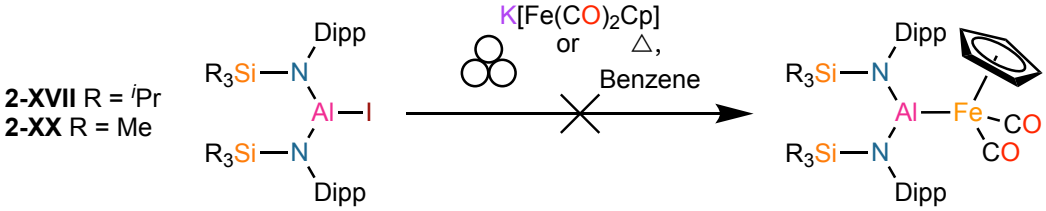

Scheme 3.12: Attempted preparation of iron-aluminyl complexes furnished with acyclic ligand scaffolds via solution state and mechanochemical methods.

Toward the preparation of analogous iron aluminyl complexes, as developed first from the groups of Nöth (**3.13**), and Aldridge and Jones (**3.14**), attempts were undertaken with K[Fe(CO)$_2$Cp] both mechanochemically and within the solution state.[4-6] Mechanochemically, aluminium(III) iodide precursors [AlI{N(Dipp)Si^{i}Pr$_3$}$_2$] **2-XVII** and [AlI{N(Dipp)SiMe$_3$}$_2$] **2-XX** were ball-milled with K[Fe(CO)$_2$Cp] in a IKA Ultra-Turrax Tube Drive fitted with a 20 mL ball mill tube, and a large number of stainless steel balls (Scheme 3.12). Following one hour milling, an aliquot was analysed by ^{1}H NMR Spectrometry. The less sterically encumbered SiMe$_3$ system showed the complete consumption of precursor **2-XX**, however, only near quantitative conversion to the associated proligand decomposition product HN(Dipp)SiMe$_3$ **2-IV**. The more bulky Si^{i}Pr$_3$ containing precursor **2-XVII** underwent similar decomposition to amine HN(Dipp)Si^{i}Pr$_3$ **2-I**. Consumption of **2-XVII** required milling for over six hours.

Following mechanochemical attempts, solution state syntheses were undertaken with K[Fe(CO)$_2$Cp] in benzene solutions at ambient and elevated temperatures (Scheme 3.12). Previously observed for the SiMe$_3$ species **2-XX**, twelve hours at ambient temperature with slight agitation afforded the complete conversion to corresponding *N*-silylaniline proligand **2-IV** and cyclopentadiene degradation species were identified via ^{1}H NMR spectroscopy. Repeating the reactions at ambient temperature with the more sterically encumbered **2-XVII** in solution led to no reaction between reactants.

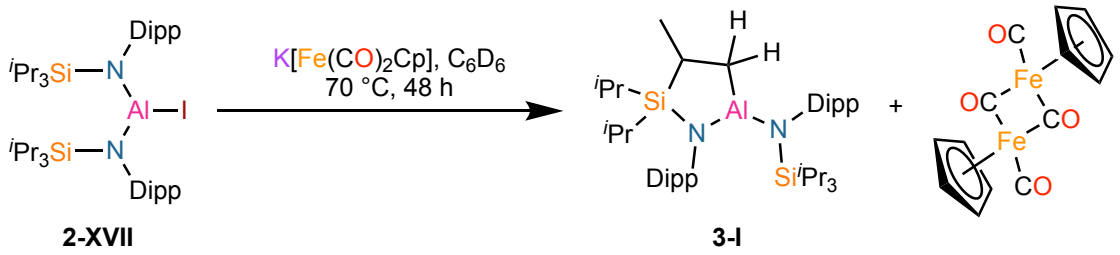

2-XVII **3-I**

*Scheme 3.13: Preparation of **3-I** from the treatment of **2-XVII** with K[Fe(CO)$_2$Cp] in the solution state.*

Combining **2-XVII** with K[Fe(CO)$_2$Cp] at 70 °C, afforded a gradual colour change over 2 hours from colourless to dark-red/orange (Scheme 3.13). Extended heating for 48 hours produced three distinct [N(Dipp)Si^{i}Pr$_3$]$^-$ signals (including *N*-silylaniline proligand) via ^{1}H NMR spectroscopy, however, no signals corresponding to the targeted iron-aluminyl complex [Cp(CO)$_2$Fe–Al{N(Dipp)Si^{i}Pr$_3$}$_2$] were present (Scheme 3.12). Subsequent purifications afforded co-crystallisation of two species in moderate yields (Scheme 3.13). Confirmed via X-ray crystallography (Figure 3.13), species included the ligand activation product [Al{N(Dipp)Si^{i}Pr$_2$CH(Me)CH$_2$}{N(Dipp)Si^{i}Pr$_3$}] **3-I** as colourless blocks, and the known cyclopentadienyliron dicarbonyl dimer [{Fe(μ-CO)(CO)Cp}$_2$] as dark-red plates. These findings could be rationalised as decomposition products of the targeted iron aluminyl complex, which may be forming *in-situ*, but undergoing an intramolecular activation of the [N(Dipp)Si^{i}Pr$_3$]$^-$ ligand scaffold.

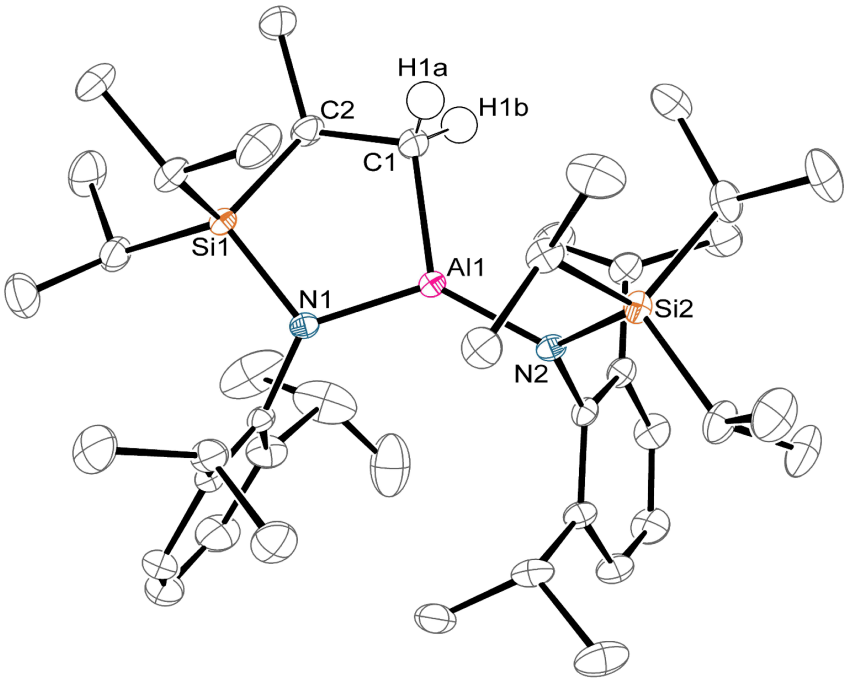

*Figure 3.13: Molecular structure of **3-I** as determined by X-ray crystallography. Thermal ellipsoids set to 50% probability. Most hydrogen atoms have been omitted for clarity. Selected bond lengths (Å) and angles (°): Al1-N1 1.8145(17), Al1-N2 1.8240(18), Al1-C1 1.965(2), Si1-N1 1.7790(17), Si2-N2 1.7709(17), Si1-C2 1.892(2), N1-Al1-N2 134.22(8), Al1-C1-C2 107.46(15), Si1-N1-Al1 108.45(9), C1-C2-Si1 107.56(15).*

Despite attempts at reduced temperatures to prevent the occurrence of ligand activation and/or decomposition, the formation of the targeted iron-aluminyl complexes could not be identified. However, greater success was achieved with the bidentate-stabilised precursor [Al(DAS)I] **2-XXXIII**, as highlighted in **Chapter 4**. Following challenges with the preparation of iron-aluminyl complexes, research focus shifted toward obtaining new alkali metal aluminyl complexes.

3.3.2. Reductions of the Bis-triisopropylsilyl(aryl)amido Aluminium(III) Iodide

3.3.2.1. Potassium-based Reductions

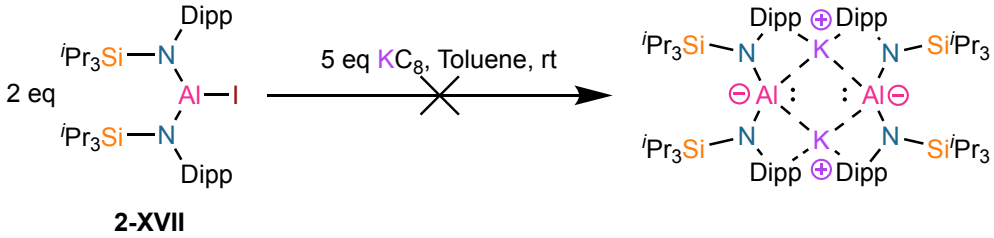

2-XVII

*Scheme 3.14: Targeted synthesis of the first acyclic aluminyl anion from **2-XVII** via reduction with potassium graphite.*

Emulating the use potassium reducing agents in the preparation of reported aluminyl anions, initial reduction studies of **2-XVII** were undertaken with potassium graphite at ambient temperature in toluene (Scheme 3.14). Following stirring at room temperature over 18 h, ^{1}H NMR spectroscopic analysis of the reaction mixture identified an indicative change compared with the diagnostic signals of **2-XVII**. This was most apparent from the generation of four septet signals of equivalent integration within the Dipp-isopropyl methine region (4.50-3.90 ppm) (Supporting Information Figure S.56), in addition to proligand **2-I** (3.56 ppm); (Figure 3.14). The observed splitting pattern was initially postulated as the formation of a highly sterically encumbered aluminium(II) dimer [(Al{N(Dipp)Si^{i}Pr$_3$}$_2$)$_2$]. Such an arrangement was hypothesised to potentially yield four different Dipp environments as observed within ^{1}H NMR spectrum, due to steric crowding and ligand restricted rotation.

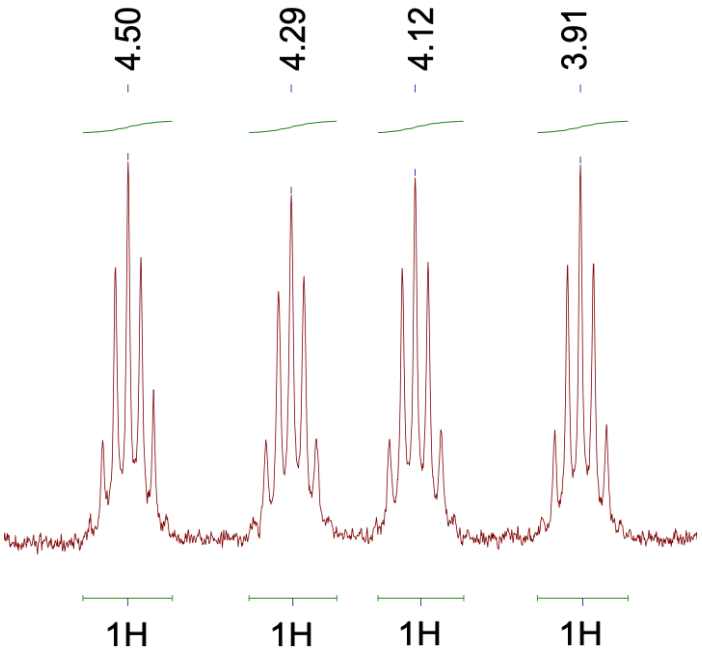

Figure 3.14:A section of the ^{1}H NMR spectrum taken from the reaction mixture generated from ***2-XVII*** *and KC_8 identifying, four equivalent septets at 4.50, 4.29, 4.23 and 3.91 ppm.*

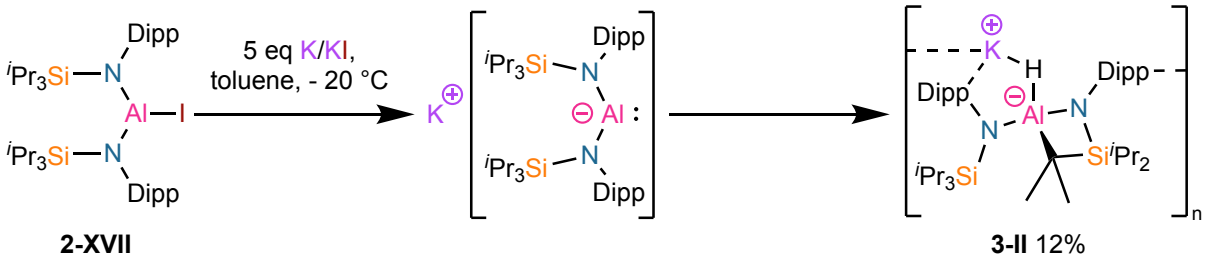

2-XVII **3-II** 12%

Scheme 3.15: Synthesis of the potassium aluminate complex ***3-II****, potentially consequent of an in-situ acyclic aluminyl anion undergoing an intramolecular oxidative addition.*

Toward substantiating the hypothesised aluminium(II) dimer, syntheses were undertaken with various potassium reagents. Performing the reaction at –20 °C with 5% w/w K/KI[62] afforded the cleanest NMR spectra. Subsequent filtrations afforded dark-yellow solutions which could be attributed to minor impurities of *N*-silylaniline proligand (isolated cleanly as an orange oil). From saturated toluene solutions, colourless SCXRD-quality crystals were afforded in minimal yield (12%). X-ray crystallography determined the solid-state structure to not be the targeted aluminyl anion or the postulated aluminium(II) dimer species, but rather, the tetracoordinate aluminate product **3-II** (Figure 3.15).

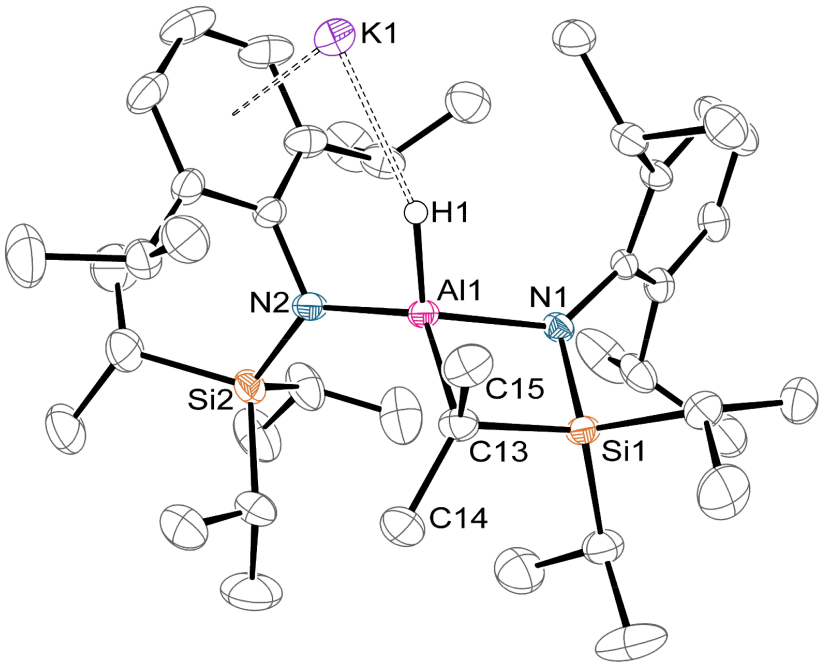

*Figure 3.15: Molecular structure of the C–H activation product **3-II** as determined by X-ray crystallography. Most hydrogen atoms are omitted for clarity. Thermal ellipsoids set to 50% probability. Selected bond lengths (Å) and angles (°): Al1-H1 1.52(4), K1-H1 2.58(4), Al1-N1 1.932(3), Al1-N2 1.924(3), Al1-C13 2.061(3) Al1-Si1 2.6934(12), Si1-N1 1.750(2), Si1-C13 1.879(3), Si2 N2 1.761(3), C13-Al1-H1 108.7(15), N1-Al1-C13 84.08(12), N1-Si1-C13 94.94(13), Si2-N2-Al1 134.68(15).*

The tetracoordinate aluminium(III) centre in **3-II** features a terminal hydride, a $[N(Dipp)Si^{i}Pr_3]^-$ and a consequentially bidentate, dianionic ligand $[N(Dipp)\{Si(^{i}Pr)_2CMe_2\}]^{2-}$. The latter is derived from a methine C–H bond cleavage involving the triisopropylsilyl moiety, likely via an oxidative addition reaction by an *in-situ*-generated aluminium(I) centre. **3-II** was isolated as a 1D coordination polymer in the solid-state, with each potassium cation closely associating with hydride and arene substituents.

As highlighted within **sub-chapter 3.1.4.2.** oxidation addition of C–H bonds is a commonly observed method of reactivity from aluminyl anions. This reactivity toward traditionally inert C–H bonds such as those in benzene sees activation across the metal centre yielding both organic and terminal hydride ligands.[11] It is hypothesised that the intended 2-electron reduction of the aluminium(III) iodide precursor **2-XVII** is realised, affording the targeted aluminyl anion *in-situ*. However, the inherent reactivity of the species contributes to an intramolecular oxidative addition upon the C–H bond of its own ligand to afford **3-II** as the more thermodynamically favourable product. It should be noted that whilst oxidative addition pathways are commonly reported with aluminyl anions,[10, 13b, 14a, 18, 23, 27, 44-45] other mechanisms (including radical) cannot be discounted, through which **3-II** and corresponding activation products may be yielded.

Having identified the structure of **3-II**, the ^{1}H NMR signal corresponding to the terminal Al-hydride ligand was identified as a very broad signal at 2.96 ppm in C_6D_6. The broadening of the signal can be attributed to the ^{27}Al nuclei (I = 5/2).[63] Moreover, the four different Dipp isopropyl environments can be attributed to the steric confinement and restricted rotation in both the monodentate and bidentate ligand frameworks incorporating the Dipp moieties.

Toward isolating the postulated transient aluminyl anion, conditions to mitigate the C–H activation were investigated. Initially pursued in toluene, ambient temperature reductions with potassium graphite, potassium mirror and potassium chunks were conducted in other non-coordinating solvents (benzene, hexane, pentane). These attempts afforded the continued formation of **3-II** with significant proligand **2-I** and varying ratios of its potassium salt K[N(Dipp)Si^{i}Pr$_3$], as determined by ^{1}H NMR spectroscopy. Investigations with coordinating solvents (tetrahydrofuran and diethyl ether) were undertaken, postulating that solvation of the metal centres (aluminium or potassium) may further stabilise the highly reactive systems. However, reactions conducted at ambient temperatures gave similar results to those attempted in non-coordinating solvents with varied ratios of proligand and K[N(Dipp)Si^{i}Pr$_3$] formation. Notably, minimal solvent coordination was observed toward the highly Lewis acidic aluminium centre, likely due to the high steric encumberment afforded by the [N(Dipp)Si^{i}Pr$_3$]$^{-}$ ligands.

Attempts to hinder the C-H activation yielding **3-II** kinetically were undertaken via conducting reductions at lower temperatures, and also attempting to trap the postulated acyclic aluminyl anion. To this end, reactions were undertaken at 0, -20 °C, and -40 °C in toluene and hexane with potassium graphite, or 5% K/KI.[62] Despite cooling, ^{1}H NMR spectra of aliquots prepared following overnight stirring at zero and sub-zero temperatures showed formation of proligand **2-I** and activated **3-II,** with no evidence of the aluminyl anion present. Moreover, using 5% K/KI at low temperatures afforded product **3-II** in increased isolated purity and yield (up to 12%). Throughout the investigation of reduction at cold temperatures, aliquot samples of the mother liquor were kept cold via a -78 °C dry ice/ethanol bath prior to placement within the pre-cooled NMR instrument. As the formation of **3-II** was still identified at -40 °C, lower temperature investigations were undertaken with the slow addition of stoichiometric potassium naphthalenide to a thf solution of **2-III** at -60 °C and -78 °C. However, these investigations saw only the generation of the potassium salt of the ligand K[N(Dipp)Si^{i}Pr$_3$], signalling decomposition of the complex. Moreover, inquiries with dropwise additions of precursor **2-XVII** solutions to suspensions of potassium graphite and 5% K/KI at -78 °C similarly led to the production of K[N(Dipp)Si^{i}Pr$_3$]. Following extensive investigations with potassium reducing agents and precursor **2-XVII** further inquiries were undertaken with other alkali metal reducing agents.

3.3.2.2. Sodium- and Lithium-based Reduction Studies

Investigations utilising sodium reducing agents were completed under various reaction conditions to explore potential improvements to target aluminyl isolation. Utilising sodium metal, 5% Na/NaCl, and sodium naphthalenide reducing agents in varied solvents (toluene, benzene, hexane, tetrahydrofuran), temperatures (ambient, -20 °C, -78 °C) and stoichiometries almost exclusively yielded sodium salt of the ligand, Na[N(Dipp)Si^{i}Pr$_3$], and **2-I** proligand. Unfortunately, evidence of a transiently generated intermediate was not observed in these reductions.

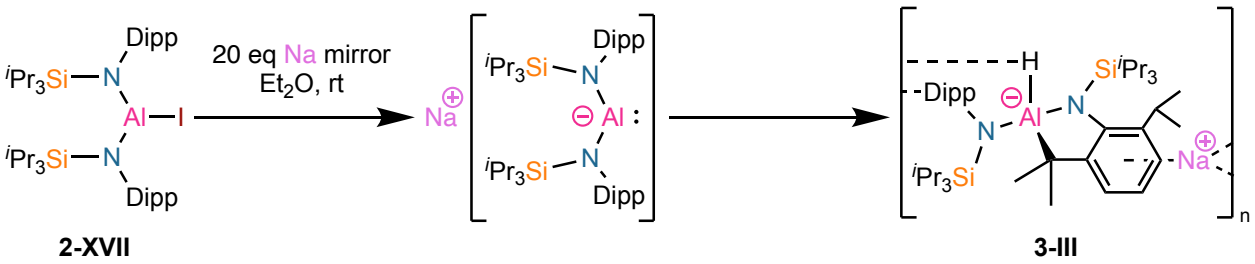

2-XVII **3-III**

*Scheme 3.16: Synthesis of the sodium aluminate **3-III** complex, potentially consequent of an in-situ acyclic aluminyl anion undergoing an intramolecular oxidative addition.*

Reductions of **2-XVII** in diethyl ether with sodium mirror at ambient temperature, led to a colour change to yellow after 5 minutes (Scheme 3.16). An aliquot was taken immediately and subjected to ^{1}H NMR spectroscopic analysis identifying a mixture of species including unreacted starting material, protonated ligand, and an unknown unsymmetrical species. Notably, evidence highlighted similarities to reactions yielding the **3-II** product, with signals corresponding to the isopropyl methine protons of the Dipp moiety (a broad septet at 3.71 ppm for **2-XVII**) presenting three defined equivalent septets in the same region (3.50 – 4.50 ppm). Following 18 hours stirring, extractions afforded a vibrant-yellow solution, which evaporated to a yellow powder and identified to containing four Dipp moiety-containing species. In attempting purification via recrystallisation, dissolution and concentration of a saturated benzene solution, afforded SCXRD quality crystals following 47 days at ambient temperature. Analysis via X-ray crystallography ascertained the solid-state structure of the analogous tetracoordinate aluminium(III) ligand C-H activation product **3-III** (Figure 3.16).

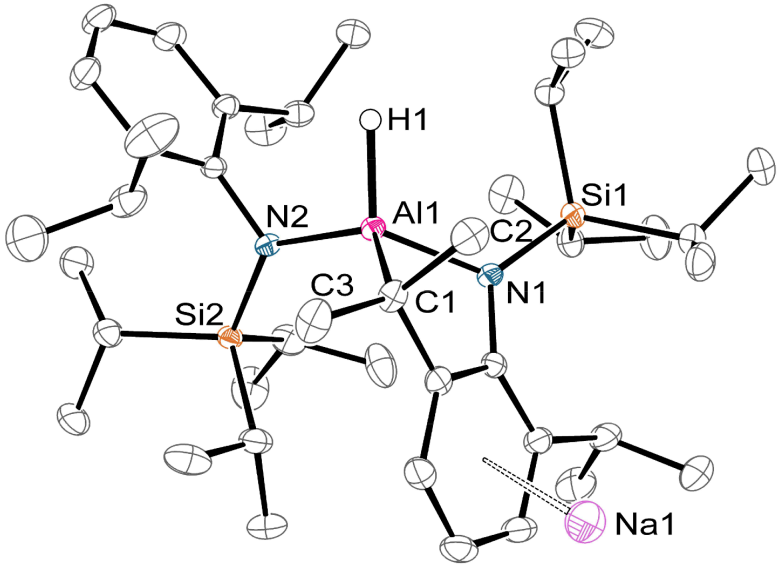

*Figure 3.16: Molecular structure of C–H activation product **3-III** as determined by X-ray crystallography. Most hydrogen atoms and solvent omitted. Thermal ellipsoids set to 50% probability. Selected bond lengths (Å) and angles (°): Al1-N1 1.9572(15), Al1-N2 1.9120(15), Al1-H1 1.60(2), Al1-C1 2.0282(18), Si-N1 1.7606(14), Si2-N2 1.7685(14), N1-Al1-H1 114.2(9), N1-Al1-C1 87.16(7), N1-Al1-N2 122.89(6).*

As proposed for the formation of **3-II**, reductions of **2-XVII** with sodium mirror likely afforded a transient aluminyl anion that subsequently activates a methine C-H bond. Differing from previous observations, this activation had occurred upon the isopropyl group of the Dipp moiety and consequently encompasses the aluminium(III) centre in a 5-membered heterocycle along with a terminal hydride ligand. As in reductions yielding **3-II**, the mechanism of formation for **3-III** is postulated as a C-H oxidative addition across an aluminium(I) centre. However, unlike the selective preparation of **3-II**, the synthesis of **3-III** also resulted in the formation of multiple other species. Notably, evidence of an analogous sodium derived triisopropylsilyl methine C–H activated species was observed by ^{1}H NMR spectroscopy, with signals matching those observed in **3-II** (Figure 3.14), but unfortunately, single crystals of this product could not be obtained.

Reductions with lithium metal were employed following the prevalence within literature toward the formation of low-valent complexes.[11, 64] However, reduction attempts of the **2-XVII** precursor complex were unsuccessful. Rather, lithium metal reductions yielded exclusively the lithium salt of the ligand, Li[N(Dipp)Si^{i}Pr$_3$], irrespective of coordinating and non-coordinating solvents at both room temperature and at –78 °C.

3.3.2.3. Single-Electron Reductions of Bis-triisopropylsilyl(aryl)amido Aluminium(III) Iodide

Throughout investigations yielding intramolecular C-H activations, the possibility of a radical mechanism was hypothesised. A radical pathway affording **3-II** and **3-III**, could be accessed via a one-electron reduction of the aluminium(III) centre of **2-XVII**, yielding a transient dicoordinate aluminium(II) radical. Within the literature, such species are exceptionally rare by virtue of their inherent instability and preferential dimerisation toward more thermodynamically stable Al−Al single-bonded compounds.[19, 65] However, due to extreme steric encumbrance about the aluminium centre presented in **2-XVII**, dimerisation is severely hindered. Consequently, the highly reactive metal centre could see degradation into a wide array of more stable products. Although the possibility of a radical pathway was hypothesised, no direct evidence of a transient aluminium(II) radical species prepared via alkali metal reductions was observed until performing the reaction below.

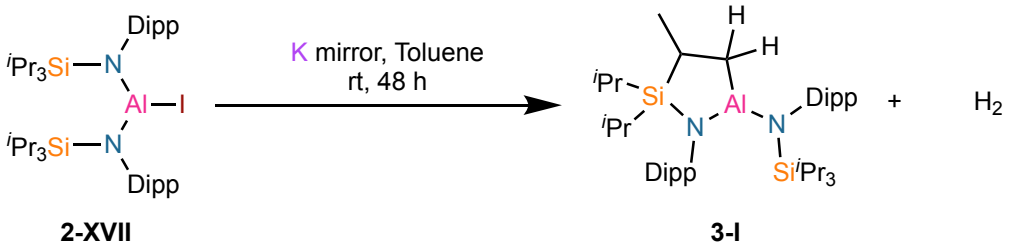

2-XVII **3-I**

*Scheme 3.17: Preparation of the 5-membered heterocycle **3-I**, proposed to be formed through a transient aluminium(II) radical complex.*

Under an N_2 atmosphere, a freshly prepared potassium mirror was treated with a toluene solution of **2-XVII** (Scheme 3.17). Following stirring for 18 h, an aliquot of the reaction mixture was taken, allowing for ^{1}H NMR spectroscopic analysis. Similarly observed in previous synthesis affording **3-I**, **3-II** and **3-III**, the ^{1}H NMR spectrum of the mother liquor identified multiple Dipp-containing species (including proligand, potassiated ligand salt, diisopropylaniline degradation and an unidentified species), and trace evidence of H_2. Extraction and concentration of the mother solution allowed for the growth of crystals from a burnt-orange oil. X-ray crystallography determined the solid-state structure of **3-I** (Figure 3.13), previously isolated from the reaction between **2-XVII** and K[Fe(CO)$_2$Cp].

Aligning with the production of H_2, it is hypothesised that a 1-electron reduction initially affords a dicoordinate aluminium(II) radical species. Following an intramolecular activation of the isopropyl methyl C-H, H$^\bullet$ is released which likely scavenges a second H$^\bullet$ from the reaction solution leading to H_2 generation.

Attempts to isolate or observe this transient aluminium(II) radical were unfortunately unsuccessful, due to its highly reactive nature.[66] Despite interesting results from an apparent single electron

reduction of the precursor complex, further investigations continued to focus on two-electron reductions toward the targeted acyclic aluminyl anion.

3.3.3. Reductions of Bis-trimethylsilyl(aryl)amido Aluminium(III) Iodide

3.3.3.1. Potassium-Based Reducing Agents

Following mixed success in the reductions of the bulkier [AlI{N(Dipp)Si^{i}Pr$_3$}$_2$] **2-XVII** precursor, the focus shifted to the smaller trimethylsilyl precursor [AlI{N(Dipp)SiMe$_3$}$_2$] **2-XX,** whereby research investigations were undertaken in close collaboration with Dr. David Liptrot and Mr. Ross Jackson of the Department of Chemistry at the University of Bath.[67]

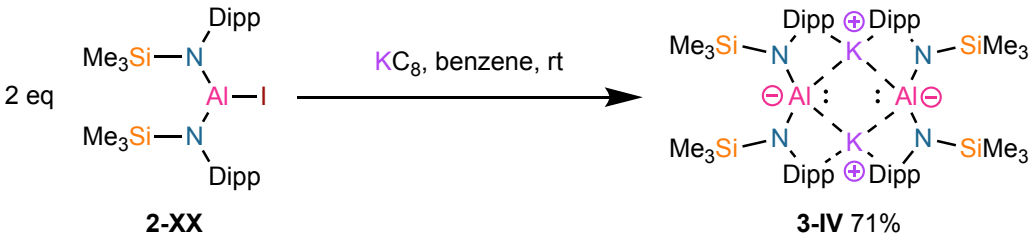

*Scheme 3.18: Synthesis of the first acyclic aluminyl anion **3-IV** from the potassium graphite reduction of **2-XX**.*

A benzene solution of **2-XX** was treated with excess (5 equiv.) of potassium graphite, affording a dark yellow solution. Filtration of the mother liquor yielded a deep- yellow solution, analogous to that described in the preparation of previously reported aluminyl systems (**3.16**-**3.18**).[10, 12-13] Following the removal of volatiles under reduced pressure, a bright-yellow powder was isolated in good yield. ^{1}H NMR spectroscopy identified clean conversion to a single new product. Dissolution of the powder (60 mg) in benzene and concentration afforded a saturated solution (0.1 mL), which was kept at ambient temperature for 5 days. This led to SCXRD quality yellow crystals of the first acyclic aluminyl anion [K$_2${Al(N{Dipp}SiMe$_3$)$_2$}$_2$] **3-IV**, which were characterised via X-ray crystallography (Figure 3.17).

Analogous to many reported CDP aluminyl anions (**3.16**-**3.22**), **3-IV** presents as a dimer featuring two [Al{N(Dipp)SiMe$_3$}$_2$]$^-$ fragments bridged by two potassium cations (**3.16**-**3.22**).[10, 12-15] Within the asymmetric unit, two fragments constituting two different aluminyl dimers of the **3-IV** molecule are present, consequently affording two sets of values for analogous atoms due to crystal packing effects. Each aluminium(I) centre is dicoordinate with a bent geometry from the lone pair of electrons and two *N*,*N*-coordination atoms. The potassium cations feature η^6-arene interactions with the Dipp groups of the bulky silyl(aryl)amido ligands. **3-IV** is the first example of a crystallographically characterised acyclic aluminyl anion.

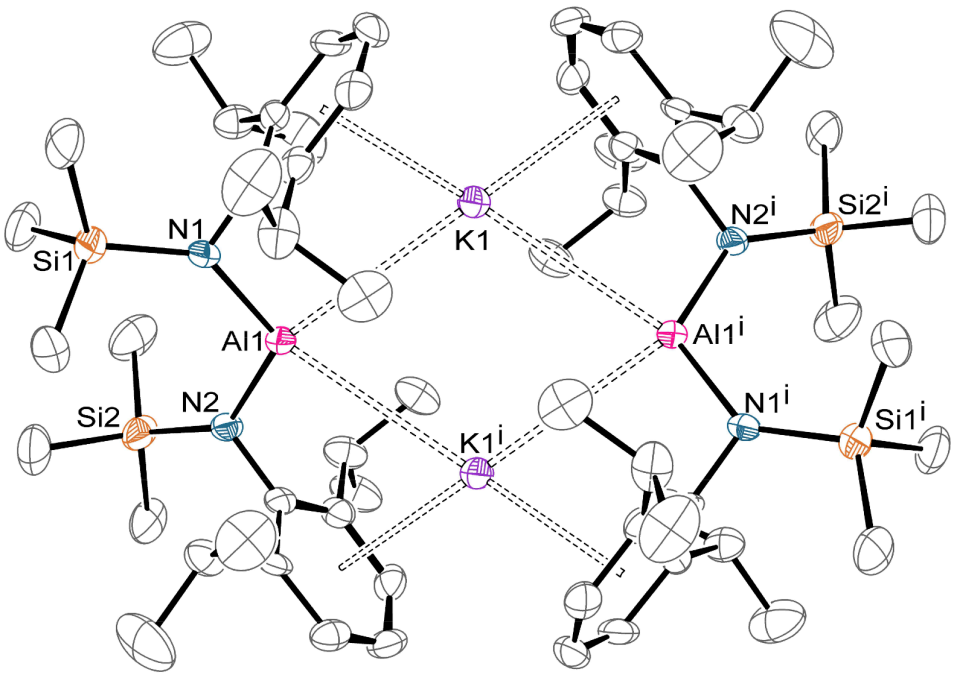

*Figure 3.17: Molecular structure of the acyclic aluminyl anion **3-IV** as determined by X-ray crystallography. The asymmetric unit contains two full molecules of **3-IV** which are essentially isostructural. Hydrogen atoms and one molecule of **3-IV** omitted for clarity. Thermal ellipsoids set to 50% probability. Selected bond lengths (Å) and angles (°) are provided for both molecules of **3-IV**: Al1···Al1^{i} 6.014(3); 6.047(3) Al1-N1 1.919(4); 1.909(4), Al1-N2 1.916(4); 1.916(4), Al1···K1 3.6483(15); 3.5993(15), N1-Si1 1.738(4), N2-Si2 1.746(3), N1-Al1-N2 116.33(16); 116.61(17), Al1-N1-Si1 137.41(19); 138.6(2), Al1-N2-Si2 135.5(5); 136.6(2).*

Identified from the solid-state structure, acyclic **3-IV** is most comparable to the 7-membered cyclic aluminyl anion [K$_2${Al(SiN^{Dipp})}$_2$] **3.18** reported by Hill, McMullin and coworkers in 2020 (Figure 3.2).[13a] Notably, **3.18** also features ligand bonding through hard *N*-based diamido donors featuring aryl and silyl substituents, but the silyl substituents are linked via a C-C backbone. Notably, the increased steric encumberment from acyclic scaffolds rather than the bidentate [SiN^{Dipp}]$^{2-}$ ligand is projected in most significantly with the greater ∠N-Al-N angles of **3-IV** (116.33(16), 116.61(17)°), with respect to **3.18** (108.84(9), 108.77(9)°).[13a] However, these angles are narrower than that identified within the corresponding precursor **2-XX** (131.35 °) due to a lack of halide substituent and more favourable Al···K interactions.

The reduced aluminium(I) metal centre could be further supported by the comparison of Al-N bond lengths. Within the precursor **2-XX**, Al-N bond lengths of Al1-N1 1.785(3) Å and Al1-N2 1.800(3) Å, were notably shorter than that of aluminyl **3-IV** Al1-N1 (1.919(4) and 1.909(4) Å) and Al1-N2 (1.916(4) and 1.916(4) Å). Given the +1 oxidation state of the aluminium centre in such complexes, the increase of Al-N bond lengths further supported the two-coordinate aluminium(I) centre, opposing the formation of a hydride aluminium(III) complex which could be difficult to identify via X-Ray

diffraction methods. Moreover, the possibility of such an aluminium hydride species could be nullified via a lack of Al-H signal present within infrared spectrometry as conducted by Liptrot and coworkers.

The employment of the acyclic ligand scaffolds was also evident in relatively widened ∠Al-N-Si angles (**3-IV**, range 135.5(2)–138.6(2); **3.18** range 132.06(12)–134.70(12)°)[13a] and staggered arrangement of trimethylsilyl moieties (Figure 3.18). Despite relatively similar Al···K distances in both complexes (**3-IV**, range 3.5995(16)–3.7380(16); **3.18** range 3.584(1)–3.625(1) Å), a substantial variation in the Al···Al distances is observed, being nearly 0.8 Å between **3-IV** (6.014(3), 6.047(3)Å) and **3.18** (5.271(1) Å). This could be attributed to the flexibility in the acyclic system, afforded via a lack of C-C backbone, allowing increased projection of Dipp groups toward potassium cations whilst supporting increased Al···Al distances between two repulsive anionic centres. As a result of these interactions, **3-IV** also features as a "twisted" CDP, previously only identified with heavier alkali metal aluminyl anions featuring rubidium **3.32** and caesium **3.33** counterions (Figure 3.18).[27] The degree of "twisting" present within the fragments could be ascertained from the least squares plane of each aluminium unit, in which the dihedral angles of ∠N-Al-N planes of acyclic fragments in **3-IV** (63.18, 63.86°) (cations = K^+), and cyclic fragments in **3.32** (66.55(4)°) (cations = Rb^+), and **3.33** (66.31(5)°) (cations = Cs^+), all of which were greatly more twisted than analogous cyclic potassium system **3.18** (33.55(4)°).[27]

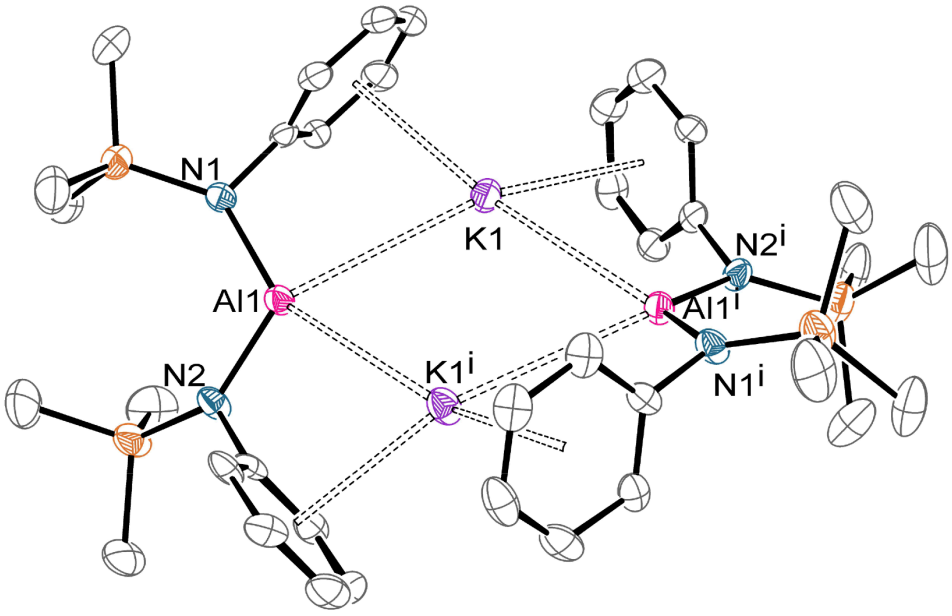

*Figure 3.18: Representation of the twisted contact dimeric pair arrangement of **3-IV**. Hydrogen atoms and isopropyl groups omitted for clarity. Thermal elipsoids set to 50% probability.*

To ascertain the structure of **3-IV** in solution, Liptrot and coworkers undertook ^{1}H DOSY NMR. The diffusion coefficient for **3-IV** was determined to be 5.87 × 10^{-10} m^2 s^{-1}, convertible to a

hydrodynamic radius of 6.74 Å.[67] This closely aligns with the calculated radius value for **3-IV** determined for the dimeric solid-state structure (6.42 Å). Comparable with that of the analogous dimeric aluminyl anion **3.18** (6.55 Å), it is evident that the dimeric arrangement of **3-IV** is maintained within solution. Consequently, as identified within other CDP aluminyl anions, the bridging potassium cations in **3-IV** further assisted with the isolation of a new donor-free dimeric aluminyl anion system.

To optimise the initially low yielding (20%) route to **3-IV**, various reaction conditions were undertaken. Synthetic precedent for chilled (~ 0 °C) reductions within the Hicks group did not afford increased yield nor purity of the product. The use of potassium metal or 5% w/w K/KI as employed within bulkier **2-XVII** reductions, afforded increased production of the potassium amide K[N(Dipp)SiMe$_3$] and the *N*-silylaniline proligand [HN(Dipp)SiMe$_3$] **2-IV** in addition to the targeted acyclic aluminyl anion in varied yields (15–55%). Notably, relatively short reaction times (1.5 h) with vigorous agitation in benzene afforded the isolation of clean material, often not requiring any additional washing or recrystallisation. However, attempts to increase yield via subsequent extractions would afford increased K[N(Dipp)SiMe$_3$] and **2-IV**.

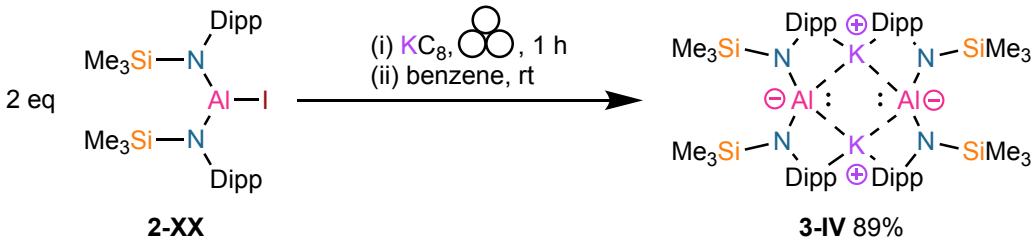

*Scheme 3.19: Synthesis of the acyclic aluminyl anion **3-IV** via ball-milling with potassium graphite.*

Inspired by the reported aluminyl preparations by Yamashita and coworkers, investigations were also undertaken in affording **3-IV** via mechanochemical routes.[60] To this end, white crystalline **2-XX** was treated with a vast excess of bronze-coloured potassium graphite powder (serving as a reductant and flux). The mixture was milled in a 20 mL ball mill tube with an IKA Ultra-Turrax Tube Drive, with 30 stainless steel balls for 1 h (Scheme 3.19). Extraction with benzene afforded **3-IV** in greater isolated yield (89%) than that prepared via optimised solution state synthesis (71%). Notably, attempts to scale the synthesis of **3-IV** via mechanochemical and solution state routes were only minimally undertaken due to bottlenecks in precursor preparation from necessitated sublimation purifications of **2-XX**.

Towards implementing relatively greener chemical preparative methods, mechanochemical processes remain a viable candidate. The preparation of potassium aluminyl systems via

mechanochemistry continues to be developed, promoting this as a powerful tool yielding highly reactive main group species.

3.3.3.2. Sodium- and Lithium-based Reduction Studies

Following the success with the potassium based-reducing agent KC_8, reductions were also attempted with lithium and sodium reductants. Utilising sodium in reduction investigations, treatment of freshly prepared sodium mirrors with hydrocarbon solutions of **2-XX** yielded evidence of the ligand sodium salt Na[N(Dipp)SiMe$_3$] and proligand **2-IV** following extended reduction times (>3 days). Investigations with 5% w/w Na/NaCl did not show sign of any reduction of the aluminium(III) iodide precursor, despite significant excesses of reducing agent and vigorous agitation. In lithium attempts, results similar to the bulkier **2-XVII** system were identified. That is, reduction attempts of **2-XVII** with lithium afforded the lithium salt Li[N(Dipp)SiMe$_3$], likely due to the over reduction of starting material. Due to a lack of time, investigations into counterion exchange affording aluminium(I) anions stabilised with non-potassium cations were not conducted.

3.3.4. *In-silico* Investigations of Acyclic Aluminyl Anions

Identifiable within solid-state structures, there is increased steric encumberment about the aluminium centres in acyclic ligand scaffolds versus cyclic. Consequently, a wider N–Al–N angle is found in the acyclic aluminyl derivatives, whereby the electronic donation effects from orbital overlap with amido donors would dictate reactivity. Therefore, in collaboration with Dr Petra Vasko of the University of Helsinki the electronic structures of the postulated aluminyl anion, [Al{N(Dipp)Si^{i}Pr$_3$}$_2$]$^-$, and observed aluminyl anion, [Al{N(Dipp)Si^{i}Pr$_3$}$_2$]$^-$ in **3-IV**, were investigated. Utilising DFT methods, calculations concerning the "free" anions were conducted, excluding the effects from corresponding alkali metals present in isolated and postulated transient acyclic aluminyl systems (Figure 3.19 and Figure 3.20).

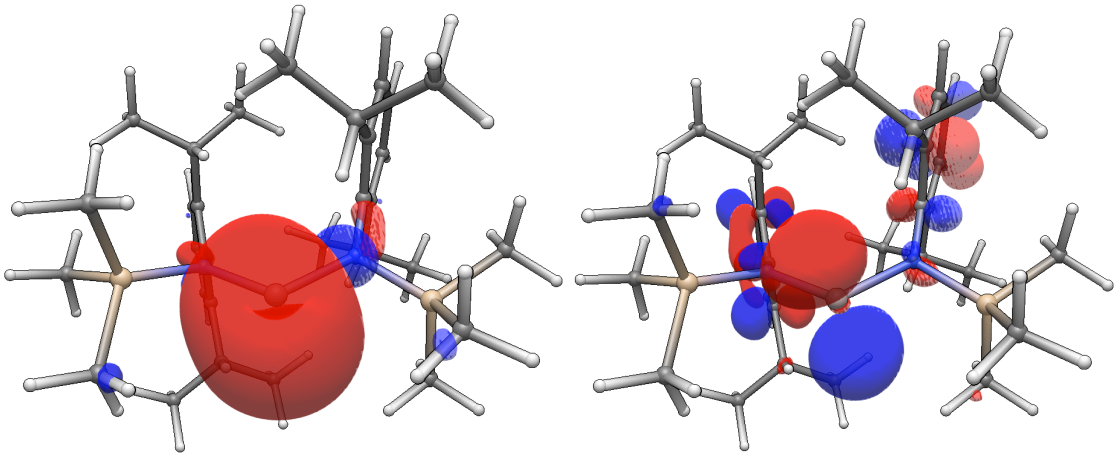

Figure 3.19: HOMO (-0.82 eV, left) and LUMO+3 (2.92 eV, right) of [Al{N(Dipp)SiMe$_3$}$_2$]$^-$ free anion, calculated at the DFT-D3, PBE0, Def-TZVP level of theory. Iso-value 0.04.

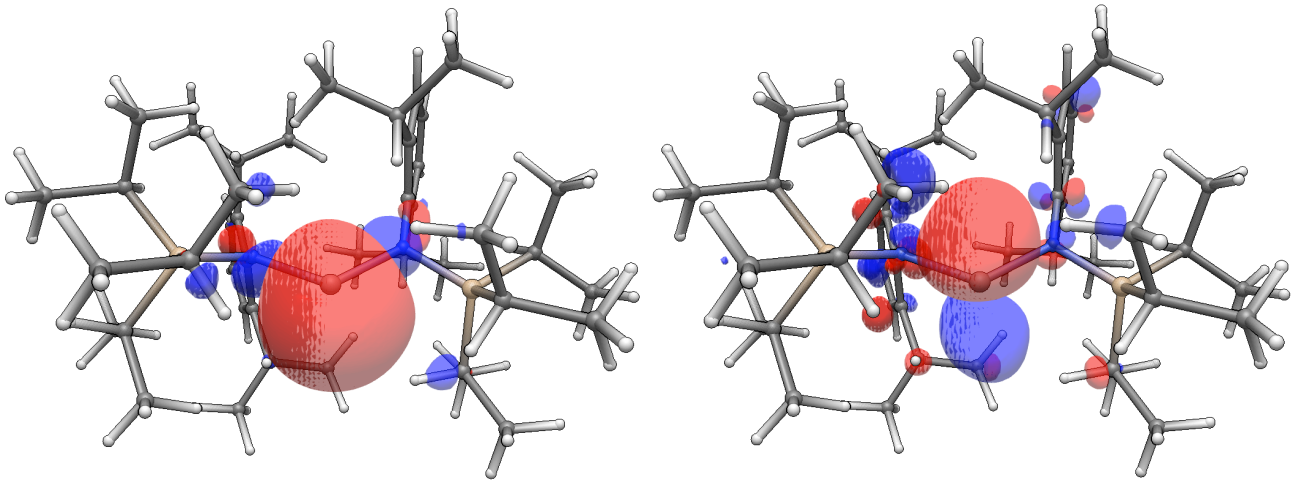

Figure 3.20: HOMO (-0.92 eV, left) and LUMO+4 (2.92 eV, right) of [Al{N(Dipp)Si^{i}Pr$_3$}$_2$]$^-$ free anion, calculated at the DFT-D3, PBE0, Def-TZVP level of theory. Iso-value 0.04.

I*n-silico* determinations of the anion electronic structures between [Al{N(Dipp)SiMe$_3$}$_2$]$^-$ and [Al{N(Dipp)Si^{i}Pr$_3$}$_2$]$^-$ identified similarities between acyclic species both isolated and postulated silylamido aluminyl systems. Comparable orbital energies and consequential HOMO-LUMO+n energy gaps between HOMO (in both the lone pair at aluminium) and LUMO+n being an aluminium *p*-orbital of significant *pz* character (energy gap for [Al{N(Dipp)SiMe$_3$}$_2$]$^-$ = 3.77 eV; [Al{N(Dipp)Si^{i}Pr$_3$}$_2$]$^-$ = 4.02 eV) were calculated. A marginally wider HOMO–LUMO gap for more sterically encumbered system [Al{N(Dipp)Si^{i}Pr$_3$}$_2$]$^-$, was observed due to the aluminium-based LUMO+n being higher in the orbital manifold (LUMO+4) than the less bulky analogue [Al{N(Dipp)SiMe$_3$}$_2$]$^-$ (LUMO+3). Notably LUMO and LUMO+n (n = 1, 2) all featured density upon the ligand scaffold with a key propensity be based within the aryl functional groups.

The optimised structures of calculated diamido acyclic aluminyl systems present a wider ∠N–Al–N angle for [Al{N(Dipp)Si^{i}Pr$_3$}$_2$]$^-$ (123.23°) than for [Al{N(Dipp)Si^{i}Pr$_3$}$_2$]$^-$ (111.26°, avg. 116.47° in solid-state structure of **3-IV**). This greater angle could score poorer π-electron density donation from nitrogen lone pairs into the aluminium *p*-orbital based LUMO. The increased prevalence of acidic C–H···M interactions within [Al{N(Dipp)Si^{i}Pr$_3$}$_2$]$^-$ rather than [Al{N(Dipp)Si^{i}Pr$_3$}$_2$]$^-$, promotes ease of C–H cleavage affording **3-II** and **3-III** not observed within the less bulky systems. The associated gaps were identified to relate closely to that of the silylamido 6-membered [Al(^{Si}NON)]$^-$ (4.06 eV), and 7-membered [Al(SiN^{Dipp})]$^-$ (3.90 eV) metallocyclic aluminyl systems.[11]

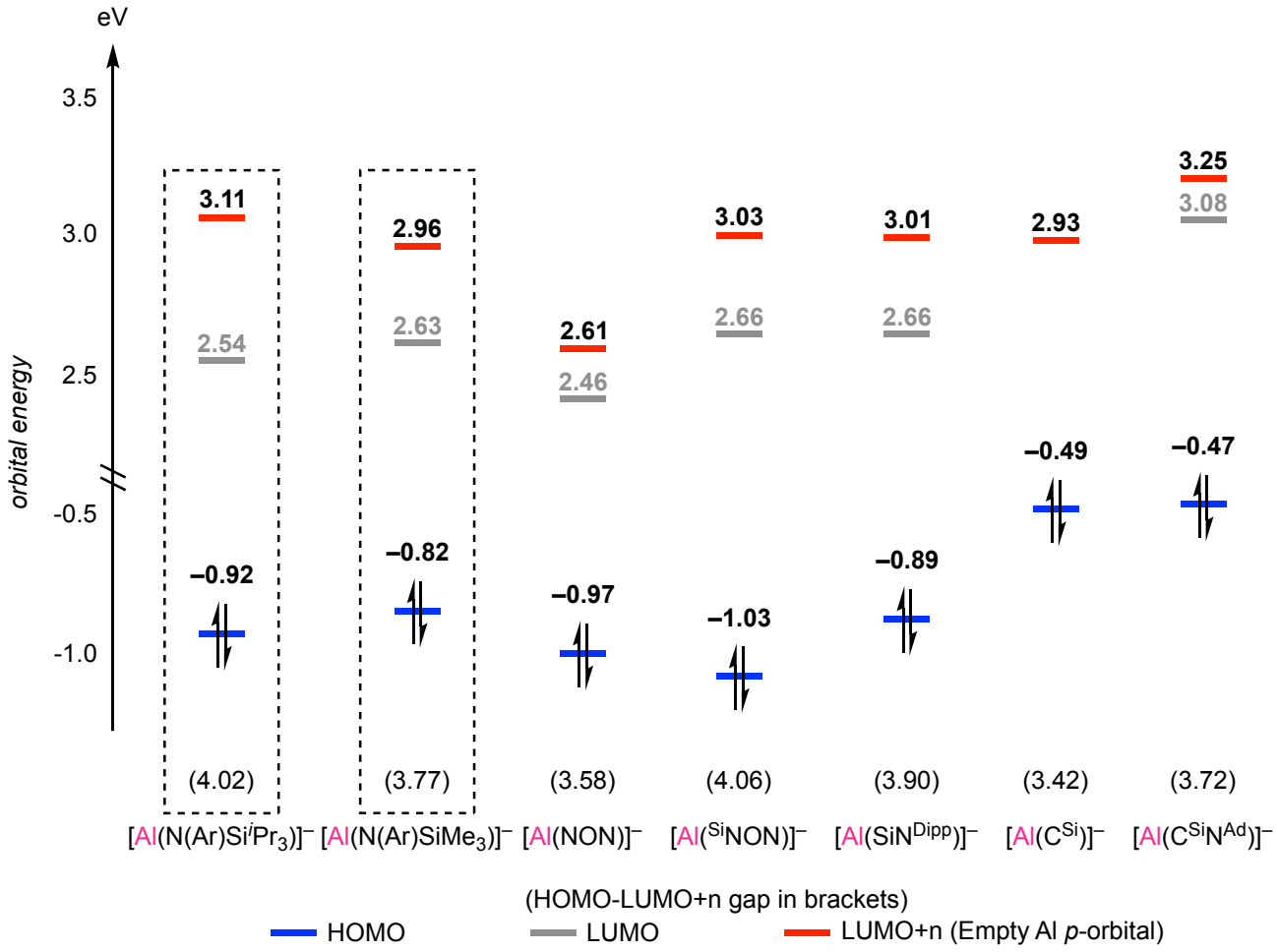

Figure 3.21: HOMO, LUMO and LUMO+n energies of selected, isolated and postulated acyclic aluminyl anions. Selected calculations previously reported by Hicks and coworkers,[11] and acyclic systems [Al{N(Dipp)SiMe$_3$}$_2$]$^-$] and [Al{N(Dipp)Si^{i}Pr$_3$}$_2$]$^-$ calculated at the DFT-D3, PBE0, Def2-TZVP level of theory. Orbital energies of calculated anions displayed in eV, HOMO-LUMO(+n) gap highlighted with in brackets. (Ar = Dipp)*

3.3.5. Initial Reactivity Studies

3.3.5.1. Aluminium(I) as a Nucleophile: Nucleophilic Substitution

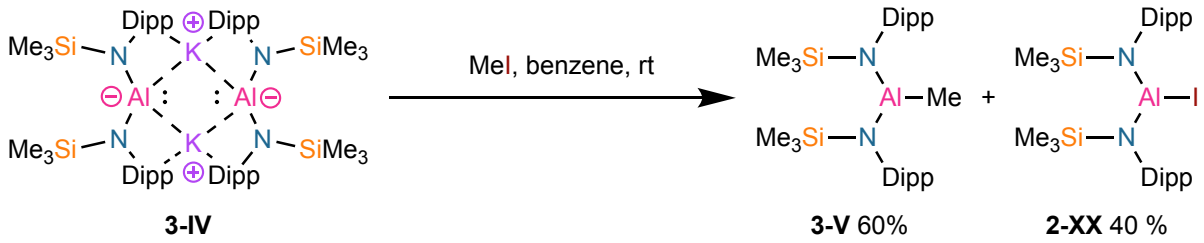

3-IV **3-V** 60% **2-XX** 40 %

*Scheme 3.20: Reaction of acyclic aluminyl **3-IV** with the carbon electrophile iodomethane.*

Highlighted with reported studies of aluminyl anions, the stabilisation of these complexes leads to a nucleophilic aluminium centre available for reactivity. With acyclic system **3-IV**, experimental verification was pursued in aluminium-element bond-forming reactions with an electrophilic carbon source. Treatment of a freshly prepared benzene solution **3-IV** with stoichiometric iodomethane led to an immediate colour change upon contact (Scheme 3.20). The initially bright-yellow solution became colourless with a visible precipitate, suggesting potassium iodide salt elimination. From the ^{1}H NMR spectrum, clean formation of targeted [AlMe{N(Dipp)SiMe$_3$}$_2$] **3-V** was identified, and isolated in a moderate yield (60%). Specifically, the appearance of a 3H integrated singlet at -0.36 ppm signified the formation of an aluminium-methyl substituent upon the aluminium(III) centre. This shift was also reflected in other aluminium-methyl species prepared from aluminyl anions **3.16**,[10] **3.18**,[13b] and **3.23**,[18] affording [AlMe(NON)] (-0.35 ppm), [AlMe(SiN^{Dipp})] (-1.08 ppm), and [AlMe(C^{Si})] (-0.09 ppm), respectively.

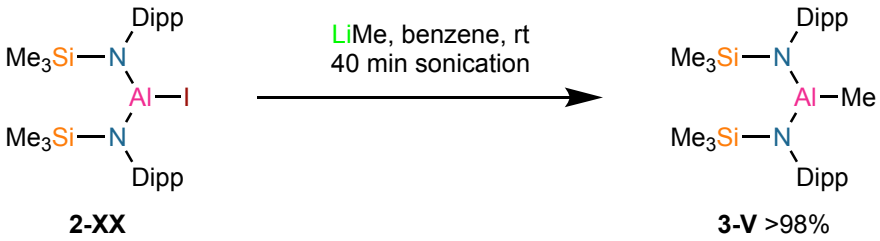

2-XX **3-V** >98%

*Scheme 3.21: Alternate preparation of diamido methylalumane **3-V** from the treatment of **2-XX** with methyllithium.*

Due to the range (-0.09 – -1.08 ppm) present for corresponding methyl signals, independent preparation of the [AlMe{N(Dipp)SiMe$_3$}$_2$] **3-V** was conducted. A benzene solution of precursor **2-XX** was treated with methyllithium powder and sonicated for 40 minutes (Scheme 3.21). Following this, the reaction proceeded cleanly by ^{1}H NMR spectroscopy, leading to a single product identified as **3-V**. This product verified the nucleophilic nature of aluminium(I) centre in **3-IV** via nucleophilic substitutions yielding **3-V**.

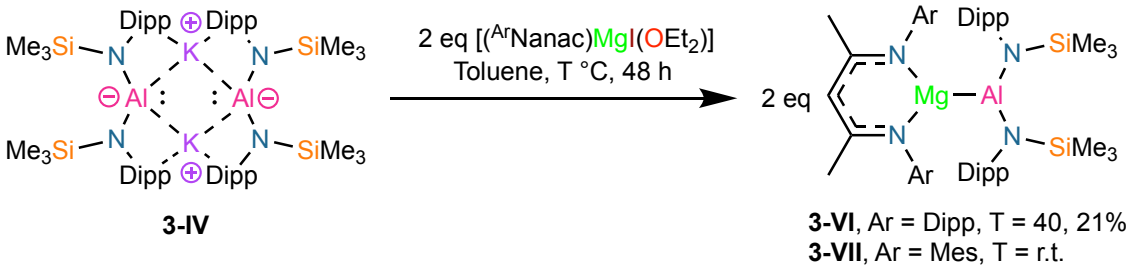

*Scheme 3.22: Synthesis of the magnesium-aluminyl species **3-VI** and postulated synthesis of **3-VII** from **3-IV**.*

To further expand nucleophilic substitution applications, focus shifted to preparing homo- and heterobimetallic complexes from the acyclic aluminyl anion. As reported for nearly all aluminyl anion species, the formation homo- and heterobimetallic complexes is possible from reactions of nucleophilic aluminium sources with metal-based electrophiles (Figure 3.10). To this end, investigations by Liptrot and Jackson involved treatment of **3-IV** with the magnesium electrophile [(^{Dipp}Nacnac)MgI(OEt$_2$)] to form a magnesium-aluminyl complex (*vis-à-vis* **3.58** – **3.60**).[67] My initial investigations in this regard started by treating a toluene solution of **3-IV** with [(^{Dipp}Nacnac)MgI(OEt$_2$)] and heating of the reaction mixture to 40 °C. Following 2 days, the bright-yellow colour of **3-IV** had attenuated and ^{1}H NMR spectroscopy identified a single new major [^{Dipp}Nacnac]$^-$ containing species. Isolation of target species through crystallisation afforded SCXRD quality material in relatively low yield (21%). Analysis via X-ray crystallography confirmed the preparation of targeted magnesium-aluminyl complex [(^{Dipp}Nacnac)Mg-Al{N(Dipp)SiMe$_3$}$_2$] **3-VI** (Figure 3.22).

3-VI represents a heterobimetallic complex featuring an acyclic aluminyl anion with a formal unsupported magnesium-aluminium bond. Within this complex, both metal centres feature trigonal planar arrangements. As highlighted in Figure 3.22, the metal-ligand trigonal planes are each essentially perpendicular to each other (interplanar angle, 94.43(4)°), an arrangement that minimises ligand steric clashing. Compared with analogous complexes, the identified magnesium-aluminium bond length (2.7888(6) Å) aligns with previously reported cyclic examples **3.58** (2.696(1) Å),[10] **3.59** (2.7711(6) Å),[32] and **3.60** (2.7980(6) Å).[13a] In observing the comparative ∠N–Al–N bond angle with the potassium bridged species **3-IV** (116.33(16), 116.61(17)°), the magnesium-aluminyl complex **3-VI** features a slightly increased angle (118.76(5)°), but notably greater than analogous cyclic system **3.60** (111.87(6)°).[13a] Highlighted within the solid-state structure of **3-VI**, the afforded arrangement flexibility from aluminium acyclic ligand scaffolds supports the rotation about Al-N bonds. This allows for the opposing orientation of the Dipp group in each of the silyl(aryl)amido ligand about the aluminium centre. This previously undescribed arrangement disallowed by constrained cyclic ligand scaffolds likely occurs to minimise steric clashing (similar perpendicular metal plane arrangements).

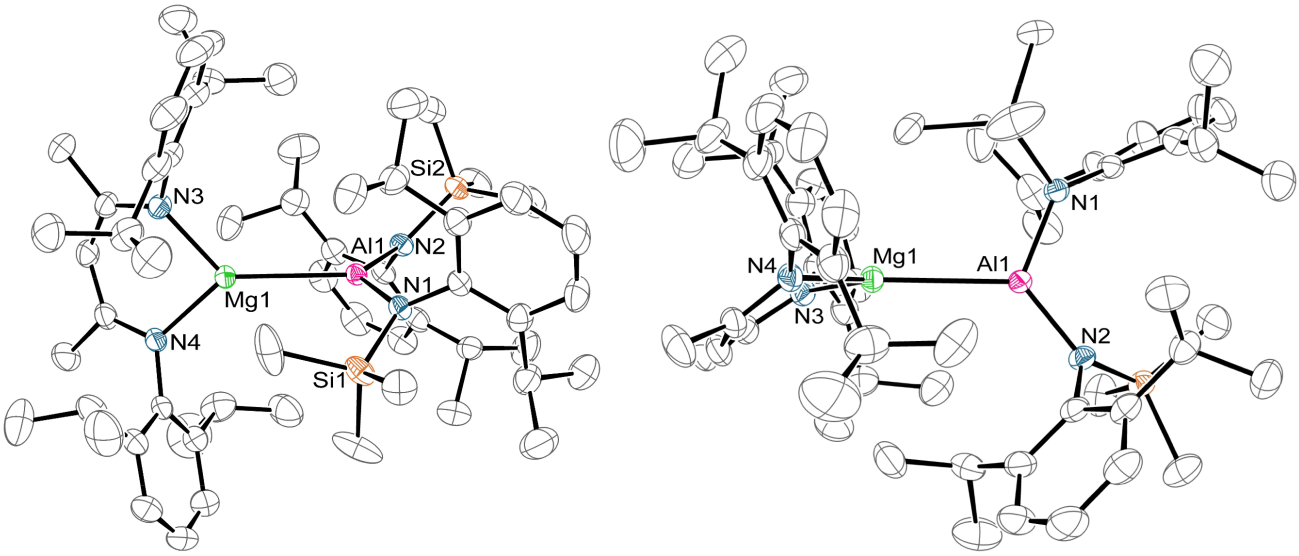

*Figure 3.22: Molecular structure of the magnesium-aluminyl complex **3-VI** as determined by X-ray crystallography represented from two rotational orientations. Hydrogen atoms omitted. Thermal ellipsoids set to 50% probability. Selected bond lengths (Å) and angles (°): Al1-Mg1 2.7888(6), Al1-N1 1.8566(12), Al1-N2 1.8555(12), Mg1-N3 2.0696(12), Mg1-N4 2.0568(12), N1-Al1-N2 118.76(5), Al1-N1-Si1 116.00(6), Al1-N2-Si2 133.64(7), N3-Mg1-N4 92.83(5).*

An analogous magnesium-aluminyl complex, [(^{Mes}Nacnac)Mg-Al{N(Dipp)SiMe$_3$}$_2$] **3-VII**, was also targeted using the less sterically encumbered [(^{Mes}Nacnac)MgI(OEt$_2$)] (Scheme 3.22). Addition of the magnesium iodide to solutions of **3-IV** at ambient, and 40 °C temperatures presented evidence of complex formation via ^{1}H NMR spectroscopy, however, reactions did not proceed cleanly, with evidence of the [^{Mes}Nacnac]$^-$ and [N(Dipp)SiMe$_3$]$^-$ decomposition species.

Investigations were also undertaken to access the potassium aluminyl **3-VI** and magnesium-aluminyl **3-VII** species through 2-electron reductions with magnesium(I) dimers featuring corresponding [^{Dipp}Nacnac]$^-$ and [^{Mes}Nacnac]$^-$ ligand scaffolds. In all cases, treatment of the acyclic aluminium(III) iodide precursors with magnesium reducing agents afforded an indiscernible mixture of decomposition products. Despite varied hydrocarbon solvents, temperatures and reaction times, crystalline material of targeted species or degradation products could not be isolated.

3.3.5.2. Oxidative Addition Investigations with an Acyclic Aluminyl Anion

Following successful preparations of nucleophilic substitution products from reactions with **3-IV**, focus shifted to the reactivity toward small molecules and relatively inert substrates. Given findings through reductions of bulkier **2-XVII** precursor affording C-H activation products **3-II** and **3-III**, anticipation of successful oxidative addition processes were elevated. To this end, investigations were undertaken with a range of small gaseous molecules (CO, CO$_2$, N$_2$, N$_2$O, C$_2$H$_4$). In nearly all examples, treatment of the vivid yellow solutions of **3-IV** with gases via *freeze-pump-thaw* method afforded rapid

fading of solution colour. Analysis of reaction mixtures via ^{1}H NMR spectroscopy identified the consistent formation of **3-IV** related degradation species. Most commonly, this was presented with the formation of proligand [HN(Dipp)SiMe$_3$] **2-IV**, highlighting the decomposition of the acyclic aluminyl species or its reaction products. Reactions were also undertaken at cooled temperatures in an attempt to isolate the kinetic products, but such investigations once again yielded the formation of proligand identified via ^{1}H NMR spectroscopy. Notably, it is hypothesised that the lack of chelate effect present within ligand coordination modes sees increased lability of bulky silyl(aryl)amido scaffolds with respect to bidentate counterparts. Consequently, the elimination of bulky ligands from metal centres reduces the likelihood of a single species being isolated.

Toward replicating the identified reactivity of the seminal aluminyl anion complex **3.18**, benzene solutions of **3-IV** were also heated to 60 and 80 °C. However, rather than the preparation of C-H activated aluminate system analogous to those previously reported **3.82** (Scheme 3.6),[10] complex **3-IV** underwent thermolysis to several intractable species and predominant proligand HN(Dipp)SiMe$_3$ **2-IV**.

3.3.6. Attempted Preparation of MIP and SIP complexes

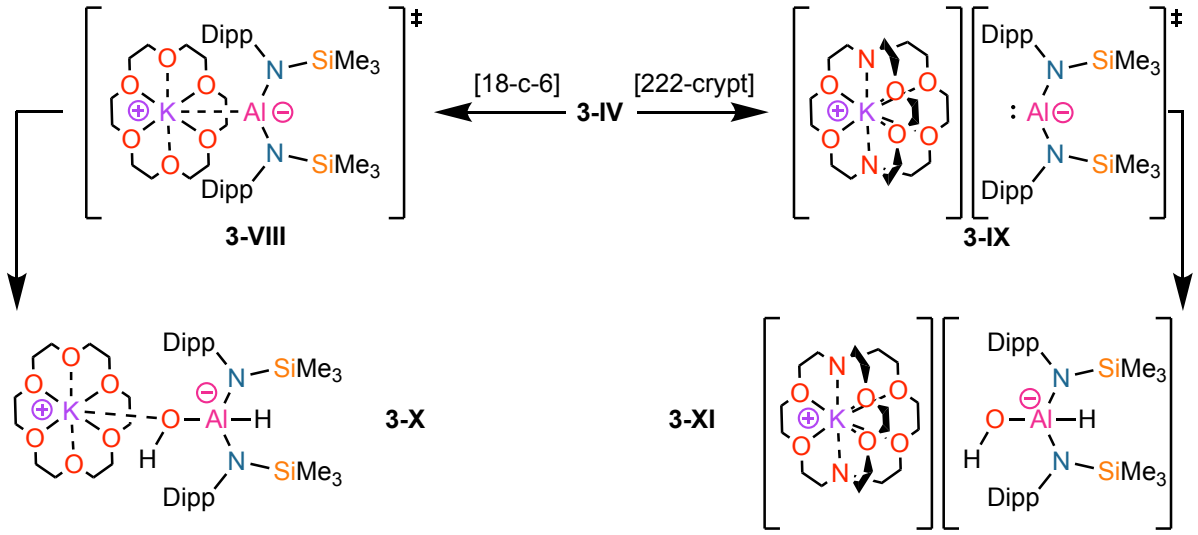

*Scheme 3.23: Investigations toward acyclic aluminyl MIP **3-VIII** and SIP **3-IX** species affording aluminate complexes featuring sequestered potassium cations.*

Investigations toward preparing the first examples of acyclic aluminyl MIP and SIP systems were inspired by reported successes with the bulky xanthene stabilised [K$_2${Al(NON)}$_2$] **3.18** complex affording the corresponding potassium MIP **3.42** and SIP **3.46**.[10, 30] Highlighted by a slightly larger HOMO-LUMO gap for the calculated acyclic aluminyl anion **3-IV** (3.77 eV) than **3.18** (3.58 eV),[11] it was hypothesized that the resultant acyclic species may be isolable at ambient temperatures and/or

yield derivatives indicative of MIP and SIP aluminyl reactivity. Accordingly, benzene solutions of **3-IV** were prepared within a glovebox and treated with stoichiometric 18-crown-6 and crypt-222 to give MIP **3-VIII** and SIP **3-IX**, respectively (Scheme 3.23). In both cases, an instantaneous colour cascade was observed whereby initially vivid-yellow solutions of **3-IV**, briefly became bright-orange, then transitioned to a pale-yellow within a 10 second timeframe. ^{1}H NMR spectroscopy was performed immediately on both reaction mixtures and identified the predominant formation of proligand **2-IV**, minor signals featuring unknown silyl(aryl)amido environments, and corresponding 18-crown-6- and crypt-222-containing species which could be attributed to hydrolysis products (5–15% consistent with adventitious moisture). Following 3 hours at ambient temperature, an orange oil had phase separated from the now colourless solution which could be postulated as the proligand. In ascertaining the identity of the species present within solution, crystallisation attempts were undertaken from benzene. SCXRD quality crystals were isolated from both reaction mixtures, with the 18-crown-6 species isolated from benzene and a corresponding crypt-222 species from cyclohexane. Respectively, both species were isolated and identified to be the formal O-H oxidative addition products of water with sequestered potassium cations; [K(18-crown-6)][HAl{N(Dipp)SiMe$_3$}$_2$(OH)] **3-X** and [K(crypt-222)][HAl{N(Dipp)SiMe$_3$}$_2$(OH)] **3-XI** (Figure 3.23).

Highlighted within their solid-solid state structures, both **3-X** and **3-XI** feature tetracoordinate aluminium(III) centres with two silyl(aryl)amido, a terminal hydride and hydroxido ligands (Figure 3.23). The negatively charged aluminium centre in each complex necessitates a +1 counterion, satisfied by the potassium present. Consequential to the nature of the introduced 18-crown-6 and crypt-222 sequestering reagents, the interactions of potassium cation with the aluminate complex are varied. Consistent with a monomeric ion pair aluminate complex **3-X** presents a weak interaction of the cation with terminal oxygen (2.7032(13) Å) and no interactions with the aluminium(III) centre (4.2810(6) Å). Conversely, **3-XI** features and formally separated ion pair aluminate with significant distance between potassium and oxygen (5.916(3) Å) or aluminium (7.5684(7) Å) atoms.

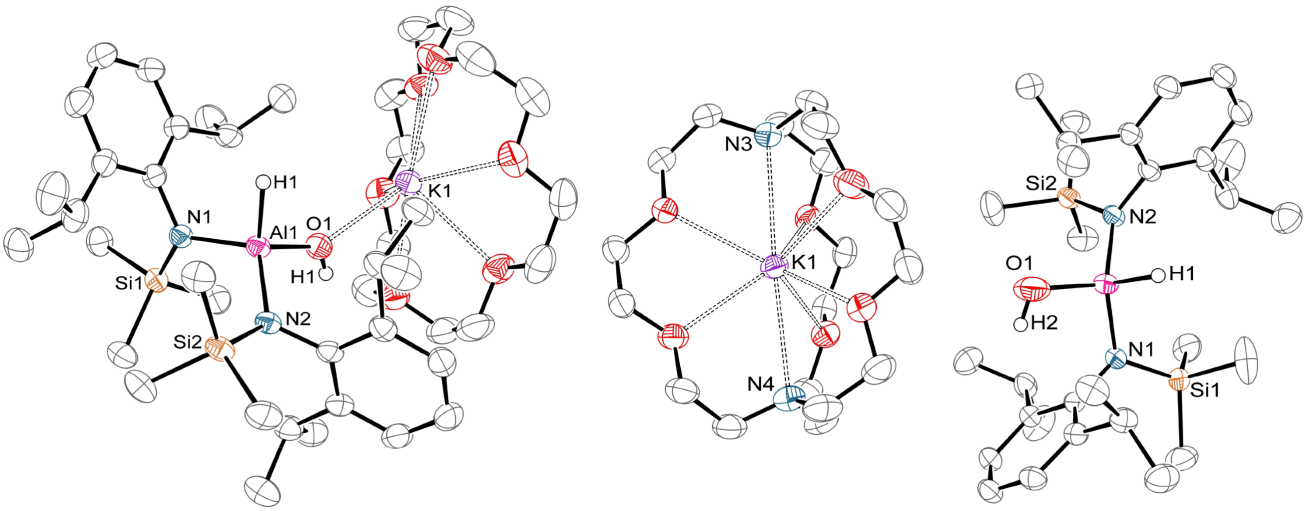

*Figure 3.23: Molecular structures of O-H oxidative addition products featuring MIP **3-X** (left) and SIP **3-XI** (right) arrangements as determined by X-ray crystallography represented from two rotational orientations. Most hydrogen atoms omitted. Thermal ellipsoids set to 50% probability. **3-X** Selected bond lengths (Å) and angles (°): K1···O1 2.7032(13), K1···Al1 4.2810(6), Al1-H1 1.64(2), Al1-O1 1.7720(14), Al1-N1 1.9008(14), Al1-N2 1.8960(14), O1-Al1-H1 108.5(7), N1-Al1-N2 115.80(6). **3-XI** Selected bond lengths (Å) and angles (°): (°): K1···O1 5.916(3), K1···Al1 7.5684(7), Al1-H1 1.61(6), Al1-O1 1.758(3), Al1-N1 1.8999(14), Al1-N2 1.9036(14), O1-Al1-H1 118.6(19), N1-Al1-N2 120.53(6).*

The products and the brief identification of the vivid orange solution suggest the transient formation of targeted **3-VIII** and **3-IX** compounds. However, these compounds quickly (if present) activated advantageous water to give MIP **3-VIII** or SIP **3-IX**. The source of water impurity still remains a mystery. However, as chemical curiosities, **3-VIII** and **3-IX** feature both a terminal hydride and a proton. If similarly furnished upon a transition metal rather than aluminium centre, complexes featuring such moieties would be reminiscent of popular catalysts utilised in (de)hydrogenations.[68] The preparation of an isolable acyclic MIP **3-VIII** or SIP **3-IX** aluminyl anion system is ongoing and requires further investigations.

Concurrent to the above-mentioned investigations, the first isolated example of a "naked" aluminyl anion **3.50** was reported by Aldridge, Sarkar and coworkers in 2024, by cation sequestration with 2,2,2-cryptand (Figure 3.8).[21] As highlighted within the calculated HOMO-LUMO gaps of monomeric aluminyl anion fragments (Figure 3.21), the employment of strongly stabilising in NHBO **3.50** (4.29 eV) rather than bulky silyl(aryl)amido ligands in $[Al\{N(Dipp)SiMe_3\}_2]^-$ (3.77 eV) has been greatly beneficial in tuning the electronics of these species.

3.4. Conclusions

Since 2018, a growing catalogue of aluminium(I) anions have been isolated, and their diverse and metallomimetic reactivity has been investigated. All previously developed species have constrained the aluminyl centre within a metallocycle of varying ring size (5- to pseudo-8-membered). Following the preparation of two acyclic aluminium(III) iodide precursors in **Chapter 2** (**2-XVII**, **2-XX**), extensive reduction and reactivity investigations have been undertaken.

Extensive reduction investigations have been undertaken with the sterically bulkier precursor [AlI{N(Dipp)Si^{i}Pr$_3$}$_2$] **2-XVII**, however, the corresponding acyclic aluminyl anion could not be isolated. Rather, products of intramolecular C-H activation with the aluminium centre were obtained and postulated to occur via radical **3-I** and oxidative addition mechanisms, **3-II** and **3-III**.

Employing the sterically diminished [AlI{N(Dipp)SiMe$_3$}$_2$] **2-XX** precursor, reductions with potassium graphite afforded the first example of an acyclic aluminyl anion **3-IV**. This species was characterised via X-ray crystallography and with heteronuclear NMR spectroscopy. Additionally, ^{1}H DOSY NMR spectroscopy ascertained **3-IV** to exist as a dimeric pair with both the solid- and solution-states. From its solid-state structure, **3-IV** exists as a twisted arrangement with the added flexibility of the acyclic ligand scaffolds supporting more favourable atomic interactions and repulsions. Synthetic optimisations via mechanochemical preparations of **3-IV** resulted in higher yields (89%) compared to solution state methods (71%).

Computational investigations identified the similarity of HOMO-LUMO gaps of acyclic aluminyl anions ([Al{N(Dipp)Si^{i}Pr$_3$}$_2$]$^-$ 4.02, [Al{N(Dipp)SiMe$_3$}$_2$]$^-$ 3.77 eV) compared to reported cyclic aluminyl anions incorporating amido and silyl groups within heterocycles ([Al(^{Si}NON)]$^-$ 4.06, [Al(SiN^{Dipp})]$^-$ 3.90 eV). Brief reactivity investigations with carbon-based electrophiles were undertaken confirming the nucleophilic nature of **3-IV**'s aluminium(I) centre. Moreover, reactions with metal electrophiles afforded the first example of a magnesium-aluminyl complex featuring an acyclic ligand scaffold **3-VI**. Attempts toward the preparation of the monomeric and separated ion pair systems **3-VIII** and **3-IX** afforded the aluminate complexes **3-X** and **3-XI**, respectively, presumably from the oxidative addition of H_2O.

Continuing investigations are being undertaken to further examine the reactivity and applications of this new variety of aluminyl anion, whilst utilising findings in directing precursor and heterobimetallic species developments.

3.5. Experimental

General Methods and Considerations

All reactions dealing with air- and moisture-sensitive compounds were carried out under an argon atmosphere using standard Schlenk line and glovebox techniques. NMR experiments using air sensitive compounds were conducted in J. Young's tap NMR tubes prepared and sealed in a glovebox under argon. Toluene, hexane, and pentane were purified using an MBraun Solvent Purification System and stored over 4Å molecular sieves or sodium mirror and degassed with argon before use. Diethyl ether was dried using sodium suspended in a benzophenone solution. C_6D_6 and toluene-d_8 were dried over potassium mirrors prior to vacuum transfer into sealed ampoules and stored in a glove box under argon. All NMR data, unless otherwise stated, were acquired at 298 K on either an Agilent ProPulse instrument for ^{1}H (500 MHz), $^{13}C\{^{1}H\}$ (126 MHz) and $^{29}Si\{^{1}H\}$ (99 MHz), a Bruker Ascend 400 for ^{1}H (400 MHz), $^{13}C\{^{1}H\}$ (101 MHz) and $^{29}Si\{^{1}H\}$ (79 MHz) or Bruker Ascend 700 for $^{13}C\{^{1}H\}$ (176 MHz) and $^{29}Si\{^{1}H\}$ (139 MHz). ^{1}H and ^{13}C NMR spectra were referenced using residual solvent resonances. Chemical shifts δ are reported in part per million (ppm), coupling constants are reported in Hertz (Hz) and coupling patterns are abbreviated as follows: m (multiplet), s (singlet), d (doublet), t (triplet), q (quartet), quin (quintet), sex (sextet), sept (septet), or combinations thereof. IR spectroscopy was acquired on a Brucker Alpha II or a PerkinElmer UATR Two FT-IR spectrometer. UV-Vis spectroscopy was acquired on a Mettler Toledo spectrophotometer UV5 and the spectra of which were collected by collaborators D. J. Liptrot and R. A. Jackson at the University of Bath.[67] **2-XVII** and **2-XX** were prepared as discussed in previous Chapters. [(^{Dipp}Nacnac)MgI(OEt_2)], [(^{Mes}Nacnac)MgI(OEt_2)], [{Mg(^{Mes}Nacnac)}$_2$], and 5% w/w Na/NaCl, 5% w/w K/KI were synthesised according to their respective literature methods.[62, 69] Methyl lithium powder was prepared from 1.6 M solution with volatiles removed under reduced pressure by Li Feng Lim. K[Fe(CO)$_2$Cp] was prepared by Dr. Fabian Kallmeier according to literature methods.[70] All other reagents were used as received. Elemental analyses of (**3-IV**) and (**3-VI**) were performed by Elemental Microanalysis Ltd., Okehampton, Devon, U.K.

Attempted synthesis of [(Cp)(CO)$_2$Fe–Al{N(Dipp)SiMe$_3$}$_2$]

Method A: [AlI{N(Dipp)SiMe$_3$}$_2$] **2-XX** (200 mg, 0.291 mmol), K[Fe(CO)$_2$(Cp)] (67 mg, 2.91 mmol), and graphite (267 mg) were charged into an IKA BMT-20-S 20 mL polypropylene vessel with stainless steel balls (28 pieces, diameter: 5 mm, weight per ball: 0.52 g, type: AISI 304). Milling was initiated on the highest setting (4000 rpm, 66.7 Hz) for 1 h using an IKA ULTRA-TURRAX® Tube Drive. This yielded a black powder, and subsequent extraction with deuterated benzene (0.5 mL) identified the generation of proligand HN(Dipp)SiMe$_3$ **2-IV** via ^{1}H NMR spectroscopy. Isolation of

the solid from the polypropylene vessel and extraction with benzene (5 mL) yielded an orange-brown mixture. Removal of volatiles under reduced pressure yielded a brown-tinged oil of proligand HN(Dipp)SiMe$_3$ **2-IV** as identified via ^{1}H NMR spectroscopy. **Method B:** To a J. Young's NMR tube, a deuterated benzene (0.5 mL) solution of [AlI{N(Dipp)SiMe$_3$}$_2$] **2-XX** (55 mg, 84.5 μmol), K[Fe(CO)$_2$(Cp)] (18.5 mg, 85.6 μmol) was charged. An immediate change from a colourless solution to a dark-orange opaque solution was observed following agitation, from which ^{1}H NMR spectroscopy identified an indiscernible mixture of species. Following 12 h at room temperature, ^{1}H NMR spectroscopy identified the predominant formation of proligand HN(Dipp)SiMe$_3$ **2-IV**, along with unreacted K[Fe(CO)$_2$(Cp)] and decomposed cyclopentadiene species.

Attempted synthesis of [(Cp)(CO)$_2$Fe–Al{N(Dipp)Si^{i}Pr$_3$}$_2$], and isolation of [Al(H){N(Dipp)Si^{i}Pr$_2$CH(Me)CH$_2$}{N(Dipp)Si^{i}Pr$_3$}] (3-I)

Method A: [AlI{N(Dipp)Si^{i}Pr$_3$}$_2$] **2-XVII** (200 mg, 291 μmol), K[Fe(CO)$_2$(Cp)] (630 mg, 2.91 mmol), and graphite (440 mg) were charged into an IKA BMT-20-S 20 mL polypropylene vessel with stainless steel balls (30 pieces, diameter: 5 mm, weight per ball: 0.52 g, type: AISI 304). Milling was initiated on the highest setting (4000 rpm, 66.7 Hz) for 1 h using an IKA ULTRA-TURRAX® Tube Drive. Yielding a black powder, and ^{1}H NMR analysis identified the majority species as unreacted [AlI{N(Dipp)Si^{i}Pr$_3$}$_2$] **2-XVII**, and an impurity of proligand HN(Dipp)Si^{i}Pr$_3$ **2-I** via ^{1}H NMR spectroscopy. Continued milling and analysis at 2.5, 5, and 6 h increments identified the progressive degradation into proligand **2-I**. Isolation of the black powder from the polypropylene vessel and extraction with benzene (3 × 5 mL) yielded an orange-brown solution. Removal of volatiles from combined extracts under reduced pressure yielded a brown-tinged oily solid of proligand HN(Dipp)Si^{i}Pr$_3$ **2-I**. **Method B:** To a J. Young's NMR tube, a C_6D_6 (0.5 mL) solution of [AlI{N(Dipp)Si^{i}Pr$_3$}$_2$] **2-XVII** (40 mg, 58.2 μmol), K[Fe(CO)$_2$(Cp)] (10.5 mg, 48.6 μmol) was charged. Following a lack of interaction of the species at ambient temperature (as determined via ^{1}H NMR spectroscopy), the reaction mixture was heated to 70 °C. Following 2 h at this temperature, a gradual colour change toward a dark-red/orange solution was observed. Following 48 h at 70 °C, reaction progression had halted, and a mixture of 3 [N(Dipp)Si(^{i}Pr)$_3$]$^-$ containing species was identified via ^{1}H NMR spectroscopy. Subsequent purification attempts were unable to separate this mixture of products, however, crystallisation afforded decomposition products including [Al(H){N(Dipp)Si^{i}Pr$_2$CH(Me)CH$_2$}{N(Dipp)Si^{i}Pr$_3$}] **3-I** as colourless blocks and [(Cp)Fe(CO)(μ-CO)]$_2$ as dark-red plates. **Method C:** To a freshly prepared potassium mirror (1 g, excess), a pale-yellow toluene (20 mL) solution of [AlI{N(Dipp)Si^{i}Pr$_3$}$_2$] **2-XVII** (208 mg, 254 μmol, 1.0 eq.) was added. No colour change was observed following stirring at ambient temperature for 20 min, but after

1 h, the reaction solution had become dark brown. Analysis of the reaction solution by ^{1}H NMR spectroscopy identified the formation of H_2, HN(DIPP)Si^{i}Pr$_3$ **2-I**, K[Al(H){N(Dipp)Si^{i}Pr$_3$}{N(Dipp)Si^{i}Pr$_2$CMe$_2$}] **3-II**, and an unknown unsymmetrical diisopropylphenyl-containing species. Separation of solution from the grey precipitate via cannula filtration afforded a dark brown solution. Removal of volatiles from the filtrate under reduced pressure yielded a brown oil. 8 days at ambient temperature saw single crystals grow from the oil that were suitable for SCXRD, which were confirmed to be [Al(H){N(Dipp)Si^{i}Pr$_2$CH(Me)CH$_2$}{N(Dipp)Si^{i}Pr$_3$}] **3-I**. Analysis of the remaining oil by ^{1}H NMR spectroscopy identified a mixture of HN(DIPP)Si^{i}Pr$_3$, K[Al(H){N(Dipp)Si^{i}Pr$_3$}{N(Dipp)Si^{i}Pr$_2$CMe$_2$}] **3-II**, and [Al(H){N(Dipp)Si^{i}Pr$_2$CH(Me)CH$_2$}{N(Dipp)Si^{i}Pr$_3$}] **3-I**. **N.B.** Attempts to purify the crystals from and oil were unsuccessful.

^{1}H NMR (400 MHz, C_6D_6, 298 K): δ = 6.96 – 6.85 (m, 6H, Dipp-aryl-*H*), 4.06 (br., 1H, Dipp-C*H*(CH$_3$)$_2$), 3.77 (br., 1H, Dipp-C*H*(CH$_3$)$_2$), 3.42 (br., 1H, Dipp-C*H*(CH$_3$)$_2$), 2.99 (br., 1H, Dipp-C*H*(CH$_3$)$_2$), 1.53 – 1.48 (m, 6H, Si{C*H*(CH$_3$)$_2$}$_3$), 1.37 – 1.28 (m, 24H, Dipp-CH(C*H*$_3$)$_2$), 1.15 – 1.08 (m, 24H, SiCH(C*H*$_3$)$_2$), 0.70 (d, 2H, $^{3}J_{HH}$ = 7.4 Hz, Si-CH(C*H*$_2$)), 0.47 (d, 3H, $^{3}J_{HH}$ = 7.3 Hz, SiCH(C*H*$_3$)$_2$), 0.05 – 0.01 (m, 6H, SiCH(C*H*$_3$)$_2$).

Synthesis of K[Al(H){N(Dipp)Si^{i}Pr$_3$}{N(Dipp)Si^{i}Pr$_2$CMe$_2$}] (3-II)

Method A: To a suspension of light blue 5% K/KI (1.05 g, 1.28 mmol K, 5.12 eq.) in toluene (20 mL) was added a pale-yellow solution of [AlI{N(Dipp)Si^{i}Pr$_3$}$_2$] **2-XVII** (205 mg, 0.25 mmol, 1.0 eq.) in toluene (10 mL) dropwise over 20 min at –20 °C. Stirred at –20 °C for 18 h, a dark-yellow solution with grey precipitate formed. Separation of the dark-yellow solution from the grey solid via cannula filtration, and removal of volatiles under reduced pressure yielded K[HAl{N(Dipp)Si^{i}Pr$_3$}{N(Dipp)Si^{i}Pr$_2$CMe$_2$}] **3-II** as a burnt-orange solid (22 mg, 12%). Following 8 days of standing at ambient temperature, a saturated toluene solution yielded SCXRD quality crystals of K[AlH{N(Dipp)Si^{i}Pr$_3$}{N(Dipp)Si^{i}Pr$_2$CMe$_2$}] **3-II**. **^{1}H NMR** (400 MHz, C_6D_6, 298 K): δ = 7.28 (dd, $^{3}J_{HH}$ = 7.5 Hz, $^{4}J_{HH}$ = 2.1 Hz, 1H, Dipp-aryl-*H*), 7.04 – 7.12 (m, 2H, Dipp-aryl-*H*), 6.56 (d, $^{3}J_{HH}$ = 8.0 Hz, 2H, Dipp-aryl-*H*), 6.38 (t, $^{3}J_{HH}$ = 7.5 Hz, 1H, Dipp-aryl-*H*), 4.50 (sept, $^{3}J_{HH}$ = 6.5 Hz, 1H, Dipp-C*H*(CH$_3$)$_2$), 4.29 (sept, $^{3}J_{HH}$ = 6.8 Hz, 1H, Dipp-C*H*(CH$_3$)$_2$), 4.12 (sept, $^{3}J_{HH}$ = 6.7 Hz, 1H, Dipp-C*H*(CH$_3$)$_2$), 3.91 (sept, $^{3}J_{HH}$ = 6.4 Hz, 1H, Dipp-C*H*(CH$_3$)$_2$), 2.96 (br., 1H, Al-*H*), 2.16 (s, 3H, SiCH(C*H*$_3$)$_2$), 2.08 (s, 3H, SiCH(C*H*$_3$)$_2$), 1.86 (d, $^{3}J_{HH}$ = 7.0 Hz, 3H, SiCH(C*H*$_3$)$_2$), 1.75 – 1.82 (m, 1H, SiC*H*(CH$_3$)$_2$), 1.60 – 1.67 (m, 4H, 1H SiC*H*(CH)$_3$, 3H SiCH(C*H*)$_3$), 1.53 (d, $^{3}J_{HH}$ = 6.7 Hz, 3H, Dipp-CH(C*H*$_3$)$_2$), 1.40 – 1.53 (m, 12H, 6H, Dipp-CH(C*H*$_3$)$_2$), 3H SiC*H*(CH)$_3$, 3H SiCH(C*H*)3), 1.33 (d, $^{3}J_{HH}$ = 7.7 Hz, 18H, SiCH(C*H*$_3$)$_2$), 1.32 (d, $^{3}J_{HH}$ = 7.4 Hz, 3H, Dipp-CH(C*H*$_3$)$_2$), 1.19 (d, $^{3}J_{HH}$ = 6.8 Hz, 3H,

Dipp-CH(CH_3)$_2$), 0.95 (d, $^3J_{HH}$ = 7.3 Hz, 3H, SiCH(CH_3)$_2$), 0.87 (d, $^3J_{HH}$ = 6.7 Hz, 3H, Dipp-CH(CH_3)$_2$, 0.49 (d, $^3J_{HH}$ = 6.5 Hz, 3H, Dipp-CH(CH_3)$_2$), 0.21 (d, $^3J_{HH}$ = 6.7 Hz, 3H, Dipp-CH(CH_3)$_2$). **^{13}C{^{1}H} NMR** (101 MHz, C_6D_6, 298 K) δ = 156.5 (Aryl-*C*), 150.5 (Aryl-*C*), 150.0 (Aryl-*C*), 148.4 (Aryl-*C*), 146.2 (Aryl-*C*), 145.0 (Aryl-*C*), 124.4 (Aryl-*C*), 123.5 (Aryl-*C*), 123.4 (Aryl-*C*), 123.4 (Aryl-*C*), 121.0 (Aryl-*C*), 120.7 (Aryl-*C*), 29.3 (Dipp-*C*H(CH$_3$)$_2$), 28.6 (Al-C-*C*H$_3$), 27.8 (Al-C-*C*H$_3$), 27.6 (Dipp-*C*H(CH$_3$)$_2$), 27.0 (Dipp-*C*H(CH$_3$)$_2$), 27.0 (Dipp-*C*H(CH$_3$)$_2$), 26.9 (Dipp-*C*H(CH$_3$)$_2$), 26.7 (Dipp-CH(*C*H$_3$)$_2$), 26.3 (Dipp-*C*H(CH$_3$)$_2$), 26.2 (Dipp-CH(*C*H$_3$)$_2$), 25.7 (Dipp-CH(*C*H$_3$)$_2$), 25.1 (Dipp-CH(*C*H$_3$)$_2$), 23.6 (Dipp-*C*H(CH$_3$)$_2$), 23.6 (Dipp-CH(*C*H$_3$)$_2$), 21.4 SiCH(*C*H$_3$)$_2$), 21.4 Si*C*H(CH$_3$)$_2$), 20.6 SiCH(*C*H$_3$)$_2$), 20.5 SiCH(*C*H$_3$)$_2$), 20.2 SiCH(*C*H$_3$)$_2$), 20.0 SiCH(*C*H$_3$)$_2$), 18.1 Si*C*H(CH$_3$)$_2$), 15.9 SiCH(*C*H$_3$)$_2$), 15.2 Si*C*H(CH$_3$)$_2$). **^{29}Si{^{1}H} NMR** (139 MHz, C_6D_6, 298 K) δ = 2.0 (N-*Si*CH(CH$_3$)$_2$), 1.0 (Al-CH$_2$-*Si*). **IR** (cm^{-1}) (Nujol): 2967(m), 2943(m), 2863(m), 2831(m), 1757(w), 1584(w), 1471(w), 1417(m), 1309(w), 1233(w), 1196(w), 1171(w), 1107(w), 1098(w), 1040(w), 1013(w), 914(w), 886(w), 914(w), 886(w), 832(w), 817(w), 794(m), 783(m), 741(w), 730(w), 689(w), 658(w), 588(w), 557(w). **E.A:** Despite attempts, conclusive elemental analysis was not possible.

Attempted synthesis of Na[Al{N(Dipp)Si^{i}Pr$_3$}$_2$], and preparation of the CH activated species (3-III)

To a freshly prepared sodium mirror (1 g, excess) in a 10 mL Schlenk flask was charged [AlI{N(Dipp)Si^{i}Pr$_3$}$_2$] **2-XVII** (154 mg, 188 μmol, 1.0 eq.). Then diethyl ether (7 mL) was added and following 5 min of stirring, a colour change to yellow was observed. After stirring for 18 h, the bright yellow reaction mixture was separated via a filter cannula and the filtrate was evaporated to dryness, yielding a pale-yellow powder (115 mg). Dissolution of the solids in deuterated benzene (0.5 mL) afforded a yellow solution. ^{1}H NMR spectroscopy identified a mixture of four diisopropylphenyl-containing products within solution. Concentration of the benzene solution under reduced pressure to a volume of 0.1 mL afforded SCXRD quality crystals of **3-III** following 47 days at ambient temperature. **N.B.** Attempts at repeating the synthesis yielded a mixture of products including decomposition to the amine HN(Dipp)Si(^{i}Pr)$_3$ **2-I**.

Synthesis of [K$_2$(Al{N(Dipp)SiMe$_3$}$_2$)$_2$] (3-IV)

Method A: In a glovebox, a Schlenk flask was charged with [AlI{N(Dipp)SiMe$_3$}$_2$] **2-XX** (350 mg, 538 μmol, 1.0 eq.) and potassium graphite (363 mg, 2.69 mmol, 5.0 eq.). The mixture was suspended in benzene (3.5 mL) and stirred for 1.5 h. Subsequent cannula filtration yielded a dark-yellow solution. Removal of the volatiles from the filtrate under reduced pressure afforded [K$_2$(Al{N(Dipp)SiMe$_3$}$_2$)$_2$] **3-IV** as a vivid-yellow powder (215 mg, 71%). **N.B.** Following 5 days of

standing at ambient temperature in a saturated benzene solution to *ca.* 0.3 mL, crystals of **3-IV** for SCXRD were isolated. **Method B:** [AlI{N(Dipp)SiMe$_3$}$_2$] **2-XX** (200 mg, 307 µmol, 1.0 eq.) and potassium graphite (820 mg, 6.07 mmol, 19.8 eq.) were added to a 20 mL IKA BM-20-S polypropylene vessel with stainless steel balls (30 pieces, diameter: 5 mm, weight per ball: 0.52 g, type: AISI 304). Milling was initiated on the highest setting (4000 rpm, 66.7 Hz) for 1 h using an IKA ULTRA-TURRAX® Tube Drive. The resulting black powder was analysed via ^{1}H NMR spectroscopy confirming the nearly quantitative formation of **3-IV**. Transfer of the black powder into a Schlenk flask, followed by extraction with benzene (3 × 5 mL) yielded a bright yellow solution. Removal of the volatiles from the combined extracts under reduced pressure afforded **3-IV** as a vivid yellow powder (154 mg, 89%). **^{1}H NMR** (400 MHz, C_6D_6, 298 K): δ = 6.90 – 6.88 (m, 8H, Dipp-aryl-*H*), 6.85 – 6.81 (m, 4H, Dipp-aryl-*H*), 3.93 (sept, $^3J_{HH}$ = 6.8 Hz, 8H, Dipp-C*H*(CH$_3$)$_2$), 1.30 (d, $^3J_{HH}$ = 7.0 Hz, 24H, Dipp-CH(C*H*$_3$)$_2$), 1.07 (d, $^3J_{HH}$ = 6.8 Hz, 24H, Dipp-CH(C*H*$_3$)$_2$), 0.41 (s, 36H, Si(C*H*$_3$)$_3$). **^{1}H NMR** (500 MHz, toluene-d_8, 298 K): δ 6.89 – 6.87 (m, 8H, Dipp-aryl-*H*), 6.84 – 6.81 (m, 4H, Dipp-aryl-*H*), 3.90 (sept, ^{3}J$_{HH}$ = 7.0 Hz, 8H, Dipp-C*H*(CH$_3$)$_2$), 1.28 (d, $^3J_{HH}$ = 6.9 Hz, 24H, Dipp-CH(C*H*$_3$)$_2$), 1.05 (d, $^3J_{HH}$ = 6.9 Hz, 24H, Dipp-CH(C*H*$_3$)$_2$), 0.35 (s, 36H, Si(C*H*$_3$)$_3$). **^{13}C{^{1}H} NMR** (125 MHz, toluene-d_8, 298 K): δ 151.6 (Dipp-aryl-*C*), 149.6 (Dipp-aryl-*C*), 123.2 (Dipp-aryl-*C*), 122.5 (Dipp-aryl-*C*), 27.9 (Dipp-*C*H(CH$_3$)$_2$), 25.7 (Dipp-CH(*C*H$_3$)$_2$), 23.9 (Dipp-CH(*C*H$_3$)$_2$), 5.3 (Si(*C*H$_3$)$_3$). **^{29}Si{^{1}H} NMR** (99 MHz, toluene-d_8, 298 K): δ –5.9 (*Si*(CH$_3$)$_3$). **UV-vis** (toluene): λ_{max} 314, 403 nm. **IR** (cm^{-1}): 3517, 2960, 1430, 1248. **E.A:** Anal. Calc. for $C_{60}H_{104}Al_2K_2N_4Si_4$: C 64.00; H 9.31; N 4.98%. Found: C 63.79; H 9.26; N 4.98%.

Synthesis of [AlMe{N(Dipp)SiMe$_3$}$_2$] (3-V)

Method A: To a freshly prepared deuterated benzene (0.5 mL) solution of [AlI{N(Dipp)SiMe$_3$}$_2$] **2-XX** (25 mg, 38.4 µmol, 1.0 eq.) in a J. Young's NMR tube, was charged potassium graphite (25 mg, 185 µmol, 4.8 eq.). The colourless solution over the KC_8 was agitated for 2.5 h, yielding a bold-yellow colour. The mixture was passed through a syringe containing Whatman glass filter paper and the black filtrate washed with deuterated benzene (0.2 mL). ^{1}H NMR spectroscopy identified the clean preparation of [K$_2$(Al{N(Dipp)SiMe$_3$}$_2$)$_2$] **3-IV**. To this NMR tube was added a colourless solution of iodomethane (96 µL solution of 0.4 M solution in benzene, 38.4 µmol, 1.0 eq.). An immediate colour change upon contact of liquid phases was observed. Inversion of the flask yielded an almost instantaneous and uniform colour change from yellow to colourless with minimal white precipitate. ^{1}H NMR spectroscopy identified the complete consumption of [K$_2$(Al{N(Dipp)SiMe$_3$}$_2$)$_2$] **3-IV**, yielding a mixture of [AlMe{N(Dipp)SiMe$_3$}$_2$] **3-V** and [AlI{N(Dipp)SiMe$_3$}$_2$] **2-XX** in a 3:2 ratio. **Method B:** To a deuterated benzene (0.5 mL) solution of [AlI{N(Dipp)SiMe$_3$}$_2$] **2-XX** (15 mg, 23.1

μmol, 1.0 eq.) in a J. Young's NMR tube, was added methyllithium powder (1.5 mg, 69.1 μmol, 3 eq.). Following 40 min of sonication, ^{1}H NMR spectroscopy identified the formation of single product [AlMe{N(Dipp)SiMe$_3$}$_2$] **3-V** (>98%). **^{1}H NMR** (400 MHz, C_6D_6, 343 K): δ = 7.01 (br., 6H, Dipp-aryl-*H*), 3.57 (sept, $^{3}J_{HH}$ = 6.8 Hz, 4H, Dipp-C*H*(CH$_3$)$_2$), 1.23 (d, $^{3}J_{HH}$ = 6.9 Hz, 12H, Dipp-CH(C*H*$_3$)$_2$), 1.08 (d, $^{3}J_{HH}$ = 6.8 Hz, 12H, Dipp-CH(C*H*$_3$)$_2$), 0.13 (s, 18H, Si(C*H*$_3$)$_3$), –0.36 (s, 3H, Al-C*H*$_3$). **^{13}C{^{1}H} NMR** (125 MHz, C_6D_6, 298 K): δ = 145.6 (Dipp-*o*-*C*), 144.3 (Dipp-*i*-*C*), 124.5 (Dipp-*p*-*C*), 124.3 (Dipp-*m*-*C*), 28.4 (Dipp-*C*H(CH$_3$)$_2$), 25.2 (Dipp-CH(*C*H$_3$)$_2$), 24.5 (Dipp-CH(*C*H$_3$)$_2$), 3.5 (Si(*C*H$_3$)$_3$), 1.4 (Al-*C*H$_3$).

Synthesis of [(^{Dipp}Nacnac)Mg-Al{N(Dipp)SiMe$_3$}$_2$] (3-VI)

In a glovebox, a sample vial was charged with [AlI{N(Dipp)SiMe$_3$}$_2$] **2-XX** (49.8 mg, 76.5 μmol) and KC_8 (41.4 mg, 306 μmol). The mixture was suspended in toluene (1 mL) and allowed to rest for 1 hour. This mixture was filtered onto a toluene solution of [(^{Dipp}Nacnac)MgI(OEt$_2$)] (29.5 mg, 45.9 mmol). The resulting mixture was heated to 40 °C for 48 hours. The resulting suspension was filtered and recrystalised. The mother liquor was decanted away from the solid which was washed three times with cold pentane (–30 °C). The resulting white solid of [(^{Dipp}Nacnac)MgAl{N(Dipp)SiMe$_3$}$_2$] **3-VI** was then dried under reduced pressure. (15.6 mg, 21%). Crystals of **3-VI** that were suitable for SCXRD were obtained from a saturated solution of toluene at –30 °C. **^{1}H NMR** (500 MHz, toluene-d_8): δ = 7.25 – 6.82 (br., 12H. Aryl-*H*), 4.79 (s, 1H, C=C*H*), 4.16 – 3.61 (br., 3H, Dipp-C*H*(CH$_3$)$_2$), 3.37 – 3.08 (br., 4H, Dipp-C*H*(CH$_3$)$_2$), 2.72 (br., 1H, Dipp-C*H*(CH$_3$)$_2$), 1.56 (s, 6H, C=C(C*H*$_3$)), 1.67 – 0.40 (br., 48H, Dipp-CH(C*H*$_3$)$_2$), 0.07 – -0.38 (br., 18H, Si(C*H*$_3$)$_3$). **^{13}C{^{1}H} NMR** (126 MHz, toluene-d_8): 169.8 (*C*-Me), 126.0 (Ar-*C*), 96.2 (C=CH), 29.0, 27.5, 26.0, 24.8 (Dipp-*C*H(CH$_3$)$_2$), Dipp-CH(*C*H$_3$)$_2$), 7.8, 3.7 (Si-(*C*H$_3$)$_3$). **EA**: Anal. Calc. for $C_{53}H_{82}AlMgN_4Si_2$: C, 73.37; H, 9.71; N, 5.80%. Found: C, 74.08; H, 9.70; N, 5.90%.

Attempted synthesis of [(^{Mes}Nacnac)Mg-Al{N(Dipp)SiMe$_3$}$_2$] (3-VII)

To a deuterated benzene (0.5 mL) solution of [K$_2$(Al{N(Dipp)SiMe$_3$}$_2$)$_2$] **3-IV** (20 mg, 17.7 μmol, 1.0 eq.) in a J. Young's NMR tube was added [(^{Mes}nacnac)MgI(OEt$_2$)] (9.9 mg, 17.7 μmol, 1.0 eq.). This was agitated for 12 h to afford a dark-yellow solution with white precipitate. ^{1}H NMR Spectroscopy identified the formation of 4 different [N(Dipp)SiMe$_3$]-containing species, with a majority species reminiscent of that identified through analogous investigations **3-VI**. Attempts to purify and crystallise postulated **3-VII** species were undertaken through extractions with benzene and washing with cold pentane (3 × 1 mL). No crystals of sufficient SCXRD quality could be grown. **NB:** Further procedure inquiries afforded proligand HN(Dipp)SiMe$_3$ as the majority product. Similarly,

crystallisation attempts afforded minimal SCXRD quality samples or the decomposition species [{MgI(^{Mes}Nacnac)}$_2$]. **^{1}H NMR** (400 MHz, C_6D_6, 343 K): δ = 7.00 – 6.95 (m, 6H. Dipp-Aryl-*H*), 6.90 (s, 4H. Mes-Aryl-*H*), 4.94 (s, 1H, C=C*H*), 3.40 (br., 4H, Dipp-C*H*(CH_3)$_2$), 2.25 (s, 18H, Mes-(C*H*$_3$)$_3$) 1.63 (s, 6H, C=C(C*H*$_3$)), 1.18 (d, $^3J_{HH}$ = 6.8 Hz, 12H, Dipp-CH(C*H*$_3$)$_2$), 0.91 (br, 12H, Dipp-CH(C*H*$_3$)$_2$), 0.01 (s, 18H, Si(CH_3)$_3$).

Attempted synthesis of [K(18-crown-6)][Al{N(Dipp)SiMe$_3$}$_2$] (3-VIII), preparation of [K(18-crown-6)][HAl{N(Dipp)SiMe$_3$}$_2$(OH)] (3-X)

To a deuterated benzene (0.5 mL) solution of [K$_2$(Al{N(Dipp)SiMe$_3$}$_2$)$_2$] **3-IV** (25 mg, 22.2 µmol, 1.0 eq.) in a J. Young's NMR tube was added 18-crown-6 (10.6 mg, 39.9 µmol, 1.9 eq.). Immediate agitation led to the formation of a vibrant orange solution becoming pale yellow after *ca*. 10 sec. ^{1}H NMR spectroscopy identified the formation of proligand HN(Dipp)SiMe$_3$ **2-IV**, an unknown diisopropylphenyl-containing species and a combination of 18-crown-6-containing species. Following 3 h at ambient temperature, an orange oil had phase-separated from the pale-yellow solution. The volatiles were removed under reduced pressure. Crystallisation of the oil from cyclohexane (0.5 mL) yielded uniform colourless crystalline plates following 18 h at ambient temperature. SCXRD identified the preparation of [K(18-crown-6)][HAl{N(Dipp)SiMe$_3$}$_2$(OH)] **3-X**.

Attempted synthesis of [K(crypt-222)][Al{N(Dipp)SiMe$_3$}$_2$] (3-IX), and preparation of [K(crypt-222)][HAl{N(Dipp)SiMe$_3$}$_2$(OH)] (3-XI)

To a deuterated benzene (0.5 mL) solution of K$_2$[Al{N(Dipp)SiMe$_3$}$_2$]$_2$ **3-IV** (25 mg, 22.2 µmol, 1.0 eq.) in a J. Young's NMR tube, was charged 2.2.2-cryptand (15.2 mg, 39.9 µmol, 1.9 eq.). Immediate agitation observed the formation of a bright-orange solution becoming pale-yellow after *ca.*10 sec. ^{1}H NMR spectroscopy identified the formation of proligand HN(Dipp)SiMe$_3$ **2-IV**, and multiple 2.2.2-cryptand-containing species. Following 3 h at ambient temperature, an orange oil had phase separated from the pale-yellow solution. After 8 days at ambient temperature, colourless crystalline material was identified as growing within the orange oil. Isolation of crystals of SCXRD quality identified the formation of [K(crypt-222)][HAl{N(Dipp)SiMe$_3$}$_2$(OH)]

3.6. References

[1] R. A. Fischer, M. M. Schulte, J. Weiss, L. Zsolnai, A. Jacobi, G. Huttner, G. Frenking, C. Boehme, S. F. Vyboishchikov, *J. Am. Chem. Soc.* **1998**, *120*, 1237-1248.

[2] R. Y. Kong, M. R. Crimmin, *Dalton Trans.* **2021**, *50*, 7810-7817.

[3] N. Hara, T. Saito, K. Semba, N. Kuriakose, H. Zheng, S. Sakaki, Y. Nakao, *J. Am. Chem. Soc.* **2018**, *140*, 7070-7073.

[4] B. N. Anand, I. Krossing, H. Nöth, *Inorg. Chem.* **1997**, *36*, 1979-1981.

[5] C. Jones, S. Aldridge, T. Gans-Eichler, A. Stasch, *Dalton Trans.* **2006**, 5357-5361.

[6] T. Agou, T. Yanagisawa, T. Sasamori, N. Tokitoh, *Bull. Chem. Soc. Jpn.* **2016**, *89*, 1184-1186.

[7] M. L. H. Green, *J. Organomet. Chem.* **1995**, *500*, 127-148.

[8] a) H. Braunschweig, M. Colling, *Coord. Chem. Rev.* **2001**, *223*, 1-51; b) U. Kaur, K. Saha, S. Gayen, S. Ghosh, *Coord. Chem. Rev.* **2021**, *446*, 214106.

[9] N. Hara, K. Semba, Y. Nakao, *ACS Catal.* **2022**, *12*, 1626-1638.

[10] J. Hicks, P. Vasko, J. M. Goicoechea, S. Aldridge, *Nature* **2018**, *557*, 92-95.

[11] J. Hicks, P. Vasko, J. M. Goicoechea, S. Aldridge, *Angew. Chem. Int. Ed. Engl.* **2021**, *60*, 1702-1713.

[12] R. J. Schwamm, M. D. Anker, M. Lein, M. P. Coles, *Angew. Chem. Int. Ed. Engl.* **2019**, *58*, 1489-1493.

[13] a) R. J. Schwamm, M. P. Coles, M. S. Hill, M. F. Mahon, C. L. McMullin, N. A. Rajabi, A. S. S. Wilson, *Angew. Chem. Int. Ed. Engl.* **2020**, *59*, 3928-3932; b) R. J. Schwamm, M. S. Hill, H.-Y. Liu, M. F. Mahon, C. L. McMullin, N. A. Rajabi, *Chem. Eur. J.* **2021**, *27*, 14971-14980.

[14] a) S. Grams, J. Eyselein, J. Langer, C. Färber, S. Harder, *Angew. Chem. Int. Ed. Engl.* **2020**, *132*, 16116-16120; b) S. Grams, J. Mai, J. Langer, S. Harder, *Organometallics* **2022**, *41*, 2862-2867.

[15] G. Feng, K. L. Chan, Z. Lin, M. Yamashita, *J. Am. Chem. Soc.* **2022**, *144*, 22662-22668.

[16] C. Cui, H. W. Roesky, H.-G. Schmidt, M. Noltemeyer, H. Hao, F. Cimpoesu, *Angew. Chem. Int. Ed. Engl.* **2000**, *39*, 4274-4276.

[17] M. P. Coles, M. J. Evans, *Chem. Commun.* **2023**, *59*, 503-519.

[18] S. Kurumada, S. Takamori, M. Yamashita, *Nature Chem.* **2020**, *12*, 36-39.

[19] K. Koshino, R. Kinjo, *J. Am. Chem. Soc.* **2020**, *142*, 9057-9062.

[20] C. Yan, R. Kinjo, *Angew. Chem. Int. Ed. Engl.* **2022**, *61*, e202211800.

[21] D. Sarkar, P. Vasko, A. F. Roper, A. E. Crumpton, M. M. D. Roy, L. P. Griffin, C. Bogle, S. Aldridge, *J. Am. Chem. Soc.* **2024**, *146*, 11792-11800.

[22] D. Sarkar, P. Vasko, T. Gluharev, L. P. Griffin, C. Bogle, J. Struijs, J. Tang, A. F. Roper, A. E. Crumpton, S. Aldridge, *Angew. Chem. Int. Ed. Engl.* **2024**, *63*, e202407427.

[23] S. Grams, J. Mai, J. Langer, S. Harder, *Dalton Trans.* **2022**, *51*, 12476-12483.

[24] T. X. Gentner, R. E. Mulvey, *Angew. Chem. Int. Ed. Engl.* **2021**, *60*, 9247-9262.

[25] M. J. Evans, M. D. Anker, C. L. McMullin, S. E. Neale, M. P. Coles, *Angew. Chem. Int. Ed. Engl.* **2021**, *60*, 22289-22292.

[26] M. M. D. Roy, J. Hicks, P. Vasko, A. Heilmann, A. M. Baston, J. M. Goicoechea, S. Aldridge, *Angew. Chem. Int. Ed. Engl.* **2021**, *60*, 22301-22306.

[27] T. X. Gentner, M. J. Evans, A. R. Kennedy, S. E. Neale, C. L. McMullin, M. P. Coles, R. E. Mulvey, *Chem. Commun.* **2022**, *58*, 1390-1393.

[28] H.-Y. Liu, M. S. Hill, M. F. Mahon, C. L. McMullin, R. J. Schwamm, *Organometallics* **2023**, *42*, 2881-2892.

[29] M. J. Evans, M. D. Anker, M. G. Gardiner, C. L. McMullin, M. P. Coles, *Inorg. Chem.* **2021**, *60*, 18423-18431.

[30] J. Hicks, P. Vasko, J. M. Goicoechea, S. Aldridge, *J. Am. Chem. Soc.* **2019**, *141*, 11000-11003.

[31] a) J. Hicks, A. Mansikkamäki, P. Vasko, J. M. Goicoechea, S. Aldridge, *Nature Chem.* **2019**, *11*, 237-241; b) K. Sugita, M. Yamashita, *Chem. Eur. J.* **2020**, *26*, 4520-4523.

[32] M. J. Evans, G. H. Iliffe, S. E. Neale, C. L. McMullin, J. R. Fulton, M. D. Anker, M. P. Coles, *Chem. Commun.* **2022**, *58*, 10091-10094.
[33] S. P. Green, C. Jones, A. Stasch, *Science* **2007**, *318*, 1754-1757.
[34] J. Emsley, *Nature's Building Blocks: an AZ Guide to the Elements*, Oxford University Press, USA, **2011**.
[35] C. McManus, A. E. Crumpton, S. Aldridge, *Chem. Commun.* **2022**, *58*, 8274-8277.
[36] H.-Y. Liu, S. E. Neale, M. S. Hill, M. F. Mahon, C. L. McMullin, *Dalton Trans.* **2022**, *51*, 3913-3924.
[37] H.-Y. Liu, R. J. Schwamm, M. S. Hill, M. F. Mahon, C. L. McMullin, N. A. Rajabi, *Angew. Chem. Int. Ed. Engl.* **2021**, *60*, 14390-14393.
[38] L. P. Griffin, M. A. Ellwanger, A. E. Crumpton, M. M. D. Roy, A. Heilmann, S. Aldridge, *Angew. Chem. Int. Ed. Engl.* **2024**, *63*, e202404527.
[39] *Oxidative Addition*, 3.0.1 ed., International Union of Pure and Applied Chemistry (IUPAC), **2019**.
[40] Y. Liu, J. Li, X. Ma, Z. Yang, H. W. Roesky, *Coord. Chem. Rev.* **2018**, *374*, 387-415.
[41] M. J. Evans, M. G. Gardiner, M. D. Anker, M. P. Coles, *Chem. Commun.* **2022**, *58*, 5833-5836.
[42] A. Heilmann, J. Hicks, P. Vasko, J. M. Goicoechea, S. Aldridge, *Angew. Chem. Int. Ed. Engl.* **2020**, *59*, 4897-4901.
[43] M. J. Evans, M. D. Anker, M. P. Coles, *Inorg. Chem.* **2021**, *60*, 4772-4778.
[44] J. Hicks, P. Vasko, A. Heilmann, J. M. Goicoechea, S. Aldridge, *Angew. Chem. Int. Ed. Engl.* **2020**, *59*, 20376-20380.
[45] S. Kurumada, K. Sugita, R. Nakano, M. Yamashita, *Angew. Chem. Int. Ed. Engl.* **2020**, *59*, 20381-20384.
[46] J. J. Cabrera-Trujillo, I. Fernández, *Chem. Eur. J.* **2020**, *26*, 11806-11813.
[47] M. D. Anker, R. J. Schwamm, M. P. Coles, *Chem. Commun.* **2020**, *56*, 2288-2291.
[48] H.-Y. Liu, M. S. Hill, M. F. Mahon, *Chem. Commun.* **2022**, *58*, 6938-6941.
[49] a) M. M. D. Roy, A. Heilmann, M. A. Ellwanger, S. Aldridge, *Angew. Chem. Int. Ed. Engl.* **2021**, *60*, 26550-26554; b) M. S. Hill, M. F. Mahon, C. L. McMullin, S. E. Neale, K. G. Pearce, R. J. Schwamm, *Z. Anorg. Allg. Chem.* **2022**, *648*, e202200224; c) K. Koshino, R. Kinjo, *Organometallics* **2020**, *39*, 4183-4186.
[50] a) M. D. Anker, M. P. Coles, *Angew. Chem. Int. Ed. Engl.* **2019**, *58*, 13452-13455; b) M. D. Anker, C. L. McMullin, N. A. Rajabi, M. P. Coles, *Angew. Chem. Int. Ed. Engl.* **2020**, *59*, 12806-12810.
[51] M. J. Evans, M. D. Anker, C. L. McMullin, N. A. Rajabi, M. P. Coles, *Chem. Commun.* **2021**, *57*, 2673-2676.
[52] J. Hicks, A. Heilmann, P. Vasko, J. M. Goicoechea, S. Aldridge, *Angew. Chem. Int. Ed. Engl.* **2019**, *58*, 17265-17268.
[53] M. D. Anker, M. P. Coles, *Angew. Chem. Int. Ed. Engl.* **2019**, *58*, 18261-18265.
[54] A. Heilmann, M. M. D. Roy, A. E. Crumpton, L. P. Griffin, J. Hicks, J. M. Goicoechea, S. Aldridge, *J. Am. Chem. Soc.* **2022**, *144*, 12942-12953.
[55] R. Y. Kong, M. R. Crimmin, *J. Am. Chem. Soc.* **2018**, *140*, 13614-13617.
[56] A. Paparo, K. Yuvaraj, A. J. R. Matthews, I. Douair, L. Maron, C. Jones, *Angew. Chem. Int. Ed. Engl.* **2021**, *60*, 630-634.
[57] a) D. Tan, F. García, *Chem. Soc. Rev.* **2019**, *48*, 2274-2292; b) N. R. Rightmire, T. P. Hanusa, *Dalton Trans.* **2016**, *45*, 2352-2362; c) D. W. Peters, R. G. Blair, *Faraday Discuss.* **2014**, *170*, 83-91; d) N. C. Boyde, N. R. Rightmire, T. P. Hanusa, W. W. Brennessel, *Inorganics* **2017**, *5*, 36; e) R. F. Koby, A. M. Doerr, N. R. Rightmire, N. D. Schley, B. K. Long, T. P. Hanusa, *Angew. Chem. Int. Ed. Engl.* **2020**, *59*, 9542-9548; f) N. Davison, J. A. Quirk, F. Tuna, D. Collison, C. L. McMullin, H. Michaels, G. H. Morritt, P. G. Waddell, J. A. Gould, M. Freitag, J. A. Dawson, E. Lu, *Chem* **2023**, *9*, 576-591; g) M. Glavinović, M. Krause, L. Yang, J. A.

McLeod, L. Liu, K. M. Baines, T. Friščić, J.-P. Lumb, *Sci. Adv.* **2017**, *3*, e1700149; h) J. V. Nallaparaju, R. Satsi, D. Merzhyievskyi, T. Jarg, R. Aav, D. G. Kananovich, *Angew. Chem. Int. Ed. Engl.* **2024**, *63*, e202319449; i) Y. Gao, K. Kubota, H. Ito, *Angew. Chem. Int. Ed. Engl.* **2023**, *62*, e202217723.

[58] a) K. J. Ardila-Fierro, J. G. Hernández, *ChemSusChem* **2021**, *14*, 2145-2162; b) J.-L. Do, T. Friščić, *ACS Cent. Sci.* **2017**, *3*, 13-19.

[59] D. Jędrzkiewicz, J. Langer, S. Harder, *Z. Anorg. Allg. Chem.* **2022**, *648*, e202200138.

[60] S. Kurumada, R. Yamanashi, K. Sugita, K. Kubota, H. Ito, S. Ikemoto, C. Chen, T. Moriyama, S. Muratsugu, M. Tada, T. Koitaya, T. Ozaki, M. Yamashita, *Chem. Eur. J.* **2024**, *30*, e202303073.

[61] F. Kallmeier, A. J. R. Matthews, G. R. Nelmes, N. R. Lawson, J. Hicks, *Dalton Trans.* **2024**, *53*, 12450-12454.

[62] J. Hicks, M. Juckel, A. Paparo, D. Dange, C. Jones, *Organometallics* **2018**, *37*, 4810-4813.

[63] M. Weller, T. Overton, J. Rourke, F. Armstrong, *Inorganic Chemistry*, 6th ed., Oxford University Press, USA, **2014**.

[64] a) Y. Segawa, Y. Suzuki, M. Yamashita, K. Nozaki, *J. Am. Chem. Soc.* **2008**, *130*, 16069-16079; b) C. Jones, *Nat. Rev. Chem.* **2017**, *1*, 0059.

[65] a) D. Mandal, T. I. Demirer, T. Sergeieva, B. Morgenstern, H. T. A. Wiedemann, C. W. M. Kay, D. M. Andrada, *Angew. Chem. Int. Ed. Engl.* **2023**, *62*, e202217184; b) I. L. Fedushkin, M. V. Moskalev, A. N. Lukoyanov, A. N. Tishkina, E. V. Baranov, G. A. Abakumov, *Chem. Eur. J.* **2012**, *18*, 11264-11276; c) P. Henke, T. Pankewitz, W. Klopper, F. Breher, H. Schnöckel, *Angew. Chem. Int. Ed. Engl.* **2009**, *48*, 8141-8145.

[66] L. F. Lim, M. Judd, P. Vasko, M. G. Gardiner, D. A. Pantazis, N. Cox, J. Hicks, *Angew. Chem. Int. Ed. Engl.* **2022**, *134*.

[67] R. A. Jackson, A. J. R. Matthews, P. Vasko, M. F. Mahon, J. Hicks, D. J. Liptrot, *Chem. Commun.* **2023**, *59*, 5277-5280.

[68] a) P. A. Dub, J. C. Gordon, *ACS Catal.* **2017**, *7*, 6635-6655; b) J. R. Khusnutdinova, D. Milstein, *Angew. Chem. Int. Ed. Engl.* **2015**, *54*, 12236-12273; c) C. Gunanathan, D. Milstein, *Science* **2013**, *341*, 1229712.

[69] S. J. Bonyhady, C. Jones, S. Nembenna, A. Stasch, A. J. Edwards, G. J. McIntyre, *Chem. Eur. J.* **2010**, *16*, 938-955.

[70] J. A. Gladysz, G. M. Williams, W. Tam, D. L. Johnson, D. W. Parker, J. C. Selover, *Inorg. Chem.* **1979**, *18*, 553-558.

4. A 4-Membered Aluminyl Anion

4.1. Preamble

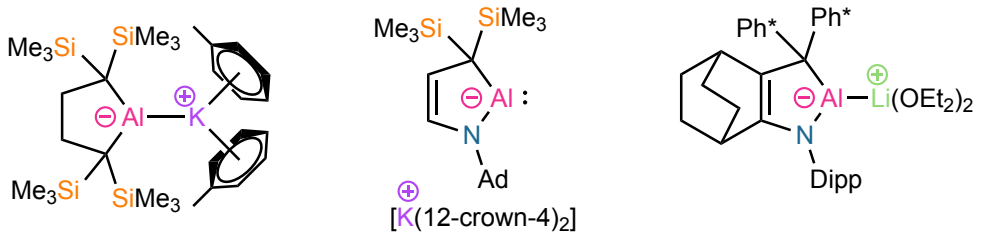

Figure 4.1: Library of 5-membered aluminyl anions as reported from groups of Yamashita ***3.23***[1] *and Kinjo* ***3.24***[2] *and* ***3.25***.[3] *(Ad = 1-adamantyl, Ph* = 3,5-^{t}Bu$_2$-phenyl).*

Since 2020, development of 5-membered aluminyl anion systems have utilised dialkyl and mixed alkylamido ligand frameworks.[4] Encompassing the aluminium(I) centre within a 5-membered metallocycle affords a narrower ∠X-Al-X bond angle (**3.23** 90.40(5),[1] **3.24** 86.8(1),[2] **3.25** 89.5(2)°)[3] than the 6- and 7-membered systems (range 96.05(4) – 108.89(9)°).[5] The narrower ∠X-Al-X angle increases the *s*-character of the lone pair at the metal centre. The bidentate silyldiamido $[DAS]^{2-}$ ($[DAS]^{2-}$ = $[Ph_2Si(DippN)_2]^{2-}$) ligand scaffold presented possibilities to develop either a contact dimeric pair (CDP) or ligand-encapsulated pair (LEP) with potassium counterions via arene interactions with the associated Dipp or phenyl moieties. Consequently, the arrangements of aluminyl anion complexes could be further expanded from reported monomeric ion pair (MIP **3.23** and **3.25**) and separated ion pair (SIP **3.24**) examples.

Prior to work within this Thesis, no diamido ligand scaffolds in the preparation of aluminyls had been employed in systems featuring smaller than 6-membered heterocycles.[6] Moreover, despite ongoing investigations, no complexes had been isolated previously featuring an anionic two-coordinate aluminium(I) centre confined within a 4-membered metallocycle.[7] Following the successful preparation of the corresponding aluminium(III) iodide precursor [AlI(DAS)] **2-XXXIII** (**Chapter 2**), attempts toward isolating the first 4-membered aluminyl anion were made to further expand the catalogue of reported aluminyl anions.

4.2. Research Rationale

4.2.1. A 4-Membered Precursor for Reduction Inquiries

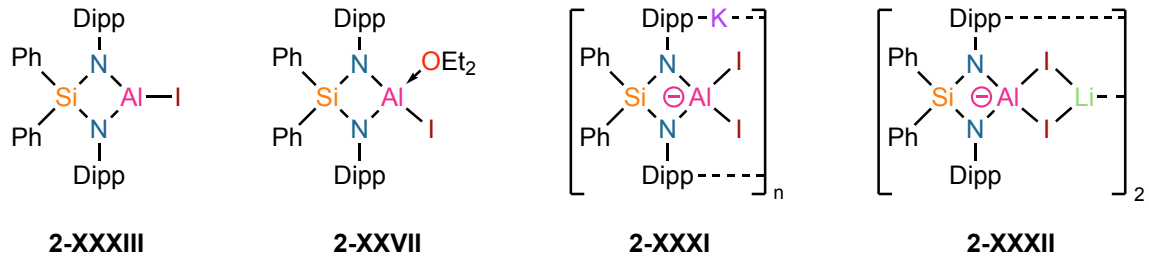

2-XXXIII **2-XXVII** **2-XXXI** **2-XXXII**

*Figure 4.2: 4-Membered aluminium(III) iodide complexes featuring a bidentate silyldiamido ligand. These include: the 3-coordinate neutral complex **2-XXXIII**, the diethyl ether solvate **2-XXVII** and the potassium- and lithium-aluminates **2-XXXI** and **2-XXXII***

Outlined within Chapter 2, a reliable synthesis of a neutral, 4-membered aluminium(III) iodide precursor system **2-XXXIII** was developed, whilst further inquiries afforded the diethyl ether solvate **2-XXVII**, and the group 1 metal aluminates **2-XXXI** and **2-XXXII** (Figure 4.2). The highly Lewis acidic nature of the aluminium(III) centre in **2-XXXIII** meant that diethyl ether coordination or aluminate formation (when exposed to alkali metal salts) was rapid. Importantly, despite the challenges and consequent inability to crystallise **2-XXXIII**, solvated and aluminate species would crystallise readily from a range of aromatic and coordinating solvents, affording tangible solid-state information about the complexes.

Capitalising upon the isolation of pure **2-XXXIII** as an iodoalane precursor, the following investigations were undertaken to develop aluminium(I) and derivative species featuring the $[DAS]^{2-}$ ligand. Initial preparations of a new 4-membered iron-aluminyl complex was investigated through both solution-state and mechanochemical routes. Alkali metal reductions of **2-XXXIII** were conducted with potassium first, and then to access analogous sodium and lithium analogues. Following successful isolations of an aluminyl anion, the consequent stabilisation of a highly reactive aluminium(I) centre within the 4-membered metallocycle was explored *in silico*. Finally, an initial catalogue of reactivity of corresponding aluminium(I) species was explored with organic and metallic electrophiles toward the preparation of bimetallic *s*- and *p*- block species.

4.3. Results and Discussion

4.3.1. Preparations of an Iron-Aluminyl Coordination Complex

*Figure 4.3: Iron-aluminyl species **3.14** featuring a 4-membered bidentate amidinate ligand system reported by Jones, Aldridge and coworkers.[8] Targeted iron-aluminyl complex **4-I** featuring silyl(bis)amido ligand.*

Reported by Jones, Aldridge and coworkers in 2006, the monoanionic 4-membered $[^{t}BuC(NCy)_2]^-$ (Cy = cyclohexyl) ligand was used to access the iron-aluminium heterobimetallic species **3.14** (**Chapter 3**) (Figure 4.3).[8] However, with the amidinate ligand being monoanionic and necessitating an additional halide, no tricoordinate iron-aluminyl complexes, where the aluminium centre is constrained within a 4-membered metallocycle, are reported.

The dianionic bidentiate $[DAS]^{2-}$ system was hypothesised to stabilise such a complex (**4-I**, Figure 4.3). Following mixed results of solution-state and mechanochemical synthetic investigations with acyclic systems (**Chapter 3**), the decreased steric encumberment within 4-membered precursors, such as **2-XXXIII** (**Chapter 2**) invited hope for the preparation of a silyl(bis)amido-ligated iron-aluminyl complex. The investigative outcomes and successful isolation of this targeted iron-aluminyl complex **4-I** are reported herein.

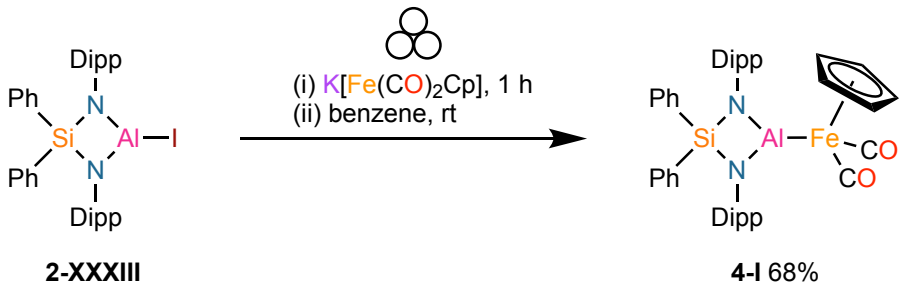

2-XXXIII **4-I** 68%

*Scheme 4.1: Mechanochemical preparation of the iron aluminyl complex $[(CO)_2(Cp)Fe\text{-}Al(DAS)]$ **4-I** furnished with a 4-membered bidentate ligand scaffold.*

Motivated by optimal yields from mechanochemical methods in the potassium acyclic aluminyl **3-IV** synthesis, ball milling investigations were initially undertaken. In an IKA Ultra-Turrax Tube Drive fitted with a 20 mL ball mill tube, the aluminium(III) iodide precursor **2-XXXIII** was ball-milled with $K[Fe(CO)_2Cp]$ and 30 stainless steel balls (Scheme 4.1). Following one hour of milling, the complete consumption of the starting material **2-XXXIII** and clean conversion to a new silyl(bis)amido and

cyclopentadienyl-containing species was identified via ^{1}H NMR spectroscopy (Supporting Information Figure S.63). Extraction and purification afforded the targeted species as a dark red solid in good yield (Scheme 4.1).

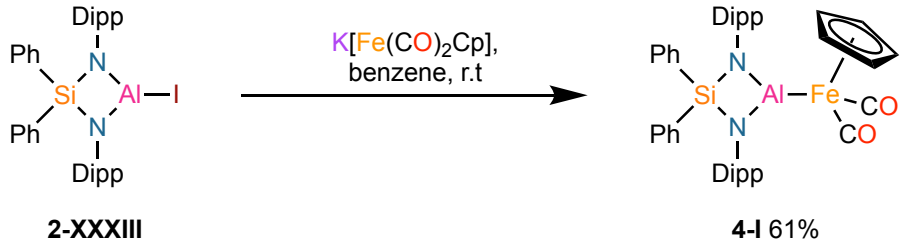

2-XXXIII **4-I** 61%

*Scheme 4.2: Solution-state preparation of **4-I**.*

Solution state reactions were undertaken between **2-XXXIII** and K[Fe(CO)$_2$Cp] in benzene at ambient temperature (Scheme 4.2). When reactions were performed on small scale (50 mg **2-XXXIII**), ^{1}H NMR spectroscopic analysis was conducted immediately following treatment of **2-XXXIII** with K[Fe(CO)$_2$Cp] showed the near quantitative conversion to the target species **4-I** with signals previously identified in the above mentioned mechanochemical syntheses. Repeating the reaction with increased scales (200 mg **2-XXXIII**) and stirring overnight, afforded **4-I** as a brown-red solid after subsequent extractions and purification. This was identified to be the pure species **4-I** via ^{1}H NMR spectroscopy. Dissolution of the isolated solid in cyclohexane and concentration to saturation afforded brown-tinged colourless crystalline blocks of SCXRD quality in a good yield. Notably, crystalline yields of **4-I** from solution-state syntheses were slightly less (61%) than that of mechanochemical methods (68%), however, this was attributed to extraction efficacy rather than synthetic conversion afforded by each method. Analysis of the colourless crystalline material via X-ray diffractometry confirmed the structure of target iron-aluminyl complex [Cp(CO)$_2$Fe–Al(DAS)] **4-I** (Figure 4.4).

An unsupported single bond is present between the two metal centres in **4-I**. Compared with the iron-aluminium species **3.14**, the iron-aluminium bond of **4-I** (2.2884(7) Å) is notably shorter than that reported by Jones, Aldridge and coworkers (2.3699(8) Å). This difference can be attributed to the tricoordinate aluminium centre in **4-I** rather than tetracoordinate aluminium centre in **3.14**.

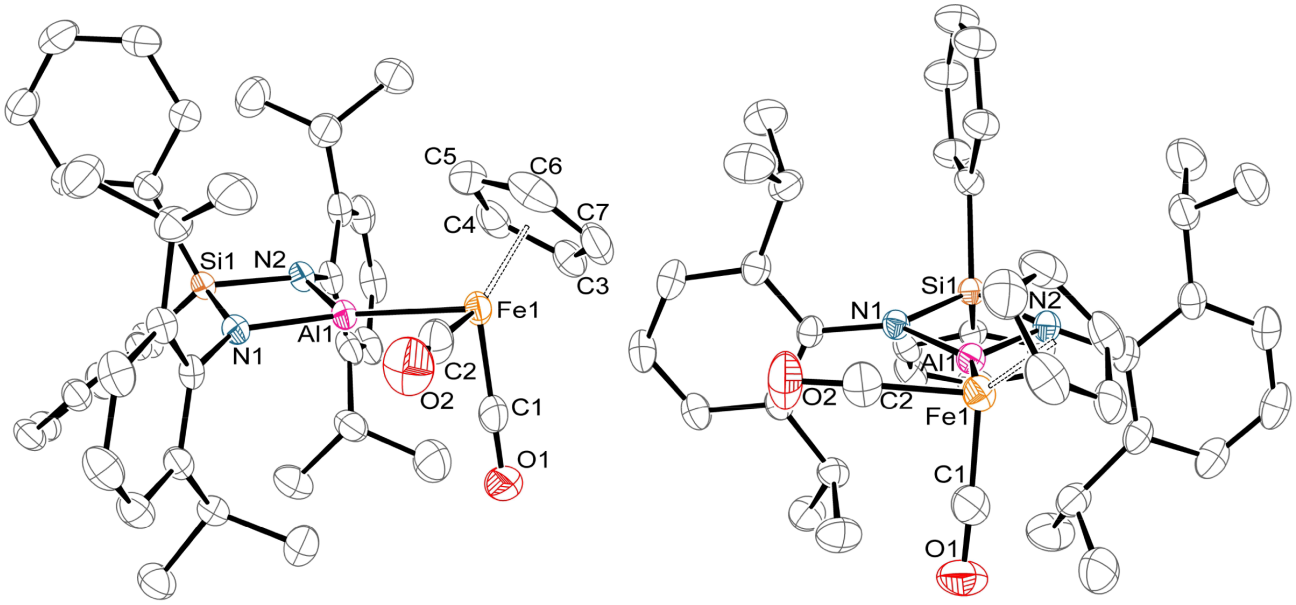

*Figure 4.4: Molecular structure of iron-aluminyl complex **4-I** as determined by X-ray crystallography, displayed from side orientation (left) and along the Fe1-Al1 bond (right). Hydrogen atoms omitted. Thermal ellipsoids set to 50% probability. Selected bond lengths (Å) and angles (°): Al1-Fe1 2.2884(7), Al1-N1 1.8135(17), Al1-N2 1.8240(18), Fe1-C1 1.750(3), Fe1-C2 1.750(3), C1-O1 1.150(3), C2-O2 1.150(3), Al1···Si1 2.5513(8), N1-Al1-N2 85.76(8), Al1-N1-Si1 91.77(8), N1-Si1-N2 90.76(8).*

Identified from the solid-state structure of **4-I**, the tricoordinate aluminium centre is constrained within a distorted trigonal planar geometry featuring the bidentate $[DAS]^{2-}$ ligand scaffold, leading to a narrow ∠N-Al-N bond angle of 85.76(8) °. The 4-membered aluminium metallocycle is planar (total angles = 359.76 °). Steric bulk about the $[DAS]^{2-}$ occurs about the 4-membered plane with the silyl-bound phenyl groups above and below the plane, and Dipp moieties extending near perpendicular to the Fe1-Al1···Si1 plane. Identifiable within the sterically constrained system, the N2 bound Dipp moiety projects further from the AlN_2Si plane than the N1 bound Dipp moiety. This could be attributed potentially to the avoidance of steric clash with Fe-based steric bulk. The iron centre was identified to have also retained its ligation of two monodentate *C*-ligated carbon monoxide ligands, and the η^5-interaction with the monoanionic cyclopentadienyl ligand.

4.3.2. Alkali Metal Reductions of a 4-Membered Aluminium(III) Iodide Precursor

4.3.2.1. Potassium-Based Reduction Investigations

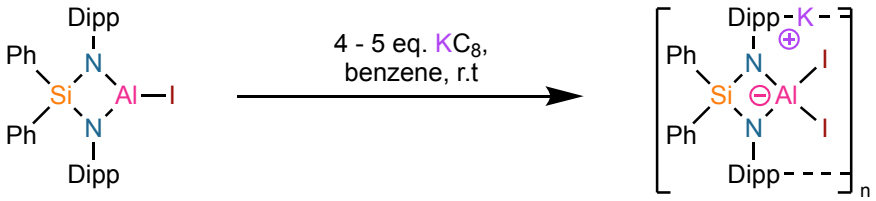

2-XXXIII **2-XXXI**

*Scheme 4.3: Attempted preparations toward first 4-membered aluminyl anion from **2-XXXIII** via reduction with potassium graphite yielding potassium aluminate **2-XXXI**.*

Toward the preparation of a 4-membered potassium aluminyl species, benzene solutions of **2-XXXIII** were treated with potassium graphite (Scheme 4.3). Initial investigations employed excesses of 4 and 5 equivalents of KC_8, however, the significant formation of potassium aluminate species K[Al(DAS)I_2] **2-XXXI** was identified via ^{1}H NMR spectroscopy in addition to a new $[DAS]^{2-}$ containing species (**2-XXXI** : new species, range 0.3 : 1 – 1 : 1). The high proclivity for **2-XXXI** to yield SCXRD crystalline quality material from hydrocarbon solutions was consistently apparent through reduction investigations affording successive crystallisation crops. A consequence of potassium reductions affording the elimination of potassium iodide, would see this salt scavenged by unreacted [Al(DAS)I] **2-XXXIII**, affording crystalline material of **2-XXXI**.

Attempting other potassium reductants and reaction methods, the application of previously advantageous 5% w/w K/KI with benzene solutions of **2-XXXIII** identified the near quantitative formation of aluminate **2-XXXI**, consequent of vast excesses of potassium iodide being present within the solution. Moreover, attempts to mitigate formation of the aluminate through inquiries od mechanochemical methods afforded a mixture of products. Whilst the formation of the aluminate species **2-XXXI** in mechanochemical syntheses could be identified within the baseline of ^{1}H NMR spectrum, the lack of selectivity in these reactions promoted the pursuit of solution state syntheses.

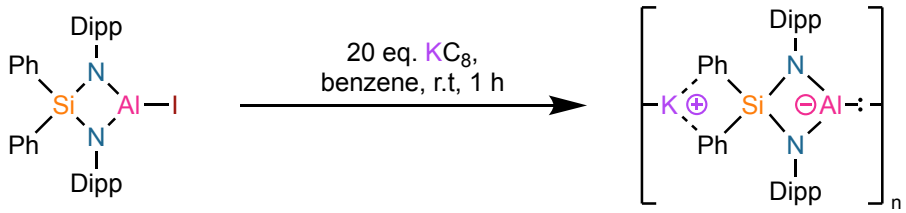

2-XXXIII **4-II** 47%

*Scheme 4.4: Synthesis of first 4-membered aluminyl anion **4-II** from **2-XXXIII** via reduction with excess potassium graphite.*

In surpassing potential aluminate formation, a vast excess of 20 equivalents of potassium graphite was identified as being preferential. Consequently, treatment of benzene and toluene solutions of **2-XXXIII** with 20 equivalents of KC_8 was undertaken on small scales (10 mg, **2-XXXIII**). Following 40 minutes of agitation within a sonication bath with frequent inversion within flask featuring a J Young's valve, conversion to a single product (postulated as **4-II**) was identified from the resulting burnt-orange solution via ^{1}H NMR spectroscopy.

Repeating the above reaction on a larger scale (100 mg, **2-XXXIII**) were undertaken along with strict timescales whereby relatively dilute solutions of **2-XXXIII** were stirred vigorously for 1 hour. The subsequent burnt-orange solution was separated via a filter cannula and removal of volatiles from the filtrate afforded **4-II** in a fair yield (47%) as a burnt-orange powder confirmed via ^{1}H NMR spectroscopy (Scheme 4.4).

To further confirm the identity of **4-II**, SCXRD quality crystals were obtained from burnt-orange benzene solutions following 40 minutes of sonication and standing at ambient temperature for 72 hours. Isolated as burnt-orange plates, the material was confirmed as the targeted 4-membered potassium aluminyl species **4-II** [K{Al(DAS)}] (Figure 4.5).

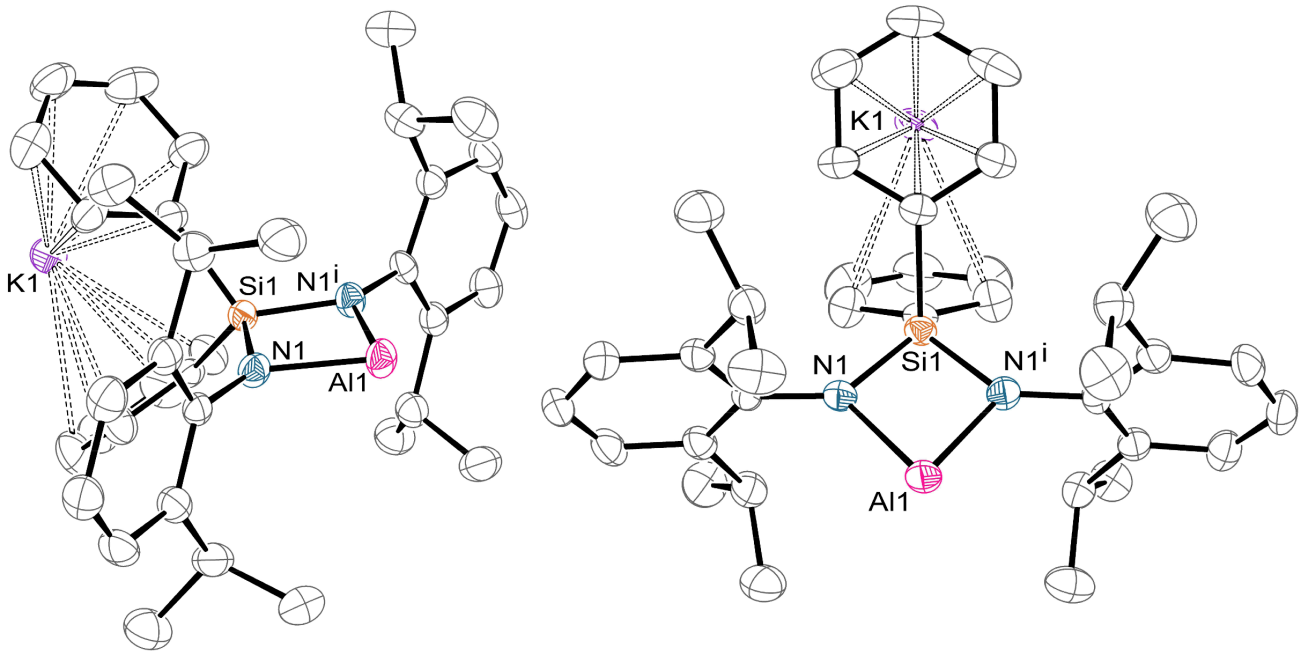

*Figure 4.5: Molecular structure of 4-membered potassium aluminyl complex **4-II** as determined by X-ray crystallography, displayed from side (left) and top-down (right) orientations. Hydrogen atoms omitted. Thermal ellipsoids set to 50% probability. Selected bond lengths (Å) and angles (°): Al1···K1 (3.404(3)), Al1-N1 (1.900(3)), Al1···Si1 (2.612), N1-Al1-N1^{i} 80.93(18), Al1-N1-Si1 92.95(14), N1-Si1-N1^{i} (93.2(2)).*

4-II crystalises as a one-dimensional coordination polymer featuring interactions between the aluminium(I) and potassium centres. The pseudo two-coordinate aluminium(I) centre has the narrowest ∠X-Al-X bond angle (80.93(18)°) reported of all aluminyl species (previous examples: **3.23** 90.40(5),[1] **3.24** 86.8(1),[2] **3.25** 89.5(2)°, **Chapter 3**)[3] imparted by the highly strained 4-membered metallocycle. The 4-membered AlN_2Si ring in **4-II** is planar and features nearly perpendicular arrangements of Dipp moieties to the Al1···Si1···K1 plane. Similarly observed within 4-membered amidiniate species, the aluminium centre is further projected and elongated out of the square arrangement compared to the Si centre. Potassium···aluminium interactions were identified as 3.404(3) Å, notably similar to MIP species [(toluene)$_2$K−Al(C^{Si})] **3.23** (C^{Si} = [{C(SiMe$_3$)$_2$CH$_2$}$_2$]$^{2-}$) 3.4549(5) Å.[1] Such distances were also slightly longer than the sum of covalent radii of aluminium and potassium (3.28 Å), highlighting a relatively weak interaction between the metal centres.

As investigated within acyclic species, the preparation of an aluminium(I) centre within the species could be supported by the comparison of Al-N bond lengths. Identified in the solid state structures of [DAS]$^{2-}$ aluminates and solvated species (**2-XXVII**; Al1-N1 1.819(3), Al1-N2 1.833(3), **2-XXX**; Al1-N1 1.822(3), Al1-N2 1.854(3), **2-XXXII**; Al1-N1 1.823(4), Al1-N2 1.849(4) Å), were notably shorter than that of aluminyl **4-II** Al1-N1 1.900(4) Å (analogous to values observed within acyclic aluminyl **3-IV**). Given the +1 oxidation state of the aluminium centre in such complexes, the increase of Al-N

bond lengths further supported the two-coordinate aluminium(I) centre, opposing the formation of a hydride aluminium(III) complex which could be difficult to identify via X-Ray diffraction methods. Moreover, the possibility of an aluminium hydride species was be nullified via a lack of Al-H signal present within infrared spectrometry.

Identifiable from potassium···ligand interactions, **4-II** is the second example of a ligand encapsulated pair (LEP) cation:anion arrangement, the first example was identified in the acyclic aluminyl anion **3.26**.[9] Similar to the range of $[DAS]^{2-}$ species previously crystallised, the steric bulk of the phenyl moieties attached to the silyl backbone is angled above and below the 4-membered plane. The phenyl rings affording a bent sandwich encapsulation of the potassium cation, and the two phenyl groups see rotation about the Si–C bond orienting to support η^6-arene interactions. Such an arrangement is akin to ansa-metallocenes previously utilised in catalysis,[10] and formative ansa-ferrocene.[11] Further interactions of the aluminium centre (3.404(3) Å) with potassium of the next unit supports arrangement to the polymeric structure.

Throughout the initial investigations affording **4-II**, variations in the optimised synthesis were undertaken with different reaction times and solvents. On larger scales (>200 mg), reaction mixtures stirred for 18 hours in aromatic solvents identified the formation of an intractable mixture of products. This was similarly identified with the extended agitation (8 hours) of small-scale syntheses (20 mg) via ^{1}H NMR spectroscopy. Furthermore, on small scales, sonication of reaction mixtures for greater than 3 hours would afford an intractable mixture of products. In all cases, this mixture was attributed to the likely activation of species via inter- or intramolecular activation pathways. Attempts to isolate degradation species present within the solution were unsuccessful, with subsequent extraction and purifications affording brown oily solids. Crystallisation attempts from the brown oily solid were identified to afford trace impurities from varied extractions and crystallisation solvents (discussed herein), along with single crystals of potassium aluminate **2-XXXI**.

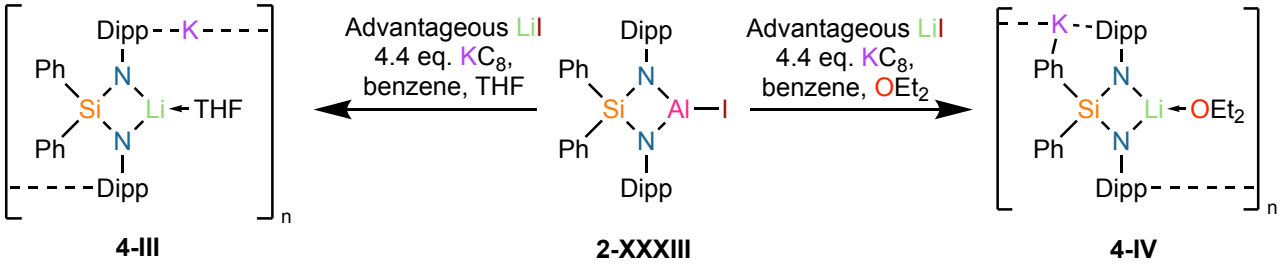

*Scheme 4.5: Extraction and crystallisation attempts from coordinating solvents affording di-alkali metal complexes **4-III** and **4-IV**.*

Toward improving extractions of the 4-membered aluminyl **4-II**, varied temperatures were first investigated to counter relatively poor complex solubility. Benzene extractions of the mother liquor performed at elevated temperatures (60 °C) and reflux gave an intractable mixture of products. The use of coordinating solvents (diethyl ether and tetrahydrofuran) was explored for the improved extraction of **4-II** (Scheme 4.5). Analogous within both attempts, the colour of the extracts were brown-black, however, ^{1}H NMR spectroscopy identified the formation of an intractable mixture of products. Attempts to isolate crystalline material confirming any species present only afforded a single crystal of degradation species **4-III** from tetrahydrofuran : hexane solutions (Figure 4.6). Similarly, a single crystal was yielded following diethyl ether crystallisation attempts and was identified as the analogous diethyl ether solvated heterobimetallic-alkali metal species **4-IV** (Figure 4.6).

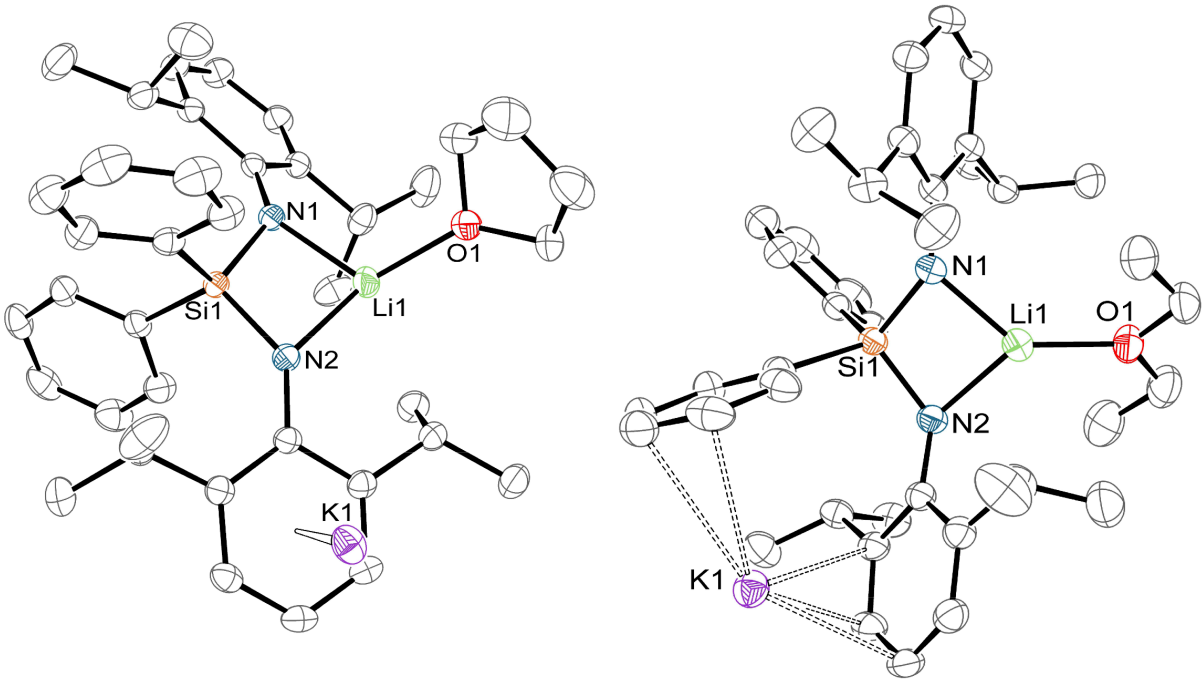

*Figure 4.6: Molecular structure of solvated heterobimetallic-alkali metal salt complexes with tetrahydrofuran **4-III** (left) and diethyl ether **4-IV** (right) as determined by X-ray crystallography. Hydrogen atoms omitted. Thermal ellipsoids set to 50% probability. **4-III** Selected bond lengths (Å) and angles (°): Li1-N1 1.984(3), Li1-N2 1.973(3), Li1-O1 1.934(3), Si1-N1 1.7070(12), Si1-N2 1.7026(12), N1-Li11-N2 (84.29(11)), N1-Si1-N2 (102.28(6)). **4-IV** Selected bond lengths (Å) and angles (°): Li1-N1 1.974(3), Li1-N2 1.973(3), Li1-O1 1.915(3), Si1-N1 1.6809(12), Si1-N2 1.6856(12), N1-Li11-N2 (83.72(11)), N1-Si1-N2 (102.96(6)).*

In the solid-state structures of **4-III** and **4-IV**, the presence of the lithium cation was initially unanticipated (Figure 4.6). However, this could be attributed to trace amounts of lithium iodide present within the starting material **2-XXXIII**. Markedly, the identification of minimal crystalline samples identified from reaction mixtures (< 3 crystals from crystallisations) highlighted these species as minor

products within preparations of **4-II**. Both species featured the arrangement of two alkali metals countering the doubly deprotonated $[DAS]^{2-}$. Within the N-Si-N pocket in each complex, a tricoordinate lithium counterion bound to both amido coordination sites and monosolvated via the *O*-coordination of the corresponding solvent molecules (**4-III** tetrahydrofuran and **4-IV** diethyl ether). Whilst both **4-III** and **4-IV** are polymeric within the solid state, each observed different engagements of potassium centres with the arene substituents. In **4-III**, potassium arene interactions are analogous with the previously isolated aluminate species **2-XXXI**, whereby explicit interactions with Dipp moieties would link alternating $[DAS]^{2-}$ containing monomers via electrostatic interactions. Similarly observed with **4-IV**, electrostatic interactions of potassium cations with Dipp moieties afforded a polymeric structure. However, additional engagements with phenyl moieties were also present. This results in the rotation about N-C(Dipp) and Si-C(Ph) bonds to support such an arrangement, but not impart significant change upon the centre SiN_2Li central fragment.

Following various reduction conditions, the optimal preparation of **4-II** was determined to be vigorously stirring dilute benzene solutions of **XXXIII** over excess KC_8 at room temperature for 1 hour. The relatively dilute mother liquor would best benefit filter cannula extractions whilst under active agitation, and the propensity for postulated inter- and intramolecular pathways subsequently promoted the immediate removal of volatiles *in vacuo*. Moreover, the relatively poor solubility of **4-II** (attributed to likely polymeric precipitation of species) promoted investigations into the generation of MIP or SIP derivatives with varied alkali metals and sequestering reagents toward minimising polymer formation and aiding solubility.

4.3.2.2. Sodium- and Lithium-Based Reduction Studies

Further reinforcing the challenges in aluminyl preparations from sodium and lithium reductions, preparation of the alkali metal salts of the $[DAS]^{2-}$ ($Li_2[DAS]$, $Na_2[DAS]$) was highly prevalent from lithium- and sodium- metal-based reductions. Consequently, the treatment of benzene solutions of **2-XXXIII** with lithium metal led to preferential formation of the previously known $Li_2[DAS]$ **2-XXIX** along with an inseparable mixture of degradation products. Repeating the reductions with excess sodium mirror gave an indiscernible mixture of products.

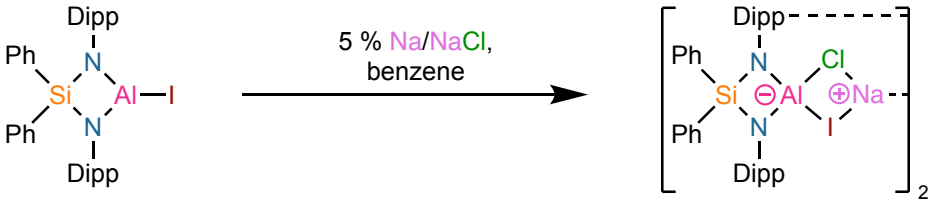

2-XXXIII **4-V**

*Scheme 4.6: Preparation of the mixed halide sodium aluminate **4-V**.*

Given the propensity of the precursor **2-XXXIII** to form aluminate complexes, it was hypothesised the treatment of [Al(DAS)I] with 5% w/w Na/NaCl would afford the corresponding sodium aluminate. Conducted on small scales, treatment of **2-XXXIII** with the dispersed reducing agent afforded an instantaneous colour change from colourless to yellow (Scheme 4.6). Following 2 hours of sonication and subsequent emboldening of the yellow colour, ^{1}H NMR spectroscopy identified the majority conversion to a single new species. Cross-referenced with the related spectrum of Li_2[Al(DAS)I_2] **2-XXXII** (Supporting Information Figure S.49), analogous signals within spectra highlighted the likely formation of a sodium-aluminate complex (Supporting Information Figure S.68). Subsequent extraction and concentration afforded SCXRD quality crystals of the hypothesised aluminate as a mixed halide system [Na_2{AlCl(DAS)I}$_2$] **4-V** (Figure 4.7)

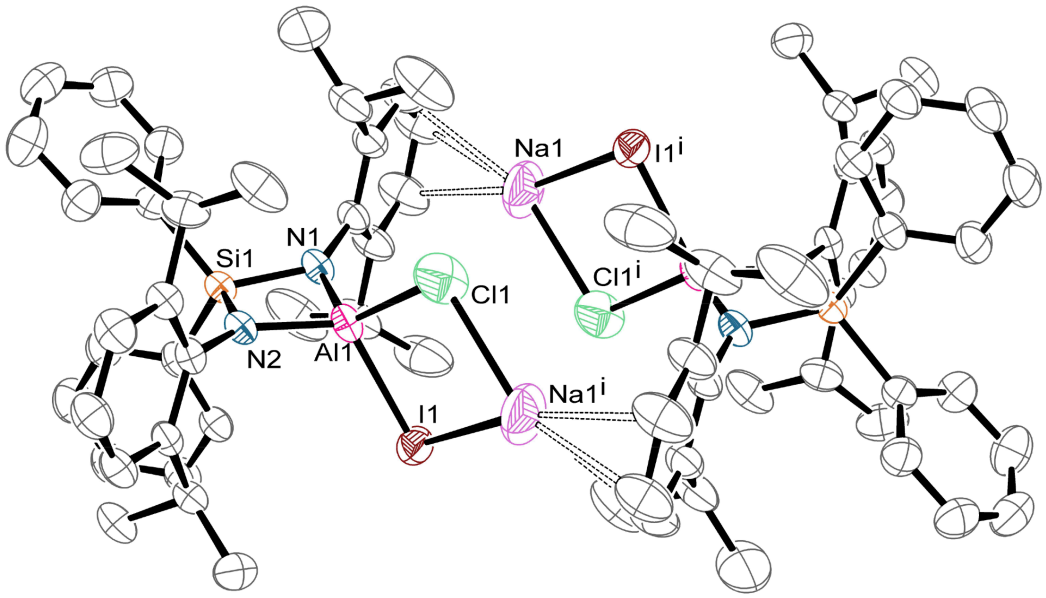

*Figure 4.7: Molecular structure of mixed halide sodium-aluminate salt Na[AlCl(DAS)I] **4-V** as determined by X-ray crystallography. Hydrogen atoms omitted. Thermal ellipsoids set to 50% probability. Selected bond lengths (Å) and angles (°):Al1-Cl1 2.2122(1), Al1-I1 2.446(5), Na1-Cl1 3.010(11), Na-I1 2.864(9), Al1-N1 1.834(2), Al1-N2 1.8263(19), Si1-N1 1.7446(19), Si1-N2 1.7344(18), N1-Al1-N2 85.35(8), Cl1-Al1-I1 95.65(7), Cl1-Na1-I1 74.5(3), N1-Si1-N2 91.00(9).*

Similarly observed with the analogous [Li{Al(DAS)I_2}] **2-XXXII** system, **4-V** crystallises as a dimer within the solid-state. Featuring a tetracoordinate aluminium(III) centre within the *N*-Si-*N* pocket, the bridging sodium cations interact with both the chlorido and iodo ligands in addition to interactions with a Dipp moiety. Featuring a distorted tetrahedral arrangement about the aluminium centre, the inclusion of a single smaller halide substituent at the aluminium centre was observed, with analogous tetrahedral angles to those identified within the diiodo species **2-XXXII** (N1-Al1-N2 **2-XXXII** 85.07(19)°, **4-V** 85.35(8)°; X1-Al1-X2 **2-XXXII** 95.94(5)°, **4-V** 95.65(7)°).

To further comprehend this new system, a combination of synthetic and *in-silico* inquiries were performed.

4.3.3. *In-silico* Investigations of a 4-Membered Aluminyl Anion

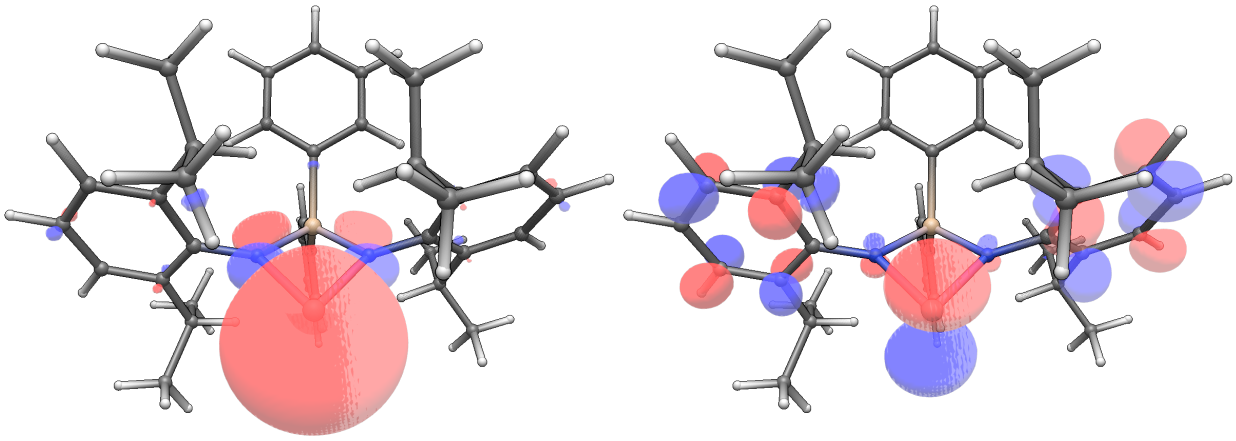

Figure 4.8: HOMO (-1.34 eV, left) and LUMO+4 (2.68 eV, right) of [Al(DAS)]$^-$ calculated at the DFT-D3, PBE0, Def-TZVP level of theory. Iso-value 0.04.

As in Chapter 3, calculations concerning the "free" anion excluding potassium cation were undertaken with the assistance of Mr Gareth Nelmes BSc (Hons) of the Hicks Group at the Australian National University (Figure 4.8). As noted within solid-state structures of **4-II**, comparatively reduced steric bulk is observed about the aluminium(I) centre rather than in acyclic system **3-IV**. However, peripheral steric bulk is featured through amido-based Dipp moieties and silyl-situated phenyl groups. Lacking potassium presence, optimisations about the backbone Si-C bond led to pseudo-perpendicular arrangement of phenyl rings. Notable within calculations, Dipp substituents do not lie coplanar to the AlN_2Si plane as observed within **4-II** in the solid-state; rather, arrangements invoke slight deviations from the plane as observed in the iron-aluminium complex **4-I**.

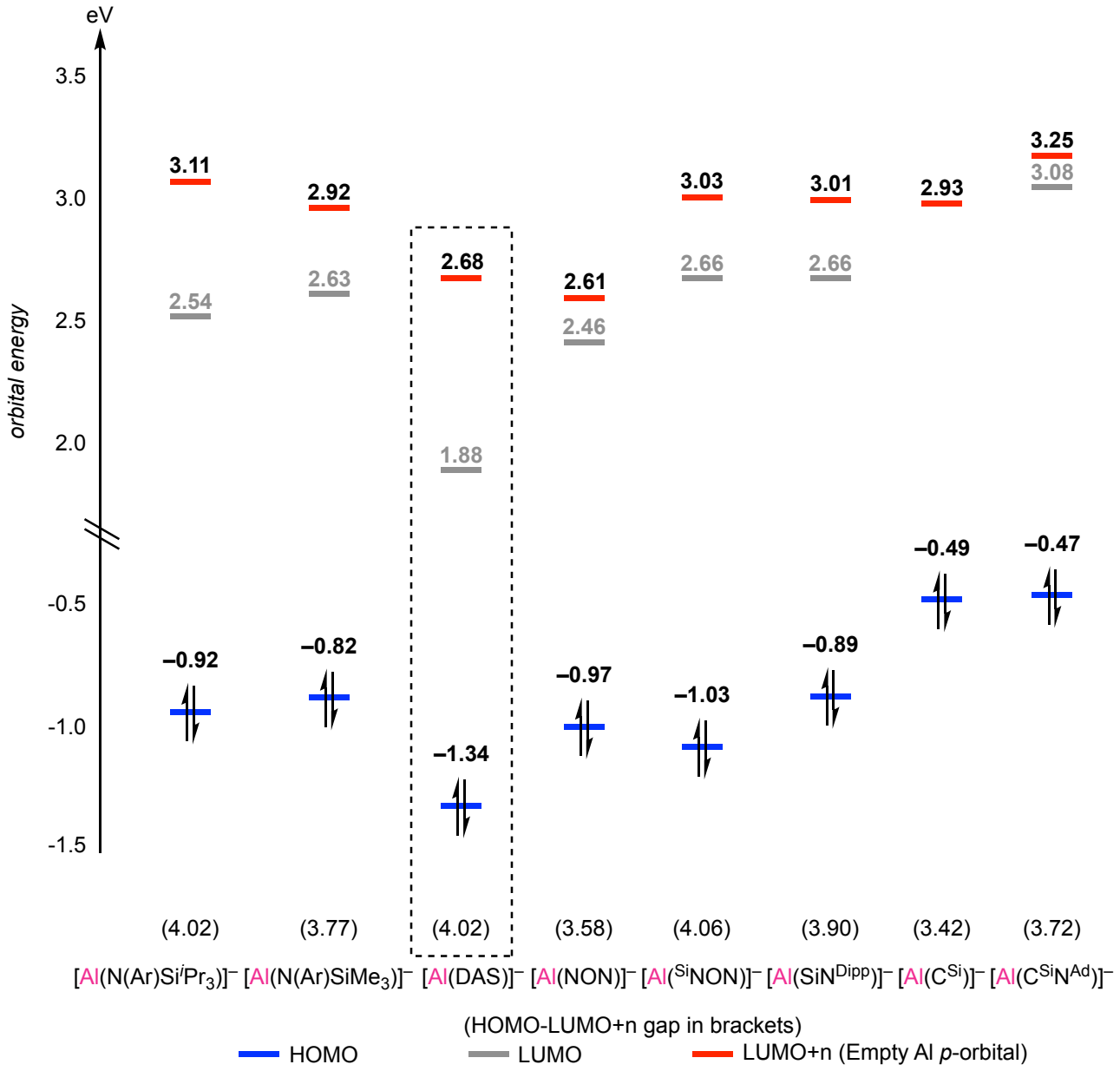

Figure 4.9: HOMO, LUMO and LUMO+n energies of selected aluminyl anions, where the LUMO+n is the energy of the empty Al-based p-orbital. Selected calculations previously reported by Hicks and coworkers calculated at the DFT-D3, PBE0, Def2-TZVP level of theory.[4] The new acyclic and 4-membered systems have been calculated at the same level of theory to allow for direct comparison. Orbital energies of calculated anions displayed in eV, HOMO-LUMO+n gap highlighted with in brackets. (Ar = Dipp).

Similarly calculated with acyclic systems, *in-silico* assertions of the [Al(DAS)]$^-$ electronic structures, corresponding orbital energies and the consequential HOMO-LUMO energy gap were identified (Figure 4.9). The optimised structure of the [Al(DAS)]$^-$ anion featured a narrower ∠N–Al–N angle (79.557°) comparative to the solid-state structures of the potassium aluminyl **4-II** (80.93(18)°), and the iron-aluminyl complex **4-I** (85.76(8)°). Resultant of this angle, the aluminium based HOMO presents the least *p*-character and most s-character of any previously calculated system. Thereby, the

HOMO of the [Al(DAS)]$^-$ aluminyl anion is also the lowest energy of all systems by greater than 0.3 eV (Figure 4.9). Of the frontier molecular orbitals, the HOMO (-1.34 eV) is centred upon aluminium(I) centre pronounced from the metal-based lone pair. The LUMO of the system is primarily centred upon the backbone diphenylsilyl substituents, thus, lacking any aluminium character. Consequently, the orbital corresponding significant Al p_z orbital character is higher in the orbital manifold (LUMO+4). Furthermore, LUMO+n (n = 1, 2, 3) all featured density upon the ligand scaffold with a key propensity be based within the aryl functional groups.

The calculated [Al(DAS)]$^-$ features a relatively large HOMO-LUMO gap (4.02 eV), similar in magnitude to that of the 6-membered [Al(^{Si}NON)]$^-$ system **3.17** (4.06 eV).[4] However, both the HOMO and LUMO+n energies are ~0.3 eV lower than those of **3.17**, potentially indicating a relatively less nucleophilic but more electrophilic aluminyl anion.

4.3.4. Initial Reactivity Studies of a 4-Membered Aluminyl Anion

4.3.4.1. Aluminium(I) as a Nucleophile: Nucleophilic Substitution

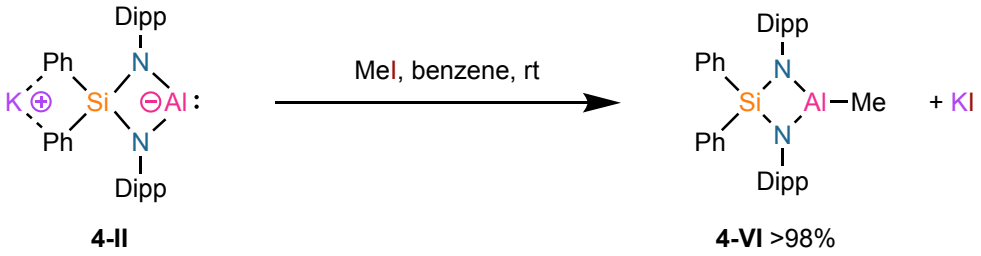

4-II **4-VI** >98%

*Scheme 4.7: Reaction of the 4-membered aluminyl anion **4-II** with methyl iodide.*

To identify the nucleophilicity of the aluminium(I) centre in , treatment of this 4-membered aluminyl with an electrophilic carbon source was undertaken. Upon addition of iodomethane to a burnt-orange benzene solution of **4-II** an immediate colour change to a colourless solution was noted. Following agitation for 5 minutes, ^{1}H NMR spectroscopy identified the clean conversion to a single species. Most tellingly, a singlet signal integrating as 3 hydrogens was identifiable within the spectral region commonly associated with aluminium methyl environments. This singlet at -0.32 ppm in C_6D_6 was also present within the range of aluminium methyl products generated from nucleophilic substitutions with aluminyl anions (**3.16**,[12] **3.18**,[13] **3.23**,[1] **Chapter 3**) (-0.09 to -1.08 ppm, in C_6D_6). Further standing of the reaction flask would also identify the precipitation of a colourless powder, attributed to potassium iodide. Notably, attempts toward the crystallisation of the target species were unsuccessful.

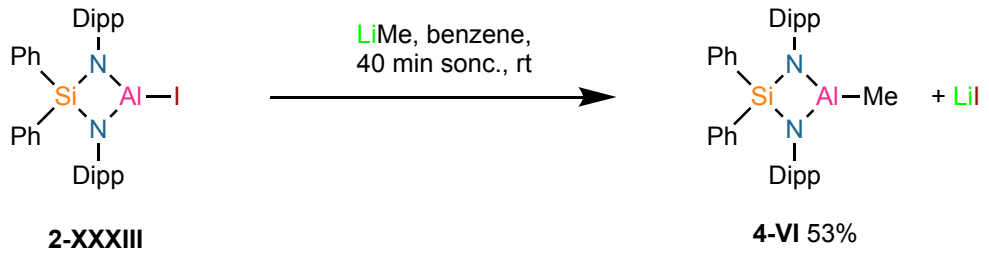

2-XXXIII **4-VI** 53%

Scheme 4.8: Synthesis of organoaluminium(III) ***4-VI*** *from treatment of aluminium(III) iodide precursor with methyllithium.*

Hypothesised as the monomethylated aluminium(III) species [Al(DAS)Me] **4-VI**, ^{1}H NMR spectra were cross-referenced with previous syntheses. Signals and splitting patterns corresponding to **4-VI** could be readily identified from previous organoaluminium investigations. Specifically, signals could be identified in the *in-situ* formation of **4-VI** from H_2DAS pro-ligand **2-XXIII** refluxed with trimethylaluminium. To further fortify the assignment of targeted methylated product **4-VI**, the formation of **4-VI** directly was conducted from the iodoalane precursor **2-XXXIII** and methyllithium. A benzene solution of **2-XXXIII** was treated with methyllithium and agitated for greater than 12 hours (Scheme 4.8). Identified as the major product within solution (53%), signals corresponding to **4-VI** were identified and aligned with preparations from both trimethylaluminium and the 4-membered aluminyl system. Contrary to acyclic investigations, the clean nor quantitative formation of the derivative methyl aluminium species was afforded. Rather, reactions also observed the retainment of unreacted precursor **2-XXXIII** and its corresponding aluminate derivative Li[Al(DAS)I_2].

4.3.4.2. Homobimetallic Aluminium(II) systems

Highlighted in the seminal work by Aldridge, Goicoechea and coworkers with the first aluminyl anion, [K_2{Al(NON)}$_2$] **3.16**,[12] the preparation of an aluminium(II) dialane species could be accessed through the treatment of aluminyl anions with stoichiometric amounts of their aluminium iodide precursor. Due to the steric encumberment located relatively peripheral to the aluminium centres (highlighted in the solid-state structures), the likelihood of aluminium(II) complex formation was postulated.

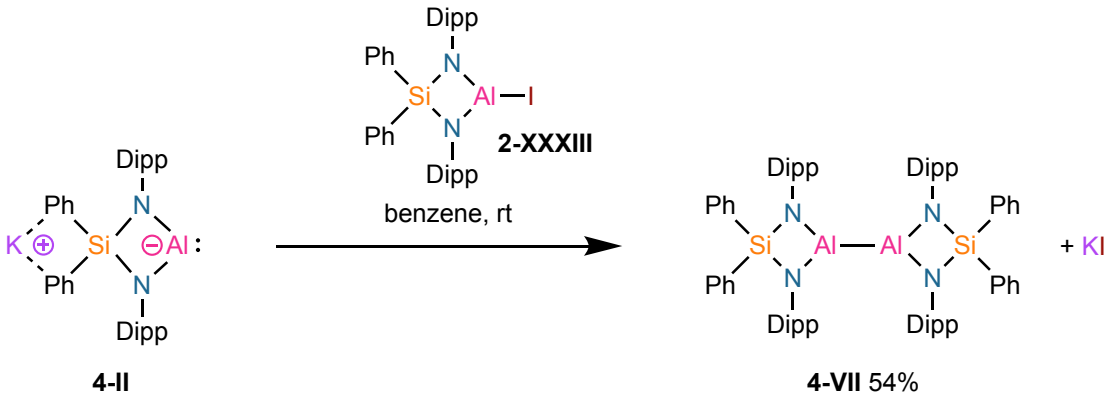

*Scheme 4.9: Synthesis of the 4-membered dialane complex **4-VII** from the 4-membered aluminyl system **4-II** and **2-XXXIII**.*

To a freshly prepared solution of aluminyl **4-II**, the iodoalane **2-XXXIII** was added as a solid, and an immediate colour change from burnt-orange to light-yellow was observed (Scheme 4.9). Extraction of the product and analysis via ^{1}H NMR spectroscopy identified the complete consumption of both starting materials. Preparations had resulted in the majority formation of a previously unidentified species **4-VII** (54%) and the potassium aluminate K[Al(DAS)I$_2$] **2-XXXI** (46%). Repeated crystallisation attempts from aromatic, aliphatic and coordinating solvents afforded varying degrees of decomposition or colourless blocks of the side product **2-XXXI**. The presence of **2-XXXI**, however, was indicative of the targeted nucleophilic substitution reaction with the eliminated potassium iodide interacting with precursor **2-XXXIII**. Despite extensive attempts toward the confirmation of **4-VII** via X-ray crystallography, no crystals could be isolated. Consequently, other methods were sought toward the formation of target species for comparative confirmation.

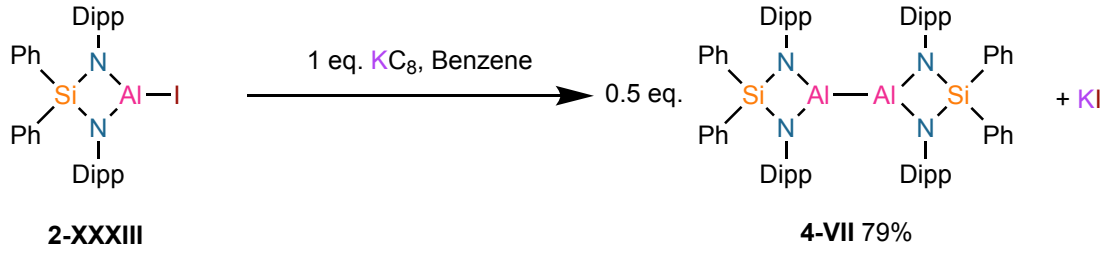

*Scheme 4.10: Synthesis of the 4-membered dialane complex **4-VII** via stoichiometric reduction of precursor **2-XXXIII**.*

Within the literature, the reported 5-membered aluminyl anion species (**3.23**-**3.25**, **Chapter 3**) were afforded by stepwise reductions (aluminium oxidation state: III → II → I).[1-3] Moreover, the steric encumberment of 4- and 5-membered systems is located more peripheral to aluminium centres, as such this reinforced the potential for synthetic similarities.

A dilute benzene solution of the iodoalane **2-XXXIII** was treated with stoichiometric potassium graphite and vigorously agitated for 1 hour (Scheme 4.10). From ^{1}H NMR spectroscopy, the formation of target species was identified as the major product in addition to the minor presence of potassium aluminate **2-XXXI**. Following separation of impurities, the targeted species **4-VII** was isolated in a good yield (79%) as a yellow-grey oil and identified via ^{1}H NMR spectroscopy. In purifying the oil product, the reaction was stood at ambient temperature for 3 days to precipitate **2-XXXI** impurities. Thereafter, extractions and crystallisation crops were undertaken to remove the remaining aluminate via two additional crystallisation crops affording clean **4-VII**.

Hinted with the isolation of **4-VII** as an oil, attempts to crystallise material from aromatic, aliphatic and coordinating solvents were unsuccessful. However, as intended, the comparative analysis of NMR spectra identified the formation of target dialane species **4-VII**, identical to that afforded by nucleophilic substitution attempts.

4.3.4.3. Heterobimetallic Aluminium(I)-Containing Systems

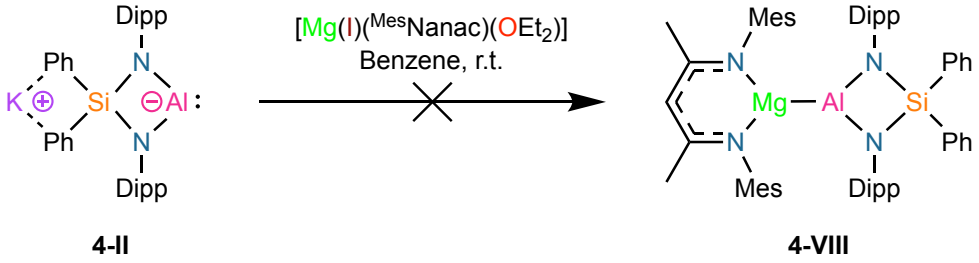

4-II **4-VIII**

*Scheme 4.11: Attempted synthesis of 4-membered magnesium aluminyl species from the potassium aluminyl **4-II** and [Mg(I)(^{Mes}Nacnac)(OEt$_2$)].*

Following successes with the acyclic system **3-IV** in the preparation of magnesium-aluminyl species, investigations were undertaken with the 4-membered aluminyl system **4-II** and its related precursor **2-XXXIII**. Initially, investigations focussed on treating **4-II** with the magnesium(II) iodide reagent [Mg(I)(^{Mes}Nacnac)(OEt$_2$)] in benzene. However, rather than the formation of the single targeted species [(DAS)Al-Mg(^{Mes}Nacnac)], the generation of an intractable mixture of products was afforded, as determined via ^{1}H NMR spectroscopy. The reaction was repeated; however, no clean preparation nor crystalline material could be isolated.

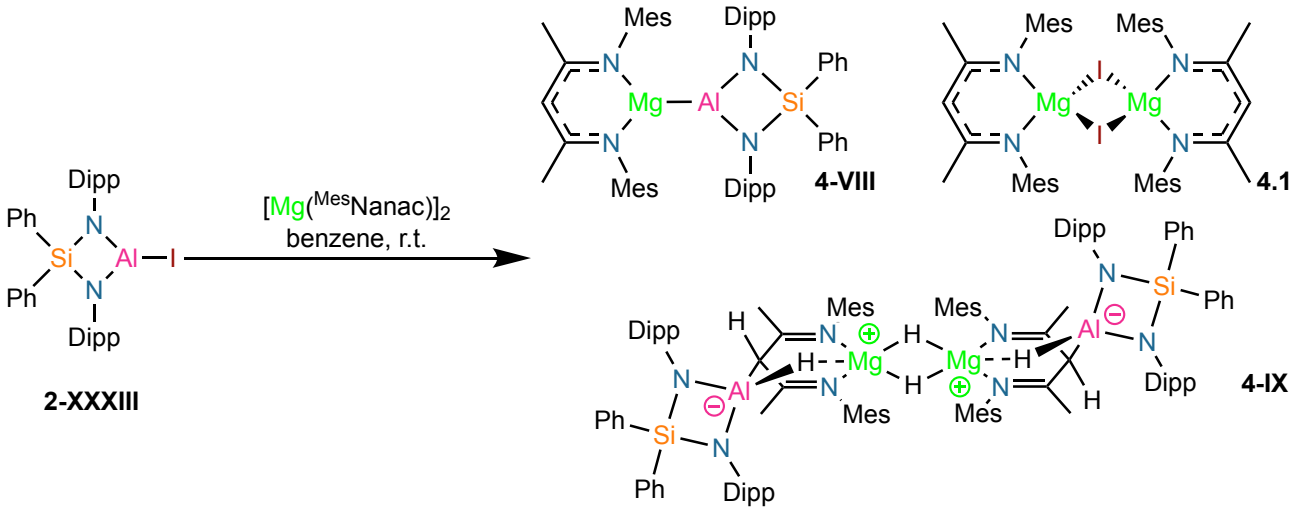

*Scheme 4.12: Identified species from magnesium(I) reductions of precursor **2-XXXIII**.*

Toward the preparation of targeted magnesium-aluminyl species, attempts were also pursued with Jones' magnesium(I) dimer [Mg(MesNacnac)]$_2$ (Scheme 4.12).[14] Such inquiries were inspired by findings reported in the optimised preparation of analogous [NON]$^{2-}$ stabilised species [(MesNacnac)Mg–Al(NON)] **3.58** via 2-electron reductions of **2.1** (**Chapter 2**) with the magnesium(I) species.[15] To this end, benzene solutions of **2-XXXIII** were treated with [Mg(MesNacnac)]$_2$ at various temperatures from ambient to reflux. Optimally, ambient temperatures were identified to afford the least number of varied side-products via ^{1}H NMR spectroscopy, whilst reflux investigations yielded a multitude of degradation and decomposition products. Within investigations, attempts were undertaken to identify the formation of target species **4-VIII** via crystallisations. Consequently, nearly all crystalline samples were identified as the known by-product [Mg(I)(MesNacnac)]$_2$ **4.1** (Scheme 4.12).[16] Positively, the preparation of this side-product reinforced the reduction of the **2-XXXIII** precursor by the magnesium(I) dimer as a halide-specific reagent. Markedly, a single crystalline example of target species **4-VIII** was grown and analysed by SCXRD, but due to poor diffraction, the structure was only sufficient to ascertain connectivity (Figure 4.10).

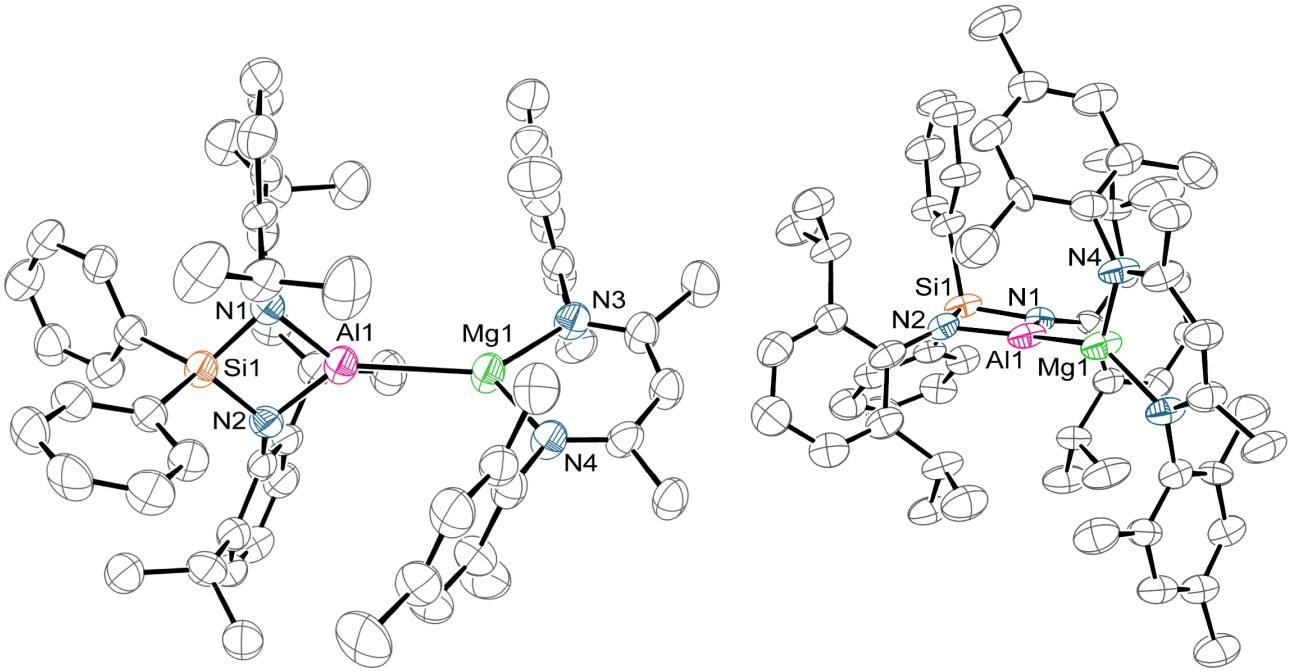

*Figure 4.10: Solid-state arrangement of 4-membered magnesium-aluminyl complex **4-VIII** connectivity as determined by X-ray crystallography depicted from side-on (left) and down the Al-Mg bond (right). Hydrogen atoms omitted. Thermal ellipsoids set to 50% probability.*

As hypothesised prior to its identification, **4-VIII** features an unsupported magnesium-aluminium bond with both metals in trigonal planar arrangements (Figure 4.10). Due to the corresponding electronegativities of the metal centres, its consequent polarisation would afford a formally aluminium(I) centred nucleophile and magnesium electrophile Al(δ–)-M(δ+). **4-VII** has an essentially perpendicular arrangement of metal-ligand planes, as identified in the previously isolated acyclic magnesium-aluminyl complex **3-VI**. This arrangement is likely due to minimisation of ligand steric clashing between the Dipp and Mes arene ligand moieties (Figure 4.10 right). Despite numerous attempts, isolation of better-quality crystals could not be achieved. However, during these attempts, a single example of a second product, **4-IX**, was isolated and analysed via X-ray diffraction (Scheme 4.12 and Figure 4.11).

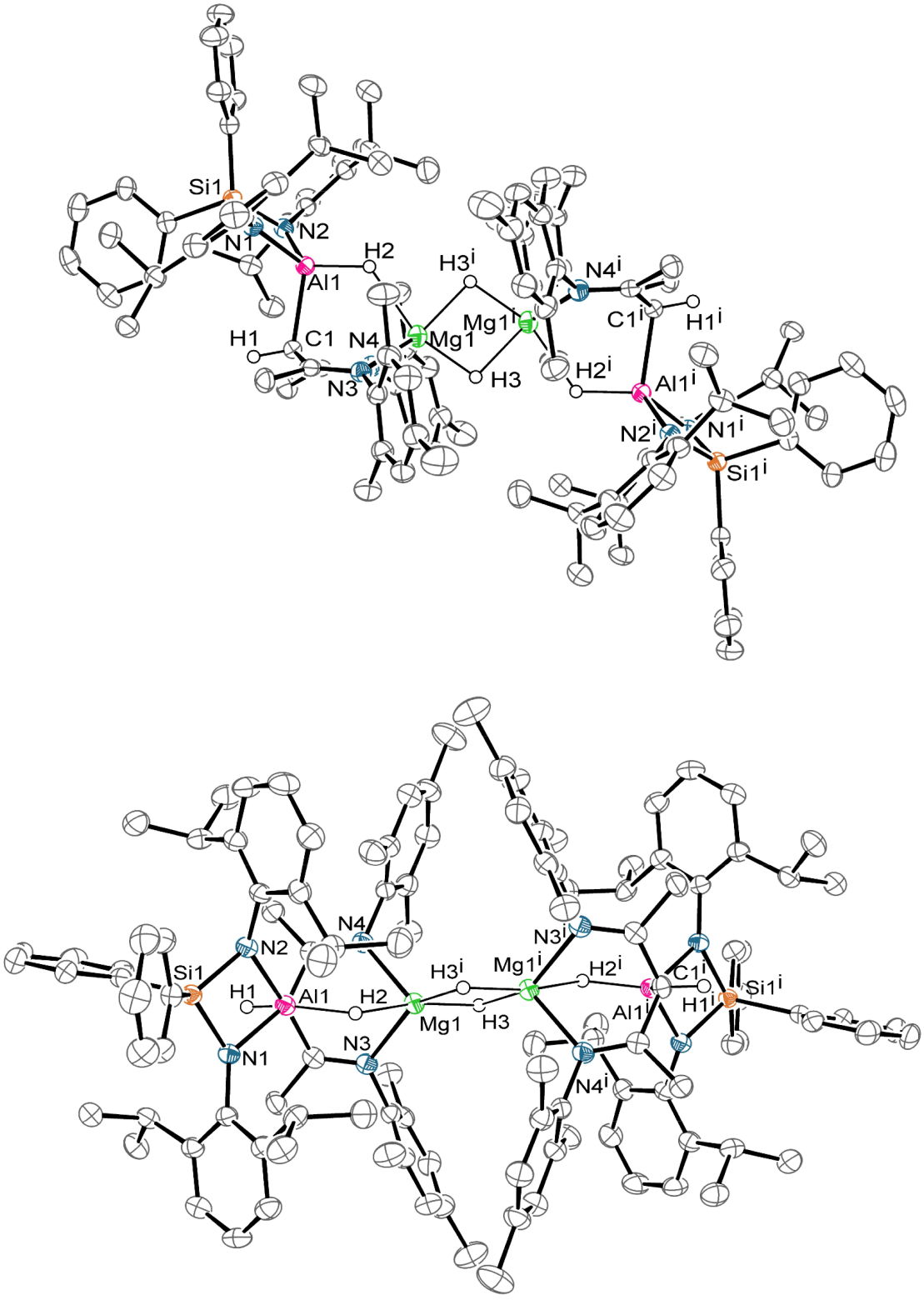

Figure 4.11: Molecular structure of magnesium-aluminium activation species ***4-IX*** *as determined by X-ray crystallography. Hydrogen atoms omitted. Thermal ellipsoids set to 50% probability. Selected bond lengths (Å) and angles (°): Mg1···Mg1 2.8032(18), Al1-C1 2.125(3), Al1-H2 1.65(3), Mg1-H2 2.12(3), Mg1-H3 1.79(4), Al1-N1 1.858(2), Al1-N2 1.842(2), Si1-N1 1.735(2), Si1-N2 1.733(2), Mg1-N3 2.140(2), Mg1-N4 2.110(2), N1-Al1-N2 84.84(10), H2-Al1-C1 97.3(10), H3-Mg1-H3^{i} 82(2), N1-Si1-N2 92.07(10), N3-Mg1-N4 87.81(9).*

Featuring both ligated aluminium and magnesium scaffolds within the asymmetric unit (Scheme 4.12), **4-IX** is a larger dimeric system featuring multiple bridging hydrides (Figure 4.11). Both metal centres feature distorted tetrahedral arrangements with 1- or 2-metal hydrides. The larger dimeric structure is supported by two hydrides bridging the two magnesium centres, with both magnesium centres also interacting with an aluminium-based hydride (Scheme 4.12). The *ß*-carbon of the formally [Nacnac]$^-$ ligand appears to have acted as a nucleophile towards the Al centre, and has consequently switched from sp^2 to sp^3 hybridisation. This affords a pseudo-boat conformation of the now diamine ligand scaffold, with both nitrogen atoms still coordinated to the magnesium centres. This arrangement directs the mesityl steric bulk upon the *N*-centres away from bridging hydride linkage.

The structural arrangement observed postulated the formation of **4-IX** from reactivity of [Nacnac]$^-$ ligand system. Whereby, electron density from the ligand system rearranges such that it is donated in to the empty p-orbital of the Lewis acidic aluminium(III) centre of the precursor **2-XXXIII**. Affording the diimine ligand scaffold, it is hypothesised that the hydride ligands are hydrogens scavenged from the solvent or decomposed material also within solution.

Indicative of the novelty of **4-IX**, attempts toward its replicative preparation were unsuccessful and impacted by approaching deadlines toward the end of the project. Furthermore, the impact of time constraints accordingly hindered opportunities to further explore the reactivity of the 4-membered aluminyl anion species with small molecules, as previously investigated with acyclic systems in **Chapter 3**.

4.3.5. Inquiries toward Isolating MIP and SIP Complexes of 4-Membered Aluminyl Systems

Throughout investigations, attempts to improve the solubility of the 4-membered potassium aluminyl species were undertaken through varied solvents, affording non-targeted solvated dialkali metal systems **4-III** and **4-IV**. Outside of solvent variation, the introduction of potassium sequestering reagents to **4-II** was pursued to increase solubility via breaking solid-state afforded polymeric chains. Inspired by the acyclic and wider aluminyl anion investigations,[4, 6, 17] inquiries were undertaken with 18-crown-6 and 2.2.2-cryptand to afford the MIP and SIP systems, respectively.

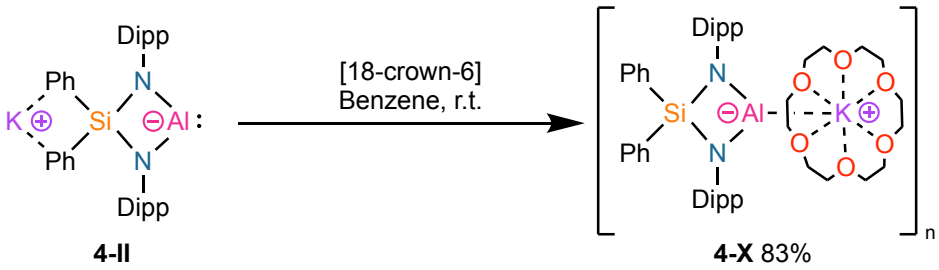

4-II **4-X** 83%

*Scheme 4.13: Preparations affording in-situ generation of a monomeric ion pair arranged 4-membered aluminyl anion **4-X**.*

Following the preparation of burnt-orange benzene solutions of **4-II**, 18-crown-6 was added as a crystalline solid. Following sonication for 10 minutes, a light-yellow solution was obtained and identified via ^{1}H NMR spectroscopy as the target MIP species **4-X** in high rate of conversion (83%) (Scheme 4.13). Notably however, was that after 16 hours at ambient temperatures within solution, **4-X** decomposed to an intractable mixture of products. Toward isolating SCXRD crystalline samples, varied results were afforded from mixtures of aliphatic and coordinating solvents, which were challenging due to the slow decomposition of the **4-X** species. That said, crystals of sufficient quality for connectivity were isolated from a benzene : diethyl ether mixture at ambient temperature (Figure 4.12).

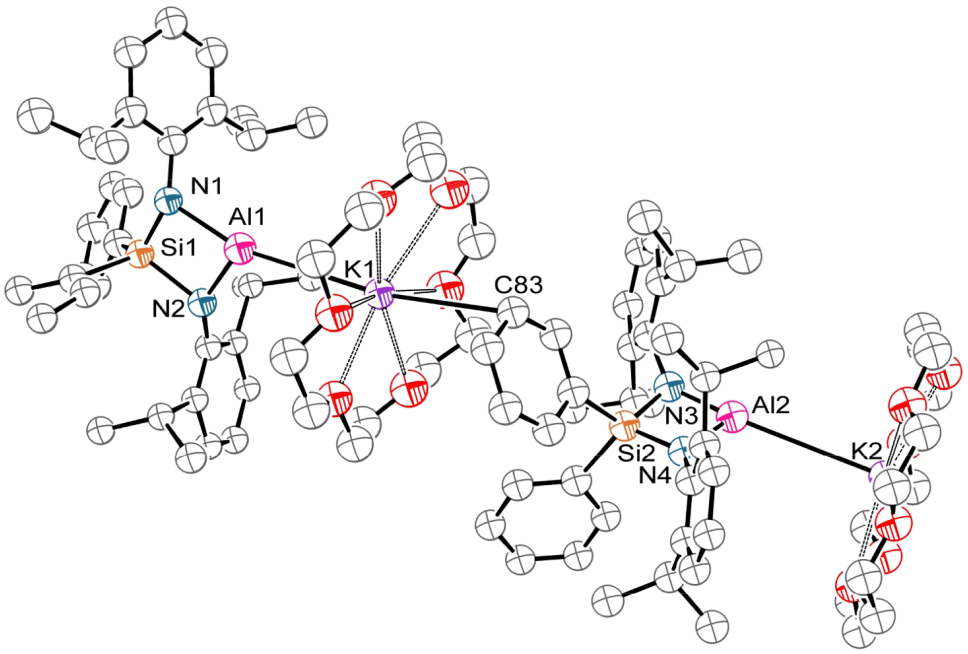

*Figure 4.12: Solid-state connectivity of 4-membered monomeric ion-pair potassium aluminyl complex **4-X** as determined by X-ray crystallography. Hydrogen atoms omitted. Thermal ellipsoids set to 50% probability.*

From the connectivity structure of **4-X**, the targeted potassium-ligand interaction and consequential targeted MIP arrangement could be identified. Thereby, the potassium cation was ligated within the 18-crown-6 fragment rather than being held by the phenyl groups of silyl backbone (as identified in **4-II**). Notably within the solid-state structure, **4-X** appeared to have crystallised as a coordination polymer, with a single potassium interaction with the aluminium centre and a single silyl backbone phenyl moiety.

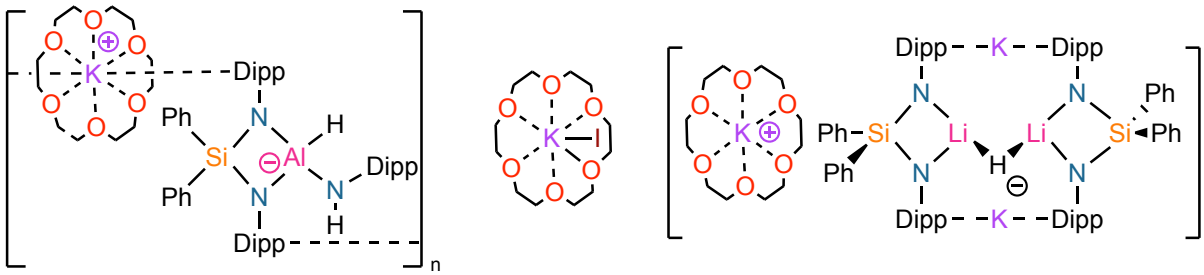

4-XI **4.2** **4-XII**

*Figure 4.13: Further species identified from treatment of **4-II** with 18-crown-6.*

Considering the singular connectivity success, the preparation of crystals of SCXRD quality of **4-X** was not reproducible. Rather, subsequent crystallisations afforded the [K(18-crown-6)] containing species: **4-XI** from the previously applied crystallisation conditions and **4-XII** with **4.2** from further investigations of varied conditions (Figure 4.13). In all crystallisation instances, only very small amounts of single crystals were afforded from saturated solutions following over 24 hours at ambient or reduced temperatures. Repeating the benzene : diethyl ether crystallisation attempt having initially afforded **4-X**, crystals of sufficient quality for connectivity were isolated, identifying the NH_2Dipp activation product **4-XI** (Figure 4.14).

From the connectivity structure of the (amido)(hydrido)aluminate species **4-XI**, the reactivity presented by **4-X** could be inferred. As such, the formation of a tetracoordinate aluminium(III) aligned with reactivity previously reported with other aluminyl systems. Highlighted by aluminyl anions **3.16** and **3.17** from Aldridge, Goicoechea and coworkers,[18] and Coles and coworkers respectively,[19] **4-XI** was indicative of an oxidative addition by an aluminyl anion toward the acidic N-H bond of diisopropylaniline, likely available from the degradation of the metal complex. Consequently, addition across the N-H bond afforded the coordination of NH(Dipp) and terminal hydride ligands to the anionic aluminium(III) centre. In stabilising this anionic charge, potassium counterion is in close proximity to the aluminate centre. As intended, the potassium centre is ligated with an 18-crown-6 ligand. The presence of diisopropylaniline in solution was attributed to the over-time solution-state degradation of the MIP **4-X**. ^{1}H NMR spectroscopy easily identified the presence of $DippNH_2$ via a septet signal at

2.66 ppm and doublet at 1.15 ppm, corresponding to the methine and methyl hydrogen environments of the isopropyl groups, respectively.

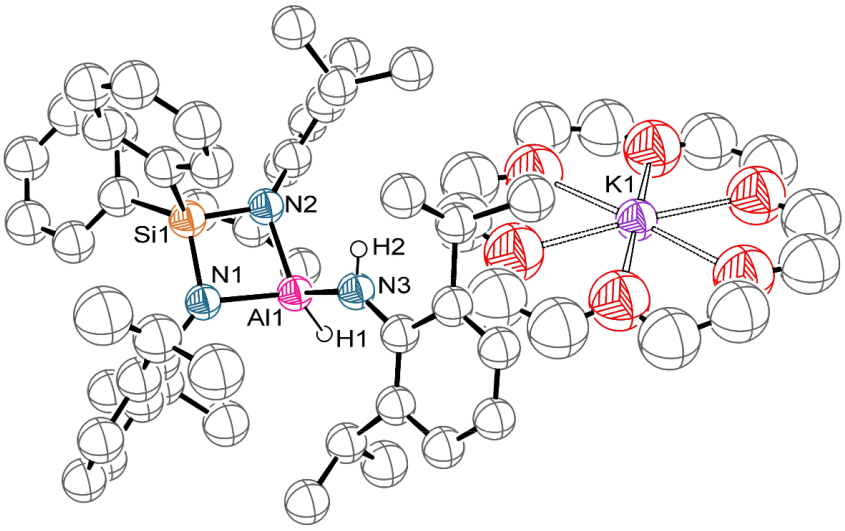

*Figure 4.14: Solid-state connectivity of $DippNH_2$ activation product **4-XI** as determined by X-ray crystallography. Hydrogen atoms omitted. Thermal ellipsoids set to 50% probability.*

Further crystallisations from saturated benzene solutions afforded the identification of additional [K(18-crown-6)]-containing species. Presenting strong diffraction patterns due to the inclusion of iodide within the system, a single example of crystalline 18-crown-6 sequestered potassium iodide **4.2** [K(I)(18-crown-6)] was identified (Figure 4.13). The preparation of this species was not attributed to the degradation of **4-X**, rather to trace amounts of potassium iodide present within reaction mixtures. Notably, the isolation of such species was not identified in subsequent investigations.

Also identified from saturated benzene crystallisation attempts and isolated as crystals of SCXRD quality, **4-XII** consisted of a heteropentametallic alkali metal salt complex incorporating two $[DAS]^{2-}$ ligands and an 18-crown-6, whilst neglecting the presence of aluminium within the species (Figure 4.15).

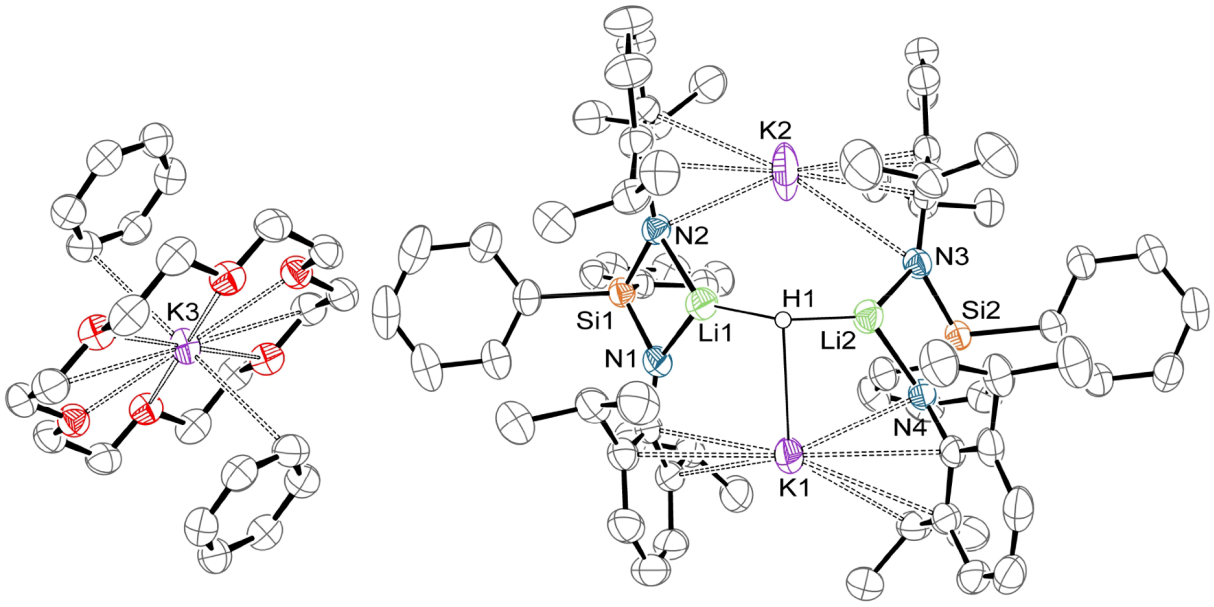

*Figure 4.15: Molecular structure of penta-alkali metal complex **4-XII** as determined by X-ray crystallography. Solvent molecules and most hydrogen atoms omitted. Thermal ellipsoids set to 50% probability. Selected bond lengths (Å) and angles (°): Li1-H1 1.84(2), Li2-H1 1.73(2). Li1···Li2 3.260(5), K1-H1 2.78(2), Li1-N1 1.948(4), Li1-N2 2.003(4), Si1-N1 1.6780(18), Si1 N2 1.6935(16), Li2-N3 1.971(4), Li2-N4 1.979(4), Si2-N3 1.6924(16), Si2-N4 1.7023(16). Li1-H1-Li2 132.19, N1-Li1-N2 84.15(15), N3-Li2-N4 85.01(14).*

As a combined contact dimeric pair and separated ion pair species, **4-XII** features an anionic bis-$[DAS]^{2-}$ alkali metal complex consisting of two potassium and two lithium cations with a bridging hydride, and a necessitated cationic sequestered $[K(18\text{-crown-6})(C_6H_6)_2]$ counterion (Figure 4.15). Within the complex, the lithium cations are within the *N*-Si-*N* binding pocket of the $[DAS]^{2-}$ ligands and are tricoordinate through interactions with both amido coordination atoms and a bridging hydride. To further balance the remaining charge of the two dianionic ligands, potassium cations support the dimeric arrangement via combinative interactions with amido coordination atoms and arene components of Dipp moieties. Moreover, due to the additional monoanionic charge of the bridging hydride, the larger bis-DAS fragment exists as a separated ion pair with an additional 18-crown-6 ligated potassium counterion, with little interaction between the two parts. In addition to the 18-crown-6 ligand, the SIP potassium centre also features η^2-arene interactions with two benzene solvent molecules located above and below the 18-crown-6 plane.

The presence of the bridging hydride within **4-XII** could not be clearly identified by ^{1}H NMR spectroscopy, nor could possible sources be identified. Moreover, attempts to repeat crystallisations affording **4-XII** were unsuccessful. To directly target the formation of the **4-XII**, syntheses incorporating Li_2DAS and K_2DAS in the presence of 18-crown-6 were hypothesised. However, due to a lack of time remaining within the project, it was not undertaken.

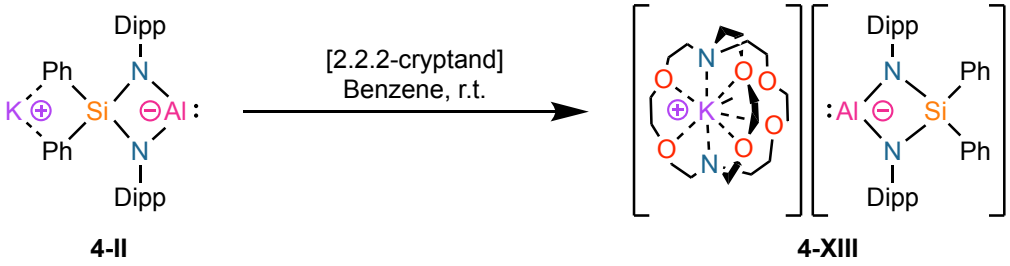

4-II **4-XIII**

*Scheme 4.14: Attempted synthesis toward the preparation of 4-membered SIP aluminyl anion **4-XIII**.*

Following the preparation of the alkali metal SIP complex **4-XII**, initial investigations were undertaken directly targeting the preparation of SIP aluminyl anions incorporating the $[DAS]^{2-}$ ligand framework. To encapsulate the potassium cation located within the phenyl moieties of the LEP-arranged potassium aluminyl **4-II**, the potassium sequestering reagent 2.2.2-cryptand was applied due to its applicability with the seminal $[NON]^{2-}$ aluminyl anion.[20]

Consequently, benzene solutions of **4-II** were treated with 2.2.2-cryptand at ambient temperature (Scheme 4.14). Following 10 seconds, the initially burnt-orange solution would observe an ostensible change to colourless. ^{1}H NMR spectroscopic analysis undertaken within 15 minutes of reaction initiation afforded a broad spectrum with clean conversion to a single product, which was identified to present visible degradation to multiple species following 12 hours. Given literature and project precedence, it was hypothesised that potentially, the targeted SIP complex **4-XIII** or a related near instantaneously afforded degradation species as identified with acyclic species affording **3-X** and **3-XI**. Toward ascertaining the species identity, crystallisation attempts were undertaken within both saturated aromatic and coordinating solvents. However, no crystalline material could be afforded from attempts. Moreover, as observed within MIP-centric investigations, the impact of minimal remaining time and the need for characterisation shifted focuses. Consequently, the preparation of **4-XIII** became a research focus for future inquiries.

4.4. Conclusion

Previously dominated with 5-, 6- and 7- membered metallocycles, initial work within this PhD project expanded the catalogue of aluminyl systems to include an acyclic example. Within the literature, all 5-membered species featured di(alkyl) or (alkyl)(amido) mixed coordination to two-coordinate aluminium centres. Consequently, all di(amido) systems are presented within 6-membered or greater metallocycles. In further advancing the catalogue of aluminyl anions, reductions afforded the first example of 4-membered aluminium(I) nucleophile $[K\{Al(DAS)\}]_n$ **4-II**.

Stabilised with a diamido ligand scaffold, **4-II** features a ligand encapsulated pair arrangement with its potassium cation held in η^6-arene interactions and crystallises as a one-dimensional polymer within the solid-state. *In silico* investigations identified the $[Al(DAS)]^-$ anion as having the most stable HOMO energy (–1.34 eV), attributed to the narrowest ∠X-Al-X bond angle (80.93(18)°) of any reported aluminyl species.[4, 6] A relatively large HOMO-LUMO gap (4.02 eV) was also identified, analogous to the previously isolated 6-membered aluminyl anion (**3.17**, **Chapter 3**) (4.06 eV) reported by Coles and coworkers.[5b]

The nucleophilicity of the aluminyl anion of **4-II** was ascertained through reaction with iodomethane affording the derivative monomethylated aluminium(III) species **4-VI**. Treatment with a homometallic electrophile precursors **2-XXXIII**, preparation of the dialane species could be afforded and its preparation confirmed via stoichiometric reductions of corresponding iodoalane **2-XXXIII**.

A variety of methods were undertaken to prepare heterobimetallic aluminyl species. An iron-aluminyl incorporating 4-membered aluminium(I) centre **4-I** was prepared in synthetically useful yield via both solution state and mechanochemical methods. Whilst the treatment of precursor **2-XXXIII** with a magnesium(I) reducing agent afforded solid-state connectivity evidence of the target magnesium-aluminyl **4-VIII**.

Inquiries were undertaken toward the preparation of corresponding MIP **4-X** and SIP **4-XIII** derivatives from the LEP potassium-aluminyl species **4-II**. As observed within magnesium-based inquiries, reactions afforded a mixture of species including activation product **4-XI**, and degradation species **4-XII**. Consequently, findings within this Chapter report the first preparation of the 4-membered potassium **4-II** and magnesium **4-VIII** aluminyl species, and highlight the further expansions and analogous reactivity possible via 4-membered aluminium(I) metallocycles.

4.5. Experimental

General Methods and Considerations

All manipulations were performed under inert conditions using standard Schlenk and glovebox techniques. n-Hexane, toluene, tetrahydrofuran (THF) and diethyl ether were pre-dried using an MBraun solvent purification system, transferred to a Schlenk tube containing a sodium mirror, and sparged with Ar. Benzene and benzene-d_6 (C_6D_6) were refluxed over potassium and transferred to a Schlenk tube containing a sodium mirror for storage. NMR samples were prepared in a glovebox using Norell NMR tubes (5 mm) fitted with a J. Young Teflon valve. NMR spectra were recorded at 298 K (unless otherwise noted) using a Bruker Avance 800 MHz or a Bruker Avance 400 MHz spectrometer and ^{1}H and $^{13}C\{^{1}H\}$ spectra were referenced internally (^{1}H: 7.16 ppm (C_6D_5H), $^{13}C\{^{1}H\}$: 128.06 ppm). Chemical shifts δ are reported in part per million (ppm), coupling constants are reported in Hertz (Hz) and coupling patterns are abbreviated as follows: m (multiplet), s (singlet), d (doublet), t (triplet), q (quartet), quin (quintet), sex (sextet), sept (septet), or combinations thereof. **2-XXIII** and **2-XXXIII** was prepared as discussed in **Chapter 2**. 5% K/KI, 5% Na/NaCl, [MgI(^{Mes}Nacnac)(OEt_2))], and [{Mg(^{Mes}Nacnac)}$_2$] were all prepared according to literature methods.[16, 21] Methyl lithium powder was prepared from 1.6 M solution with volatiles removed under reduced pressure by Li Feng Lim. K[Fe(CO)$_2$Cp] (Cp = cyclopentadienyl) was prepared by Dr. Fabian Kallmeier according to literature methods.[22] All other reagents were used as received.

Synthesis of [Cp(CO)$_2$Fe–Al(DAS)] (4-I)

Method A: [Al(DAS)I] **2-XXXIII** (200 mg, 0.291 mmol, 1.0 eq.) and K[Fe(CO)$_2$(Cp)] (630 mg, 2.91 mmol, 10.0 eq.) were charged into an IKA BMT-20-S 20 mL polypropylene vessel with stainless steel balls (30 pieces, diameter: 5 mm, weight per ball: 0.52 g, type: AISI 304). Milling was initiated on the highest setting (4000 rpm, 66.7 Hz) for 1 h using an IKA ULTRA-TURRAX® Tube Drive. A light-brown powder was yielded, which was confirmed to be the clean preparation of [(Cp)(CO)$_2$Fe–AlDAS] via ^{1}H NMR spectroscopy. Isolation from the polypropylene vessel and extraction with benzene (3 × 4 mL) yielded a dark-red solid, which was washed with (–80 °C) cold hexane (3 × 3 mL). Removal of volatiles under reduced pressure yielded [Cp(CO)$_2$Fe–AlDAS] **4-I** as a dark-red solid (146 mg, 68%). **Method B:** To a 25 mL Schlenk flask, **2-XXXIII** (200 mg, 0.291 mmol, 1.0 eq.) and K[Fe(CO)$_2$(Cp)] (63 mg, 0.291 mmol, 1.0 eq.) were charged. Following the cannula addition of benzene (10 mL), the reaction mixture was stirred for 19 h at room temperature. A transparent brown-red solution was separated from a colourless precipitate via cannula filtration. The volatiles were removed from the filtrate *in vacuo,* yielding a foam-like solid, which was dissolved in cyclohexane (3 mL). The resultant brown solution was concentrated under reduced pressure (*ca.* 0.5 mL). Following

16 h standing at ambient conditions, SCXRD quality crystals of [Cp(CO)$_2$Fe–AlDAS] could be isolated as off-white blocks. The crystalline material was washed with cold hexane (3 × 3 mL), and isolated as off-white crystalline blocks of **4-I** (131 mg, 61%). **^{1}H NMR** (400 MHz, C_6D_6, 298 K): δ = 7.50 (d, $^3J_{HH}$ = 6.2 Hz, 4H, Ph-*o*-C*H*), 7.18 (d, $^3J_{HH}$ = 7.4 Hz, 4H, Dipp-*m*-C*H*), 7.13 – 7.01 (m, 2H, Dipp-*p*-C*H*, 4H, Ph-*m*-C*H*, 2H Ph-*p*-C*H*), 4.12 (s, 5H, Cp*H*), 4.09 (sept, $^3J_{HH}$ = 6.8 Hz, 4H, Dipp-C*H*(CH$_3$)$_2$), 1.37 (d, $^3J_{HH}$ = 6.9 Hz, 12H, Dipp-CH(C*H*$_3$)$_2$), 0.90 (d, $^3J_{HH}$ = 6.7 Hz, 12H, Dipp-CH(C*H*$_3$)$_2$). **^{13}C{^{1}H} NMR** (101 MHz, C_6D_6, 298 K): δ = 212.6 (Fe-(*C*O)$_2$), 144.8 (Dipp-*o*-*C*), 142.5 (Dipp-*i*-*C*), 138.1 (Ph-*i*-*C*), 135.7 (Ph-*o*-*C*), 129.6 (Ph-*p*-*C*), 127.5 (Ph-*m*-*C*), 123.8 (Dipp-*p*-*C*), 123.3 (Dipp-*m*-*C*), 80.6 (Fe-*C*$_5$H$_5$), 29.3 (Dipp-*C*H(CH$_3$)$_2$), 25.6 (Dipp-CH(*C*H$_3$)$_2$), 23.9 (Dipp-CH(*C*H$_3$)$_2$). **^{29}Si NMR** (79 MHz, C_6D_6, 298 K): δ = –29.5 ((NDipp)$_2$*Si*Ph$_2$). **IR** ν_{max} (cm^{-1}) (Nujol): 3070(w), 3051(w), 2001(s), 1957(s), 1943(s), 1785(w), 1588(w), 1427(m), 1381(w), 1312(m), 1251(m), 1203(m), 1100(m), 1041(w) 931(m), 827(s), 782(s), 740(w) 727(m), 708(m), 700(m), 682(w), 643(m), 587(s), 532(m), 501(s), 485(m), 456(m), 435(w).

Synthesis of [K{Al(DAS)}] (4-II)

Method A: To a 50 mL Schlenk flask, [Al(DAS)I] **2-XXXIII** (100 mg, 146 μmol, 1.0 eq.) and potassium graphite (400 mg, 2.96 mmol, 20.3 eq.) were added. Benzene (25 mL) was added rapidly via cannula, and the reaction mixture was stirred vigorously for strictly 1 h at ambient temperature. After allowing the precipitate to settle over 10 min, a dark burnt-orange solution was separated from the black precipitate via cannula filtration. Removal of volatiles from the filtrate under reduced pressure yielded [K{Al(DAS)}] **4-II** as a burnt-orange (40.4 mg, 47%). **N.B.** To afford SCXRD quality crystals, the reactants were charged into a J. Young's NMR tube and placed in a sonication bath for 40 min. Following the generation of a dark burnt-orange solution, the flask was stood at ambient temperature for 3 days. X-ray quality crystals could be isolated as small burnt-orange plates from the tube. **Attempted Method B:** [Al(DAS)I] **2-XXXIII** (190 mg, 277 μmol, 1.0 eq.), potassium graphite (200 mg, 1.48 mmol, 5.3 eq.) and graphite (240 mg, 19.9 mmol, excess) were charged into an IKA BMT-20-S 20 mL polypropylene vessel with stainless steel balls (30 pieces, diameter: 5 mm, weight per ball: 0.52 g, type: AISI 304). Milling was initiated on the highest setting (4000 rpm, 66.7 Hz) for 1 h using an IKA ULTRA-TURRAX® Tube Drive. The resulting black powder was transferred to a Schlenk flask, extracted with benzene (20 mL), and the solution was analysed via ^{1}H NMR spectroscopy, which found a complex mixture of products. **N.B.** Attempts to purify a single species were unsuccessful.

Characterisation data for 4-membered aluminyl anion (**4-II**):

^{1}H NMR (400 MHz, C_6D_6, 298 K): δ = 7.56 (dd, $^{3}J_{HH}$ = 7.6 Hz, 2.4 Hz, 4H, Ph-*o*-C*H*), 7.13 – 7.07 (m, 10H, Aryl-C*H*), 6.89 – 6.83 (m, 2H, Aryl-C*H*), 4.20 (sept, $^{3}J_{HH}$ = 7.0 Hz, 4H, Dipp-C*H*(CH_3)$_2$), 1.17 (br, 24H, Dipp-CH(C*H*$_3$)$_2$). **^{13}C{^{1}H} NMR** (101 MHz, C_6D_6, 298 K): δ = 147.9 (Dipp-*o*-*C*), 145.6 (Dipp-*i*-*C*), 141.7 (Ph-*i*-*C*), 135.3 (Ph-*o*-*C*), 128.6 (Ph-*p*-*C*), 127.3 (Ph-*m*-*C*), 123.5 (Dipp-*p*-*C*), 120.7 (Dipp-*m*-*C*), 28.3 (Dipp-*C*H(CH$_3$)$_2$), 25.8 (Dipp-CH(*C*H$_3$)$_2$). **IR** ν_{max} (cm^{-1}) (Nujol): 3502(w), 3046(w), 1587(w), 1459(m), 1425(s), 1360(w), 1317(w), 1250(m), 1203(m), 1099(m), 1040(w), 927(m), 823(m), 782(s), 785(m), 701(s), 674(m), 548(w), 498(m), 449(w), 433(w).

Preparation of Li(THF)K(DAS) (4-III)

To a deuterated benzene (0.6 mL) solution of [Al(DAS)I] **2-XXXIII** (20 mg, 29.1 μmol, 1.0 eq.) in a J. Young's NMR tube was added potassium graphite (36 mg, 266 μmol, 9.2 eq.). The reaction mixture was sonicated for 2 h, which yielded the targeted [K{Al(DAS)}] **4-II** by analysis via ^{1}H NMR spectroscopy. Volatiles were removed under reduced pressure, and the residue was extracted with tetrahydrofuran (0.4 mL). No colour change was observed. The dark brown solution was concentrated (*ca.* 0.1 mL); however, no crystals were observed after 48 h at ambient temperature. Following, hexane (0.2 mL) was layered on top of the THF solution, and the mixture was left to stand for 19 days. From the resultant brown oil, a small number of small single colourless crystals of SCXRD quality could be isolated and identified as Li(THF)K[DAS] **4-III**. **N.B.** Purification attempts to isolate **4-III** as a target major species were unsuccessful.

Preparation of Li(OEt$_2$)K(DAS) (4-IV)

In a J. Young's NMR tube, [Al(DAS)I] **2-XXXIII** (20 mg, 29.1 μmol, 1.0 eq.) and potassium graphite (36 mg, 266 μmol, 9.2 eq.) were charged and deuterated benzene (0.5 mL) was added. The suspension was sonicated for 25 min, after which [K{Al(DAS)}] was identified as the major product via ^{1}H NMR spectroscopy. In a glovebox, the dark burnt-orange solution was filtered and concentrated (*ca.* 0.1 mL). Following a lack of crystallisation after 3 days, volatiles were removed under reduced pressure. The resultant red-brown foam was dissolved in diethyl ether (0.1 mL) and stood at ambient temperature. Following 11 days, SCXRD quality crystals could be picked from within a brown oily solid and confirmed as Li(OEt$_2$)K[DAS] **4-IV** via X-ray diffraction. **N.B.** Purification attempts to isolate **4-IV** as a target major species were unsuccessful.

Synthesis of Na[AlCl(DAS)I] (4-V)

To a solution of [Al(DAS)I] **2-XXXIII** (25 mg, 34.6 μmol, 1.0 eq.) in deuterated benzene (0.5 mL), 5% Na/NaCl (87 mg, 182 μmol Na, 5.3 eq.) was charged. The off-white solution observed a colour change towards yellow. Following 2 h of sonication, near quantitative conversion to Na[AlCl(DAS)I] **4-V** was observed via ^{1}H NMR spectroscopy (90%). **N.B.** Subsequent filtration and concentration of the reaction mixture (*ca*. 0.1 mL) yielded SCXRD quality crystals of **4-V** as small colourless plates. **^{1}H NMR** (400 MHz, C_6D_6, 298 K): δ = 7.60 (br, 2H, Aryl-*H*), 7.11 (d, $^{3}J_{HH}$ = 7.6 Hz, 4H, Aryl-*H*), 7.09 – 7.01 (m, 6H Aryl-*H*), 6.93 (t, $^{3}J_{HH}$ = 7.6 Hz, 4H, Aryl-*H*), 4.30 (sept, $^{3}J_{HH}$ = 6.8 Hz, 4H, Dipp-C*H*$(CH_3)_2$), 1.17 (br, 24H, Dipp-CH(C*H*$_3)_2$). **^{13}C{^{1}H} NMR** (101 MHz, C_6D_6, 298 K): δ = 147.2 (Dipp-*o*-*C*), 144.0 (Dipp-*i*-*C*), 143.5 (Ph-*o*-*C*), 136.3 (Ph-*i*-*C*), 129.4 (Ph-*p*-*C*), 127.3 (Ph-*m*-*C*), 124.0 (Dipp-*p*-*C*), 122.6 (Dipp-*m*-*C*), 28.4 (Dipp-*C*H$(CH_3)_2$), 25.7 (Dipp-CH(*C*H$_3)_2$).

Preparation of [Al(DAS)Me] (4-VI)

Method A: To a deuterated benzene (0.5 mL) solution of [K{Al(DAS)}] **4-II** (4.8 mg, 8.01 μmol, 1.0 eq.) within a J. Young's NMR tube, excess of MeI (10 μL, excess) was added under inert conditions. Agitation of the previously dark brown solution observed a colour change toward transparent yellow. Analysis via ^{1}H NMR spectroscopy ascertained the consumption of the **4-II** and formation of [Al(DAS)Me] **4-VI** and potassium iodide as a precipitated white powder (>98%) **Method B:** In a 50 mL J. Young's reaction flask, H_2[DAS] **2-XXIII** (535 mg, 1.00 mmol, 2.0 eq.) was charged. Dissolution in toluene (5 mL) yielded a colourless solution. Trimethylaluminium (500 μL of 1.1 M solution in toluene, 550 μmol, 1.0 eq.) was added dropwise at ambient temperature. Once the bubbling had subsided, the colourless solution was stirred vigorously at 100 °C for 24 h. At this stage, analysis of the reaction mixture by ^{1}H NMR spectroscopy identified complete consumption of the trimethylaluminium, giving the target compound **4-VI** and unreacted **2-XXIII** in a 1:1 ratio. Addition of further trimethylaluminium (500 μL of 1.1 M solution in toluene, 550 μmol, 1.0 eq.) and subsequent heating to 100 °C for 24 h yielded a mixture of products as identified via ^{1}H NMR spectroscopy. **N.B.** Attempts to isolate species through crystallisation gave mixtures of products from which only H_2(DAS) **2-XXIII** and [Al_2(DAS)Me_4] **2-XXIV** could be isolated. **Method C:** In a J. Young's NMR tube, to a deuterated benzene (0.5 mL) solution of [Al(DAS)I] **2-XXXIII** (25 mg, 36.4 μmol, 1.0 eq.) was added methyllithium powder (0.8 mg, 36.4 μmol, 1.0 eq.). This was placed on an NMR flask rotating apparatus and slowly agitated for 12 h. ^{1}H NMR spectroscopy identified the majority conversion toward the targeted [Al(DAS)Me] **4-VI** (53%), in addition to side product Li[Al(DAS)I_2] **2-XXXII** (26%) and unreacted starting material **2-XXXIII** (21%). Attempts to isolate or crystallise the targeted species yielded an indiscernible mixture of decomposition products.

Characterisation data for [Al(DAS)Me] (**4-VI**):

^{1}H NMR (400 MHz, C_6D_6, 298 K): δ = 7.44 (d, $^{3}J_{HH}$ = 6.4 Hz, 4H, Ph-*o*-C*H*), 7.13 – 7.08 (m, 6H, Aryl-C*H*), 6.99 (t, $^{3}J_{HH}$ = 7.5 Hz, 6H, Aryl-C*H*), 3.76 (sept, $^{3}J_{HH}$ = 6.8 Hz, 4H, Dipp-C*H*(CH_3)$_2$), 1.03 (d, $^{3}J_{HH}$ = 6.7 Hz, 24H, Dipp-CH(C*H*$_3$)$_2$), –0.31 (s, 3H, Al-C*H*$_3$). **^{13}C{^{1}H} NMR** (101 MHz, C_6D_6, 298 K): δ = 144.3 (Dipp-*o*-*C*), 141.8 (Dipp-*i*-*C*), 137.0 (Ph-*o*-*C*), 135.5 (Ph-*i*-*C*), 129.8 (Ph-*p*-*C*), 127.6 (Ph-*m*-*C*), 123.8 (Dipp-*p*-*C*), 123.2 (Dipp-*m*-*C*), 29.7 (Dipp-*C*H(CH$_3$)$_2$), 26.2 (Dipp-CH(*C*H$_3$)$_2$), –12.9 (Al-*C*H$_3$).

Synthesis of [{Al(DAS)}$_2$] (4-VII)

Method A: To a 50 mL Schlenk flask was added [Al(DAS)I] **2-XXXIII** (150 mg, 218 µmol, 1.0 eq.) and potassium graphite (29.5 mg, 218 µmol, 1.0 eq.). Benzene (30 mL) was added via cannula, and the resulting suspension was stirred at ambient temperature for 1 h. After allowing for precipitate to settle, the burnt yellow solution was stood at ambient temperature for 18 h. Following concentration (*ca.* 5 mL), the reaction solution stood for a further 3 d to precipitate K[Al(DAS)I$_2$] **2-XXXI**. With minimal agitation, the burnt yellow solution was separated from the colourless and black precipitate via cannula filtration. From an aliquot, ^{1}H NMR spectroscopy identified the majority formation of targeted [{Al(DAS)}$_2$] **4-VII**. The solution was further concentrated (*ca*. 1 mL), yielding two crystalline crops of K[Al(DAS)I$_2$] **2-XXXI**; as identified via X-ray diffraction. The remaining volatiles were removed *in vacuo,* and within a glovebox, the mass of the yellow-grey oil was isolated (97 mg, 79%). **N.B.** For crystallisation, the yielded material was transferred to a 10 mL Schlenk flask and attempts were undertaken with concentrated solutions of benzene and diethyl ether; however, no crystals of SCXRD quality could be grown. **Method B:** To a J. Young's NMR tube containing a deuterated benzene (0.5 mL) solution of [Al(DAS)I] **2-XXXIII** (30 mg, 43.7 µmol, 1.0 eq.), was charged potassium graphite (5.8 mg, 43.7 µmol, 1.0 eq.). Following 1 h of sonication, the yielded light-yellow solution was identified via ^{1}H NMR spectroscopy to contain [{Al(DAS)}$_2$] **4-VII** (87%), side-product K[Al(DAS)I$_2$] **2-XXXI** (7%), and decomposition impurities (6%). The solution was passed through a syringe containing Whatman glass filter paper and the black graphite residue was washed with deuterated benzene (0.2 mL). ^{1}H NMR spectroscopy identified purification from decomposition products yielding only [{Al(DAS)}$_2$] **4-VII** (88%) and side-product K[Al(DAS)I$_2$] **2-XXXI** (12%) within solution. **N.B.** The yellow benzene solution was concentrated (*ca*. 0.1 mL) and kept at ambient temperature. Following 18 h, attempts to isolate the targeted species via crystallisation afforded only crystals of the potassium aluminate K[Al(DAS)I$_2$] **2-XXXI**. **Method C:** To a freshly prepared deuterated benzene (0.5 mL) solution of [K{Al(DAS)}] **4-II** (7.9 mg, 12.5 µmol, 1.0 eq.), was charged [Al(DAS)I] **2-XXXIII** (7.6 mg, 11.1 µmol, 0.9 eq.). An immediate colour change from burnt-orange

to light yellow was observed. The solution was passed through a syringe containing Whatman glass filter paper and the colourless precipitate washed with benzene (0.1 mL). ^{1}H NMR spectroscopy identified the formation of [{Al(DAS)}$_2$] **4-VII** (54%) and K[Al(DAS)I$_2$] **2-XXXI** (46%). **N.B.** The transparent light-yellow solution was concentrated (*ca.* 0.1 mL) and stood at ambient temperature. Following 18 h, crystals of SCXRD quality were grown, however, all samples grown were identified as **2-XXXI**. **^{1}H NMR** (400 MHz, C_6D_6, 298 K): δ = 7.38 (dd, $^{3}J_{HH}$ = 8.0 Hz, $^{4}J_{HH}$ = 1.5 Hz, 4H, Ph-*o*-C*H*), 7.03 (s, 6H, Dipp-aryl-C*H*), 6.95 (t, $^{3}J_{HH}$ = 7.2 Hz, 6H, Ph-aryl-C*H*), 3.74 (sept, $^{3}J_{HH}$ = 6.7 Hz, 4H, Dipp-C*H*(CH$_3$)$_2$), 0.96 (br, 24H, Dipp-CH(C*H*$_3$)$_2$). **^{13}C{^{1}H} NMR** (101 MHz, C_6D_6, 298 K): δ = 144.0 (Dipp-*o*-*C*), 141.4 (Dipp-*i*-*C*), 136.8 (Ph-*i*-*C*), 135.3 (Ph-*o*-*C*), 130.0 (Ph-*p*-*C*), 127.6 (Ph-*m*-*C*), 123.7 (Dipp-*p*-*C*), 123.4 (Dipp-*m*-*C*), 29.4 (Dipp-*C*H(CH$_3$)$_2$), 24.6 (Dipp-CH(*C*H$_3$)$_2$).

Attempted preparation of [(^{Mes}Nacnac)Mg-Al(DAS)] (4-VIII) and isolation of magnesium aluminium activation species (4-IX)

To a J. Young's NMR tube containing a deuterated benzene (0.5 mL) solution of [Al(DAS)I] **2-XXXIII** (30 mg, 43.7 μmol, 1.0 eq.), was charged [(^{Mes}Nacnac)MgI(OEt$_2$)] (31.3 mg, 43.7 μmol, 1.0 eq.). Following 2 h of agitation, minimal colour change from the initial yellow solution was identified. ^{1}H NMR spectroscopy identified an indiscernible mixture of products including three [^{Mes}Nacnac] and four [DAS]$^{2-}$ containing species could be identified. Following standing for 48 h at ambient temperature, the mother liquor was decanted and the crystalline material identified as [{MgI(^{Mes}Nacnac)}$_2$] via X-ray diffraction. Extraction with hexane afforded further impurities including further crops of [{MgI(^{Mes}Nacnac)}$_2$]. Removal of volatiles and recrystallisation from benzene afforded a single crystalline example of target [(^{Mes}Nacnac)Mg-Al(DAS)] **4-VIII** which was of only sufficient quality to determine connectivity. **NB:** Variations of synthetic conditions and variation of solvent afforded crystalline material of [{MgI(^{Mes}Nacnac)}$_2$] indicative of reaction progression. A subsequent inquiry and crystallisation from a saturated hexane solution afforded a single SCXRD sample of magnesium aluminium activation species **4-IX**, which could not be reproduced.

Synthesis of [K(18-crown-6)][Al(DAS)] (4-X), and isolation of activation (4-XI) and degradation (4-XII) species

To a J. Young's NMR tube containing a deuterated benzene (0.5 mL) solution of [Al(DAS)I] **2-XXXIII** (32 mg, 46.6 μmol, 1.0 eq.), was charged potassium graphite (64 mg, 474 μmol, 10.2 eq.). Following 1.5 h of agitation, ^{1}H NMR spectroscopy identified the majority formation of [K{Al(DAS)}] **4-II** (85%) with side product K[Al(DAS)I$_2$] **2-XXXI** (15%). Within the glovebox, the

dark brown-red solution was charged with 18-crown-6 (11.8 mg, 46.6 μmol, 1.05 eq.) and then sonicated for 10 min. ^{1}H NMR spectroscopy identified the conversion to the targeted species [K(18-crown-6)][Al(DAS)] **4-X** (83%). **N.B.** Following 16 h at ambient temperature, decomposition of the targeted species was observed via ^{1}H NMR spectroscopy. Crystallisation attempts yielded a mixture of co-crystallised species of quality sufficient for connectivity. Grown from a concentrated solution of diethyl ether (*ca*. 0.1 mL) and benzene (*ca*. 0.1 mL), these including the targeted [K(18-crown-6)][Al(DAS)] **4-X** and K[Al(DAS)(H)(NHDipp)] **4-XI**. An attempted crystallisation from a concentrated solution of benzene yielded crystals of SCXRD quality identified as penta-alkali metal complex **4-XII**, however, this result could not be replicated.

Characterisation data for **4-X**: **^{1}H NMR** (400 MHz, C_6D_6, 298 K): δ = 7.30 (d, $^{3}J_{HH}$ = 7.5 Hz, 4H, Ph-*o*-C*H*), 7.16 – 7.13 (m, 6H, Dipp-aryl-C*H,* 4H, Ph-aryl-C*H*), 7.04 (t, $^{3}J_{HH}$ = 7.5 Hz, 2H, Ph-*p*-C*H*), 4.56 (sept, $^{3}J_{HH}$ = 6.8 Hz, 4H, Dipp-C*H*(CH_3)$_2$), 2.90 (s, 24H, 18-crown-6 C*H*$_2$), 1.36 (br, 24H, Dipp-CH(C*H*$_3$)$_2$). **^{13}C{^{1}H} NMR** (101 MHz, C_6D_6, 298 K): δ = 148.7 (Dipp-*i*-*C*), 145.2 (Dipp-*o*-*C*), 144.0 (Ph-*o*-*C*), 135.8 (Ph-*i*-*C*), 127.8 (Ph-*p*-*C*), 126.9 (Ph-*m*-*C*), 122.7 (Dipp-*m*-*C*), 119.4 (Dipp-*p*-*C*), 69.8 (18-crown-6 *C*H$_2$), 28.4 (Dipp-CH(*C*H$_3$)$_2$), 25.9 (Dipp-*C*H(CH$_3$)$_2$).

Attempted synthesis of [K(crypt-222)][Al(DAS)] (4-XIII)

To a J. Young's NMR tube containing a deuterated benzene (0.5 mL) solution of [K{Al(DAS)}] **4-II** (21.8 mg, 36.4 μmol, 1.0 eq.), was charged 222-cryptand (12 mg, 32.8 μmol, 0.9 eq.). The burnt-orange solution immediately identified a colour change to near colourless. ^{1}H NMR spectroscopic analysis was immediately completed. This afforded a broad ^{1}H NMR spectrum with a major new product (>80%), treatment of [K{Al(DAS)}] **4-II** with sequestering reagent formation of [K(crypt-222)][Al(DAS)] **4-XIII** species was postulated, however, could not be confirmed via X-Ray crystallography. **NB:** Attempts to isolate target species **4-XIII** by crystallisation were unsuccessful. Following the standing of benzene solution at ambient temperature for 24 h identified the degradation of species to multiple indiscernible species.

Characterisation data for [K(crypt-222)][Al(DAS)] (**4-XIII**):

^{1}H NMR (400 MHz, C_6D_6, 298 K): δ = 7.85 (br, 2H, Ph-*o*-C*H*), 7.35 (d, $^{3}J_{HH}$ = 7.2 Hz, 2H, Ph-*o*-C*H*), 7.14 – 7.02 (br, 6H, Dipp-aryl-C*H,* 6H, Ph-aryl-C*H*), 4.72 (br, 4H, Dipp-C*H*(CH_3)$_2$), 3.01 (s, 12H, OC*H*$_2$crypt.), 2.93 (br, 12H, NCH$_2$C*H*$_2$crypt.), 1.95 (br, 12H, NC*H*2-crypt.), 1.71 (br, 3H, Dipp-CH(C*H*$_3$)$_2$), 1.48 – 1.42 (br, 12H, Dipp-CH(C*H*$_3$)$_2$), 1.28 – 1.12 (br, 9H, Dipp-CH(C*H*$_3$)$_2$).

4.6. References

[1] S. Kurumada, S. Takamori, M. Yamashita, *Nature Chem.* **2020**, *12*, 36-39.
[2] K. Koshino, R. Kinjo, *J. Am. Chem. Soc.* **2020**, *142*, 9057-9062.
[3] C. Yan, R. Kinjo, *Angew. Chem. Int. Ed. Engl.* **2022**, *61*, e202211800.
[4] J. Hicks, P. Vasko, J. M. Goicoechea, S. Aldridge, *Angew. Chem. Int. Ed. Engl.* **2021**, *60*, 1702-1713.
[5] a) S. Grams, J. Eyselein, J. Langer, C. Färber, S. Harder, *Angew. Chem. Int. Ed. Engl.* **2020**, *132*, 16116-16120; b) R. J. Schwamm, M. D. Anker, M. Lein, M. P. Coles, *Angew. Chem. Int. Ed. Engl.* **2019**, *58*, 1489-1493; c) R. J. Schwamm, M. P. Coles, M. S. Hill, M. F. Mahon, C. L. McMullin, N. A. Rajabi, A. S. S. Wilson, *Angew. Chem. Int. Ed. Engl.* **2020**, *59*, 3928-3932.
[6] M. P. Coles, M. J. Evans, *Chem. Commun.* **2023**, *59*, 503-519.
[7] M. Asay, C. Jones, M. Driess, *Chem. Rev.* **2011**, *111*, 354-396.
[8] C. Jones, S. Aldridge, T. Gans-Eichler, A. Stasch, *Dalton Trans.* **2006**, 5357-5361.
[9] D. Sarkar, P. Vasko, A. F. Roper, A. E. Crumpton, M. M. D. Roy, L. P. Griffin, C. Bogle, S. Aldridge, *J. Am. Chem. Soc.* **2024**, *146*, 11792-11800.
[10] B. Wang, *Coord. Chem. Rev.* **2006**, *250*, 242-258.
[11] A. Lüttringhaus, W. Kullick, *Angew. Chem.* **1958**, *70*, 438-438.
[12] J. Hicks, P. Vasko, J. M. Goicoechea, S. Aldridge, *Nature* **2018**, *557*, 92-95.
[13] R. J. Schwamm, M. S. Hill, H.-Y. Liu, M. F. Mahon, C. L. McMullin, N. A. Rajabi, *Chem. Eur. J.* **2021**, *27*, 14971-14980.
[14] a) S. P. Green, C. Jones, A. Stasch, *Science* **2007**, *318*, 1754-1757; b) C. Jones, *Nat. Rev. Chem.* **2017**, *1*, 0059.
[15] M. M. D. Roy, J. Hicks, P. Vasko, A. Heilmann, A. M. Baston, J. M. Goicoechea, S. Aldridge, *Angew. Chem. Int. Ed. Engl.* **2021**, *60*, 22301-22306.
[16] S. J. Bonyhady, C. Jones, S. Nembenna, A. Stasch, A. J. Edwards, G. J. McIntyre, *Chem. Eur. J.* **2010**, *16*, 938-955.
[17] R. A. Jackson, A. J. R. Matthews, P. Vasko, M. F. Mahon, J. Hicks, D. J. Liptrot, *Chem. Commun.* **2023**, *59*, 5277-5280.
[18] A. Heilmann, J. Hicks, P. Vasko, J. M. Goicoechea, S. Aldridge, *Angew. Chem. Int. Ed. Engl.* **2020**, *59*, 4897-4901.
[19] M. J. Evans, M. D. Anker, M. P. Coles, *Inorg. Chem.* **2021**, *60*, 4772-4778.
[20] J. Hicks, P. Vasko, J. M. Goicoechea, S. Aldridge, *J. Am. Chem. Soc.* **2019**, *141*, 11000-11003.
[21] J. Hicks, M. Juckel, A. Paparo, D. Dange, C. Jones, *Organometallics* **2018**, *37*, 4810-4813.
[22] J. A. Gladysz, G. M. Williams, W. Tam, D. L. Johnson, D. W. Parker, J. C. Selover, *Inorg. Chem.* **1979**, *18*, 553-558.

5. Developments of Group 13 Metalloles

5.1. Introduction

5.1.1. Hückel Antiaromatic Metalloles and their Initial Reports

Developed from the 1960's,[1] the concept of antiaromaticity further expanded upon Hückel's original calculations describing thermodynamic stability within cyclic hydrocarbons.[2] As described by Hückel, *aromaticity* entails the extra thermodynamic stability afforded within planar cyclic π-conjugated hydrocarbon systems containing $4n + 2$ π-electrons, comparative to analogous localised resonance structures.[2-3] Comparably, *antiaromaticity* relates to closed-shell cyclic planar conjugated species with $4n$ π-electrons, whereby species feature elevated reactivity and instability from the distinct destabilisation of the cyclic π-delocalisation.[1, 4] Antiaromatic compounds, initially based upon energetic, geometric and magnetic criteria set by the model ground-state triplet cyclopentadienyl cation ($C_5H_5^+$) **5.1**, have since been expanded to encompass π-conjugated systems featuring main group heteroatoms and transition metal centres.[5] Electronic analogues, heterocyclic group 13 element-based parent borole **5.2** and alumole **5.3** species have been the target of fundamental investigations (Figure 5.1).

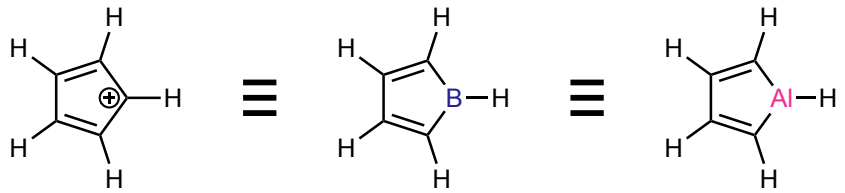

*Figure 5.1: Valence isoelectronic antiaromatic species cyclopentadienyl cation **5.1**, and parent metalloles 1H-borole **5.2** and 1H-alumole **5.3**.*

Boroles (boracyclopentadienes) and their lesser developed alumoles (aluminacyclopentadiene) congeners, are members of the class metalloles featuring a 5-membered heterocycle and an electron-deficient, commonly tricoordinate group 13 centre.[3] Aligning with IUPAC nomenclature, the parent metallole (HEC_4H_4) is defined as a 1*H*-borole **5.2** (E = B) or 1*H*-alumole **5.3** (E = Al).[3] These terms are highlighted within this work whereby "free" metallole define tricoordinate E species derivatives of the general formula [R′EC_4R_4] (R′ = substituent at the group 13 centre, R = ring backbone substituents). Notably, within the preparation of alumoles, Lewis-base stabilisation is prevalent lending to the isolation of tetracoordinate E species aligning [LR′EC_4R_4] (L = Lewis base).

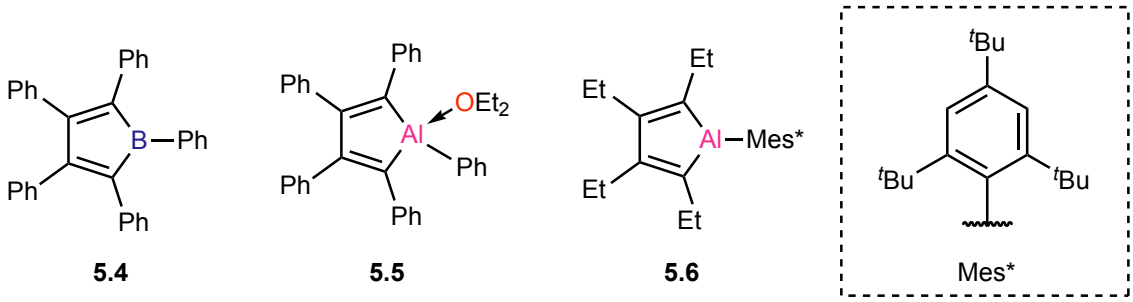

Figure 5.2: Initial reports of selected metallole species from the groups of Eisch ***5.4****,*[6] *Hoberg and Krüger* ***5.5****,*[7] *and Tokitoh* ***5.6****.*[8]

Indicative of antiaromaticity within their "free" arrangement, metalloles have served as fundamental group 13 comprehensions since the initial report of a "free" borole **5.4** in 1969 from the group of Eisch (Figure 5.2),[6] and postulation of "parent" alumole **5.3** in 1962 (Figure 5.1).[9] Expanding literature comprehensions, the first crystallographically characterised alumole was the Lewis base stabilised alumole [(Et_2O)PhAlC_4Ph_4] **5.5** in 1977 (Figure 5.2),[7] and the first report of a "free" alumole system was **5.6**, reported by Tokitoh in 2013.[8]

5.1.2. Boroles: A Structural Overview

The antiaromatic parent borole **5.2** presents a highly reactive heterocycle, the isolation of which consequently remains elusive. Since the synthesis of pentaphenylborole [PhBC_4Ph_4] **5.4** by Eisch and Kaska in 1969 as a deep-blue solid (Figure 5.2),[6] extensive studies relating to the borole [R′EC_4R_4] scaffold have been reported.

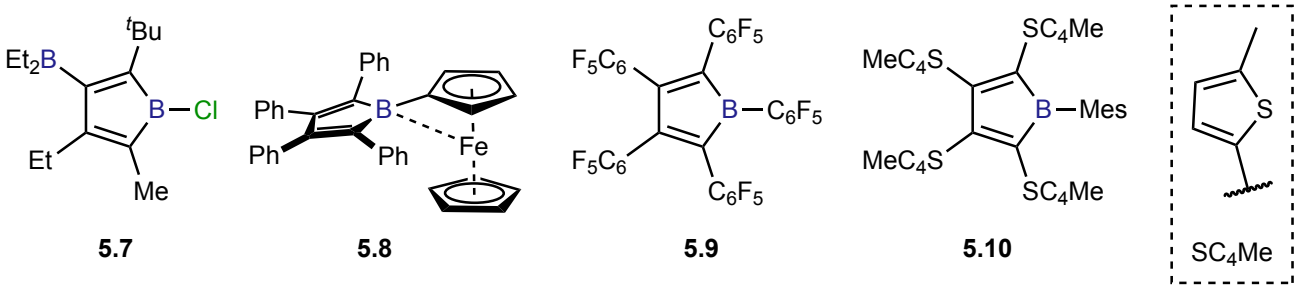

Figure 5.3: Selected examples of borole species featuring variation of boron and backbone-bound substituents.

Following reports of pentaaryl borole systems, further developments have been sought to include variations upon the boron-based (R′) and backbone (R) substituents and combinations thereof (Figure 5.3). In 1978, Killian and Wrackmeyer reported the first example of a free borole [ClBC_4(BEt_2)(ᵗBu)(Et)(Me)] **5.7** (Figure 5.3).[10] This system also featured the first example of a monomeric haloborole featuring a terminal chloride substituent upon the boron centre. Furthermore,

5.7 featured the inclusion of alkyl (Me, Et, ^{t}Bu) and heteroatom (BEt_2) substituents about the C_4 backbone and dissolved to give a deep-red colour. Since the report of **5.7**, haloborole species have served as valuable reagents capable of furnishing further boroles via halide substitution.

Despite fundamental developments involving boroles up until the 1990's, inquiries into these species were on hiatus until 2008.[3] Modern theoretical studies by Braunschweig, Frenking and coworkers have promoted a resurgence in this field.[11] Further expanding the substituents upon the boron centre, Braunschweig and coworkers reported the ferrocenylborole **5.8** in 2008, which was isolated as a deep-red solid.[11] The Lewis acidity presented by the borole centre is noticable within the solid-state structure via a strong Fe-B interaction, given the closeness of arranged boron to the iron centre and the dip of the borole derivative. Highlighted through UV/Vis spectroscopy and X-ray crystallography, this interaction also results in the less pronounced antiaromatic character of the borole derivative due to the interruption of π-conjugation.

In 2009, the groups of Piers and Tilley reported the isolation of the perfluoropentaphenylborole **5.9** (Figure 5.3) featuring modification with highly electron-withdrawing groups.[12] This species was the fully fluorinated analogue of the pentaphenylborole **5.4**. Upon isolation, the 4π-electron, antiaromatic **5.9** was isolated as a purple solid. Notably, the highly Lewis acidic nature of the planar species has been since highlighted through Diels-Alder cycloaddition and electrophilic attack reactivity modes.[13]

Conversely, the group of Yamaguchi in 2012 reported the preparation of a highly electron donating borole system **5.10** (Figure 5.3).[14] Furnished with thienyl substitution about the C_4 ligand scaffold, these moieties serve to heighten the electron-donating character of the borole ring. This results in the narrowing of the HOMO–LUMO gap and the onset of a new bright-green colour. Notably, this species is the first heteroaryl-substituted borole derivative featuring the inclusion of a mesityl (Mes, = 2,4,6-trimethylphenyl) group upon the boron centre.

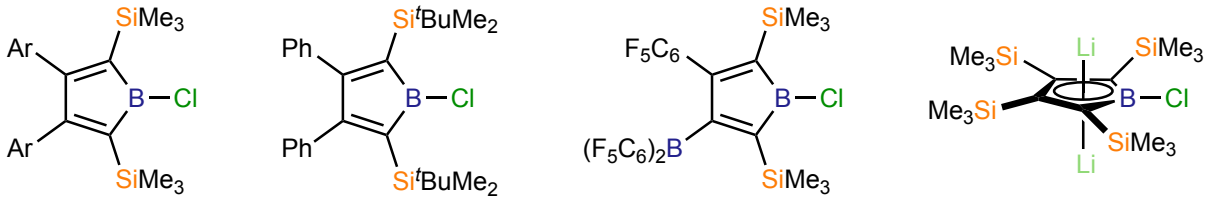

5.11 Ar = Ph*
5.12 Ar = *m*Xyl

5.13

5.14

5.15

Figure 5.4: Selected library of 2,5-disilyl-borole species including varied boron and backbone substituents. (Ph = 3,5-^{t}Bu$_2$(C$_6$H$_3$),* m*Xyl = 3,5-Me$_2$(C$_6$H$_3$).*

Relevant to this Chapter, the report of highly versatile 2,5-disilyl chloroborole systems (**5.11** and **5.12**) has been exemplified by the Sindlinger group (Figure 5.4).[15] These 1-chloro-2,5-(SiMe$_3$)$_2$-3,4-(Ar)$_2$-borole species feature a combination of bulky arene (Ar = Ph* **5.11**,[16] *m*Xyl **5.12**[17]) and trimethylsilyl groups about the C$_4$ scaffold, and form bright red/orange species upon isolation. Notably, these 2,5-bis-trialkylsilyl-substituted boroles were developed following the reports from the groups of Saito **5.13**,[18] and Erker **5.14**,[19] as well as the borole motif identified in the work of Sekiguchi and Lee **5.15** (Figure 5.3).[20]

5.1.3. Boroles: Synthesis

As a consequence of various electronic and steric environments present within boroles, a variety of methods are applied to afford these highly reactive and antiaromatic species. Notably, the most commonly preparations have involved two common synthetic processes; i) transmetalation with templated metals, and ii) direct salt metathesis with alkali metal salts and halogenated reagents.[3]

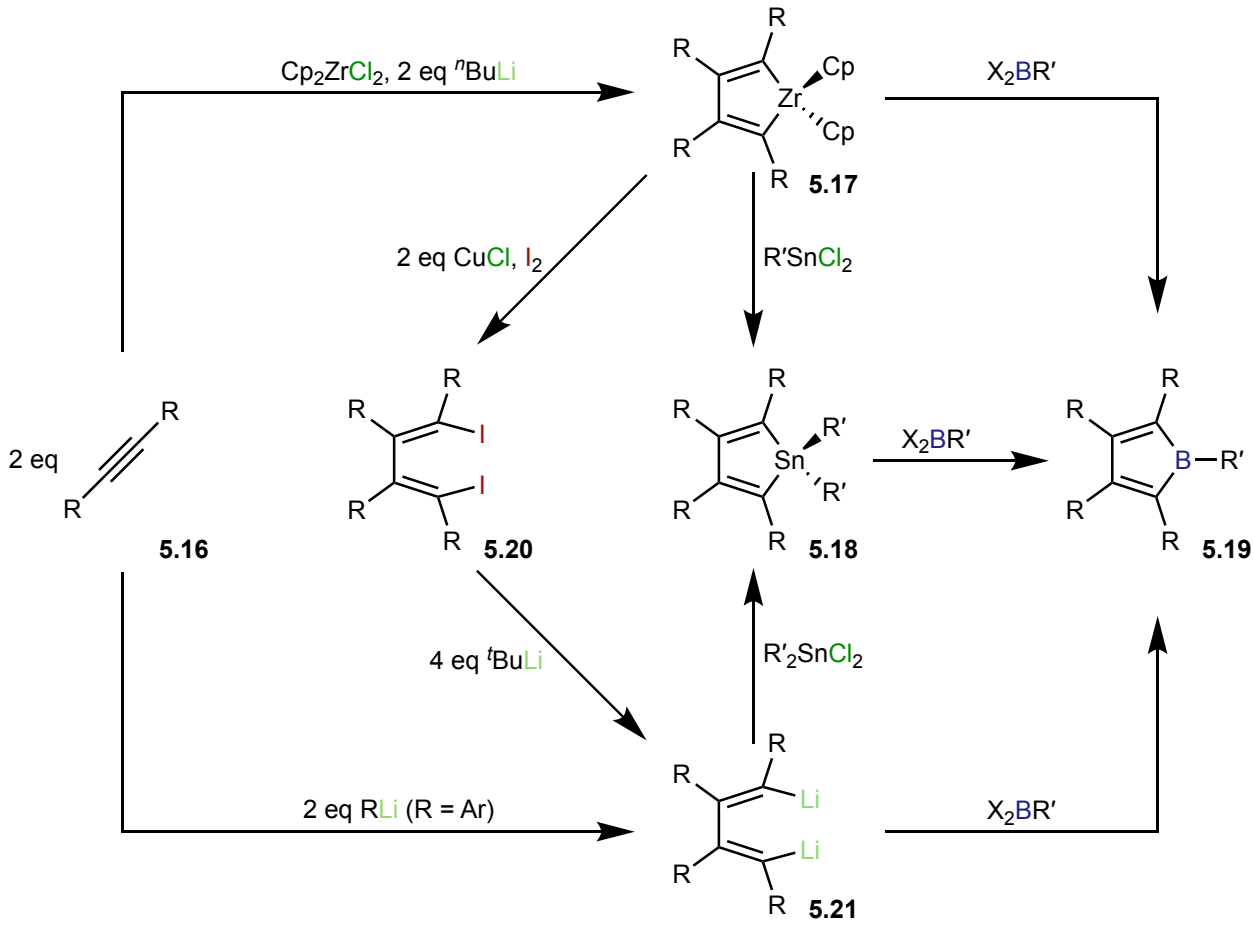

*Scheme 5.1: Selected synthetic methodologies affording substituted borole species **5.19**.*

Commonly, substituted alkyne reagents **5.16** serve as valuable starting materials in the preparation of boroles, via the two main routes shown in Scheme 5.1. As sources of steric complexity, alkyne species are commercially available or accessible via Sonogashira cross-coupling reactions.[21] Being readily prepared from other metalloles, routes have been sought in the preparation of varied transmetalation reagents.[22] Consequently, the preparation of heterocyclic zirconium templated species **5.17** from *in-situ* generated zirconium-based Negishi,[23] or Rosenthal reagents,[12a, 24] have been established as viable transmetalating reagents in preparations yielding the related stannole **5.18**, other group 14 metalloles,[25] and eventually borole species via Sn/B exchange (Scheme 5.1).[3] Importantly, the inclusion of silyl groups at the 2,5-positions within ligand scaffolds is reported to interfere with the propensity for stannole **5.18** to undergo reactivity with dihalogenated boranes to afford the related borole derivatives **5.19**.[16, 26] As a result, other preparative methods for 2,5-silyl substituted species are employed.

The cyclised zirconium templated species **5.17** may also undergo iodination in the presence of copper(I) chloride, affording the corresponding diiodobutadiene species **5.20**.[27] In the subsequent treatment of **5.20** with organolithium reagents, the analogous dilithiobutadiene species **5.21** may be

isolated. Preparations of boroles via iodination and lithiation routes are commonly related to the relevant 2,5-silyl species, as the synthesis of dilithiobutadiene **5.21** species are accessible via direct lithiation routes of symmetric aryl-substituted alkynes **5.17**.[3, 28] Notably, lithiation routes were also described in the conventional preparation of the seminal pentaphenylborole **5.4** via reductive coupling of diphenylacetylene.[3, 6]

When treated with dihalogenated boranes [X_2BR'], targeted borole species of varying ligand frameworks are accessible from zirconium-based templated species **5.17**,[23, 29] stannole transmetalating reagents **5.18**,[6, 30] and dilithiobutadiene **5.21** species (Scheme 5.1).[6, 16, 31] Notably, the synthetic routes applied in the preparation of borole species **5.19** are also applicable and synonymous with those applied in the preparation of other metalloles, such as alumoles.[3, 26]

5.1.4. Boroles: Reactivity

Due to small HOMO-LUMO energy gaps, boroles are highly reactive and versatile reagents in various chemical applications.[3] Representatively, the highest occupied molecular orbital (HOMO) of the parent borole system is relatively high in energy, whilst the lowest unoccupied molecular orbital (LUMO) is comparatively low-lying. The antiaromatic nature of boroles is manifest by pronounced electrophilicity at the boron centre, consequentially allowing the formation of Lewis acid-base adducts.[32] Further transformations can be attributed to the impacts of the included C_4 scaffold. Boroles and their activated carbon backbone may participate within cycloadditions and Diels-Alder chemistry with unsubstituted substrates, and present a propensity for redox chemistry in the preparation of five and six π-electron species.[3]

5.1.4.1. Reactivity: Lewis Acid-Base Adduct Formation

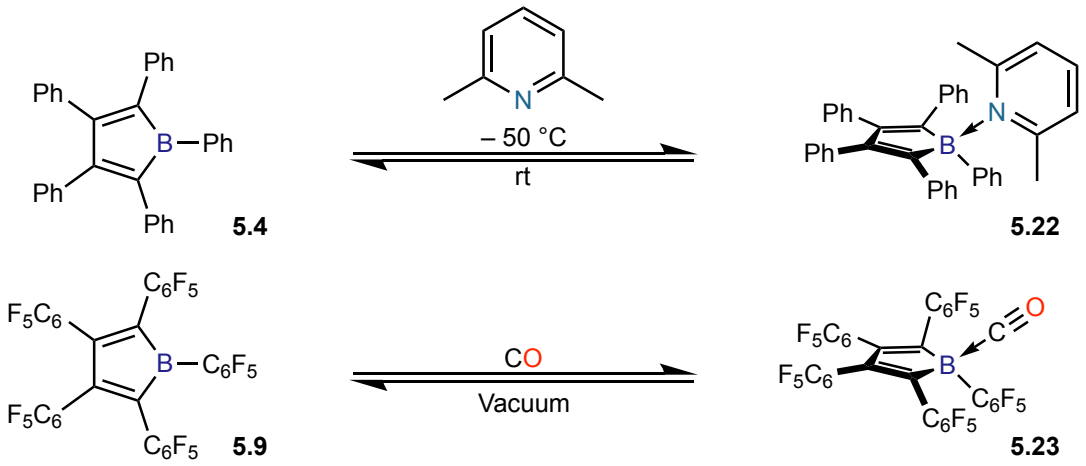

*Scheme 5.2: Selected examples of Lewis base-adduct formation from borole species **5.4** and **5.9**.*

Highlighted in the seminal report of pentaphenylborole **5.4**,[6] the pronounced Lewis acidity at boron enables preparation of numerous base-stabilised borole compounds.[32] In coordinating a Lewis base, the donation of two electrons leads to pyramidalization of the boron centre, alleviating the destabilising overlap of valence π-orbitals and ring strain within the initially planar 5-membered ring (Scheme 5.2).[3] Borole adducts are known with ethers,[33] nitrogen bases,[34] phosphines,[33] carbon monoxide,[35] and carbenes.[33, 34b]

Indicative of complexation, apparent colour changes are identified following the treatment of boroles with Lewis bases, however, adduct formation can be impacted by both temperature and the nature of the substituents about the boroles. Consequently, as presented with the relationship of "free" **5.4** and the pyridine "adduct" **5.22**, the variation of temperature shifts the equilibrium between these species, leading to the observed thermochromic change from blue to yellow, respectively.[34a] Moreover, the CO adduct of **5.4** is reported as isolable only at low temperatures. However, when employing the purple perfluorinated species **5.9**, the corresponding colourless CO adduct **5.23** was isolated as a crystalline solid at ambient temperatures.[35] Identified through the ongoing synthesis of various base-stabilised borole compounds, the prymaidalisation at boron centre is indicative of the strength of the Lewis acid-base interaction.

5.1.4.2. Reactivity: Diels-Alder Reactivity and Cycloadditions

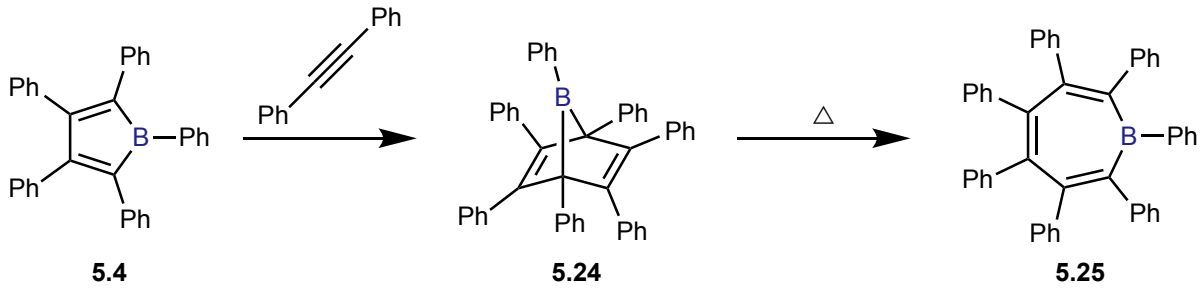

*Scheme 5.3: [4+2] cycloaddition reaction of pentaphenylborole 5.4 to afford a strained bicyclic Diels-Alder adduct **5.24**, and subsequent thermal rearrangement to heptaphenylborepine **5.25**.*[3]

Eisch and Kaska's pentaphenylborole **5.4**, shows the propensity for the novel system to undergo [4+2] cycloaddition self-dimerisation (Scheme 5.3).[6] Capitalising upon the high energy HOMO and low energy LUMO, exposure of **5.4** to diphenylacetylene afforded the strained bicyclic Diels-Alder adduct **5.24**. This bicyclic adduct has since been shown to perform a thermal rearrangement to afford the ring-expanded species heptaphenylborepine **5.25**.[3] Consequently, the reactivity presented identified the conversion of antiaromatic **5.4**, to a down-stream aromatic product **5.25** in the form of a 6 π-electron heterocycle.[3]

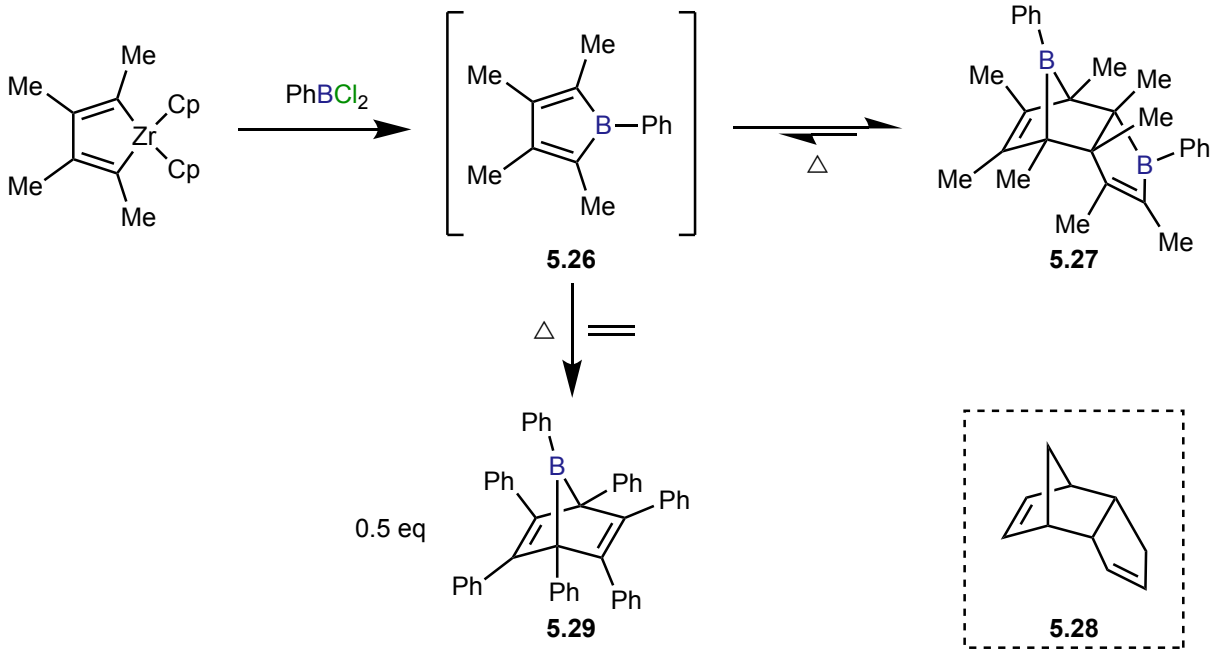

*Scheme 5.4: Seminal report of Diels-Alder cycloaddition products **5.27** and **5.29** as performed by in-situ borole species **5.26**. Related cyclopentadiene dimerisation product **5.28**.*

Representative of traditional Diels-Alder reactivity, borole-promoted cycloadditions can be undertaken with "unactivated" alkenes (Scheme 5.4). Initially and most notably, preparations targeting the isolation of less sterically encumbered (comparative to **5.4**) species [$PhBC_4Me_4$] **5.26** by Fagan and coworkers in 1988 afforded the self-addition dimer product **5.27** (Scheme 5.4), attributed to the insufficient steric shielding about the C_4 scaffold.[36] This product was indicative of an endo addition resultant from interaction of the electron-deficient boron centre in **5.26** with a C=C double bond, is reminiscent of the Diels–Alder dimerization of cyclopentadiene **5.28**.[3] Subsequent investigations highlighted the possibility for **5.27** to undergo thermally promoted retro-Diels-Alder reaction to afford the *in-situ* preparation of borole **5.26**. Elevated temperature investigations with **5.27** as a source of monomeric **5.26** were conducted in the presence of unactivated alkenes, a catalogue of expected consequential bicyclic Diels-Alder adducts could be afforded, including with poor dienophiles, such as ethylene (**5.29**), in high yields.

From reports, the role of frontier orbitals involved in cycloaddition reactions borole (diene) and reactive substrates (dienophile, alkene, alkyne) has been explored. Consequently, in manipulating the steric and electronic effects of various borole species, the respective orbital HOMO/LUMO pair energies have yielded a variety of reagent substitution patterns.

5.1.4.3. Reactivity: Bond Activation Chemistry

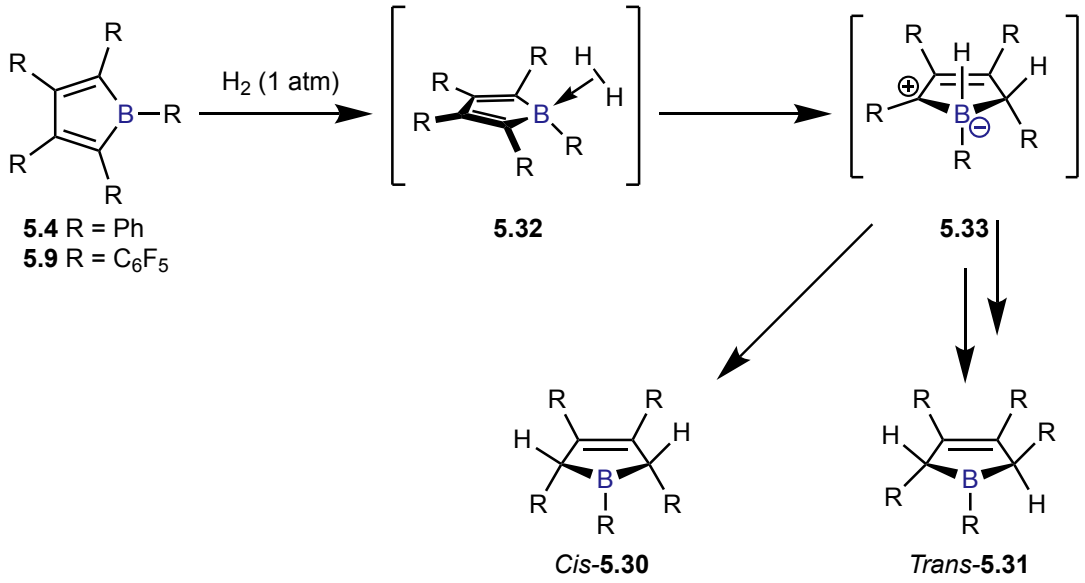

*Scheme 5.5: Seminal report of metal-free H_2 activation by **5.4** and **5.9** from Piers and coworkers in 2010.*[37]

The potential for transition metal metallomimetics has motivated explorations of boroles for the activation of small molecules and traditionally inert substrates.[38] Aligning with the emergence of new fields of research, developments of "frustrated Lewis pairs" (FLP's) are notable.[39] Within this field, cooperative interactions of bulky Lewis acids with sterically encumbered Lewis bases are reported to activate a library of small molecules.[40] The "frustration" within species terminology refers the steric hinderance induced inability of species to form stable Lewis acid–base adducts.

Inspired by FLP reports with the strong electrophilicity of antiaromatic boroles hypothesised to present comparable reactivity, Piers and coworkers published the metal-free activation of H_2 with **5.4** and **5.9** in 2010.[37] Of key focus with **5.9**, the exceptionally high Lewis acid strength of this complex led to its rapid reaction with stoichiometric molecular hydrogen under atmospheric pressure and ambient temperature to afford the 3-borolene dihydro derivatives as a mixture of isomers, *cis*-**5.30** and trans-**5.31** (Scheme 5.5).[37] Ascertaining proposed mechanisms, studies including kinetic experiments have highlighted the initial adduct formation with H_2 (**5.32**) and subsequent heterolytic addition across the endocyclic B–C bond affording the zwitterionic intermediate with anionic borate and positively charged carbocationic centres **5.33**.[3] The intermediate could then undergo a 1,2-hydride shift, or a thermodynamically preferable ring-open and -closing process to afford the *cis*-**5.30** and trans-**5.31** isomers, respectively (Scheme 5.5).[41] Notably, a similar mechanism is attributed to the analogous reactivity of **5.4** toward H_2 is postulated,[37] suggesting the growing potential for the application of boroles in activating substrates featuring non-polar bonds.

5.1.5. Borole Reduction and Derivatisation

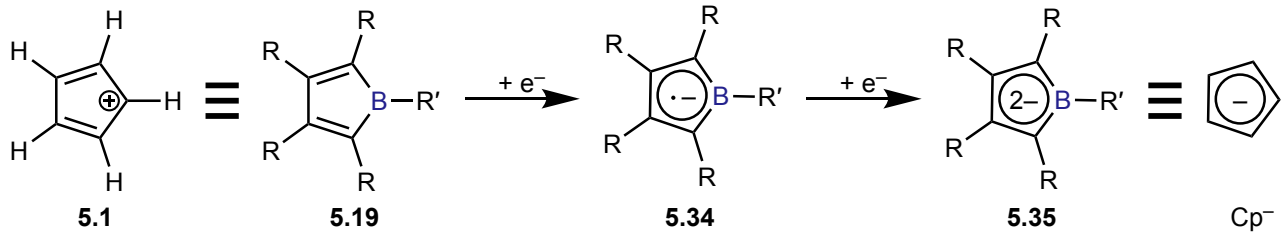

Scheme 5.6: Sequential reduction of boroles and their isoelectronic organic analogues.[3]

Accessible via the low-lying LUMO of systems centred at the empty *p*-orbital of the boron centre in **5.19**, the addition of one- and two-electrons have been reported to afford the reduced borole radical anion **5.34**, and boroledиide dianion **3.35**, respectively (Scheme 5.6).[32] Initially spurred through investigations implementing borole **5.4** as a pentahapto η^5–ligand to late transition metals species could be viewed as 6π-electronic systems electronically analogous to the cyclopentadienyl anion (Cp^-) (Scheme 5.6).

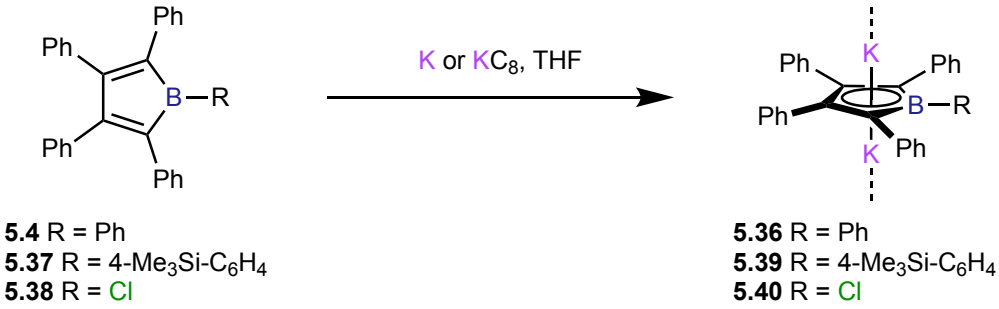

Scheme 5.7: Synthesis of dianionic potassium boroledиides reported by Herberich ***5.36****,*[42] *Yamaguchi* ***5.39****,*[43] *and Braunschweig* ***5.40****.*[44]

Reported first in the 1980's by Herberich and coworkers, the potassium boroledиide **5.36** species was isolated as a red solid (Scheme 5.7).[42] At the time, characterisation of this species was achieved by elemental analysis and its reactivity with metal halides to generate η^5-borole complexes. Notably, the solid-state structure of **5.36** was not reported until 2008 by Yamaguchi and coworkers, which confirmed the 6π-electron species.[43] This boroledиide system featured a planar BC_4 ring with potassium counterions above and below the plane, with η^5-interactions with the ring and neighbouring molecules. Further expansions developed efficient syntheses for the selective 2-electron reduction of boroles [(4-Me_3Si-C_6H_4)BC_4Ph_4] **5.37** and [$ClBC_4Ph_4$] **5.38**, to their respective boroledиides **5.39** and **5.40** following treatment with potassium metal or potassium graphite (Scheme 5.7). Interestingly, the synthesis of **5.40** involved the reduction of the chloroborole 4π-electron system, rather than cleavage of B–Cl bond, contrasting attempts with haloboranes previously yielding mixtures of reduced products

from unspecified radical-type reactions.[45] The targeted boroledиide species **5.36**, **5.39**, **5.40** all were reported as red solids that were extremely air- and moisture-sensitive.[42-44] Identified experimentally, these borole dianion species remain highly reactive despite increased stability afforded by imparted aromaticity; rather, the electrostatic repulsion of negative charges in the five-membered ring affords a strikingly reactive class of main group species.[3] Subsequent reports have included the complexation of boroledиide species as ligands to a range of main group metals including *p*-block elements,[46] however, these examples are outside the scope of this Thesis.

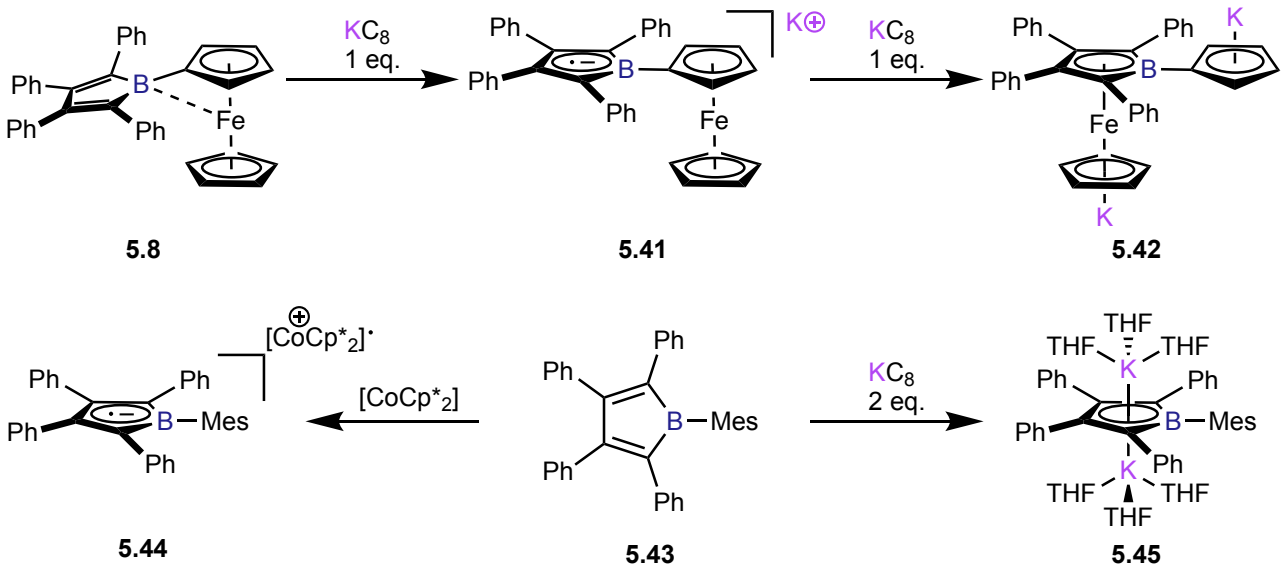

Scheme 5.8: Selected synthesis affording dianionic boroledиide and monoanionic borole radical complexes.

Despite a prior report of 2-electron reduced boroledиide species, the related monoanionic 1-electron reduced species served a notably important intermediate in dianionic species synthesis. To date, inquiries into neutral borole species indicated the possibility for the formation of monoradical anion species constituting 5π-electrons.[3, 47] Electronically, this would align with the neutral cyclopentadienyl radical. Reinforced through cyclic voltammogram investigations, the first reduction event of the investigated borolylferrocene derivative [$FcBC_4Ph_4$] **5.8** (Fc = σ-5-C_5H_4FeCp) was attributed to a 1-electron reduction and corresponding radical formation **5.41** (Scheme 5.8).[48] Further synthetic investigations characterised the postulated paramagnetic species **5.41** via EPR spectroscopy, following the *in-situ* reduction of **5.8** with potassium graphite (Scheme 5.8).[48] The EPR spectrum presented characteristics indicative of an unpaired electron coupling to ^{11}B (I = 3/2), identifiable via four equally spaced hyperfine lines (isotropic g value = 2.0037). Moreover, hyperfine values of $A(^{11}B)$ = 3.73 G aligned with expectations of the delocalisation of spin density about the 5-membered ring with a planar boron substituent. Notably, attempts to isolate and characterise **5.41** crystallographically

were unsuccessful due to the highly reactive nature of the species. A further 1-electron reduction to the dianion **5.42** was also possible following treatment with excess potassium graphite. Identifiable from crystallisations **5.42** features the intramolecular migration of the [CpFe] fragment to boron (Scheme 5.8).

In 2012, Braunschweig and coworkers described the preparation and 1-electron reduction of the 1-mesityltetraphenylborole [$MesBC_4Ph_4$] **5.43** (Scheme 5.8).[49] Markedly, the reduction of green-coloured **5.43** with decamethylcobaltocene [$CoCp^*_2$] afforded the formation of paramagnetic 5 π-electron species **5.44** as a red-brown solid, which was stable in the solid-state at ambient temperature. Following the isolation of crystalline material from the diffusion of hexane into a tetrahydrofuran solution of **5.44** at –30 °C, **5.44** was identified as the first crystallographically characterised borole radical anion.[49] From the solid-state structure, the borole framework was confirmed as cyclic, planar, and π-conjugated system hosting five electrons. In balancing the monoanionic charge of the borole framework, this species exists as a separated ion pair with the cationic decamethylcobaltocene radical $[CoCp^*_2]^+$. Similarly identified with **5.41**, EPR spectroscopy confirmed the presence of a radical in **5.44**, with four equally spaced hyperfine lines (isotropic g value = 2.0025). Furthermore, small hyperfine coupling constants of $A(^{11}B)$ = 3.43 G and $A(^{10}B)$ = 1.08 G was evident of anticipated unpaired electron spin delocalisation about the central role BC_4 ring.

As similarly identified with **5.8** and **5.42**,[48] treatment of neutral borole **5.43** with two equivalents of potassium graphite could afford the corresponding dianion species **5.45** (Scheme 5.8). However, rather than the intramolecular migration observed in **5.42**, boroledиide **5.45** presented η^5-interactions with the ring in arrangements, analogous to boroledиides **5.36**, **5.39** and **5.40**.

5.1.6. Boroles: An Outlook

Reports on a growing catalogue of boroles highlight these antiaromatic 4π electron species as being highly reactive. Variation of substituents corresponds to the manipulation of steric and electronic effects and the resulting diverse reactivity of these species is highlighted by the formation of Lewis acid-base adducts, cycloadditions, and activation of chemically-relevant feedstocks (including H_2). Redox applicability in boroles is highlighted through the introduced aromaticity in 6π electron dianion complexes via alkali metal reductions, and one-electron reductions having afforded the isolation of a new class of isolable π-conjugated boron radical species.

5.1.7. Alumoles: A Structural Overview

As a heavier element congener of the extensively explored boroles, alumoles are a relatively underexplored class of group 13 antiaromatic species. Notably, computational analyses have shown that the parent alumole **5.3** has decreased antiaromaticity relative to the parent borole **5.2**.[8] However, inherently high reactivity and instability of many alumoles made their study challenging.[50]

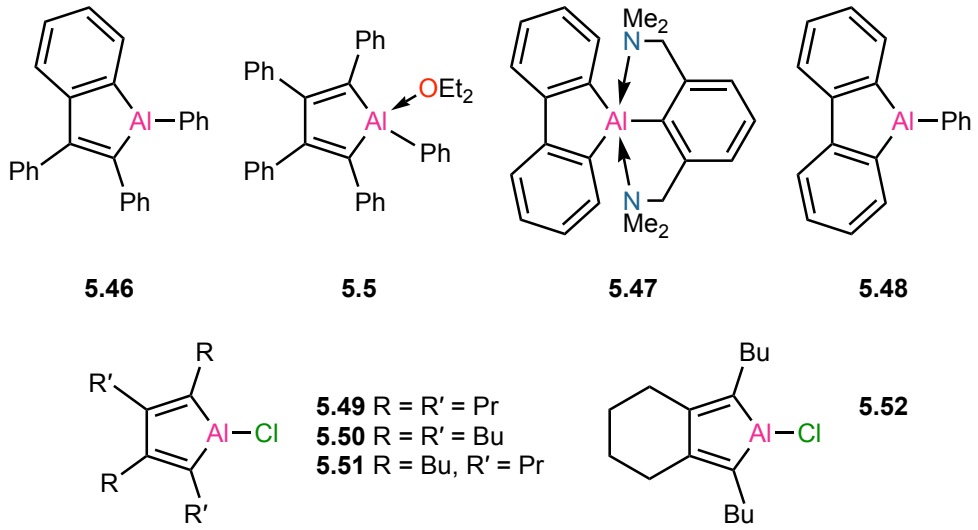

Figure 5.5: Selected isolated alumoles and related species, including 9-aluminafluorenes.

Varied structural classes are presented in the alumole literature with a variety of species based on their aluminium and C_4 scaffold substituents. Moreover, the foundational C_4 scaffold can serve a site of variation influencing species reactivities and isolation. Borole-inspired investigations heavily featured developments into initial pentaphenylalumole species and their related derivatives. However, rather than the synthesis of "free" alumole species, *in-situ* preparations and reports initially identified the benzo-fused C_4 scaffolds **5.46** in 1966 (Figure 5.5),[51] and the first crystallographically characterised Lewis base-stabilised alumole adduct **5.5** in 1977 (Figure 5.2).[7]

Similarly employing benzo-fused C_4 scaffolds, 9-aluminafluorenes have seen growing development since the class crystallographic authentication of **5.47** in 2015,[52] after the novel preparation of the base-free alumole **5.48** in 1962.[9] Despite the unique electronic effects employed in these aluminium analogues of boron-doped fluorenes, their relevancy falls outside the scope of this work.[53]

Expanding the applications of alumoles within organic synthesis saw the *in-situ* preparation of haloalumoles featuring aluminium-based chloride substituents **5.49-5.52** (Figure 5.5).[54] Notably, these species presented varied steric bulk (**5.49**, **5.50**), alternation of substituents (**5.51**), and the inclusion of 3,4-C centres within a greater cyclic group (**5.52**). Inquiries identified such alumoles as

valuable reagents in the preparation of the cyclopentadiene derivatives from various aldehydes, however, were not isolated nor crystallographically characterised.[54]

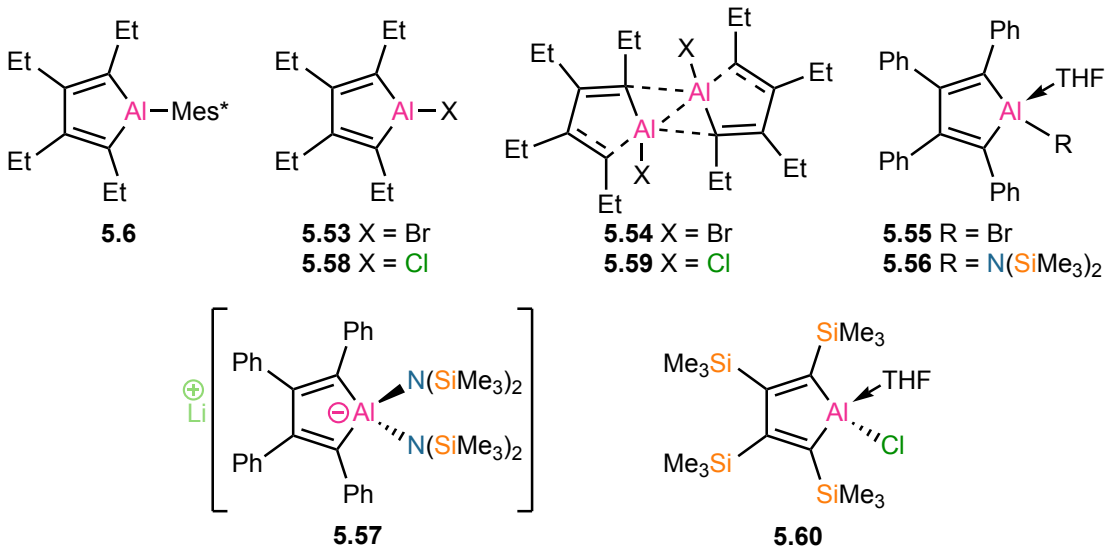

Figure 5.6: Selected alumole species including species with ethyl, phenyl, and silyl C_4 substitution patterns.

Spurred by the isolation of the first "free" alumole [Mes*AlC$_4$Et$_4$] **5.6** in 2013,[8] subsequent investigations have reported further analogues similarly employing the C$_4$Et$_4$ scaffold. Expanding methods affording **5.6**, Tokitoh and coworkers then reported the isolation of the bromoalumole **5.53** as a precursor for further functionalisation in 2014 (Figure 5.6).[55] However, due to the lack of steric encumberment about the aluminium centre, **5.53** existed as a dimer **5.54** in the solid-state. Consequently, the preparation of the tetrahydrofuran Lewis-base stabilised species **5.55** was accomplished by the treatment of **5.53** with the coordinating solvent. **5.53** was further applied as a precursor for the preparation of *N*-substituted aminoalumoles both as a Lewis acid-base adduct **5.56** and corresponding lithium aluminate complex **5.57**, which featured coordination of two N(SiMe$_3$)$_2$ moieties to an aluminium centre.[56]

Expanding the reported derivatives of haloalumoles, the C$_4$Et$_4$ scaffold was utilised by Tokitoh and coworkers to give the isolable chloride analogue **5.58** in 2016,[57] which was also identified to crystallise in a dimeric **5.59** fashion akin to the bromoalumole.[55] Moreover, a report from Sekiguchi, Lee and coworkers further extended chloroalumole examples to include the silyl-substituted system **5.60**, which could be crystallised as the tetrahydrofuran adduct.[58]

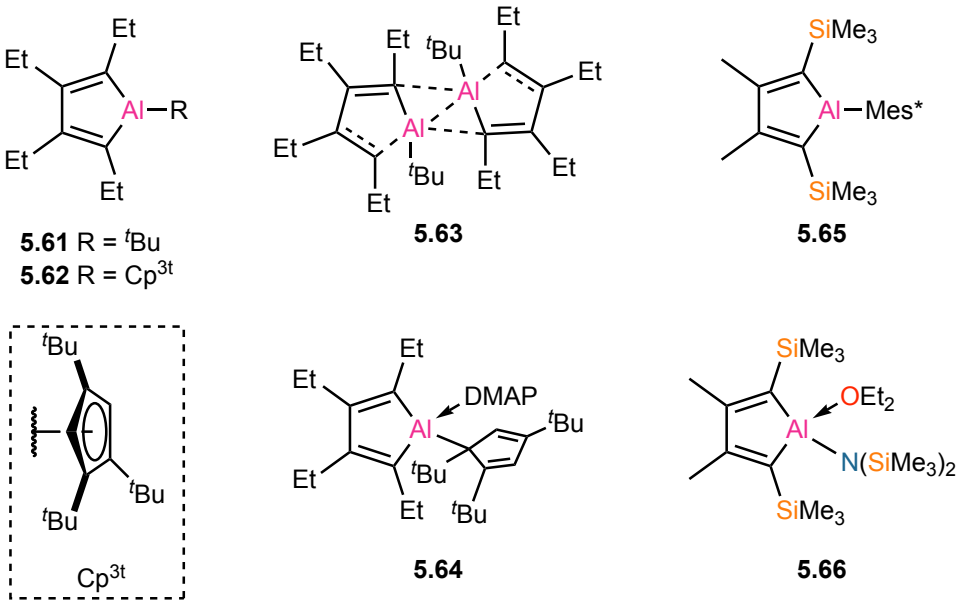

Figure 5.7: Selected library of isolated and pursued "free" alumoles, and Lewis acid-base adduct derivatives.

In the preparation of further "free" alumole examples, the C_4Et_4 scaffold has been applied in the preparation of both alkyl **5.61** and η^5-haptic **5.62** coordination at the aluminium centre (Figure 5.7).[50] Analogous to the bromoalumole species **5.54** reported by Tokitoh,[55] the solid-state structure of **5.63** is stabilized by the interactions of an endocyclic carbon of one alumole monomer to the Lewis acidic aluminium centre of the other. However, the monomeric form of **5.61** is preferential in solution at elevated temperatures. This monomer-dimer equilibrium contrasts with **5.62** (Figure 5.7), which does not form dimeric species. Whilst neither species may be isolated as adducts of tetrahydrofuran at ambient temperatures, **5.62** affords the corresponding Lewis acid-base species **5.64** upon treatment with DMAP (DMAP = 4-dimethylaminopyridine).[50]

In 2024,[59] further reports of afforded alumole species continued to expand C_4 scaffold substituents, building upon previous aluminate and Lewis acid-base adduct developments from 2015.[60] Müller and coworkers reported the preparation of alumoles species **5.65** and **5.66**, consequential of formation and skeletal rearrangements, with dipotassium germacyclopentadienediide and aluminium(III) dichloride reagents and subsequent treatments.[59] These species possessed the 2,5-silyl-3,4-methyl substituted C_4 scaffold, incorporating both alkyl and silyl-based steric encumberment. Through the variation on the third substituent of the aluminum(III) dichloride and thermal elevation, the aluminium-substituted aryl **5.65** and amido diethyl etherate **5.66** complexes could be afforded.

5.1.8. Alumoles: Synthesis

Synthetic preparations of alumoles have been significantly inspired by the methodologies used to prepare boroles (**Chapter 5.1.3**). Widely applied in modern developments,[8, 50, 53] salt metathesis routes have proven to be useful in the preparation of various alumole species. However, synthesis via salt metathesis routes has not exclusively afforded the formation of target "free" alumole species, rather the additional preparation of notable derivatives.

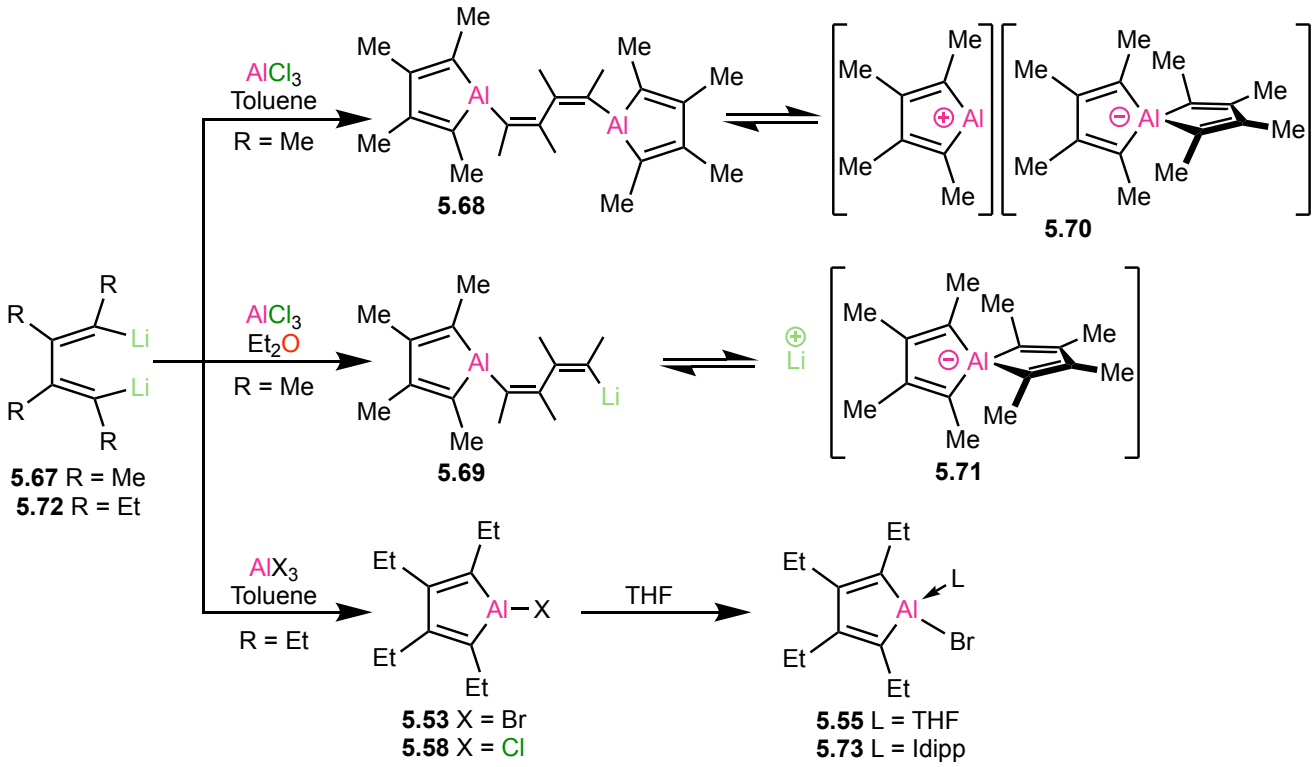

Scheme 5.9: Selected preparations of haloalumoles and corresponding aluminate derivatives.

Reported in 1980, Hoberg and Richter reported the impacts of solvent and minimal steric encumberment upon attempts to prepare chloroalumoles (Scheme 5.9).[61] From the same starting materials of methyl-substituted 1,4-dilithiodibutadiene **5.67** and aluminium chloride, the authors proposed products within an equilibrium from mass spectrometry. Upon preparations, equilibria of tricoordinate alumoles (**5.68**, **5.69**) with aluminate species (**5.70**, **5.71**) of varied counterions were proposed, with aluminate species balanced with an alumole anion **5.70** and lithium cation **5.71** obtained from solutions of toluene and diethyl ether respectively. Of note, the preparations of aluminates **5.70** and **5.71** were indicative of the minimal steric bulk afforded by the 2,5-substitution with methyl groups. Consequently, the exposed Al–Cl bond and aluminium centre were postulated to undergo further reactivity to more thermodynamically favourable species.

The preparation of analogous and isolable haloboroles was reported first in 2014, featuring the minor increase in steric bulk via the furnishing of a C_4 scaffold with ethyl substituents (Scheme 5.9).[55] The treatment of the ethyl-substituted 1,4-dilithiobutadiene **5.72** with aluminium halides in toluene led to the corresponding bromide **5.53**,[55] and chloride **5.58** alumoles (Scheme 5.9).[57] Furthermore, following the preparation of the bromoalumole **5.53**, this species served as a precursor to the Lewis-base coordinated tetrahydrofuran-solvated species **5.55** and the first crystallographically characterised alumole carbene adduct species **5.73**, furnished with an Idipp carbene (NHC = *N*-heterocyclic carbene, Idipp = $C\{N(C_6H_3\text{-}2,6\text{-}^iPr_2)CH\}_2$).[57]

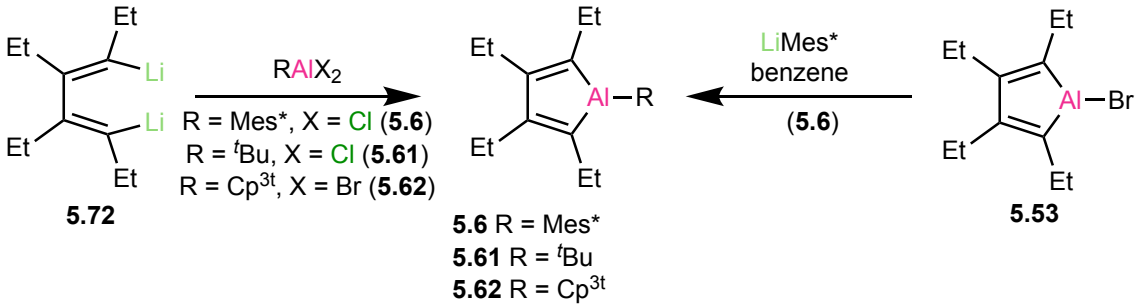

Scheme 5.10: Syntheses affording "free" alumole species from 1,4-dilithiobutadiene and bromoalumole reagents.

Further capitalising upon the application of 1,4-dilithiobutadiene reagents, syntheses with aluminium(III) dichloride reagents have been reported to ensure pre-instalment of organoaluminium substituents within alumoles (Scheme 5.10).[8, 50] Consequently, salt metathesis routes conducted in aromatic solvents (toluene **5.6**, benzene **5.61**, **5.62**) gave the corresponding alumoles in varying yields **5.6** (48%),[8] **5.61** (6%) and **5.62** (30%).[50] Acknowledged by Braunschweig and coworkers, the relatively poor yields isolated of **5.61** and **5.62** were attributed to the potential for poor selectivity in such cyclometalation reactions and the corresponding oily nature and facile hydrolysis of the products.[50] Notably, in the preparation of the first crystallographically characterised alumole species **5.5**, the synthesis was also undertaken with the corresponding phenyl-substituted 1,4-dilithiobutadiene and phenylaluminium(III) dichloride in diethyl ether.[7a] Being conducted with coordinating ethereal solvent assured the preparation of the Lewis acid-base adduct $[PhAlC_4Ph_4(OEt_2)]$ **5.5**, later crystallographically characterised in the same year.[7b] Further establishing routes to the seminal free alumoles species **5.6**, Tokitoh and coworkers reported the preparation of target alumole through the single salt metathesis of the bromoalumole **5.53** (Scheme 5.10).[57] Treatment of **5.53** with mesityl lithium at 60 °C for 48 hours afforded **5.6** in yields identical to those prepared via the aluminium(III) dichloride route (48%) (Scheme 5.10).[57]

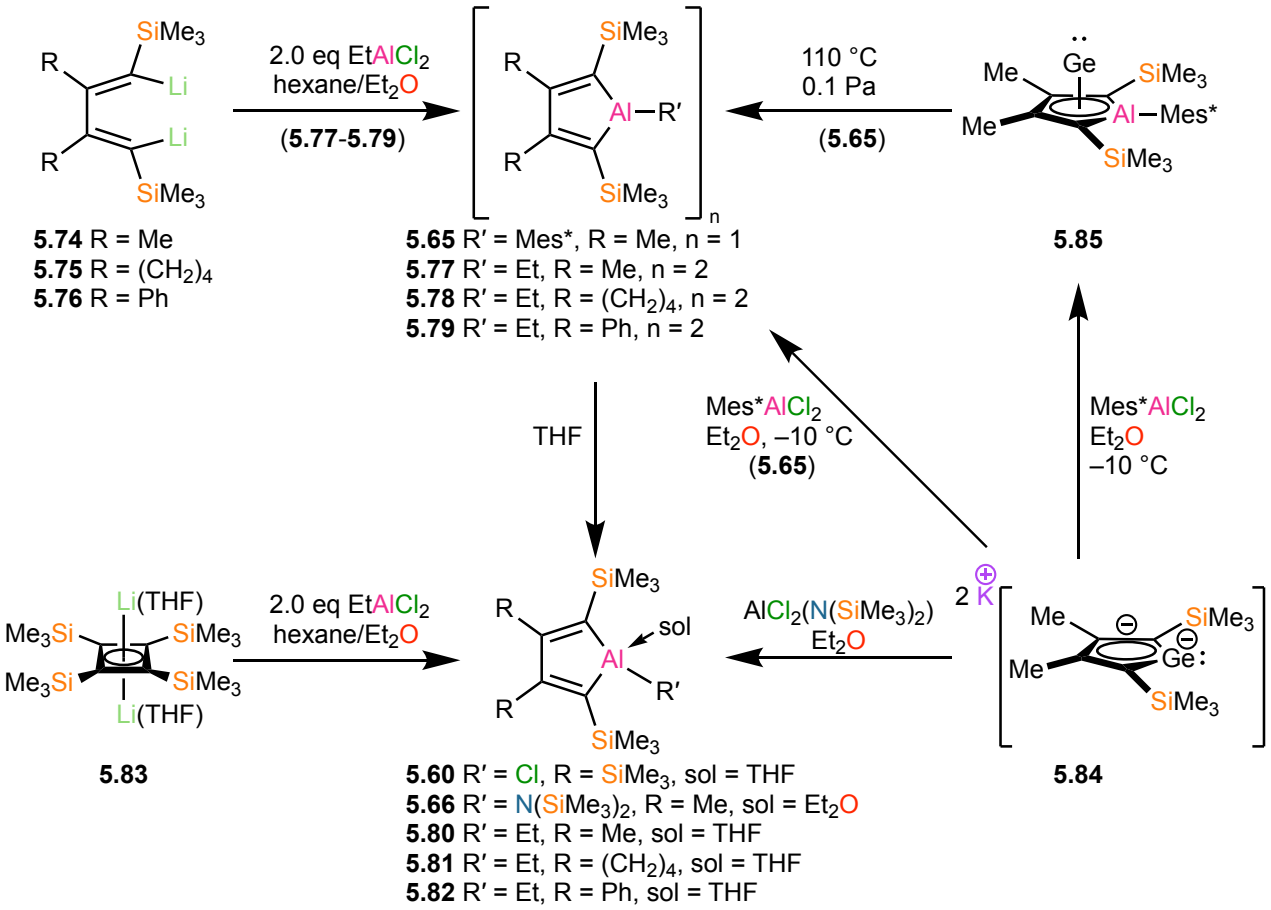

Scheme 5.11: Preparation of alumole species featuring 2,5-silyl substitution.

The preparation of 2,5-silyl-substituted alumoles have been reported from salt metathesis routes, however, they may be obtained from more exotic starting materials. Expanding the preparation of haloalumoles (**5.53**, **5.58**) and "free" alumole species (**5.6**, **5.61**, **5.62**), Xi and coworkers reported the synthesis of a library of 2,5-silyl substituted alumoles and their tetrahydrofuran adduct derivatives (Scheme 5.11).[60] The treatment of sterically varied 1,4-dilithiobutadiene **5.74-5.76**, with two equivalents of diethylaluminium(III) chloride in a hexane/diethyl ether mixture gave the corresponding dimeric alumole species.[60] Within the solid-state, **5.77** - **5.79** feature an analogous dimeric arrangement to previously identified alumoles (**5.54**, **5.59**, **5.63**), whereby the dimer is supported via interactions with the endocyclic carbon of one alumole and the Lewis acidic aluminium centre the other. These dimeric species were similarly isolated in variable yields (**5.77** 70%, **5.78** 85%, **5.79** 36%), however, treatment with tetrahydrofuran afforded THF adducts in yields greater than 95% (**5.80-5.82**) (Scheme 5.11).[60]

Employing the more exotic tetrakis(trimethylsilyl)cyclobutadiene dianion **5.83**, as a reagent Sekiguchi, Lee and coworkers reported the preparation of the monomeric tetrahydrofuran adduct chloroalumole **5.60** featuring exclusively trimethylsilyl substitution about the C_4 scaffold.[58]

Moreover, investigations with a dipotassium germacyclopentadienediide metallole species **5.84**, led Müller and coworkers to prepare two 2,5-silyl-substituted alumole species **5.65** and **5.66**.[59] Toward the preparation of the tricoordinate alumole species **5.65**, treatment of **5.84** with substituted aluminium(III) dichloride afforded the rearrangement species **5.85**, featuring alumole fragment serving as an η^5-ligand to the Ge(II) complex as an alumole dianion. Moreover, this synthesis also affords **5.65** as a reaction side-product, however, heating **5.85** to 110 °C under reduced pressure (1×10^{-6} bar) led to its quantitative conversion into the tricoordinate alumole **5.65**. Notably, treatment of **5.84** with $[AlCl_2N(SiMe_3)_2(Et_2O)]$ similarly affords a mixture of products, from which only single crystals of amidoalumole **5.66** could be isolated.[59] Consequently, more robust synthetic methods towards amidoalumole analogues are reported within the literature.[56]

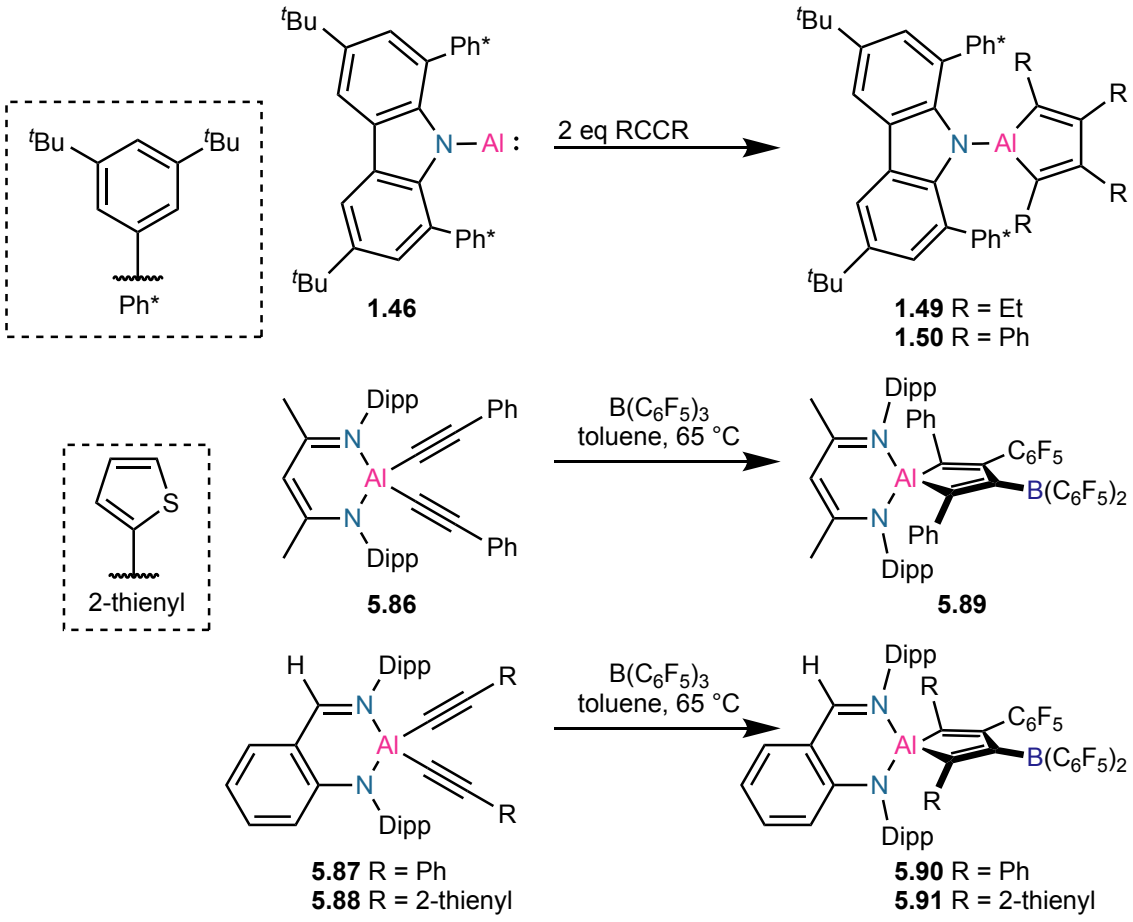

Scheme 5.12: Preparation of alumole species via unconventional non-salt metathesis methods.

Highlighted within **section 1.5.2.**, the most recent decade has presented the capability for alumole species to be prepared in the final-step furnishing aluminium centres with ligands via ring-forming reactions (Scheme 5.12). In 2023, products **1.49** and **1.50** were obtained from [2+2+1] cycloaddition and ring expansions conducted by *N*-aluminylene **1.46** with unsaturated hydrocarbons, as a novel method of alumole synthesis (Scheme 5.12).[62] Roesky and coworkers in 2020 reported a new facile

synthesis to afford alumoles.[63] Treatment of starting reagent aluminum dialkynyls **5.86** - **5.88** with the strongly Lewis-acidic borane $B(C_6F_5)_3$, afforded 3 different alumoles featuring aluminium centres coordinated with a β-diketiminato **5.89** or anilido-imino **5.90**, **5.91** ligands all with good isolated yields (> 75%) (Scheme 5.12). Markedly, this synthetic method had also been employed in the preparation of borole systems,[19] however, this falls outside the scope of this work. Whilst the alumole preparations via non-salt metathesis routes can be used to access new systems, the wider applicability of such preparations is of still ongoing.

5.1.9. Alumoles: Reactivity

As a predominantly under investigated field of inquiry, the reactivity of alumoles is developing through the report of each new species. Within the literature and highlighted previously, the prevalence of aluminate and Lewis-acid base adduct formation often serves as an aid to complex isolation. Moreover, "free" alumoles as highly reactive aluminium species have highlighted the propensity for ring expansion,[50] and redox chemistry to afford aromatic aluminium-containing heterocycles.[8, 64]

5.1.9.1. Reactivity: Alumole Ring Expansion

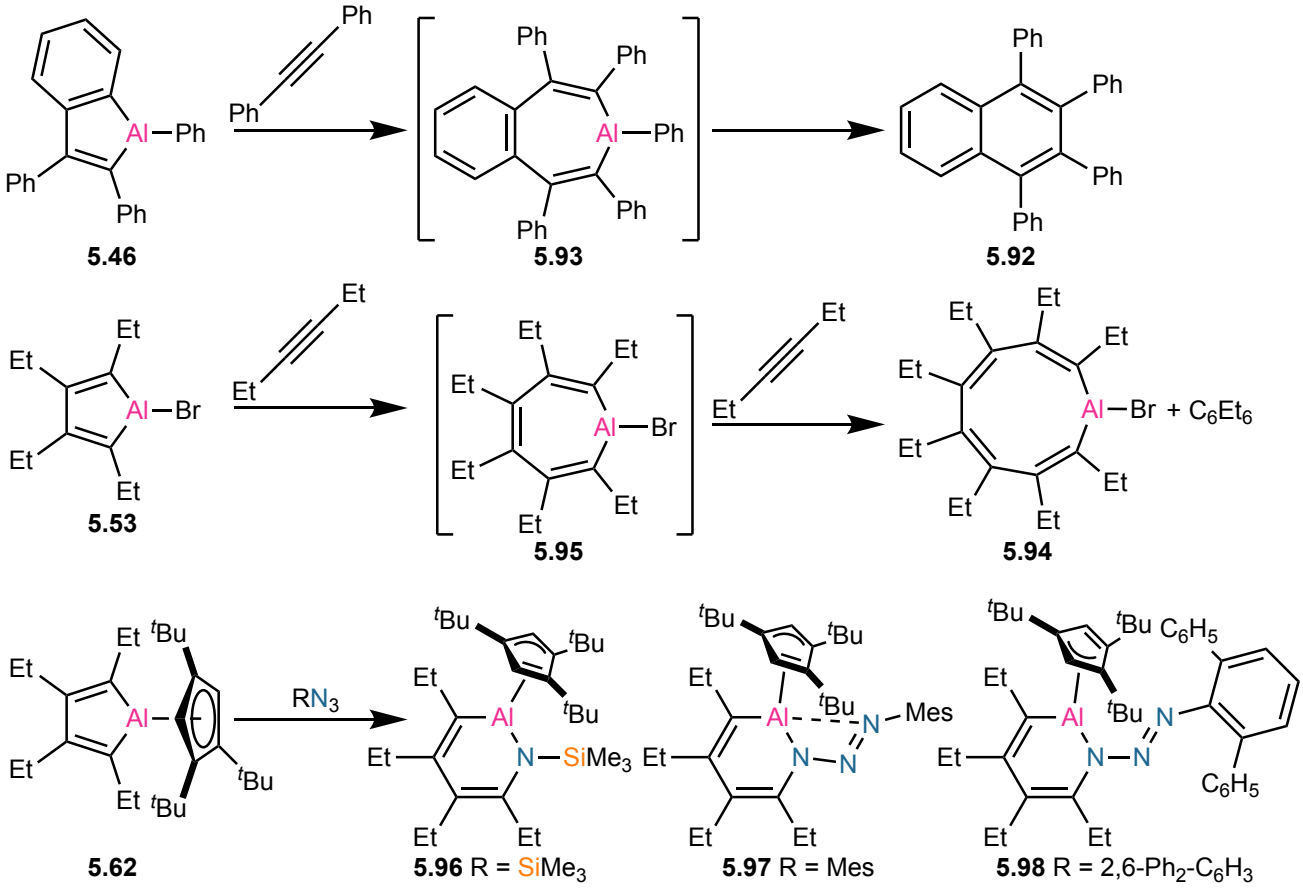

Scheme 5.13: Alumoles that participate in ring expansions to afford C-C coupled products and azide species.

The capability for alumole ring expansions was originally proposed following the initial report of the benzoalumole **5.46** in 1966 (Scheme 5.13).[51] Specifically, treatment of **5.46** with diphenylacetylene at elevated temperatures afforded a mixture of species, including the substituted naphthalene **5.92**.[65] Following the isolation of **5.92**, the authors hypothesised its formation to occur via an *in-situ* ring expanded system **5.93**; however, this intermediate was not isolated.[65]

The subsequent resurgence of modern alumole chemistry has afforded various species obtained from ring expansion routes involving both halo- and "free" alumoles (Scheme 5.13).[66] Bromoalumole **5.53**, reported by Tokitoh and coworkers in 2015, was found to undergo ring expansions with 3-hexyne affording the 9-membered aluminacycle **5.94** from excess treatment or the C-C coupled product C_6Et_6 from only two equivalents.[67] Similar to original reports, both species were attributed to a 7-membered ring expanded intermediate **5.95**, which could not be isolated nor spectroscopically identified. In 2020, Braunschweig and coworkers reported further alumole ring expansion propensities with organic azides and the "free" alumole **5.62**, leading to the formation of the 6-membered aluminium-nitrogen heterocycles **5.96**-**5.98**.[50] The alumole derivatives afforded were steric bulk dependent, with **5.96** yielded from the loss of N_2 and the formal trimethylsilyl nitrene insertion into the endocyclic Al–C bond. **5.97** and **5.98** retained the N-N bonds of aryl azides; however, the reduced steric bulk in the Mes-substituted species **5.97** led to added interactions between the N_3-chain and the aluminium centre.[50]

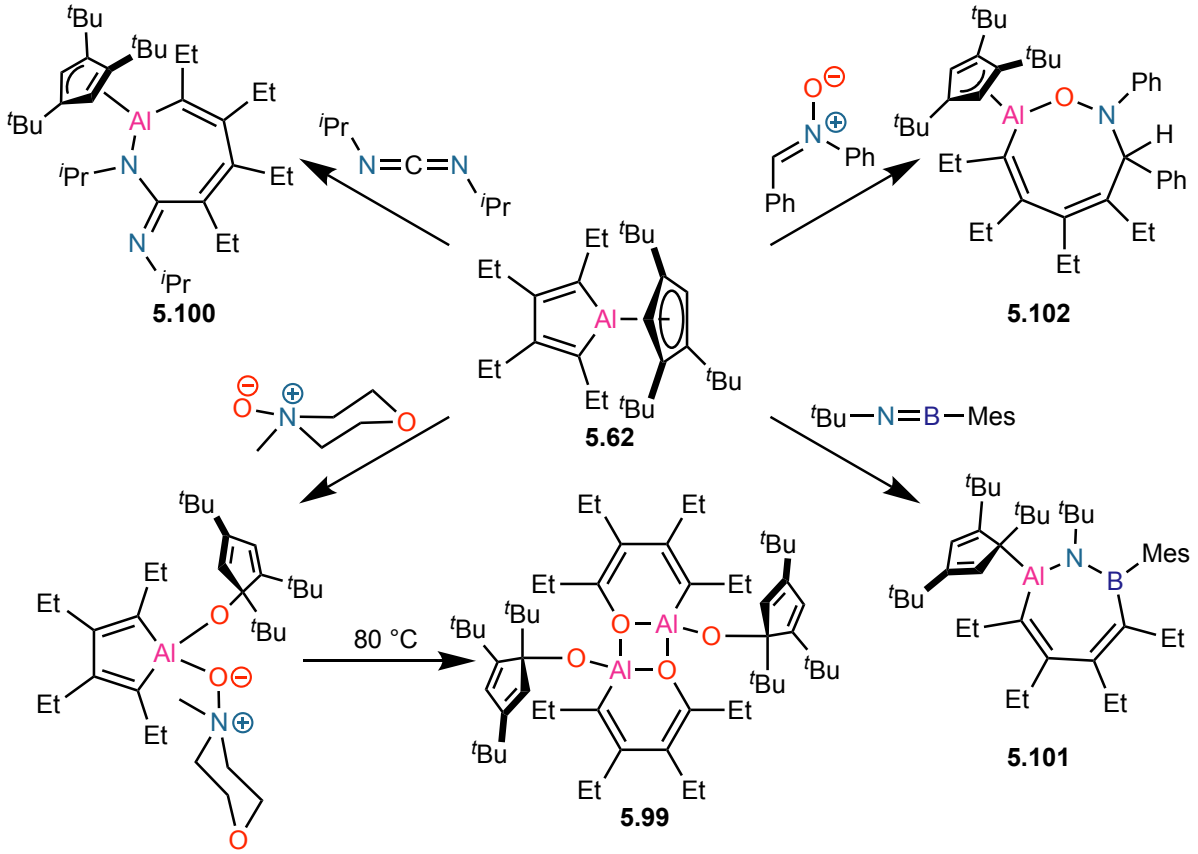

Scheme 5.14: Further ring expansion examples via reactions with heteroatom-containing unsaturated species.

Following, Braunschweig and coworkers further ascertained the reactivity of the **5.62**. Through reaction with heteroatom-containing unsaturated species, the reproducible preparation of further novel six- **5.99**, seven- **5.100**, **5.101**, and eight-membered **5.102** cyclic products with high heteroatom content were reported.[66] The successful isolation of these products was attributed to the Al-Cp^{3t} fragment (Cp^{3t} = 1,2,4-tris(*tert*-butyl)cyclopentadienyl), as flexibility in steric and electronic saturation is possible by the degree of C_5 ligand ring-slippage at the Al centre.[66] The degree of ring slip and subsequent aluminium centre saturation was reported in η^1, η^2, and η^3 arrangements. Consequently, this reinforces the impact of the aluminium substituents upon the isolation alumoles and their related derivatives.

5.1.9.2. Reactivity: Alumole Redox Chemistry

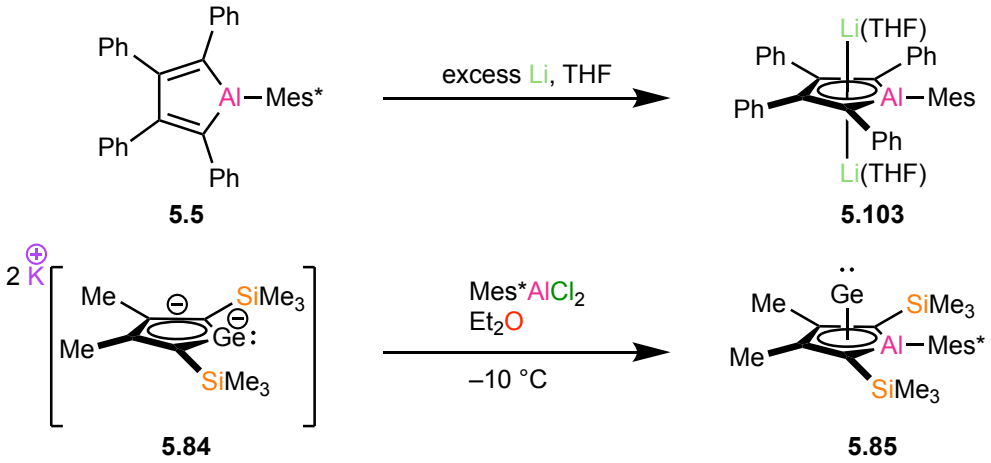

*Scheme 5.15: Preparation of dilithioalumole dianion **5.103** and related dianionic germanium complex **5.85**.*

The preparation of aromatic aluminium-containing heterocyclic species from antiaromatic alumole starting materials is currently underexplored.[64] First reported by Tokitoh and coworkers the dilithioalumolediide dianion **5.103** was prepared from the reduction of alumole **5.5** with lithium.[8] Analogous to boroledиide species, **5.36** features η^5 coordination of the lithium counterions above and below the 5-membered alumole core (Scheme 5.15).[57] Variation of the counterion of **5.5** through reductions with sodium, potassium or potassium graphite were unsuccessful, affording complicated mixtures and no evidence of the corresponding metal salts. Moreover, further alumole dianion examples are currently limited, with **5.85** afforded from dipotassium germacyclopentadienediide metallole **5.84** following treatment with Mes*$AlCl_2$ (Scheme 5.15). Alumoldiide dianions may further extend the reactivity of aluminium-containing heterocycles, and further explorations into their preparations of research interest.

5.1.10. Alumoles: An Outlook

Despite being a relatively underdeveloped field, alumoles have seen ongoing investigation since their outset in 1962.[9] The report of the first isolable "free" alumole **5.5** in 2013 by Tokitoh and coworkers has since prompted a resurgence within this field. Consequential variations of aluminium- and C_4-based substituent identities have further translated into diverse reactivity profiles. Lewis acid-base adducts have proven imperative in the isolation of monomeric alumoles and their subsequent derivatives, whilst ring expansion and redox transformations constitute a growing focus within the field.

5.2. Research Rationale

5.2.1. Applying an Acyclic Aluminyl Anion with Boroles

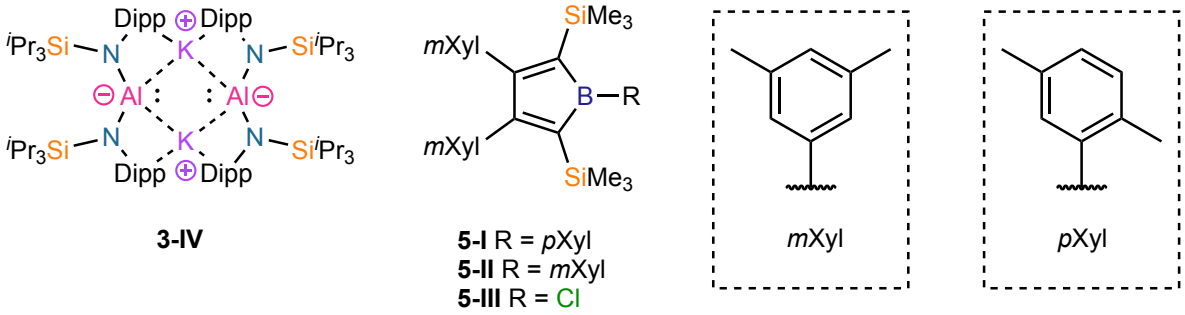

*Figure 5.8: Acyclic aluminyl species **3-IV** to be explored with multiple borole analogues (**5-I** - **5-III**).*

Following the preparation of a catalogue of known "free" and haloborole reagents **5-I** - **5-III**, investigations were undertaken towards their reactivity with the acyclic aluminyl anion **3-IV** (Figure 5.8). With both borole and aluminyl systems presenting varied reactivity, the literature did not show a precedent for transformations afforded by the interaction of both species. Notably, the aluminyl anion **3-IV** and its associated potassium cations present viable reagents for Lewis acid-base adduct formations, aluminium metal available for borole ligation, or as aluminyl promoted reducing agents in the preparation of reduced derivatives.

5.2.2. Expanding the Alumole Catalogue

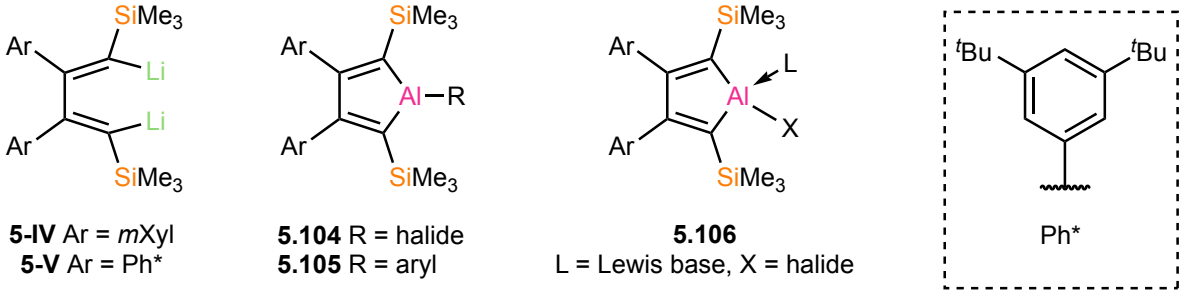

*Figure 5.9: 1,4-Dilithiodibutadiene starting materials and related target "free" **5.104**, halo-, Lewis acid-base adduct alumoles.*

As established by Sindlinger and coworkers through previous investigations,[16-17] the optimised synthesis of two 1,4-dilithiobutadiene materials (**5-IV** and **5-V**) were developed in the preparation of boroles. Within the target metallole complexes, the impact of varied steric bulk of the 3,4-substituted aryl groups was to be investigated towards the crystallisation, isolation and reactivity of aluminium complexes (Figure 5.9). The preparation of alumoles with both aromatic and coordinating solvents were undertaken to further aid in the isolation of target products (**5.104 and 5.105**, and **5.106** respectively), with solvent coordination leading to Lewis acid-base adducts aiding in formation.

5.3. Results and Discussion: Boroles

5.3.1.1. Preparation of Borole and 1,4-Dilithiobutadiene Reagents

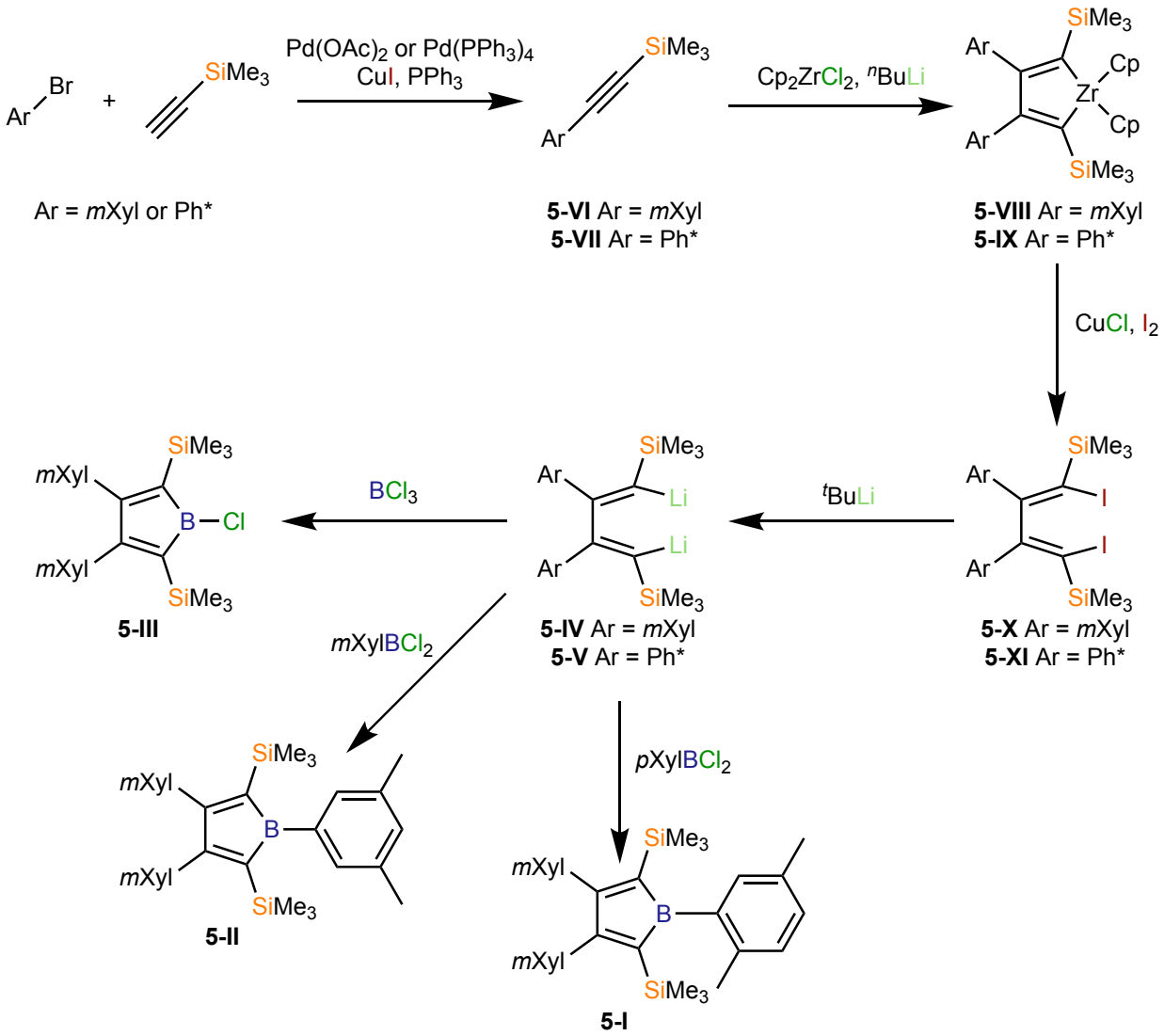

*Scheme 5.16: Synthetic procedures to afford **5-I** – **5-III** boroles, and **5-IV** and **5-V** 1,4-dilithiobutadiene reagents from commercially available reagents.*

The preparation of boroles **5-I** – **5-III**, and 1,4-dilithiobutadiene reagents **5-IV** and **5-V** were completed according to literature methodologies (Scheme 5.16).[15-17, 28, 68] Due to time limitations, **5-III** and **5-V** were supplied by coworkers MSc. Michael Jochum and Dr. Tobias Heitkemper, respectively.

As highlighted previously (Scheme 5.1), substituted alkynes serve as common starting materials in metallole synthese. To afford the corresponding alkynes **5-VI** and **5-VII**, Sonogashira cross couplings were undertaken with palladium(II) acetate and tetrakis(triphenylphosphine)palladium(0), respectively, with the corresponding methyl substituted bromobenzene and trimethylsilylacetylene as

coupling partners. Subsequent synthetic transformations were undertaken in tetrahydrofuran solutions, affording the target boroles **5-I** – **5-III** (Scheme 5.16).

Next, alkynes **5-VI** and **5-VII** were treated with zirconocene dichloride and *n*-butyllithium to afford the corresponding cyclised zirconium-templated species **5-VIII** and **5-VIX**. Forthwith, the zirconium metalloles could be iodinated with copper(I) chloride and elemental iodine to yield the 1,4-diiodobutadiene species **5-X** and **5-XI** (Scheme 5.16), which were isolated following a one-pot reaction.

The 1,4-dilithiobutadiene reagents **5-IV** and **5-V** could be prepared following the lithiation of **5-X** and **5-XI**. Treatment with *t*-butyllithium and subsequent workup would afford the lithiated species **5-IV** and **5-V** as dark orange to red, and orange sticky solids, which could be utilised in subsequent reactions undertaken within a glovebox (Scheme 5.16).

The preparation of the aryl-substituted systems 1-(3,6-dimethylphenyl)-3,4-bis(3,5-dimethylphenyl)-2,5-bis(trimethylsilyl)borole **5-I** and 1-(3,5-dimethylphenyl)-3,4-bis(3,5-dimethylphenyl)-2,5-bis(trimethylsilyl)borole **5-II** by combining the requisite borane with the 1,4-dilithiobutadiene **5-IV** (Scheme 5.16).[15] Notably, the varying the substitution pattern of methyl groups from *para*- to *meta*-Xylyl impacted the physical characteristics the final borole species. **5-II** was isolated as a red crystalline solid, whereas **5-I** is highly soluble and was consequently isolated as a highly viscous dark-red oil. The 1-chloro-3,4-bis(3,5-dimethylphenyl)-2,5-bis(trimethylsilyl)borole **5-III** was prepared via a salt metathesis between boron trichloride and **5-IV** on a multigram scale, as per a literature procedure (Scheme 5.16).[17] Following the purification of species, chloroborole **5-III** was isolated as a deep-red crystalline solid.

5.3.2. Reduction Chemistry of Boroles with an Acyclic Aluminyl Anion

5.3.2.1. 1-Electron Reductions of a *para*-Xylyl Substituted Borole

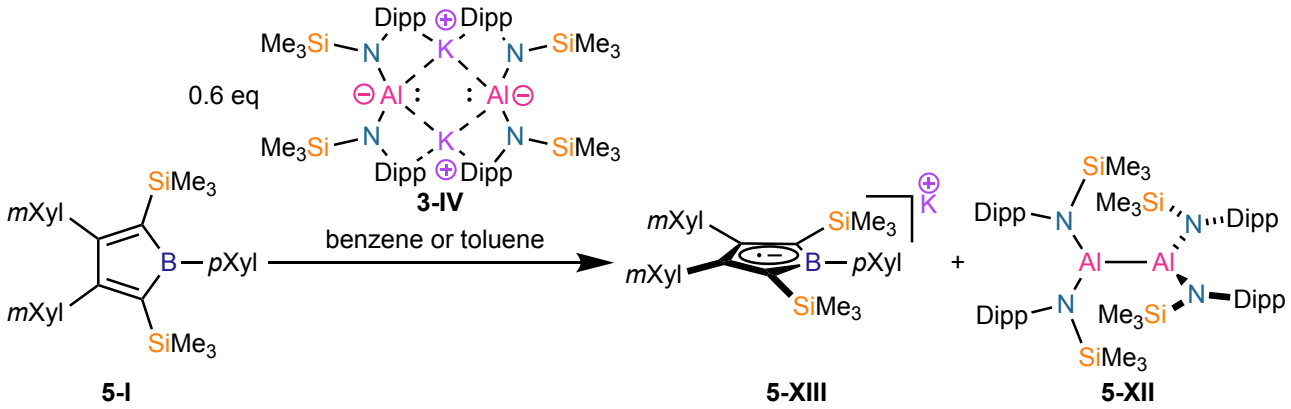

*Scheme 5.17: Stoichiometric 1-electron reduction of **5-I** with an acyclic aluminyl anion **3-IV** to afford a postulated borole radical **5-XIII** and dialane **5-XII**.*

Following the preparation of the aluminyl anion **3-IV** in benzene via ^{1}H NMR spectroscopy, a deep-yellow solution of **3-IV** was treated with **5-I** within a glovebox. This led to an immediate colour change to an orange solution, from which no precipitate was afforded (Scheme 5.17). Immediate ^{1}H NMR spectroscopic analysis identified the formation of a highly sterically crowded $[N(Dipp)SiMe_3]^-$ containing species. This was identifiable by the signals corresponding to Dipp moieties featuring two different isopropyl methine proton environments, and four different isopropyl methyl proton environments, but only one trimethylsilyl signal. Similarly observed in the reductions of bulkier acyclic aluminium(III) iodide precursors mentioned previously (**3-I**–**3-III**, **Chapter 3**), these signals were attributed to the formation of previously postulated dialane **5-XII**. However, most apparent from the spectra was the complete absence of signals related to borole **5-I** and its related derivatives. Consequently, all borole species were assumed as now being the paramagnetic borole radical monoanion **5-XIII** afforded from the acyclic aluminyl species promoted stoichiometric reduction. The removal of volatiles from the NMR tube resulted in an orange powder, which was extracted with hexane. Ensuing purification attempts afforded a yellow-red foam, which when dissolved in deuterated benzene, identified the formation of a mixture of dialane and borole degradation species.

To gain further comprehension of postulated paramagnetic species in solution, the reaction of **5-I** and **3-IV** was repeated in toluene (Scheme 5.17). Following the filtration of the reaction mixture into a quartz tube, EPR spectroscopy was completed, identifying the presence of a paramagnetic species (Figure 5.10).

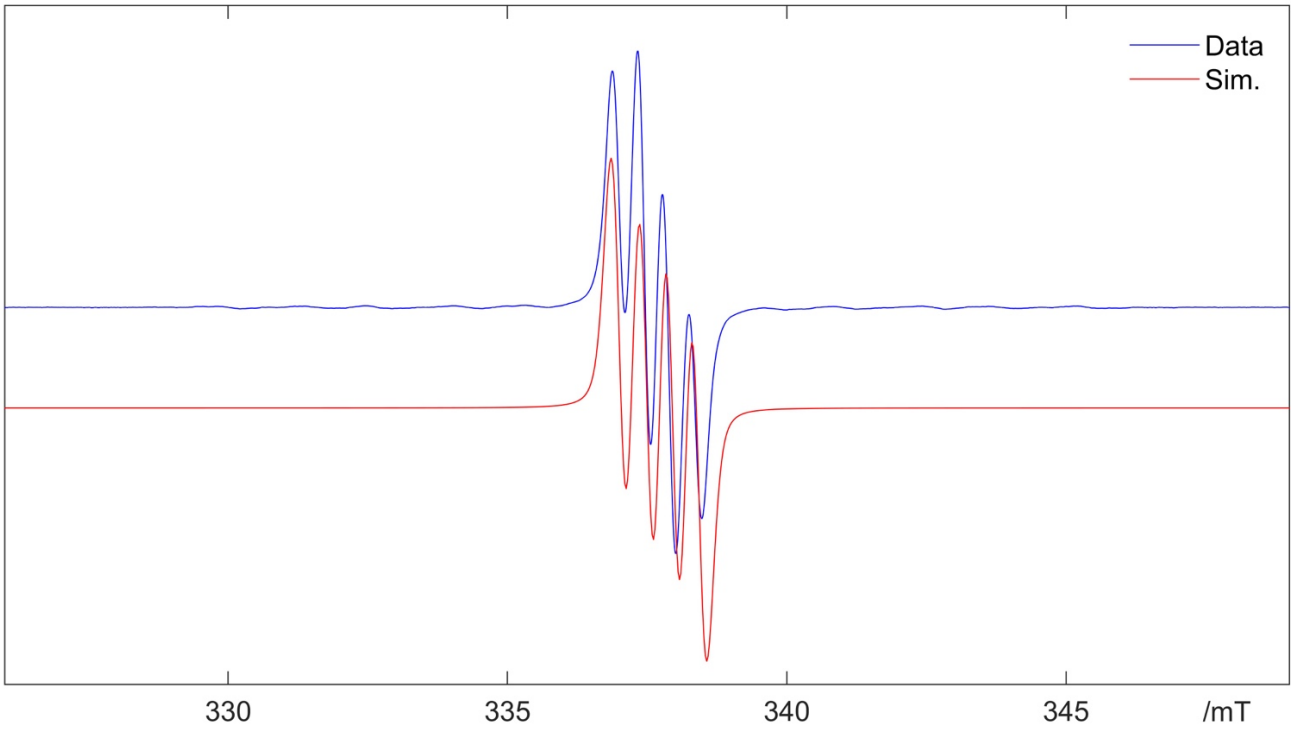

Figure 5.10: EPR spectrum of the para-Xylyl-substituted borole radical monoanion ***5-XIII****.*

From the resulting EPR spectrum the presence of the *para*-Xylyl substituted borole radical anion **5-XIII** is proposed. Signals associated with an unpaired electron near a ^{11}B centre (nuclear spin of I = 3/2), appeared as four equally spaced hyperfine lines (isotropic g value = 1.9620). This was further emphasised via signal indicative of unpaired electron spin delocalisation about the central borole BC_4 ring from relatively small hyperfine coupling constants of $A(^{11}B)$ = 4.73 G. These values could be compared with the literature-reported ferrocene-substituted borole radical anion **5.41** (Scheme 5.8),[48] and the 1-mesityltetraphenylborole radical anion **5.44**,[49] both reported by Braunschweig and coworkers. Consequently, a lower comparable isotropic g value was identified for **5-XIII** comparable to reported in **5.41** (2.0037) and **5.44** (2.0025), and a relatively larger hyperfine coupling constant ($A(^{11}B)$ = 3.73 G **5.41**; 3.43 **5.44**). Markedly, these values were analogous for borole radical species, and notably smaller than values observed in triarylborane radical anions ($[Ph_3B]^{\cdot-}$ $A(^{11}B)$ = 7.84 G; $[Mes_3B]^{\cdot-}$ $A(^{11}B)$ = 10.32 G),[69] due to the increase electronic delocalisation about the metallole heterocycle in **5-XIII**.

To further identify species afforded from reactions, repeated preparations in toluene were undertaken, targeting the formation of SCXRD-quality crystals. To this end, a deep-yellow toluene solution of **3-IV** was added dropwise to a dark red toluene solution of **5-I** (Scheme 5.17). On contact of the two solutions afforded the immediate precipitation of an orange solid. Moreover, agitation of the reaction vial observed the deposition of crystalline material on the glass walls. The saturated

solution was placed in a –40 °C freezer to crystallise overnight. Following 18 hours, orange powder-coated colourless crystalline prisms of SCXRD quality of **5-XII** were isolated and washed until the powder coating was removed. From the washings and toluene mother liquor, all volatiles were removed, affording an orange powder, which was isolated in a moderate yield (62%, based upon quantitative formation of **5-XII** and **5-XIII**).

^{1}H NMR spectroscopic analysis of the orange powder identified the preparation of postulated dialane **5-XII** (in combination with paramagnetic and NMR silent borole radical **5-XIII**), which was characterised via heteronuclear NMR spectroscopy. From the isolated crystalline material, the identity of postulated acyclic dialane could be confirmed as [{Al(N{Dipp}SiMe$_3$)$_2$}$_2$] **5-XII** (Figure 5.11).

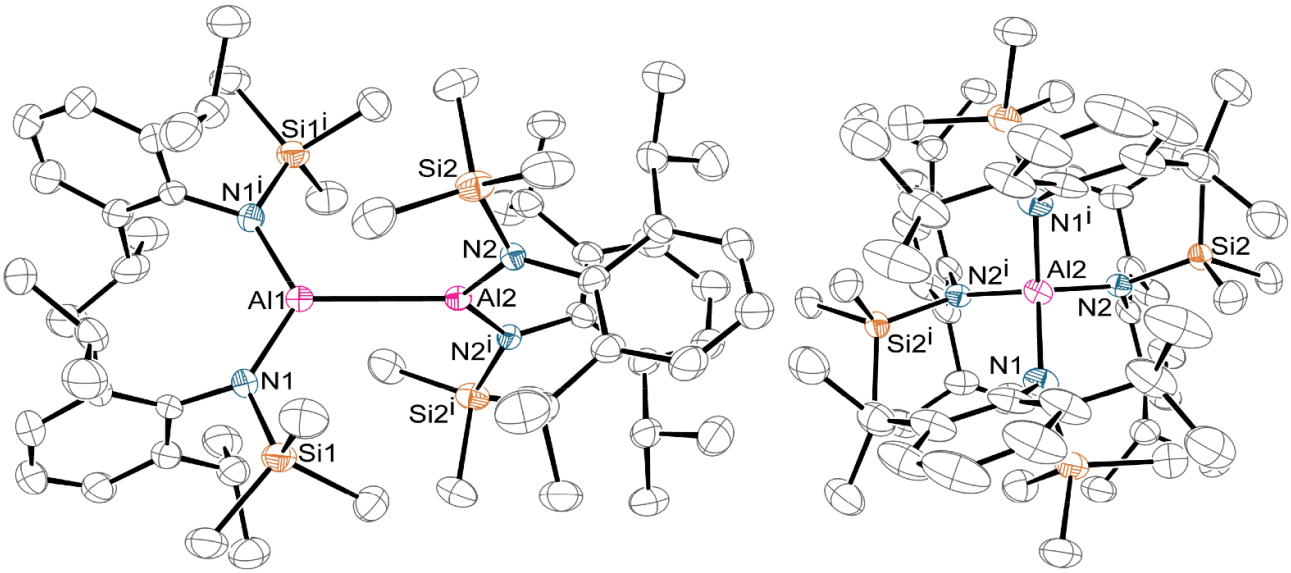

*Figure 5.11: Molecular structure of [{Al(N{Dipp}SiMe$_3$)$_2$}$_2$] **5-XII**, shown from two different orientations, as determined by X-ray crystallography. Thermal ellipsoids set to 50% probability. Protons and toluene solvent molecules omitted for clarity. Selected bond lengths (Å) and angles (°): Al1-Al2 2.759(3), Al1-N1 1.828(4), Al2-N2 1.833(4), N1-Si1 1.759(4), N2-Si2 1.777(4), N1-Al1-N1^i 120.4(3), N2-Al2-N2^i 119.79(14), Si1-N1-Al1 124.8(2), Si2-N2-Al2 125.9(2).*

From the solid-state structure of **5-XII**, the formation of an unsupported aluminium(II)-aluminium(II) bond could be identified. In comparison with the reported dialane structures in the CCDC, the Al-Al bond in **5-XII** (2.759(3) Å) was identified as the second longest unsupported Al-Al bond, with the longest example (2.8790(8) Å) found in complex [{Al(Iipr*)(Mes)$_2$}$_2$] (Iipr* = C{N(^{i}Pr)CMe}$_2$) with each aluminium centre bound to an NHC to give 4-coordinate environments.[70] Moreover, the Al-Al bond length in **5-XII** is notably longer than the range of dialane Al-Al bond length as prepared from aluminyl species (2.5850(5) - 2.7330(6) Å).[71] Both Al centres consequently feature trigonal planar arrangements with minimal distortion about the aluminium centre identifiable via ∠N-

Al-N bond angles (Al1 120.4(3)°, Al2 119.79(14)°, trigonal planar 120°). Rather the steric encumberment of the ligands was identifiable via wide ∠Si-N-Al (N1 124.8(3)°, Al2 125.9(2)°), bond angles highlighting the distorted trigonal planar arrangement of silyl and aryl moieties around N-coordination atoms. Moreover, the dihedral angle afforded via the arrangement of N-Al-N fragments was nearly perpendicular (88.31°) to accommodate the steric constraint of the trimethylsilyl groups. Similarly observed within previous acyclic aluminyl derivatives, to accommodate for steric impacts within the $[N(Dipp)SiMe_3]^-$ ligands, rotations about the Al-N bonds allowed for the location of silyl groups toward the Al-Al bond, opposed to the projection of Dipp groups in the aluminyl **3-IV**.

5.3.2.2. 2-Electron Reductions of a *para*-Xylyl Substituted Borole

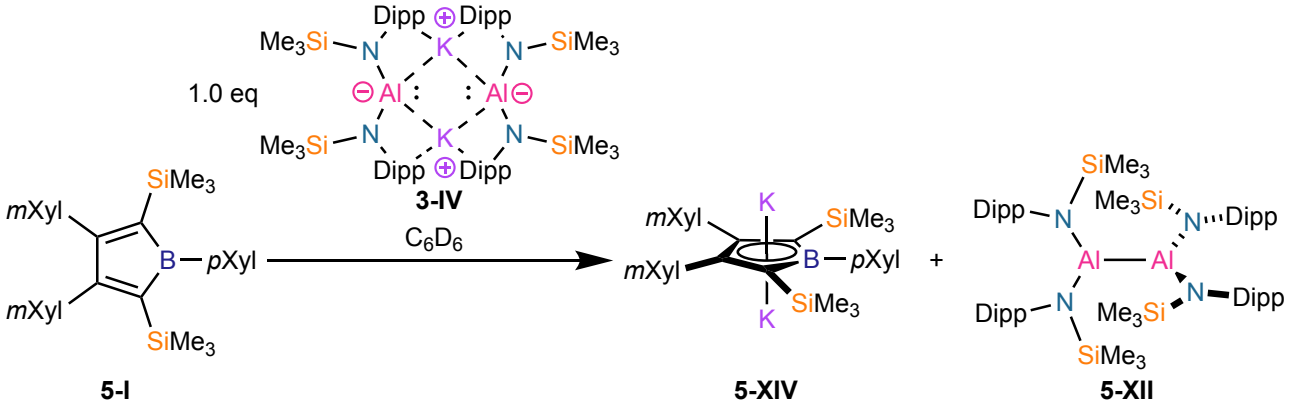

*Scheme 5.18: Stoichiometric 2-electron reduction of **5-I** with an acyclic aluminyl anion **3-IV** to afford the dipotassium boroledиide dianion **5-XIV** and dialane **5-XII**.*

Following the preparation of a fresh, deep-yellow toluene solution of **3-IV**, **5-I** was added leading to an immediate colour change to orange (Scheme 5.18). Immediate ^{1}H NMR spectroscopic analysis identified the complete consumption of the aluminyl anion and formation of the dialane **5-XII**. Moreover, signals relating to the known *p*Xyl-borole **5-I** similarly presented quantitative conversion from starting reagents to the boroledиide dianion **5-XIV**. Within the ^{1}H NMR spectra, all CH_3-related signals observed more downfield shifts relative to the starting material **5-I**. Notably, changes were most pronounced in signals related to 2,5-trimethylsilyl (**5-I** -0.06 ppm, **5-XIV** 0.12 ppm) and 3,4-*m*Xylyl (**5-I** 2.02 ppm, **5-XIV** 2.32 ppm) substituents about the C_4 scaffold.

Concurrently within the Sindlinger group, investigations conducted by Michael Jochum MSc. afforded the preparation of the tetrahydrofuran solvated analogue dipotassium boroledиide analogue $[\{K(THF)\}_2\{p\text{Xyl-BC}_4(2,5\text{-SiMe}_3)_2(3,4\text{-}m\text{Xyl})_2\}]$. Comparison between the data of **5-XIV** and solvated species, identified analogous signals relating all proton environments, excluding potassium-coordinated tetrahydrofuran signals at 3.46 and 1.37 ppm.

Following 18 hours at ambient temperature an orange precipitate was observed within the deuterated benzene reaction solution of **5-I** and **3-IV**. The corresponding ^{1}H NMR spectra observed the lack of signals related to the presence of any *p*Xyl-borole related species (**5-I**, or **5-XIV**). Despite efforts, attempts to recrystallise the target dianion **5-XIV** or associated dialane **5-XII** were unsuccessful. Over the period of 5 days, the prevalence of proligand NH(Dipp)SiMe$_3$ **2-IV** and multiple unidentified species suggested degradation of **5-XIV** and dialane **5-XII**. Due to the observed degradation of species within the reaction mixture, isolation of material was not sought and further treatment with coordinating solvents was instead focussed on other borole investigations.

5.3.2.3. 1-Electron Reductions of a *meta*-Xylyl Substituted Borole

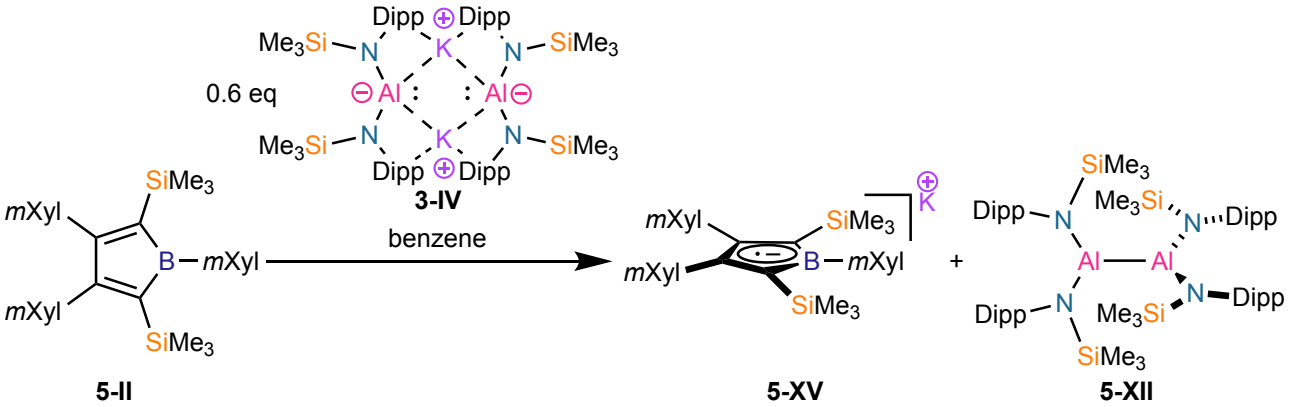

*Scheme 5.19: Stoichiometric 1-electron reduction of **5-II** with acyclic aluminyl anion **3-IV** to afford a postulated mXyl-borole radical **5-XV** and dialane **5-XII**.*

A deuterated benzene solution of **3-IV** was prepared and treated with *m*Xyl-borole **5-II**, to give a yellow-brown preciptate (Scheme 5.19). ^{1}H NMR spectroscopic analysis afforded an indiscernible and broad spectrum, prompting EPR spectroscopy to be undertaken. The presence of a radical species (postulated as **5-XV**) was identifiable.

Targeting the borole radical **5-XV**, diluted reaction investigations was pursued for analysis with EPR spectroscopy in toluene solutions. Following preparation of **3-IV**, the reaction was undertaken in a vial in the glovebox and the mixture filtered into a quartz EPR tube. Analysis was sequentially undertaken at varied temperatures ranging from 20 °C to –40 °C, and with freezing down to –180 °C. However, the clearest hyperfine coupling was observed at room temperature (Figure 5.12).

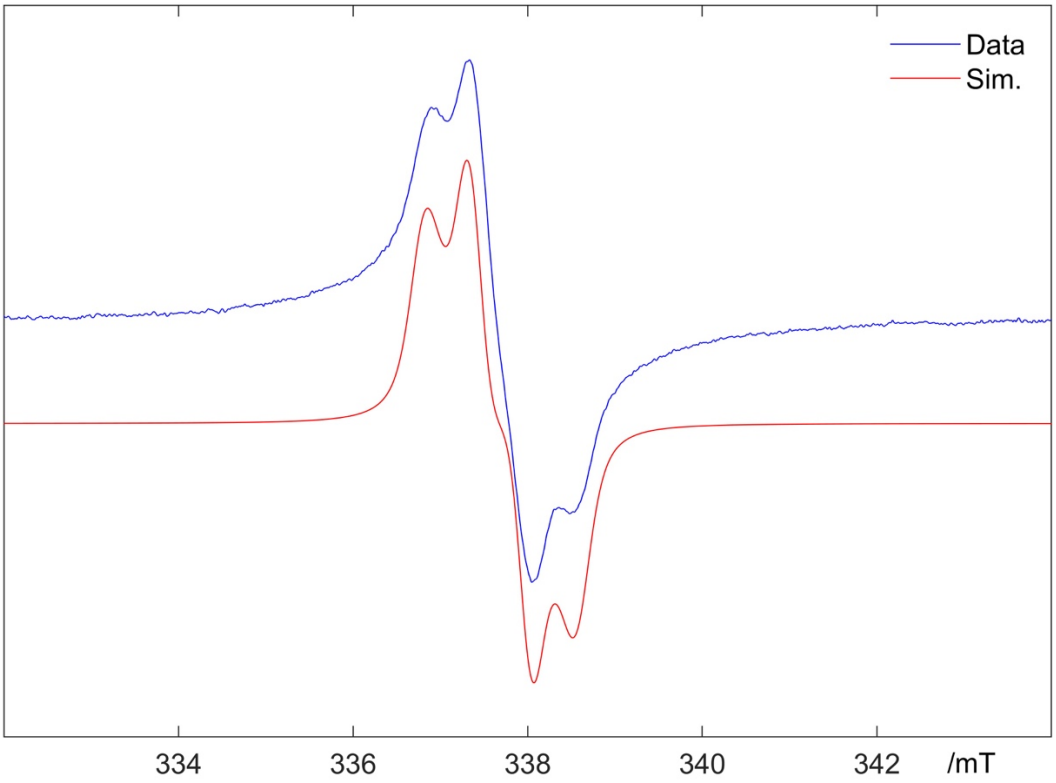

*Figure 5.12: EPR spectrum of meta-Xylyl substituted borole radical monoanion **5-XV**.*

Similarly identified within EPR investigations of *para*-Xylyl species **5-XIII**, the presence of postulated *meta*-Xylyl borole radical anion **5-XV** could be identified from EPR spectra. A signal was identified closely correlating to literature values, relating to an unpaired electron coupling to a ^{11}B nucleus (I = 3/2) was observed in an isotropic g value = 2.0034 (**5-XIII** 1.9620; **5.41** 2.0037; **5.44** 2.0025). However, Gauss values relating the hyperfine coupling constants of ^{11}B nucleus ($A(^{11}B)$ = 1.78 G) were notably lower than in the reported borole radical anions: **5-XIII** (4.73), **5.41** (3.73) and **5.44** (3.43).[48-49] Moreover, the simulated hyperfine coupling constant associated with the ^{1}H nucleus was also identified ($A(^{1}H)$ = 5.25 G), as highlighted within the signal via the stepped arrangement of hyperfine lines as presented within Figure 5.12. Taken on its own, the large ^{1}H hyperfine coupling can be connected to the two aromatic protons in the *ortho*- position of the *meta*-xylyl substituent, which are disposed orthogonally on either side of the aromatic BC_4 ring (on which the unpaired electron is delocalised across). This would act to enhance the hyperfine couplings to the two ^{1}H nuclei via the Overhauser effect,[72] and would account for their presence in the EPR spectrum. However, the absence of ^{1}H hyperfine coupling in the EPR spectrum of **5-XIII**, as well the markedly smaller ^{11}B coupling for **5-XV**, leaves room for uncertainty in its electronic structure particularly in the absence of similarly substituted-borole radicals within literature. The signal further emphasised the presence of an unpaired electron spin delocalisation about the central borole BC_4 ring from relatively small hyperfine coupling

constants of $A(^{11}B)$ = 4.73 G. This value could be compared with literature reported ferrocene-substituted borole radical anion **5.41**,[48] and the 1-mesityltetraphenylborole radical anion **5.44**,[49] both reported by Braunschweig and coworkers (Scheme 5.8). Consequently, a lower comparable isotropic g value was identified for **5-XIII** versus in **5.41** (2.0037) and **5.44** (2.0025), and a relatively larger hyperfine coupling constant ($A(^{11}B)$ = 3.73 G **5.41**; 3.43 **5.44**). These values were analogous for borole radical species, and notably smaller than values observed in triarylborane radical anions ($[Ph_3B]^{\cdot-}$ $A(^{11}B)$ = 7.84 G; $[Mes_3B]^{\cdot-}$ $A(^{11}B)$ = 10.32 G),[69] due to the increase in electronic delocalisation about the metallole heterocycle.

With increased time of reaction, clearer spectra could not be afforded when allowing suspended material to settle for multiple hours. To this end, the reaction mixture was kept further at ambient temperatures over the weekend. Subsequent ^{1}H NMR spectroscopy identified the complete consumption of **3-IV** to majority proligand **2-IV**. This matched prior observations, whereby the dialane species **5-XII** would degrade in the solution state to majority amine proligand and identifiable decomposition species following 48 hours at ambient temperature. Additionally, starting material **5-II** was identified as the only borole-related species present within solution. Toward the isolation of the yellow-brown precipitate, the reaction mixture was filtered and retentate washed with hexane until washings were colourless. Extraction with tetrahydrofuran afforded a bright red-orange solid, which was identified via ^{1}H NMR spectroscopy to feature a mixture of solvated dipotassium boroldiide $[\{K(THF)\}_2\{m\text{Xyl-BC}_4(2,5\text{-SiMe}_3)_2(3,4\text{-}m\text{Xyl})_2\}]$ and starting material **5-II**. Consequently, it was hypothesised that the radical target species **5-XV** had undergone a disproportionation to the corresponding dianion boroldiide **5-XVI** and starting material **5-II**.

5.3.2.4. 2-Electron Reductions of a *meta*-Xylyl Substituted Borole

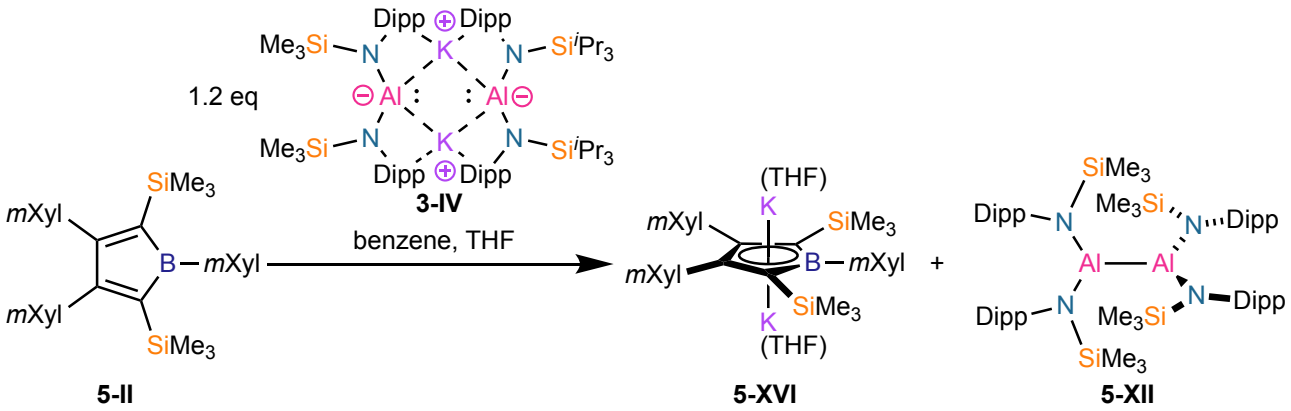

*Scheme 5.20: Stoichiometric 2-electron reduction of **5-II** with an acyclic aluminyl anion **3-IV** to afford the dipotassium boroldiide dianion **5-XVI** and dialane **5-XII**.*

A benzene solution of **3-IV** was prepared was treated with *m*Xyl-borole **5-II** (Scheme 5.20). An immediate orange colour change was identifiable, and the reaction mixture was then stirred for 1 hour in a vial within a glovebox. Removal of volatiles afforded an orange solid, which was washed with hexane until the washings were colourless. The isolated orange solid was dried and then taken up in tetrahydrofuran, affording a vibrant red solution that could be evaporated to give a red powder. ^{1}H NMR spectroscopy of this product in C_6D_6 identified the formation of the solvated dipotassium borolediide [{K(THF)}$_2${*m*Xyl-BC$_4$(2,5-SiMe$_3$)$_2$(3,4-*m*Xyl)$_2$}] **5-XVI**.

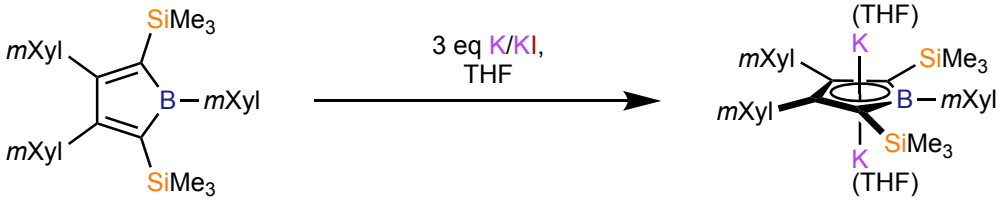

5-II **5-XVI**

*Scheme 5.21: Preparations of dipotassium borolediide dianion **5-XVI** from reductions with potassium reducing agents.*

Following the preparation of the solvated dipotassium borolediide **5-XVI** through reductions with the acyclic aluminyl species **3-IV**, the group's regular method to prepare **5-XVI** via potassium reducing agents was completed (Scheme 5.21). Treatment of a tetrahydrofuran solution of **5-II** with 5% w/w K/KI afforded an initial dark red oily solid. Hexane washings afforded an orange solid, which was dried *in vacuo* for two hours. ^{1}H NMR spectroscopic analysis was conducted on a deuterated benzene solution with two drops of deuterated tetrahydrofuran and identified the clean formation of **5-XVI**. Comparatively, spectra from both the 5% w/w K/KI and acyclic aluminyl reductions identified the formation same species with tetrahydrofuran present following washing and additions to aid in solubility. Notably, minor differences in chemical shift could be attributed to a greater concentration of tetrahydrofuran within analysis from aluminyl species rather than in potassium reductions.

5.3.2.5. 1-Electron Reductions of a Chloroborole

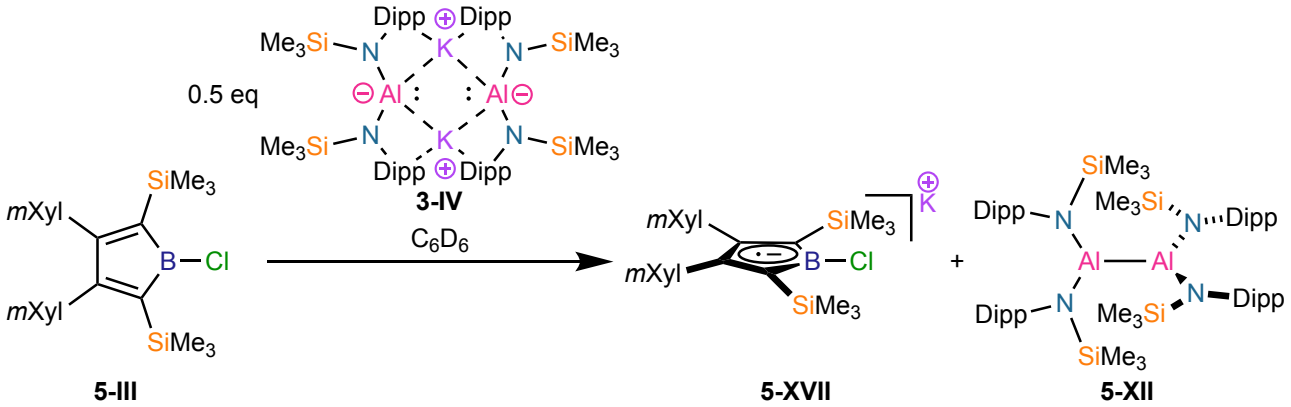

*Scheme 5.22: Stoichiometric 1-electron reduction of **5-III** with an acyclic aluminyl anion **3-IV** to afford a postulated borole radical **5-XVII** and dialane **5-XII**.*

Continuing the reactivity studies, the Xyl-substituted chloroborole **5-III** and **3-IV** a solution of **3-IV** was treated with solid **5-III** (Scheme 5.22). Upon addition of the chloroborole **5-III**, an immediate colour change to a maroon solution was identified. Immediate ^{1}H NMR spectroscopic analysis of the reaction solution identified the formation of the dialane **5-XII** species and residual unreacted chloroalumole within solution. Similarly observed with the formation of **5-XVII** radical species, the lack of signals corresponding borole-related species was attributed to paramagnetic nature of the target species **5-XVII**. It was not possible to undertaken analysis via EPR spectroscopy to confirm the presence and nature of paramagnetic species, due to a lack of time.

Markedly, the storage of reaction mixtures for multiple days at ambient temperature led to the growing prevalence of signals within the ^{1}H NMR spectra. Following 6 days, an indiscernible mixture of species was afforded. However, signals relating to borole **5-III** were observed to be notably greater than initial preparations. This was rationalised via the degradation of postulated formed target species **5-XVII**, to a mixture of diamagnetic decomposition products. Attempts to purify any species via crystallisation attempts from benzene or tetrahydrofuran were unsuccessful.

5.3.2.6. 2-Electron Reductions of a Chloroborole

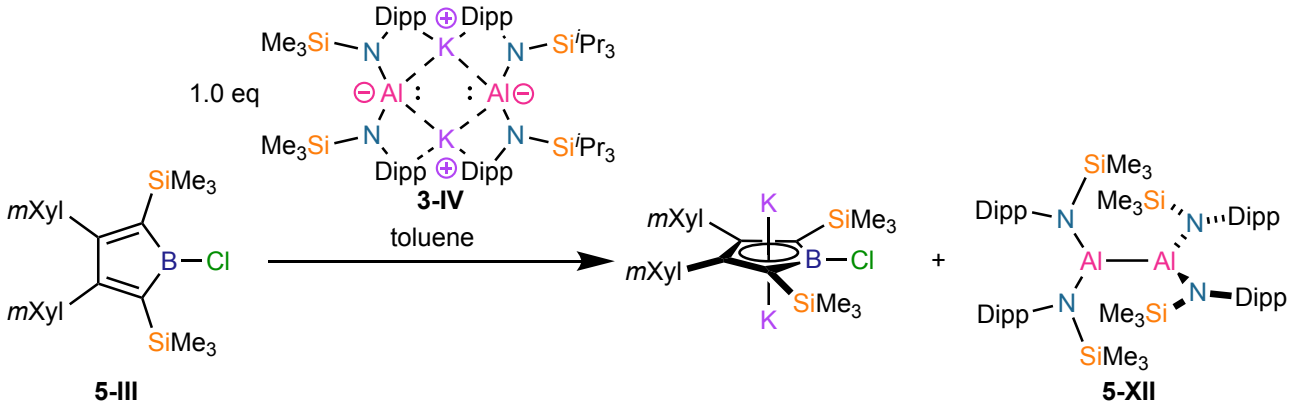

*Scheme 5.23: Stoichiometric 2-electron reduction of **5-III** with an acyclic aluminyl anion **3-IV** postulated to afford a dipotassium boroledиide dianion **5-XVIII** and dialane **5-XII**.*

To a freshly prepared solution of **3-IV** was added chloroborole **5-III**, yielding a very dark-red solution (Scheme 5.23). ^{1}H NMR spectroscopic analysis detected the formation of multiple species. Notably, evidence of the formation of target species **5-XVIII** could be identified in addition to dialane **5-XII**, however, multiple other species including unreacted **5-III** starting material were also afforded. Attempts to target a thermodynamic product by heating the tube to 60 °C for 18 h. From ^{1}H NMR spectroscopy, the complete degradation of the dialane species **5-XII** to single, unisolable [N(Dipp)SiMe$_3$]$^-$ containing species was observed. Moreover, multiple borole-related degradation derivatives identified as featuring aryl and trimethylsilyl functional groups could be observed within the indiscernible mixture of species. Crystallisation attempts from saturated benzene, hexane and tetrahydrofuran solutions were unsuccessful to afford any crystalline material.

5.3.3. Targeted Preparations of an Acyclic Aluminium(II) Dimer

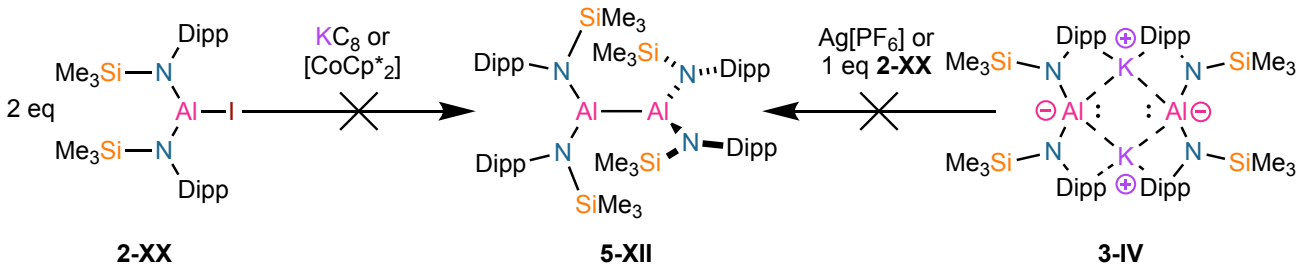

*Scheme 5.24: Attempted syntheses to afford acyclic dialane species **5-XII**.*

Following the replicable and consistent formation of dialane **5-XII** in the abovementioned borole reductions, more direct preparations of the dialane were undertaken (Scheme 5.24). As eluded to in **Chapter 3**, the preparation of dialane species via the treatment of aluminyl anions with their associated aluminium iodide precursors are often a reliable synthetic approach. Markedly, this could not be

replicated with acyclic species whereby, rather than undergoing comproportionation from aluminium(I) and aluminium(III) to the target aluminium(II) species, no evidence of the dialane **5-XII** could be identified. Instead, the proligand amine degradation species (HN(Dipp)SiMe$_3$ **2-IV**) as the major product by ^{1}H NMR Spectroscopy.

Attempting to perform a 1-electron oxidation of the aluminium(I) **3-IV** with silver hexaflurophosphate, similarly the oxidation of aluminyl species as observed with boroles was also unsuccessful, leading to the majority formation of the proligand **2-IV** as the major product.

The majority formation of **2-IV** was similarly identified via ^{1}H NMR spectroscopy following stoichiometric attempts to reduce the aluminium(III) iodide **2-XX** with potassium graphite. Moreover, reduction attempts of **2-XX** with a single equivalent of decamethylcobaltocene to afford a corresponding aluminium(II) radical for dimeric coupling to the dialane species **5-XII** were also attempted. Notably, despite elevated temperatures, no reaction was observed by ^{1}H NMR spectroscopy. This could be attributed to the high degree of steric encumberment afforded from the bulky acyclic ligand systems and/or the lower reduction potential of the reducing agent.

Despite attempts, the preparation of dialane **5-XII** was not possible other than from the reduction of boroles. Irrespective of reduction or oxidation attempts, the majority species afforded from various investigations was the proligand **2-IV**.

5.3.4. Summary of Borole Reductions with an Acyclic Aluminyl Anion

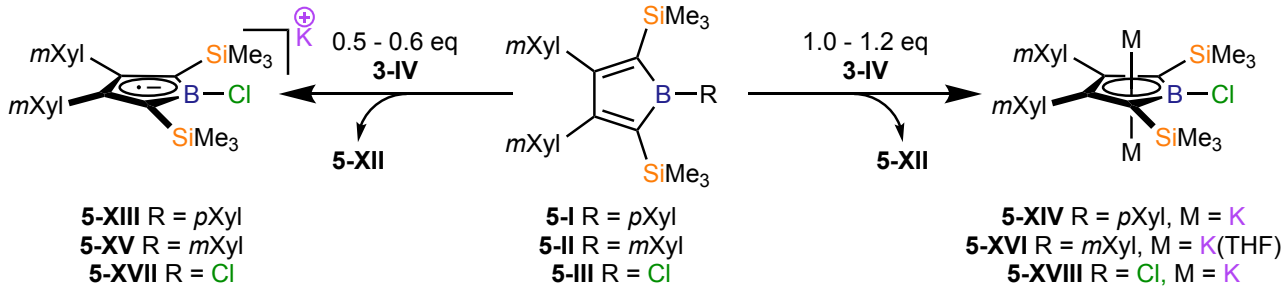

*Scheme 5.25: Summary of reactions with the acyclic aluminyl anion **3-IV** and the boroles **5-I** – **5-III**.*

The applications of an acyclic aluminyl system as a reducing agent with three borole species of the same C$_4$ scaffold were explored (Scheme 5.25). Borole products indicative of 1- and 2-electron reductions were afforded from boroles **5-I**–**5-III**, with evidence of both monoanion borole radicals (**5-XIII**, **5-XV**, **5-XVII**), and dianionic boroledиide (**5-XIV**, **5-XVI**, **5-XVIII**) species through NMR and EPR spectroscopy. Of the radical species, **5-XIII** and **5-XV** were characterised via EPR spectroscopy and found to present isotropic g values of 1.9620 and 2.0034 respectively, aligning with previously identified borole radical species (**5.41** 2.0037; **5.44** 2.0025). Moreover, hyperfine ^{11}B coupling

constants ($A(^{11}B)$ = **4.73 5-XIII**; 1.78 G **5-XV**) were lower than values presented by triarylborane radical anions ($[Ph_3B]^{\cdot-}$ $A(^{11}B)$ = 7.84 G; $[Mes_3B]^{\cdot-}$ $A(^{11}B)$ = 10.32 G),[69] relating the delocalisation of electron density about the planar BC_4 heterocycle. Following the preparation of dianionic species, the acyclic aluminyl anion was found to be an effective reducing agent. Even though the boroledиide species were not isolated, their ^1H NMR spectra were cross-referenced with reactions with other potassium-based reducing reagents, confirming their formation.

Syntheses affording reduced borole species all saw the oxidation of the aluminyl species **3-IV** from aluminium(I) to aluminium(II) in the dialane **5-XII**. **5-XII** was isolated via crystallisations and further confirmed via SCXRD. Attempts to rationally target **5-XII** were undertaken via the stoichiometric reduction of corresponding precursor [AlI{N(Dipp)SiMe$_3$}$_2$] **2-XX** with potassium graphite or decamethylcobaltocene, and stoichiometric oxidation of acyclic aluminyl with Ag[PF_6], however, all were unsuccessful.

5.4. Results and Discussion: Alumoles

5.4.1. Synthesis of Haloalumoles and their Lewis Acid-Base Adducts

Previous investigations to prepare alumoles species from the 1,4-dilithiobutadiene starting materials had been explored by Dr. Tobias Heitkemper. Utilising the Ph* furnished **5-V**, afforded the preparation of a Lewis base stabilised chloroalumole etherate **5-XIX**. However, the less bulky **5-IV** had not been utilised to access alumoles. Moreover, given the literature prevalence for Lewis acid-base alumole adducts,[7, 56-60] initial investigations centred upon utilising diethyl ether and tetrahydrofuran as coordinating solvents.

5.4.1.1. Synthesis of Lewis Base Stabilised Chloroalumole Etherate Adduct

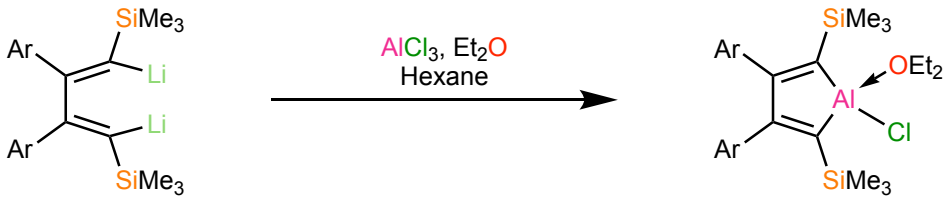

5-V Ar = Ph*
5-IV Ar = *m*Xyl

5-XIX Ar = Ph*, 19%
5-XX Ar = *m*Xyl, 75%

*Scheme 5.26: Syntheses affording Lewis base stabilised chloroalumole etherate species **5-XIX** and **5-XX**.*

Following the reported synthesis of **5-XIX**, a parallel synthetic route was pursued to afford the analogous Lewis-base stabilised chloroalumole etherate adduct **5-XX** (Scheme 5.26). To this end, a colourless diethyl ether solution of aluminium trichloride was treated with a dark-red solution of **5-IV**. After stirring the mixture for 2.5 hours at ambient temperature, the solution had become yellow with

a colourless precipitate, from which volatiles were removed and products extracted with hexane. Concentration of the hexane solution under reduced pressure afforded the initial deposition of crystalline material. Subsequent crystallisations and concentrations would afford crops of **5-XX** (75%) as a collection of light-yellow crystalline plates, which were characterised via heteronuclear NMR spectroscopy. Moreover, SCXRD analysis confirmed the formation of the targeted chloroalumole etherate adduct **5-XX** (Figure 5.13).

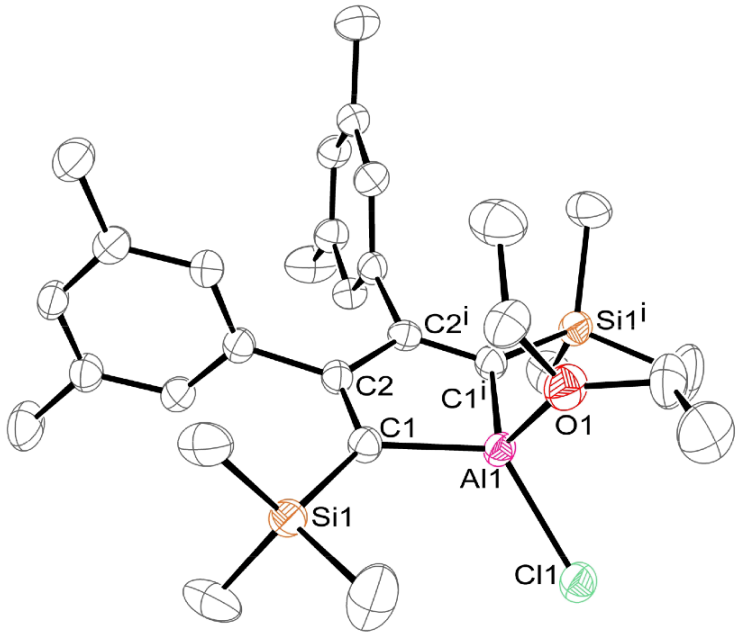

*Figure 5.13: Molecular structure of [ClAl{C_4(2,5-$SiMe_3$)$_2$(3,4-mXyl)$_2$}(OEt_2)] **5-XX** as determined by X-ray crystallography. Thermal ellipsoids set to 50% probability. Hydrogen atoms and toluene solvent molecules omitted for clarity. Selected bond lengths (Å) and angles (°): Al1-Cl1 2.2248(14), Al1 O1 1.889(3), Al1-C1 1.955(3), C1-C2 1.355(3), C2-C2 1.527(5), O1-Al1-Cl1 102.06(10), C1-Al1-C1 94.51(15).*

5-XX is monomeric in the solid state and features a tetracoordinate aluminium(III) centre, due to the coordination of an equivalent of diethyl ether. A distorted tetrahedral arrangement is presented with the solvent molecule and chloride ligand located above and below the AlC_4 metallocyclic plane. Identifiable from C-C (1.527(5) Å) and C=C (1.355(3) Å) bond lengths, the installed butadiene arrangement within the backbone is retained within the alumole species. Moreover, to accommodate the steric bulk of *meta*-Xylyl moieties, these are arranged in a nearly perpendicular alignment to the AlC_4 plane.

5.4.1.2. Preparative Investigations of a Lewis Acid-Base Stabilised Iodoalumole Etherate

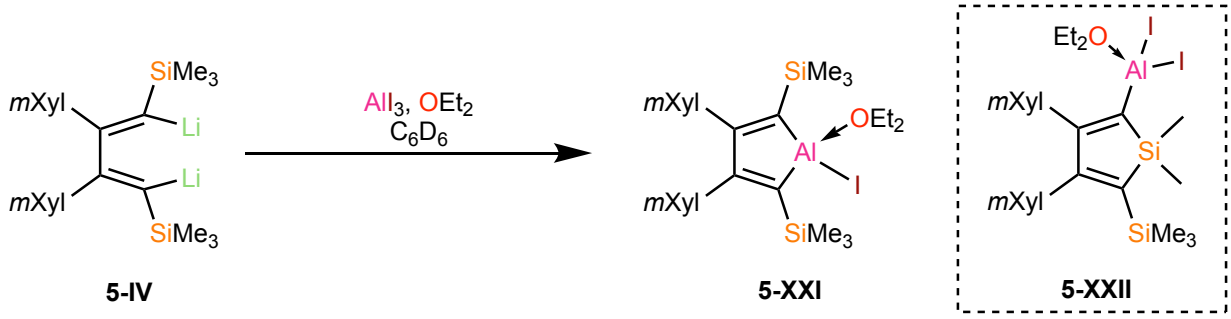

5-IV **5-XXI** **5-XXII**

*Scheme 5.27: Synthetic attempt to diethyl ether-solvated iodoalumole species **5-XXI**, and crystallographically isolated rearrangement product **5-XXII**.*

Seeking to expand the minimal number literature-reported iodoalumole examples,[55, 57-58] investigations toward affording such a species were undertaken. Initial investigations within a J. Young's NMR tube entailed the dissolution of **5-IV** and aluminium triiodide in a solution of deuterated benzene solution and diethyl ether. Following a brief period of agitation and confirmation of conversion via ^{1}H NMR spectroscopy, the volatiles were then removed. Addition of further deuterated benzene to the sample and analysis via heteronuclear NMR spectroscopy identified the synthesis of a species featuring near identical signals and splitting patterns to solvated chloroalumole **5-XX** in high yields (91%). Consequently, the targeted solvated iodoalumole species **5-XXI** was postulated as having formed. Attempts to afford SCXRD quality crystals from the dark red-orange solution were attempted and further pursued in coordinating and non-coordinating solvents, but were unsuccessful.

Subsequent scaled reactions were also undertaken toward the isolation of **5-XXI,** yielding varied results. In a single example, additional dilithiodibutadiene **5-IV**, aluminium triiodide and diethyl ether was added to the mother liquor following the poor conversion initially to **5-XXI**. This poor conversion was attributed to potential solvent effects with less diethyl ether relative to reagents than in high conversion reactions. Consequently, the scaling of the reaction afforded the subsequent isolation of target **5-XXI** in poor but isolated yields as a light brown solid (24%). From scaled reaction investigations, crystallisations were also attempted but unable to isolate SCXRD quality crystals of target iodoalumole **5-XXI**. Rather, crystallisations afforded a single crystalline example of an unexpected rearrangement product **5-XXII** (Figure 5.14).

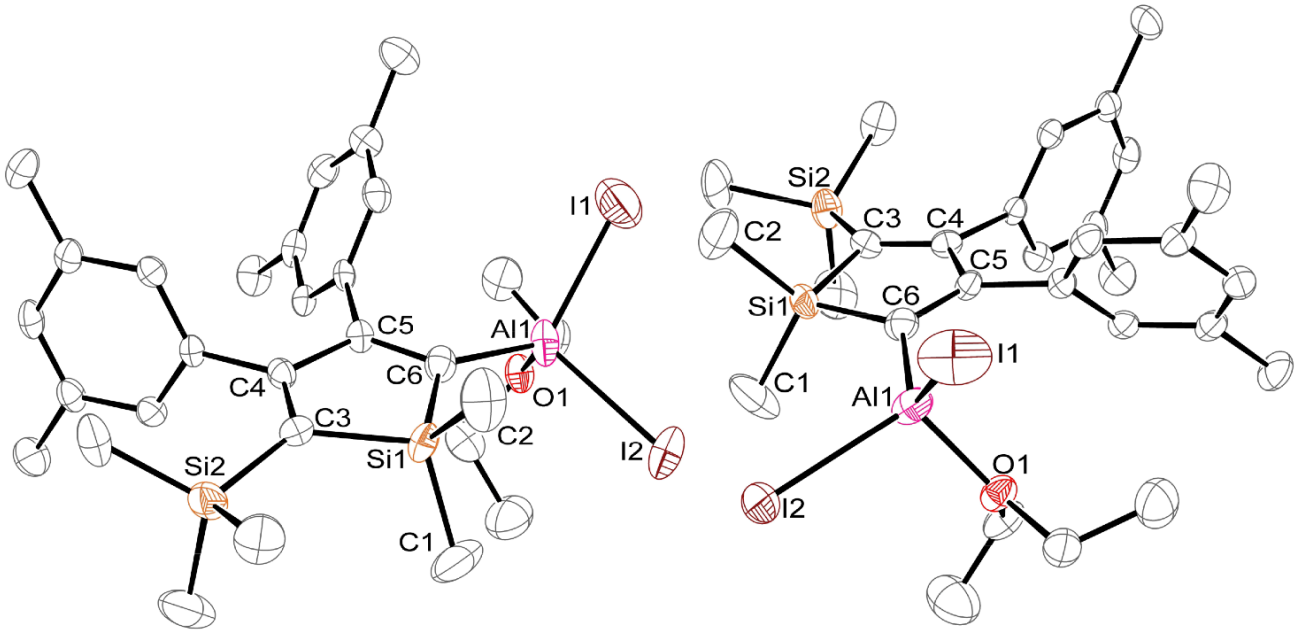

*Figure 5.14: Molecular structure of rearrangement species **5-XXII** as determined by X-ray crystallography and shown from two orientations. Thermal ellipsoids set to 50% probability. Hydrogen atoms and toluene solvent molecules omitted for clarity Selected bond lengths (Å) and angles (°): Si1-C1 1.851(9), Si1-C2 1.868(9), Si1-C3 1.866(7), Si2-C3 1.868(7), Si1-C6 1.859(7), Al1-C6 1.936(7), Al1-O1 1.867(5) Al1-I1 2.478(2), Al1-I2 2.583(4), C4-C3 1.339(9), C5-C6 1.355(9), C5-C4 1.508(9), C1-Si1-C2 109.9(5), C3-Si1-C6 94.4(3), O1-Al1-I1 105.49(18).*

Shown in Figure 5.14, **5-XXI** had undergone a rearrangement to afford a dimethyl-substituted silacyclopentadiene (silole) species **5-XXII**, a heavier group 14 analogue of cyclopentadiene.[73] The central silicon atom in **5-XXII** features a 4-coordinate geometry with two methyl groups, and is contained within the greater C_4 ligand scaffold. The identity of this central silicon(IV), given its substituents, may be attributed to it previously being one of the two trimethylsilyl groups originally found at the 2- and 5- positions within **5-XXI**. Consequently, the 2-position of the C_4 scaffold features a tetracoordinate aluminium(III) centre with two iodo substituents and a diethyl ether solvate. Despite rearrangement of the aluminium and silicon centres, the butadiene C_4 backbone arrangement in **5-XXII** is retained within the silole species as identifiable from C-C (1.508(9) Å) and C=C (1.339(9), 1.355(9) Å) bond lengths. Due to the increased sterics of diethyl ether adduct upon the aluminium centre, one backbone *meta*-Xylyl moiety observes rotation that is not perpendicular to the SiC_4 heterocyclic plane. Despite attempts, reproducing the synthesis and isolating **5-XXII** was not realised due to the formation of indiscernible mixtures of species.

5.4.1.3. Preparation of a Tetrahydrofuran Chloroalumole Adduct

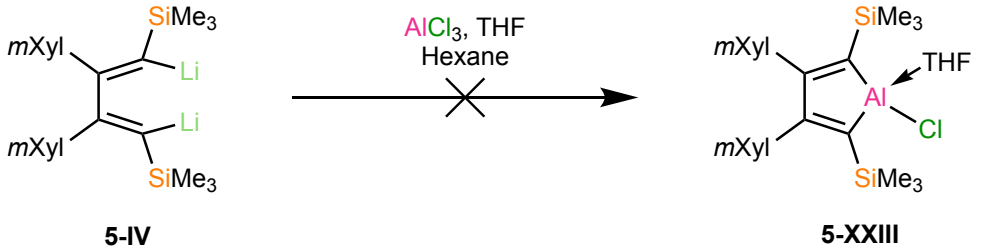

5-IV **5-XXIII**

*Scheme 5.28: Attempted synthesis of tetrahydrofuran analogue **5-XXIII** of **5-XX** via an analogous salt metathesis.*

Inspired by successes afforded via diethyl ether synthetic routes affording **5-XIX** and **5-XX**, attempts to make the tetrahydrofuran adduct of **5-XX** were pursued (Scheme 5.28). In a glovebox, colourless aluminium iodide and dark red **5-IV** tetrahydrofuran solutions were combined within a reaction vial. Following 18 hours of stirring at ambient temperature, volatiles were removed under reduced pressure from the now yellow solution. Dried as a yellow oil, the formation of **5-XXIII** was postulated following extractions with hexane affording a colourless precipitate attributed to the lithium chloride by-product. Subsequent crystallisation attempts to afford SCXRD quality samples of **5-XXIII** were unsuccessful, with only initial NMR data collected to identify species afforded.

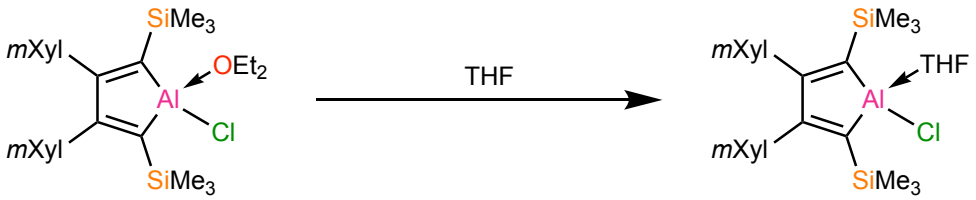

5-XX **5-XXIII** >98%

*Scheme 5.29: Preparation of tetrahydrofuran adduct **5-XXI** via displacement of diethyl ether.*

In addition to salt metathesis routes, attempts to displace the coordinated diethyl ether from the aluminium centre in **5-XX** with tetrahydrofuran were explored (Scheme 5.29). To a benzene solution of **5-XX** was added tetrahydrofuran, and the reaction mixture was agitated for 2 hours. Following confirmation of conversion via ^{1}H NMR spectroscopy, volatiles were removed under reduced pressure for multiple hours. To the afforded yellow oil, further deuterated benzene was added and ^{1}H NMR spectroscopy identified the clean conversion to tetrahydrofuran solvated target species **5-XXIII** (>98%). Similarly observed from salt metathesis routes, attempts to crystallise target alumole species from aliphatic and coordinating solvents were unsuccessful. Attempts toward remove the coordinating solvents diethyl ether and tetrahydrofuran under reduced pressure for an extended multiple hours and overnight were unsuccessful. Further attempts undertaken at elevated temperatures (50 – 80 °C) led to the degradation into an indiscernible mixture of species.

5.4.1.4. Synthesis of NHC-Stabilised Chloroalumoles

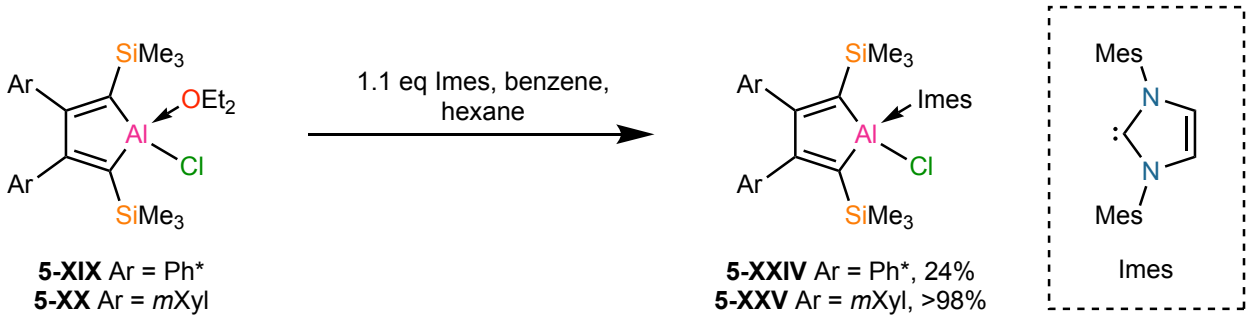

5-XIX Ar = Ph*
5-XX Ar = *m*Xyl

5-XXIV Ar = Ph*, 24%
5-XXV Ar = *m*Xyl, >98%

*Scheme 5.30:Preparations of the NHC-coordinated chloroalumoles **5-XXIV** and **5-XXV**.*

Toward expanding NHC-furnished alumole examples from Idipp bromoalumole **5.73** reported by Tokitoh and coworkers,[57] investigations were undertaken with the analogous Imes carbene (Imes = C{N(C_6H_2-2,4,6-Me_3)CH}$_2$). Addition of Imes to both of the diethyl ether-solvated chloroalumole species **5-XIX** and **5-XX**, led to quantitative conversion to the corresponding Imes adducts species **5-XXIV** and **5-XXV**, as determined by ^{1}H NMR spectroscopy.

Increasing the scale and attempting to isolate **5-XXIV** and **5-XXV** was conducted within reaction vials in a glovebox (Scheme 5.30). Following the treatment of solvated chloroalumole species **5-XIX** and **5-XX**, with a slight excess of Imes afforded dark yellow and colourless solutions, respectively. Following stirring, evaporation of the solvent was conducted. Consequential of unsuccessful crystallisation attempts from hexane, removal of volatiles under reduced pressure afforded **5-XXV** as a colourless needle-like solid in near quantitative yields (>98%). Crystallisation of the bulkier **5-XXIV** from hexane yielded SCXRD quality material as large colourless crystals (Figure 5.15). Heteronuclear NMR spectroscopy was conducted in the characterisation of both **5-XXIV** and **5-XXV**, presenting similar ^{1}H NMR signals associated with coordinated Imes and ^{29}Si signals related to trimethylsilyl groups situated upon each C_4 scaffold. The collection of SCXRD quality crystals of **5-XXIV** allowed for its structural confirmation via X-ray diffraction (Figure 5.15).

Similarly identified within previously discussed alumole solid-state structures, the aluminium(III) centre of **5-XXIV** is tetracoordinate featuring the C_4 scaffold bidentate ligand, a terminal chloride and furnished with Imes NHC (Figure 5.15). Similarly, as observed with the molecular structure of diethyl ether solvated **5-XX**, the chloride and Lewis-base are situated above and below the C_4 scaffold. Comparative the installed Al-C interaction with NHC moiety in Idipp furnished **5.73** (2.081(2) Å), is akin in **5-XXIV** with slight bond elongation (2.107(2) Å) likely attributed to a slight steric increase in 2,5-trimethylsilyl substituents in **5-XXIV** relative to 2,5-ethyl moieties in **5.73**.[57]

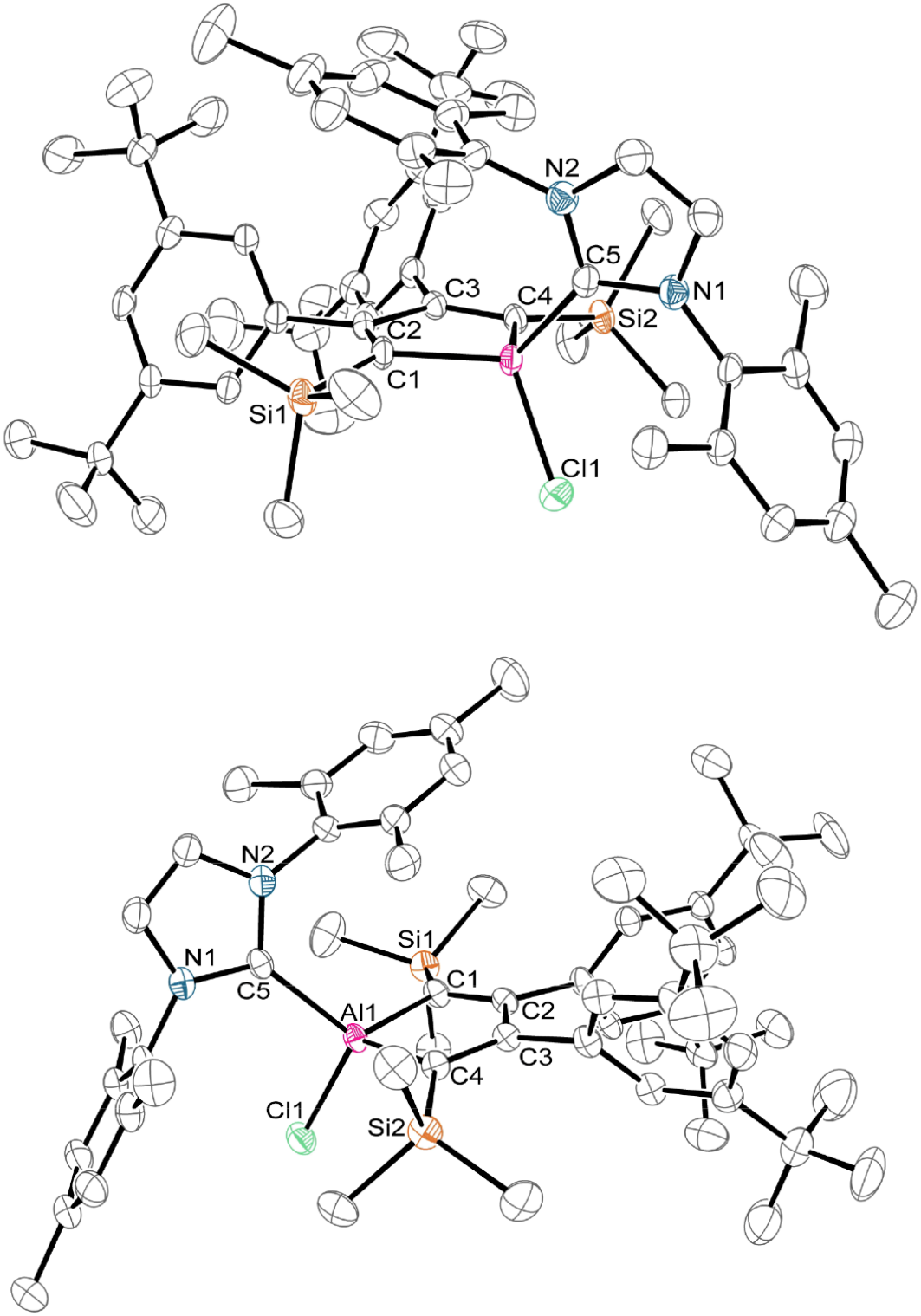

*Figure 5.15: Molecular structure of [ClAl(C$_4${2,5-SiMe$_3$}$_2${3,4-*Ph**}$_2$)(Imes)]* ***5-XXIV*** *as determined by X-ray crystallography and shown from two orientations.. Thermal ellipsoids set to 50% probability. Hydrogen atoms and toluene solvent molecules omitted for clarity. Selected bond lengths (Å) and angles (°): Al1-C5 2.107(2), Al1-Cl1 2.1781(9), Al1-C1 1.974(2), Al1-C4 1.983(2), C1-C2 1.347(3), C3-C4 1.364(3), C2-C3 1.531(3), C5-Al1-Cl1 106.12(7), C1-Al1-C4 92.50(10).*

5.4.1.5. Synthesis of Lithium Dichloroalumole Aluminate

To expand successes with solvated haloalumole species (**5-XX**, **5-XXI**, **5-XXIII**), investigative focusses sought the preparation of "free" haloalumoles, analogous to the chloroalumole [$ClAlC_4Et_4$] **5.58** reported by Tokitoh and coworkers.[57] To this end, salt metathesis investigations were undertaken in aromatic solvents (benzene, toluene) between the dilithiodibutadiene **5-IV** and aluminium halides (chloride, iodide). Notably, investigations with both aluminium halide reagents in toluene afforded indiscernible mixtures of products.

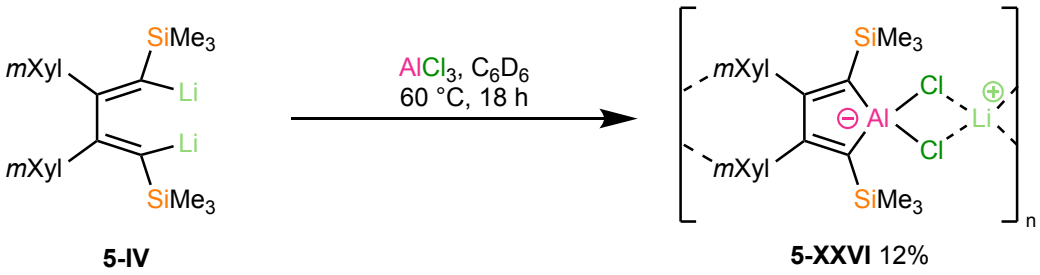

5-IV **5-XXVI** 12%

*Scheme 5.31: Preparation of lithium dichloroalumole aluminate species **5-XXVI**.*

Salt metathesis preparations of aluminium chloride and **5-IV** in benzene at 60 °C afforded the formation of a new species (Scheme 5.31). Prepared via the dissolution of reagents in benzene and subsequent sonication to assist with solubility, the reaction mixture was heated to 60 °C overnight. Following heating, the initially dark red solution had become a burnt-orange solution with a colourless suspension. Allowing the reaction mixture to cool undisturbed to ambient temperatures gave colourless crystals of sufficient quality for SCXRD, which confirmed the preparation of dichloroaluminate aluminate species **5-XXVI** (Figure 5.16 and Scheme 5.31).

Isolation of crystals following the decanting of the burnt-orange solution and suspending and washing the material with toluene afforded clean, uniform samples in a low yield (12%). Notably, attempts to isolate further material from toluene washings and subsequent crystallisations were unsuccessful. Moreover, the notably decreased solubility of **5-XXVI** in aromatic solvents at ambient temperatures made undertaking heteronuclear NMR spectroscopy challenging, whereby only ^1H spectra could be collected.

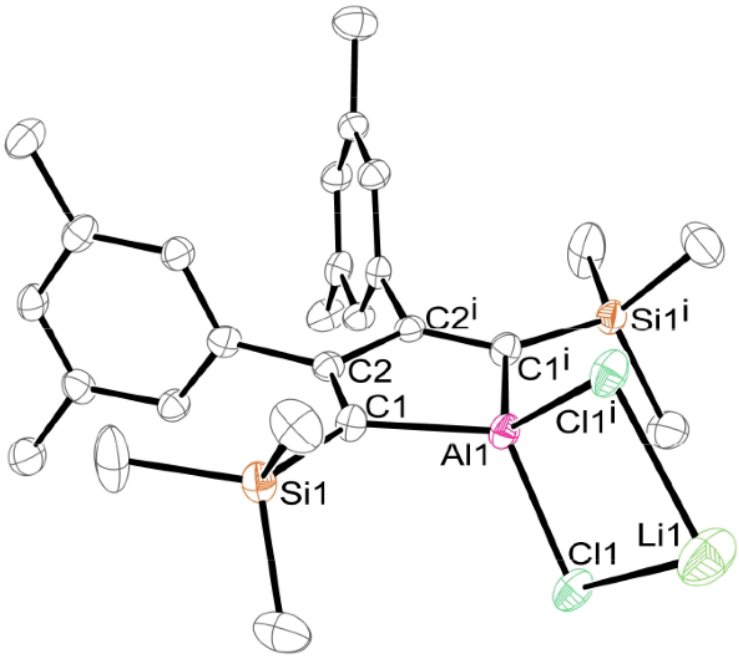

*Figure 5.16: Molecular structure of [Li(Cl$_2$Al{C$_4$(2,5-SiMe$_3$)$_2$(3,4-m*Xyl*)$_2$})]$_n$* ***5-XXVI*** *as determined by X-ray crystallography. Thermal ellipsoids set to 50% probability. Hydrogen atoms omitted for clarity. Selected bond lengths (Å) and angles (°): Al1-Cl1 2.2366(11), Li1-Cl1 2.515(7), Al1-C1 1.978(3), C1-C2 1.354(4), C2-C2^i 1.522(5), Cl1-Li1-Cl^i 82.3(3), Cl1-Al1-Cl^i 95.39(6), C1-Al1-C^i 93.27(18).*

Identifiable within the solid-state structure, **5-XXVI** features the installation of an aluminium centre into the C$_4$ scaffold. Similarly observed within prepared alumoles and silole species, the unsaturated butadiene backbone is retained (C=C 1.354(4), C–C 1.522(5) Å). As the four-coordinate aluminium(III) centre features 4 anionic donors, a lithium cation is present balancing the monanionic charge of the aluminate. Notably, **5-XXVI** exists as a 1-dimensional coordinational polymer, whereby the lithium cation associated with both chloride centres featured arene-interactions with the *meta*-Xylyl backbone groups of the next alumole monomer.

Further reinforced by **5-XXVI**, preparative attempts toward the isolation of "free" alumole species necessitate the need for increased steric bulk about the aluminium centre. Consequently, investigative focussed sought to utilise aryl substituents to further explore accessible alumole complexes featuring a 2,5-disilyl ligand scaffold.

5.4.2. Investigations to Afford Aryl-Coordinated Alumoles

With the reliable synthesis of the diethyl ether chloroalumole adducts **5-XIX** and **5-XX**, initial investigations were undertaken towards the preparation of "free" alumoles. Inspired by the preparation of **5.6** [Mes*AlC_4Et_4] by Tokitoh and coworkers, investigations were conducted with an aryllithium reagent to install a bulky aryl group to the aluminium centre.[8]

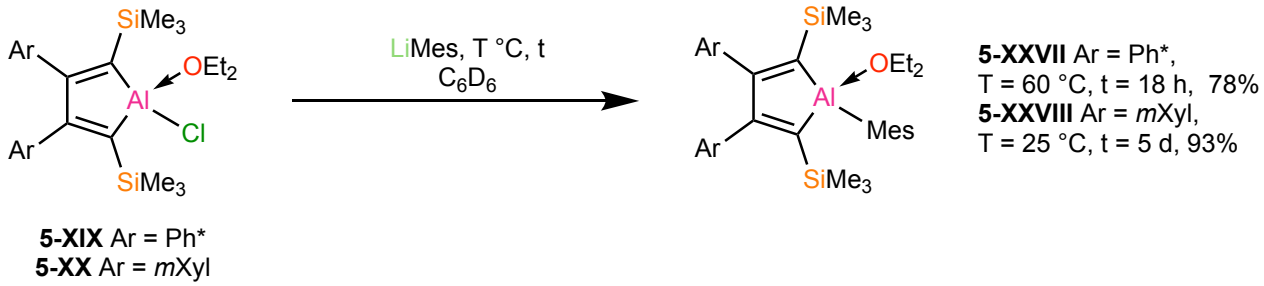

Scheme 5.32: Preparation of aryl substituted alumole complexes and ^1H NMR identified conversion yields.

Replicating NHC-based investigations, attempts toward furnishing aluminium centres with aryl groups were explored with the corresponding chloroalumole species **5-XIX** and **5-XX**. 20 mg scale inquiries in J. Young's NMR flasks featured the treatment of **5-XIX** and **5-XX** with mesityl lithium and conversion to the target aryl furnished species **5-XXVII** and **5-XXVIII** was identified by ^1H NMR spectroscopy (Scheme 5.32). The less sterically encumbered species, **5-XXVIII** was obtained after 5 days of being agitated at ambient temperature. Larger scale preparations were completed in a vial afforded a moderate isolated yield (50%). Conversely, Ph* furnished species **5-XXVII** was afforded following 18 hours of heating at 60 °C, however, investigations at larger scales were not conducted. Notably, attempts to shorten reaction times through elevated temperatures (80 °C) did not afford the target *m*Xyl species **5-XXVIII**.

All attempts to crystallise **5-XXVII** and **5-XXVIII**, were undertaken from saturated aromatic and aliphatic solutions. Whilst these efforts to crystallise **5-XXVII** were unsuccessful, a saturated hexane solution of **XXVIII** cooled to –40 °C yielded crystals of sufficient quality for X-ray diffraction (Figure 5.17).

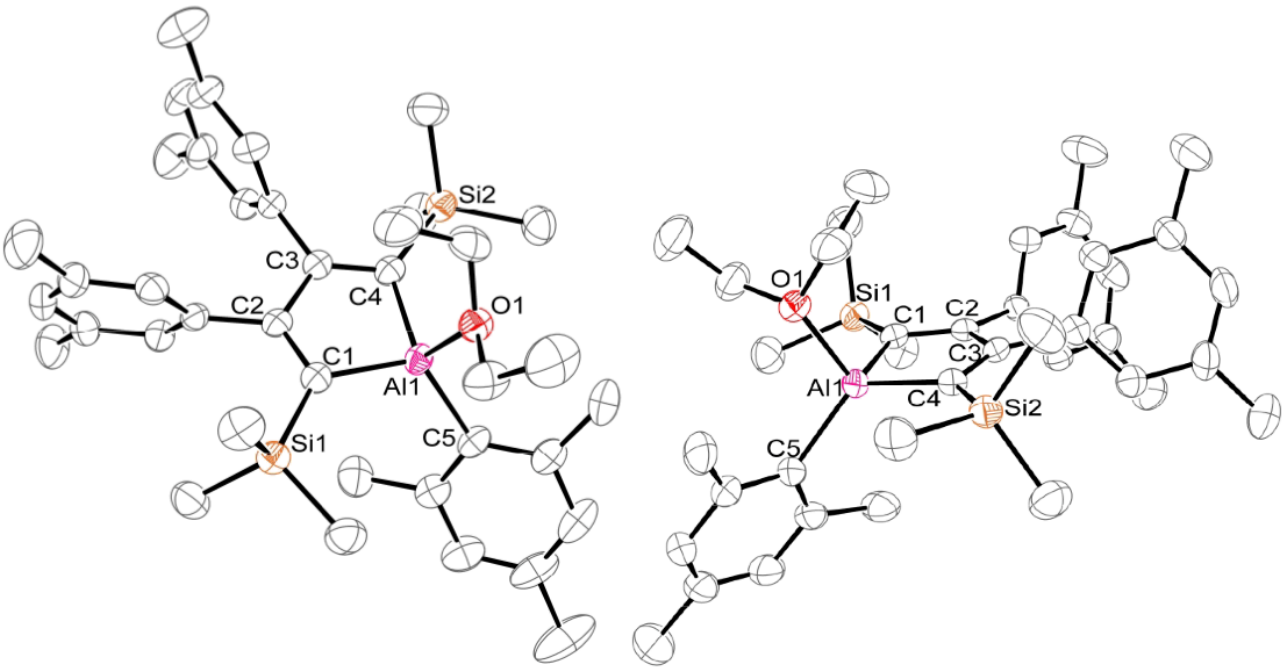

*Figure 5.17: Molecular structure of [(Mes)Al{C_4(2,5-$SiMe_3$)$_2$(3,4-m*Xyl*)$_2$}(OEt_2)]* ***5-XXVIII*** *as determined by X-ray crystallography. Thermal ellipsoids set to 50% probability. Hydrogen atoms and hexane solvent molecules omitted for clarity. Selected bond lengths (Å) and angles (°): Al1-C5 1.999(3), Al1-O1 1.937(2), Al1-C1 1.984(3), Al1-C4 1.968(3), C1-C2 1.355(4), C3-C4 1.358(4), C2-C3 1.526(4), O1-Al1-C5 107.39(12), C1-Al1-C4 93.63(13).*

From solid state structure, the aluminium(III) centre of **5-XXVIII** is 4-coordinate, featuring a diethyl ether molecule and a further 3 organoaluminium bonds. A single mesityl group has been installed upon the aluminium centre, following the substitutiuon of terminal chloride ligand in starting material **5-XX**. Similar to previous species, the unsaturated C_4 butadiene scaffold is retained, incorporating the metal centre into a planar 5-membered heterocycle. Accommodating for the steric encumberment of the retained diethyl ether solvent and installed aryl group, these moieties are each positioned above and below the heterocycle plane.

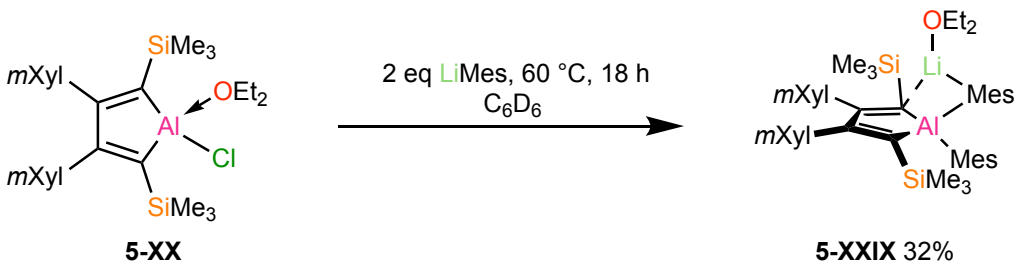

5-XX **5-XXIX** 32%

Scheme 5.33: Synthesis of dimesityl substituted alumole complex ***5-XXIX****.*

As highlighted above, attempts to reproduce the synthesis of **5-XXIX** with the less sterically encumbered *m*Xyl analogue **5-XX** through elevated temperatures (60 – 80 °C) did not yield the

preferential formation of monoaryl species **5-XXVIII**. Rather, ^{1}H NMR spectroscopy identified the formation of a previously unidentified product. Consequently, crystallisation attempts were successful in identifying the formation of dimesityl substituted alumole complex **5-XXIX** via X-ray diffraction (Figure 5.18). Consequently, the stoichiometry could be adjusted toward the targeted preparation of **5-XXIX** with 2 equivalents of mesityl lithium (Scheme 5.33). A high rate of conversion (88%) to targeted species **5-XXIX** occurred after the mixing of reagents at 60 °C for 22 hours. After the removal of volatiles from the reaction mixture, a bright-yellow residue could be extracted in hexane, following 1 week at –40 °C isolated in a relatively low crystalline yield (32%). This was then confirmed as **5-XXIX** via X-ray crystallography (Figure 5.18).

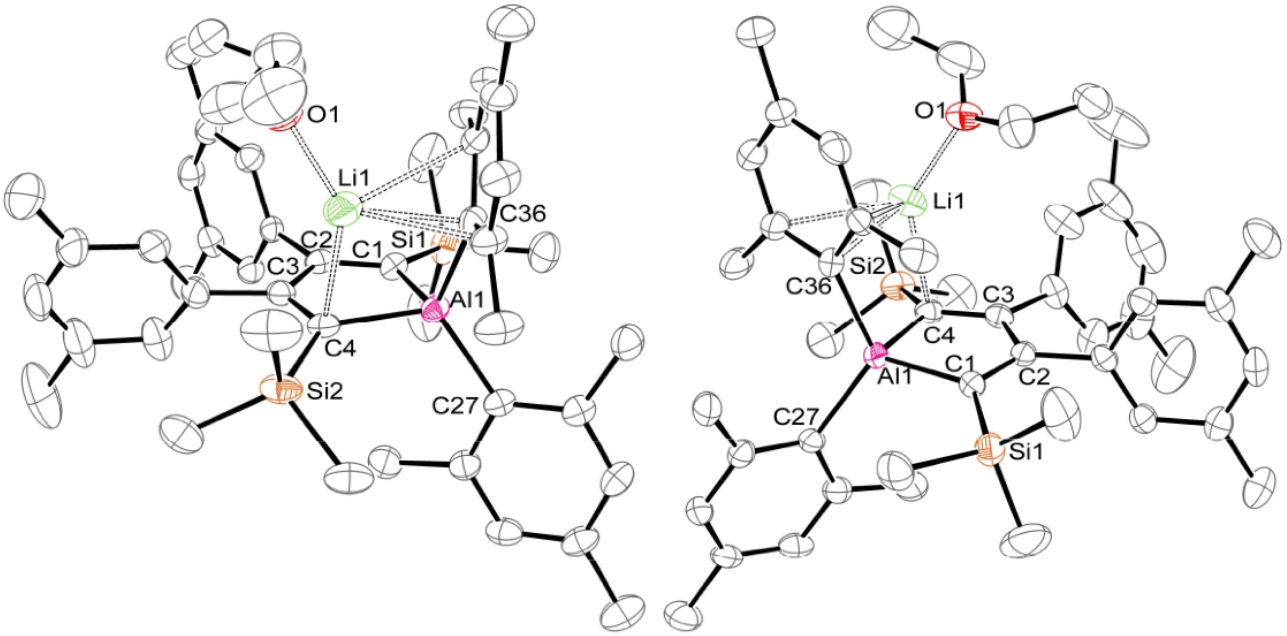

*Figure 5.18: Molecular structure of [Li(OEt$_2$)({Mes}$_2$Al{C$_4$(2,5-SiMe$_3$)$_2$(3,4-m**Xyl**)$_2$})] **5-XXIX** as determined by X-ray crystallography. Thermal ellipsoids set to 50% probability. Hydrogen atoms and toluene solvent molecules omitted for clarity. Selected bond lengths (Å) and angles (°): Al1-C36 2.070(2), Al1-C27 2.023(2), Al1-C1 1.998(2), Al1-C4 2.052(2), O1-Li1 1.917(5), Li1-C4 2.351(5), C1-C2 1.357(3), C4-C3 1.367(3), C2-C3 1.520(3), C27-Al1-C36 119.69(9), C1-Al1-C4 89.38(9).*

Featuring a tetracoordinate aluminium(III) with 4 Al-C single bonds, **5-XXIX** is an aluminate complex necessitating an alkali metal counterion. About the aluminium centre, the distorted tetrahedral is implicit from the narrow angle imparted by the C$_4$ scaffold (89.38(9) °) and subsequent arrangement of mesityl groups above and below AlC$_4$ heterocycle plane (119.69(9) °). The tricoordinate lithium cation features diethyl ether coordination in addition to interactions with the C$_4$ scaffold via the aluminium ligating α-carbon and η^3-interactions with the mesityl moiety. This was notably dissimilar

to interactions presented with both aluminium coordinated substituents as in dichloroalumole aluminate **5-XXIX**.

From the solid-state structure, the preparation of **5-XXIX** from corresponding diethyl ether chloroalumole adduct **5-XX** is rationalised to occur initially via salt metathesis of terminal chloride ligand. This would yield the preparation of mono-mesityl substituted product. Incumbent upon the elevated temperatures (60 °C), the diethyl ether solvate is more labile and consequently yields the Lewis acidic aluminium centre more accessible. Thereafter, the second equivalent of mesityl lithium serving carbon-centred nucleophile affords the second installed Al-C bond. In doing so, the afforded aluminate complex retains the associated lithium of the second mesityl species as a counterion. A diethyl ether molecule then preferentially coordinates to the lithium cation due to the saturated coordination sphere of the aluminium centre.

5.4.3. Reactivity of NHC-Stabilised Chloroalumoles toward a Cationic Alumole

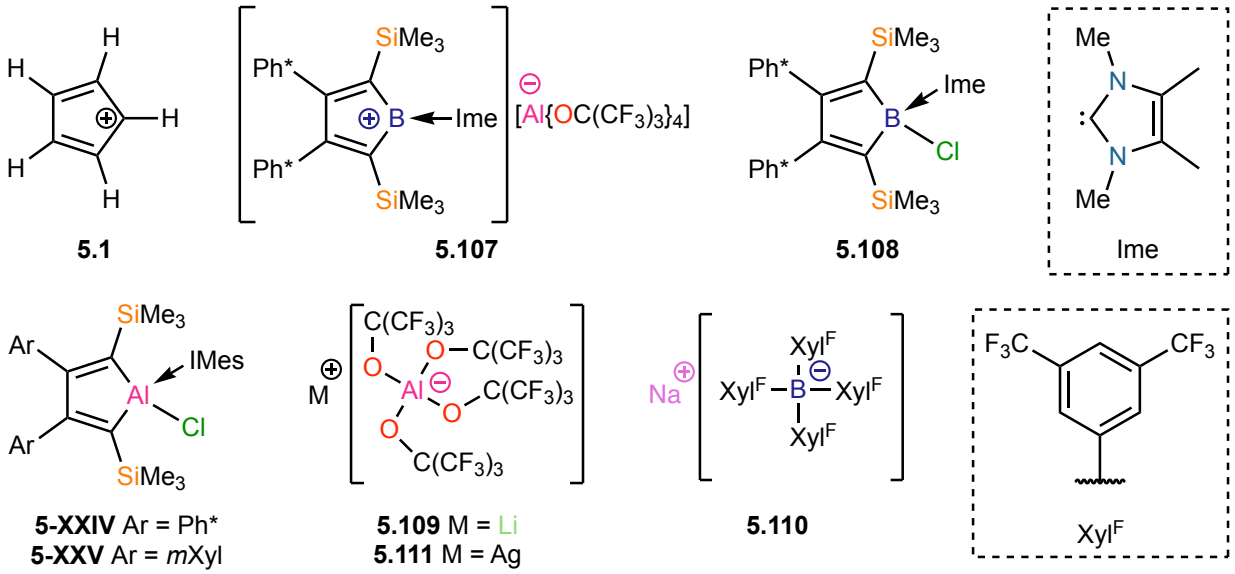

Figure 5.19: Library of selected species related to the preparation of isolable borole cation and subsequent alumole inquiries.

In 2020, Sindlinger and Heitkemper expanded the catalogue of isolable "free" boroles to include a cationic system **5.107** (Figure 5.19).[68] This borenium cation was included within a 5-membered BC_4 heterocycle featuring cyclic conjugation of a 4π-electron arrangement and cationic charge. Consequently, **5.107** is isoelectronic to the fundamental example of antiaromaticity: the elusive cyclopentadienyl cation **5.1**.[5, 68] The highly reactive **5.107** featured a tricoordinate boron centre, and an NHC (Ime) coordinated to the boron centre. Prepared from an NHC-chloroborole adduct **5.108** (analogous to alumole species **5-XXIV** and **5-XXV**), the terminal chloride was abstracted with

Krossing's weakly coordinating anion salt Li[Al{OC(CF$_3$)$_3$}$_4$] **5.109**.[74] The dissolution of the two reagents in dichloromethane leads to the immediate formation of the cation **5.107,** which could be isolated in a near quantitative crystalline yield (>98%).[68] Moreover, explorations with another halide abstraction reagent Na[B(Xyl^F)$_4$] **5.110** (Xyl^F=3,5-(CF$_3$)$_2$(C$_6$H$_3$)) would similarly lead to complete consumption of NHC-chloroborole adduct. However, the resulting species decomposed at 25 °C. Further investigations highlighted the reactivity of BC$_4$ moiety with small molecules (carbon monoxide, acetylene) through the combination of cationic charge and frontier π-orbitals.

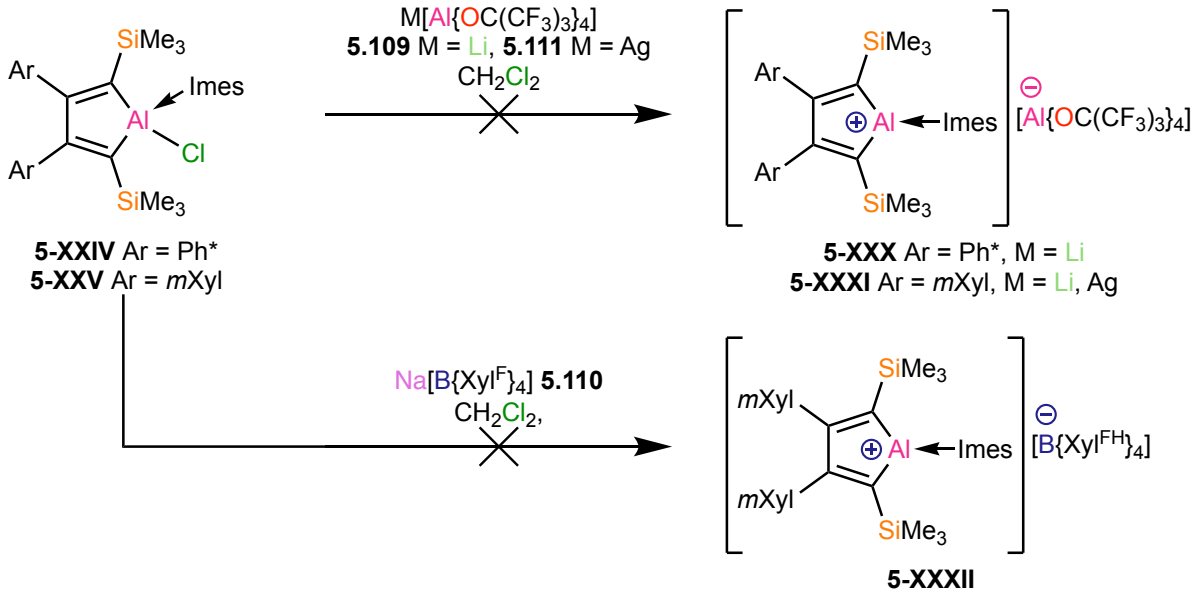

*Scheme 5.34: Attempted preparations of cationic alumole species **5-XXX** - **5-XXXII** with various halide abstraction reagents **5.109** - **5.111**.*

Inspired by the preparation of the NHC-alumole **5.107**, the preparation of related species **5-XXIV** and **5-XXV** were conducted toward cationic alumoles of varied steric bulk (Scheme 5.34). Investigations were conducted within CH_2Cl_2 and CD_2Cl_2 across temperatures ranging -40 to 40 °C.

From investigations of **5-XXIV** with lithium salt **5.109** (Scheme 5.34), the immediate consumption of starting materials could be identified from ^{1}H NMR spectroscopy. However, the confirmation of product generation was greatly hindered by the generation of multiple products and the lack of species crystallisation. Evolving slowly over time, distinct shifts in colour (starting from orange and transitioning to turquoise) aligned with signal product transformation identifiable via ^{1}H NMR spectroscopy. However, in all cases convergence into a singular identifiable product was not identified or possible to be promoted via elevated temperatures.

Combining **5-XXV** with the lithium salt **5.109** (Scheme 5.34) afforded the immediate consumption of starting materials and generation of multiple products according to ^{1}H NMR Spectroscopy. The

reaction solutions consistently changed colour, often darkening from yellow starting materials to a vibrant blue, dark green, or black and frequently with the precipitation of colourless solid attributed to lithium chloride. These colour changes correlated with the formation of new products, however, purified products could not obtained.

From inquiries, a variety of trends could be identified. Notably, in **5-XXV** reactions, the consistent generation of two unknown species was highlighted via new signals within the ^{1}H NMR spectra, postulating the formation of a new symmetric and unsymmetric system about the C_4 heterocycle scaffold identified from signals corresponding to the trimethylsilyl environments. Evidence of unsymmetric products within the NMR spectra was rationalised due to rearrangements yielding the 2,3- or 3,5- organisation of trimethylsilyl moieties about the AlC_4 heterocycle.

All attempts toward crystallisation of postulated degradation or target species from inquiries with **5-XXIV** and **5-XXV** were unsuccessful, often affording dark blue or black oils. Notably, when crystalline material could be grown, it was either not single or of insufficient quality for SCXRD. To aid crystallisations attempts, DMAP was added to reaction mixtures. From such inquiries, crystalline material could be afforded from reactions with both **5-XXIV** and **5-XXV**. In attempts concerning **5-XXIV**, initial crystallisations afforded samples of insufficient quality, only diffracting to 1.4 Å. Recrystallisation of samples following 2 weeks at –40 °C afforded 2 mm cube crystals from saturated CD_2Cl_2 solutions. However, samples melted upon picking with a spatula prior to analysis via X-ray diffraction. For **5-XXV**, upon picking within a glovebox and transport under an inert atmosphere, thermal degradation of crystalline material was observed within 2 minutes. Moreover, further attempts to crystallise and transport at –40 °C could not be conducted due to a lack of time.

Further expanding investigations of **5-XXV**, reactions were explored with halide abstraction reagents of varying cations. With **5-XXIV**, the silver salt **5.111** identified the formation of the same symmetric and unsymmetric products species previously identified via ^{1}H NMR Spectroscopy. However, reactions were observed to progress under a notably shorter time scale (18 hours) compared to lithium investigations (2 weeks) at ambient temperatures. Utilising **5.111** observed the preferential formation of a symmetric species, however, crystalline material to confirm product identities could not be afforded. Investigations of **5-XXV** with sodium regent **5.110** were also conducted to vary the corresponding weakly coordinating anion (Scheme 5.34). Upon addition of **5.110** to a dichloromethane solution of **5-XXV**, colour changes from yellow to a very bright yellow immediately, and then to black was identified following 10 minutes. Analysis via ^{1}H NMR spectroscopy identified the preparation of multiple species within the spectra, postulating the transient formation of target species **5-XXXII,** which consequently underwent degradation or activations at room temperature to afford an indiscernible mixture of species. Following 18 hours, the majority formation of a previously

unidentified unsymmetric product could be observed via ^{1}H NMR spectroscopy, however, attempts to isolate or identify target species **3-XXXII** or related degradation compounds via crystallisations were unsuccessful.

5.5. Conclusion

The reactivity of an acyclic aluminyl system **3-IV** towards three borole species of the same C_4 scaffold was conducted, identifying trends in reactivity (Scheme 5.25). These reactions gave reduced borole derivatives, monoanionic borole radicals (**5-XIII**, **5-XV**, **5-XVII**) and dianionic boroledііde (**5-XIV**, **5-XVI**, **5-XVIII**) indicative of 1- and 2-electron reductions, respectively. Whilst crystallisation attempts to confirm borole derivative identities and bonding modes were unsuccessful, the species prepared were identified through NMR and EPR spectroscopy. Further inquiries of the newly reported acyclic aluminyl system **3-IV** highlighted borole reductions as the only current method towards affording the oxidised aluminyl product dialane species **5-XII**, which was characterised via heteronuclear NMR spectroscopy and X-ray crystallography.

Broadening group 13 species accessible from the bulky silyl-substituted dibutadienes **5-IV** and **5-V**, investigations have afforded the preparation of aryl- and halide-substituted alumole complexes of varying degrees of steric encumberment. Expanding upon the initial species prepared within the Sindlinger group, further examples of NHC-furnished alumoles **5-XXIV** and **5-XXV**, haloalumole complexes (**5-XIX**, **5-XX**), and aryl-substituted alumoles **5-XXVIII** and **5-XXIX** have extended examples of alumole species as part of the accelerating field of alumole chemistry. The varied steric hindrance of **5-XIX** and **5-XX** chloroalumoles presented varied products accessible via analogous reaction conditions (**5-XXVIII**, **5-XXIX**). Moreover, the preparation of cationic alumole species **5-XXX** - **5-XXXII** was attempted via halide abstraction from NHC-furnished alumoles **5-XXIV** and **5-XXV** with a range of weakly coordinating anions. Whilst the isolation of target species **5-XXX** - **5-XXXII** was not achieved during the shortened timeframe in Germany, this challenge serves as a new and interesting line of inquiry to further extend alumole complexes.

5.6. Experimental

General Methods and Considerations

All reactions dealing with air- and moisture-sensitive compounds were carried out under an argon atmosphere using standard Schlenk line and glovebox techniques. NMR experiments using air sensitive compounds were conducted in J. Young's tap NMR tubes prepared and sealed in a glovebox under argon. Prior to use, solvents were prepared using an SPS system or distilled over a suitable drying agent (C_6D_6 over potassium, hexane over NaK, THF/diethyl ether/pentane/toluene over sodium wire and CH_2Cl_2 over calcium hydride). The solvents used in the glovebox were also degassed three times using the *Freeze-Pump-Thaw* method. All NMR data, unless otherwise stated, were acquired at 298 K on either an Bruker Avance AV 250 instrument for ^{1}H (250 MHz), a Bruker Avance AV 400 for ^{1}H (400 MHz), $^{13}C\{^{1}H\}$ (126 MHz), $^{27}Al\{^{1}H\}$ (130 MHz), and $^{29}Si\{^{1}H\}$ (99 MHz) or Bruker Avance 500 for ^{1}H (500 MHz). ^{1}H and ^{13}C NMR spectra were referenced using residual solvent resonances. Chemical shifts δ are reported in part per million (ppm), coupling constants are reported in Hertz (Hz) and coupling patterns are abbreviated as follows: m (multiplet), s (singlet), d (doublet), t (triplet), q (quartet), quin (quintet), sex (sextet), sept (septet), or combinations thereof. Crystal structure analyses were measured on a Bruker Kappa APEXII Duo diffractometer (Mo Kα, λ = 0.7107 ˚A) at 150 K by Dr W. Frey at the University of Stuttgart. The elemental analyses were carried out by the Institute of Inorganic Chemistry, University of Stuttgart on an ELEMENTAR (VarioMicro cube). Continuous Wave (CW) X-band solution-phase EPR spectra were collected by Fridolin Hennhöfer on a Freiberg Instruments Magnettech MS-5000 with a field modulation of 0.1 mT (for **5-XIII**) and 0.2 mT (for **5-XV**) with a microwave power of 1 mW. Simulations were performed by Li Feng Lim using the fast-motion CW EPR program "*garlic*" in the EasySpin package in MATLAB.[75]

5-XIX was first prepared and characterised by Dr. Tobias Heitkemper. **2-XX** and **3-IV** was prepared as discussed in previous Chapters (**Chapter 2**, **Chapter 3**). **5-II**, **5-III**, **5-IV**, and AlI_3 were prepared as per literature methods.[17, 71a] **5-I** was prepared by MSc. Michael Jochum as per a literature method.[15] **5-V** and Imes were prepared by Dr. Tobias Heitkemper as per literature method.[16, 76] 5% K/KI, **5.109**, **5.110**, and **5.111** were prepared by Dr. Tobias Heitkemper and MSc. Julijan Sarcevic as per literature method.[74b, 77] All other reagents were used as received.

Synthesis of acyclic dialane [{Al(N{Dipp}SiMe$_3$)$_2$}$_2$] (5-XII) and preparation of the radical anion of *para*-Xylylborole (5-XIII) with an aluminyl anion (3-IV).

In a glovebox, to a 10 mL vial containing dark-red oily solid of *para*-Xylylborole **5-I** (50 mg, 96.0 µmol, 1.0 eq.) was added dropwise a deep-yellow toluene solution (0.4 mL) of [K_2(Al{N(Dipp)SiMe$_3$}$_2$)$_2$] **3-IV** (64.8 mg, 57.6 µmol, 0.60 eq.). Upon addition, a crystalline material

was immediately identified as growing on the walls of the vial. Further toluene (0.2 mL) was utilised to dissolve the crystals. Immediate precipitation of a yellow-brown solid visible from burnt-orange solution. Following brief agitation, the vial was placed within a –40 °C freezer. Following 12 days, [{Al(N{Dipp}SiMe$_3$)$_2$}$_2$] **5-XII** was isolated as colourless rectangular crystals of SCXRD quality that were characterised via X-ray diffraction (80.9 mg, 71%). ^{1}H NMR spectroscopy identified complete conversion of **3-IV** to targeted **5-XII**. **N.B.** Following 48 h at ambient temperature, signals corresponding to degradation of the paramagnetic radical anion of *para*-Xylylborole **5-XIII** were identified, highlighting the equivalent *in-situ* preparation of targeted **5-XIII** with **5-XII**. An investigation within a J. Young's NMR tube in deuterated toluene (0.5 mL) underwent EPR spectroscopy and identified an active signal corresponding to a boron-centred radical anion within the borole framework.

Characterisation data for [{Al(N{Dipp}SiMe$_3$)$_2$}$_2$] (**5-XII**):

^{1}H NMR (500 MHz, C$_6$D$_6$, 298 K): δ = 7.07 (d, $^3J_{HH}$ = 6.8 Hz, 4H, Dipp-*m*-*H*), 6.95 (t, $^3J_{HH}$ = 6.8 Hz, 4H, Dipp-*p*-*H*), 6.87 (d, $^3J_{HH}$ = 6.8 Hz, 4H, Dipp-*m*-*H*), 3.93 (br, 4H, Dipp-C*H*(CH$_3$)$_2$), 3.09 (br, 4H, Dipp-C*H*(CH$_3$)$_2$), 1.42 (d, $^3J_{HH}$ = 6.5 Hz, 12H, Dipp-CH(C*H*$_3$)$_2$), 1.38 – 1.35 (m, 12H, Dipp-CH(C*H*$_3$)$_2$), 1.18 (d, $^3J_{HH}$ = 7.2 Hz, 12H, Dipp-CH(C*H*$_3$)$_2$), 0.37 (s, 36H, Si(C*H*$_3$)$_3$, 0.16 – 0.14 (m, 12H, Dipp-CH(C*H*$_3$)$_2$). **^{13}C{^{1}H} NMR** (126 MHz, C$_6$D$_6$, 298 K): δ = 147.5 (Aryl-*C*), 146.6 (Aryl-*C*), 145.0 (Aryl-*C*), 125.8 (Aryl-*C*), 125.2 (Aryl-*C*), 124.5 (Aryl-*C*), 28.4 (Dipp-*C*H(CH$_3$)$_2$), 27.0 (Dipp-CH(*C*H$_3$)$_2$), 26.7 (Dipp-CH(*C*H$_3$)$_2$), 26.5 (Dipp-CH(*C*H$_3$)$_2$), 25.3 (Dipp-CH(*C*H$_3$)$_2$), 8.4 (Si(*C*H$_3$)$_3$). **^{29}Si{^{1}H} NMR** (99 MHz, C$_6$D$_6$, 298 K): δ = 8.4 (N-*Si*(*C*H$_3$)$_3$).

Characterisation data for radical anion of *para*-Xylylborole (**5-XIII**):

EPR (toluene, 298 K, 9.4 GHz): g_{iso} = 1.9620. **MS/LIFDI *m/z* (%) $^-$ve:** 529.0 (Xyl-BH$_2${CH(SiMe$_3$)CH(Xyl)CH(Xyl)CH(SiMe$_3$)$^-$, 3), 339.2 (CH$_3$CH(Xyl)CH(Xyl)CH(SiMe$_3$)$^-$, 2), 325.2 (CH$_2$(Xyl)CH(Xyl)CH(SiMe$_3$)$^-$, 2). **MS/LIFDI *m/z* (%) $^+$ve:** 522.3 (Xyl-B{C$_4$H$_2$(SiMe$_3$)$_2$Xyl$_2$}$^+$, 100), 519.3 (Xyl-B{C$_4$ (SiMe$_3$)$_2$Xyl$_2$}$^+$, 5), 305.2 (CH(SiMe$_3$)CH(Xyl)CH$_2$CH$_2$(SiMe$_3$)$^+$, 24).

Preparation of the potassium boroldiide of *para*-Xylylborole (5-XIV) with an aluminyl anion (3-IV)

In a J. Young's NMR tube, to a freshly prepared deuterated benzene (0.5 mL) solution of **3-IV** (14.9 mg, 13.2 μmol, 1.25 eq.) was added *para*-Xylylborole **5-I** (5.50 mg, 10.6 μmol, 1.0 eq.). Upon addition, the deep-yellow transparent solution darkened, and an orange precipitate was observed. ^{1}H NMR spectroscopy of the reaction mixture revealed the complete consumption of both the **3-IV** and **5-I**, yielding clean conversion to the potassium boroldiide **5-XII** and the targeted **5-XIV** (in addition

to retained impurities of [Al{N(Dipp)SiMe$_3$}$_2$] **2-XX** and HN(Dipp)SiMe$_3$ **2-IV** yielded from the preparation of **3-IV**). **N.B.** ^{1}H NMR spectroscopy identified no change within species distribution at ambient temperature over 1.5 h. However, a decrease in **5-XIV** signal integrations correlated with increased precipitate present within the tube. Following 18 h at ambient temperature, further precipitation was observed as an orange powder and a lack of corresponding **5-XIV** signals identifiable via ^{1}H NMR spectroscopy. Crystalline material was grown within the flask from concentrated benzene solutions, however, attempts to isolate SCXRD quality samples were unsuccessful.

Characterisation data for potassium boroldiide of *para*-Xylylborole (**5-XIV**):

^{1}H NMR (250 MHz, C_6D_6, 298 K): δ = 7.33 (d, $^3J_{HH}$ = 7.5 Hz, 1H, Aryl-*H*), 7.25 (br, 1H, Aryl-*H*), 7.10 (s, 1H, Aryl-*H*), 6.67 (br, 6H, Aryl-*H*), 2.57 (s, 3H, B-Xyl-C*H*$_3$), 2.55 (s, 3H, B-Xyl-C*H*$_3$), 2.32 (s, 12H, *meta*-Xyl-C*H*$_3$), 0.12 (s, 18H, Si(C*H*$_3$)$_3$).

Characterisation data for solvated potassium boroldiide of *meta*-Xylylborole:

^{1}H NMR (250 MHz, C_6D_6, 298 K): δ = 7.31 (d, $^3J_{HH}$ = 7.5 Hz, 1H, Aryl-*H*), 7.25 (br, 1H, Aryl-*H*), 7.12 (s, 1H, Aryl-*H*), 6.67 (br, 6H, Aryl-*H*), 3.46 (br, 6H, THF-OC*H*$_2$CH$_2$), 2.57 (s, 3H, B-Xyl-C*H*$_3$), 2.54 (s, 3H, B-Xyl-C*H*$_3$), 2.32 (s, 12H, *meta*-Xyl-C*H*$_3$), 2.32 (br, 6H, THF-OCH$_2$C*H*$_2$), 0.12 (s, 18H, Si(C*H*$_3$)$_3$).

Preparation of radical anion of *meta*-Xylylborole (5-XV) with an aluminyl anion (3-IV)

In a J. Young's NMR tube, to a freshly prepared deuterated benzene (0.5 mL) solution of **3-IV** (18.1 mg, 16.0 μmol, 0.5 eq.) was charged *meta*-Xylylborole **5-II** (5.50 mg, 32.1 μmol, 1.0 eq.). Upon addition, a burnt-orange solid precipitated from the yellow solution. ^{1}H NMR spectroscopy acquired on the solution identified an immensely broad spectrum from which no structural information could be elucidated. Subsequent analysis of the solution via EPR spectroscopy identified evidence of a radical, postulated to be the targeted radical anion **5-XV**. However, due to the suspended solid and concentration, the signal was too broad to ascertain clear structural information. Following 72 h at ambient temperature, the dark yellow precipitate had settled to the bottom of flask and ^{1}H NMR spectroscopy identified a mixture of species within solution. In a glovebox, the precipitate was isolated as a yellow powder and washed with hexane (3 × 2 mL) until white. Dissolution within tetrahydrofuran (1 mL) led to an immediate colour change to bright red-orange. Further tetrahydrofuran washings of residue were collected, and consecutive crops were dried *in vacuo* as isolated as a red powder (20 mg). Analysis via ^{1}H NMR spectroscopy identified a mixture of products, of which the major species present was solvated **5-XVI**. Data was consistent with that previously collected in the Sindlinger research group. **NB**: Preparations ascertained EPR spectra from which isotropic g values could be identified.

EPR (toluene, 298 K, 9.4 GHz): g_{iso} = 2.0034.

Synthesis of the potassium boroldiide of *meta*-Xylylborole (5-XVI)

In a glovebox, *meta*-Xylylborole **5-II** (150 mg, 288 μmol, 1.0 eq.) and 5% K/KI (705 mg, 864 μmol, 3.0 eq.) were charged into a 20 mL vial. Tetrahydrofuran (10 mL) was added, yielding an orange suspension that became a burgundy solution with precipitate after 18 h stirred at ambient temperature. The mixture was passed through a filter, and the volatiles were removed from the filtrate *in vacuo*. The dark-red oily solid was washed with hexane (2 × 5mL) and dried under reduced pressure to yield **5-XVI** as an orange powder (160 mg, 93%). **N.B.** ^{1}H NMR spectroscopy was completed in a C_6D_6 solution (0.5 mL) with two drops of THF-d_8 due to poor aromatic solubility.

Characterisation data for potassium boroldiide of *meta*-Xylylborole (**5-XVI**):

^{1}H NMR (250 MHz, C_6D_6, 298 K): δ = 7.58 (br, 2H, Aryl-*H*), 6.94 (s, 1H, Aryl-*H*), 6.81 (br, 4H, Aryl-*H*), 6.69 (br, 2H, Aryl-*H*), 2.55 (s, 6H, B-Xyl-CH_3), 2.32 (s, 12H, *meta*-Xyl-CH_3), 0.27 (s, 18H, Si(CH_3)$_3$).

Attempted preparation of the potassium boroldiide of *meta*-Xylylborole (5-XVI) with an aluminyl anion (3-IV)

In a J. Young's NMR tube, to an *in-situ* prepared deuterated benzene (0.5 mL) solution of **3-IV** (13.8 mg, 12.3 μmol, 1.25 eq.) was charged *meta*-Xylylborole **5-II** (5.1 mg, 9.84 μmol, 1.0 eq.). Upon addition to the deep-yellow transparent solution, a darkening of the colour and an increase in opacity, due to the formation of an orange precipitate, was observed. ^{1}H NMR spectroscopy identified the complete consumption of both **3-IV** and **5-II** reactants, yielding complete conversion to **5-XII** and the targeted **5-XVI** (in addition to retained impurities of [Al{N(Dipp)SiMe$_3$}$_2$] **2-XX** and HN(Dipp)SiMe$_3$ **2-IV** yielded from **3-IV** preparation). **N.B.** ^{1}H NMR spectroscopy identified no change within species distribution at ambient temperature over 1.5 h. Following 18 h at ambient temperature, precipitation of **5-XVI** was observed and confirmed via ^{1}H NMR spectroscopy. Attempts to isolate the targeted species yielded a yellow-brown powder (2.9 mg), identified as an indiscernible mixture of products.

Attempted preparation of radical anion of chloroborole (5-XVII) with an aluminyl anion (3-IV)

In a J. Young's NMR tube, to a deep-yellow solution of **3-IV** (5.1 mg, 28.3 μmol, 2.5 eq.) was added chloroborole **5-III** (5.1 mg, 11.3 μmol, 1.0 eq.). Immediate analysis via ^{1}H NMR spectroscopy identified the majority consumption of reactants and production of the dialane **5-XII**. Following 1 h at ambient temperature, further analysis via ^{1}H NMR spectroscopy identified the consumption of all borole staring material, but with next to no signals corresponding to borole products identified. From this the formation of the targeted paramagnetic radical anion of chloroborole **5-XVII** was postulated.

N.B. Following 5 days at ambient temperature, analysis of the solution via ^{1}H NMR spectroscopy identified a significant increase in the integration of chloroborole **5-III** related signals, where previously no signals had been present. In combination with signals corresponding to the decomposition of the **5-XVII** species, the dark-brown solution consisted of an indiscernible mixture of products.

Attempted preparation of the potassium boroldiide of chloroborole (5-XVIII) with an aluminyl anion (3-IV)

In a J. Young's NMR tube, to a red deuterated benzene (0.1 mL) suspended solution of chloroborole **5-III** (15 mg, 33.3 μmol, 1.0 eq.) was added a deep-yellow deuterated benzene (0.5 mL) solution of **3-IV** (37.5 mg, 33.3 μmol, 1.0 eq.). Upon addition, a very dark red solution with bright yellow edges was obtained. ^{1}H NMR spectroscopy undertaken on the reaction mixture identified the formation of a multitude of products, including **5-XII** and the targeted potassium boroldiide **5-XVIII** (11%), however, majority species within solution was unreacted chloroborole **5-III** (30%). **N.B.** Following 1 h at ambient temperature, the solution had become black. The NMR flask was heated to 60 °C for 2 h, during which no colour change was observed. ^{1}H NMR spectroscopy identified the formation of an indiscernible mixture of products. Attempts to isolate any species via crystallisation were unsuccessful.

Characterisation data for potassium boroldiide of chloroborole (**5-XVIII**):

^{1}H NMR (250 MHz, C_6D_6, 298 K): δ = 6.64 (br, 2H, Aryl-*H*), 6.53 (br, 4H, Aryl-*H*), 2.25 (s, 12H, *meta*-Xyl-C*H*$_3$), 0.45 (s, 18H, Si(C*H*$_3$)$_3$).

Attempted synthesis of [{Al(N{Dipp}SiMe$_3$)$_2$}$_2$] (5-XII)

Method A: To a freshly prepared deuterated benzene (0.5 mL) solution of [K$_2$(Al{N(Dipp)SiMe$_3$}$_2$)$_2$] **3-IV** (23.1 mg, 41.0 μmol, 1.0 eq.) in a J. Young's NMR tube, was added [AlI{N(Dipp)SiMe$_3$}$_2$] (26.7 mg, 41.0 μmol, 1.0 eq.). Immediate analysis of the bright-yellow solution via ^{1}H NMR spectroscopy identified minor formation of the proligand HN(Dipp)SiMe$_3$ **2-IV** and an equivalence of [K$_2$(Al{N(Dipp)SiMe$_3$}$_2$)$_2$] **3-IV** and [AlI{N(Dipp)SiMe$_3$}$_2$] **2-XX** reactants. The reaction mixture was agitated for 72 h, after which ^{1}H NMR spectroscopy identified the majority consumption of [K$_2$(Al{N(Dipp)SiMe$_3$}$_2$)$_2$] **3-IV**, and the generation of a variety of unknown species in addition to [AlI{N(Dipp)SiMe$_3$}$_2$] **2-XX** and proligand. After heating to 80 °C for 24 h, ^{1}H NMR spectroscopy identified consumption of all [K$_2$(Al{N(Dipp)SiMe$_3$}$_2$)$_2$] **3-IV**, producing a mixture of products including three [N(Dipp)SiMe$_3$]$^-$ containing species, [AlI{N(Dipp)SiMe$_3$}$_2$] **2-XX** (40%) and HN(Dipp)SiMe$_3$ **2-IV** (20%) species. **N.B.** Attempts to isolate a single product were unsuccessful. Repeating the reaction gave the formation of the proligand as a majority product following agitation

for 48 h at ambient temperature. **Method B:** To a deuterated benzene (0.4 mL) solution of [AlI{N(Dipp)SiMe$_3$}$_2$] **2-XX** (30 mg, 46.1 μmol, 1.0 eq.) in a J. Young's NMR tube, was added [Co(Cp*)$_2$] (15.2 mg, 46.1 μmol, 1.0 eq.). An immediate colour change from colourless to a dark red-orange solution with bright yellow edges was observed. Agitation of the NMR flask for 16 h yielded a burnt-orange solution retaining the bright yellow edges. ^{1}H NMR spectroscopy identified minimal change to that of the starting material [AlI{N(Dipp)SiMe$_3$}$_2$] **2-XX**. Following heating of the NMR tube to 60 °C for 6.5 h, ^{1}H NMR spectroscopy identified the slow but clean decomposition of the starting material [AlI{N(Dipp)SiMe$_3$}$_2$] **2-XX** (75%) to proligand HN(Dipp)SiMe$_3$ **2-IV** (25%). **N.B.** Despite further manipulations and attempts toward the formation of a single product, only further decomposition was observed. **Method C:** To a freshly prepared deuterated benzene (0.5 mL) solution of [AlI{N(Dipp)SiMe$_3$}$_2$] **2-XX** (24 mg, 36.9 μmol, 1.0 eq.) in a J. Young's NMR tube, was added potassium graphite (27 mg, 199 μmol, 5.4 eq.). The reaction mixture was agitated at ambient temperature for 2 h, before being passed through a syringe containing a Whatman glass filter. The black precipitate was washed with deuterated benzene (0.2 mL). ^{1}H NMR spectroscopy identified the clean formation of [K$_2$(Al{N(Dipp)SiMe$_3$}$_2$)$_2$] **3-IV**. To the deep-yellow solution was added silver hexafluorophosphate (8.4 mg, 33.2 μmol, 0.9 eq.), which turned the reaction mixture yellow-black in colour. ^{1}H NMR spectroscopy identified evidence of targeted [{Al(N{Dipp}SiMe$_3$)$_2$}$_2$] **5-XII** species in the baseline; however, the majority of [K$_2$(Al{N(Dipp)SiMe$_3$}$_2$)$_2$] **3-IV** remained unreacted. The NMR tube was agitated at ambient temperature for a further 1 h and yielded an orange-black solution. ^{1}H NMR spectroscopy identified the majority consumption of [K$_2$(Al{N(Dipp)SiMe$_3$}$_2$)$_2$] **3-IV**, with a slight increase in [{Al(N{Dipp}SiMe$_3$)$_2$}$_2$] **5-XII** but an additional indiscernible mixture of products. Further agitation and attempts to isolate products via crystallisation were unsuccessful.

Synthesis of Chloroalumole Etherate Adduct (5-XIX)

In a glovebox, a colourless diethyl ether (4 mL) solution of aluminium choride (111 mg, 833 μmol, 1.0 eq.) was added dropwise to a dark-red diethyl ether (4 mL) solution of dilithiobutadiene **5-V** (487 mg, 833 μmol, 1.0 eq.). This addition led to fading of the initial red colour to an opaque green-yellow mixture. Following 19 h stirring at ambient temperature, the volatiles were removed from the reaction mixture under reduced pressure. The colourless solid was extracted with hexane (3 × 3 mL), at which stage the extractions were colourless. The hexane solutions combined and concentrated (*ca*. 3 mL) and placed within a –40 °C freezer. This gave **5-XIX** as colourless SCXRD quality crystals over 2 crops (130 mg, 19%). **^{1}H NMR** (500 MHz, C$_6$D$_6$, 298 K): δ = 7.18 (t, $^4J_{HH}$ = 1.9 Hz, 2H, Ph*-*o*-*H*), 6.85 – 6.80 (br, 4H, Ph*-aryl-*H*), 3.74 (q, 4H, Al-OC*H*$_2$CH)$_3$, 1.24 (br, 36H, Ph*-C(C*H*$_3$)$_3$), 0.90 (t, $^3J_{HH}$ = 7.0 Hz, 6H, Al-OCH$_2$C*H*$_3$), 0.14 (s, 36H, Si(C*H*$_3$)$_3$). **^{13}C{^{1}H} NMR** (126 MHz, C$_6$D$_6$, 298 K): δ =

172.3 (Ph*-*aryl*-*C*), 149.4 (Ph*-*aryl*-*C*), 148.8 (Ph*-*aryl*-*C*), 123.8 (Ph*-*aryl*-*C*), 123.0 (Ph*-*aryl*-*C*), 119.4 (Ph*-*aryl*-*C*), 68.3 (Al-O*C*H_2CH$_3$), 34.7 (Ph*-*C*(CH$_3$)$_3$), 31.7 (Ph*-C(*C*H$_3$)$_3$), 13.9 (Al-OCH$_2$*C*H$_3$), 1.7 (Si(*C*H$_3$)$_3$). **^{29}Si{^{1}H} NMR** (99 MHz, C_6D_6, 298 K): δ = –10.6 (C-*Si*(*C*H$_3$)$_3$). **MS/LIFDI *m/z* (%) ⁻ve:** 601.0 (H$_2$[**5-XIX**]}$^-$, 3), 529.0 (AlH{C$_4$H(SiMe$_3$)(Ph*)$_2$}$^-$, 2), 279.9 (AlCl{C$_4$H$_2$(SiMe$_3$)$_2$}(OH)$^-$, 100), 197.0 (AlH{C$_4$H(SiMe$_3$)$_2$(Ph*)$_2$}(OEtH)$^-$, 4). **MS/LIFDI *m/z* (%) ⁺ve:** 680.5 ((OHEt)[**5-XIX**]$^+$, 1), 576.4 (C$_4$H$_4$(SiMe$_3$)$_2$Ph*$_2^+$, 15), 574.4 (C$_4$H$_2$(SiMe$_3$)$_2$Ph*$_2^+$, 100), 518.4 (AlH$_2${C(SiMe$_3$)C(Ph*)(CH$_2$-Ph*)}$^+$, 4).

Synthesis of Chloroalumole Etherate Adduct (5-XX)

In a glovebox, to a colourless diethyl ether (4 mL) solution of aluminium chloride (95.6 mg, 717 μmol, 1.0 eq.) was added a dark red diethyl ether (6 mL) solution of dilithiobutadiene **5-IV** (300 mg, 717 μmol, 1.0 eq.). Following 1 h of stirring at ambient temperature, the solution had become yellow with a colourless precipitate. Following a further 2.5 h of stirring at ambient temperature, the volatiles were removed under reduced pressure. The colourless solid was extracted with hexane (8 mL) and concentrated until the deposition of crystalline material upon the glass wall (*ca.* 3 mL). Following placement within –40 °C freezer for 8 days, the mother liquor was decanted and further concentrated to isolate a second crop of crystalline material from a –40 °C freezer. Crystalline crops of SCXRD quality **5-XX** were isolated and dried *in vacuo* (292 mg, 75%). **^{1}H NMR** (500 MHz, C_6D_6, 298 K): δ = 6.64 (s, 4H, Xyl-*o*-*H*), 6.51 (s, 2H, Xyl-*p*-*H*), 3.74 (br., 4H, Al-OCH_2CH$_3$), 2.07 (s, 12H, Xyl-CH_3), 0.91 (t, $^3J_{HH}$ = 7.2 Hz, 6H, Al-OCH$_2$CH_3), 0.14 (s, 18H, Si(CH_3)$_3$). **^{13}C{^{1}H} NMR** (126 MHz, C_6D_6, 298 K): δ = 172.7 (Xyl-*o*-*C*), 146.4 (Xyl-*i*-*C*), 135.7 (Xyl-*p*-*C*), 127.3 (Xyl-*m*-*C*), 68.4 (Al-O*C*H_2CH$_3$), 21.3 (Xyl-*C*H$_3$), 14.0 (Al-OCH$_2$*C*H$_3$), 1.8 (Si(*C*H$_3$)$_3$). **^{29}Si{^{1}H} NMR** (99 MHz, C_6D_6, 298 K): δ = –10.7 (C-*Si*(*C*H$_3$)$_3$). **^{27}Al{^{1}H} NMR** (130 MHz, C_6D_6, 298 K): δ = 103.2. **MS/LIFDI *m/z* (%) ⁻ve:** 546.0 (AlCl{C$_4$H$_4$(SiMe$_3$)$_2$Xyl$_2$}OEt$_2^-$, 3), 527.0 (AlCl{C$_4$H(SiMe$_3$)$_2$Xyl$_2$}(OEtMe)$^-$, 3), 502.0 (AlCl$_2${C$_4$H(SiMe$_3$)$_2$Xyl$_2$}$^-$, 2), 279.9 (AlCl{C$_4$H$_2$(SiMe$_3$)$_2$}(OH)$^-$, 100), 147.0 (AlCl{C$_4$H$_2$OH}(OH)$^-$, 35). **MS/LIFDI *m/z* (%) ⁺ve:** 504.4 (Al{C$_4$(SiMe$_3$)$_2$Xyl$_2$}OEt$_2^+$, 10), 494.3 (Al{C$_4$H$_3$(SiMe$_3$)$_2$Xyl$_2$}$^+$, 26), 406.3 (C$_4$H$_2$(SiMe$_3$)$_2$Xyl$_2^+$, 100), 408.3 (C$_4$H$_2$(SiMe$_3$)$_2$Xyl$_2^+$, 30).

Synthesis of Iodoalumole Etherate Adduct (5-XXI) and Isolation of Rearrangement Product (5-XXII)

In a J. Young's NMR flask, aluminium iodide (31 mg, 76.4 μmol, 1.0 eq.) and dilithiobutadiene **5-IV** (32 mg, 76.4 μmol, 1.0 eq.) were charged, and deuterated benzene (0.5 mL) and diethyl ether (0.1 mL) were added. Following brief agitation, a dark-red solution was obtained. Standing at ambient temperature for 18 h,^{1}H NMR spectroscopy of the reaction solution identified minimal conversion to the targeted compound. In a glovebox, additional aluminium iodide (73 mg, 179 μmol, 2.3 eq.), dilithiobutadiene **5-IV** (74 mg, 184 μmol, 2.4 eq.) and diethyl ether (6 mL) were added to the reaction mixture mixture, which was stirred at ambient temperature for 18 h, before volatiles being removed under reduced pressure yielding a yellow-orange powder. Extracted with hexane (5 mL), the yellow-orange solution was concentrated (2 mL) and placed within –40 °C freezer. Following 5 days, the brown solution was decanted from a precipitated light brown solid. The solid was washed with cold hexane (-40 °C) (1 mL), dried *in vacuo* and identified via NMR spectroscopy as **5-XXI** (39.5 mg, 24%). **N.B.** Despite attempts, SCXRD quality crystals of the targeted species could not be grown; however, crystals of the rearrangement product **5-XXII** could be grown from the mother liquor and hexane washings in a –40 °C freezer.

Characterisation data for Iodoalumole Etherate Adduct (**5-XXI**):

^{1}H NMR (500 MHz, C_6D_6, 298 K): δ = 6.62 (s, 4H, Xyl-*o*-*H*), 6.50 (s, 2H, Xyl-*p*-*H*), 3.81 (br., 4H, Al-OC*H*$_2$CH$_3$), 2.08 (s, 6H, Xyl-C*H*$_3$), 2.04 (s, 6H, Xyl-C*H*$_3$), 0.89 (br, 6H, Al-OCH$_2$C*H*$_3$), 0.18 (s, 18H, Si(C*H*$_3$)$_3$). **^{13}C{^{1}H} NMR** (126 MHz, C_6D_6, 298 K): δ = 172.1 (Xyl-*o*-*C*), 146.1 (Xyl-*i*-*C*), 127.4 (Xyl-*p*-*C*), 126.7 (Xyl-*m*-*C*), 69.1 (Al-O*C*H$_2$CH$_3$), 21.3 (Xyl-*C*H$_3$), 13.9 (Al-OCH$_2$*C*H$_3$), 2.1 (Si(*C*H$_3$)$_3$). **^{29}Si{^{1}H} NMR** (99 MHz, C_6D_6, 298 K): δ = –10.5 (C-*Si*(*C*H$_3$)$_3$). **^{27}Al{^{1}H} NMR** (130 MHz, C_6D_6, 298 K): δ = 37.0.

Synthesis of the Tetrahydrofuran Chloroalumole Adduct (5-XXIII)

Method A: In a J. Young's NMR tube, a light-yellow deuterated benzene (0.5 mL) solution of chloroalumole etherate adduct **5-XX** (16.4 mg, 30.3 μmol, 1.0 eq.) was prepared. To the solution, tetrahydrofuran (50 μL) was added, and the reaction mixture was agitated. Following 2 h of stirring at ambient temperature, the volatiles were removed *in vacuo* and *a* dynamic vacuum was applied for a further 20 min. The residue was dissolved in deuterated benzene (0.5 mL) and ^{1}H NMR spectroscopy confirmed the near quantitative conversion to targeted **5-XXIII** species (>98%). **Attempted Method B:** In a glovebox, to a colourless tetrahydrofuran (4 mL) solution of aluminium chloride (95.6 mg, 717 μmol, 1.0 eq.) was added a dark red tetrahydrofuran (6 mL) solution of dilithiobutadiene **5-IV** (300 mg, 717 μmol, 1.0 eq.). Following 1 h of stirring at ambient temperature, the solution had become a

light orange-red colour. After stirring for a further 18 h at ambient temperature, the solution became yellow. Volatiles were removed under reduced pressure, yielding a dark yellow oil. Suspension in hexane (8 mL) yielded a colourless precipitate that was isolated via filtration. The mother liquor was concentrated (*ca.* 3 mL). The colourless precipitate was dissolved with tetrahydrofuran (3 mL), then concentrated (*ca.* 2 mL), and placed within a –40 °C freezer along with the concentrated mother liquor. Despite further attempts, no crystalline of target **5-XXIII** could be isolated. **^{1}H NMR** (250 MHz, C_6D_6, 298 K): δ = 6.67 (s, 4H, Xyl-*o*-*H*), 6.52 (s, 2H, Xyl-*i*-*H*), 3.85 (br, 4H, THF-OCH_2CH$_2$), 2.08 (s, 24H, Xyl-CH_3), 1.11 (br, 4H, THF-OCH$_2$CH_2), 0.13 (s, 18H, Si(CH_3)$_3$).

Synthesis of the NHC-Coordinated Chloroalumole (5-XXIV)

Method A: In the glovebox, chloroalumole etherate adduct **5-XIX** (82 mg, 116 μmol, 1.0 eq.) and Imes (40 mg, 131 μmol, 1.10 eq.) were mixed within a 10 mL vial. The addition of benzene (2 mL) followed by 10 min of stirring yielded a colourless solution. Volatiles from the reaction mixture were removed *in vacuo,* and the residue dissolved in hexane (0.5 mL). Allowing this solution to stand at ambient temperature for 12 h yielded NHC-coordinated chloroalumole **5-XXIV** as a colourless solid (26 mg, 24%). **Method B:** In a J. Young's NMR tube, to a colourless deuterated benzene (0.5 mL) solution of chloroalumole etherate adduct **5-XIX** (20 mg, 28.1 μmol, 1.0 eq.) was added Imes (9.4 mg, 30.8 μmol, 1.10 eq.) as an orange crystalline solid. Agitation for 10 min yielded a pale-orange solution which ^{1}H NMR spectroscopy identified the near quantitative conversion to the targeted species **5-XXIV** (>98%). **^{1}H NMR** (500 MHz, C_6D_6, 298 K): δ = 7.13 (t, $^{4}J_{HH}$ = 1.9 Hz, 2H, Ph*-*o*-*H*), 6.93 (s, 4H, Mes-*m*-*H*), 6.84 (br, 2H, Ph*-*o*-*H*), 6.51 (br, 2H, Ph*-*o*-*H*), 5.91 (s, 2H, Imes-C*H)*, 2.23 (s, 6H, Mes-*p*-CH_3), 2.20 (s, 12H, Mes-*o*-CH_3), 1.35 (br, 18H, Ph*-C(CH_3)$_3$), 1.22 (br, 18H, Ph*-C(CH_3)$_3$), 0.10 (s, 18H, Si(CH_3)$_3$). **^{1}H NMR** (250 MHz, CD_2Cl_2, 298 K): δ = 7.15 (s, 2H, Imes-C*H)*, 7.07 (s, 4H, Mes-*m*-*H*), 6.91 (t, $^{4}J_{HH}$ = 1.9 Hz, 2H, Ph*-*o*-*H*), 6.53 (br, 2H, Ph*-*o*-*H*), 6.26 (br, 2H, Ph*-*o*-*H*), 2.39 (s, 6H, Mes-*p*-CH_3), 2.25 (s, 12H, Mes-*o*-CH_3), 1.17 (br, 18H, Ph*-C(CH_3)$_3$), 1.09 (br, 18H, Ph*-C(CH_3)$_3$), –0.33 (s, 18H, Si(CH_3)$_3$). **^{13}C{^{1}H} NMR** (126 MHz, C_6D_6, 298 K): δ = 172.7 (Ph*-*aryl*-*C*), 169.6 (Imes-:*C*N$_2$), 148.4 (Ph*-*aryl*-*C*), 148.1 (Ph*-*aryl*-*C*), 139.8 (Mes-aryl-*C*), 135.3 (Mes-aryl-*C*), 135.3 (Mes-aryl-*C*), 129.7 (Mes-aryl-*C*), 124.5 (Imes-C*H*), 123.3 (Ph*-*aryl*-*C*), 118.8 (Ph*-*aryl*-*C*), 34.8 (Ph*-*C*(CH$_3$)$_3$), 32.1 (Ph*-C(*C*H$_3$)$_3$), 31.9 (Ph*-C(*C*H$_3$)$_3$), 21.5 (Mes-*p*-*C*H$_3$), 19.4 (Mes-*o*-*C*H$_3$), 3.2 (Si(*C*H$_3$)$_3$). **^{29}Si NMR** (99 MHz, C_6D_6, 298 K): δ = –11.9 (C-*Si*(*C*H$_3$)$_3$). **MS/LIFDI** *m/z* (%) $^{+}$ve: 938.6 (**5-XXIV**$^{+}$, 8), 671.3 (AlCl{C(SiMe$_3$)(CH$_2$-Ph*)}(OH)(Imes)$^{+}$, 12), 573.4 (C_4(Ph*)$_2$(SiMe$_3$)$_2^{+}$, 24), 305.2 (ImesH^{+}, 100).

Synthesis of the NHC-Coordinated Chloroalumole (5-XXV)

In the glovebox, chloroalumole etherate adduct **5-XX** (100 mg, 185 μmol, 1.0 eq.) and Imes (56.2 mg, 185 μmol, 1.10 eq.) were charged in a 10 mL vial. The addition of benzene (2 mL) followed by stirring at room temperature for 10 min yielded a dark-yellow solution. Volatiles were removed *in vacuo,* and hexane (2 mL) was added. The reaction mixture was placed within the –40 °C freezer to precipitate. Following 18h, volatiles were again removed, and hexane (3 × 1 mL) was added and removed *in vacuo* to remove residual diethyl ether. The residue was dissolved in minimal hexane and left to stand at ambient temperature to give NHC-coordinated chloroalumole **5-XXV** as colourless needle-like solid (142 mg, >98%). **^{1}H NMR** (500 MHz, C_6D_6, 298 K): δ = 6.90 (s, 4H, Mes-*m*-*H*), 6.47 (s, 2H, Xyl-*p*-*H*), 6.43 (s, 4H, Xyl-*o*-*H*), 5.98 (s, 2H, Imes-C*H*), 2.26 (s, 6H, Mes-*p*-CH_3), 2.15 (s, 12H, Mes-*o*-CH_3), 2.13 (s, 12H, Xyl-CH_3), 0.12 (s, 18H, Si(CH_3)$_3$). **^{1}H NMR** (250 MHz, CD_2Cl_2, 298 K): δ = 7.18 (s, 2H, Xyl-*p*-*H*), 7.09 (s, 4H, Mes-*m*-*H*), 6.50 (br, 2H, Imes-C*H*), 6.22 (br, 4H, Xyl-*o*-*H*), 2.45 (s, 6H, Mes-*p*-CH_3), 2.21 (s, 12H, Mes-*o*-CH_3), 2.10 (s, 12H, Xyl-CH_3), -0.33 (s, 18H, Si(CH_3)$_3$). **^{13}C{^{1}H} NMR** (126 MHz, C_6D_6, 298 K): δ = 172.0 (Xyl-aryl-*C*), 169.3 (Imes-:*C*N$_2$), 147.3 (Xyl-aryl-*C*), 139.7 (Mes-aryl-*C*), 135.3 (Xyl-aryl -*C*), 135.0 (Mes-aryl-*C*), 135.0 (Mes-aryl-*C*), 129.8 (Mes-aryl-*C*), 126.5 (Xyl-aryl-*C*), 124.4 (Imes-C*H*), 21.4 (Xyl-*m*-*C*H$_3$), 21.3 (Mes-*p*-*C*H$_3$), 19.2 (Mes-*o*-*C*H$_3$), 3.3 (Si(*C*H$_3$)$_3$). **^{29}Si{^{1}H} NMR** (99 MHz, C_6D_6, 298 K): δ = –11.9 (C-*Si*(*C*H$_3$)$_3$). **MS/LIFDI *m/z* (%) $^{-}$ve:** 665.0 (Al{$C_4H_3(SiMe_3)Xyl_2$}Imes^{-}, 3), 564.2 (Al{$C_4H_4(SiMe_3)$(Xyl)}Imes^{-}, 3), 539.1 (Al{$C_4H_3(SiMe_3)_2Xyl_2$}Xyl^{-}, 100), 537.1 (Al{$C_4H(SiMe_3)_2Xyl_2$}Xyl^{-}, 81), 501.2 ($AlCl_2${$C_4(SiMe_3)_2Xyl_2$}, 55). **MS/LIFDI *m/z* (%) $^{+}$ve:** 770.4 (**5-XXV**$^{+}$, 10), 566.3 (AlCl{$C_4H_6(SiMe_3)_2$}Imes^{+}, 1), 305.2 (ImesH^{+}, 100).

Attempted Synthesis of a "Free" Chloroalumole in Toluene

In a glovebox, to a vial containing a colourless toluene (5 mL) solution of aluminium trichloride (128 mg, 960 μmol, 1.0 eq.) was added a dark-red toluene (4 mL) solution of dilithiobutadiene **5-IV** (402 mg, 960 μmol, 1.0 eq.). Following 1 h stirring at ambient temperature, the solution had lightened to red-orange. A further 18 h of stirring identified the majority of dilithiobutadiene **5-IV** remained unreacted via ^{1}H NMR spectroscopy. Following 96 h stirring, the reaction mixture was filtered, and volatiles were removed *in vacuo.* A red-orange oil and colourless solid were extracted with hexane (5 mL). The dark red filtrate was concentrated (*ca.* 1 mL) and placed in a –40 °C freezer. Subsequent concentrations did not yield any crystalline material of SCXRD quality.

Attempted Synthesis of a "Free" Iodoalumole in Toluene

In a glovebox, to a vial containing a pale-yellow toluene (5 mL) solution of aluminium triiodide (310 mg, 960 μmol, 1.0 eq.) was added a dark red toluene (4 mL) solution of dilithiobutadiene **5-IV** (328 mg, 960 μmol, 1.0 eq.). Following 1.5 h of stirring at ambient temperature, the solution had not undergone any notable colour change from the initially observed purple-red colour. Following 18 h stirring, ^{1}H NMR spectroscopy identified majority of dilithiobutadiene **5-IV** as unreacted. Following 96 h stirring, the reaction mixture was filtered, and volatiles from the filtrate were removed *in vacuo.* A red-orange oil and colourless solid were extracted with hexane (5 mL). The dark red filtrate was concentrated (*ca.* 1 mL) and placed in a –40 °C freezer. Subsequent concentrations did not yield any crystalline material of SCXRD quality.

Synthesis of the Lithium Dichloroalumolate (5-XXVI)

In a J. Young's NMR tube, to a dark orange-red deuterated benzene (0.5 mL) solution of dilithiobutadiene **5-IV** (48.0 mg, 115 μmol, 1.0 eq.) was added aluminium chloride (15.3 mg, 115 1μmol, 1.0 eq.). Following 20 min of sonication, the solution had lightened in colour and the flask was heated to 60 °C for 4 h. A burnt-orange solution with a colourless precipitate was yielded, and ^{1}H NMR spectroscopy identified the consumption of dilithiobutadiene **5-IV** starting material. Following 18 h at 60 °C, the reaction mixture was stood at ambient temperatures to afford crystallisation. The dark burnt-orange solution was decanted, and the subsequent yellow crystalline material was washed with toluene (3 × 1 mL). Isolation of the uniform crystalline material and analysis via SCXRD confirmed the formation of lithium dichloroalumolate **5-XXVI**. The yellow crystalline material was dried under reduced pressure and isolated as targeted **5-XXVI** (7.1 mg, 12%). **N.B.** Attempts to yield further product from washings were unsuccessful. **^{1}H NMR** (250 MHz, C_6D_6, 298 K): δ = 6.92 (s, 1H, Xyl-*p-H*), 6.78 (s, 1H, Xyl-*p-H*), 6.61 (s, 2H, Xyl-*o-H*), 6.44 (s, 2H, Xyl-*o-H*), 2.00 (br, 6H, Xyl-CH_3), 1.97 (br, 6H, Xyl-CH_3), 0.40 (br, 18H, Si(CH_3)$_3$), 0.30 (br, 18H, Si(CH_3)$_3$). **E.A:** Anal. Calc. for $C_{26}H_{36}AlCl_2LiSi_2$: C 61.28; H 7.12%. Found: C 60.83; H 7.18%.

Synthesis of Mesitylalumole Etherate Adduct (5-XXVII)

A J. Young's NMR tube was charged with chloroalumole etherate adduct **5-XIX** (26.4 mg, 37.2 μmol, 1.0 eq.) and mesityllithium (7.0 mg, 55.5 μmol, 1.5 eq.). Dissolution in deuterated benzene (0.4 mL) yielded an opaque yellow mixture, which was heated at 60 °C for 22 h. The deep-yellow solution was identified via ^{1}H NMR spectroscopy to yield the targeted product mesitylalumole etherate adduct **5-XXVIII** (93%). **N.B.** In a glovebox, the reaction mixture was filtered, and the volatiles were removed from the filtrate under reduced pressure. The material was extracted with hexane (2 mL), concentrated

(*ca.* 0.5 mL), and the yellow transparent solution was placed within a –40 °C freezer. Following 17 days, crystalline material could be isolated, however, were not of sufficient SCXRD quality. Attempts to recrystallise material were unsuccessful. **^{1}H NMR** (500 MHz, C_6D_6, 298 K): δ = 7.19 (t, $^4J_{HH}$ = 1.9 Hz, 2H, Ph*-*o*-*H*), 6.93 – 6.83 (m, 6H, Mes-aryl-*H*, Ph*-aryl-*H*), 3.31 (br, 4H, Al-OCH_2CH$_3$), 2.77 (s, 6H, Mes-*o*-*H*), 2.69 (s, 3H, Mes-*p*-*H*), 1.28 (s, 18H, Ph*-C(CH_3)$_3$), 1.24 (s, 18H, Ph*-C(CH_3)$_3$), 0.84 (t, $^3J_{HH}$ = 7.0 Hz, 6H, Al-OCH$_2$CH_3), 0.04 (s, 9H, Si(CH_3)$_3$), –0.01 (s, 9H, Si(CH_3)$_3$).

Synthesis of Mesitylalumole Etherate Adduct (5-XXVIII)

Method A: In a glovebox, to a solution of lithium mesityl (11.7 mg, 92.8 μmol, 1.0 eq.) in diethyl ether (4 mL) was added a diethyl ether (4 mL) solution of chloroalumole etherate adduct **5-XX** (50.2 mg, 92.8 μmol, 1.0 eq.). The colourless solution with a colourless precipitate was stirred at ambient temperature for 5 days before volatiles were removed *in vacuo*. The residue was extracted with hexane (5 mL), concentrated (2 mL) and placed within a –40 °C freezer. Following 1 month, an off-white crystalline material was isolated and washed with –40 °C hexane (3 × 0.3 mL). Dried under reduced pressure, this gave mesitylalumole etherate adduct **5-XXVIII** as a colourless powder (29 mg, 50%). **Method B:** To a J. Young's NMR tube containing a suspension of mesityllithium (4.7 mg, 37.3 μmol, 1.0 eq.) in deuterated benzene (0.5 mL) was added **5-XX** (20.2 mg, 37.3 μmol, 1.0 eq.). Following 5 days at ambient temperature with incremental agitation and sonication, ^{1}H NMR spectroscopy identified the conversion to the targeted **5-XXVIII** (78%). **N.B.** In a glovebox, the yellow mixture was filtered and the filtrate concentrated to *ca.* 0.2 mL. Following 1 month at ambient temperature, volatiles were removed *in vacuo* and hexane added (1 mL). The solution was concentrated (*ca*. 0.3 mL) and placed within a –40 °C freezer. Following 18 h, **5-XXVIII** was isolated as SCXRD quality crystals. **^{1}H NMR** (250 MHz, C_6D_6, 298 K): δ = 6.95 (s, 2H, Xyl-*m*-*H*), 6.76 (s, 4H, Xyl-*o*-*H*), 6.53 (s, 2H, Xyl-*p*-*H*), 3.77 (br., 4H, Al-OCH_2CH$_3$), 2.70 (s, 6H, Xyl-*o*-CH_3), 2.26 (s, 3H, Xyl-*p*-CH_3) 2.12 (s, 12H, Xyl-*m*-CH_3), 0.92 (t, $^3J_{HH}$ = 7.0 Hz, 6H, Al-OCH$_2$CH_3), 0.06 (s, 18H, Si(CH_3)$_3$). **MS/LIFDI *m/z* (%) $^-$ve:** 539.1 (AlCl{C$_4$(SiMe$_3$)$_2$Xyl$_2$}(OEt$_2$)-H$^-$, 100), 583.1 (Al{C$_4$H$_4$(SiMe$_3$)$_2$Xyl$_2$}(OEt$_2$)$_2^-$, 2), 540.1 (AlCl{C$_4$(SiMe$_3$)$_2$Xyl$_2$}(OEt$_2$)$^-$, 34), 501.1 (AlCl$_2${C$_4$(SiMe$_3$)$_2$Xyl$_2$}$^-$, 1), 278.0 (C$_4$(H)(OH)Xyl$_2^-$, 10). **MS/LIFDI *m/z* (%) $^+$ve:** 568.3 (Al{C$_4$H(SiMe$_3$)$_2$Xyl$_2$}(Mes)(OH), 2), 405.2 (C$_4$H(SiMe$_3$)$_2$Xyl$_2^+$, 100), 335.2 (C$_4$H$_3$(SiMe$_3$)(Xyl), 40), 317.2 (C$_4$(OH$_2$)(SiMe$_3$)$_2$(Xyl), 63), 203.1 (CH(SiMe$_3$)C(Xyl), 10).

Synthesis of the Lithium Dimesitylalumolate (5-XXIX)

To a J. Young's NMR flask containing a deuterated benzene (0.5 mL) solution of chloroalumole etherate adduct **5-XX** (20.2 mg, 37.3 μmol, 1.0 eq.) was added mesityllithium (9.2 mg, 74.7 μmol, 2

eq.). The colourless solution was heated to 60 °C for 22 h, which yielded a deep-yellow precipitate. ^{1}H NMR spectroscopy identified the high conversion to targeted lithium dimesitylalumolate **5-XXIX** (88%). In a glovebox, the solution was filtered, and the volatiles removed from the filtrate under reduced pressure. Subsequent addition and concentration of hexane (*ca.* 1 mL) yielded a yellow-green solution, which was placed in a –40 °C freezer. Crystalline material was isolated following 1 week at –40 °C and confirmed via SCXRD and ^{1}H NMR spectroscopy as **5-XIX** (8 mg, 32%). **^{1}H NMR** (250 MHz, C_6D_6, 298 K): δ = 6.89 (s, 2H, Xyl-*m*-*H*), 6.69 (s, 4H, Xyl-*o*-*H*), 6.55 (s, 2H, Xyl-*p*-*H*), 2.77 (s, 12H, Xyl-*o*-C*H*$_3$), 2.18 (s, 6H, Xyl-*p*-C*H*$_3$) 2.10 (s, 12H, Xyl-*m*-C*H*$_3$), 0.06 (s, 18H, Si(C*H*$_3$)$_3$).

Attempted Synthesis of 5-XXX with Li[Al{OC(CF$_3$)$_3$}$_4$]

In a J. Young's NMR tube, a lightorange deuterated dichloromethane (0.5 mL) solution of NHC-coordinated chloroalumole **5-XXIV** (30.1 mg, 31.9 µmol, 1.0 eq.) was charged with Li[Al{OC(CF$_3$)$_3$}$_4$] (31.2 mg, 31.9 µmol, 1.0 eq.). A colour change to an opaque yellow was observed. Following 18 h at ambient temperature, the reaction mixture had become light green in colour. Despite 7 days at ambient temperature, the reaction mixture remained turquoise. ^{1}H NMR spectroscopy identified the solution as an indiscernible mixture of species. **N.B.** Attempts to crystallise the targeted species from aromatic and coordinating solvents were undertaken. Microcrystalline material was identified as growing within the concentrated dichloromethane solution, and recrystallisation of this material was also attempted, but without success. Repeating of the reaction with the inclusion of 1 equivalent of DMAP was also attempted to promote crystallisation. Initial crystalline crops were isolated from the reaction mixture following 7 days at –40 °C, however, they were not of sufficient quality for analysis by SCXRD. Recrystallisation of this solid from CH_2Cl_2 following 14 days at –40 °C yielded single crystals of SCXRD quality to be grown. However, samples degraded upon contact with a spatula when isolating for analysis via SCXRD.

Attempted Synthesis of 5-XXXI from Li[Al{OC(CF$_3$)$_3$}$_4$]

In a J. Young's NMR tube, NHC-coordinated chloroalumole **5-XXV** (28.5 mg, 36.9 µmol, 1.0 eq.) and Li[Al{OC(CF$_3$)$_3$}$_4$] (35.9 mg, 36.9 µmol, 1.0 eq.) were dissolved in deuterated dichloromethane (0.5 mL) at ambient temperature. An immediate colour change to dark-yellow was observed, which transitioned to a vibrant blue after standing at room temperature for 16 hours. ^{1}H NMR spectroscopic analysis of the reaction solution revealed the reaction had not yet reached competition, so it was left to stand for a further 2 weeks at room temperature. ^{1}H NMR spectroscopic analysis at this point revealed that the reaction had reached completion, giving a 1:1 mixture of a new symmetrical and unsymmetrical product. **N.B.** Attempts to isolate the equivalent symmetrical and unsymmetrical

products via crystallisation from concentrated deuterated dichloromethane (*ca.* 0.1 mL) solutions were unsuccessful. Layering the reaction mixture with pentane (0.4 mL) yielded an oily dark blue-black product. Investigations to yield crystals from aromatic and coordinating solvents were undertaken. Repeating of the reaction with the inclusion of 1 equivalent of DMAP was also attempted to promote crystallisation. Following 2 weeks at –40 °C, single crystals of SCXRD could be grown, however, degraded in time required to transport to diffractometer despite storage within Schott bottle under inert atmosphere. **MS/LIFDI *m/z* (%) $^{-}$ve:** 966.9 ($Al(O\{C(CF_3)_3\}_4^-$, 100), 537.1 ($AlH\{C_4(SiMe_3)_2Xyl_2\}Xyl^-$, 1). **MS/LIFDI *m/z* (%) $^{+}$ve:** 637.4 ($AlCl\{C_4H_5(SiMe_3)_2(Xyl)\}Imes^+$, 2), 563.3 ($AlCl\{C_4H_4(SiMe_3)(Xyl)\}Imes^+$, 2), 448.3 ($Al\{C_4(SiMe_3)_2Xyl_2\}OH^+$, 1), 305.2 ($ImesH^+$, 100).

Attempted Synthesis of 5-XXXI from Li[Al{OC(CF$_3$)$_3$}$_4$] at Elevated Temperature.

In a J. Young's NMR tube, a transparent deuterated dichloromethane (0.5 mL) solution of NHC-coordinated chloroalumole **5-XXV** (27.1 mg, 35.1 µmol, 1.0 eq.) was charged with Li[Al{OC(CF$_3$)$_3$}$_4$] (34.2 mg, 35.1 µmol, 1.0 eq.). An immediate colour change was observed toward an opaque yellow mixture. The reaction mixture was heated to 40 °C for 18 h, yielding a vibrant dark blue colour. Heating to 40 °C for a further 72 h yielded a mixture of products as identified via ^{1}H NMR spectroscopy. A further 2 weeks at 40 °C with concurrent tracking by NMR spectroscopy identified no further change to the mixture of products, which included the major symmetrical and minor unsymmetrical species. These species were identified at a ratio of symmetrical 1.5 : 1 unsymmetrical. Attempts to isolate either species via crystallisation from saturated deuterated dichloromethane solution (*ca.* 0.1 mL) yielded only SCXRD quality crystals of Li[Al{O-C(CF$_3$)$_3$}$_4$]. Further attempts did not afford the isolation of either species.

Attempted Synthesis of 5-XXXI from Li[Al{OC(CF$_3$)$_3$}$_4$] at Decreased Temperature.

In a glovebox, a 10 ml reaction vial containing a dichloromethane (1 mL) solution of NHC-coordinated chloroalumole **5-XXV** (51 mg, 67.5 µmol, 1.0 eq.) was charged with Li[Al{OC(CF$_3$)$_3$}$_4$] (64 mg, 65.7 µmol, 1.0 eq.) and briefly agitated. The subsequent pale green solution was placed in a –40 °C freezer. Following 18 h, no colour change was observed. The colourless precipitate was removed from the reaction mixture via filtration, and the filtrate returned to –40 °C freezer, with the precipitate kept at ambient temperature. Following 7 days at ambient temperature, the precipitate had become dark blue and identified via ^{1}H NMR spectroscopy to have yielded a mixture of the unknown symmetrical and unsymmetrical products in a ratio of 1 : 2. From the mother liquor at –40 °C, microcrystalline samples were isolated and attempts to recrystallise toward SCXRD quality crystals were unsuccessful despite multiple attempts.

Attempted synthesis of 5-XXXI from Ag[Al{OC(CF$_3$)$_3$}$_4$] at Ambient Temperature.

In a J. Young's NMR tube, a deuterated dichloromethane (0.5 mL) solution of NHC-coordinated chloroalumole **5-XXV** (21.5 mg, 27.9 µmol, 1.0 eq.) was charged with Ag[Al{OC(CF$_3$)$_3$}$_4$] (30.0 mg, 27.9 µmol, 1.0 eq.). An immediate colour change was observed to orange. Following 10 min sonication, the reaction mixture became black with yellow edges and precipitated a colourless solid. ^{1}H NMR spectroscopy identified partial conversion of the **5-XXV**. Following 14 h at ambient temperature, ^{1}H NMR spectroscopy identified complete conversion of **5-XXV** to the previously identified symmetrical major and unsymmetrical minor products at a ratio of 4.5 : 1 respectively. Comparatively, a greater mixture of species and potential decomposition products were also present within the solution. Crystallisation attempts were undertaken in saturated aromatic and halogenated solvents at –40 °C, however, no crystals of SCXRD quality could be grown.

Attempted synthesis of 5-XXXII from Na[{3,5-(CF$_3$)$_2$C$_6$H$_3$}$_4$B] at Ambient Temperature.

In a J. Young's NMR tube, a deuterated dichloromethane (0.5 mL) solution of NHC-coordinated chloroalumole **5-XXV** (30 mg, 39.5 µmol, 1.0 eq.) was charged with Na[{3,5-(CF$_3$)$_2$C$_6$H$_3$}$_4$B] (35 mg, 39.5 µmol, 1.0 eq.). The transparent solution was observed to briefly become a bright-yellow colour, which rapidly transitioned to black upon inversion of the tube. ^{1}H NMR spectroscopy identified an indiscernible mixture of products within the solution. Following 16 h at ambient temperature, ^{1}H NMR spectroscopy speculated the number of species within the solution to have decreased. However, minimal precipitation within the flask was observed. A further 18 h at ambient temperature afforded three distinct species within the solution. This a new unsymmetrical product, and both previously observed unsymmetrical and symmetrical products in a ratio of 8 : 4 : 1 respectively. **N.B.** Attempts were made to isolate a single of the three species, including crystallisation attempts from halogenated and aliphatic solvents.

5.7. References

[1] a) R. Breslow, *C&EN Archives* **1965**, *43*, 90-100; b) R. Breslow, J. Brown, J. J. Gajewski, *J. Am. Chem. Soc.* **1967**, *89*, 4383-4390; c) R. Breslow, *Acc. Chem. Res.* **1973**, *6*, 393-398.

[2] E. Hückel, *Z. Phys. Chem.* **1931**, *70*, 204-286.

[3] H. Braunschweig, I. Krummenacher, J. Wahler, in *Advances in Organometallic Chemistry, Vol. 61* (Eds.: A. F. Hill, M. J. Fink), Academic Press, **2013**, pp. 1-53.

[4] C. A. Tsipis, *Coord. Chem. Rev.* **2005**, *249*, 2740-2762.

[5] D. Y. Zubarev, B. B. Averkiev, H.-J. Zhai, L.-S. Wang, A. I. Boldyrev, *Phys. Chem. Chem. Phys.* **2008**, *10*, 257-267.

[6] J. J. Eisch, N. K. Hota, S. Kozima, *J. Am. Chem. Soc.* **1969**, *91*, 4575-4577.

[7] a) H. Hoberg, R. Krause-Göing, *J. Organomet. Chem.* **1977**, *127*, C29-C31; b) C. Krüger, J. C. Sekutowski, H. Hoberg, R. Krause-Göing, *J. Organomet. Chem.* **1977**, *141*, 141-148.
[8] T. Agou, T. Wasano, P. Jin, S. Nagase, N. Tokitoh, *Angew. Chem. Int. Ed. Engl.* **2013**, *52*, 10031-10034.
[9] J. J. Eisch, W. C. Kaska, *J. Am. Chem. Soc.* **1962**, *84*, 1501-1502.
[10] L. Killian, B. Wrackmeyer, *J. Organomet. Chem.* **1978**, *148*, 137-146.
[11] H. Braunschweig, I. Fernández, G. Frenking, T. Kupfer, *Angew. Chem. Int. Ed. Engl.* **2008**, *47*, 1951-1954.
[12] a) C. Fan, W. E. Piers, M. Parvez, *Angew. Chem. Int. Ed. Engl.* **2009**, *48*, 2955-2958; b) K. Huynh, J. Vignolle, T. D. Tilley, *Angew. Chem. Int. Ed. Engl.* **2009**, *48*, 2835-2837.
[13] C. Fan, W. E. Piers, M. Parvez, R. McDonald, *Organometallics* **2010**, *29*, 5132-5139.
[14] T. Araki, A. Fukazawa, S. Yamaguchi, *Angew. Chem. Int. Ed. Engl.* **2012**, *51*, 5484-5487.
[15] J. Sarcevic, T. Heitkemper, P. N. Ruth, L. Naß, M. Kubis, D. Stalke, C. P. Sindlinger, *Chem. Sci.* **2023**, *14*, 5148-5159.
[16] T. Heitkemper, L. Naß, C. P. Sindlinger, *Dalton Trans.* **2020**, *49*, 2706-2714.
[17] J. Sarcevic, T. Heitkemper, C. P. Sindlinger, *Chem. Commun.* **2022**, *58*, 246-249.
[18] M. Saito, T. Akiba, M. Kaneko, T. Kawamura, M. Abe, M. Hada, M. Minoura, *Chem. Eur. J.* **2013**, *19*, 16946-16953.
[19] F. Ge, G. Kehr, C. G. Daniliuc, G. Erker, *J. Am. Chem. Soc.* **2014**, *136*, 68-71.
[20] V. Y. Lee, H. Sugasawa, O. A. Gapurenko, R. M. Minyaev, V. I. Minkin, H. Gornitzka, A. Sekiguchi, *J. Am. Chem. Soc.* **2018**, *140*, 6053-6056.
[21] R. Chinchilla, C. Nájera, *Chem. Rev.* **2007**, *107*, 874-922.
[22] A. Steffen, R. M. Ward, W. D. Jones, T. B. Marder, *Coord. Chem. Rev.* **2010**, *254*, 1950-1976.
[23] E.-I. Negishi, T. Takahashi, *Acc. Chem. Res.* **1994**, *27*, 124-130.
[24] U. Rosenthal, A. Ohff, W. Baumann, A. Tillack, H. Görls, V. V. Burlakov, V. B. Shur, *Z. Anorg. Allg. Chem.* **1995**, *621*, 77-83.
[25] S. Yamaguchi, Y. Itami, K. Tamao, *Organometallics* **1998**, *17*, 4910-4916.
[26] J. L. Bohlen, L. Endres, R. Drescher, K. Radacki, M. Dietz, I. Krummenacher, H. Braunschweig, *Chem. Sci.* **2023**, *14*, 9010-9015.
[27] C. Xi, S. Huo, T. H. Afifi, R. Hara, T. Takahashi, *Tetrahedron Lett.* **1997**, *38*, 4099-4102.
[28] T. Heitkemper, C. P. Sindlinger, *Chem. Eur. J.* **2019**, *25*, 6628-6637.
[29] a) J. F. Araneda, B. Neue, W. E. Piers, M. Parvez, *Angew. Chem. Int. Ed. Engl.* **2012**, *51*, 8546-8550; b) P. J. Fagan, W. A. Nugent, J. C. Calabrese, *J. Am. Chem. Soc.* **1994**, *116*, 1880-1889.
[30] A. Iida, S. Yamaguchi, *J. Am. Chem. Soc.* **2011**, *133*, 6952-6955.
[31] Z. Zhang, R. M. Edkins, M. Haehnel, M. Wehner, A. Eichhorn, L. Mailänder, M. Meier, J. Brand, F. Brede, K. Müller-Buschbaum, *Chem. Sci.* **2015**, *6*, 5922-5927.
[32] H. Braunschweig, T. Kupfer, *Chem. Commun.* **2011**, *47*, 10903-10914.
[33] H. Braunschweig, C.-W. Chiu, A. Damme, K. Ferkinghoff, K. Kraft, K. Radacki, J. Wahler, *Organometallics* **2011**, *30*, 3210-3216.
[34] a) K. Ansorg, H. Braunschweig, C.-W. Chiu, B. Engels, D. Gamon, M. Hügel, T. Kupfer, K. Radacki, *Angew. Chem. Int. Ed. Engl.* **2011**, *50*, 2833-2836; b) H. Braunschweig, C.-W. Chiu, D. Gamon, K. Gruß, C. Hörl, T. Kupfer, K. Radacki, J. Wahler, *Eur. J. Inorg. Chem.* **2013**, 1525-1530.
[35] A. Fukazawa, J. L. Dutton, C. Fan, L. G. Mercier, A. Y. Houghton, Q. Wu, W. E. Piers, M. Parvez, *Chem. Sci.* **2012**, *3*, 1814-1818.
[36] P. J. Fagan, E. G. Burns, J. C. Calabrese, *J. Am. Chem. Soc.* **1988**, *110*, 2979-2981.
[37] C. Fan, L. G. Mercier, W. E. Piers, H. M. Tuononen, M. Parvez, *J. Am. Chem. Soc.* **2010**, *132*, 9604-9606.
[38] P. P. Power, *Nature* **2010**, *463*, 171-177.

[39] a) D. W. Stephan, *J. Am. Chem. Soc.* **2015**, *137*, 10018-10032; b) N. Li, W.-X. Zhang, *Chin. J. Chem.* **2020**, *38*, 1360-1370; c) D. W. Stephan, *J. Am. Chem. Soc.* **2021**, *143*, 20002-20014.
[40] D. W. Stephan, G. Erker, *Angew. Chem. Int. Ed. Engl.* **2010**, *49*, 46-76.
[41] A. Y. Houghton, V. A. Karttunen, C. Fan, W. E. Piers, H. M. Tuononen, *J. Am. Chem. Soc.* **2013**, *135*, 941-947.
[42] G. E. Herberich, B. Buller, B. Hessner, W. Oschmann, *J. Organomet. Chem.* **1980**, *195*, 253-259.
[43] C.-W. So, D. Watanabe, A. Wakamiya, S. Yamaguchi, *Organometallics* **2008**, *27*, 3496-3501.
[44] H. Braunschweig, C.-W. Chiu, J. Wahler, K. Radacki, T. Kupfer, *Chem. Eur. J.* **2010**, *16*, 12229-12233.
[45] a) H. Braunschweig, R. D. Dewhurst, *Angew. Chem. Int. Ed. Engl.* **2013**, *52*, 3574-3583; b) K. H. Hermannsdörfer, E. M. Und, H. Nöth, *Chem. Ber.* **1970**, *103*, 516-527.
[46] a) C. P. Sindlinger, P. N. Ruth, *Angew. Chem. Int. Ed. Engl.* **2019**, *58*, 15051-15056; b) P. E. Romero, W. E. Piers, S. A. Decker, D. Chau, T. K. Woo, M. Parvez, *Organometallics* **2003**, *22*, 1266-1274; c) P. Tholen, Z. Dong, M. Schmidtmann, L. Albers, T. Müller, *Angew. Chem. Int. Ed. Engl.* **2018**, *57*, 13319-13324.
[47] A. D. Allen, T. T. Tidwell, *Chem. Rev.* **2001**, *101*, 1333-1348.
[48] H. Braunschweig, F. Breher, C.-W. Chiu, D. Gamon, D. Nied, K. Radacki, *Angew. Chem. Int. Ed. Engl.* **2010**, *49*, 8975-8978.
[49] H. Braunschweig, V. Dyakonov, J. O. C. Jimenez-Halla, K. Kraft, I. Krummenacher, K. Radacki, A. Sperlich, J. Wahler, *Angew. Chem. Int. Ed. Engl.* **2012**, *51*, 2977-2980.
[50] R. Drescher, S. Lin, A. Hofmann, C. Lenczyk, S. Kachel, I. Krummenacher, Z. Lin, H. Braunschweig, *Chem. Sci.* **2020**, *11*, 5559-5564.
[51] J. J. Eisch, W. C. Kaska, *J. Am. Chem. Soc.* **1966**, *88*, 2976-2983.
[52] T. Matsumoto, H. Takamine, K. Tanaka, Y. Chujo, *Chem. Lett.* **2015**, *44*, 1658-1660.
[53] R. Drescher, L. Wüst, C. Mihm, I. Krummenacher, A. Hofmann, J. Goettel, H. Braunschweig, *Dalton Trans.* **2021**, *50*, 10400-10404.
[54] H. Fang, C. Zhao, G. Li, Z. Xi, *Tetrahedron* **2003**, *59*, 3779-3786.
[55] T. Wasano, T. Agou, T. Sasamori, N. Tokitoh, *Chem. Commun.* **2014**, *50*, 8148-8150.
[56] T. Agou, T. Wasano, T. Sasamori, N. Tokitoh, *Organometallics* **2014**, *33*, 6963-6966.
[57] N. Tokitoh, T. Agou, T. Wasano, T. Sasamori, *Phosphorus, Sulfur, Silicon Relat. Elem.* **2016**, *191*, 584-587.
[58] V. Y. Lee, H. Sugasawa, O. A. Gapurenko, R. M. Minyaev, V. I. Minkin, H. Gornitzka, A. Sekiguchi, *Organometallics* **2022**, *41*, 467-471.
[59] L. Bührmann, L. Albers, M. Beuße, M. Schmidtmann, T. Müller, *Angew. Chem. Int. Ed. Engl.* **2024**, *63*, e202401467.
[60] Y. Zhang, J. Wei, W.-X. Zhang, Z. Xi, *Inorg. Chem.* **2015**, *54*, 10695-10700.
[61] H. Hoberg, W. Richter, *J. Organomet. Chem.* **1980**, *195*, 347-353.
[62] X. Zhang, H. Wang, X. Lan, Y. Mei, D. A. Ruiz, L. L. Liu, *CCS Chem.* **2023**, *5*, 2059-2068.
[63] J. Li, P. Wu, W. Jiang, B. Li, B. Wang, H. Zhu, H. W. Roesky, *Angew. Chem. Int. Ed. Engl.* **2020**, *59*, 10027-10031.
[64] J. Wei, W.-X. Zhang, Z. Xi, *Chem. Sci.* **2018**, *9*, 560-568.
[65] J. J. Eisch, R. L. Harrell Jr, *J. Organomet. Chem.* **1969**, *20*, 257-260.
[66] R. Drescher, B. Ritschel, R. D. Dewhurst, A. Deißenberger, A. Hofmann, H. Braunschweig, *Chem. Commun.* **2021**, *57*, 7505-7508.
[67] T. Agou, T. Wasano, T. Sasamori, J.-D. Guo, S. Nagase, N. Tokitoh, *Angew. Chem. Int. Ed. Engl.* **2015**, *54*, 9568-9571.
[68] T. Heitkemper, C. P. Sindlinger, *Chem. Eur. J.* **2020**, *26*, 11684-11689.

[69] a) J. E. Leffler, G. Watts, T. Tanigaki, E. Dolan, D. S. Miller, *J. Am. Chem. Soc.* **1970**, *92*, 6825-6830; b) C. Elschenbroich, P. Kuhlkamp, A. Behrendt, K. Harms, *Chem. Ber.* **1996**, *129*, 1407-3160.
[70] L. Werner, J. Hagn, U. Radius, *Chem. Eur. J.* **2023**, *29*, e202303111.
[71] a) J. Hicks, P. Vasko, J. M. Goicoechea, S. Aldridge, *Nature* **2018**, *557*, 92-95; b) H.-Y. Liu, M. S. Hill, M. F. Mahon, C. L. McMullin, R. J. Schwamm, *Organometallics* **2023**, *42*, 2881-2892; c) S. Kurumada, R. Yamanashi, K. Sugita, K. Kubota, H. Ito, S. Ikemoto, C. Chen, T. Moriyama, S. Muratsugu, M. Tada, T. Koitaya, T. Ozaki, M. Yamashita, *Chem. Eur. J.* **2024**, *30*, e202303073.
[72] a) A. W. Overhauser, *Phys. Rev.* **1953**, *92*, 411-415; b) T. R. Carver, C. P. Slichter, *Phys. Rev.* **1953**, *92*, 212-213.
[73] S. Santra, *ChemistrySelect* **2020**, *5*, 9034-9058.
[74] a) T. A. Engesser, M. R. Lichtenthaler, M. Schleep, I. Krossing, *Chem. Soc. Rev.* **2016**, *45*, 789-899; b) I. Krossing, *Chem. Eur. J.* **2001**, *7*, 490-502.
[75] S. Stoll, A. Schweiger, *J. Magn. Reson.* **2006**, *178*, 42-55.
[76] X. Bantreil, S. P. Nolan, *Nat. Protoc.* **2011**, *6*, 69-77.
[77] J. Hicks, M. Juckel, A. Paparo, D. Dange, C. Jones, *Organometallics* **2018**, *37*, 4810-4813.

6. Conclusions

This Thesis concerns the development of new aluminyl anions stabilised by acyclic and four-membered metallocyclic ligands. Following their successful synthesis and isolation, the reactivity of these highly reactive main-group species was explored. In the preparation of the reported aluminium(I) nucleophiles, synthesis was achieved through the reduction of corresponding aluminium(III) iodide precursors.

Once reproducible and reliable methods for synthesising aluminium(III) iodide precursors were established, reduction studies afforded two new aluminyl compounds featuring previously unreported ligand arrangements. Contrasting previously reported aluminyl systems featuring a nucleophilic aluminium(I) centre within metallocycles of various sizes (ranging from 5- to pseudo-8-membered rings), this work achieved the isolation of the first acyclic and four-membered aluminyl systems. Further optimization of synthetic methods reinforced the effectiveness of mechanochemical preparation, giving higher yields of the acyclic aluminyl species (89%) compared to solution-state methods (71%). Density Functional Theory (DFT) calculations determined the electronic structure of these compounds, revealing key information about their highest occupied molecular orbitals (HOMOs), lowest unoccupied molecular orbitals (LUMOs), and corresponding energy gaps. Notably, the orbital energies of the isolated and postulated acyclic aluminyl systems showed a close correlation with analogous seven-membered cyclic diamido aluminyl species. In 4-membered aluminyl anion, the high s-character of the metal centre identified the most stable calculated HOMO energy.

The reactivity of these aluminyl species was investigated towards various substrates. Reinforcing the umpolung (polarity inversion) reactivity of the aluminyl centre, aluminium methyl derivatives were synthesised by exposing these species to the electrophilic carbon source methyliodide. Additionally, nucleophilic substitutions with electrophilic metal sources (magnesium and aluminium) produced unsupported aluminium-metal bonded compounds. Emulating transition metals, oxidative addition products were identified through C-H and N-H activations using acyclic and four-membered aluminyl species. The acyclic aluminyl species was utilised as a novel reducing agent in the preparation of aromatic boroldiide dianions and borole radical monoanions from antiaromatic borole reagents.

Finally, the preparation and reactivity of alumole complexes targeting halo- and aryl-substituted species were explored. The predominant species obtained from these investigations were tetracoordinate compounds, often in the form of Lewis acid-base adducts or aluminate complexes, which serve as viable and applicable reagents for further chemical transformations.

7. Future Work

In synthesising the first acyclic and four-membered cyclic aluminyl anions, this Thesis has opened several investigative avenues. Key areas of further investigation are highlighted for their potential to expand the coordination motifs, structural arrangements, and reactivity of aluminyl systems reported in this work.

Minor variations in the sterically bulky groups used within ligand systems present opportunities to tailor the reactivity and stability of the aluminyl species. In the acyclic systems, smaller aryl groups on amido centres may aid in the preparation of precursors and enhance the reactivity of the aluminyl centre. On the other hand, exploring non-aryl substituents on the silyl backbone of the four-membered systems could prevent the formation of polymeric solid-state structures, while larger aryl substituents on amido centres may promote the formation of contact dimeric pair systems.

Alongside acyclic and 4-membered ligand system expansions, investigating variations in alkali metal cations has a precedent in the literature for synthetic applications through extending metal centre reactivity. The use of varied counterions, such as smaller cations (lithium, sodium) and larger ones (rubidium, caesium), could be applied to both acyclic and four-membered species. These changes may lead to different structural arrangements and reactive behaviours, which could be compared spectroscopically and synthetically across a range of substrates, including small molecules.

Due to time constraints, only limited studies were conducted to assess the reactivity of the new aluminyl anion species with small molecules. In future work, a catalogue of small molecules (e.g., CO, CO_2, NO, N_2O, SO_2) should be tested with the new aluminyl systems. These experiments would be conducted in a variety of aromatic, aliphatic, and coordinating solvents to aid in the stabilisation and isolation of potential activation derivatives. The findings could guide further refinements to aluminyl species by varying the kinetics and electronic properties of the ligands. Specifically, the potential use of the acyclic aluminyl species in a masked aluminylene reactive mode could be explored, where reactions with sterically demanding substrates drive the displacement of one of the monoanionic amido ligands, further enhancing the species' reactivity.

Finally, as briefly explored in this work, the coordination chemistry of acyclic and four-membered aluminyl anions with transition metals, rare-earth elements, and main group elements warrants further exploration. Beyond the conducted iron investigations, the use of these aluminyl systems as monoanionic, monodentate ligands to stabilise low-oxidation state and structurally diverse complexes in the broader *d*- and *f*-blocks could be investigated. Furthermore, the role of aluminyl anions as ligands in the *p*-block would also be examined. Specifically, the preparation of an acyclic aluminyl species stabilised by two aluminyl ligands would be an exciting avenue for future study.

8. Appendix

8.1. Publications in Support of this Thesis

1. A. J. R. Matthews, R. A. Jackson, P. Vasko, M. F. Mahon, J. Hicks, D. J. Liptrot, *Chem. Commun.* **2023**, *59*, 5277-5280

2. F. Kallmeier, A. J. R. Matthews, G. R. Nelmes, N. R. Lawson, J. Hicks, *Dalton Trans.* **2024**, *53*, 12450-12454

8.2. X-ray Crystallography

X-ray diffraction experiments were performed using a Rigaku Supernova dual-source diffractometer using Cu Kα which was upgraded from a CCD detector to a Rigaku Hybrid Pixel 2-dimensional detector (HyPix-6000HE) during this work, or Rigaku Xcalibur using Mo Kα radiation for compounds in Chapters 2 – 4. Crystals were suspended in immersion oil, mounted on Micromount loops, and quench-cooled to 150 K using an Oxford Cryostream N_2 cooler at the Australian National University. Crystal structure analyses of compounds in Chapter 5 were measured on a Bruker Kappa APEXII Duo diffractometer (Mo Kα, λ = 0.7107 ˚A) at 150 K by Dr. W. Frey at the University of Stuttgart. Data was processed using the CrysAlisPro package,[1] solved using the SHELX software package,[2] refined using Olex2,[3] and visualised using ORTEP-3.[4]

8.3. Computational Studies

All theoretical calculations in Chapter 3 were obtained in collaboration with Dr Petra Vasko of the University of Helsinki. All theoretical calculations in Chapter 4 were obtained in collaboration with BSc. Gareth Nelmes of the Australian National University. All Density Functional Theory work presented here was done using Gaussian16 (Revision C.01).[5] Geometry optimizations and frequency calculations were done by using the PBE1PBE functional,[6] Def2-TZVP basis set for all atoms,[7] Grimme's empirical dispersion correction with Becke-Johnson damping (GD3BJ) and an ultrafine integration grid.[8] The stationary points found were confirmed to be minima on the potential energy surface (no imaginary frequencies).

8.4. Summary of Crystallographic Data

8.4.1. Crystallographic and Refinement Parameters for the Structures in Chapter 2

	2-VII	**2-IX**	**2-X**	**2-XIII**	**2-XIV**	**2-XV** •2(benzene)	**2-XVI**
Empirical formula	$C_{27}H_{54}AlNOSi$	$C_{40}H_{76}Al_2N_2O_2Si_2$	$C_{25}H_{48}AlI_2NOSi$	$C_{18}H_{32}KNSi$	$C_{36}H_{64}Li_2N_2Si_2$	$C_{33}H_{50}AlI_3KNSi$	$C_{21}H_{38}AlI_3LiNSi$
Formula weight	463.78	727.16	687.51	329.63	594.95	935.61	747.23
Cell setting	monoclinic	monoclinic	triclinic	orthorhombic	triclinic	monoclinic	monoclinic
Space group	$P2_1/c$	$P2_1/c$	P-1	Pnma	P-1	$P2_1/c$	$P2_1$
a [Å]	10.9320(3)	11.0482(2)	10.3104(4)	11.4989(4)	9.1598(4)	10.2460(4)	9.5082(3)
b [Å]	24.2783(7)	18.6340(3)	11.6091(5)	14.8969(5)	11.8755(5)	12.8910(5)	14.8600(3)
c [Å]	11.0531(3)	22.0233(3)	12.6535(4)	11.1469(3)	18.2762(8)	29.2185(11)	10.4674(3)
α [°]	90	90	87.061(3)	90	95.592(4)	90	90
β [°]	91.005(3)	96.2850(10)	80.876(3)	90	97.468(4)	92.756(3)	102.547(3)
γ [°]	90	90	87.551(3)	90	103.302(4)	90	90
Volume [$Å^3$]	2933.16(14)	4506.73(13)	1492.50(10)	1909.44(11)	1901.51(15)	3854.8(3)	1443.64(7)
Z	4	4	2	4	2	4	2
Unique / I > 2σI	8217/6615	8854/6990	5853/5094	1998/1672	7483/5845	9295/7575	4023/3923
R_{int}	0.0505	0.0308	0.0312	0.0428	0.0382	0.0288	0.0350
Parameters	294	451	292	110	393	347	263
R1 (all data / I > 2σI)	0.0593/0.0442	0.0562/0.0403	0.0423/0.0354	0.0468/0.0381	0.0742/0.0563	0.0453/0.0323	0.0395/0.0382
wR2 (all data / I > 2σI)	0.1218/0.1119	0.1010/0.0935	0.0886/0.0844	0.1033/0.0974	0.1498/0.1403	0.0678/0.0609	0.1017/0.1005
GooF	1.020	1.025	1.023	1.063	1.079	1.066	1.043
Residual max / min	0.442/-0.342	0.317/-0.222	0.815/-0.940	0.280/-0.265	0.066/-0.335	1.118/-0.783	1.135/-1.1638
T [K]	149.99(10)	150.00(10)	150.01(10)	150.01(10)	150.00(10)	150.00(10)	150.00(10)

	2-XVII	**2-XVIII** •2(benzene)	**2-XIX** •2(toluene)	**2-XX**	**2-XXIV**	**2-XXV**	**2-XXVI**
Empirical formula	$C_{42}H_{76}AlIN_2Si_2$	$C_{82}H_{134}I_2Li_4N_4Si_4$	$C_{75}H_{126}I_2Li_4N_4Si_4$	$C_{30}H_{52}AlIN_2Si_2$	$C_{40}H_{56}Al_2N_2Si$	$C_{41}H_{57}AlN_2OSi$	$C_{41}H_{55}AlN_2OSi$
Formula weight	819.10	1569.84	1477.71	650.79	646.91	648.95	646.94
Cell setting	Monoclinic	triclinic	triclinic	triclinic	monoclinic	monoclinic	monoclinic
Space group	$P2_1/c$	P-1	P-1	P-1	$P2_1$	$P2_1/c$	$P2_1/c$
a [Å]	18.8006(2)	9.9121(2)	17.9377(4)	10.1072(6)	9.6684(11)	10.806(2)	10.737(2)
b [Å]	13.66544(13)	12.9378(6)	18.7085(3)	10.2573(6)	17.0863(12)	18.722(4)	18.632(4)
c [Å]	18.6649(2)	17.0804(7)	19.8445(5)	17.9608(8)	12.0616(13)	19.408(4)	19.238(4)
α [°]	90	82.617(3)	80.455(2)	89.292(4)	90	90	90
β [°]	112.8002(15)	81.555(2)	85.466(2)	83.539(4)	110.583(12)	103.46(3)	103.95(3)
γ [°]	90	89.278(2)	67.426(2)	66.374(6)	90	90	90
Volume [$Å^3$]	4420.64(10)	2148.66(13)	6063.3(2)	1694.04(18)	1865.3(3)	3818.6(14)	3735.1(14)
Z	4	1	3	2	2	4	4
Unique / I > 2σI	8869/8446	8370/7299	23755/20790	8652/6769	6973/5306	11219/9544	10938/9505
R_{int}	0.0379	0.0367	0.0305	0.0244	0.0423	0.0420	0.0392
Parameters	504	480	23755/20790	339	420	446	424
R1 (all data / I > 2σI)	0.715/0.0696	0.0477/0.0404	0.0469/0.0400	0.0678/0.0479	0.0828/0.0551	0.0535/0.0469	0.0525/0.0468
wR2 (all data / I > 2σI)	0.2058/0.2034	0.1027/0.0971	0.1055/0.1004	0.1280/0.1162	0.1068/0.0921	0.1356/0.1263	0.1355/0.1297
GooF	1.034	1.025	1.032	1.035	1.031	1.072	1.053
Residual max / min	1.523/-2.418	1.115/-1.023	1.370/-0.746	0.785/-1.286	0.322/-0.305	0.296/-0.425	0.431/-0.463
T [K]	150.00(10)	150.00(10)	150.00(10)	149.9(7)	150.00(10)	100.0(2)	100.0(2)

	2-XXVII	**2-XXIX** •(benzene)	**2-XXX** •(hexane)	**2-XXXI**	**2-XXXII** •5(benzene)	**2-XXXIV** •2(benzene)
Empirical formula	$C_{40}H_{54}AlIN_2OSi$	$C_{78}H_{94}Li_4N_4Si_2$	$C_{78}H_{100}Li_6N_4Si_2$	$C_{36}H_{44}AlI_2KN_2Si$	$C_{102}H_{118}Al_2I_4Li_2N_4Si_2$	$C_{84}H_{100}Al_2I_4N_4Si_2$
Formula weight	760.82	1171.51	1191.43	852.70	2031.62	1783.41
Cell setting	monoclinic	monoclinic	Triclinic	monoclinic	triclinic	monoclinic
Space group	Cc	$P2_1/c$	P-1	$P2_1/c$	P-1	$P2_1/c$
a [Å]	12.45690(10)	13.28090(10)	12.1726(2)	10.64990(10)	10.6936(6)	10.8298(5)
b [Å]	17.08710(10)	11.90680(10)	12.3490(2)	17.6051(2)	13.9672(9)	23.1883(11)
c [Å]	19.0922(2)	21.3402(2)	12.7768(3)	19.5193(2)	16.6076(11)	16.4445(8)
α [°]	90	90	76.876(2)	90	80.535(5)	90
β [°]	107.0410(10)	91.7900(10)	68.798(2)	94.1860(10)	87.099(5)	94.961(4)
γ [°]	90	90	74.742(2)	90	89.498(5)	90
Volume [$Å^3$]	3885.40(6)	3372.94(5)	1708.81(6)	3649.96(7)	2443.6(3)	4114.1(3)
Z	4	2	1	4	1	2
Unique / I > 2σI	6128/5901	7110/6217	7172/6290	7682/7053	11517/7872	8632/6675
R_{int}	0.0449	0.0334	0.0326	0.0572	0.0434	0.0326
Parameters	445	405	429	401	507	429
R1 (all data / I > 2σI)	0.0291/0.0275	0.0414/0.0364	0.0489/0.0435	0.0469/0.0441	0.0986/0.0647	0.0695/0.0478
wR2 (all data / I > 2σI)	0.0660/0.0655	0.1003/0.0964	0.1212/0.1162	0.1210/0.1182	0.1759/0.1490	0.0949/0.0849
GooF	1.079	1.064	1.065	1.060	1.065	1.050
Residual max / min	0.386/-0.439	0.263/-0.331	0.464/-0.271	1.267/-1.875	2.237/-1.563	0.847/-0.536
T [K]	150.00(10)	150.00(10)	148(3)	150.01(10)	200.00(10)	149.99(10)

8.4.2. Crystallographic and Refinement Parameters for the Structures in Chapter 3

	3-I	**3-II**	**3-III** •4(benzene)	**3-IV**	**3-VI** •(toluene)	**3-X** •0.5(cyclohexane)	**3-XI**
Empirical formula	$C_{42}H_{75}AlN_2Si_2$	$C_{42}H_{76}AlKN_2Si_2$	$C_{54}H_{88}AlN_2NaSi_2$	$C_{36}H_{58}AlKN_2Si_2$	$C_{66}H_{101}AlMgN_4Si_2$	$C_{45}H_{84}AlKN_2O_7Si_2$	$C_{48}H_{90}AlKN_4O_7Si_2$
Formula weight	691.20	731.30	871.41	641.10	1057.97	887.40	957.49
Cell setting	triclinic	orthorhombic	orthorhombic	orthorhombic	triclinic	monoclinic	monoclinic
Space group	P-1	$P2_12_12_1$	Pbca	$P2_12_12_1$	P-1	$P2_1/c$	$P2_1/c$
a [Å]	10.7132(3)	13.1992(4)	17.0226(2)	22.1102(5)	12.8772(5)	14.03370(10)	18.4500(3)
b [Å]	17.4975(4)	14.9863(3)	24.8233(3)	33.7684(8)	14.6377(6)	17.9311(2)	14.3596(2)
c [Å]	23.2424(8)	22.2794(3)	25.2815(3)	10.7300(3)	17.2412(6)	20.8039(2)	21.8271(3)
α [°]	88.161(2)	90	90	90	87.531(3)	90	90
β [°]	89.527(3)	90	90	90	83.372(3)	91.1720(10)	106.9570(10)
γ [°]	84.609(2)	90	90	90	84.087(3)	90	90
Volume [$Å^3$]	4335.3(2)	4407.02(15)	10682.9(2)	8011.3(3)	3209.3(2)	5233.99(9)	5531.34(14)
Z	4	4	10	8	2	4	4
Unique / I > 2σI	17067/13595	8623/8105	10440/8171	14148/13016	12477/11296	10886/9121	11476/9503
R_{int}	0.0324	0.0258	0.0330	0.0785	0.0176	0.0443	0.0410
Parameters	896	456	565	678	732	571	622
R1 (all data / I > 2σI)	0.0722/0.0558	0.0470/0.0438	0.0623/0.0450	0.0616/0.0578	0.0466/0.0426	0.0552/0.0447	0.0549/0.0435
wR2 (all data / I > 2σI)	0.1496/0.1377	0.1149/0.1118	0.1247/0.1142	0.1595/0.1562	0.1224/0.1183	0.1197/0.1133	0.1104/0.1051
GooF	1.017	1.021	0.983	1.073	1.008	1.031	1.034
Residual max / min	1.281/-0.807	0.543/-0.257	0.424/-0.260	0.6714/-0.263	0.556/-0.306	0.442/-0.229	0.270/-0.462
T [K]	150.00(10)	150.00(10)	150.01(10)	150.00(10)	150.01(10)	150.00(10)	150.00(10)

8.4.3. Crystallographic and Refinement Parameters for the Structures in Chapter 4

	4-I	**4-II** •2(benzene)	**4-III**	**4-IV**	**4-V** •5(benzene)	**4-VIII**	**4-IX** •5(benzene)
Empirical formula	$C_{92}H_{110}Al_2Fe_2N_4O_4Si_2$	$C_{48}H_{56}AlKN_2Si$	$C_{40}H_{52}KLiN_2OSi$	$C_{40}H_{54}KLiN_2OSi$	$C_{102}H_{118}Al_2Cl_{2.9}I_{1.1}N_4Na_2Si_2$	$C_{59}H_{73}AlMgN_4Si$	$C_{148}H_{180}Al_2Mg_2N_8Si_2$
Formula weight	1557.67	755.11	650.96	652.98	1798.51	917.59	2229.75
Cell setting	Orthorhombic	Monoclinic	triclinic	Monoclinic	triclinic	triclinic	monoclinic
Space group	Pbca	C2/c	P-1	$P2_1/c$	P-1	P-1	$P2_1/c$
a [Å]	19.4527(2)	18.9921(7)	9.69020(10)	21.0310(2)	10.5898(2)	12.3143(9)	19.1216(4)
b [Å]	19.4412(2)	9.9605(3)	10.3466(2)	18.2366(2)	13.9711(2)	13.1653(9)	15.6628(3)
c [Å]	44.6082(6)	24.6950(9)	18.3791(2)	21.2866(2)	16.3013(3)	18.9356(14)	22.1485(5)
α [°]	90	90	90.4910(10)	90	98.5680(10)	77.761(6)	90
β [°]	90	109.403(4)	94.2510(10)	109.7240(10)	93.146(2)	76.025(6)	103.034(2)
γ [°]	90	90	94.5650(10)	90	90.0640(10)	66.714(7)	90
Volume [$Å^3$]	16870.1(3)	4406.3(3)	1831.61(4)	7685.14(14)	2381.18(7)	2712.9(4)	6462.5(2)
Z	8	4	2	8	1	2	2
Unique / I > 2σI	17462/14131	4677/4000	7580/6540	15984/13489	9990/8681	3394/2702	13391/9289
R_{int}	0.0528	0.0791	0.0330	0.0585	0.0415	0.0277	0.0890
Parameters	1017	282	423	849	540	632	729
R1 (all data / I > 2σI)	0.0611/0.0464	0.0893/0.0792	0.0457/0.0384	0.0529/0.0454	0.0562/0.0502	0.0633/0.0466	0.1050/0.0668
wR2 (all data / I > 2σI)	0.1204/0.1126	0.2209/0.2120	0.0950/0.0917	0.1294/0.1229	0.1411/0.1364	0.1221/0.1142	0.1462/0.1315
GooF	1.028	1.056	1.055	1.047	1.068	1.060	1.029
Residual max / min	0.734/-0.310	0.436/-0.358	0.249/-0.277	0.382/-0.352	0.794/-0.642	0.226/-0.166	0.548/-0.294
T [K]	150.00(10)	150.01(10)	150.00(10)	150.15(10)	150.00(10)	150.00(10)	150.00(10)

	4-X •0.5(benzene)	**4-XI** •0.5(benzene)	**4-XII** •3.5(benzene)
Empirical formula	$C_{51}H_{71}AlKN_2O_6Si$	$C_{66}H_{93}AlKN_3O_6$ Si	$C_{114}H_{143}K_3Li_2N_4O_6Si_2$
Formula weight	902.26	1118.60	1852.68
Cell setting	triclinic	orthorhombic	triclinic
Space group	P-1	Fdd2	P-1
a [Å]	14.108(2)	37.146(4)	12.7165(2)
b [Å]	18.223(3)	31.124(3)	16.8876(2)
c [Å]	19.969(3)	22.127(3)	25.5441(4)
α [°]	91.882(13)	90	78.6030(10)
β [°]	91.205(13)	90	85.2240(10)
γ [°]	90.746(13)	90	85.1240(10)
Volume [$Å^3$]	5129.2	25581(5)	5345.58(14)
Z	4	16	2
Unique / I > 2σI	8865/2145	3225/1471	22293/18488
R_{int}	0.2168	0.0946	0.0421
Parameters	809	280	1218
R1 (all data / I > 2σI)	0.4002/0.1677	0.2166/0.1228	0.0660/0.0548
wR2 (all data / I > 2σI)	0.5013/0.33457	0.3724/0.3053	0.1525/0.1451
GooF	0.966	1.027	1.026
Residual max / min	0.495/-0.420	0.430/-0.406	0.536/-0.463
T [K]	293(2)	150.00(10)	150.00(10)

8.4.4. Crystallographic and Refinement Parameters for the Structures in Chapter 5

	5-XII •2(toluene)	**5-XX**	**5-XXII**	**5-XXIV**	**5-XXVI** •(benzene)	**5-XXVIII** •(pentane)	**5-XXIX**
Empirical formula	$C_{74}H_{120}Al_2N_4Si_4$	$C_{30}H_{46}AlClOSi_2$	$C_{29}H_{43}AlI_2OSi_2$	$C_{62}H_{87}AlClN_2Si_2$	$C_{32}H_{42}AlCl_2LiSi_2$	$C_{44}H_{69}AlOSi_2$	$C_{48}H_{68}AlLiOSi_2$
Formula weight	1232.05	541.28	744.59	978.94	587.65	697.15	751.12
Cell setting	monoclinic	orthorhombic	triclinic	Monoclinic	monoclinic	Monoclinic	triclinic
Space group	C2/c	Pnma	P-1	$P2_1/c$	C2/c	$P2_1/c$	P-1
a [Å]	18.4947(17)	15.0480(5)	8.0171(4)	24.4407(19)	14.5110(7)	17.5283(12)	10.4927(4)
b [Å]	22.672(2)	21.2692(9)	13.1362(6)	14.1465(11)	9.8560(4)	17.0204(12)	12.0045(4)
c [Å]	18.3490(16)	10.2361(3)	16.8110(8)	18.1735(14)	22.6767(9)	15.6775(9)	21.1854(7)
α [°]	90	90	74.983(3)	90	90	90	77.225(2)
β [°]	105.885(6)	90	79.185(3)	108.989(3)	90.810(2)	101.785(2)	89.529(2)
γ [°]	90	90	86.174(3)	90	90	90	66.924(2)
Volume [$Å^3$]	7400.2(12)	3276.2(2)	1679.30(14)	5941.6(8)	3242.9(2)	4578.6(5)	2385.05(15)
Z	4	4	2	4	4	4	2
Unique / I > 2σI	6860/3301	3441/2735	6186/4349	14672/9852	3288/2554	8382/5134	9744/6403
R_{int}	0.1149	0.0356	0.0453	0.0773	0.0347	0.0564	0.0392
Parameters	365	188	337	730	178	463	504
R1 (all data / I > 2σI)	0.1780/0.0805	0.0700/0.0531	0.0904/0.0624	0.1071/0.0660	0.0776/0.0578	0.1104/0.0610	0.1001/0.0557
wR2 (all data / I > 2σI)	0.2553/0.1994	0.1629/0.1486	0.2034/0.1837	0.1947/0.1610	0.1627/0.1509	0.1979/0.1621	0.1404/0.1208
GooF	1.025	1.030	1.042	1.031	1.059	1.026	1.014
Residual max / min	0.857/-0.676	1.382/-0.360	1.249/-2.534	0.664/-0.473	0.808/-0.337	0.653/-0.308	0.340/-0.267
T [K]	150(2)	150.00(2)	150.00(2)	150(2)	150.01(2)	150.01(2)	150(2)

8.5. References

[1] R. O. Diffraction, **2021**.

[2] a) G. M. Sheldrick, *Acta Cryst.* **2015**, *71*, 3-8; b) G. M. Sheldrick, *Acta Cryst.* **2015**, *71*, 3-8.

[3] O. V. Dolomanov, L. J. Bourhis, R. J. Gildea, J. A. K. Howard, H. Puschmann, *J. App. Cryst.* **2009**, *42*, 339-341.

[4] L. J. Farrugia, *J. App. Cryst.* **2012**, *45*, 849-854.

[5] M. J. Frisch, G. W. Trucks, H. B. Schlegel, G. E. Scuseria, M. A. Robb, J. R. Cheeseman, G. Scalmani, V. Barone, G. A. Petersson, H. Nakatsuji, X. Li, M. Caricato, A. V. Marenich, J. Bloino, B. G. Janesko, R. Gomperts, B. Mennucci, H. P. Hratchian, J. V. Ortiz, A. F. Izmaylov, J. L. Sonnenberg, Williams, F. Ding, F. Lipparini, F. Egidi, J. Goings, B. Peng, A. Petrone, T. Henderson, D. Ranasinghe, V. G. Zakrzewski, J. Gao, N. Rega, G. Zheng, W. Liang, M. Hada, M. Ehara, K. Toyota, R. Fukuda, J. Hasegawa, M. Ishida, T. Nakajima, Y. Honda, O. Kitao, H. Nakai, T. Vreven, K. Throssell, J. A. Montgomery Jr., J. E. Peralta, F. Ogliaro, M. J. Bearpark, J. J. Heyd, E. N. Brothers, K. N. Kudin, V. N. Staroverov, T. A. Keith, R. Kobayashi, J. Normand, K. Raghavachari, A. P. Rendell, J. C. Burant, S. S. Iyengar, J. Tomasi, M. Cossi, J. M. Millam, M. Klene, C. Adamo, R. Cammi, J. W. Ochterski, R. L. Martin, K. Morokuma, O. Farkas, J. B. Foresman, D. J. Fox, Wallingford, CT, **2016**.

[6] a) J. P. Perdew, K. Burke, M. Ernzerhof, *Phys. Rev. Lett.* **1997**, *78*, 1396-1396; b) J. P. Perdew, K. Burke, M. Ernzerhof, *Phys. Rev. Lett.* **1996**, *77*, 3865-3868; c) C. Adamo, V. Barone, *J. Chem. Phys.* **1999**, *110*, 6158-6170.

[7] F. Weigend, R. Ahlrichs, *Phys. Chem. Chem. Phys.* **2005**, *7*, 3297-3305.

[8] S. Grimme, S. Ehrlich, L. Goerigk, *J. Comput. Chem.* **2011**, *32*, 1456-1465.